NOTICE

The quality of this microform is heavily dependent upon the quality of the original thesis submitted for microfilming. Every effort has been made to ensure the highest quality of reproduction possible.

If pages are missing, contact the university which granted the degree.

Some pages may have indistinct print especially if the original pages were typed with a poor typewriter ribbon or if the university sent us an inferior photocopy.

Reproduction in full or in part of this microform is governed by the Canadian Copyright Act, R.S.C. 1970, c. C-30, and subsequent amendments.

AVIS

La qualité de cette microforme dépend grandement de la qualité de la thèse soumise au microfilmage. Nous avons tout fait pour assurer une qualité supérieure de reproduction.

S'il manque des pages, veuillez communiquer avec l'université qui a conféré le grade.

La qualité d'impression de certaines pages peut laisser à désirer, surtout si les pages originales ont été dactylographiées à l'aide d'un ruban usé ou si l'université nous a fait parvenir une photocopie de qualité inférieure.

La reproduction, même partielle, de cette microforme est soumise à la Loi canadienne sur le droit d'auteur, SRC 1970, c. C-30, et ses amendements subséquents.

CONSTRUCTIONAL AND ALTERATION FEATURES AND THEIR RELATIONSHIPS TO SULFIDE DEPOSITS IN THE UPPER PART OF THE TROODOS OPHIOLITE, CYPRUS

by

JING-SUI YANG

Submitted in partial fulfillment of the requirements
for the degree of Doctorate of Philosophy

at

Dalhousie University
Halifax, Nova Scotia
December, 1991

ISBN 0-315-71417-4

DALHOUSIE UNIVERSITY

FACULTY OF GRADUATE STUDIES

The undersigned hereby certify that they have read and recommend to the Faculty of Graduate Studies for acceptance a thesis entitled: " Constructional and Alteration Features and their Relationships to Sulfide Deposits in the Upper Part of the Troodos Ophiolite, Cyprus"

by Jingsui Yang

in partial fulfillment of the requirements for the degree of Doctor of Philosophy.

Dated _____

External Examiner

Research Supervisor

Examining Committee

D A L H O U S I E U N I V E R S I T Y

DATE: Dec. 19, 1991

AUTHOR: YANG, Jing-sui

TITLE: CONSTRUCTIONAL AND ALTERATION FEATURES AND THEIR RELATIONSHIPS TO SULFIDE DEPOSITS IN THE UPPER PART OF THE TROODOS OPHIOLITE, CYPRUS

DEPARTMENT OR SCHOOL: Department of Earth Sciences

DEGREE: PhD CONVOCATION: February YEAR: 1992

Permission is herewith granted to Dalhousie University to circulate and to have copied for non-commercial purposes, at its discretion, the above title upon the request of individuals or institutions.

Signature of Author

TABLE OF CONTENTS

LIST OF FIGURES

LIST OF TABLES

LIST OF MAPS

(in back pocket)

ABSTRACT

The well developed Troodos ophiolite, Cyprus, is preserved within a regular anticline structure, allowing the study of constructional features of the Troodos-type oceanic crust and the examination of relationships between constructional features of ophiolite and in-situ oceanic crust. Field observations and measurements were carried out along 18 profiles spaced at about 2.5 km, and oriented approximately normal to the average spreading direction in the Extrusive Sequence, i.e., between the sediment-extrusive interface (SEI) and the Sheeted Dikes Complex (SC), on the northeastern part of the ophiolite.

A number of important features of the upper part of this type of oceanic crust have been recognized in this study: (1) Within the 45 km of spreading distance covered by the 18 lines, the proportion of pillowed lava flows at different stratigraphic levels is remarkably constant and a high proportion of pillows and thick pillowed sequences are generally concentrated at the top of extrusive sequence. At least two volcanic cycles are present in vertical section of the central part of the area. (2) Dikes occur throughout the extrusive sequence but increase in abundance with depth at different rates from place to place. (3) Three regional hydrothermal alteration zones can be recognized within the extrusive sequence. They are, from top to bottom, the brownstone (approximating to the zeolite facies), transition, and greenstone (approximating to the greenschist facies) alteration zones. A transition in alteration, from a clay-carbonate brownstone facies to a chlorite-quartz greenschist facies takes place at between dike abundance of 25% and 50%. (4) The 13 sulfide deposits in the study area, comparable with that observed on the present oceanic spreading ridges, occur in four groups in the extrusive sequence and generally occur just above the 25% dike abundance contour on the flanks of major areas of sheet flows.

Features are closely linked on a regional scale to dike abundance, suggesting that dike abundance is the most important factor in controlling many features of the uppermost 1-2 km of Troodos and perhaps in-situ oceanic crust. An average of 41% of pillowed flows in the extrusives, combined with some other characteristics in the ophiolite, suggests that the Troodos oceanic crust was formed at a relatively intermediate-fast spreading rate (4-7.5 cm/yr half rate). It is likely that differential preservation has played a role in present distribution of sulfide deposits and dikes were possibly a major heat source responsible for the hydrothermal alteration and sulfide mineralization accompanying crustal formation in the ancient ocean represent by the Troodos ophiolite.

ACKNOWLEDGEMENTS

I sincerely thank Dr. Jim Hall, my thesis supervisor, for the original idea for the thesis, constant support and great help during this study.

Drs. Pat Ryall, Nick Culshaw, Marcos Zentilli and Becky Jamieson in the department of Earth Sciences, Dr. Randy Koski of the Geological Survey of United States, and Dr. James Franklin of the Geological Survey of Canada are much appreciated for their careful reviews, critical comments, and vital suggestions, which have significantly improved the thesis.

I am grateful to Charlie Walls for the assistance in the field and much help in the laboratory work. Thanks are also due to Gordon Brown for good quality thin sections, Bob Mackay for guidance in microprobe analyses, and Tom Duffett for the preparation of the photos in the thesis. Alice Giddy, Darlene Van de Rijt, Norma Keeping, Jane Barrett, and Brant Laidler are thanked for the kindness and help.

Field work for the thesis received great support from people in Cyprus. I wish to thank Dr. Panayiotou and Vassos Nicolaou and the people of the Geological Survey of Cyprus for their help and allowing me to use air photos and unpublished geological and mining data. I would like to express my great regards to the people living in the Mathiatis village, especially to Andreas and his family and grandma and grandpa, and to the people lived in the Ayia Marina village, especially to Andreas and his family restaurant, Demetris and his friend, for their warm friendship and hospitality, and for so many great times I spent with them. The Embassy of the People's Republic of China in Nicosia, Cyprus, is acknowledged for the help during the field work.

Thanks also to all the friends in Halifax for their friendship and help during this studying period. The discussions on computer usage and geology with doctorates and current doctoral students, especially Dr. Zhang Min (Biology Department), Long Changxin (Earth Sciences Department), Dr. Huang Zehui (Bedford Institute of Oceanography), Xu Zhigang (Oceanography Department), Qian Deping (Oceanography Department), and Zhang Jun (Physics Department), were helpful.

The Institute of Geology, Chinese Academy of Geological Sciences Beijing, China, and my colleagues there, especially Profs. Bai Wenji and Jiang Chunfa, are appreciated for their assistance and encouragement during this study.

Finally, I thank Lata for much help and the drafting. Thanks also to Mair and James for the field assistance, and to my wife, Fu Xiu-yin and both of our families for their support.

Financial support for experimental and field studying was from NSERC operating support to Dr. Jim Hall. Fellowship support was received from the Faculty of Graduate Studies and Faculty of Science at Dalhousie University.

Chapter 1 INTRODUCTION

This thesis project is to study first and second order constructional and alteration features in the upper part of the Troodos ophiolite and to examine relationships between constructional features of ophiolite and in-situ oceanic crust. By comparing these features in ophiolites and in present oceanic crust, it may be possible to understand better the environment of ophiolite crustal construction, as well as to provide guidance for the study of the oceanic crust.

Generally, in a well-developed ophiolite complex, the uppermost Extrusive Sequence is dominated by pillowed and sheeted basalts, beneath which is a sheeted dike complex, in turn underlain by a cumulate gabbro/ultramafic layer and upper mantle tectonites. These regional pseudo-stratigraphical layers may be described as the first order structures of the oceanic crust represented in the ophiolite. The variations within these layers can then be described as second order features. Examples of second order features are the lateral variations in the thickness and lithological types of the extrusive sequence, variation in the abundance of dikes laterally and with depth, variation of alteration zonation, and in spatial relationships between the distribution of sulfide deposits and other constructional features. (Hall et al., 1989a; Yang et al., 1988). Variations can be sought in

both the spreading and axial directions.

1.1 Review of current knowledge of and questions regarding in-situ oceanic crust

Since present oceanic crust is analogous to ophiolites, remainders of ancient oceanic crust, in many aspects, such as pseudo-stratigraphical sequences, physical properties of individual sequences, and their formation by spreading process, then, before starting a description of a research project on the Troodos ophiolite, it is essential to review our knowledge of, and unsolved questions regarding, present oceanic crust.

In last two decades, the study of present oceanic crust has made striking progress in the understanding of formational processes that take place in the rift valleys and ridges and constructional features in three dimensions. Today scientists can descend into even the deepest parts of the oceans in small research submarines. They can observe features directly or take photographs of them. Most submersibles also are equipped with mechanical arms to select geological and biological samples. These observations have greatly improved our knowledge about the present oceanic crust both along the spreading ridges and off-axes.

Generally, direct observation or photography of the seafloor, seismic reflection and refraction, and deep drilling on the seafloor are the three most effective methods in modern ocean investigations. Some of the main new results from application of these methods are briefly described below.

1. Results from direct observation on the seafloor

(1) One of the most significant results from recent studies is the direct observation and sampling of a section of crust and upper mantle exposed at the Vema fracture zone in the slow spreading Atlantic (Auzende et al., 1989). The section consists of (from bottom to top) 1) upper-mantle-derived peridotites (exposed for a thickness of about 1 km); 2) a lower-crust gabbroic unit (thickness of about 500 m); 3) a mid-crust dike complex (thickness of 700-1100 m); (4) an upper-crust eruptive basalt unit (thickness of up to 800 m) (Fig. 1.1.1). The observed sequence is similar in kind to those inferred from seismic-refraction experiments, deep-sea drilling on the seafloor and observations from ophiolites (e.g., Stoffa and Talwani, 1978; Coleman, 1977).

(2) High-resolution images covering large areas of the seafloor reveal numerous discontinuities along the mid-ocean ridges. These discontinuities occur at a range of scales of 10-1,000 km and define a fundamental segmentation of seafloor

(a)

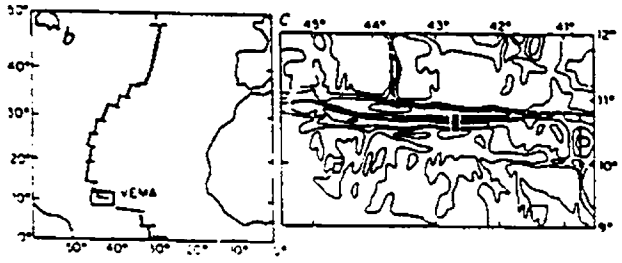

(b)

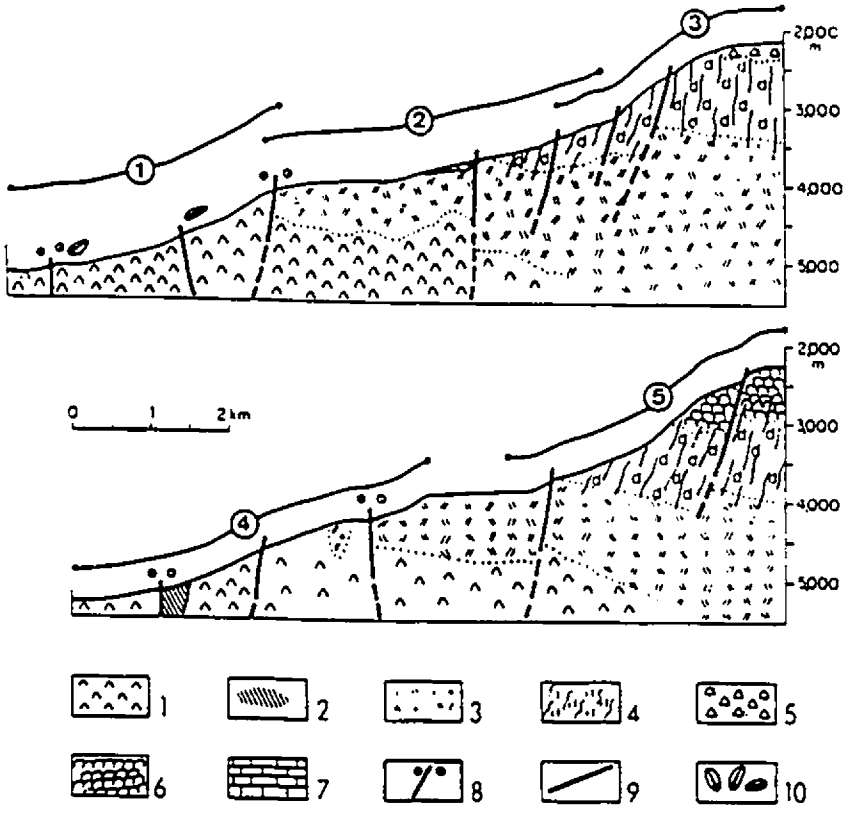

Fig. 1.1.1 A section of oceanic crust and upper mantle directly observed at the Vema fracture zone in the Atlantic using the French submersible Nautile. (a) location maps; (b) two synthetic geological sections consisting of 5 small profiles. 1-serpentinites; 2-amphibolites; 3-gabbros; 4-dikes complex; 5-basalt pavement; 6-pillows; 7-indurated sediments; 8-strike-slip faults; 9-normal faults; 10-clams (After Auzende et al., 1990).

spreading centres (Fig. 1.1.2) (Macdonald, 1986; Macdonald et al., 1988). Langmuir et al. (1986) find geochemical evidence for segmentation on an even finer scale along the crest (10-50 km) of the EPR. They propose that all discontinuities of the ridge represent boundaries between regions or ridge segments with separate magma supplies. Results from chemical analyses of over 200 glasses by Langmuir et al. indicate that one-third of the length of the East Pacific Rise (EPR) in this section contains at least some basalts more enriched than normal MORB. In addition, it is significant that glasses ranging in composition from basaltic andesite with 53% silica to dacite with almost 70% silica were recovered in three on-axis dredges and one off-axis dredge in their study. These data challenge the models which attempt to explain normal basalts on axis and both normal and enriched basalts off-axis and, furthermore, indicate that the general concept of fast-spreading ridges being more homogeneous than slow-spreading ridges such as the Mid-Atlantic Ridge is no longer valid (Langmuir et al., 1986).

(3) Along the strike of a spreading ridge a cyclic process of seafloor spreading occurs, expressed, for example, by a periodic cycle of volcanic processes during oceanic crust construction (Stakes et al., 1984). A typical example is at the Mid-Atlantic Ridge (MAR), where the FAMOUS and AMAR areas represent two different stages of a cyclic process of seafloor spreading (Fig. 1.1.3) (Stakes et al., 1984; Macdonald, 1982;

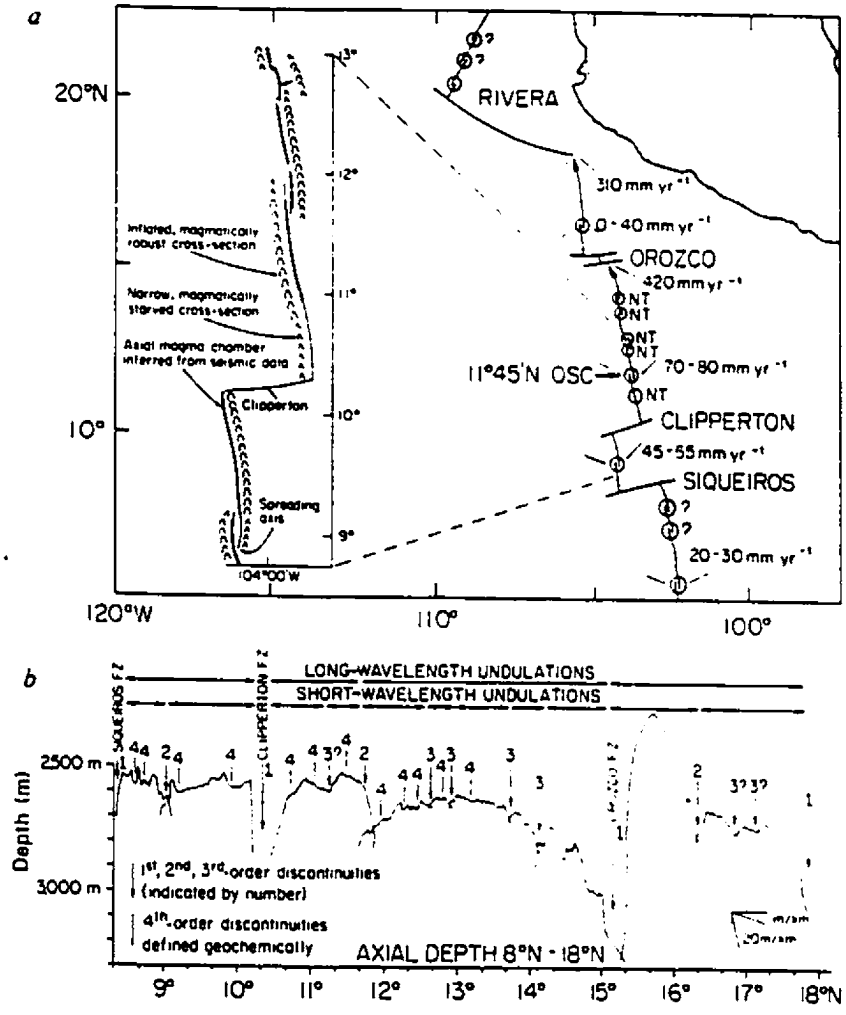

Fig. 1.1.2 Recently mapped section of the East Pacific Rise by SeaMARC II and Sea Beam sonar systems reveals several orders of ridge discontinuities (After Macdonald et al., 1988).

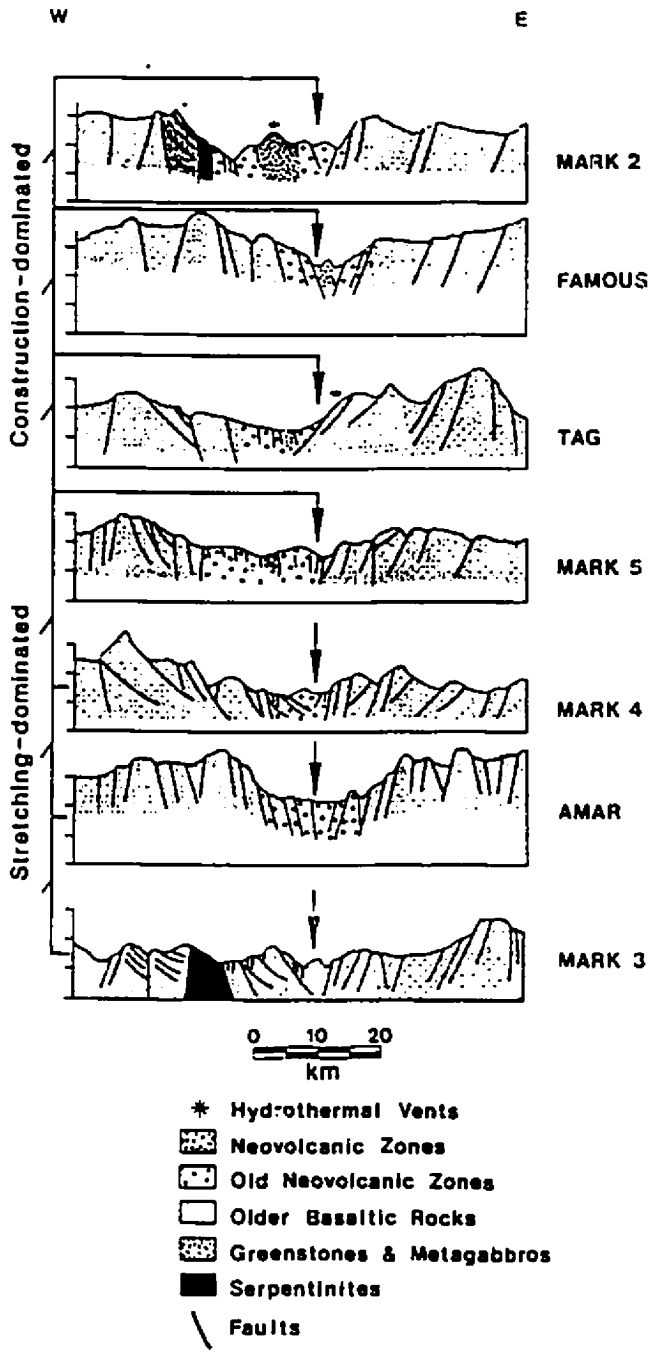

Fig. 1.1.3 Recent investigations with the submersible Alvin and the Angus deep-towed camera indicate cyclic process of volcanic activity and spreading along the Mid-Atlantic Ridge (after Karson et al., 1987).

Crane and Ballard, 1981; Karson et al., 1987). The former represents an area which has experienced a relatively recent volcanic constructional event and the latter represents an area in which tectonic extension dominates. These different median valley structures have been interpreted as alternates between two stages with more or less continuous tectonic extension and periodic magmatism (Karson et al., 1987).

The cyclicity of eruption style in the slow and fast spreading ridges has been noted since the earlier 1980's (e.g., Francheteau and Ballard, 1983; Lichtman and Eissen, 1983; Macdonald, 1982; and Lewis, 1979). The cyclic volcanic episodes are characterized by the repeated emplacement of both early-stage, high-eruptive-rate, sheet flow lavas and late-stage, low-effusion-rate, pillow lavas (Ballard and Francheteau, 1983). The amplitude of an individual eruptive event on the ocean floor is variable. Individual eruptions may cover an area as large as 220 km^2 (with a volume of 15±4 km^3) as found for a recently erupted lava field on the EPR near lat 8°S. The lava field extends up to 18 km off-axis and inundates scarps up to 100 m high (Macdonald et al., 1989). Again, Davis (1982) and Holcomb et al. (in Macdonald, 1989) have found that submarine lavas erupted at hotspot volcanoes may travel as much as 60 km from their vents under optimal conditions of very gentle slopes (0.001) and minimal roughness. In contrast, many pillowed flows extend for a much more limited distance

from vents, which may be related to a slow eruptive rate.

(4) Hydrothermal mineralization at seafloor spreading centres is currently one of the most actively researched subjects. Being irregularly distributed it is, by definition, a second order feature of oceanic crust construction. Known hydrothermal mineralization at seafloor spreading centres occurs in different host-rock lithologies (volcanic- and sediment-hosted), at ridges with different rates of seafloor spreading, and at different stages of opening of an ocean basin (e.g., Thompson et al., 1988; Kappel and Franklin, 1989; Horibe et al., 1986; Scott, 1987; Fouquet et al., 1991; Crane et al., 1985). Some of the hydrothermal mineral occurrences are large ($\geq 1 \times 10^6$ tonnes), but most are very small. The most extensive hydrothermal deposit (1.5- 3.8 Mt) was found near 12°43'N on an off-axis volcano located at 6 km from the axial graben of the EPR (Hekinian and Bideau 1985).

Marchig et al. (1988) reported that, on the EPR between 18° and 24°S (at a spreading rate of 162 mm/yr, Macdonald, 1986), large occurrences of sulfide are restricted to zones in which there is more tectonic strain, i.e., high volcanic production and fracture, than usual for sea-floor spreading centres. These sites are also characterised by a relatively shallow bathymetric position and greater coverage with sheet lava than with pillow lava. The highest parts of the spreading

zone are those that are particularly rich in hydrothermal massive sulfides. Rona and Clague (1989) found that present and past hydrothermal discharge on the northern Gorda Ridge is controlled by the intersection of faults and fissures near the shallowest part of the ridge segment where magmatic sources are most accessible. Kappel and Franklin (1989) note that some deposits in the Northeast Pacific Ocean do not occur in areas of the youngest lavas and are found in areas dominated by pillowed flows rather than sheet lava flows. Karson and Rona (1990) distinguished three episodes for hydrothermal outflow driven by separate magmatic events in the TAG area, MAR 26°N.

2. Results from geophysical methods

Relatively speaking, geophysical methods are traditional and useful in the investigation of ocean floor, e.g., the seismic-reflection and refraction techniques provide a basis for general understanding of the construction of oceanic crust at depth.

(1) Toomey et al. (1990) report the three-dimensional seismic velocity structure of the EPR near 9°30'N, which reveals the specific relation between sites of vertical injection of magma and the tectonic segmentation of the rise axis (Fig. 1.1.4). A linear high-velocity anomaly, approximately 1-2 km in width and restricted to the uppermost

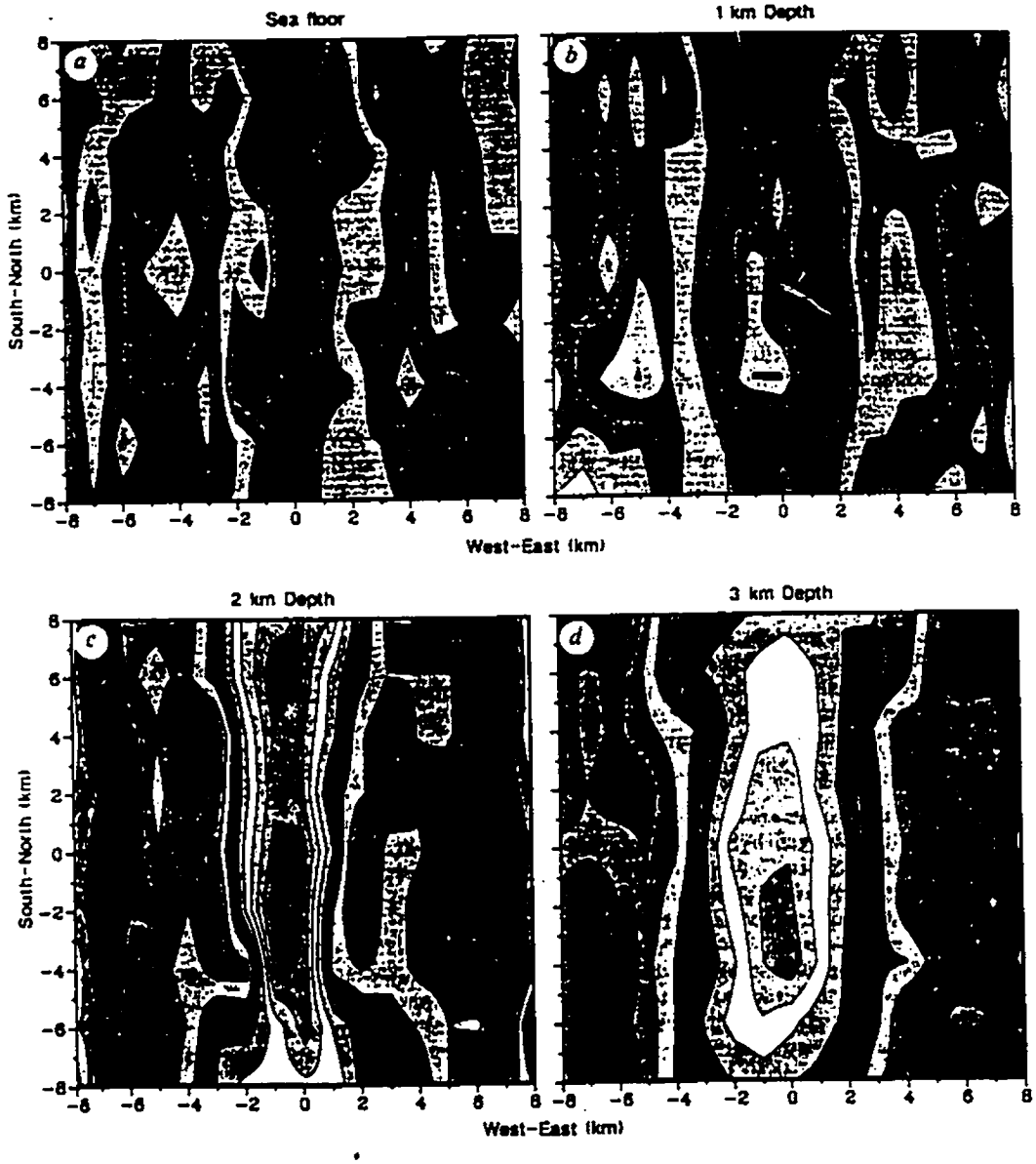

Fig. 1.1.4 Horizontal cross-sections through a 3-D P-wave velocity structure resulting from tomographic inversion. 3-D images of crustal seismic structures beneath the East Pacific Rise near lat 9°30'N show pronounced axial heterogeneity over distances of a few kilometres (after Toomey et al., 1990).

1 km of the crust, is centred on the rise axis. The three-dimensional images of crustal seismic structure show pronounced axial heterogeneity over distances of a few kilometres. Also, a morphological analysis of the Juan de Fuca Ridge (JDFR) by Kappel and Ryan (1986) led them to propose that ridge crest topography is not steady-state but is evolutionary with different stages in a cycle of oceanic crust accretion.

White et al. (1990) reported remarkable new images of the internal structure of oceanic crust that had been recorded from a two-ship multichannel seismic survey in the western North Atlantic (Fig. 1.1.5). The internal structure of the crust records the magmatic and tectonic history of the crust as it was generated at, and then moved away from, the spreading centre. On the other hand, a recent result from 2-D seismic refraction tomography reveals three layers for the upper crust beneath the Juan de Fuca Ridge, but the data preclude the existence of a significant shallow-level magma chamber (White and Clowes, 1990).

(2) An important result in the recent study of the first-order constructional features in the present oceanic crust is the improvement of the knowledge of magma chambers beneath the present spreading ridges (e.g., Detrick et al., 1987; Kent et al., 1990; Smith and Cann, 1990).

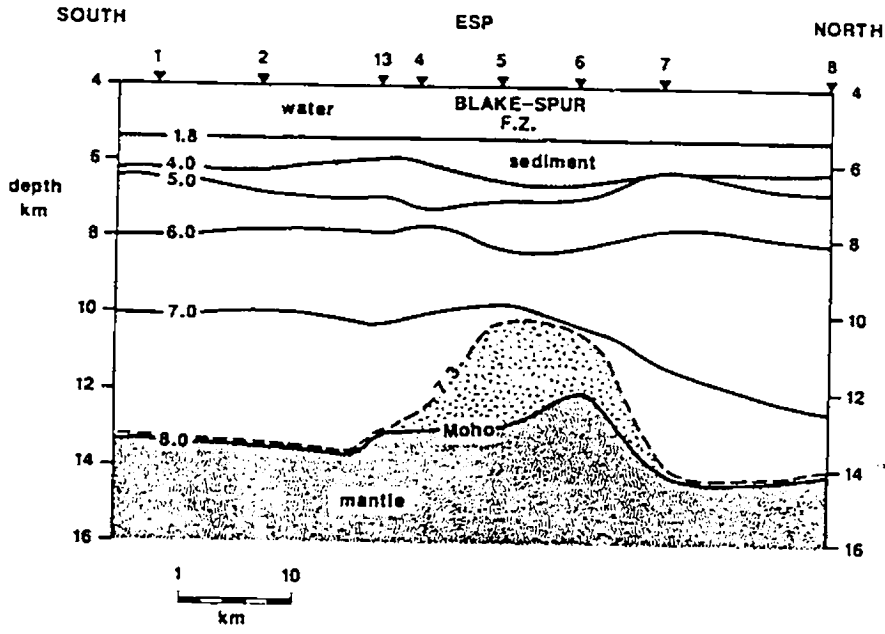

Fig. 1.1.5 A two-ship multichannel seismic survey in the western North Atlantic recorded new images of the internal structure of oceanic crust. Hachured area with velocities above 7.3 km/s shows extent of inferred partial serpentinization of mantle (after White et al., 1990).

Detrick et al. (1987) and Burnett et al. (1989) reported cross-axis seismic reflection profiles and tomographic images from the EPR between 8°50'N and 13°30'N for the first time provide evidence of a magma chamber located 1.2-2.4 km below the sea floor. The magma chamber is quite narrow (<4-6 km wide), but can be traced as a nearly continuous feature for tens of kilometres along the rise axis. The Lau Basin, where a magma chamber has also been imaged, is a small back-arc basin associated with subduction at the Tonga Trench. The magma chamber reflector is at a depth of 3 km beneath the sea floor and varies in width between 1 and 2.5 km (Collier and Sinha, 1990).

Recently, many new results obtained from multi-technical methods seem clearly to preclude the existence of large, steady-state magma chambers under the entire MAR rift valley; however, it is suggested that smaller, localized crustal magma bodies could be present, at least intermittently (e.g., Detrick et al., 1990). Smith and Cann (1990) report that the ridge axis is riddled by a multitude of recently active volcanoes which are far more numerous than on the EPR. This can be regarded as another important feature of crustal construction on slow spreading ridges. Smith and Cann (1990) report 481 seamounts, interpreted as being small volcanoes, recently found from a ~6000 km^2 survey of the median valley floor of the Mid-Atlantic Ridge between 24 and 30°N (Fig.

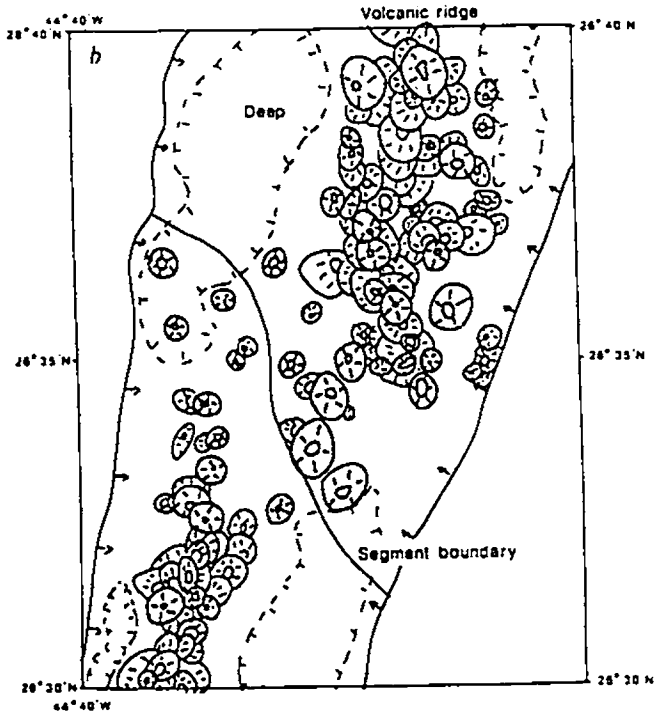

Fig. 1.1.6 Hundreds of small volcanoes identified from Sea Beam swaths on the median valley floor of the Mid-Atlantic Ridge at 24-30°N show that the magmatic style at the MAR contrasts with that of the EPR (after Smith and Cann, 1990).

1.1.6). The abundant seamounts suggest that, at least on this section of the MAR, seamount volcanism plays an important part in the formation of new oceanic lithosphere. Since large magma chambers are thought to be absent along the MAR (e.g., Detrick et al., 1990), it is possible that the MAR seamounts represent the products of individual batches of magma rising from the mantle, evolving in small magma chambers and erupting from point sources, or more probably, produced from intermediate-sized magma chambers which are not large enough to sustain fissure eruptions but may feed several small volcanos (Smith and Cann, 1990). Since the seamounts are so numerous, one might expect oceanic crust created at slow-spreading centres to be far more heterogeneous than at fast-spreading centres, and, accordingly, Macdonald (1990) suggests possible differences between sources of volcanism for fast- and slow-spreading ridges (Fig. 1.1.7).

3. Results from deep-sea drilling

Sampling material from on and below the seafloor is a most effective method in the study of the present oceanic crust. Generally, larger and shallower exposed samples were collected by dredging, which is still used because it collects large samples relatively inexpensively. However, deep-sea drilling can provide continuous, stratigraphically correct information on the deep crust, especially where it is sediment

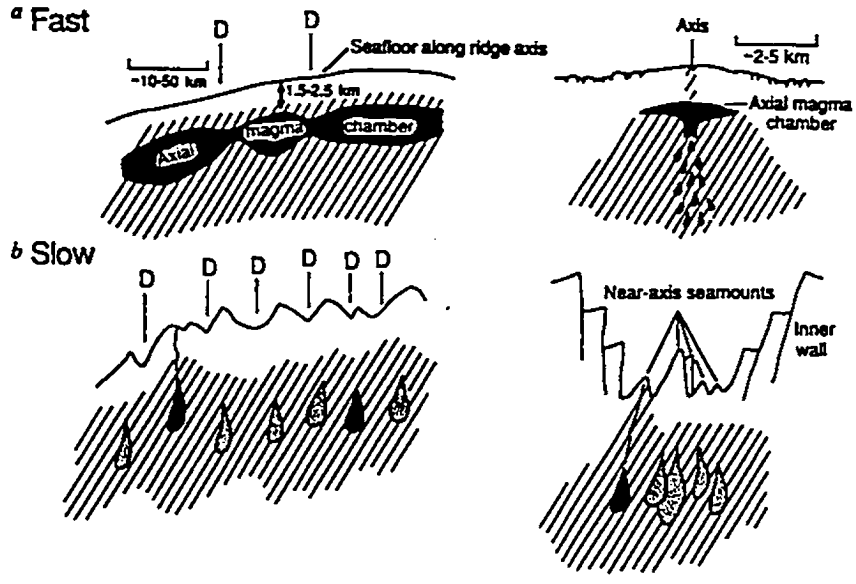

Fig. 1.1.7 Possible differences between sources of volcanism for (a) fast and (b) slow-spreading ridges. Hatched areas indicate regions of hot rock, dark areas indicate magma; in b, stippled areas indicate recently frozen magma pockets and 'D's' indicate very small ridge-axis discontinuities (after Macdonald, 1990).

covered. The Deep Sea Drilling Program (DSDP) and the subsequent Ocean Drilling Program (ODP) are the two worldwide ocean study projects concerned with drilling the seafloor. The DSDP started in 1968 and obtained cores from 624 sites through 1983, using the Glomar Challenger. In 1983 the ODP continued the work, using the drilling ship JOIDES Resolution. As of April 1990, the ODP had completed drilling at 184 sites (Coch and Ludman, 1991). However, only a very limited numbers of holes have penetrated to over 500 m in oceanic crust. In addition, because these limited deep holes are usually widely separated, information on second order features, in particular of crustal construction is limited.

(1) The results from early deep-sea drilling in the North Atlantic Ocean were summarized by Hall and Robinson (1979). Penetration of basement to depths greater than 500 m was achieved at three sites and a number of shallower holes had also been drilled (Fig. 1.1.8). Pillowed and massive basalts are the major lithological types in the drilled sections, and, relatively, pillows are abundant. Other rocks are gabbros and ultramafic rocks, but neither sheeted dikes nor greenschist facies alteration were observed from the drillcores. Several lines of evidence suggested that crustal construction at the Mid-Atlantic Ridge is episodic rather than continuous. Volcanic activity in the median rift appeared to be strongly episodic for time periods of less than $\sim 10^5$ years. In some

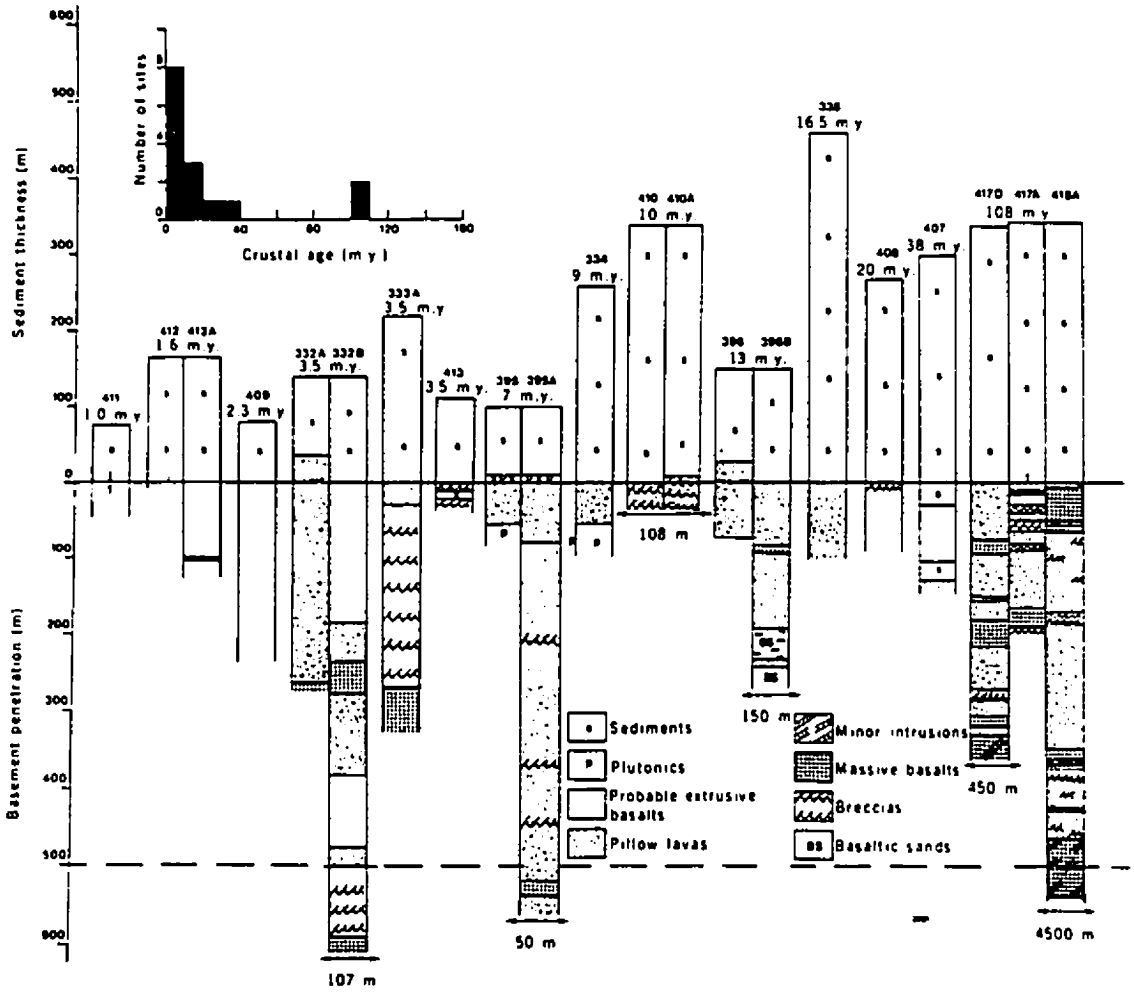

Fig. 1.1.8 Lithologic profiles for North Atlantic basement drill holes, providing information of construction of in-situ oceanic crust (after Hall and Robinson, 1979).

instances, palaeomagnetic characteristics suggest that two or more magma chambers of restricted size coexisted beneath the rift valley and erupted essentially contemporaneously (Fig. 1.1.9). The almost complete lack of lateral lithologic and stratigraphic continuity in the crust suggests that eruptions onto the seafloor are very local. Alteration in drilled basalts has proved almost everywhere to be due to low temperature seawater-rock interaction. Evidence for higher temperature hydrothermal alteration has been found only at two holes that are over 500 m deep in basement. One is Hole 504B (e.g., Backer et al., 1989). The other is Hole 786B, which is located at a convergent margin in the Bonin/Mariana Region (Shipboard Scientific Party, Site 786, 1990).

(2) The study of the hydrothermal alteration of seafloor volcanics has also made great progress since samples have been collected from DSDP/ ODP drillholes. Specifically, Hole 504B, by far the deepest hole yet drilled into the oceanic crust in situ, which extends through 274.5 m of sediment and 1725.9 m into basement to late 1991, provides the most complete section for hydrothermal alteration studies of about 571.5 m of extrusive lavas and 945.4 m of intrusive sheeted dikes, as well as a 209 m transition between them (Becker et al., 1989; ODP Leg 140 Scientific Party, 1991, personal communication). Three alteration zones in hole 504B are recognized with distinct assemblages of secondary minerals (Honnorez et al.,

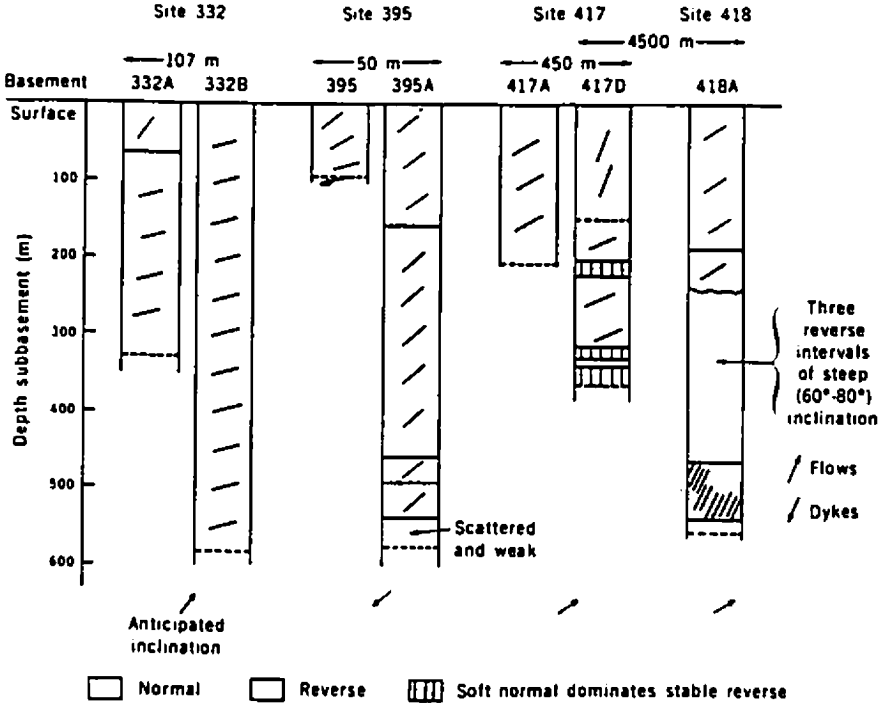

Fig. 1.1.9 Palaeomagnetic inclinations and polarities in basalts recovered from the four basement sites in the North Atlantic show a remarkable scatter implying a complex construction of the crust (Hall and Robinson, 1979).

1983; Alt et al., 1986; Shipboard Scientific Party, Hole 504B, Leg 111, 1988; Alt et al., 1989; ODP Leg 140 Scientific Party, 1991, personal communication).

From the above statement, it is evident that studies of construction of the ocean floor have been greatly extended recently. These include the division of spreading phases and eruptive cycles, the recognition of magma chambers and magmatic features, hydrothermal alteration zonation, and sulfide deposit distribution. Episodic spreading processes and volcanic activity with associated hydrothermal sulfide mineralization along the ridges are typically widely observed on the present ocean floors. Such favourable conditions at the present ocean ridges, i.e., extending up to several thousands kilometres exposure with almost bare surfaces and no post-constructional tectonically disturbed sequences, are lacking in ophiolites, ancient oceanic crust on land, which usually have both limited exposure and tectonically disturbed sequences.

However, it is noted that the features of crustal construction observed at present spreading ridges are mostly limited to axial directions, where the crust is not covered by sediments, and can be traced for long distances along the ridge crests. In contrast, knowledge of crustal constructional features at depth at seafloor spreading centres is generally

limited such that complete information is available only for the surface, and almost unknown in the depth dimension. The reasons for this situation are quite understandable. Away from the ridges, newly formed crust will quickly be covered by sediments. Therefore, to study this part of the crust, we need drilling or geophysical methods.

There are many technical difficulties involved with deep sea drilling on the ocean floor, especially for holes deep in the basement. In addition, the costs of drilling are extremely high. As a result, although deep sea drilling has been carried out continuously for over two decades, and over 1000 holes have been drilled, there are only very few deep holes (over 500 m deep in basement), e.g., only three holes among hundreds in the North Atlantic Ocean and one hole (504B) over 1000 m deep in the basement in the Pacific Ocean. Knowledge of the character of the rest of the crust has been based largely on the results of marine refraction work and correlation of the seismic velocities determined in these experiments with possible rock types.

Knowledge of some deep constructional features in the oceanic crust can be obtained from seismic work, e.g., layers with different velocities and the presence of magma chambers. However, these methods mostly yield first order features rather than the second order ones of in-situ oceanic crust,

and can not determine directly lithology, alteration history or volcanic massive sulfide mineralization.

In these circumstances, a well developed and preserved ophiolite may possibly provide more information in the spreading and depth dimensions than studies of present oceanic ridges.

In summary, definitive knowledge or ideas regarding the lithological construction in the vertical dimension of oceanic crust, including the nature of the extrusive layer as a whole, and its contact with or transition to a supposed underlying sheeted dike zone, is not yet generally available. Deep sea drilling, except at Hole 504B, has not so far provided much information on the questions of deeper structure. The reason for this is, in part, that the lithological features along spreading axes are much more easily observed than those perpendicular or vertical to the axis. With continuous detailed seismic data either sparse or difficult to interpret, and drilling in the main still too shallow or widely spaced, it is reasonable to turn to ophiolitic sections on land for further insight into variations in oceanic crust in all dimensions on scales from a few kilometres to a few tens of kilometres.

Since only a few ophiolites are known definitely to have

a MORB affinity and, as a consequence, there is a tendency to conclude that most ophiolites are derived from island arc-back arc environments (Nicolas, 1989), then how do ophiolites compare with oceanic lithosphere? Coleman (1984) points out that MORB chemistry is based on samples from the vicinity of active ridges, that very little is known of older oceanic crust, and emphasizes the limits of present knowledge. Also, Nicolas (1989), taking the Oman ophiolite as an example, proposes that this question of the environment of origin for ophiolites is still open. On the other hand, although oceanic crust preserved in ophiolites may sometimes represent a special environment of crustal construction (e.g., Moores et al., 1984), and spreading rate was thought to be the single most influential parameter explaining the diversity of oceanic lithosphere and ophiolites (Boudier and Nicolas, 1985; Nicolas, 1989), at least for some ophiolites the special environment of crustal construction appears to modify the chemical rather than the physical aspect of construction, sediment-sealing, fluid-flow, and alteration characteristics of the crust so formed (Hall et al., 1989a). For this reason this thesis is based on study of a well preserved ophiolite, i.e., the Troodos ophiolite of Cyprus, with many similarities to in-situ oceanic crust, to gain further insight into the constructional nature of oceanic crust at depth.

1.2 The Troodos ophiolite of Cyprus

Cyprus is a 9300 km^2 island in the north-east corner of the Mediterranean. The Troodos ophiolite lies in the southwestern part of Cyprus. Including the inliers of the Akamas Peninsula and Troulli, the ophiolite has an east-west extent of almost 130 km, which is approximately in the spreading direction during crustal construction, and from north to south a maximum width of just over 30 km (Fig. 1.2.1).

The Troodos ophiolite may be one of the remnants of a Mesozoic ocean basin (Neotethys) that formed between the Eurasian and Afro-Arabian plates, and it is still being emplaced onto the northern margin of Africa at present (Dilek et al., 1990). The ophiolite is one of the best preserved and most thoroughly studied ophiolite complexes in the world. It comprises two parts separated by the nearly east-west tending Arakapas fault zone. The northern part, which constitutes the main Troodos massif, includes a broad, east-west tending elongate dome that consists of a central core of tectonized peridotite and serpentinite overlain successively by a pseudo-stratigraphic sequence consisting of mafic-ultramafic cumulate plutonic sequence, a sheeted dike complex, extrusive rocks, and sedimentary rocks. The southern part, including the Limassol Forest complex, consists of tectonized peridotite and

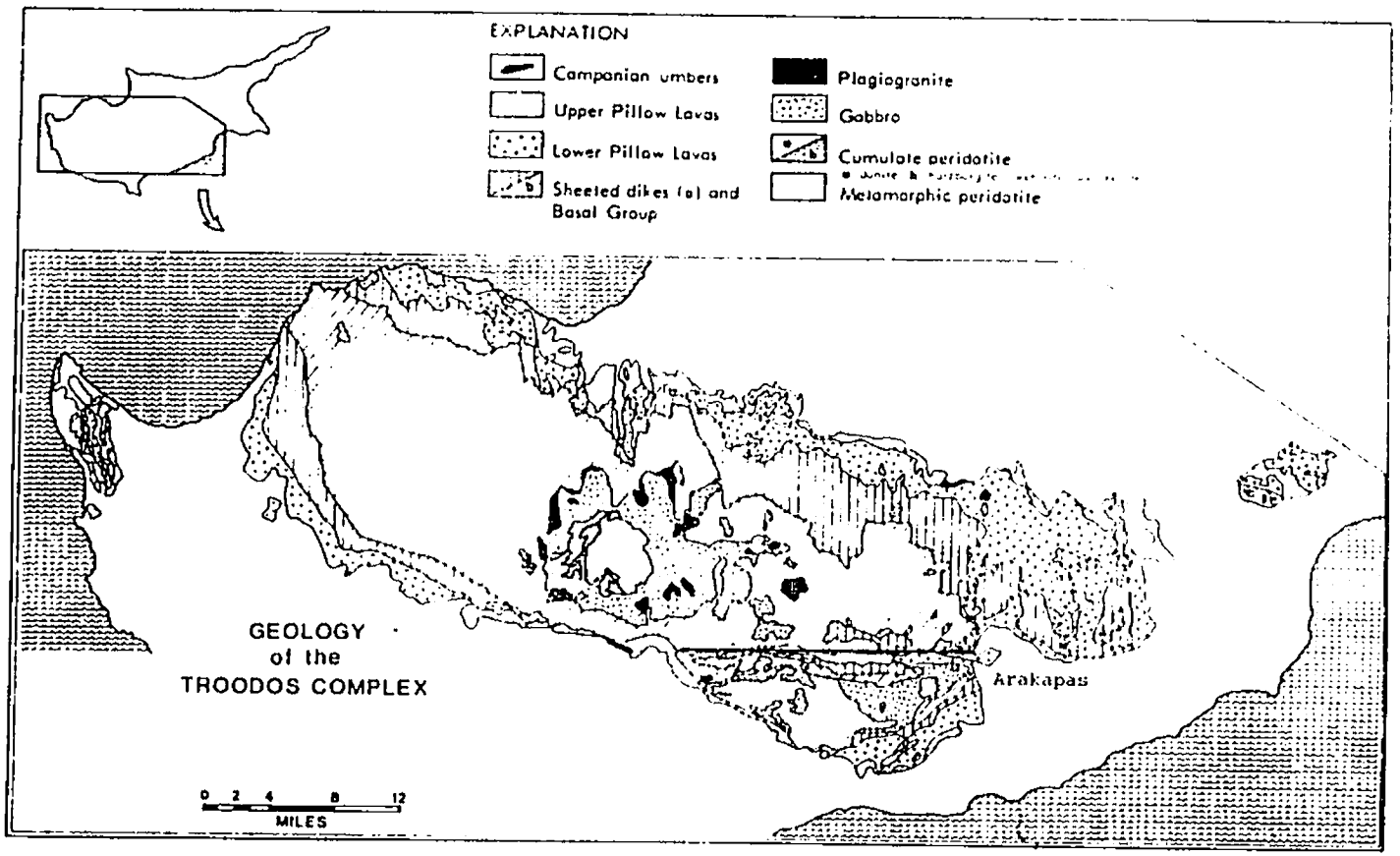

Fig. 1.2.1 Geological Map of the Troodos ophiolite, Cyprus (after Malpas and Langdon, 1984, original from Bear, 1960).

serpentinite, mafic plutons and dikes, pillowed and massive basaltic lavas, and volcaniclastic rocks (Simonian and Gass, 1978; Dilek et al., 1990).

The pseudo-stratigraphic sequences are well preserved and exposed in the northern part of the ophiolite, which includes the study area of this thesis. The western end of this northern area is inaccessible for political reasons.

The central part of the plutonic sequence of main Troodos massif is mostly occupied by tectonized harzburgite and subordinate dunite containing economic chrysolite asbestos deposits and chromite lenses (Constantinou, 1980), and is called mantle sequence by Gass (1990). The mantle sequence consists largely of variably serpentinised peridotites, mainly (85%) tectonised harzburgites with associated lherzolites and dunites (5-15%). Serpentinization is pervasive throughout the peridotite mass within the vicinity of Mt. Olympus, approaching 80-100% in most of the rock units.

The plutonic complex overlies tectonized harzburgite (i.e., the mantle sequence) and contains a series of cumulates ranging from dunite at the base, through wehrlite and pyroxenite to gabbro (Thy, 1987a). The gabbroic rocks, including olivine gabbro and pyroxene gabbro, are extensively exposed and completely surround the ultramafic outcrop.

Numerous small ultramafic bodies, up to several hundred meters across, intrude the high level gabbros (Searle and Panayiotou, 1980). These small bodies consist of layered wehrlite, lherzolite and olivine gabbro and are believed to represent the magma chambers from which the upper mafic lavas were erupted (Malpas and Langdon, 1984). In addition, an older series of deformed plutonic rocks intruded by a series of undeformed cumulate rocks is recognized (Benn and Laurent, 1987; Thy, 1987; Malpas et al., 1989). Plagiogranites are exposed on the margins of some areas between the gabbro and sheeted dike complex. Zircon populations from two plagiogranites yield U-Pb dates between 90.3±0.7 and 92.4±0.7 Ma (Mukasa and Ludden, 1987).

The sheeted dike complex is a dense linear dike swarm virtually consisting of 100 per cent dikes, surrounding the outcrops of plutonic rocks on all sides and covering the biggest part of the massif (Constantinou, 1980). The lower boundary of the sheeted dikes is complex. Gabbro and plagiogranite of the plutonic complex both cut and are cut by dikes. In Hole CY-4 of the Cyprus Crustal Study Project (CCSP), the proportion of dikes to gabbro screens decreases markedly within a vertical distance of about 100-200 m (Hall et al., 1989b). Dikes have a large range in thickness but complete dikes are most commonly 1-1.5 m thick. Most of the chilled margins are well preserved and the cooling

relationships are clear (Baragar et al., 1990). Studies have demonstrated considerable variations in both the strike and dip of the dikes (e.g., Searle and Panayiotou, 1980; Smith and Vine, 1990), although approximately N-S is the dominant direction, and have revealed cross-cutting relationships between some dike swarms. The majority of dikes are basalts (or basaltic andesites) and andesites (Desmons et al., 1980; Baragar et al., 1988). The dikes pass upward into the volcanic assemblage through a mixed zone of dikes and lava screens variously estimated to be a few tens of meters thick (Gass, 1980) to a few hundred meters (Baragar et al., 1990).

The extrusive sequence occupies the periphery of the Troodos ophiolite complex and, since it is the object of this study, will be described in detail in Chapter 2.

1.3 Aims of this study

The well preserved regular anticlinal structure of the Troodos, Cyprus, ophiolite and its continuous exposure allows quantitative measurements of a number of primary constructional components of the Troodos-type oceanic crust (Hall et al., 1989a). The section above the Sheeted Complex, which is equivalent to the Upper Pillow Lavas (UPL), the Lower Pillow Lavas (LPL), and the Basal Group (BG) field mapping divisions, outcrops as a gently tilted annular belt around the

core of the ophiolite, and is overlain by Cretaceous and younger sedimentary rocks. This section is well suited for studying the three-dimensional aspects of oceanic crustal construction because of its relatively simple structure, and locally excellent exposures along river canyons, new highways, and elsewhere.

The study of the constructional features in the Extrusive Sequence of the Troodos ophiolite was started by Hall, Walls and Yang in 1986 on the basis of analyses of the existing geological maps of Cyprus (Geological Survey department, Cyprus, 1960) and drillhole data of Cyprus Crustal Study Program (CCSP). They identified some second order, cyclic features such as variation in the thickness and nature of the UPL, LPL, BG and combinations of them and found cyclic lateral variations in all the units examined (Figs. 1.3.1 and 1.3.2). Five groups of economic ore bodies, spaced at an average of 12 km, are related to a relatively depressed sediment surface and a shallow sheeted complex, and with the occurrence of abundant gossans, umbers, Fe-Mn-Si rich sediments (Hall et al., 1989a).

However, information, such as the pillowed/sheet lava ratio, the rate of dike increase with depth, hydrothermal alteration variation in the sequence, as well as their relationship with the spatial distribution of sulfide deposits, are not sufficiently quantitatively described on the

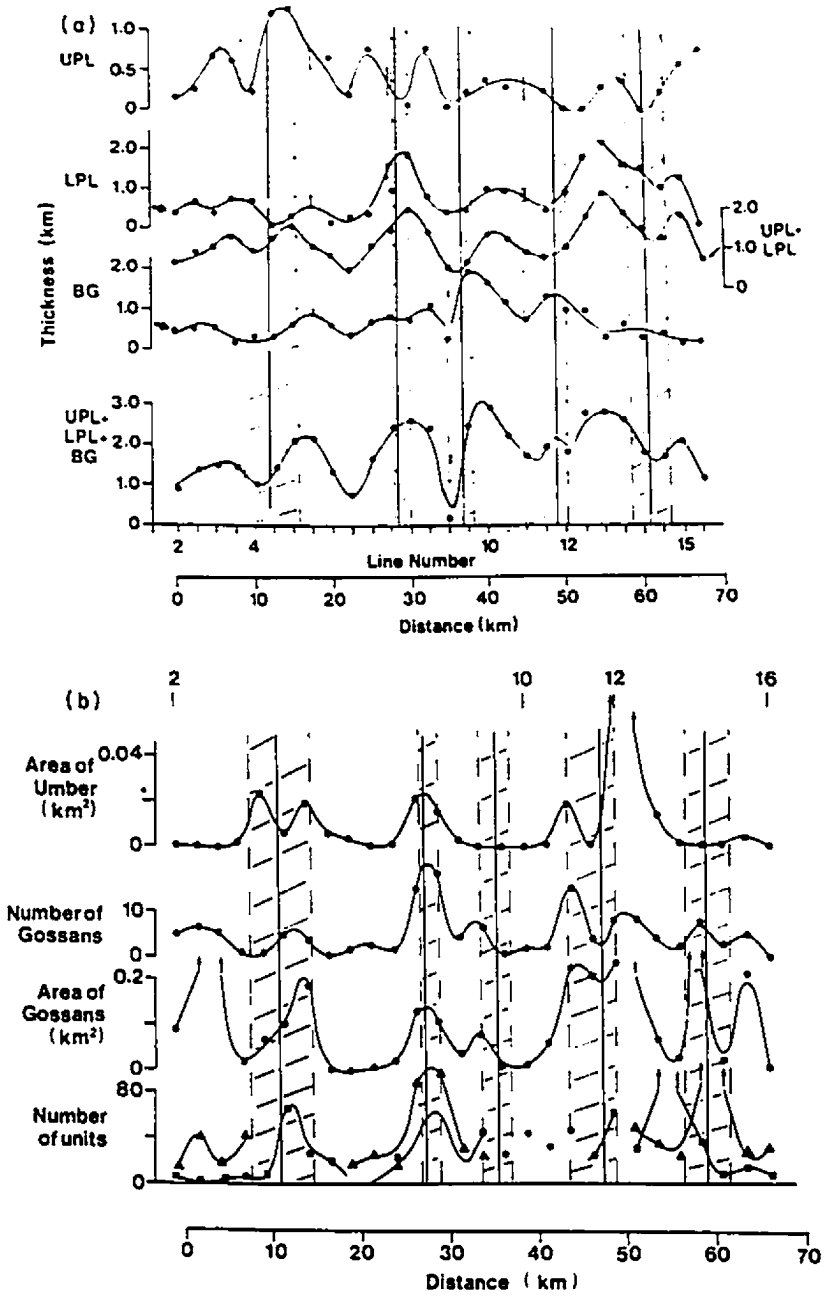

Fig. 1.3.1 Variation approximately in the spreading direction of the thickness of crustal constructional components. Thickness variations of the stratigraphic units all show cyclicity to varies degrees. Hatched areas represent locations of groups of massive sulfide deposit (Hall et al., 1989a).

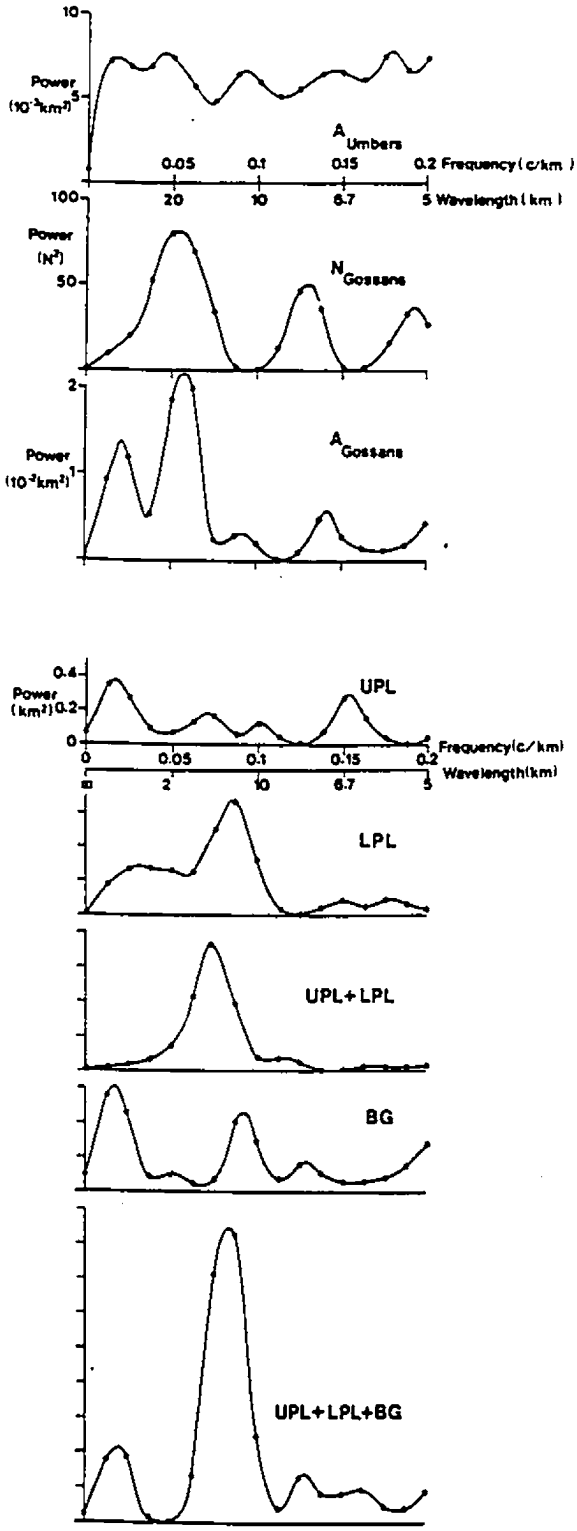

Fig. 1.3.2 Power spectra correspond to the cyclicity of profiles shown in Fig. 1.3.1. (Hall et al., 1989a).

Geological Survey of Cyprus maps. Again, the CCSP drillholes are too few and far apart to allow second order features to be defined. For these reasons it was essential to map key features in the field in a quantitative way.

This thesis project, then, is to study first and second order features of construction of oceanic crust as seen in the Troodos ophiolite and to provide relevant information for in-situ, typical oceanic crust. The study focuses on the variation of the features within the Extrusive Sequence of the ophiolite, including 1) volcanic cyclicity, e.g., variations of lava styles and thickness; 2) variation of dike density both laterally and with depth; 3) alteration zonation and controls; and 4) relationships between constructional features and the distribution of sulfide deposits.

Chapter 2 Previous Knowledge of the Extrusive Sequence of the Troodos Ophiolite

In this chapter, knowledge to date of the Extrusive Sequence of the Troodos ophiolite is reviewed. This includes stratigraphy, lithology, geochemistry and magma suites, and their contribution to the discussion of the genesis of ophiolite. The Extrusive Sequence is defined as that part of the ophiolite stratigraphy occurring between the sediment/igneous contact (SEI) and the top of the Sheeted Dike Complex (SC).

2.1 Stratigraphy of the Extrusive Sequence

The Extrusive Sequence of the Troodos ophiolite used to be known as the Volcanic Complex on the geological maps of Cyprus (e.g., Geological Survey Department of Cyprus, 1979). Stratigraphically, the Extrusive Sequence traditionally has been divided, in upward sequence, into the Basal Group (BG), the Lower Pillow Lavas (LPL) and the Upper Pillow Lavas (UPL) by early workers (e.g., Wilson and Ingham, 1959; Bear, 1960; Gass, 1960; Carr and Bear, 1960; Pantazis, 1967) (Fig. 2.1.1). This subdivision was established on the basis of field criteria, the broad petrological, mineralogical and geochemical differences between the lavas of the three series, and the presence of supposed local unconformable contact

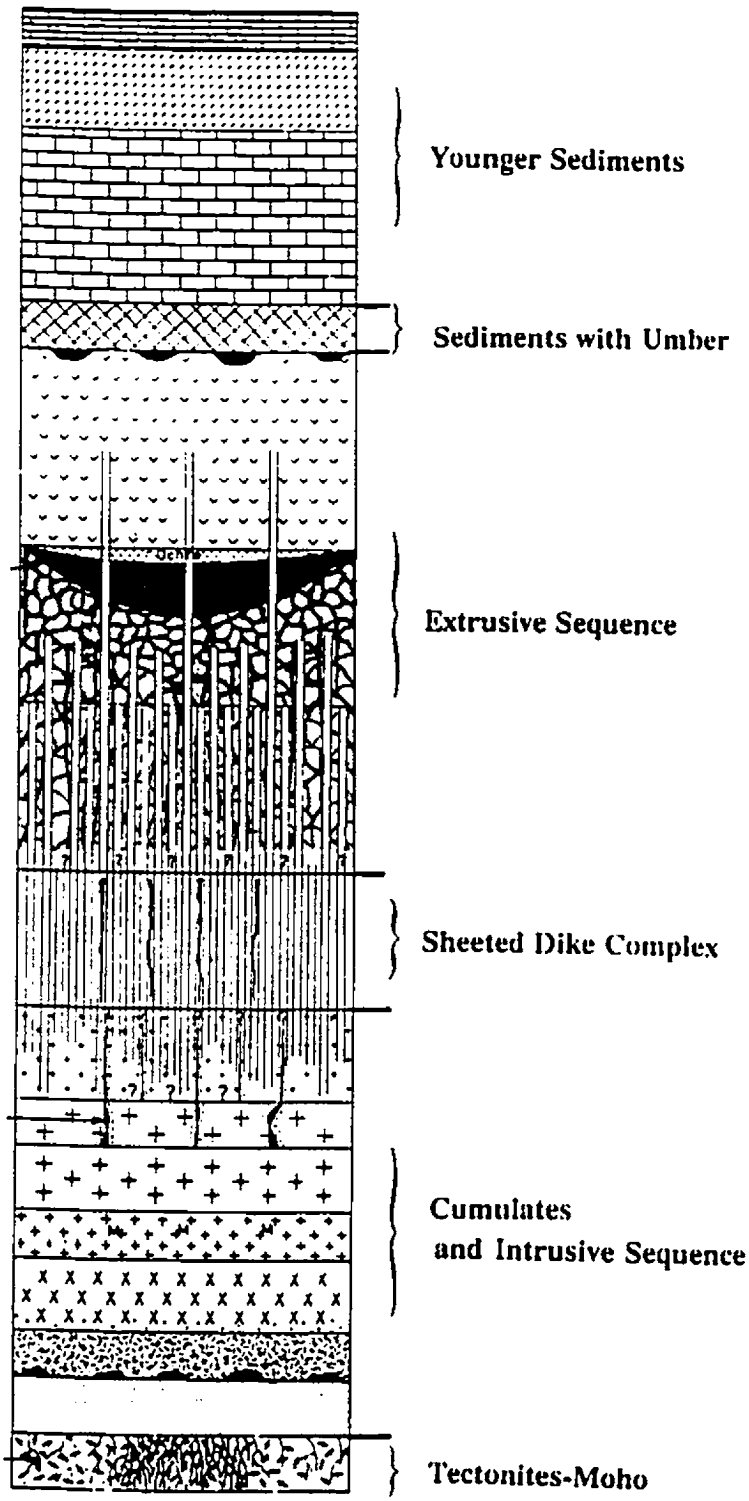

Fig. 2.1.1 Stratigraphy of Troodos ophiolite and overlying sediments (after Constantinou, 1980).

between the divisions (Constantinou, 1976; Gass, 1980). The Basal Group consists almost entirely of interlayered extrusives and intrusives, the former occurring as narrow screens of pillowed or massive flows, and the latter in the form of steeply inclined dikes. Their relative proportions vary considerably but generally the amount of extrusive material increases away from the Sheeted Dike Complex contact and towards the Lower Pillow Lavas (Carr and Bear, 1960). The BG is distinguished from the Sheeted Dikes only by the presence of remnants of lava screens (Govett and Pantazis, 1971). The amount of intrusive material in the BG generally exceeds the amount of lavas, and in places constitutes 90 percent of the interval. The BG is distinguished from the LPL by virtue of a much greater proportion of lavas in the latter division. Generally, the BG is separated with difficulty from the Sheeted Dikes below or the LPL above- it represents an intermediate zone between the two divisions.

It needs to be pointed out that there are two views of the appropriate attribution of the Basal Group in the stratigraphic sequence. Wilson and Ingham (1959) and Carr and Bear (1960) included the BG in the Pillow Lava Series (i.e., the Extrusive Sequence), Pantazis (1967) regarded the BG as the base of the Pillow Lava Series and the Sheeted Dikes as genetically related to, and essentially contemporaneous with, the Pillow Lava Series. On the other hand, Bagnall (1960)

stated that the BG had more affinities to the Sheeted Dikes (e.g., high proportion of dikes) and therefore was genetically related to it. Subsequent researchers attribute the BG either to the Extrusive Sequence (e.g., Searle and Panayiotou, 1980; Rautenschlein et al., 1985; Robinson and Malpas, 1990), or to the Sheeted Dikes (e.g., Thy and Moores, 1988). In this study, the BG is considered as a portion of the Extrusive Sequence, as the earliest manifestation of an extrusive phase is seen in the BG pillowed and sheet flow screens (Searle, 1972).

The Lower Pillow Lavas are usually highly weathered, and generally form hummocky low-lying ground sharply delineated from the Basal Group by the abrupt steepening in slope as the latter is approached (Bagnall, 1960). The LPL was defined as mainly oversaturated, often intensely silicified with common celadonite, aphyric basalt, while the Upper Pillow Lavas division was described as generally undersaturated, often olivine-bearing basalts with more ultrabasic varieties occurring at the top of the sequence (e.g., Gass and Smewing, 1973; Smewing, 1975). The boundary between the UPL and the LPL has also been difficult to place since, for the most part, it has been defined as being dependent on the degree of intrusion or difference in alteration facies, both of these showing broad transitions, accordingly most workers have suggested a transitional contact (Bagnall, 1960; Gass, 1960; Pantazis, 1967). Smewing et al. (1975) concluded that the boundary

between the Upper and Lower Pillow Lavas is largely a metamorphic discontinuity and they reported geochemical overlap between the two suites.

Gass and Smewing (1973) and Smewing et al. (1975) noted statistical separation (but with extensive overlap) in Ti-Zr ratios for the UPL and LPL (Fig. 2.1.2) and, alternatively, divided the sequence into an Axis Sequence, consisting of the LPL and BG as well as the underlying Sheeted Dike Complex, and an Off-Axis Sequence consisting of the UPL (Fig. 2.1.3), with boundary varying laterally from unconformity to transitional between these two subdivisions.

A different division was suggested by Robinson et al. (1983), Schmincke et al. (1983), Mehegan (1988) and Mehegan and Robinson (1985). Using major element data from both glasses and whole rock samples, they showed that, on the northern flank of the ophiolite, the Extrusive Sequence can be divided into two geochemical suites: a lower, island-arc type tholeiite suite (Suite A), consisting of basalt, andesites, dacites, and rhyodacites; and an upper, depleted-arc tholeiitic suite (Suite B with subdivisions of B1 and B2 groups), containing basalts and basaltic andesites (Fig. 2.1.4). In addition, a highly depleted boninitic suite (Suite C) is recognized in the Extrusive Sequence on the southern flank of the ophiolite. In stratigraphic order, Suite A

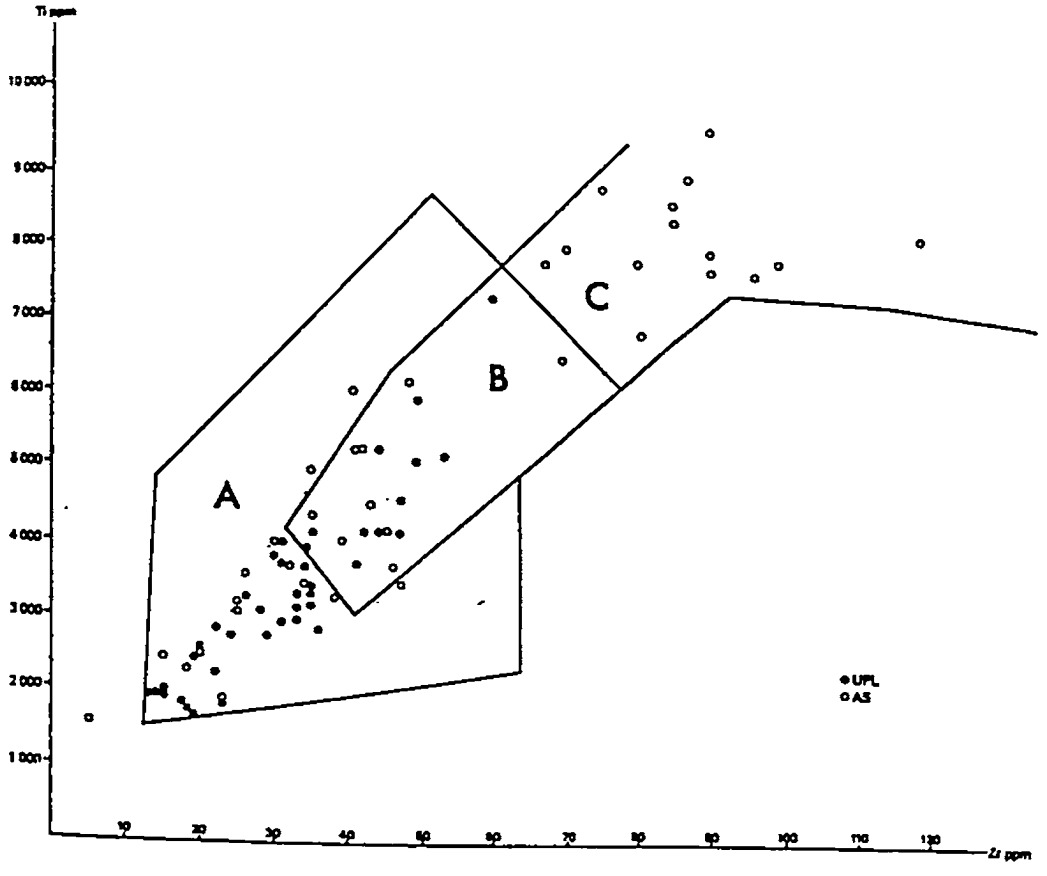

Fig. 2.1.2 Ti-Zr plot lavas from the Axis Sequence (AS) and UPL. Present day ocean floor basalts plot in Fields B and C, and island arc tholeiites in Fields A and B (Smewing et al., 1975).

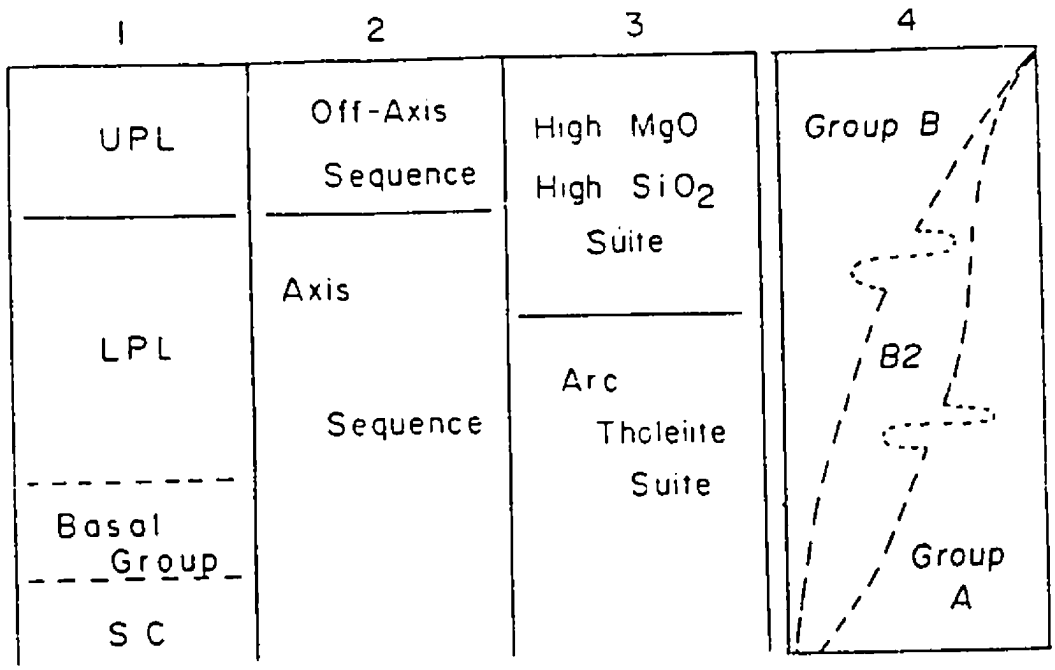

Fig. 2.1.3 A comparison of stratigraphic divisions for the Extrusive Sequence of the Troodos ophiolite. 1- Bear (1960); 2- Gass and Smewing (1973); 3- Robinson et al. (1983); 4- Northern Troodos compositional (magma) groups (Mehegan, 1988).

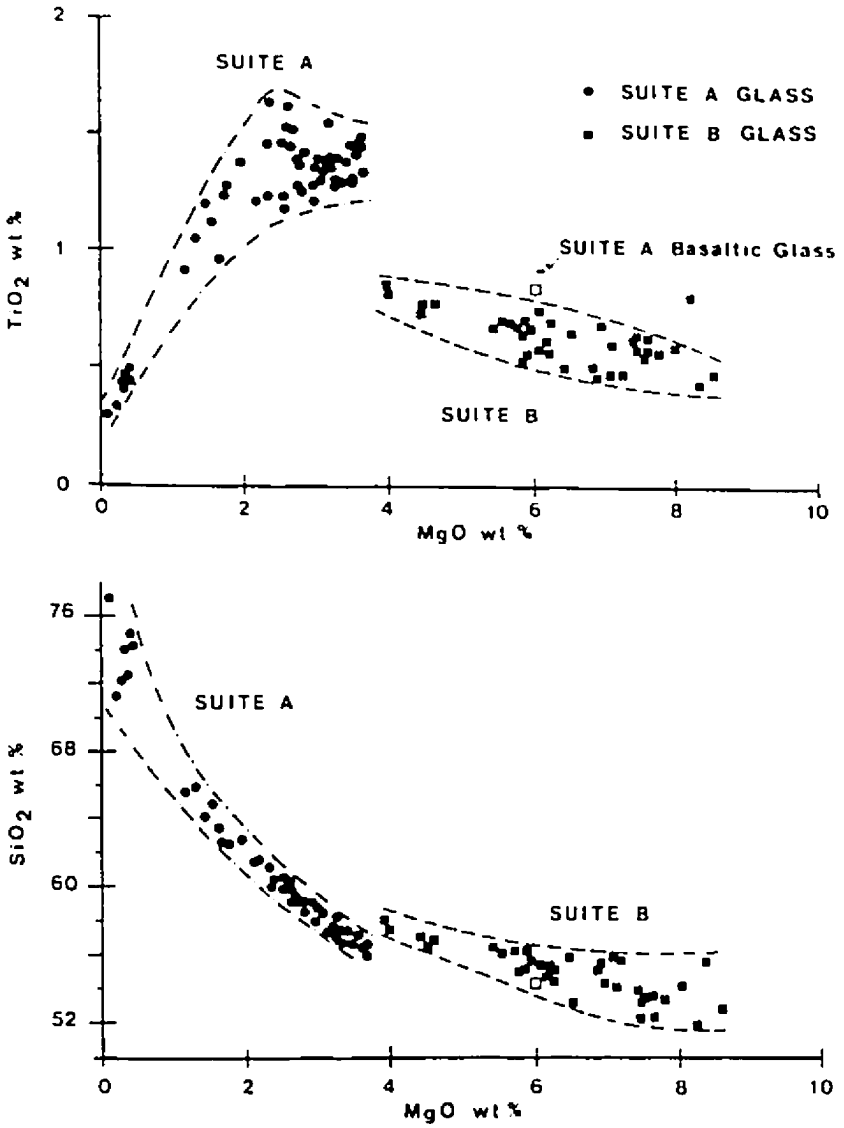

Fig. 2.1.4 Mehegan (1988) and Robinson and Malpas (1990), based on volcanic glass analyses from lavas on the northern flank of Troodos, recognized an island-arc tholeiitic suite (suite A) and a depleted arc tholeiite suite (suite B).

corresponds approximately to the Axis Sequence (i.e., BG and LPL) of Gass and Smewing (1973) and Suite B approximately to the Off-axis sequence (i.e., UPL), but the boundaries rarely coincide (see Fig. 2.1.3).

From the comparison of these different divisions of the sequence, it is obvious that the field-based division of Bear (1960) does not correspond to the geochemical division. Recent studies have pointed out that the supposed contact between UPL and LPL shows no evidence of an erosional break but, instead, different degrees of alteration (e.g., Gillis and Robinson, 1985, 1990; Hall et al., 1987). The results from petrological, geochemical and geophysical studies indicate that although the distinction between BG, LPL and UPL is useful as a field classification and as an indication of general stratigraphic relations, it should not be used for a rigid and absolute interpretation of the stratigraphic sequence (e.g. Robinson et al., 1983; Mehegan, 1988; Hall et al., 1989a). However, it should be noted that, due to the ease of distinction in the field and simple spatial distribution, the terms UPL, LPL and BG are still commonly used, even in recent publications (e.g., Cameron, 1985; Thy and Moores, 1988; Dilek et al., 1990). One possible reason is that the new divisions have not been accepted by most workers, or, that one cannot distinguish geochemical divisions in the field and, therefore, it is not convenient, at least for the time being, to use the newer

divisions for easy communication.

2.2 Lithology

Field observation and previous work indicated that the rocks in the Extrusive Sequence occur morphologically as pillowed flows, sheet flows, and dikes, and as very minor hyaloclastites and breccias. This is also well demonstrated, for example, in the four drill holes in the extrusives of the Cyprus Crustal Study Project (CCSP) which was carried out in the early 1980s by the International Crustal Research Drilling Group (ICRDG). In holes CY-2 (226 m in the extrusives) and CY-2a (689 m in the extrusives with abundant dikes in the lower part) there is only 0.43 m of sills according to the drillcore description of Robinson (1987) and only one 0.45 m thick unit of hyaloclastite in Hole CY-2a (Bednarz et al., 1987a). Pillowed flows make up 26% and sheet flows 74% of the section in Hole CY-2, while, from the histograms of Bednarz et al. (1987a), 7% of pillows, 40% of sheet flows and about 50% of dikes occur in CY-2a (Fig. 2.2.1 and Table 2.2.1). Some very glassy flows were observed in the cores. Several mechanisms have been suggested for the formation of these flows (Bednarz et al., 1987a; Hall et al., 1991), but there is general agreement that they are a type of sheet flow. Similar situations, in which pillowed and sheet flows and dikes are dominant (above 95%), are observed in two other CCSP drillcore

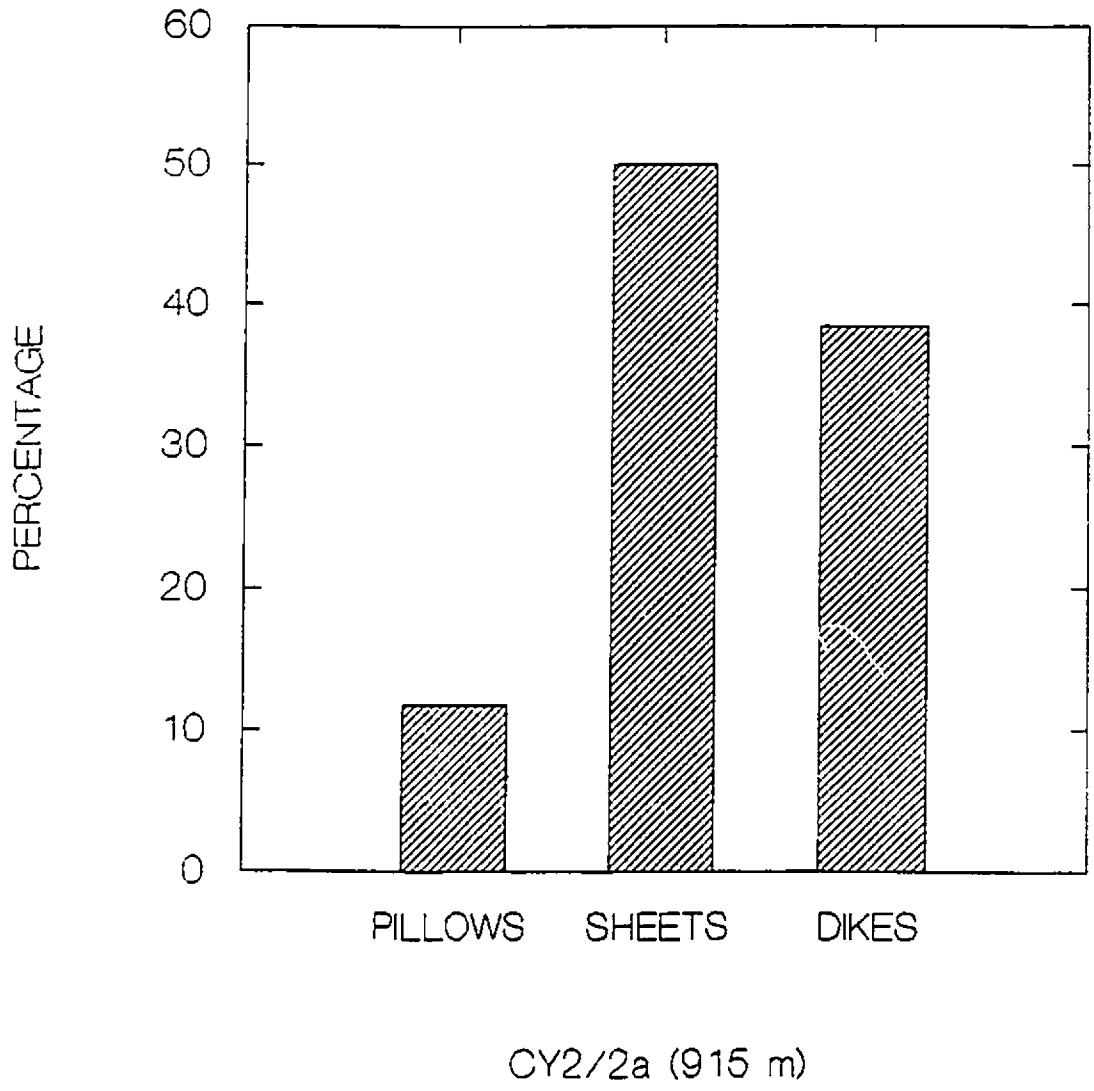

Fig. 2.2.1 Histogram of morphological types in the 915 m total drillcore sections of CCSP holes CY-2 and CY-2a in the Extrusive Sequence of the Troodos ophiolite. Pillows-pillowed flows; Sheets-sheet flows; Dikes-dikes in the extrusives. (Data from Bednarz et al., 1987)

Table 2.2.1 Lithological Types in Four Drillholes of CCSP

	CY-1	CY-1a	CY-2	CY-2a
Core Depth	485 m	701 m	226 m	689 m
Pillowed Flows	233 (48%)	51 (7.3%)	59 (26%)	48 (7%)
Pillow Breccias	68 (14%)			
Sheet Flows	174 (36%)	324 (46.2%)	115 (51%)	104 (15%)
Glassy Sheet Flows			52 (23%)	186 (27%)
Hyaloclastites		36 (5.1%)		
Dikes	10 (2%)	244 (34.7%)		351 (51%)
Undivided Flows/Dikes		47 (6.7%)		

	CY-1/1a	CY-2/2a
Pillowed Flows	351 m (29.3%)	107 m (11.7%)
Sheet Flows	498 (42.1%)	457 (50.0%)
Hyaloclastites	36 (3.1%)	
Dikes	254 (21.6%)	351 (38.4%)
Undivided Flows/Dikes	47 (4.0%)	

1) Data CY-1 from Douma and Robinson (1984), Gillis (1986).
2) Data CY-1a from Horne and Robinson (1986), Gillis (1986).
3) Data CY-2 and CY-2a from Bednarz et al. (1987).

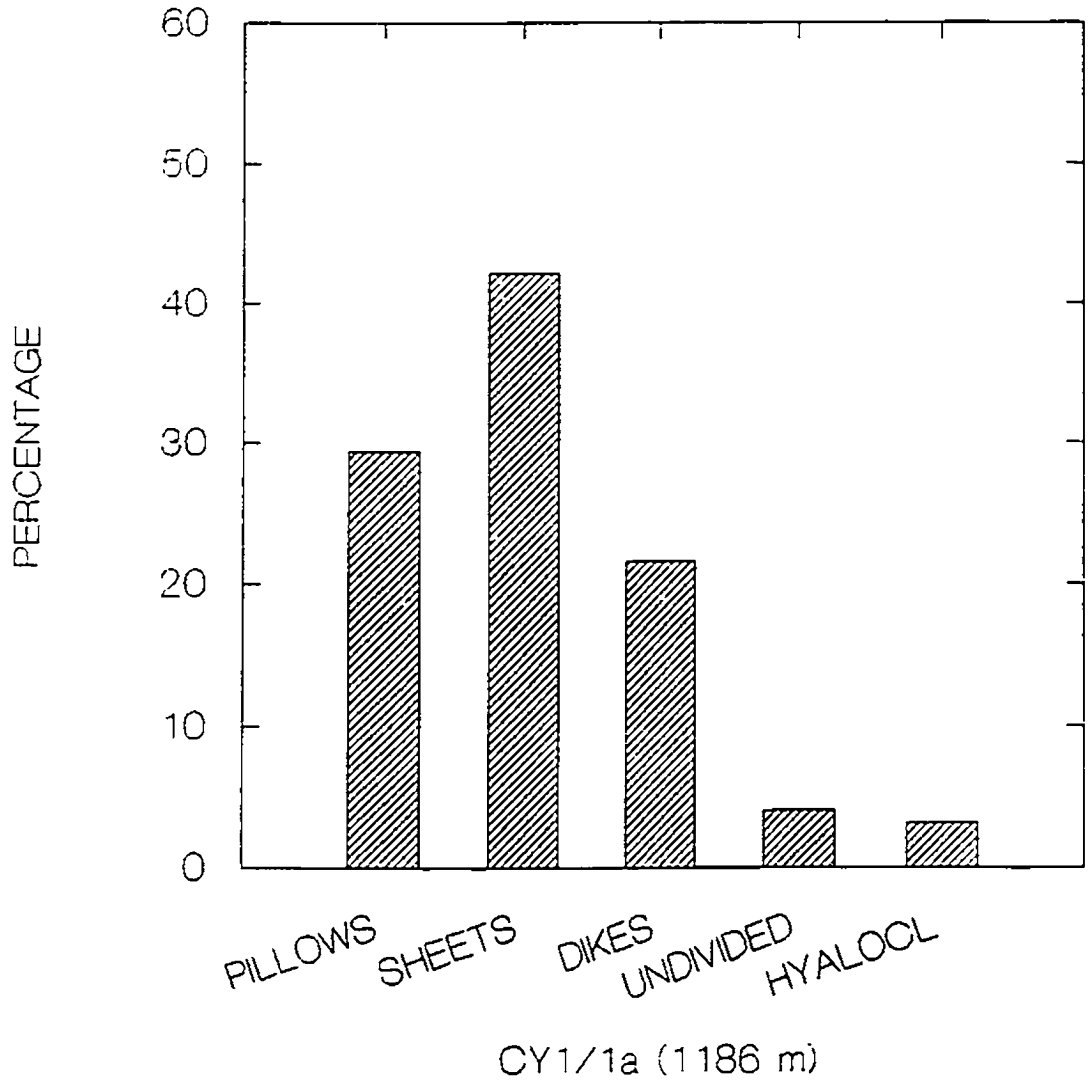

Fig. 2.2.2 Histogram of morphological types in the 1186 m total drillcore sections of CY-1 and CY-1a of CCSP in the Extrusive Sequence of the Troodos ophiolite. Undivided-undivided sheet flows and dikes; Hyalocl-hyaloclastites; rest of symbols are same as in Fig. 2.2.1. (Data from Douma and Robinson, 1984; Horne and Robinson, 1986; Gillis, 1986).

sections, for Holes CY-1 (depth 485 m) and CY-1a (depth 701 m) (Fig. 2.2.2) (Douma and Robinson, 1984; Horne and Robinson, 1986; Gillis, 1986).

2.3 Geochemistry and magma suites

The examination of temporal variations in lava geochemistry can provide useful constraints on the constructional history and petrogenesis of volcanic centres (Taylor, 1990). Similarly, it would be useful for the discussion of the constructional features of the extrusives of the Troodos ophiolite and their eruptive styles if the characteristics of the magma suites involved were known. This information might have a bearing on comparisons with in-situ oceanic crust.

As mentioned above, based on major-element analyses of glasses and of whole rock samples of extrusive rocks, Robinson et al. (1983) and Schmincke et al. (1983) proposed the existence of two major magma suites in the extrusives, a lower, arc-tholeiite suite and an upper, more mafic suite with affinities with high-Mg andesites or boninites. The analyses of the fresh glasses from the differentiated LPL and UPL (Robinson et al., 1983) generally lie on smooth chemical trends (Figure 2.3.1), with a distinct break in TiO_2 content at the level of 3.8% MgO. Cameron (1985) argued, however, that

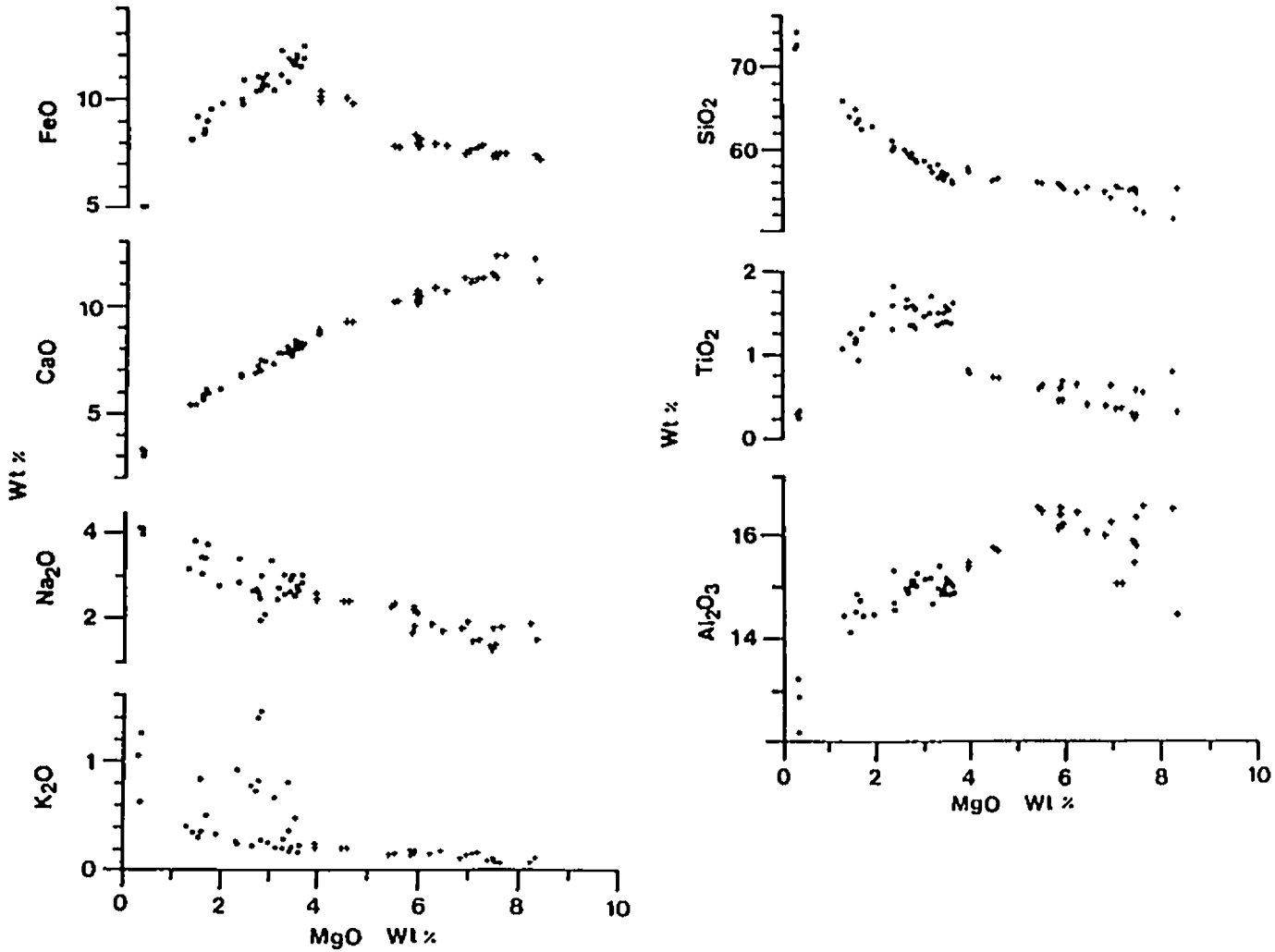

Fig. 2.3.1 Two compositional groups divided by Robinson et al. (1983), based on 59 samples of Troodos glasses. Crosses = basalts and basaltic andesites; circles = andesites, dacites, and rhyodacites.

this break may reflect a sampling problem. It is noted that there is no structural or metamorphic discontinuity between the two suites and, moreover, in places these two suites are interfingered with each other, as has been demonstrated in a number of studies, e.g., Pearce (quoted in Robinson et al., 1983), Rautenschlein et al. (1985), Mehegan (1988), and Mehegan and Robinson (in press).

A detailed stratigraphic analysis of the Extrusive Sequence in the southwest of Margi village in Troodos (Taylor, 1990), reveals a semicyclical eruptive sequence of the two main geochemical suites (Fig. 2.3.2) recognized by Robinson et al. (1983). In the study area, samples of low-Ti lavas (i.e., olivine phyric units) were recovered from pillowed screens within the dike complex located at the base of the Akaki river section as well as in the upper extrusive sequence. The low-Ti lavas had earlier been reported to be characteristic only of the upper, younger sequence of the extrusives (Schmincke et al., 1983; Robinson et al., 1983).

Glasses from Troodos have been compared by Thy et al. (1985) with boninites from different locations. However, the glasses do not show the characteristic boninite REE patterns but in fact, are closer to the MORB pattern, at least for Troodos dacites (Fig. 2.3.3a). The Troodos andesite glasses show the same general REE patterns as the dacitic and MORB

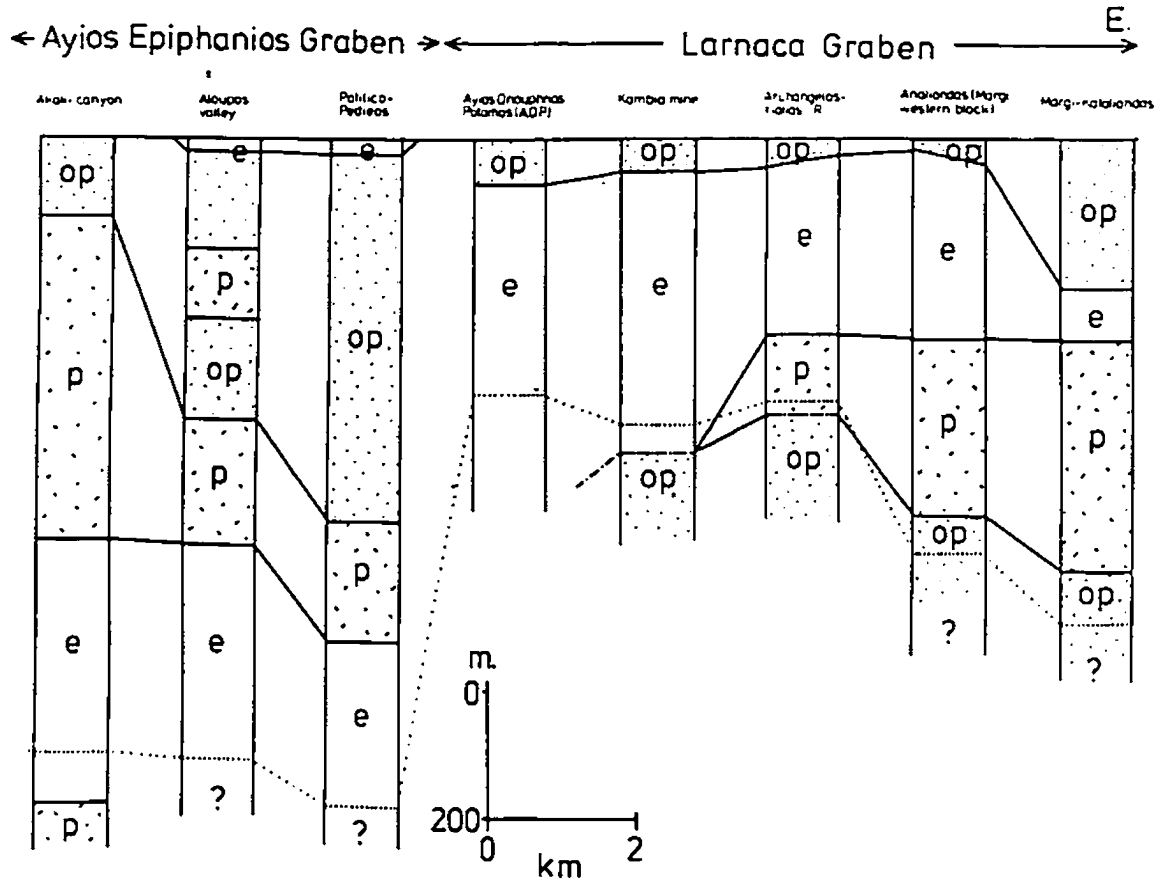

op = Olivine phyric low-Ti lavas
p = Generally aphyric low-Ti lavas
e = Generally aphyric high-Ti lavas
Dotted line represents the transition from extrusive dominated to intrusive dominated lithologies.

Fig. 2.3.2 Geochemical and petrographic variations within the extrusives of the Troodos ophiolite, showing the two suites of low-Ti and high-Ti lavas interlayered in the stratigraphic sequence (after Taylor, 1990).

glasses, i.e., the patterns are offset but generally subparallel with a clear but weak negative Eu anomaly (Fig. 2.3.3b). It is suggested that the sequence of Troodos glasses could be regarded as one interrelated sequence. This is based on the good correlation shown on all variation diagrams, the close correspondence to other basaltic andesite series (Meijer et al., 1981), and is also suggested by the parallel REE patterns of similar form.

Auclair and Ludden (1987) found that low temperature altered samples of UPL from Hole CY-1 show rare earth element patterns and abundances similar to those found for the fresh glasses and CY-2a LPL samples. In conjunction with the conclusion of Rautenschlein et al. (1985) that there is no difference in isotopic composition and incompatible trace element ratios between UPL and LPL fresh glasses, Auclair and Ludden (1987) have assumed that the patterns and abundances found in the CY-2a and fresh glass samples are typical of the whole volcanic suite of the Troodos ophiolite. They suggested that all the lavas of the Troodos ophiolite are related to either one, or to a series of episodes, of fusion which melted an isotopically and geochemically homogeneous mantle. This conclusion is also supported by the results of Adamides (1987).

On the other hand, Thy (1987a, 1987b), based on the

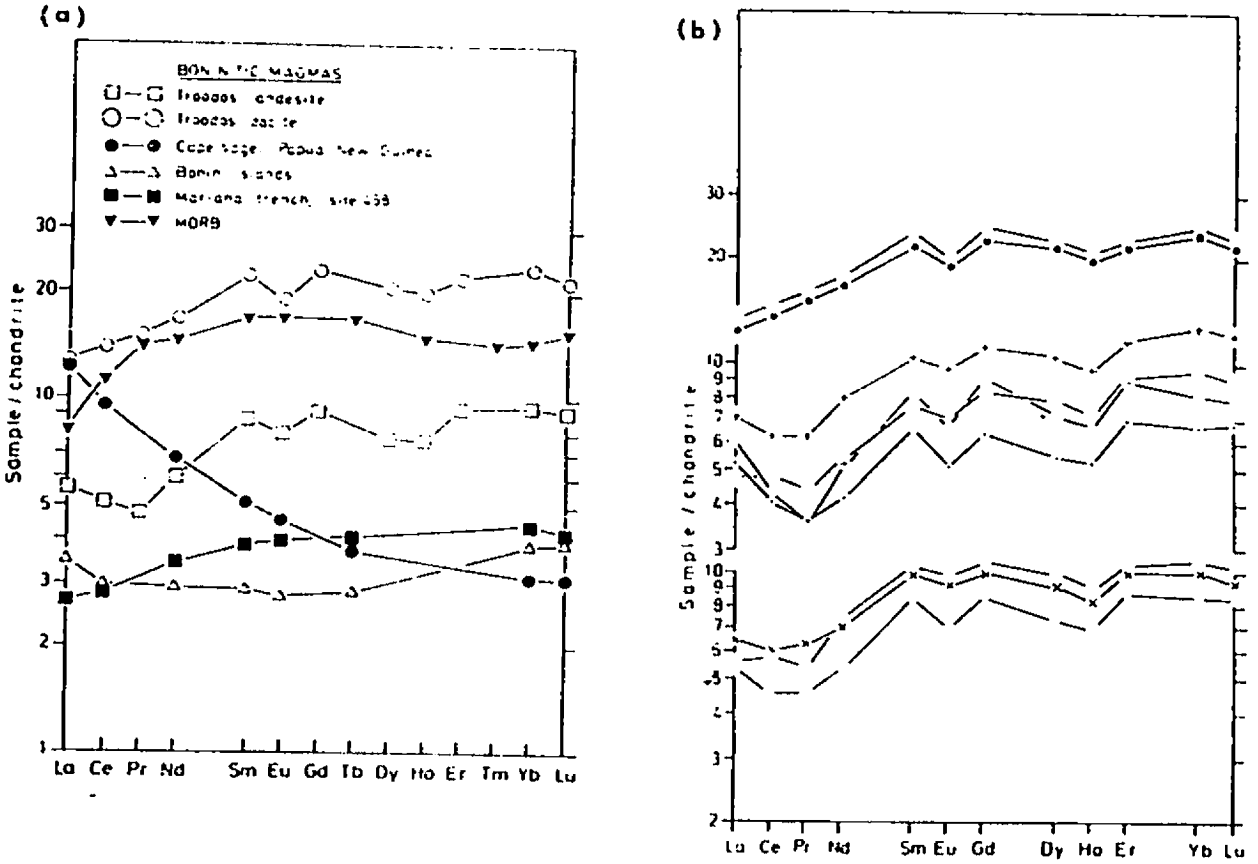

Fig. 2.3.3 Thy et al. (1985) summarized REE data from Troodos glasses and concluded: a) The Troodos andesites do not show the characteristic boninite REE pattern; b) The almost identical patterns of the REE abundances in the Troodos glasses (basaltic andesites to dacitic andesites) point to either a common source or to an interrelationship by crystal fractionation (after Thy et al., 1985).

mineralogy of the cumulates sampled in CCSP Hole CY-4, has recently proposed that two distinct cumulate sequences are present, a stratigraphically lower websteritic and gabbroic cumulate sequence, and an upper gabbroic cumulate sequence, which originated from chemically unrelated magmatic systems. The upper gabbros, the sheeted dike complex, and lower (andesitic to dacitic) pillow lavas are related genetically by Thy to the upper gabbroic magmatic system and are supposed to have formed in a regular spreading episode. Either during a late-stage spreading event, or after termination of active spreading, a large magma chamber is supposed by Thy to have accumulated at the mantle-crust boundary. The upper (low Ti, magnesian andesitic) pillow lavas are supposed to have originated from this late, non-spreading or off-axis event and are best correlated with the ultramafic cumulates. Benn and Laurent (1987), from observations of the cumulates in the Mount Troodos region, also concluded that two magmatic systems were represented.

Two questions thus arise. One is that if the sheeted dikes are only related to the lower pillow lavas, where are the dikes which were, as conduits, related to the upper pillow lavas? The second is that if there were indeed two magmatic systems, one representing a spreading episode and the other a late, non-spreading or off-axis event as suggested by Thy (1987a), how could the products of the two series be

interfingered? As an improvement on the above, inconsistent picture, Thy and Moores (1988) and Thy et al. (1989) propose that the extrusion of the basaltic andesites of the upper pillow lavas occurred simultaneously with still active evolving volcanic centres belonging to the earlier magmatic suite. In this model, the upper extrusives are supposed to have formed in a relatively slow-spreading or non-spreading tectonic environment.

However, results from the study of the sheeted dikes, both from CCSP Hole CY-4 drillcores and surface profiles, provide a different scenario (Baragar et al., 1989; 1990). First, the results show that the dikes can be divided into depleted and non-depleted suites and that the two suites correspond to the chemical characteristics of Upper and Lower Pillow Lava types. The new factor is while the range and distribution of dike compositions parallel those of the lavas, they lack the break in continuity, between 4-5.5% MgO, shown in glasses from pillows, a break that divides the lavas into distinctive upper and lower suites (Fig. 2.3.4). Robinson and Malpas (1990) argue that the absence of sharp geochemical breaks in the dikes may be due to in part to their relatively high grade of metamorphism. Secondly, among the elements of generally low mobility such as Zr, Ti and Y, the distribution of analyses are virtually identical for both lavas (from the drillhole sections from CY-1 and CY-1a) and sheeted dikes

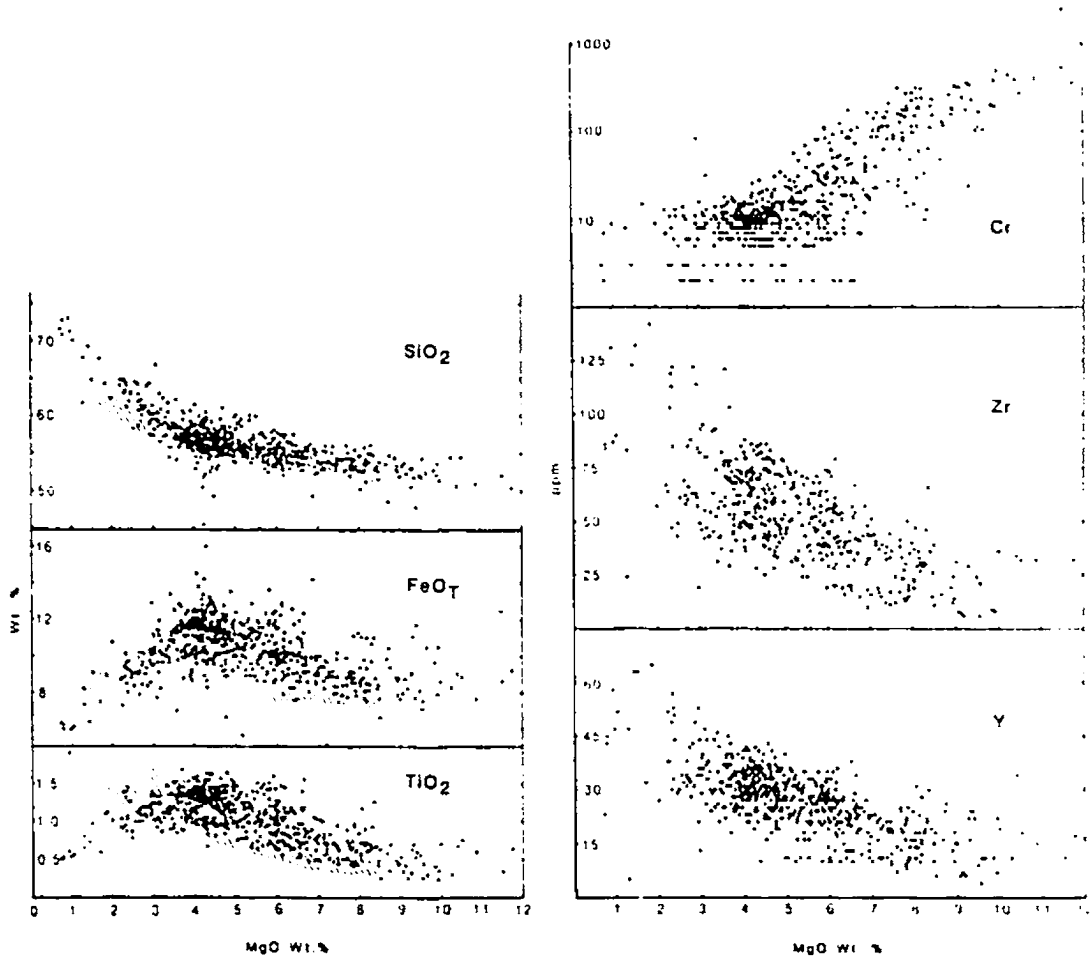

Fig. 2.3.4 MgO variation diagrams for the Troodos sheeted dikes (Baragar et al., 1990). Cross-hatching marks the field of lava glasses (Robinson et al., 1983). Compositions of the Troodos sheeted dikes display fairly coherent trends for those of lava glasses but lack a break of MgO abundances.

(Fig. 2.3.5) and no break is evident in their distributions. The third is that the REE (Fig. 2.3.6) analyses show a complete gradation through the entire spectrum of compositions in both abundance and degree of LREE depletion and, therefore, division into depleted and non-depleted suites is considered to be entirely arbitrary. The generally similarity of REE patterns throughout the compositional range and their gradual systematic change with degree of differentiation suggests a common origin for all the dike magmas. The fourth is that Baragar et al. (1989) demonstrate that the dikes, which can be divided chemically into depleted and non-depleted suites, show no age preference as determined by cross-cutting relationships. The depleted suite dikes are not consistently younger than those of the non-depleted suite as might be expected from their reported disposition in the lava sequence. On the contrary, they commonly form screens to non-depleted suite dikes. Baragar et al. (1990) note that although the depleted suite is on the top of the stratigraphic sequence, there is considerably more overlap between the two suites than is shown by general surface mapping.

The conclusion by Baragar et al. (1990) is that, given the continuity of major and trace element compositions, the similarity of Zr/Y and TiO2 -Zr ratios, and the gradational change in REE abundance and pattern throughout the composition range of the sheeted dikes, it is difficult to avoid the view

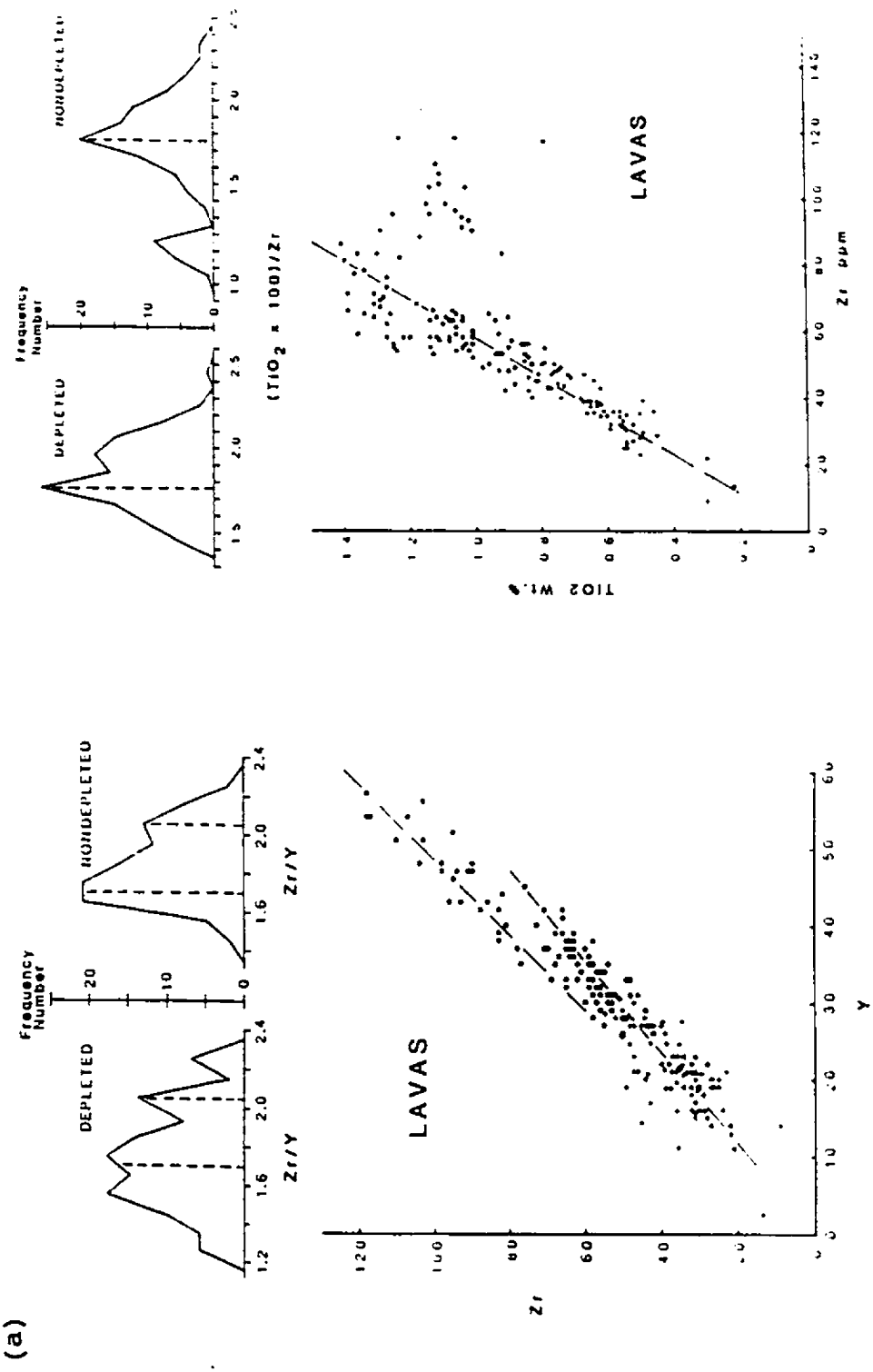
(a)
Frequency Number
DEPLETED
NONDEPLETED
Zr/Y
Zr
Y
LAVAS
(TiO2 x 100)/Zr
TiO2 Wt.%
Zr ppm

Fig. 2.3.5a

(b)

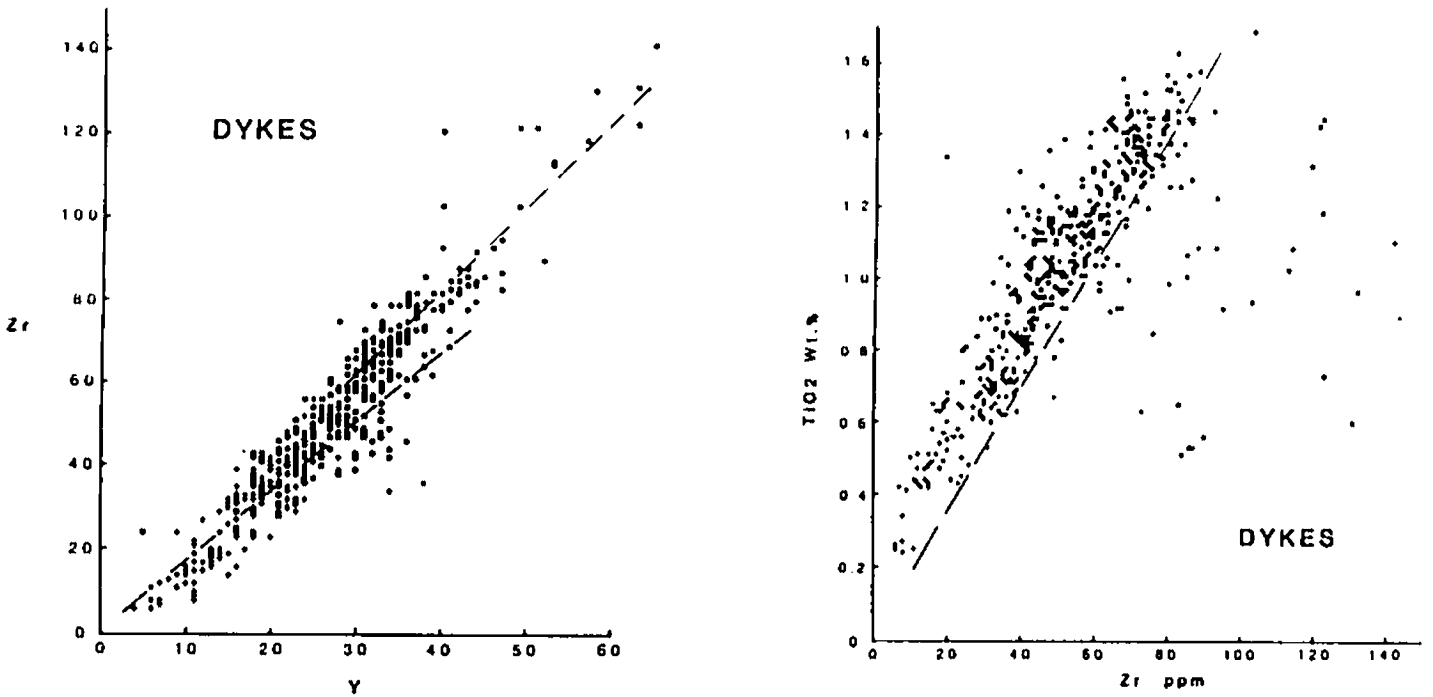

Fig. 2.3.5a,b Baragar et al. (1990) further show that no break is evident in distributions of trace elements of both lava flows and sheeted dikes, although the depleted (marked by crosses) and nondepleted (marked by circles) suites are distinguishable on Zr-Y plots.

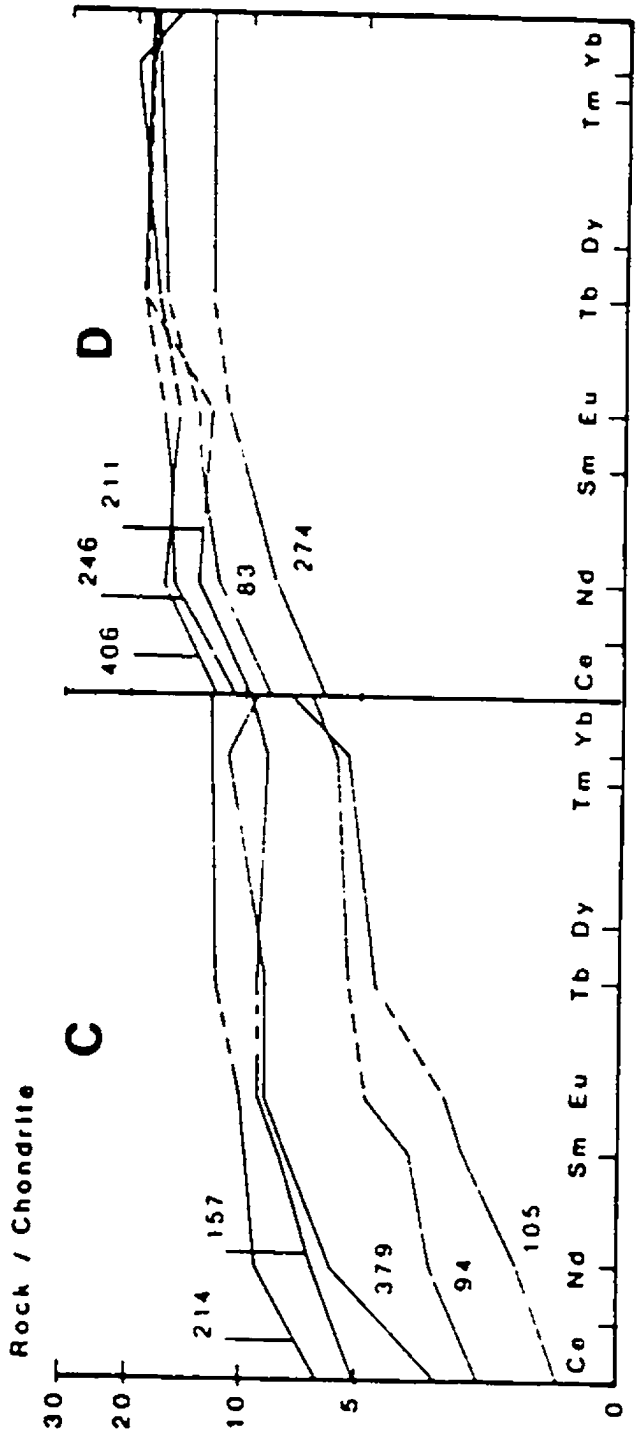

Fig. 2.3.6 REE patterns for (a) depleted and (b) nondepleted suite samples of sheeted dikes (Baragar et al., 1990).

that all compositions share a common or closely-related development history. The two suites, which appear to be of independent derivation in the lava sequence, can only be separated in the dikes by an arbitrary division of what seems to be a continuous series. The same conclusion is recently given by Laurent (1990), based on the study of plutonic rocks in CCSP Hole CY-4 in Troodos, that the plutonic rocks are comagmatic, forming a single and continuous suite of differentiation.

In summary, it is evident that there is still disagreement on the number of magmatic systems responsible for the extrusives of the ophiolite. It is still too early to give a final conclusion on the question of whether there were one or two magma systems, or more. However, some phenomena observed by author and his colleagues indicate that the extrusives and underlying sheeted dikes form a single crustal constructional unit, with continuous variation with depth. Properties such as hydrothermal alteration, dike density (Hall et al., 1987; Yang et al., 1988; Yang and Hall, 1990), and physical properties (Salisbury et al., 1989; Hall et al., 1990a), together with the interfingering of lavas from the different compositional groups (Rautenschlein et al., 1985; Mehegan, 1988; Taylor, 1990; Mehegan and Robinson, in press) could, at least, indicate that all volcanism was related to one magmatic event. In addition, since the UPL form almost

continuous belts along the 80 km long northern and southern flanks of the Troodos emplacement anticline, and in the absence of off-axis volcanism with this form in the present ocean basins, it seems most unlikely that the UPL formed in an off-axis environment (Hall et al., 1990b).

2.4 Structure of the Troodos ophiolite

First, it needs to point out that, although the Troodos ophiolite has been extensively studied since early 1980's, there are only very limited publications about the structure in the ophiolite. In this section, structures in the northern part of the ophiolite, i.e., this thesis study area, will be discussed.

Figure 2.4.1 displays the main faults in the area. Earlier workers demonstrated that most faults in the area dip steeply and that few are vertical. They comprise three sets which strike northeast, northwest and north, respectively. The northeast and north sets predominate in the central and eastern parts of the area (Carr and Bear, 1960; Bagnall, 1960; Bear, 1960). Regionally, the dominant fault trend is directed towards the northeast, i.e., approximately parallel to the axial direction. It is reported that the bulk of the faulting has taken place along the contacts of the intrusives (e.g., Bear, 1959) within the ophiolitic sequence accompanied by a

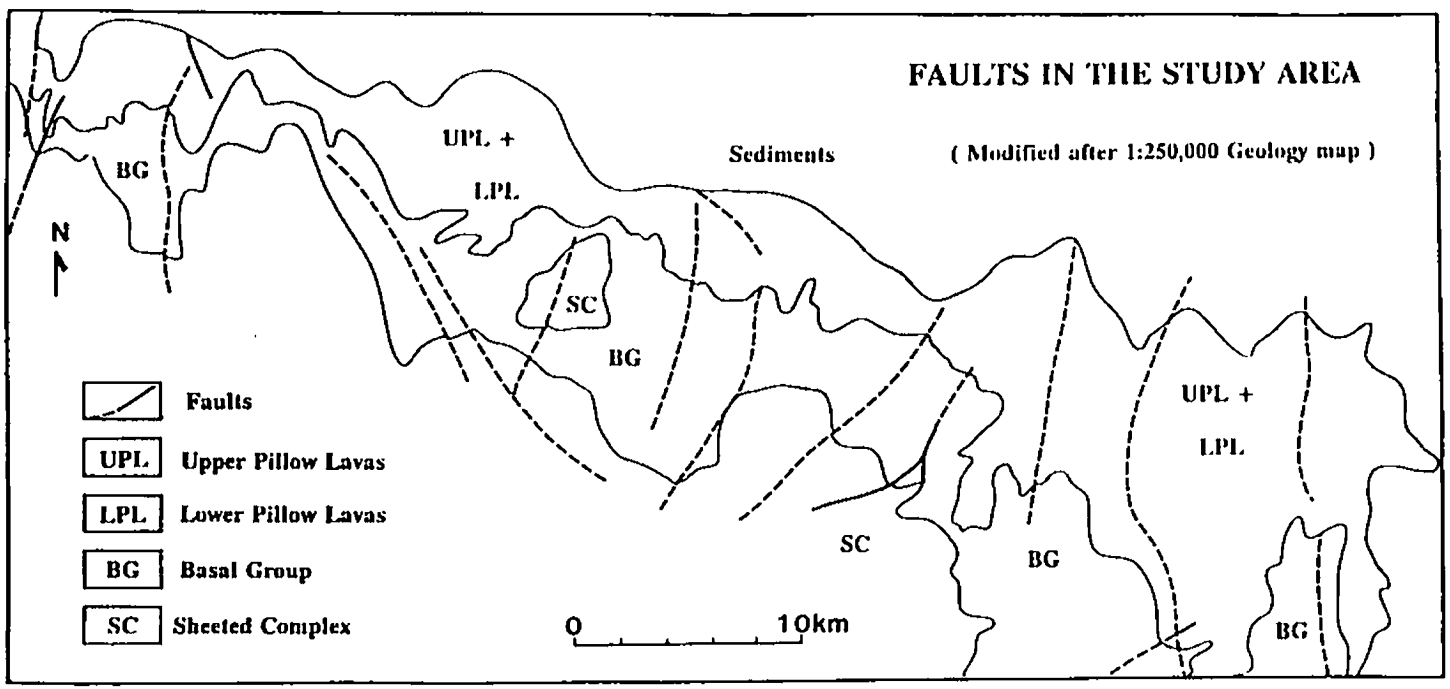

Fig. 2.4.1 Main faults in the northern part of the Troodos ophiolite (after Geology Survey of Cyprus, 1979).

very limited displacement of geological boundaries and they are mostly considered as syn-constructional faults.

Boyle and Robertson (1984), based on field relations and comparisons with modern spreading ridges, first recognized the axis of a well-defined median valley with small grabens and half-grabens in the eastern part of the Troodos ophiolite. They determined that a major transverse fault and two generations of normal faults predate pelagic sediments above the umbers in the area south of Margi village (Fig. 2.4.2). The Mathiati massive sulfide body formed in the vicinity of ridge-parallel fractures towards the margin of the rift valley. They believed that the gross lava succession, the position of the sulfide orebodies and the style of faulting in the Mathiati-Margi area are very similar to many other parts of the Troodos ophiolite.

By means of statistical analysis of the orientation of dikes within the Sheeted Complex of the Troodos ophiolite, and the recognition of primary spreading structures, such as listric and planar normal faults, Varga and Moores (1985, 1990) proposed the existence of three grabens, which are believed to have acted as separate spreading centres (Fig. 2.4.3). It is proposed that faults flatten at depth into a detachment within the upper parts of the plutonic complex. The grabens are proposed to be fossil axial valleys produced by

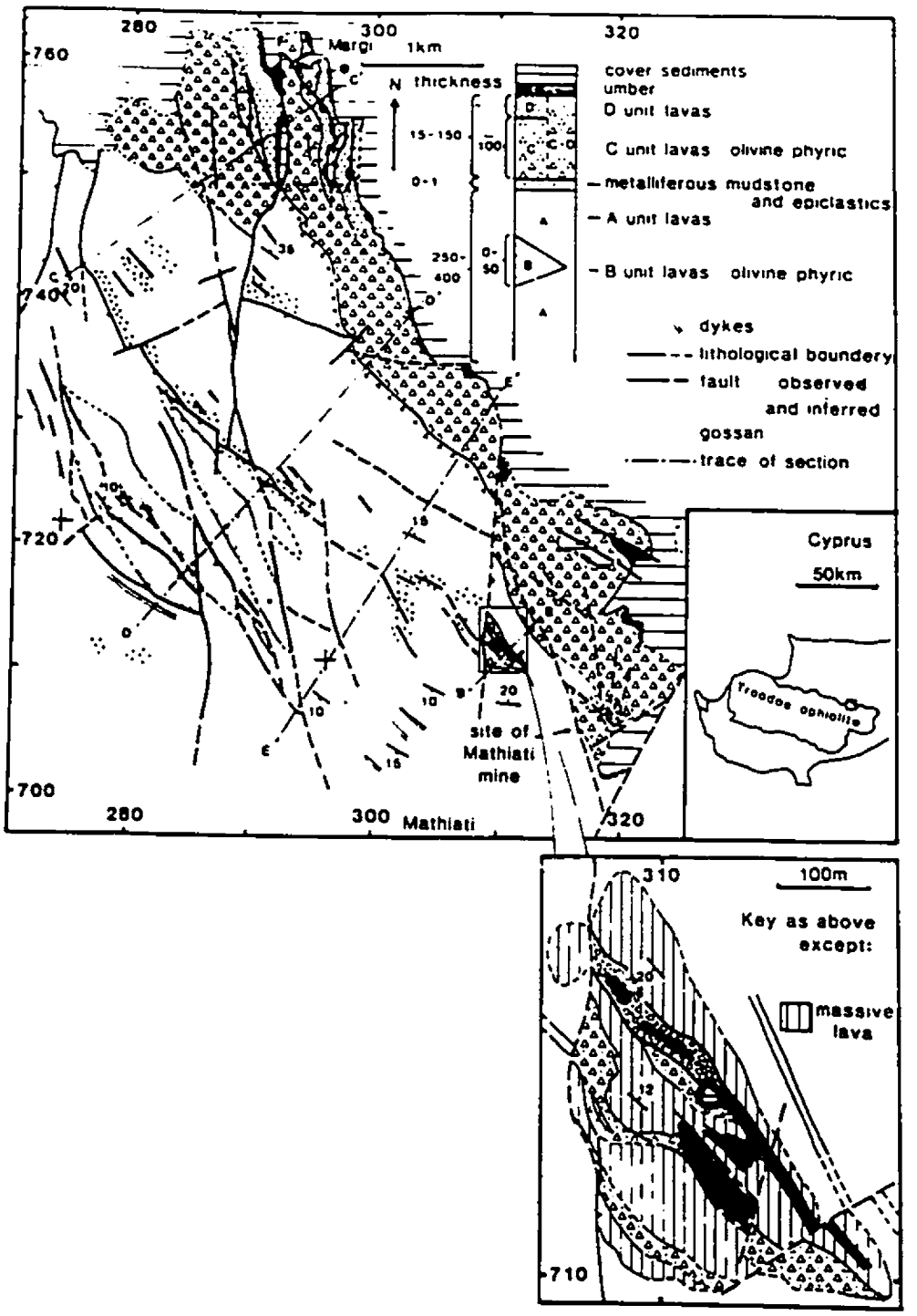

Fig. 2.4.2 Geological map of the Mathiati-Margi area, showing major faults in the area and accompanied massive sulfides (after Boyle and Robertson, 1984).

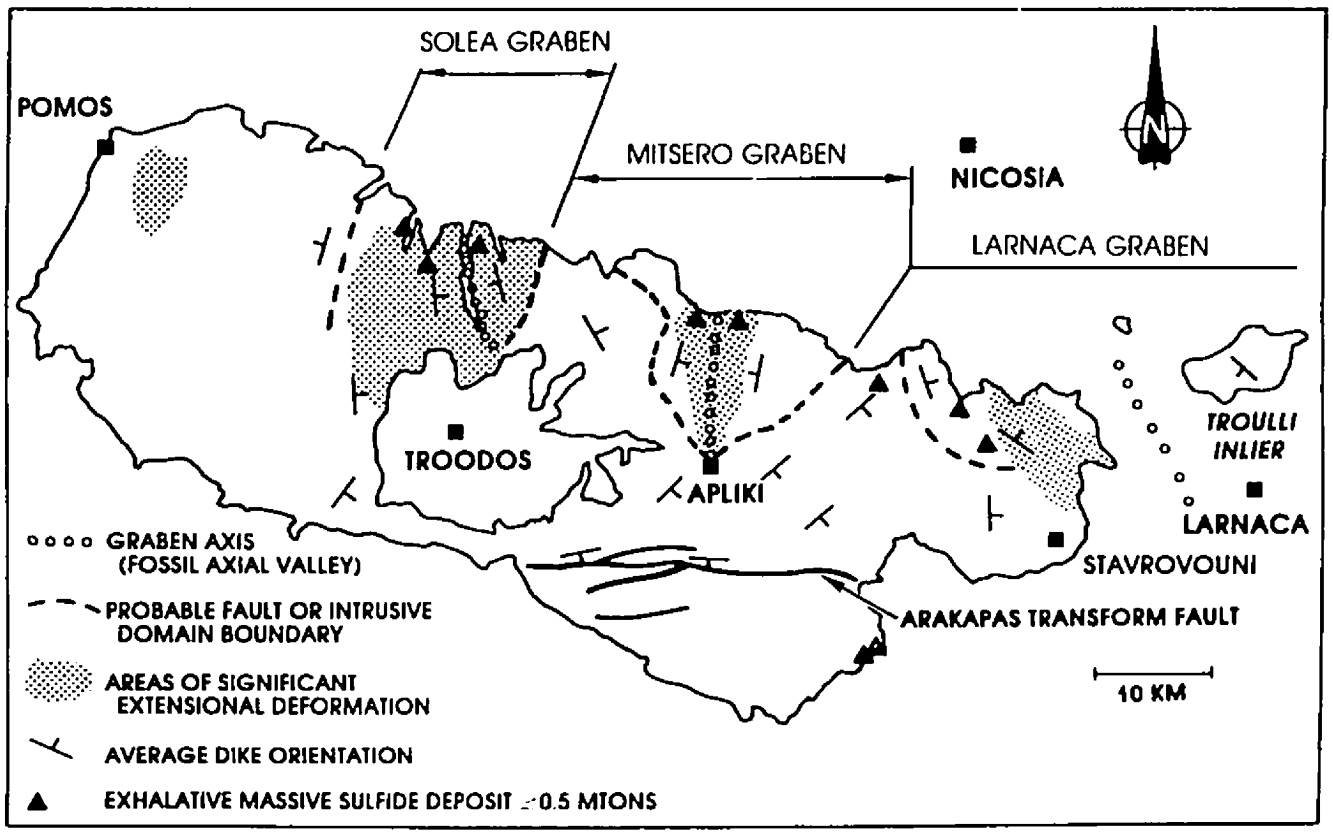

Fig. 2.4.3 Dike orientation domain map of the Troodos ophiolite, showing three grabens recognized in the north (after Varga and Moores, 1985, 1990).

successive eastward jumps of the spreading axis in steps of 8-13 km. They also noted that three of the largest exhalative massive sulfide deposits in the Troodos ophiolite occur within or near the Solea graben, and suggested that large normal faults within the grabens have provided significant channels of ascending geothermal fluids.

2.5 Contribution to the discussion of the tectonic origin of the Troodos ophiolite

Ophiolites are widely believed to represent fragments of oceanic crust formed at constructive plate margins. However, it is now recognized that many ophiolites have petrological and, particularly, geochemical characteristics different from oceanic crust observed at modern, major ocean basin, spreading ridges. Back-arc or marginal basins are an alternative site for the generation of much ophiolitic oceanic crust. Another possible situation is that rifting/spreading events take place in the early stages of island arc evolution, above subduction zones at destructive plate margins, creating oceanic crust formed in a tensional environment, as suggested for Troodos by Rautenschlein et al. (1985). The geochemistry of the lavas in ophiolites usually plays an important role in discussion of the origin of an ophiolite.

In earlier discussions, it was suggested that the Troodos

ophiolite formed at an old Tethyan ridge as a fragment of oceanic crust and mantle and that the magmatic evolution of the Troodos massif required multiple magmatic events (e.g., Moores and Vine, 1971). Since then, many different ideas and models for the origin of the Troodos ophiolite and for the tectonic setting of formation have been suggested.

One is represented by Smewing (1975), Gass and Smewing (1973) and Gass (1980). They divide the extrusive sequence into an Axis Sequence and an Off-axis Sequence. They proposed that the LPL is part of the Axis Sequence, erupted at a minor spreading axis in a marginal sea above a subduction zone. The UPL, although produced by the same primary processes, was supposed to be erupted slightly off-axis after the Axis Sequence had been metamorphosed. Smewing et al. (1975) demonstrated that there was no significant geochemical trace element break between the two divisions and that the metamorphic event divided an essentially continuous upward geochemical variation. It is suggested that the ophiolite evolved with a continually replenished magma chamber (Gass, 1980).

Mukasa and Ludden (1987), however, on the basis of their U-Pb dates and in conjunction with some previous observations, such as the lack of extensive sediment accumulation between the lower and upper pillow lavas, the conformable field

relations (Schmincke et al., 1983), and the established age limitations, virtually eliminate any possibility that the high-Mg basalts of the Upper Pillow Lavas are an off-axis volcanic sequence.

Miyashiro (1973, 1975) argued that, based on bulk lava compositions, the Troodos ophiolite might have formed in an island arc setting. Although the geochemistry and petrology of the LPL point to an arc setting, opposing evidence is that several geological features, e.g., a well-developed sheeted dike complex, graben structures and the transform fault zone recognized by some authors (e.g., Moores et al., 1984; Varga and Moores, 1985), strongly suggest a spreading centre origin, and have never been reported from an arc. In addition, the rarity of pyroclastic products (Schmincke et al., 1983), as well as the regional geology, do not support the existence of an arc.

Recently, Muenow et al. (1990) use volatiles, such as H_2O, Cl, F, S, CO_2, CO, CH_4, in submarine glasses as a discriminant of tectonic origin. Their results indicate that K_2O and TiO_2 contents and K_2O/H_2O rations in some fresh glasses from the Troodos ophiolite display a back-arc-basin affinity distinct from an island-arc original ophiolite.

Many authors hold the view that both the Nd- and Sr-

isotope and geochemical evidence confirm that the primitive lavas of Troodos have affinities with boninites and therefore are subduction-related (Cameron et al., 1979, 1983; McCulloch and Cameron, 1983; Schmincke et al., 1983; Robinson et al., 1983; Robinson and Malpas, 1990). Similar evidence was obtained by Rautenschlein et al. (1985). They found that all geochemical characteristics of the Troodos volcanic glasses are similar to those observed in supra-subduction zone volcanics and suggested that the Troodos ophiolite formed in the earliest stages of island arc development. Flower and Levine (1987), from their work on the Ayios Mamas section, obtained the same conclusion as Rautenschlein et al. (1985).

Furthermore, Thy and Moores (1988), while repeatedly stating that the Troodos ophiolite is composed of two distinct magmatic suites, stress that the extrusion of the basaltic andesites of the Upper Pillow Lavas occurred simultaneously with still active evolving volcanic centres belonging to the earlier magmatic suite. They argued that all the available data for the Troodos ophiolite are consistent with its formation in a short-lived spreading basin formed by the splitting of an immature, submarine arc.

Recently, Dilek et al. (1990) reconciled conflicting structural and geochemical evidence for the origin of the Troodos ophiolite, as well as the regional tectonic

environment, with the following conclusions: Grabens and normal faults within the sheeted dike complex and the extrusive sequence of the Troodos ophiolite resemble those of oceanic spreading centres. Coupled with the existence of the Arakapas transform fault to the south, these structural and intrusive relationships suggest an origin at an intersection between a spreading centre and a transform fault. Geochemical evidence from both the extrusives and intrusives argues for generation of at least part of the ophiolite within a subduction zone environment. Regional reconstructions suggest that the Mesozoic Neotethys, of which Troodos is thought to have been a part, may have evolved as a marginal basin over an active or recently active south dipping subduction zone.

It needs to be pointed out that, although many people have related the silicic Troodos glasses to an island-arc tholeiite suite, abyssal silicic glasses were also recovered from the Galapagos spreading centre (Schmincke, 1983) and from several locations along the EPR (Langmuir et al., 1986), the Iceland spreading centre (Walker, 1966), and from island-arc environments (Maaloe and Petersen, 1981; Jenner, 1981). Thy et al. (1985) accordingly argued that the possibility that the dacitic Troodos glasses belong to an oceanic suite cannot be fully excluded by the present data.

To conclude the preceding discussion, the use of

geochemical discriminant diagrams to identify the oceanic environment of origin of a given ophiolite should be treated with much caution. Eventually, more attention should be paid to the nature of the sediments deposited on the ophiolitic crust as already pointed by Moores (1982) and Nicolas (1989). Present day sedimentary sequences overlying the volcanic basement of arc systems are predominantly greywackes or andesitic tuffs (Leitch, 1984). Alternatively, when the sediments are only umbers or radiolarites as in Troodos, suggesting an environment below the carbonate compensation level and away from sedimentary sources, a mid-oceanic ridge situation should not be dismissed (Nicolas, 1989), although radiolarites may also form in small basins, transform-dominated or arc-related (Jenkyns and Winterer, 1982).

2.6 Basic ideas followed in this study

The tectonic setting and environment of the formation of an ophiolite has always proved to be a controversial topic and in general no single answer is forthcoming. The apparent conflict between a spreading-related geology and the arc petrology and geochemistry of the Troodos ophiolite may be an artifact of the lack of detailed studies of the geology and chemistry of oceanic and back-arc rifting environments (Thy and Moores, 1988). Nevertheless, although the tectonic setting of formation of the Troodos ophiolite is still undecided, for

many aspects of the ophiolite most workers have nc agreed that:.

1. Regardless of its exact tectonic setting, the Troodos ophiolite represents a kind of oceanic crust which formed in a spreading environment. Even if the environment was similar to that of the Mariana arc (Hussong and Uyeda, 1982), the lithology and structure of the crustal sections drilled by ICRDG or by ODP do not notably differ from that of "normal" ocean crust.

2. All the pseudo-stratigraphical sequences in the ophiolite, and characteristics such as lithology, lava morphology and dikes, physical properties, alteration and mineralization, as well as those of the overlying submarine sediments, can be compared closely with those of present oceanic crust.

3. Although in geochemical terms there may have been different divisions of magmatic systems in the ophiolite, neither a time break and nor a single spatially abrupt boundary exists between the field mapping division of the UPL and LPL, or between the low-Ti and high-Ti suites, a geochemical division. In contrast, the occurrence of fractionated lavas at the base and primitive lavas at the top suggests a broad zone of accretion (Schmincke et al., 1983).

Therefore, no matter how many arguments exist for origin of the Troodos ophiolite, the working hypothesis of this thesis is that the geochemical differences do not have significant bearing on the processes of construction and alteration of what is probably very close to the crust of at least some parts of the present ocean basins.

Chapter 3 Constructional features of the Extrusive Sequence

3.1 Field Geology

The field area is about 40 km long in the spreading direction (N110E) on the north flank of the Troodos anticline between Nikitari in the west and Mathiatis in the east, and is about 10 km long in the axial direction (N20E) between the SEI (the sediments/extrusive interface) and the top of the Sheeted Dike Complex (SC) (Fig. 3.1.1). The spreading direction is defined by the major strike direction of sheeted dikes, as suggested by early workers (e.g. Moores and Vine, 1971) and accepted by most subsequent researchers. The Extrusive Sequence shown in the diagram contains the three traditional stratigraphical subdivisions of the extrusive, i.e., the Upper Pillow Lavas (UPL), the Lower Pillow Lavas (LPL) and the Basal Group (BG) established by early workers (e.g., Wilson and Ingham, 1959; Gass, 1960). Since these subdivisions may mainly represent alteration features (Gillis and Robinson, 1985; Hall et al., 1987), they will not be used as stratigraphical units in this study. Below the Extrusive Sequence, sheeted dikes are continuously exposed to the south of the study area, except the eastern part, where no SC is exposed. A flexure leading to a depression in the anticline occurs here such that erosion has not yet exposed the SC.

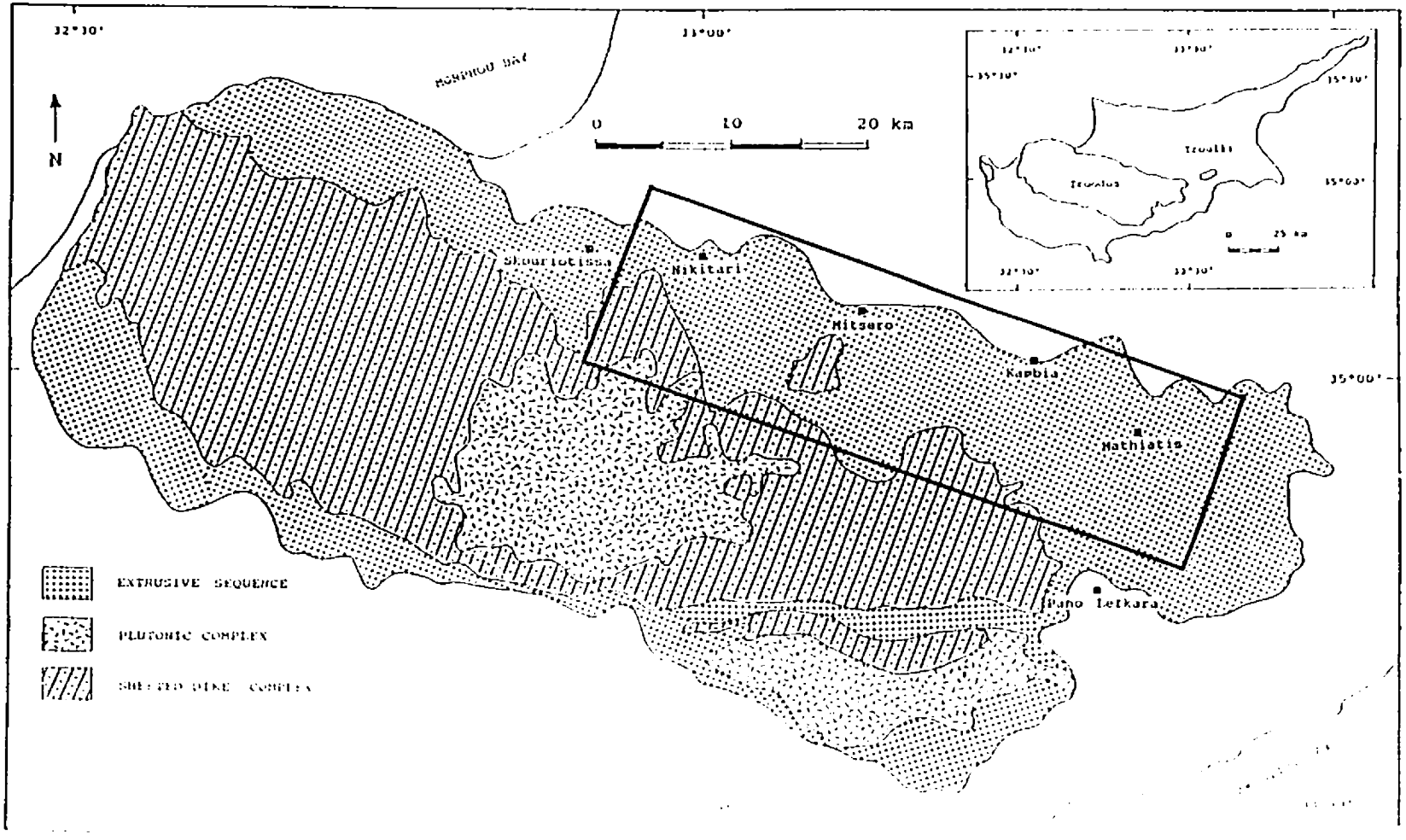

Fig. 3.1.1 Simplified geologic map of the Troodos ophiolite. The area within the rectangle outlined by a heavy line is the study area (after Geological Survey Department, Cyprus, 1979).

In most of the area the extrusives are well exposed, especially along roadcuts and streams, as well as on many bare ridges and slopes. Field work was carried out, as close as available exposure allowed, on 18 lines in the axial direction with a spacing of about 2.5 km between adjacent lines. Most measurements were carried out along streams and roadcuts where outcrops are continuous over distances of the order of a hundred meters.

The rocks in the extrusive sequence occur morphologically as pillowed flows, sheet flows, and dikes, and as very minor sills and hyaloclastites. Since the latter two types are very low in proportion (<1%) as observed in the field and demonstrated in drillcores in Chapter 2, hyaloclastites, a type of sheet flow, and sills, a type of intrusives, are not separated from other sheet flows and dikes, respectively. Therefore, the morphologies of rocks in the Extrusive Sequence can be simply regarded as consisting of three types, pillowed flows, sheet flows and dikes. The variation in relative abundance of these three morphological types, including their variation in thickness and spatial distribution, are examined in this chapter.

3.2 Measurement of the P value

Since the Extrusive Sequence in the study area consists

dominantly of two flow types: high-eruptive-rate (Ballard et al., 1979) sheet flows and low-eruptive-rate pillowed flows, one of the major field measurements made was of the ratio between pillowed flows and sheet flows. This ratio is called the P value and is defined as follows:

P = Net thickness of pillowed flows in a section/ Total thickness of extrusive rocks in the section.

Here P is used as a measure of the style of seafloor volcanicity.

This ratio is probably related to the rate of magma supply and therefore provides a measure of the condition and environment of the formation of extrusive units (Ballard et al., 1979) as well as features of the magma supply system.

In the field, pillowed flows are readily distinguished from sheet flows. The upper part of the extrusive sequence, the "Upper Pillow Lavas" (UPL, field mapping division), consists of fairly indurated volcanic rocks that are relatively resistant to subaerial weathering. For this reason the UPL outcrops well, both within and away from streams (Fig. 3.2.1). In contrast, in the less altered "Lower Pillow Lavas" (LPL) pillowed flows weather rapidly, but their presence can, with experience, be recognized by their characteristic

(a)

(b)

Fig. 3.2.1 Indurated pillow lavas of the UPL; a-in the sides of a stream valley (station no. 10.41); b-away from a stream valley (station no. 11.35).

subdued, earthy, topography (Fig. 3.2.2). Sheet flows in the LPL are relatively resistant to weathering and can be recognized readily, both in and away from streams, by their high relief and common columnar jointing (Fig. 3.2.3). Because the sheet flows, where abundant, are commonly fragmented and tectonically rotated, they frequently outcrop in such areas as short systems of ridges (Fig. 3.2.4).

Field observations and measurements were carried out along profiles approximately normal to the spreading direction. Values of P, at outcrops as close as possible to each line, were obtained both by visual estimation and by measurement with a tape (or pace) in continuous outcrop sections. The length of measured sections depended on the degree of outcrop. Generally, outcrops along the eighteen lines are locally well developed and most P values were obtained from sections of more than 100 m long. Examples of detailed measurements of P and F (dike abundance) are described in Appendix 1. A total of 547 measurements in the field were obtained and 690 samples were collected for alteration and magnetic studies (Fig. 3.2.5 and Appendix 2).

3.3 Characteristics of the Extrusive Sequence

The results of the P ratio measurements are plotted and contoured by linear interpolation (see Appendix 1) with an

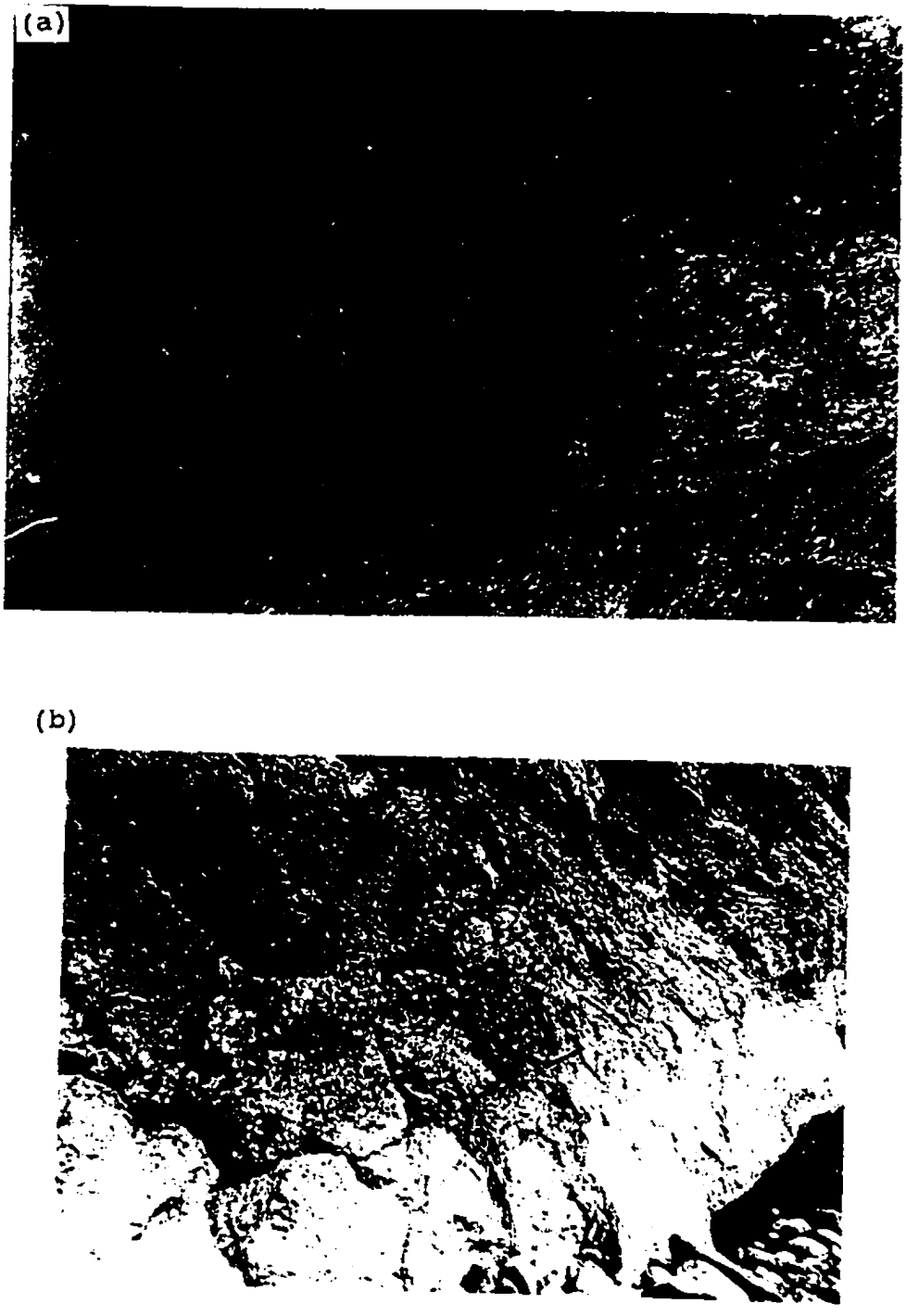

Fig. 3.2.2 Earthy weathered pillow lavas in LPL; a-away from a stream (station no. 11.31); b-in a stream (station no. 11.28).

(a)

(b)

Fig. 3.2.3 Sheet flows in LPL; a-showing generally prominent outcrops (station no. 20.41); b-showing columnar jointing in a cross section in a stream valley (station no. 21.19).

Fig. 3.2.4 Sheet flows forming short systems of ridges.

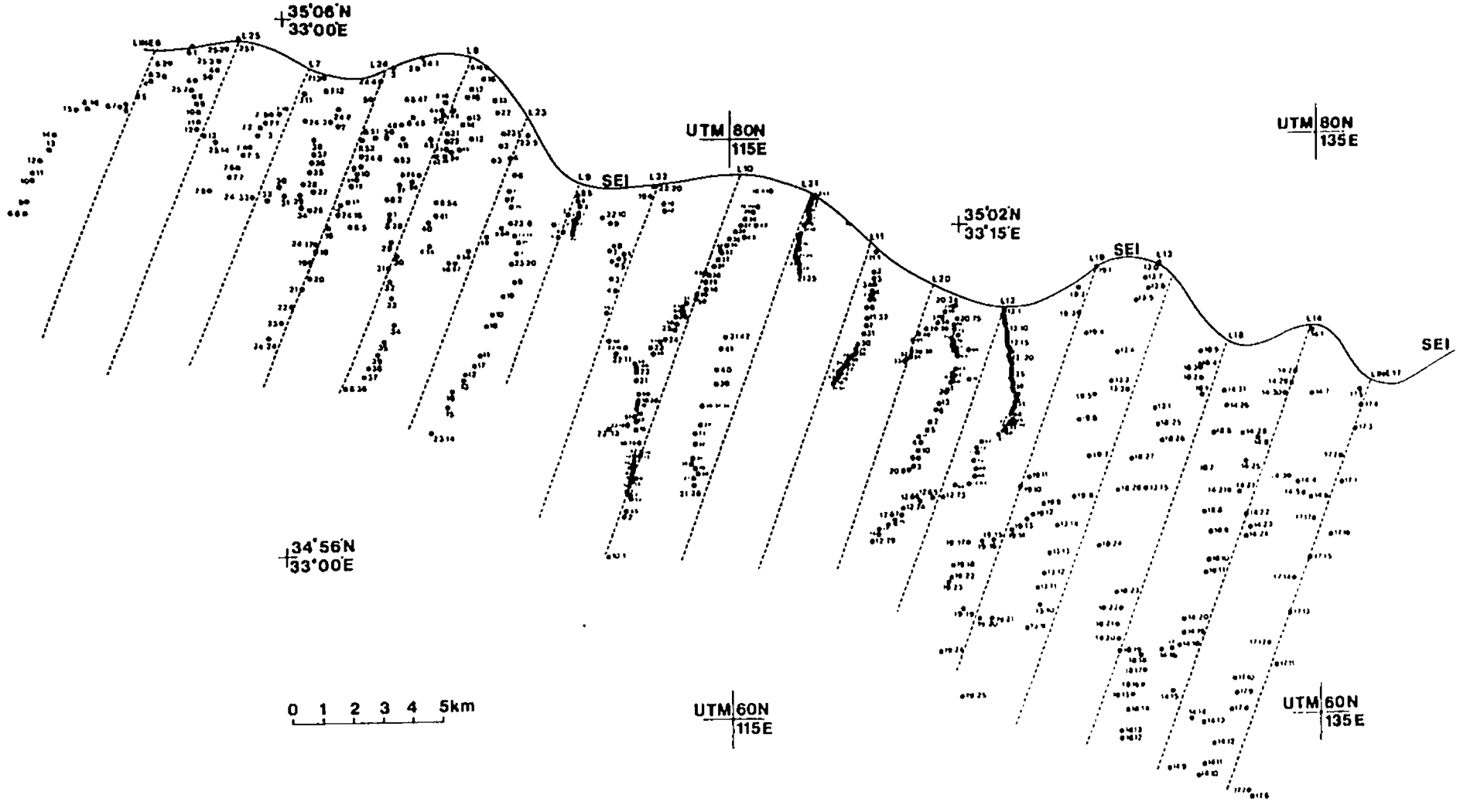

Fig. 3.2.5 Location of stations measured in the field.

interval of 0.25 in Fig. 3.3.1a (A map with all P measurements is attached in the back pocket). From the diagram, continuity of variation of lava flow morphologies is evident on scales of the order of one to ten kilometres. Because erosion shows a deeper part of the section, the lava flows can be observed at different stratigraphic levels in the spreading direction, especially in the central part of the area, i.e., between the longitudes of Mitsero and Kambia. Here, relatively thick intervals of high P value are generally concentrated at the top of extrusive sequence and P values show proportional variation with depth. To the east and west of the central area, the P contours are distinctly complex in their distribution and a number of isolated areas of high and low P occur, for example, in the vicinities of Ayia Marina in the west and Mathiatis in the east. These are indications of variability in the original construction of the crust.

Several characteristics of the eruptive processes, such as cyclicity of eruption, as well as individual features for each eruptive cycle, are discussed below.

3.3.1 Cyclicity

In the study area, because of differential erosion, crustal construction can be observed either along the spreading direction or along the axial direction. The central

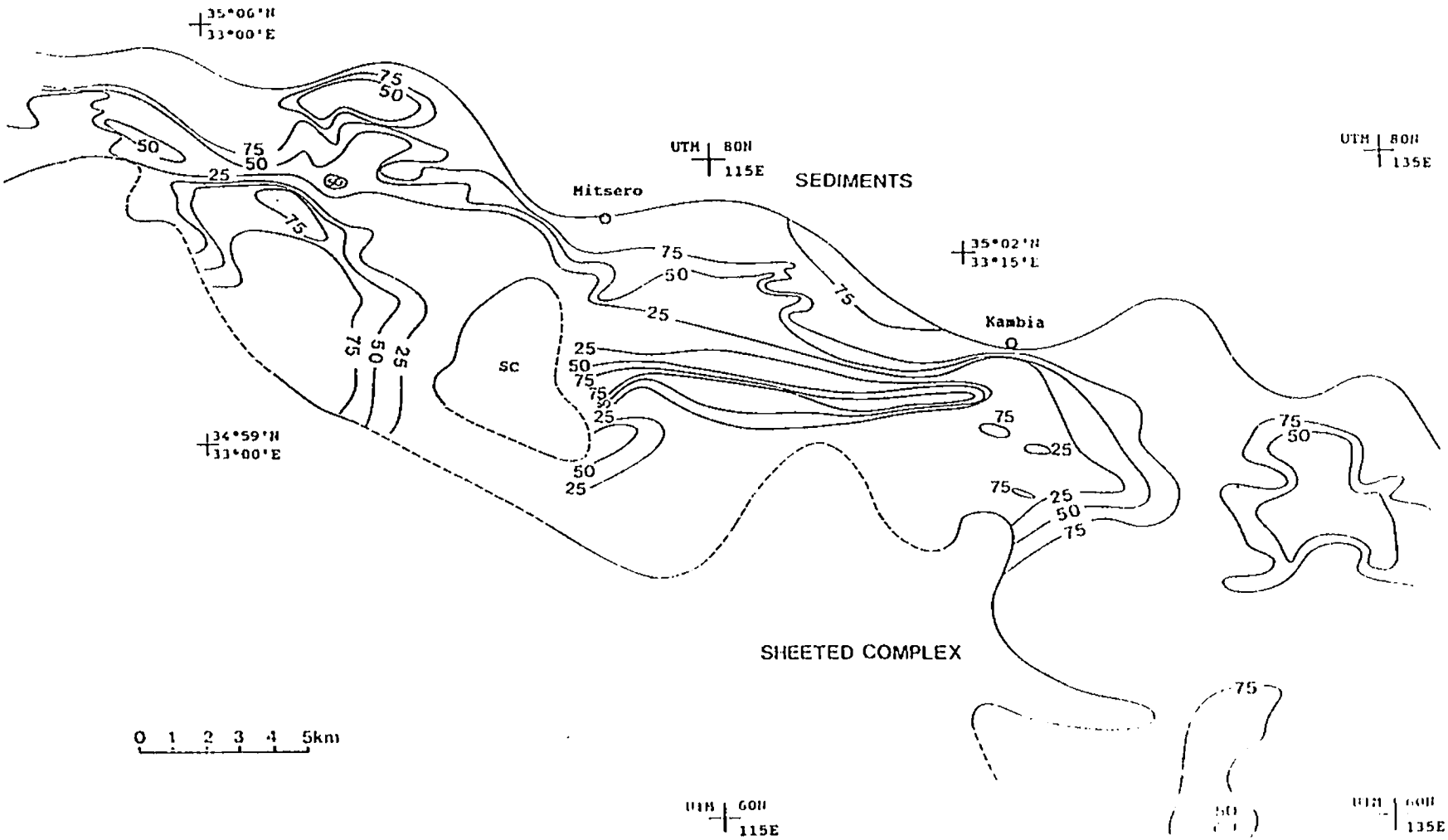

Fig. 3.3.1a Contour of P at intervals of 25%, 50%, 75% (see text for definition of P); SC- sheeted dike complex.

part of the area (UTM 110-125E), about 15 km long in the spreading direction, provides relatively much more crustal constructional information at depth. However, in the western and eastern parts of the area, where due to only slight erosion, the deeper sequence has not been exposed as yet, crustal construction along the axis can better be observed.

At least two temporal volcanic cycles are apparently represented in the middle part of the area between Mitsero and Kambia. This temporal cyclicity extends over a distance of close to 12 km in the spreading direction. Each cycle begins with a high content of sheet flows (low P) and ends with a high proportion of pillowed flows (high P). Still earlier cycles may be represented by fragments of extrusive units deeper in the section, e.g., deep in the central part of the area. Sections of screens of pillowed and sheet flows occur occasionally at depth. These sections are now isolated from higher, more continuous sections of extrusive rocks by thick sections of dikes. These isolated sections may represent a lower or earlier cycle or cycles, or have been downfaulted from higher crustal levels.

In the axial direction, cyclicity of volcanic activity is also evident both in the western and eastern areas in Fig. 3.3.1b. The distances between two adjacent peaks of activity along the axis are about 6 km in the west and 8 km in the

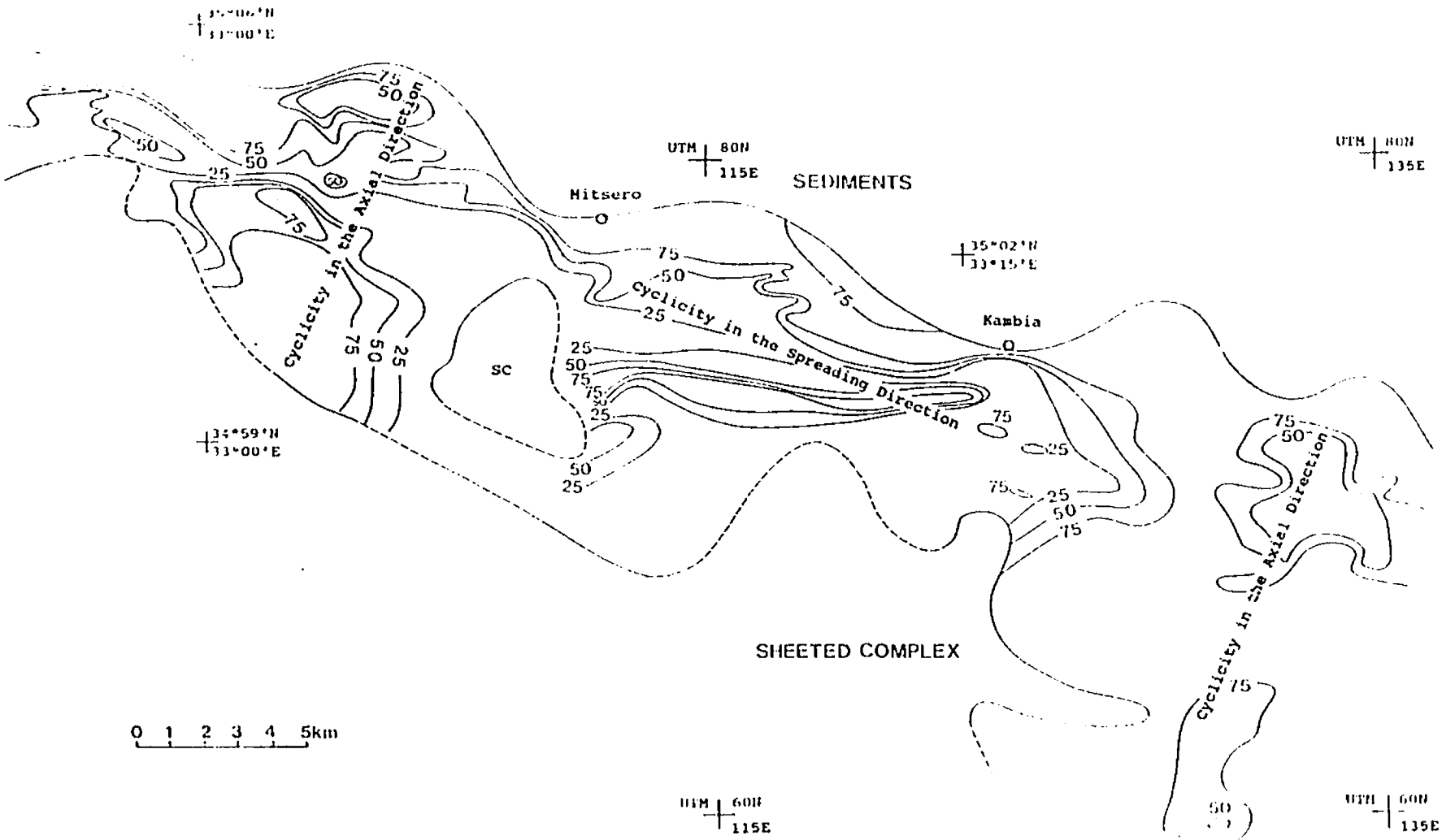

Fig.3.3.1b Cyclicity of eruptions both in the spreading direction and axial direction.

east, respectively.

To justify the contour map of P, 5 adjacent profiles from the central part of the area are drawn side by side for P values (Fig. 3.3.2). These profiles show, although considerable scatter in the data is evident, the main features on the contour map. For example, for the profiles of P the first and second volcanic cycles can be seen quite easily, although variation of P locally exists. It is also possible to see the large area of sheet lava flows in the sections at the eastern end, where P values are zero.

Since the Troodos ophiolite occurs in a regular anticlinal structure over much of its area, Hall et al. (1991) have proposed a quantitative geometric model, MODEL 2, for the structure. For the area under consideration, extending from Skouriotissa in the west tc a line through Pano Lefkara and Mathiatis (for locations see Fig. 3.1.1) in the east, a sinusoidal model was found to provide the best fit to the surface of sheeted complex. The expression for MODEL 2, assuming an average depth of the Sheeted Dike Complex (SC) beneath the SEI of about 1.1 km, is:

$$D=1.128+1.299\cos(0.128(N-(98.993-0.324E)))-H$$

where D is the depth of location in kilometres beneath the

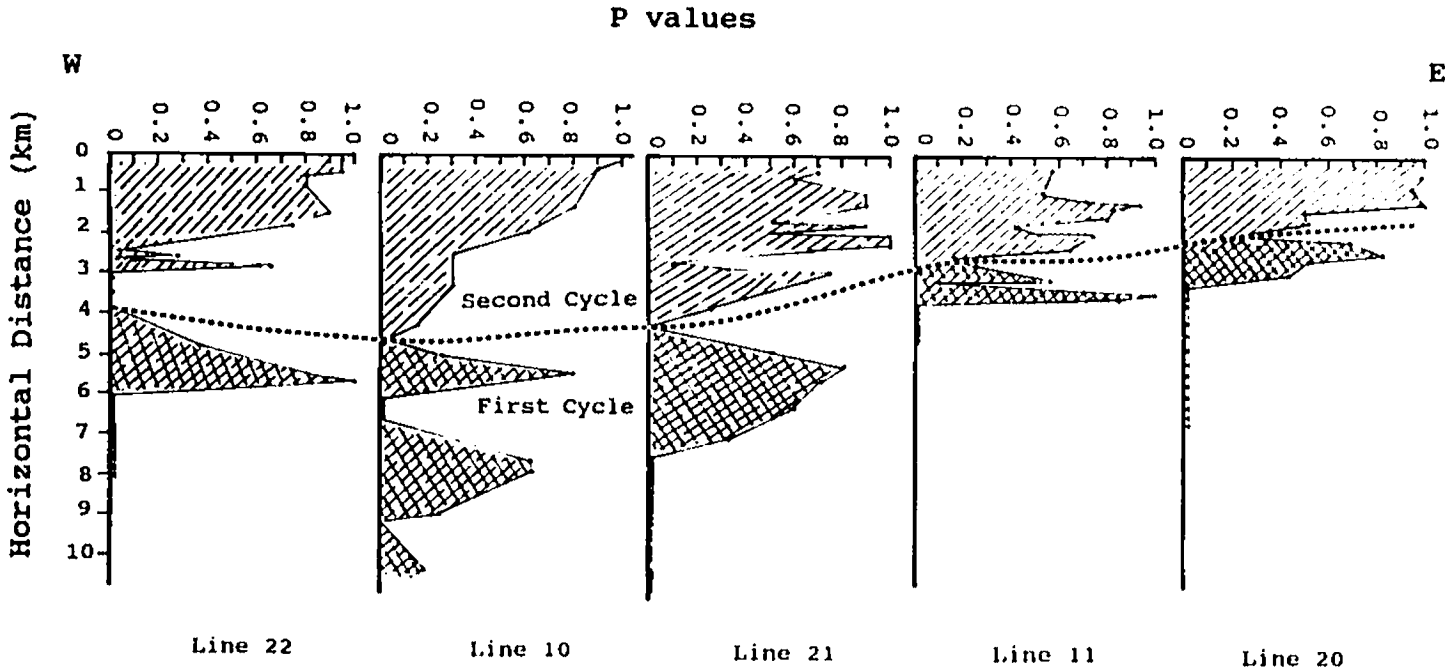

Fig. 3.3.2 Two volcanic cycles are identified based on the P values from five lines in the central part of the area. Black spot- observation station; the dashed line separates the two cycles.

SEI. N and E are, respectively, the north and east partial UTM coordinates of a location, and H is the elevation above sea level of the location. The model indicates a dip for the SEI (or SC) of close to 9° at the current outcrop position of the SEI, reducing to 0° at the crest of the anticline (Fig. 3.3.3). This model has been used to obtain all depths beneath the SEI given in this thesis.

Figure 3.3.4 is a depth diagram of the central part of the area and the depth data are listed in Appendix 3. In the diagram P is seen to generally increase upward from <0.25 to >0.75 much more rapidly in first, older, cycle than in second, younger, cycle. For the sake of detailed comparison between the two cycles, thicknesses of individual P values for each cycle are measured from 5 stratigraphic profiles Fig. 3.3.5) and the data are listed in Table 3.3.1. The average thicknesses of the dominantly pillowed intervals (P 0.75-1.0) in the two cycles are 0.04 ±0.01 km and 0.14 ±0.05 km, respectively. The thickness of the sheet flow sequence forming the lower part of the second, younger cycle generally decreases eastward.

Four possibilities for the formation of the observed cycles in crustal construction can be envisioned (Fig. 3.3.6). In the first two, continuous lava morphology layers extend in the spreading direction, but in the first the morphological

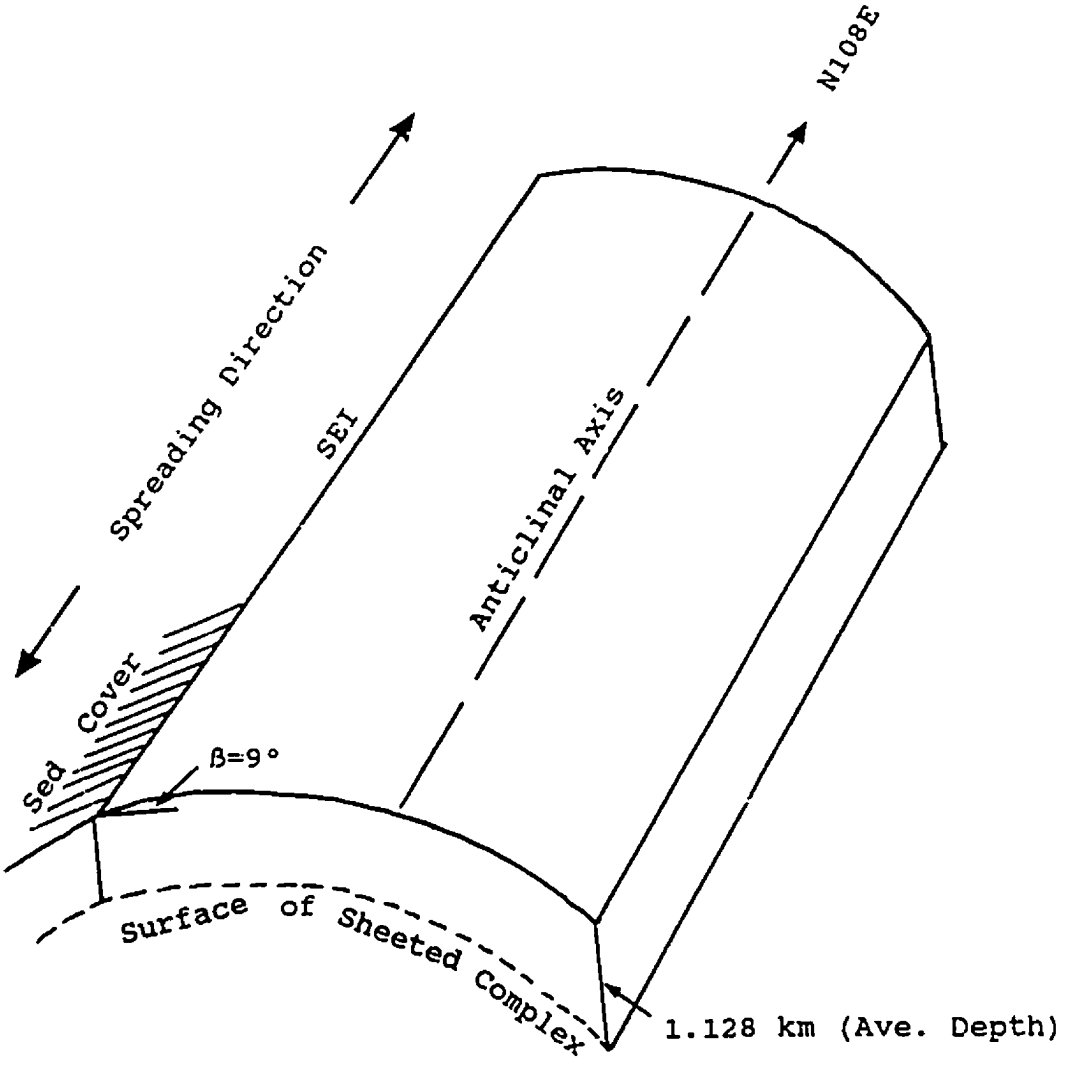

Fig. 3.3.3 Sketch of the form of the emplacement structure for the Troodos ophiolite as expressed by MODEL 2 (see text). SEI-sediment extrusive interface.

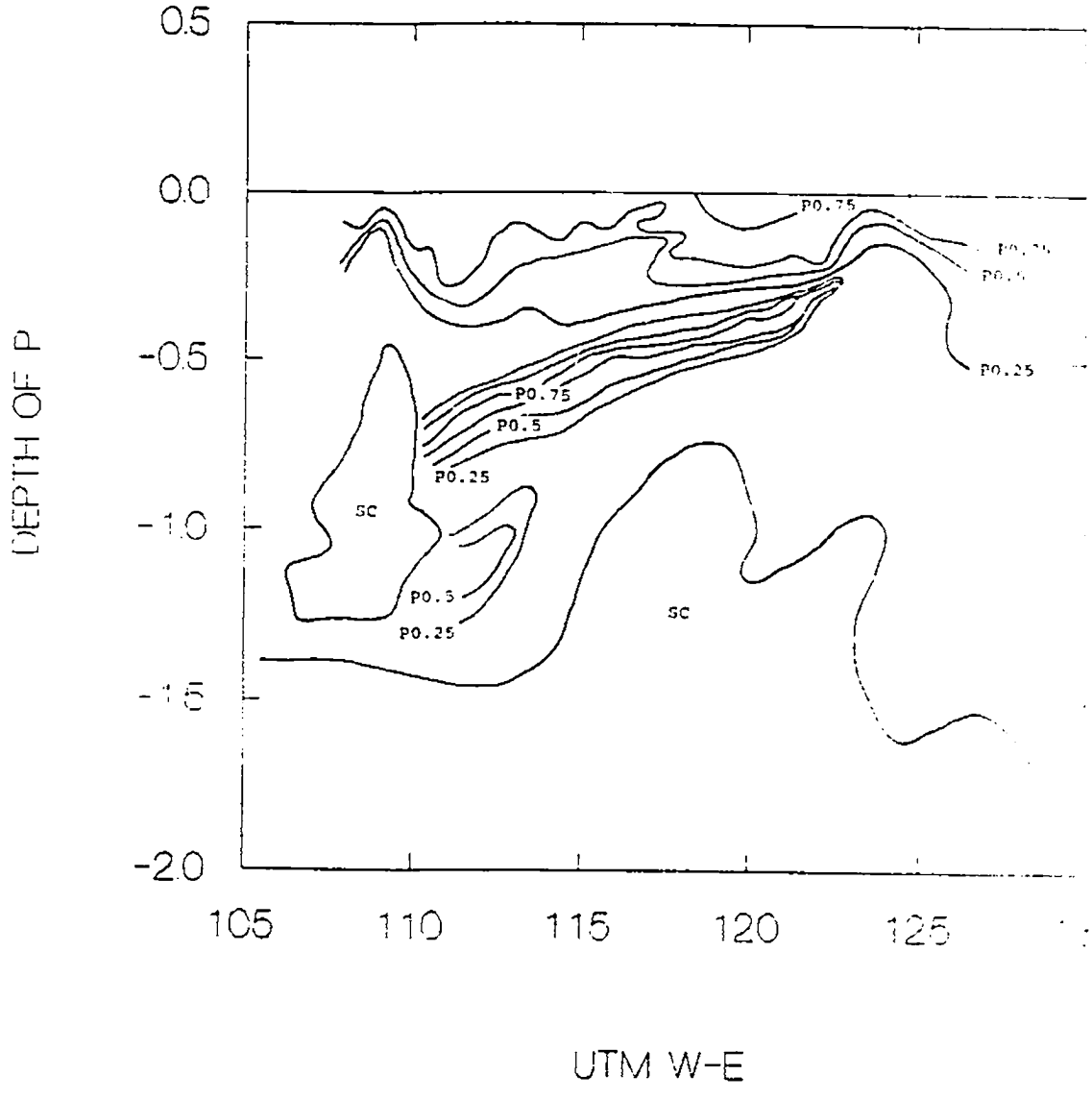

Fig. 3.3.4 Depth within the Extrusive Sequence in the central part of the study area. Contours are of P in intervals of 0.25. X-axis using UTM coordinates (see text).

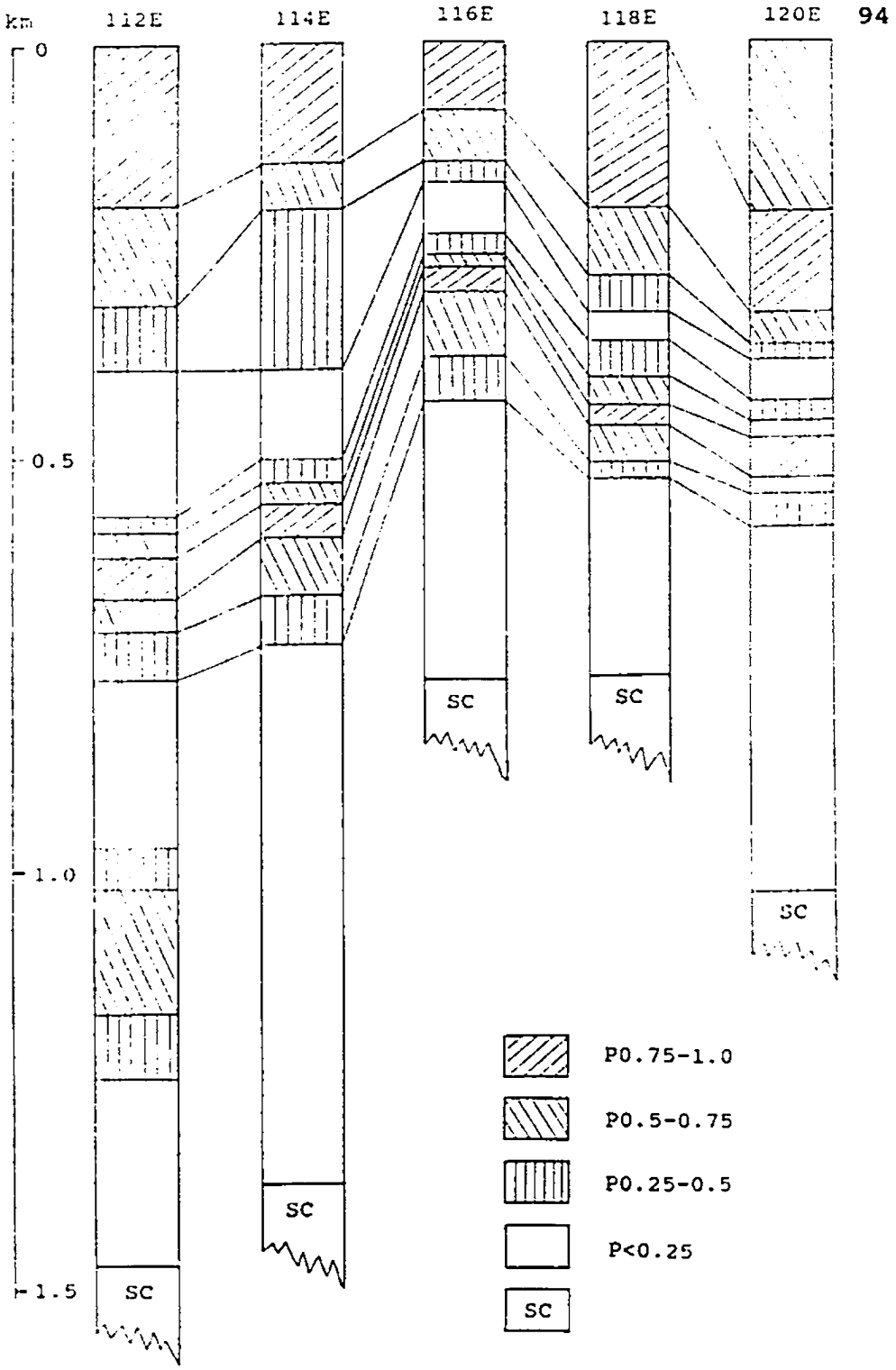

Fig. 3.3.5 Five depth cross sections showing variations of intervals of P. Sections, at a spacing of 2 km, are all crossing the two cycles of eruptions. 112E-UTM coordinates. SC-sheeted dike complex.

Table 3.3.1 Statigraphic Columns Through the Two Cycles of the Central Part of the Study Area

Columns	112E	114E	116E	118E	120E
P0.75-1.0	0.19	0.14	0.08	0.19	0.12
P0.5-0.75	0.12	0.06	0.06	0.08	0.04
P0.25-0.5	0.08	0.19	0.02	0.04	0.02
P<0.25	0.18	0.10	0.06	0.05	0.05
P0.5-0.25	0.02	0.03	0.02	0.04	0.02
P0.75-0.5	0.03	0.03	0.02	0.04	0.02
P1.0-0.75	0.05	0.04	0.03	0.02	0.05
P0.75-0.5	0.04	0.07	0.08	0.04	0.02
P0.5-0.25	0.06	0.06	0.05	0.02	0.04
P<0.25	0.70	0.65	0.34	0.24	0.44
Total	1.47	1.38	0.76	0.76	0.82

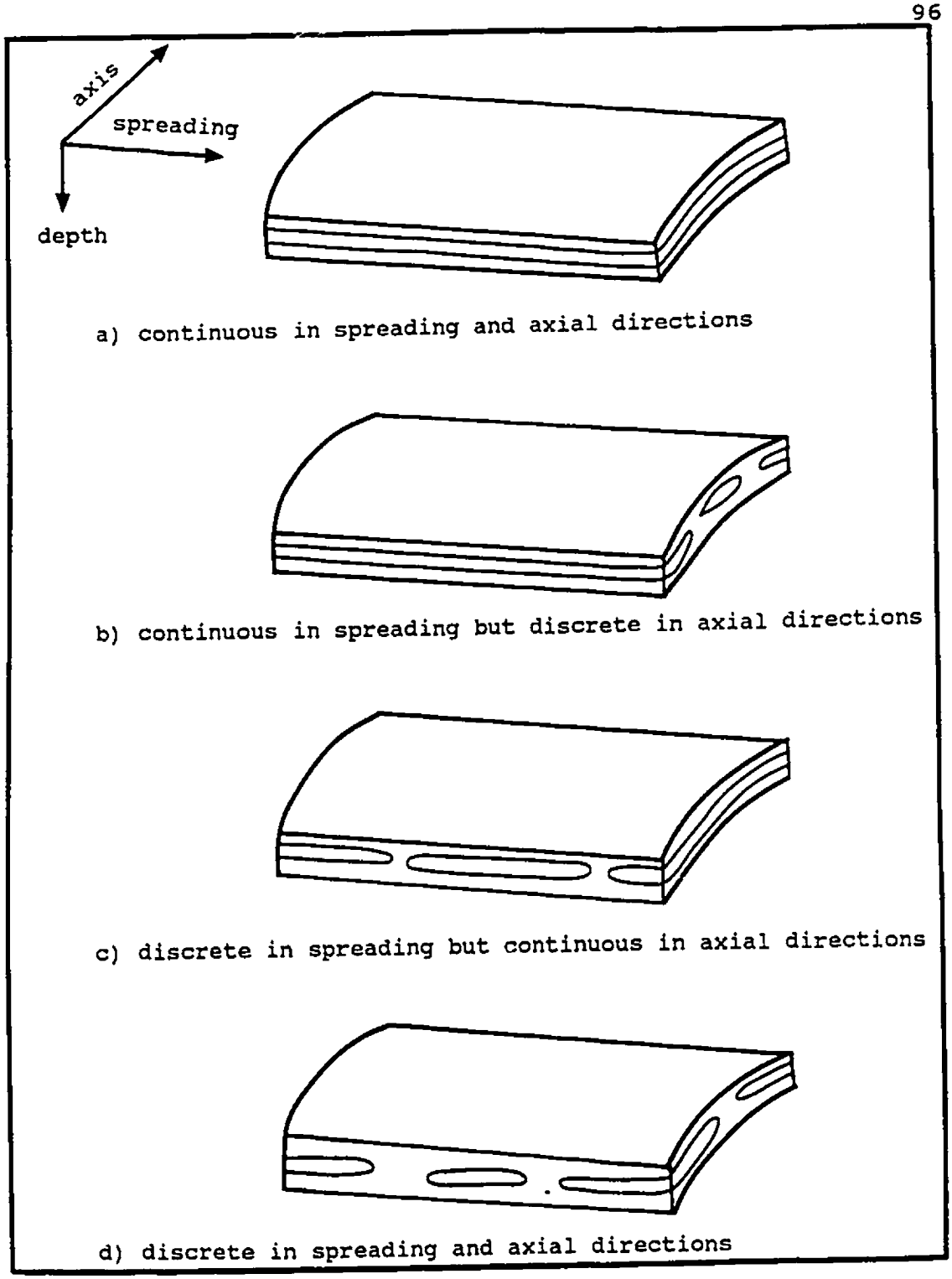

Fig. 3.3.6 Four possibilities for construction of the pillow-rich sequence in the central area.

types also continue for a considerable distance in the axial direction while in the second the morphological groups only extend for a limited distance in the axial direction as seen on present ridges, e.g., at EPR 21° N (e.g., Ballard et al., 1981). In the latter two possibilities, flow morphological layers are discrete in the spreading direction but may be continuous or discrete in the axial direction. Possibility one reflects long-lived spreading processes at the ridge. Possibilities two and three reflect, respectively, spatial and temporal variability on the spreading ridge while four is the result of variability in both space and time. Either possibility one and two could account for the cyclicity observed in the central part of the study area while possibility four appears to account for the situations in the eastern and western areas.

3.3.2 Individual lava formations

In the study area as a whole, four areas occur in which there are thick sheet flows with very thin development of pillow flows. These areas mark the locations of high magma productivity at the spreading axis during crustal construction. It is also evident that hydrothermally circulated, modified seawater arrived on the seafloor and sulfides were deposited preferentially in or near to these areas (see chapters 5 and 6). In addition, these are areas

where sheeted dikes occur at a relatively high level in the crust. The areas are separated by an average of 12 ±2 km (1sd) in the spreading direction (Fig. 3.3.7). From west to east, these are designated the Nikitari Formation, the Xyliatos Formation, the Kambia Formation and the Mathiatis Formation.

The sequences of the two middle formations, i.e. the Xyliatos and Kambia formations, are exposed most completely. The eastern, Mathiatis Formation, is located in the structurally depressed part of the emplacement structure and erosion has only exposed the upper part of the formation. Only half of the western, Nikitari Formation is contained in the study area.

Two characteristics of volcanic processes involved in crustal construction in the areas of these formations can be observed clearly in the two middle examples.

Firstly, the high P layer that characterises the uppermost part of the Extrusive Sequence is very thin or absent at the centre of these formations. The high P interval gradually increases in thickness laterally while downward it is quickly replaced by a relatively thick, high sheet flow sequence.

Secondly, the surface of the sheeted complex at the

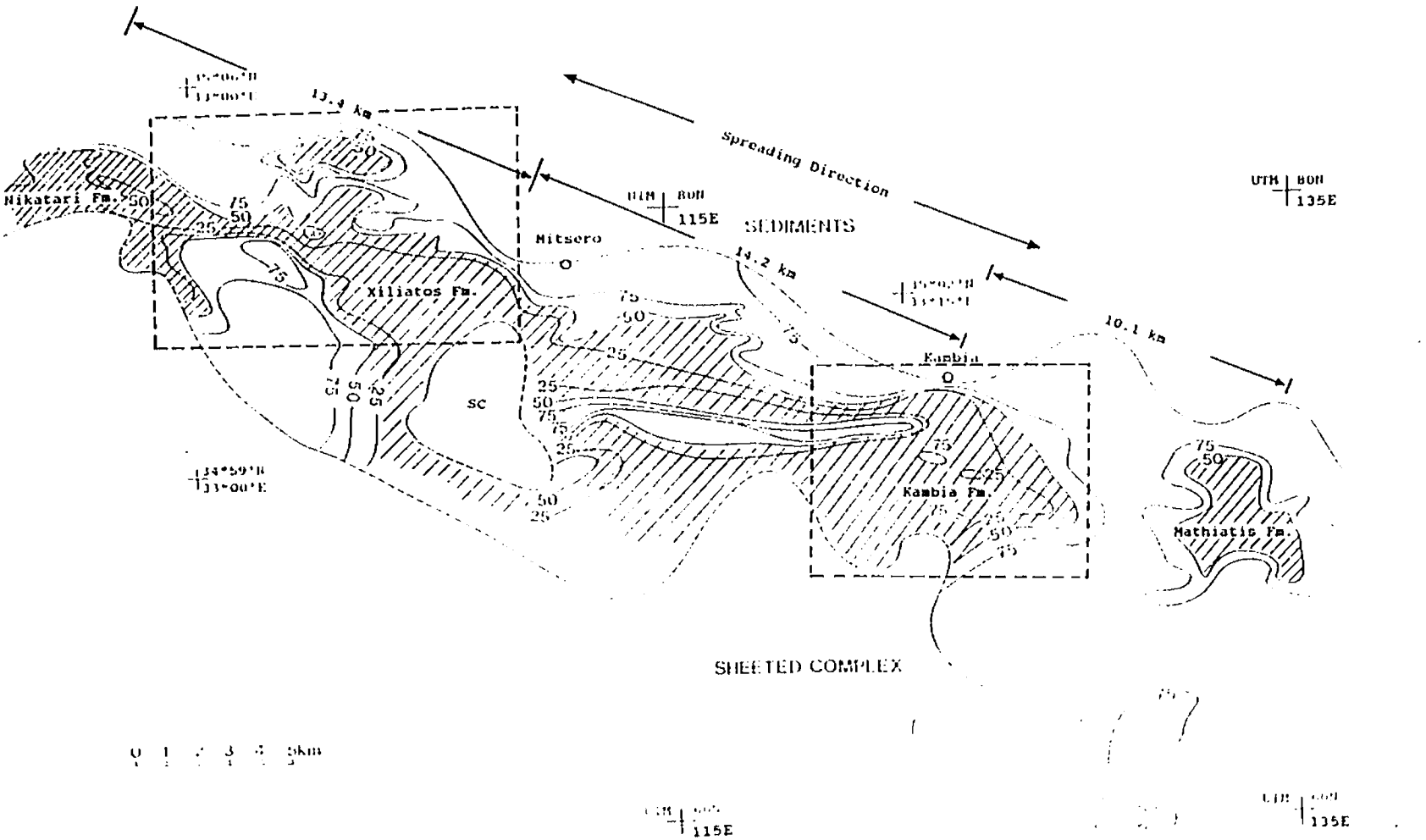

Fig. 3.3.7 Location of four formations of high eruptive activity in the area. The two blocks outlined by dashed lines indicate the locations of the areas shown in Figs. 3.3.9 and 3.3.13.

centre of the outcrop area of the formations is at a relatively high constructional level, i.e. these areas are marked by the peaks of the undulations of the surface of the sheeted complex. This feature is also obvious for the western formation and is predicted to occur under the eastern formation. In contrast, the surface of sediment/ extrusive boundary at all these formations appears to be at the relatively most depressed points in the original seafloor. The amplitudes of horizontal variation between SEI and SC are 2.7 ±1.1 km at high points of SC and 11.1 ±1.0 km at low points of SC, respectively.

3.3.3 Eruptive characteristics

The appearance of thick sheet flow sequences observed in the field is everywhere characteristic, that is, short sequences of sheet flows displaying opposing dips occur within short distances of one another. It is notable that the large majority of strikes are closely parallel to the axial direction (Fig. 3.3.8). This phenomenon is well seen in the high sheet flow areas of the Kambia and Xiliatos formations.

The occurrence of syntectonic structures in the sheet flows along the observation line in the Kambia Formation is shown in Fig. 3.3.9. The evidence for the syntectonic nature of these structures is that demonstratively synconstructional

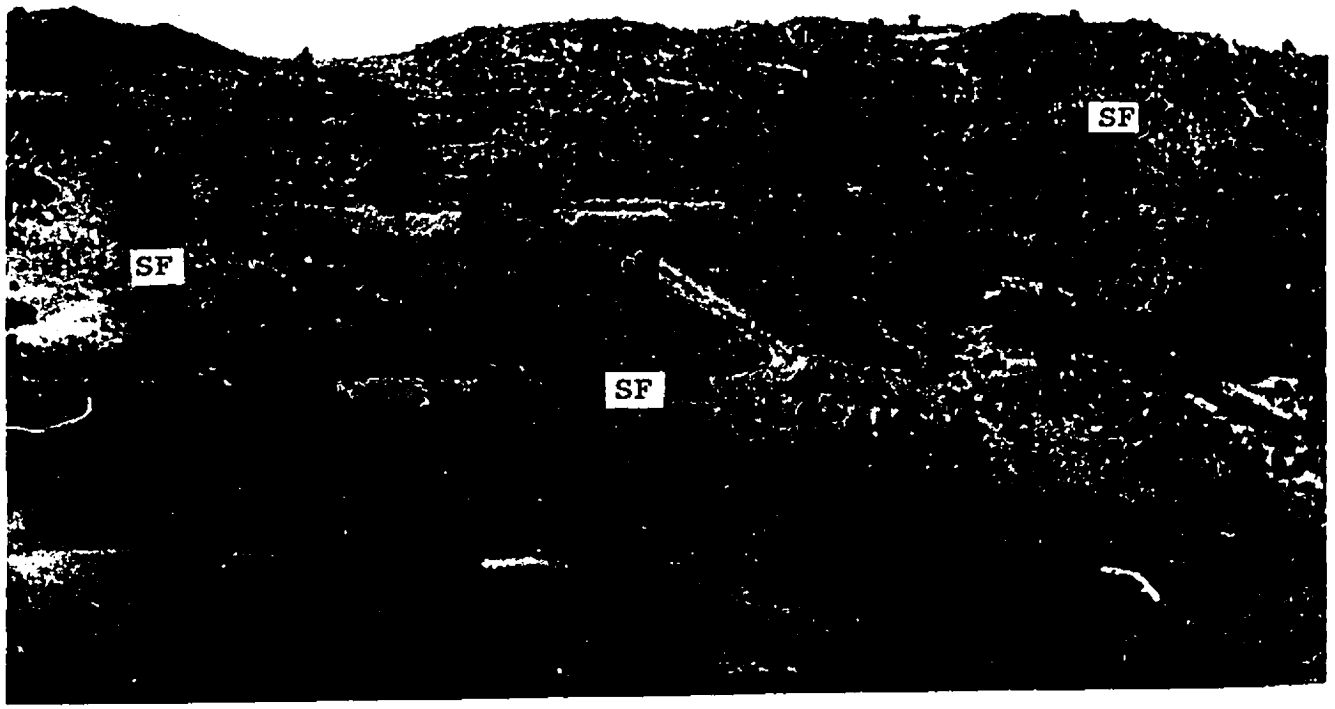

Fig. 3.3.8 Sheet flows show opposing dips in a short distance in the Kambia Formation.

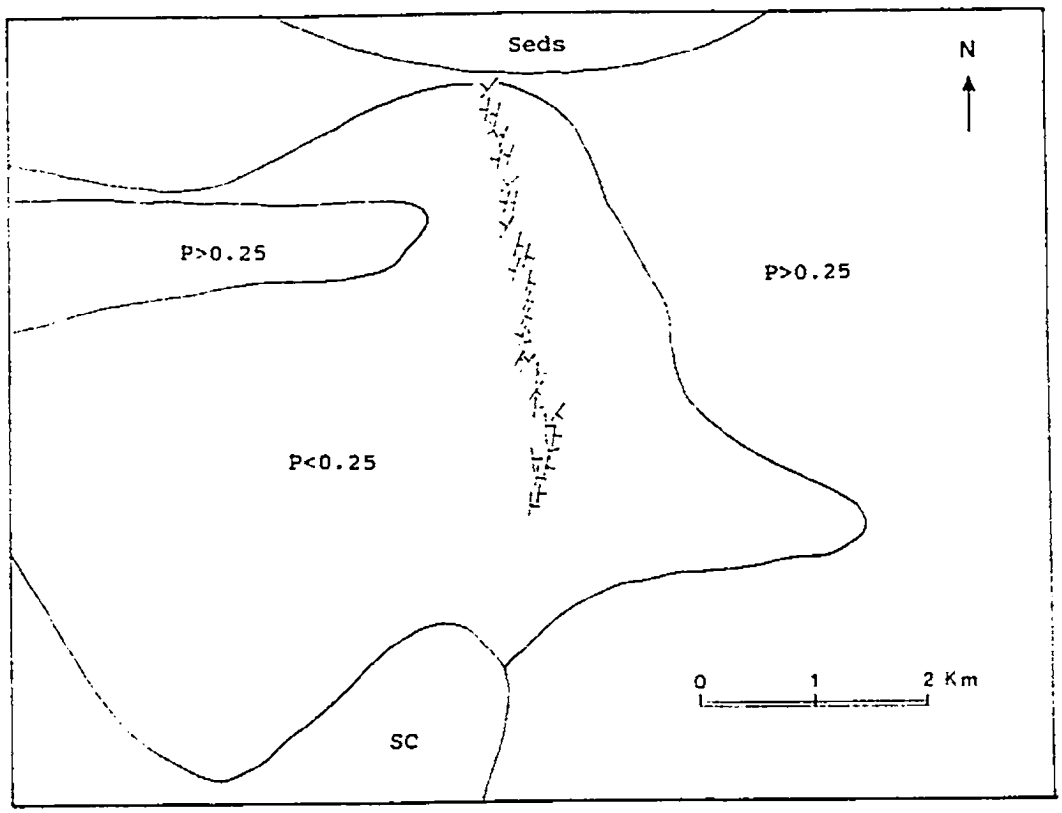

Fig. 3.3.9 Occurrence of dips in the SF of the Kambia Formation, showing two groups of opposing dips. For location of the area see Fig. 3.3.7.

umbers occur within depressions on the SEI formed by the opposing surfaces of rotated blocks of sheet flows. In this area there are 34 measurements of sheet flow dip in a profile from the SEI to the SC approximately in the axial direction (Table 3.3.2). They are interesting for their implications for crustal construction.

First, the major strike of these measured sheet flows dips is in N-NNE direction, approximate 71% of values are between 000° and NE 030° (Fig. 3.3.10), i.e., closely consistent with the expected axial direction during spreading as predicted from the strike of the dikes in the extrusives and in the Sheeted Complex. The histogram (see Fig. 3.3.10) shows an asymmetric distribution of these strikes, i.e., a narrower variation of strikes in the NW direction and a wider variation in the NE. A similar feature also appears in the western, Xiliatos Formation. At present there is no explanation for this phenomenon.

Second, the dips of these sheet flows show two groups with opposing direction, i.e., NW-NWW and NE-NEE. The opposing dips may occur at a very close distances from each other as seen at several places in the diagram. Most interesting is that the dips at the lower part of the sequence are dominantly NE-NNE and at the upper, NW-NWW, with a mixed zone in between them. The diagram showing dip distribution with depth (Fig.

Table 3.3.2 Strikes and Dips of Part Sheet Flows in the Kambia Formation

Station No.	Strike	Dip Direction*	Dip Angle
12.03,	40.00,	2.00,	30.00
12.05,	10.00,	2.00,	60.00
12.06,	10.00,	2.00,	36.00
12.07,	160.00,	2.00,	40.00
12.08,	20.00,	2.00,	35.00
12.09,	10.00,	2.00,	30.00
12.10,	20.00,	2.00,	25.00
12.12,	50.00,	2.00,	30.00
12.13,	20.00,	2.00,	22.00
12.14,	10.00,	2.00,	30.00
12.15,	30.00,	2.00,	45.00
12.17,	20.00,	1.00,	55.00
12.18,	15.00,	1.00,	45.00
12.19,	20.00,	2.00,	35.00
12.21,	10.00,	1.00,	50.00
12.22,	15.00,	1.00,	75.00
12.23,	200.00,	1.00,	52.00
12.24,	15.00,	2.00,	40.00
12.25,	170.00,	2.00,	80.00
12.26,	30.00,	1.00,	35.00
12.27,	40.00,	2.00,	30.00
12.29,	5.00,	1.00,	55.00
12.30,	30.00,	1.00,	70.00
12.31,	5.00,	1.00,	85.00
12.32,	35.00,	1.00,	80.00
12.33,	360.00,	1.00,	80.00
12.34,	5.00,	1.00,	65.00
12.35,	170.00,	1.00,	80.00
12.36,	10.00,	1.00,	70.00
12.37,	175.00,	1.00,	45.00
12.38,	10.00,	1.00,	50.00
12.39,	5.00,	1.00,	45.00
12.40,	5.00,	1.00,	50.00

* Dip Direction: 1-east; 2-west.

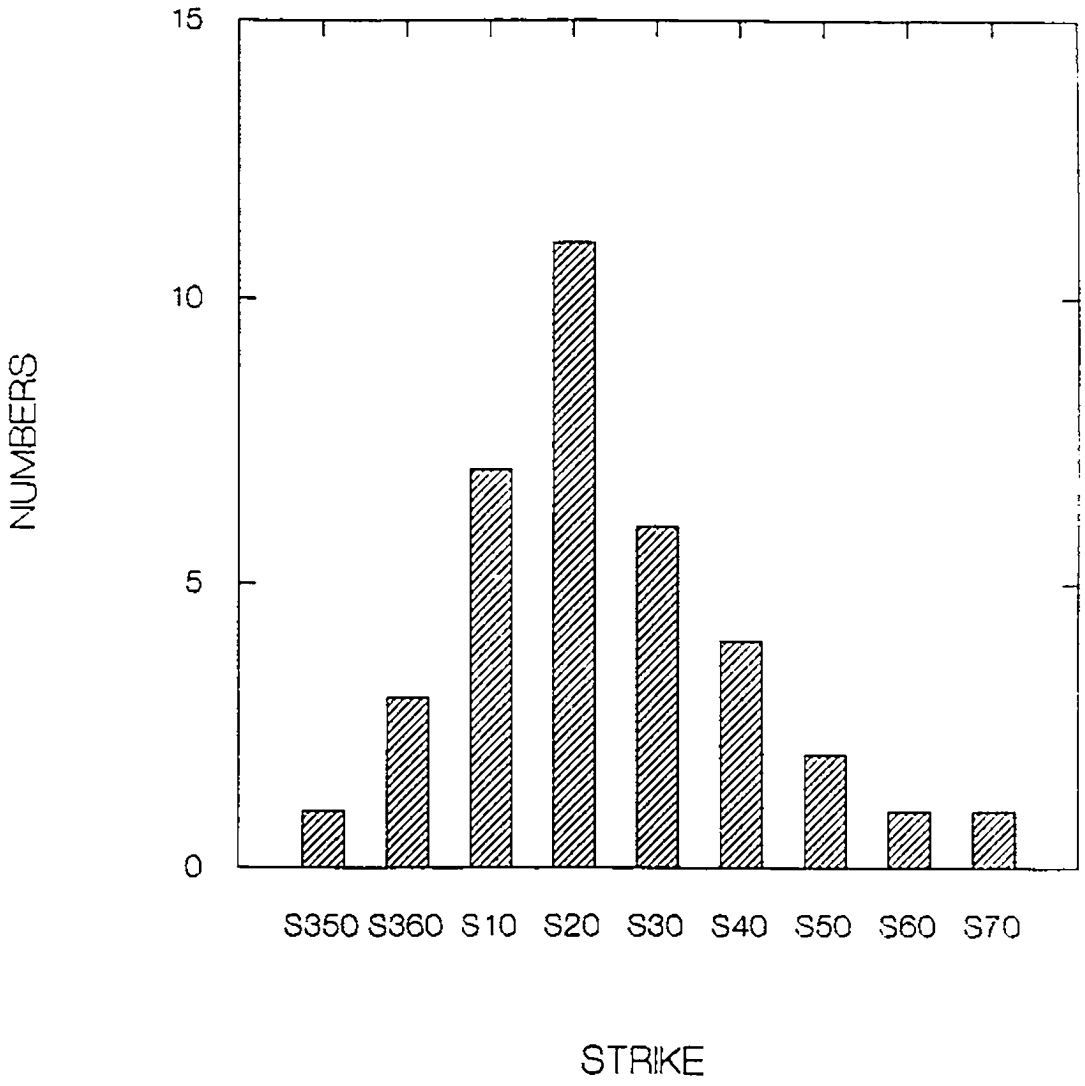

Fig. 3.3.10 Histogram of strikes of SF in the Kambia Formation.

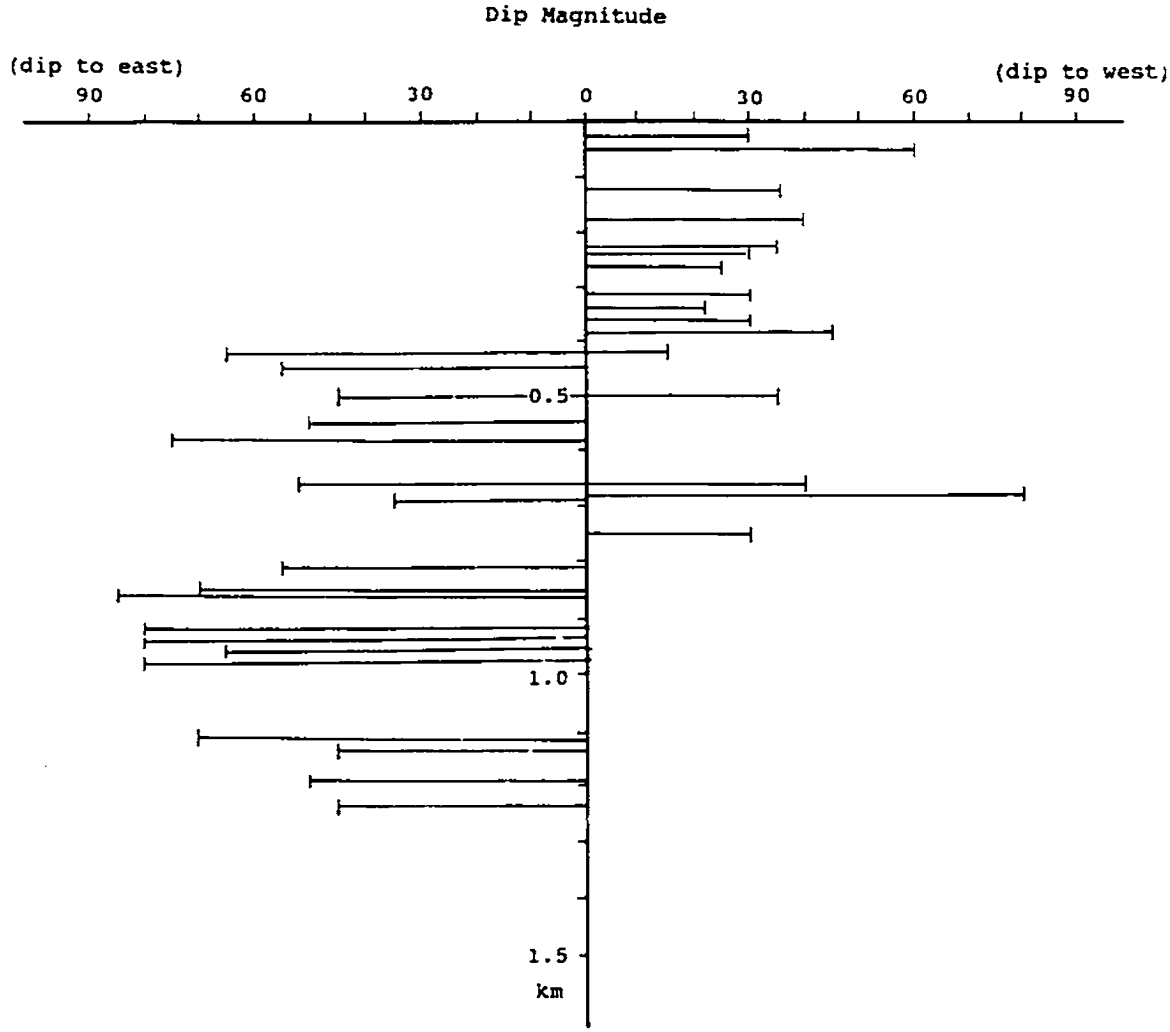

Fig. 3.3.11 Distribution of dip directions and variations of dip angles in the Kambia Formation.

3.3.11) reveals that the three zones are almost the same in thickness, i.e., 0.4 km for the upper west-dipping zone, 0.4 km for the middle mixed zone, and 0.45 km for the lower east-dipping zone.

One possible explanation for the opposition of dips is that synconstructional faults, probably listric normal faults, have played a major role during the eruptive period at the spreading ridge. It is interesting that, generally, dip angles in the upper part of the sequence are relative smaller, then downwards they gradually become larger (see Fig. 3.3.11). This may suggest rotation of lava blocks by listric normal faults, that is, the earlier formed lava flows after their formation will be rotated more leading to steeper dips than the younger lava flows. Similar small size dipping blocks of sheet flows which may rotate along faults, probably axis-parallel listric normal faults, have been found on mid-ocean ridges (e.g., Kappel and Normark, 1987).

Features quite similar to those in the Kambia Formation are also observed in the Xiliatos Formation. While measurement of dips is constrained by limited outcrops, the restriction of dip orientation is also very evident in this latter area. A quantitative analysis of dip directions in the Xiliatos area can be obtained since it was noted in the field that the units called "shallow dipping units" on the 1:31,680 geological map

of the area (Geological Survey of Cyprus, 1960) are actually inclined sheet flows. This is clear from the fact that the vesicles, joints, and alteration in these rocks are quite distinct from those of dikes or sills intruded at shallow levels (Fig. 3.3.12). In sheet flows vesicles are relatively abundant and are generally elongated with tubular shape. Many vesicles have no fillings, or are filled by celadonite. Cooling joints are often present in sheet flows but are not quite even or flat in contrast with the geometrically regular joints of dikes or sills. Although minor glass also can be observed at the margin of shallow dikes, most marginal glass is believed to be characteristic of sheet flows. The authors of the map and memoir, working in the area during the 1950s, had no knowledge of the morphology of submarine extrusives on the present mid-ocean ridges. It is thought that they assumed such extrusives were all pillowed in form due to the known rapid cooling rate in subaqueous conditions. In these circumstances it was reasonable for them to consider the similarity of the external form of sheet flows and sills as evidence that the forms were some type of minor intrusion.

Based on these observations, the sheet flows in the Xiliatos Formation and in the westernmost area of high sheet flows (see Fig. 3.3.7) which are described as "shallow dipping intrusions", show quite similar structural features to those observed in the Kambia Formation. There are 442 strikes and

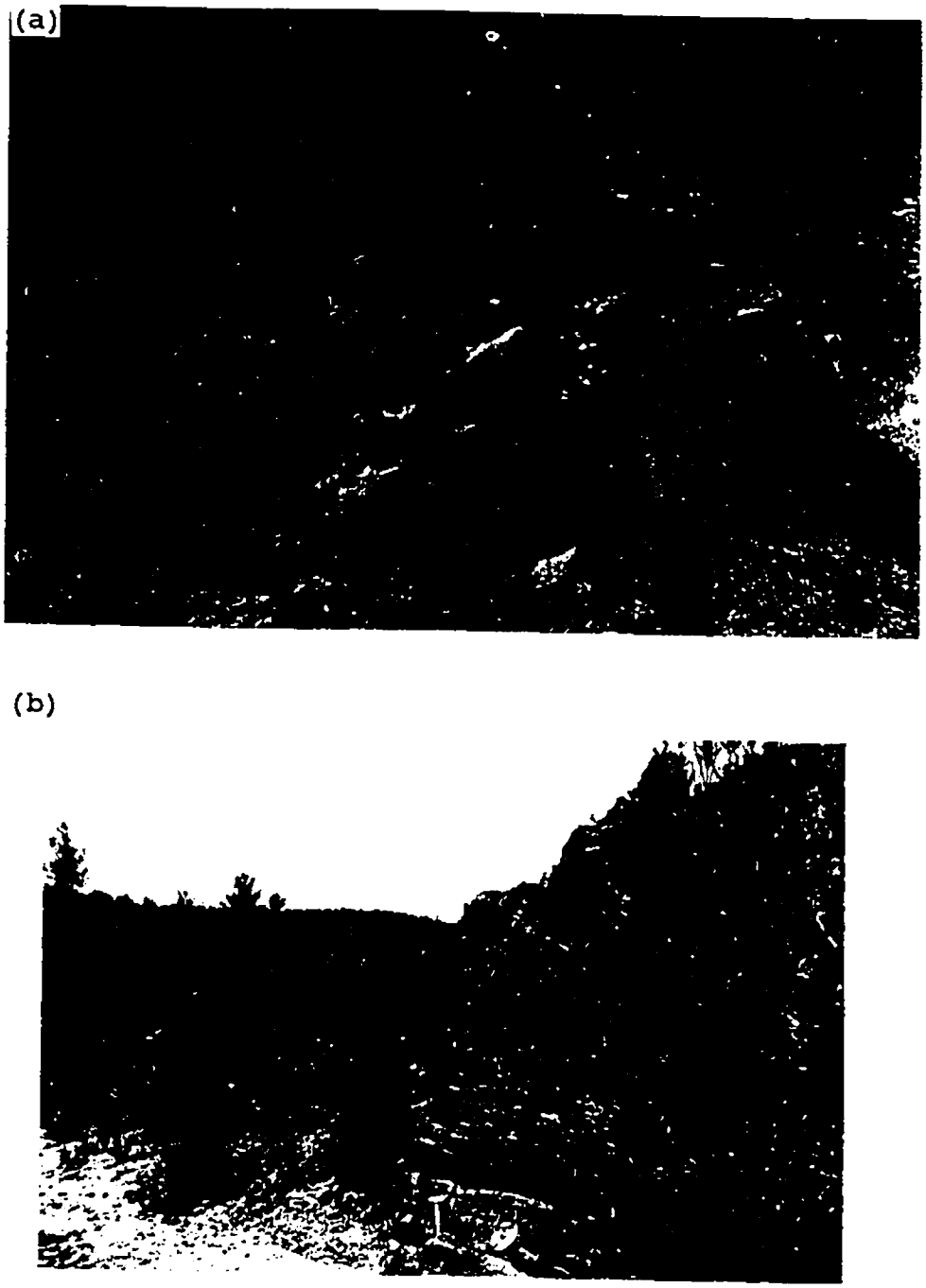

Fig. 3.3.12 Dikes and sheet flows generally distinguished by jointing, vesicles, and alteration appearance. a-sheet flows (station no. 20.74); b-dikes (station no. 20.30).

Table 3.3.3 Distribution of Strikes of Sheet Flows in the Xiliatos Formation

Direction	Total	Group 1	Group 2	Group 3
001-010	80	9	39	32
011-020	61	7	32	22
021-030	55	5	37	13
031-040	45	4	28	13
041-050	30	0	16	14
051-060	25	4	11	10
061-070	27	3	9	15
071-080	7	1	2	4
081-090	13	5	0	8
291-300	6	1	2	3
301-310	7	4	1	2
311-320	7	1	1	5
321-330	7	2	0	5
331-340	4	1	0	3
341-350	24	9	6	9
351-360	44	17	9	18
Sum	442	73	193	176

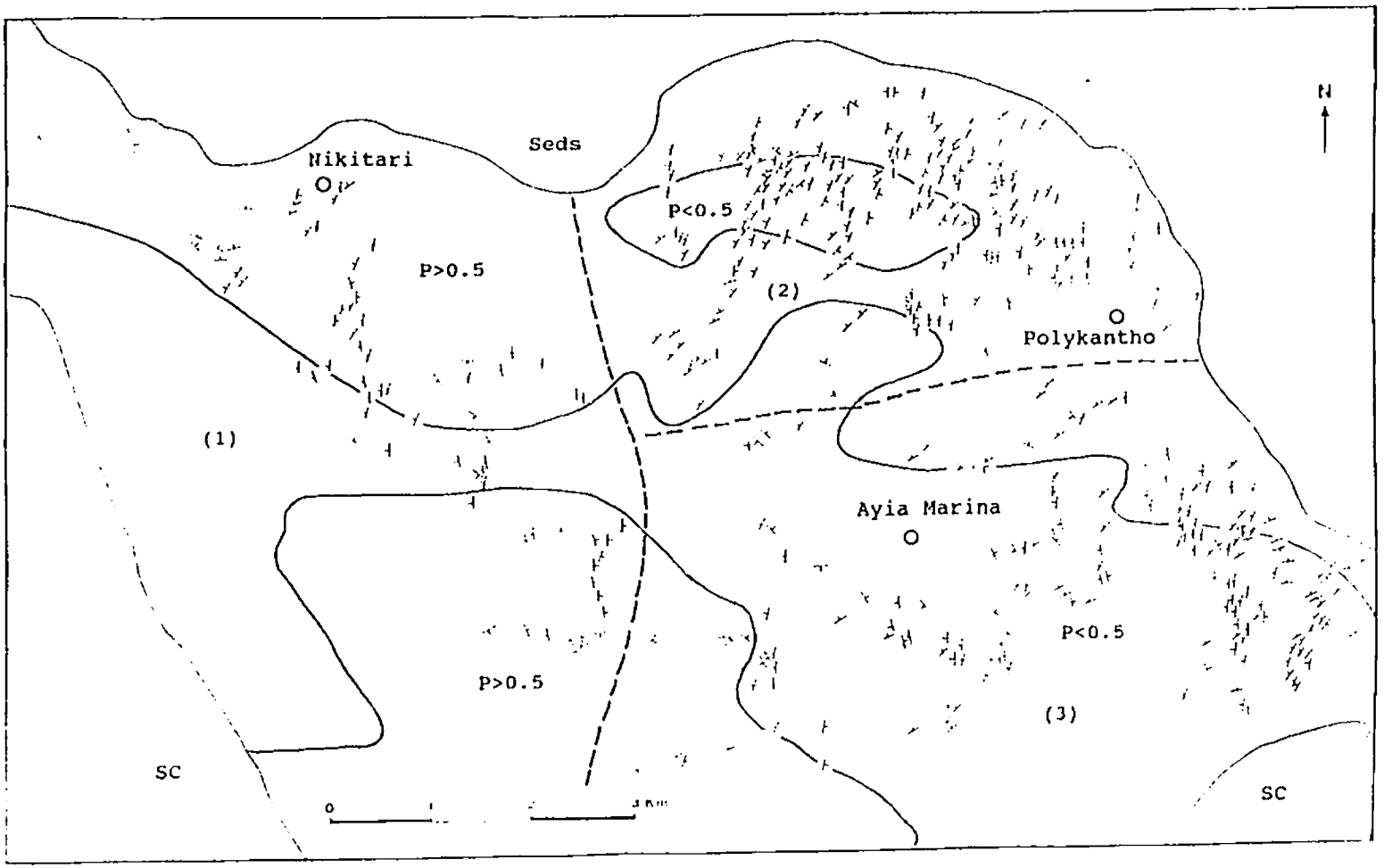

Fig. 3.3.13 Occurrence of SF, termed "shallow dipping intrusives" in the Geology Map of the Presterona-Lagouhera Area (1:31,680) (Geological Survey Department, Cyprus, 1960), in the Xiliatos Formation. Dashed line-boundary of three subdivision of the area: (1) Nikitari area, (2) Polykantho area, (3) Ayia Marina area.

dip directions extracted from the 1:31,680 geological map of the area, listed in Appendix 3 and summarized in Tables 3.3.3, and plotted in Fig. 3.3.13. The dip values, however, are not given in the map, precluding comparison of dip magnitudes between the Xiliatos and Kambia. Figure 3.3.13 shows dips in opposing directions, i.e., toward the southeast or, locally, towards the northwest. A histogram (Fig. 3.3.14a) of all measured strikes of flows shows a general orientation towards NNE, which is again parallel to the expected axial direction and is similar to that observed for the Kambia Formation. The histogram displays a degree of asymmetry with strikes to the east of the peak more scattered than to the west of the peak. In the Xiliatos Formation the histograms (Fig. 3.3.14b, c, d) of strikes of three separate subareas all show the same asymmetry; the only difference is that proportions of the NW strikes vary.

3.4 Controls on lava flow morphology

When various eruptive styles or morphologies of lava flows are observed on the present seafloor or in ophiolites, a first question always is how are the different morphologies of lava flows, such as pillowed and sheet flows, formed?

Lava flow morphologies may be related to one or more of: viscosity of magma, differences in extrusion rate, topography

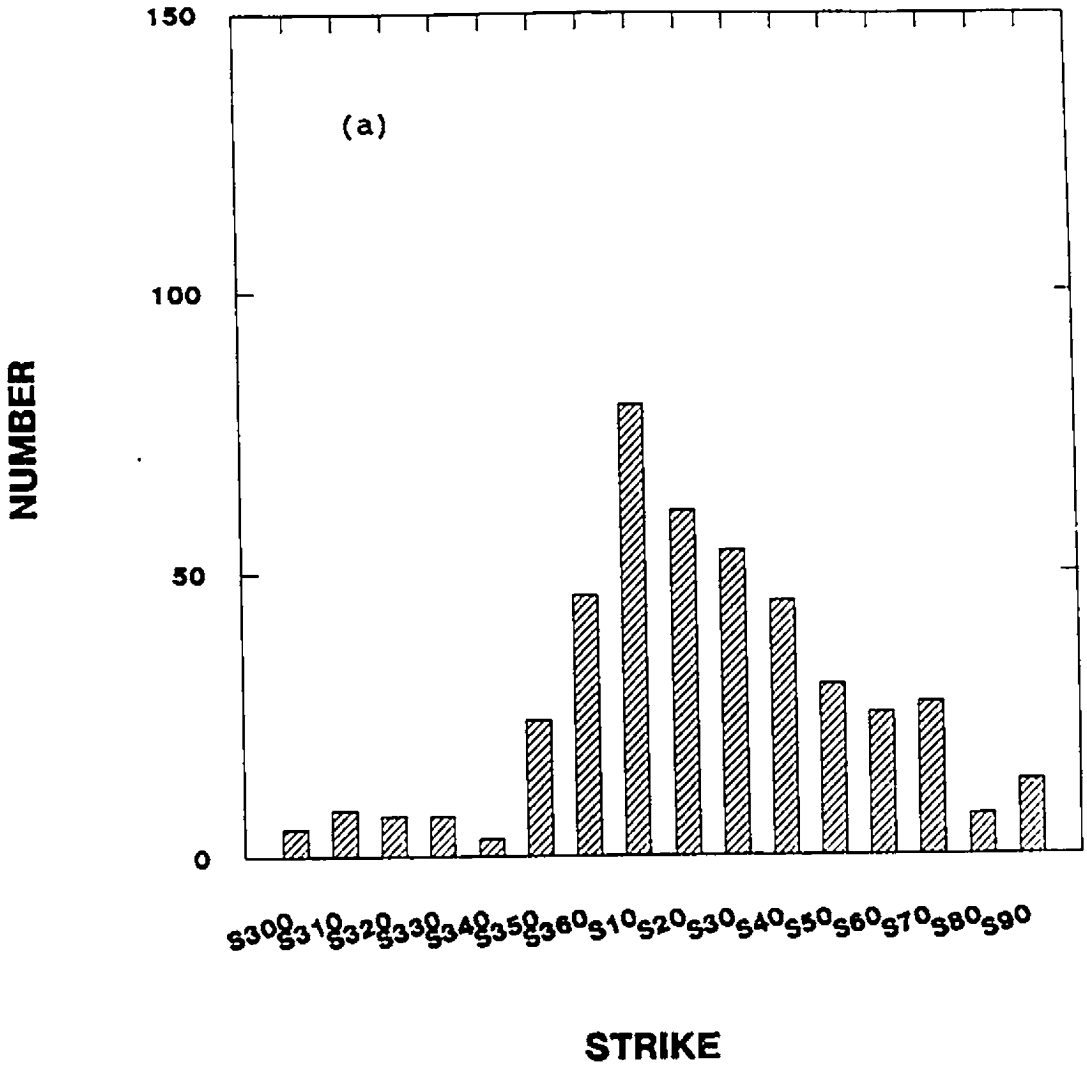

Fig. 3.3.14a Histograms of strikes of SF in the Xiliatos Formation, S300=strike in N300W. (a) total of 442 values; (b) 195 values in the Nikitari area; (c) 176 values in the Polykantho area; (d) 75 values in the Ayia Marina area (for discussion see the text).

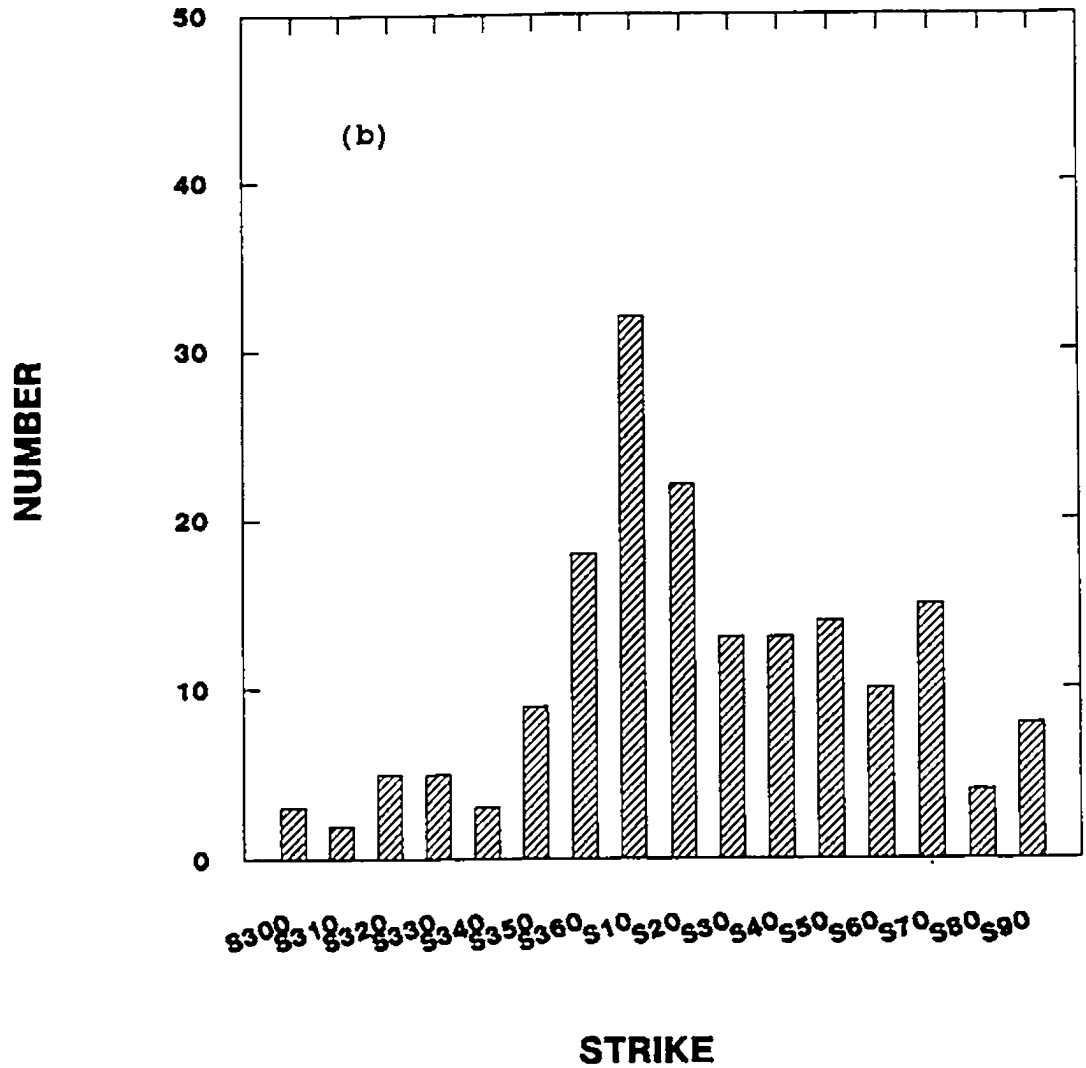
(b)
NUMBER
50
40
30
20
10
0
S300 S310 S320 S330 S340 S350 S360 S10 S20 S30 S40 S50 S60 S70 S80 S90
STRIKE

Fig. 3.3.14b

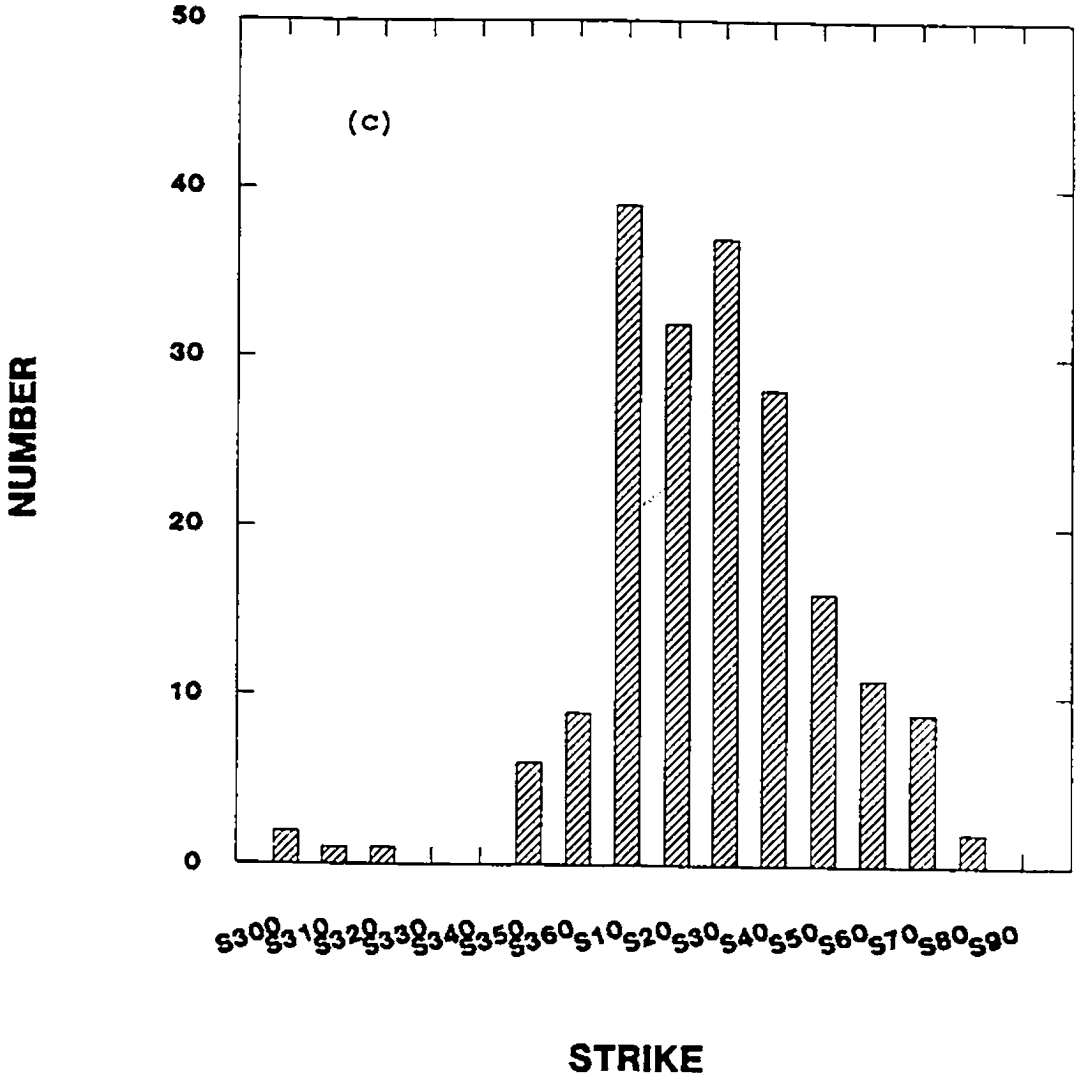
50
40
30
20
10
0
(c)
NUMBER
S300 S310 S320 S330 S340 S350 S360 S10 S20 S30 S40 S50 S60 S70 S80 S90
STRIKE

Fig. 3.3.14c

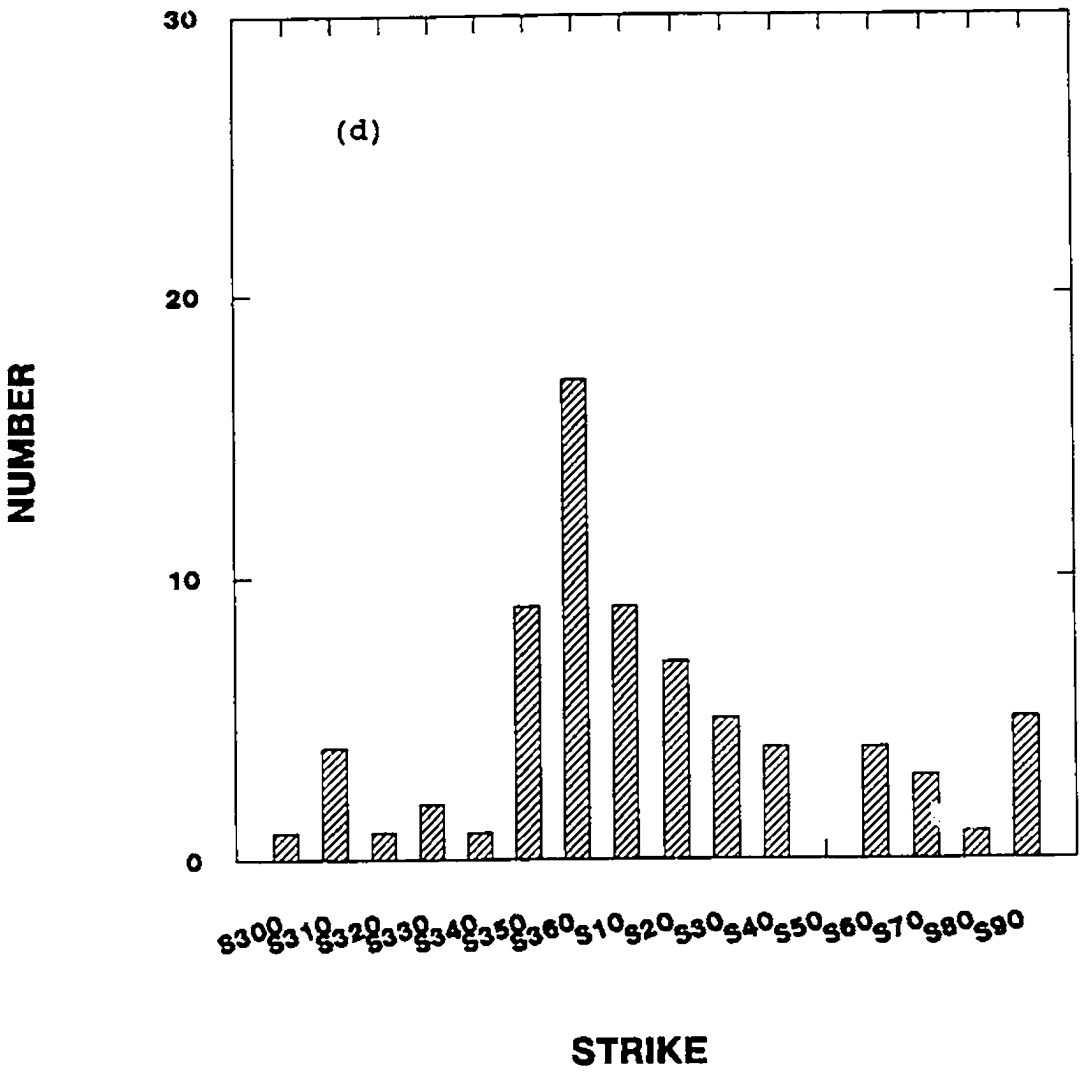
30
20
10
0
(d)
NUMBER
S300 S310 S320 S330 S340 S350 S360 S10 S20 S30 S40 S50 S60 S70 S80 S90
STRIKE

Fig. 3.3.14d

of the underlying surface, or other factors. These factors are discussed below.

1. Viscosity of magma

It is known that viscosity depends on pressure, major element composition, temperature and volatile content. Small amounts of volatiles can change the viscosity of magma and a major difference in the volatile content could then account for different lava forms (Campsie et al., 1984).

Byers et al. (1986) analyzed volatiles in pillow-rim glasses from lavas erupted along the axis of the East Pacific Rise (EPR) at 21°N. They found that sheet flow and pillow basalts contain identical volatile contents. Thus, the formation of both sheet and pillow lavas cannot be related to volatile content, i.e., volatile abundance is not a factor controlling flow morphology. As major element composition, pressure, temperature and volatile content do not vary between sheet flows and pillows at 21°N (Spiess et al., 1980; Juteau et al., 1980; Byers et al., 1986), eruption rate and/or surface topography are probably the most important factors in determining whether a submarine flow will have sheet or pillow morphology.

In Troodos, the case is complex, since there may be a

wider range of composition types in the Troodos extrusives than in in-situ oceanic crust. The extrusives contain dominantly basalt, basaltic andesite and andesite, with minor (about 5%) dacite and rhyodacite and picrite (Mehegan, 1988; Bear, 1960). Glass compositions by Robinson et al. (1983) indicated that the upper two thirds of the UPL and LPL sequence are basalts and basaltic andesites and one third are andesites, dacites and rhyodacites. This is consistent with the result of Taylor (1990) who estimates that the proportions of the low-Ti and high-Ti lavas for the extrusive sequence above the dike complex is 65:35, i.e., the low-Ti primitive suite is the most abundant in the area. Although no fresh glass are found in the BG, due to the extensive hydrothermal alteration, whole rock compositions were used to subdivide the rock types into basalts, andesites and dacites from previous studies (e.g., Bagnall, 1960; Bear, 1960; Bednarz et al., 1987a; Mehegan, 1988).

Question here is: are there any general relationships between morphological styles and magma compositions? Although this is obviously an important question, there are several difficulties involving in giving a final answer to this question.

First, there is possibly uncertainty regarding the distinction of rock types in the extrusives in Troodos. It is

a fact that fresh glasses demonstrate unambiguously the existence of the different rock types in the extrusives. However, the data provided by the limited glass samples are not likely to be representative of the composition of whole sequence, because fresh glass is only occasionally preserved and was not collected throughout the sequence, e.g., in the BG where the lavas are extensively altered and, as a result, workers have to use whole rock analyses for chemical classification (e.g., Bednarz et al., 1987a; Mehegan, 1988). This has been necessary although the rocks in the sequence have mostly been altered to some degree; in particular, basalts in the BG have been intensely hydrothermally altered. In these circumstances, since we know that during alteration mobile elements have moved out of or into the extrusives (e.g., Gillis, 1986), a first important question here to ask is whether there are influences of alteration on the supposed identification of primary rock types? For example, Gillis (1986), by comparison with fresher samples in the CY-1 sample set, suggested that SiO_2 has been reduced from initial values by 3.9 wt% for extrusives in the Smectite-Palygorskite-Calcite alteration zone at the top of Hole CY-1. Therefore, the conclusion here is that the influence of alteration on the discrimination of types is likely to be significant, and as a result, the present classification of rock types based on whole rock analyses is questionable. As an extension of this conclusion, the questionable classification of rock types

affected by alteration becomes one of the difficulties in testing for correlation between different lava morphological styles and rock types.

However, the question then to be asked is might the local fresh glass samples be used as standards to remove the effect of alteration of the extrusives in general and to classify the whole sequence of extrusive rocks? Apparently, a relevant question is how representative are these fresh glasses of the whole sequence of the extrusives? These questions are a prerequisite to seeking any relationship between the rock types and their morphologies. Unfortunitly, no general answer has been made from the data of previous studies.

The second difficulty is that we know little about volatiles in the extrusive rocks on the viscosity of the magma(s), other than the data reported by Muenow et al. (1990) for volatiles from five basaltic glass samples (including two altered samples), of which one is from a dike and four from lava flows. In spite of the absence of an indication whether these samples are pillowed or sheet flow, the sample number is also too small to be representative of the whole extrusives in Troodos.

Another difficulty is that there is no data on magma temperature and pressure for the Troodos extrusives,

particularly for different rock types and morphological forms. On the other hand, although we know that acid melts are several orders more viscous than basic melts, for example, at 1200°C, a typical basalt has a viscosity of ~500 P, a typical andesite 3 x 10^4 P, and a typical rhyolite 10^7 P (Hughes, 1982), unfortunately, there is no any experimental data to define correlation between magma types and lava morphological forms, especially in a marine environment.

For the situation in Troodos, it is known that the two prominent lava flow styles, pillowed lavas and sheet flows, occur within all rock types. For example, the histograms of lithological types from both holes CY-2 and CY-2a of CCSP (Bednarz et al., 1987a) for each main chemical division show this partitioning (Fig. 3.4.1). From this diagram, it is seen that pillow lavas occur in all the three rock types, i.e., basaltic andesite, andesite, and dacite, and at different depths in the holes, as do sheet flows. Also, basalts in Troodos occur both in the forms of pillow and sheet flows, e.g., in the upper 200 m of CY-1 drillcores of CCSP, there are approximate 175 m basaltic pillow lavas (88%) and 25 m basaltic sheet flows (12%) (Gillis, 1986), which is consistent with observations on the ground. Besides, minor ultramafic picritic sheet and pillowed flows, as well as picritic dikes, were observed in the field by the author and others (e.g., Bailey, 1984).

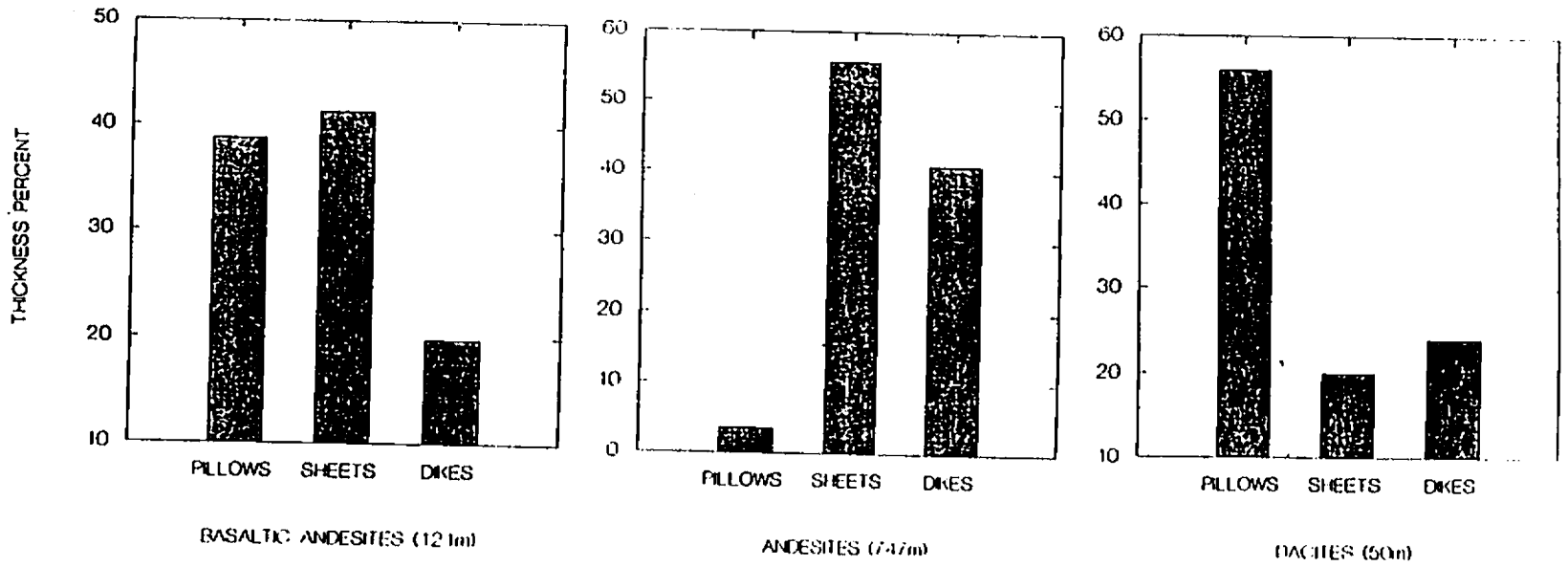

Fig. 3.4.1 Histograms of the thickness of different occurrences of different rock type in holes CY-2/2a (compilations based on data of Bednarz et al., 1987).

Since all the extrusive rocks, basaltic to dacitic, occur in the forms of both pillowed and sheet flows, and the proportions of pillow flows are higher in the basaltic and dacitic (two extreme members) than in the andesitic (middle member), this at least suggests that, although the volatiles as well as viscosity varied in the Troodos magma(s), they were not decisive factors for the formation of pillowed and sheet flows.

2. Eruptive rate of extrusives

Based on a wealth of new high-resolution observations of the seafloor, it has been suggested that sheet lavas are produced by large and rapid outpouring of liquid magma, while pillow lavas are formed preferentially by slower and less voluminous eruptions (Ballard et al., 1979, 1981; Bonatti and Harrison, 1988). Emplacement of crust at the axis of the Galapagos Rift (Ballard et al., 1981), in the FAMOUS-AMAR area of the MAR (Stakes et al., 1984), and on the EPR at 21°N (Ballard et al., 1981) follows cycles with sheet flows being produced by initial brief but voluminous eruptions of magma from long, continuous vents, whereas pillow lavas result from subsequent slower, but steadier eruptive phases originating from small vents.

Juteau et al. (1980) found systematic differences in crystal/liquid ratio among lava lake pillars (which are not separated in Troodos but may be attributed to the sheet flows), sheet flow, and pillow basalt samples in the EPR 21°N area, i.e., the lava lake pillar samples are essentially devoid of crystals, sheet flow basalt is typically subaphyric (<5% crystals), and pillows range from aphyric to moderately phyric (up to 12% crystals). Therefore, the crystal/liquid ratio at eruption is thought to have influenced the sheet/pillow ratio (Thompson et al., 1985) and correlates with the eruptive rate. The average crystal/liquid ratio at eruption is substantially higher in the slow spreading MAR than in the fast spreading EPR axial basalt (i.e., 9.8% versus 6.4%-by Bryan and Grove, 1986).

In Troodos, it is obvious that the crystal/liquid ratio in pillow flows was higher than that in sheet flows, based on the observation of samples in this study. Although no systematic statistical data have been reported, a higher proportion of phenocrysts, such as olivine and pyroxene, are usually observed in pillowed lavas, while sheet flows are usually aphyric or have a very low proportion of phenocrysts. A high crystal/liquid ratio is especially observed in the thick pillow flows at the top of the Extrusive Sequence, the interval approximately equal to the traditional Upper Pillow Lavas. These characteristics are consistent with the

systematic differences in crystal/liquid ratio between sheet flows and pillow basalt samples in the EPR 21°N area reported by Juteau et al. (1980), and therefore is possibly related to local variations of eruptive rate during the construction of Troodos crust.

Bonatti and Harrison (1988), on a world-wide scale, considered that initial temperature, crystal/liquid ratio, viscosity, and discharge rate of the lava at eruption on spreading ridges are likely to depend statistically on spreading rate. They proposed that on going from fast to slow spreading ridges (i.e., from the East Pacific Rise to Mid-Atlantic Ridge), the probability of forming lava lakes and sheet flows decreases and the probability of forming pillow flows increases. This idea is possibly consistent with the deep-sea drilling results from holes 504B, 418A, and 395A which will be discussed in Chapter 7.

On the other hand, although topography may be one of the factors in controlling the lava forms (Byers et al., 1986), it may only be responsible for local variation of lava forms rather than regional variation as seen in Troodos. In summary, for Troodos, the discharge rate of the lava on eruption, which most likely depends on spreading rate (Bonatti and Harrison, 1988), is most probably the only important factor in controlling lava form.

3.5 Relationship between P value and topography

To see the relationship between P value and topography, it is necessary to make a 3-d perspective diagram to give a cleaner view of these features. The perspective diagram is based on the 1:50,000 topographic maps. First, the study area of 45x15 km was divided by straight lines at 0.5 km intervals both parallel to the spreading and axial directions, and then the elevations at each intersection on the grid measured. A total of 2,821 intersections were measured. The 3-D diagram was plotted using the method of 3-D mesh plotting ("PLT3D" software, version 1.4, by David Crossley, 1988). Finally, the contours of P and F, which were obtained from the field observations and measurements, were plotted on the 3-d topographic maps, respectively.

The topography in the study area shows a general trend towards high elevation and relief in the south and low elevation and relief in the north. If the whole ophiolite massif is seen as an anticline, the study area is only equal to the lower half of the northern flank of the anticline. From the diagram (Fig. 3.5.1), it seems that P values show no definite relation with the variation of topography. High-P values may occur at the upper part of extrusive sequence, i.e., the section where the dike abundance and elevation are relatively low ($F<0.5$), as well as at the lower part of the

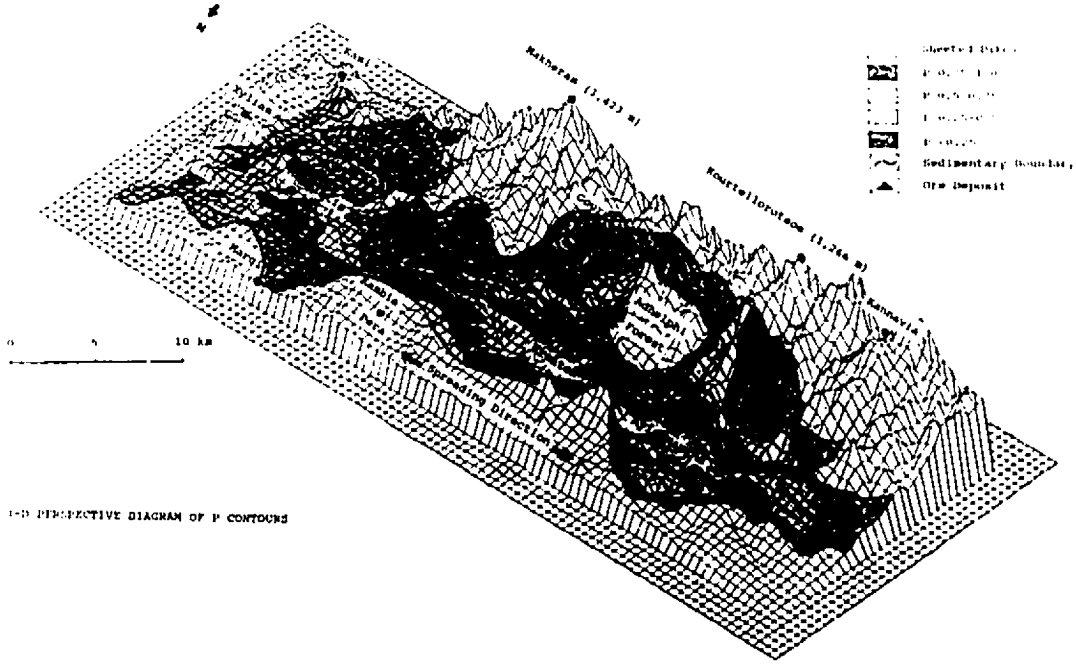

Fig. 3.5.1 3-D perspective diagram of P contours, showing that the distribution of P values has no relation with the variation of the topography, i.e., high P, as well as low P, are distributed at a either high or low relief.

section where dike abundance and elevation are relatively high. Diagrams of P values vs. elevations of four profiles from the central part of the area provide detailed evidence (Fig. 3.5.2). In the diagrams, for each profile P is clearly independent of elevation. The high elevation for many of these very high values of sheet lava flows, e.g., along the horizontal axis for Line 20, is explained by their occurrence as weathering-resistant greenschist facies screens between similar weathering-resistant dikes.

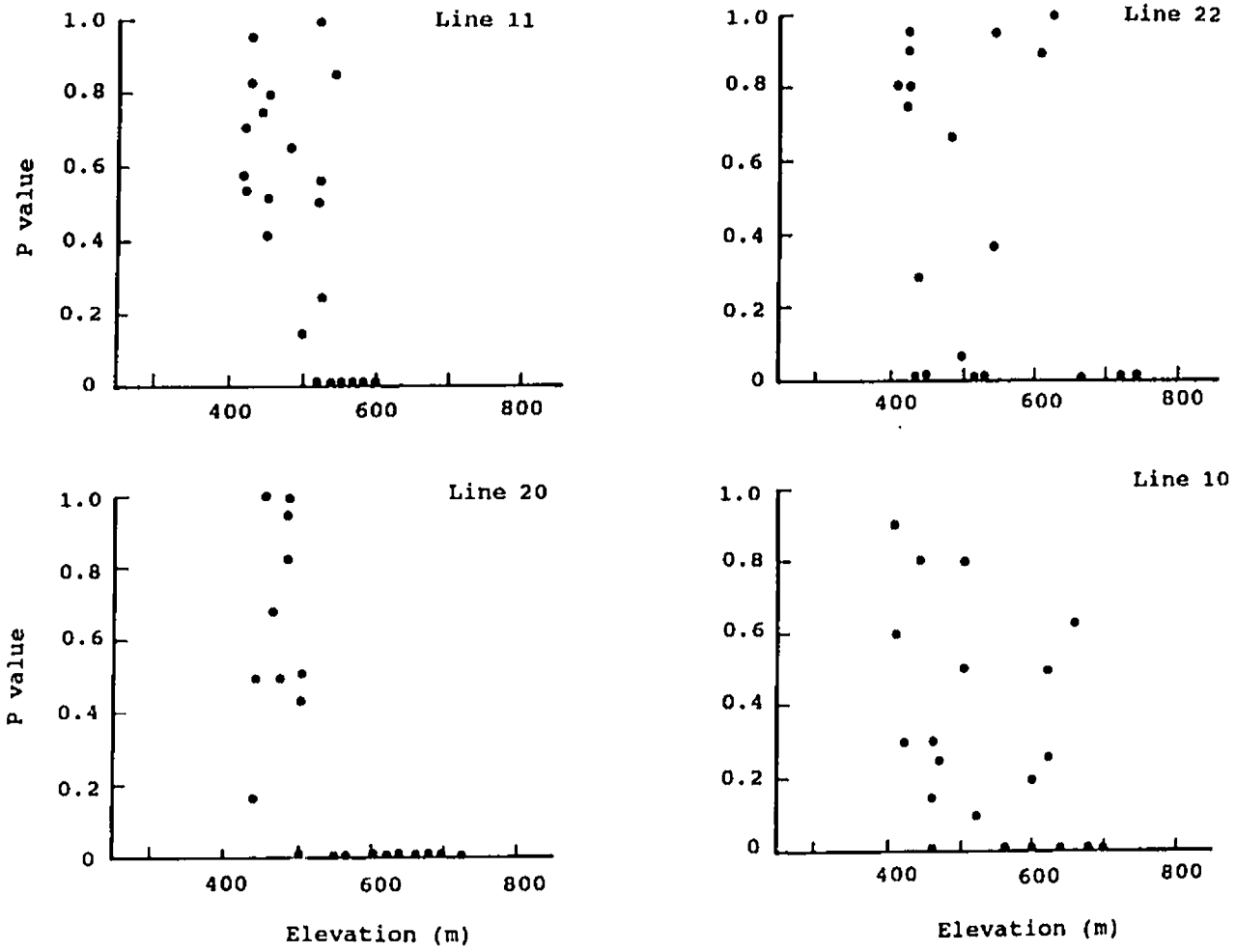

Fig. 3.5.2 P values vs. elevation (m) diagrams of Lines 10, 11, 20, and 22, showing no linear relationship between P value and elevation.

Chapter 4 The Distribution of Dikes in the Extrusives

4.1 Measurement of F value

Dikes occur throughout the Extrusive Sequence but generally increase in abundance downward, reaching a maximum of 100% in the Sheeted Complex. The ratio of thickness between dikes and extrusives is another important parameter of crustal construction and is called dike abundance (e.g., Baragar et al., 1989), or dike density (e.g., Gass and Smewing, 1973). This ratio is obtained in an analogous manner to the P value.

The abundance of dikes is defined here as the ratio of the net thickness of dikes to the total thickness of the sequence in a measured section, and is represented by the fractional value, F.

F = Thickness of dikes / Thickness of the measured section.

F was obtained in a similar manner to P, but the measured outcrop sections were normal to the lines rather than parallel, i.e., across the strike of the dikes. The measured sections were mostly from 10 to 100 m long with an average section length of close to 60 m. Dike abundance values from

sections at the low end of the range are probably still valid since individual dikes or screens are typically ≤ 1 m in width.

In the upper part of the Extrusive Sequence, i.e., in the brownstone alteration facies (see Chapter 5), dikes commonly have relatively low resistance to weathering and their presence in a section is detectable, with experience, as gaps in lava flow outcrops (Fig. 4.1.1). Towards the base of the brownstone alteration interval, where dikes form from 30 to 50% of the sequence, indurated, purplish, baked lava flows adjacent to dikes, which are highly resistant to weathering, form very distinctive castellated outcrops, in which a dike (or dikes) occurs in every gap.

In the lower part of the Extrusive Sequence, i.e., in the greenschist alteration facies, dikes and intervening screens of extrusive rocks have a similar resistance to subaerial weathering and, unless the screens consist of clearly pillowed flows, which is relatively uncommon, they cannot generally be distinguished from dikes in subaerially weathered outcrops. For this reason quantitative data on dike abundance in the greenschist facies were obtained only from stream sections, where brownstone surface weathering products are absent as a result of active annual mechanical erosion, and new road cuts, of which there are a substantial number. Within outcrops of

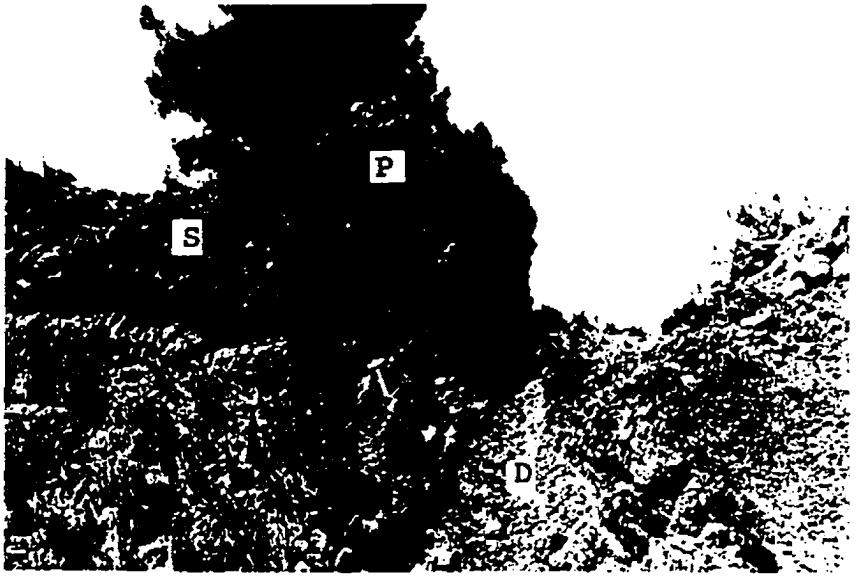

Fig. 4.1.1 Dikes occur in gaps between PL and SF. P-pillow lavas; S-sheet lavas; D-dikes (station no. 11.32).

fresh, blue-grey-green greenschist facies dikes and screens, the screens are usually clearly distinguishable from dikes even where they consist of fragments of sheet flows (Fig. 4.1.2). Characteristics which can be used to identify massive lava screens, even where chilled contacts are not evident, include 1) irregular jointing as opposed to the regular, cross jointing of dikes, 2) irregular vesicularity or ophitic texture as opposed to the vesicles in dikes which are commonly restricted to subvertical zones parallel to dike contacts, 3) abundant sulfides with either or both rusty or white sulfide weathering products in lava screens, and 4) a tendency to a paler grass green color in lavas compared with the darker blue-grey-green dikes. Color and alteration differences are sufficiently marked that dike abundance can, in places, be estimated with confidence at a distance, such as across a canyon.

4.2 Characteristics of dike abundance

4.2.1 Continuity laterally and with depth

Field measurements confirm a previous conclusion that dikes occur throughout the extrusive sequence and generally increase in abundance downward, reaching a maximum in the Sheeted Complex. However, routine field mapping of dike abundance makes available a much more detailed and

(a)

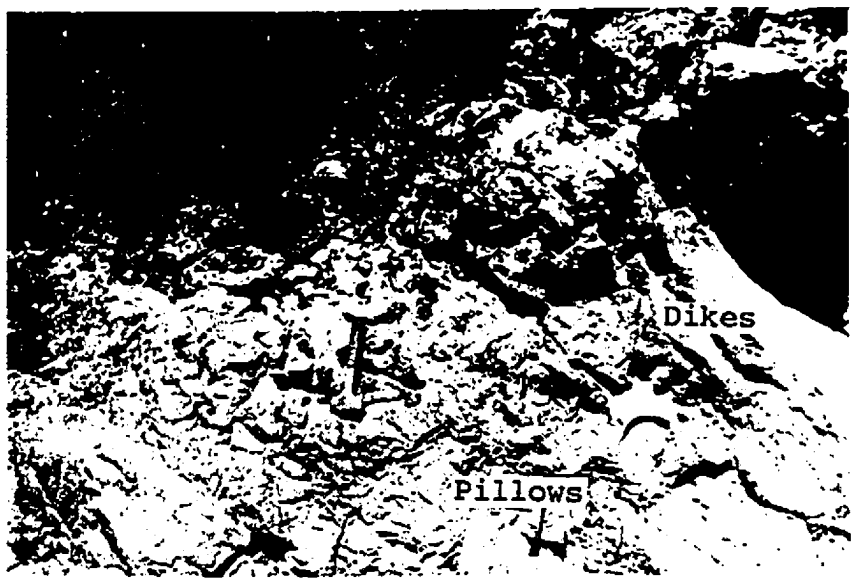

(b)

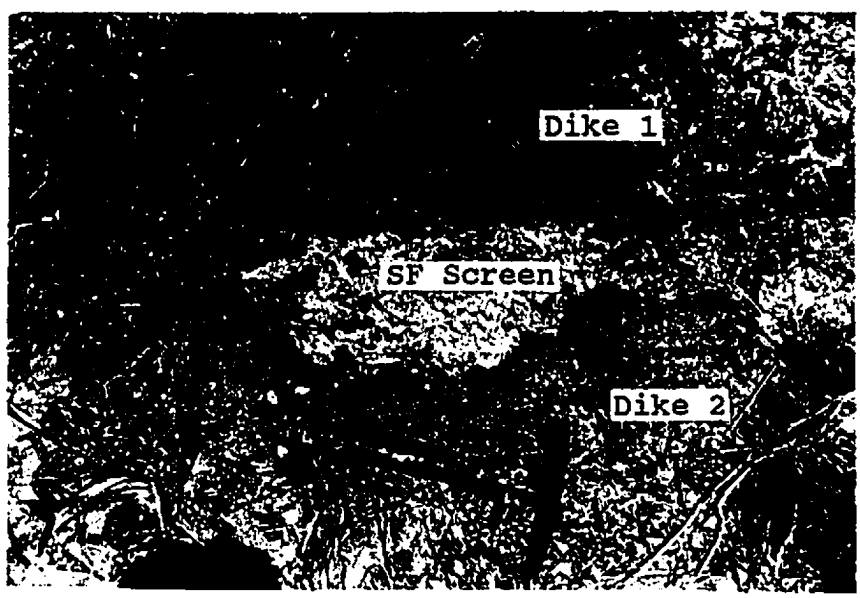

Fig. 4.1.2 Screens of PL and SF between dikes in Greenstone facies rock. a-PL screens (station no. 20.6); b-SF screens (station no. 22.3).

quantitative view of the variation of dike abundance both in the spreading direction and with depth.

Figure 4.2.1 shows the distribution of F contours with an interval of 0.25. F value measurement points were showed in Map 2 (in back pocket) and the contouring method was described in Appendix 1.

The contour pattern shows continuous variation in dike abundance in the spreading direction, except locally where some isolated highs occur. To justify the contour map of F, 5 adjacent profiles from the central part of the area are drawn side by side for F values (Fig. 4.2.2). In these profiles, the increase of dike abundance to the south is generally well seen. The variation from place to place in the increase of F with depth can also be seen, e.g., between Lines 21, 11 and 20. Also, some locally isolated areas of high dike abundance on the north of Lines 10 and 21 can be observed from the profiles.

Large scale undulations in the contour pattern are termed highs and lows here. A total of 16 highs and lows are recognized and named in Fig. 4.2.3.

In the diagram, it can be seen that although five of 16 highs are highs in the upper surface of the SC, two of them

Fig. 4.2.1 Contours of dike abundance (F value), contour interval 0.25. SEI-sediment extrusive interface; SC-sheeted dike complex; CY-2-location of CCSP drillholes; Solid line-measured; Dashed line-inferred.

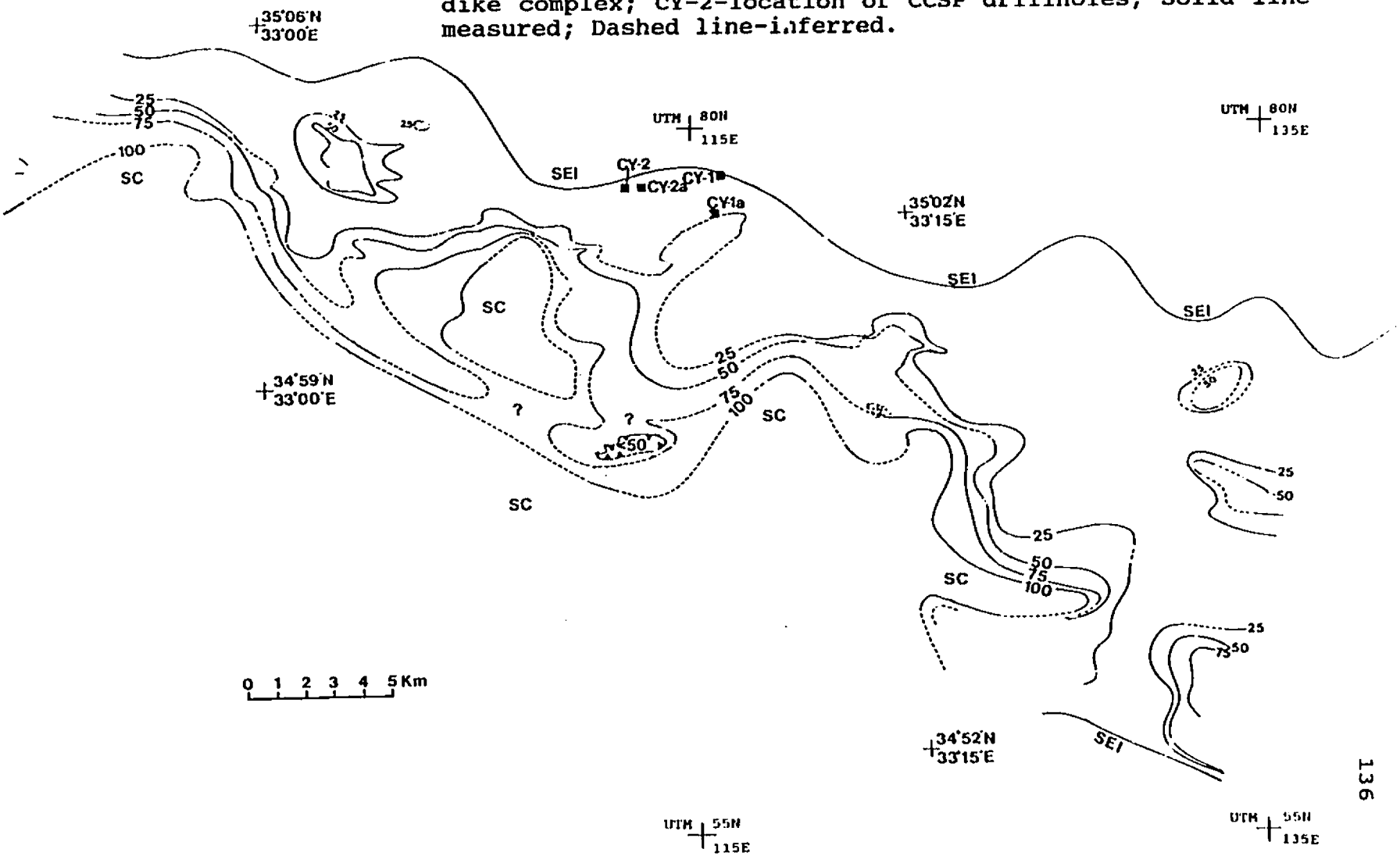

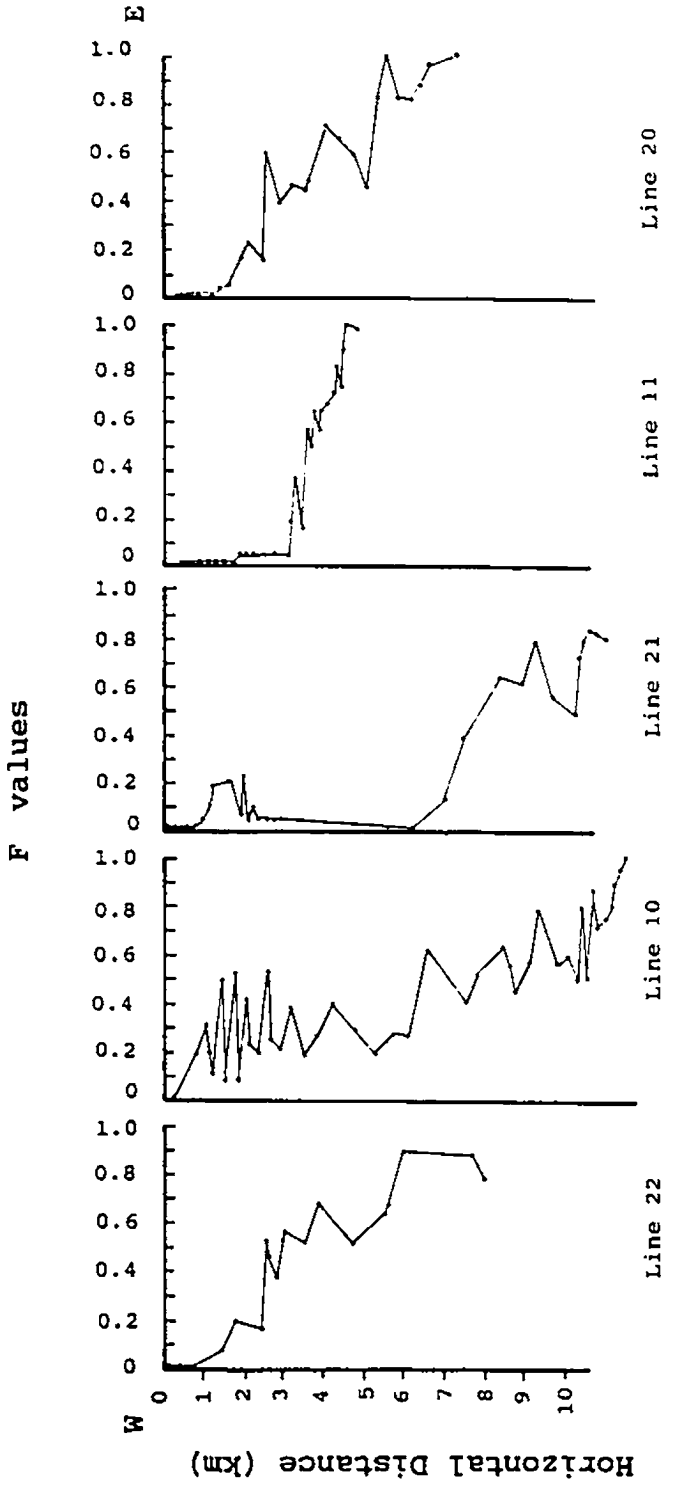

Fig. 4.2.2 Dike abundance increases with depth based on F values from five lines in the central part of the area. Black spot- observation station; detailed discussion see text.

Fig. 4.2.3 Highs and lows of dike density in the area.

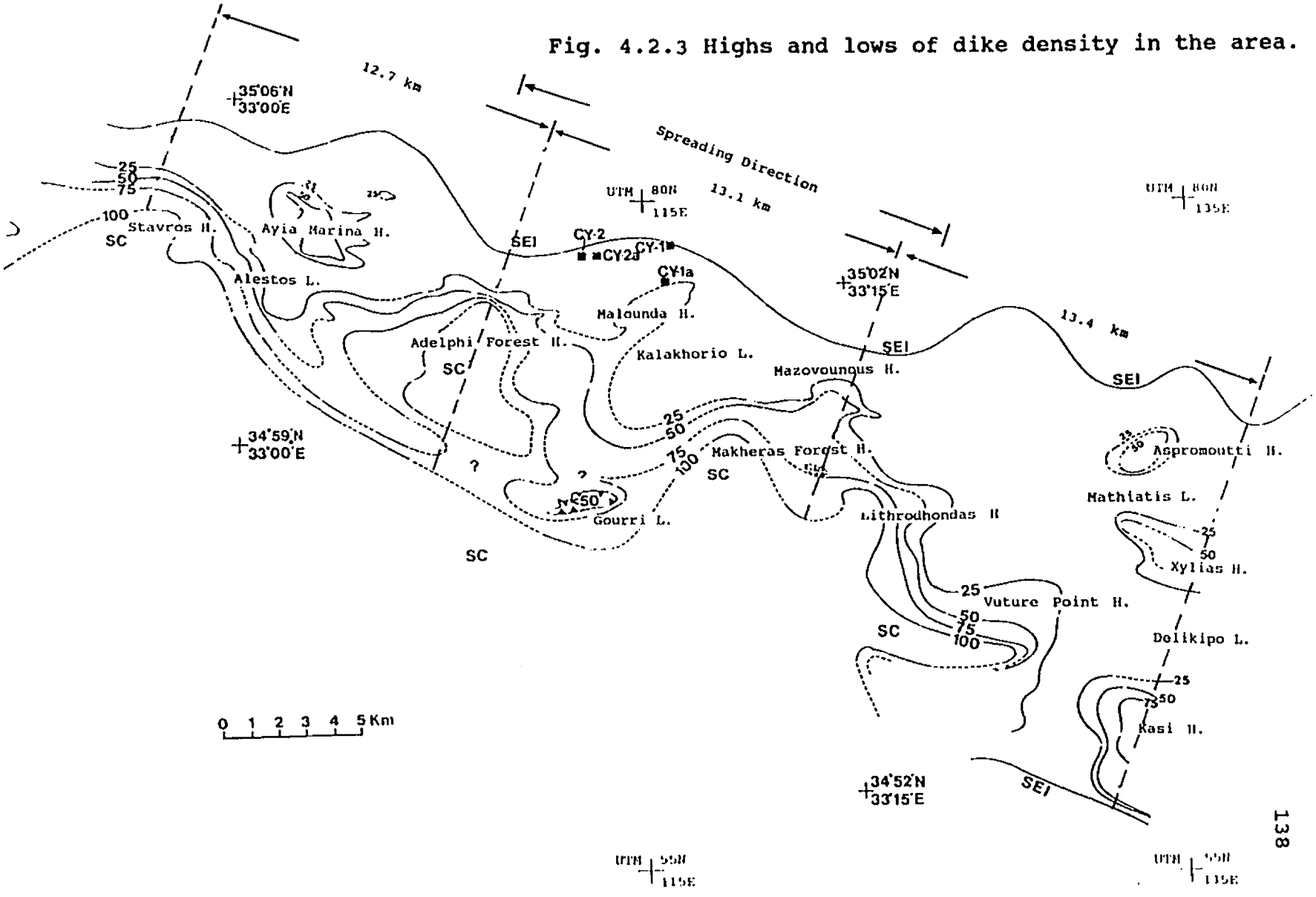

are relatively subordinate. The three major SC-highs are named from west to east, the Stavros High, the Adelphi Forest High and the Makheras Forest High. In addition, in the east of the area, although the SC surface is not exposed on the ground, there are three separated localities of high dike abundance aligned in the axial direction suggesting that there is most probably a general high in the SC beneath the area. As a consequence, four major highs are considered to exist in the area, including the east one.

The average spacing of the four adjacent major highs in the spreading direction is 13.1 ±0.4 km (1sd), i.e., indistinguishable from the average spacing of the high productivity sheet flow formations of 12.6 ±2.2 km. This suggests that the high volumes of sheet flow eruption are accompanied by a high level of the upper surface of the sheeted dikes. This relationship might be expected since both features indicate a high rate of magma supply to the seafloor.

Beside the four major highs on the SC surface, there are a number of smaller highs and lows in the F-contour surface, both along spreading and axial directions, as shown in Figure 4.2.3. These are the Ayia Marina H., the Lithrodhondas H., the Malounda H., the Mazovounous H., the Vulture Point H., the Aspromoutti H., the Kasi H., the Alestos L., the Kalakhorio

L., the Gourri L., the Mathiatis L., and the Delikipo L.. These represent small-scale variation of dike abundance both in the spreading direction and in the axial direction, and thus reflect original constructional features of the crust. The 8 highs which are distributed in the spreading direction have a range of horizontal spacing of 5-7 km and an average of 5.6 ±0.9 km, i.e, the distance is almost close to half the spacing of major highs (13.1 ±0.4 km). The three eastern highs distributed in the axial direction have a range of horizontal spacing of 3.8-6.3 km and in average of 5.0 ±1.8 km (Table 4.2.1). The spacing of small highs along spreading direction is a little larger than that in the axial direction but of almost the same amplitude. Evidently, all small highs are located between the major highs of SC except in the eastern area where the assumed major high in the SC is not as yet exposed. This suggests that relatively weak peaks in magmatic productivity occurred between each part of first-order intervals of magma supply to the crust.

4.2.2 Increase of dike abundance with depth

As in the case of P, the F data have also been converted to depth sections (Fig. 4.2.4 and Appendix 4.1) using MODEL 2. From such conversions the amplitude between peaks and swells in the surface of the SC, or of different F-contour surfaces,

Table 4.2.1 Distance Between Two adjacent Highs

In Axial Direction:	(Average)	5.83 ±0.86 km
Aspromoutti H. - Xylias H.		3.75 km
Xylias H. - Kasi H.		6.25 km
In Spreading Direction:	(Average)	5.64 ±1.04 km
Kasi H. - Vuture Point H.		5.00 km
Vuture Point H. - Lithrodhondas H.		5.00 km
Lithrodhondas H. - Mazovounous H.		5.00 km
Mazovounous H. - Malounda H.		7.00 km
Malounda H. - Adelphi Forest H.		6.00 km
Adelphi Forest H.- Ayia Marina H.		6.80 km
Ayia Marina H. - Stavros H.		6.00 km

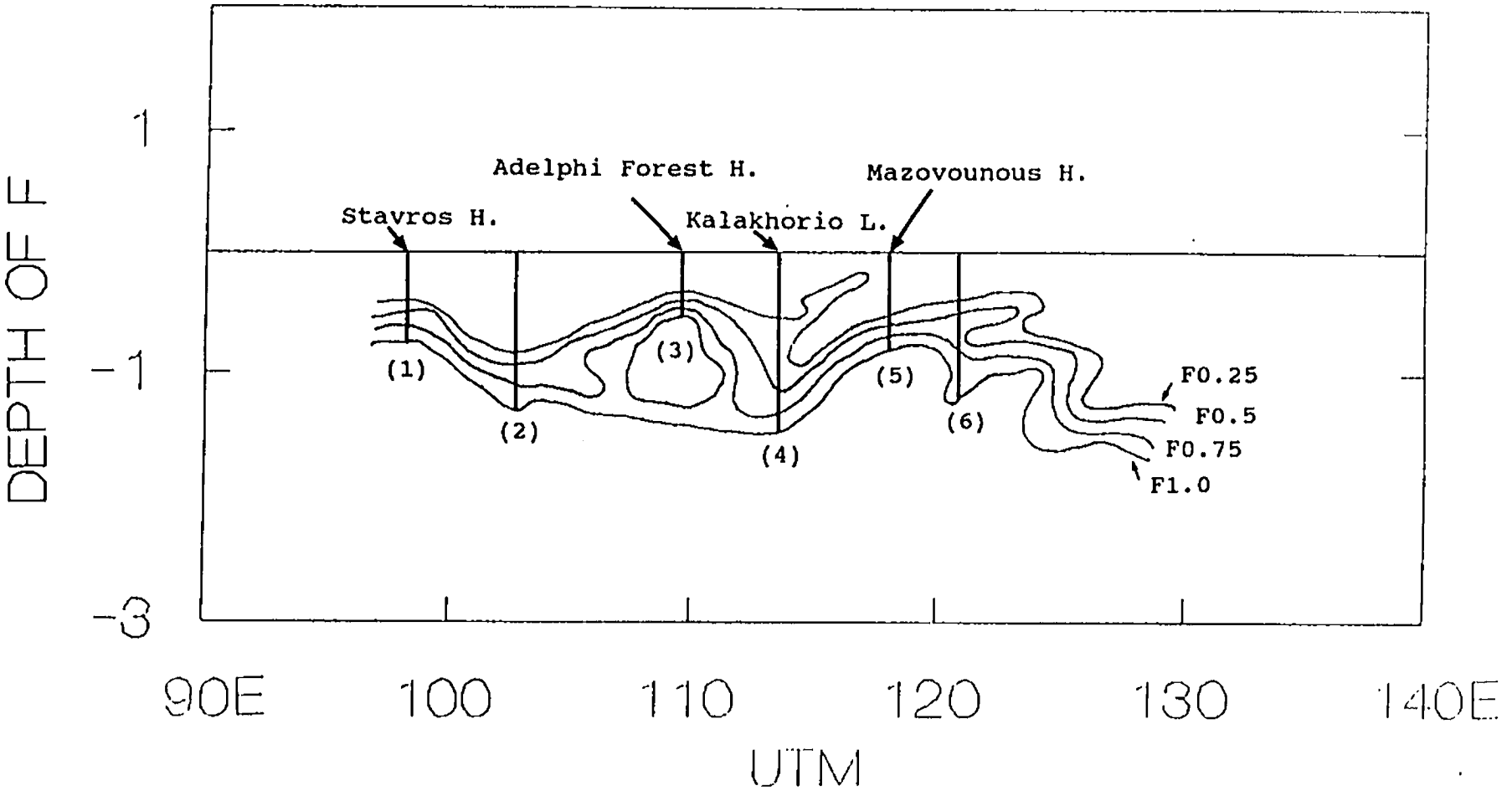

Fig. 4.2.4 Depth to various F value levels based on MODEL 2 for the form of the Troodos emplacement structure (Hall et al., 1991). Thicknesses obtained form six cross sections are listed in Table 4.2.2.

can be measured.

From Fig. 4.2.4, we first see the general variation of apparent thickness of the sequence between the SEI and SC. While generally the abundance of dikes increases with depth, the apparent gradients differ greatly in different areas. The term apparent is used because it is not possible to distinguish between the effects of a real increase in thickness and local undulations in the dike abundance surface. There are large lateral variations in the onset and rate of increase of dikes. There are at least three highs and three lows of SC surface, ranging in depth between 0.56 and 1.52 km, i.e., the apparent depth at the lows of SC is twice as great as at the highs. Six sections through the sequence between SEI and SC have an average of 1.03 ±0.37 km, while the average depth interval between SEI and F0.25 contour is 0.49 ±0.17 km and between the F0.25 to 1.0 contours is 0.53 ±0.31 km, respectively. The latter two are almost at of same amplitude (Table 4.2.2), suggesting a general limitation in dikes intruded into the upper part of the extrusive sequence.

The shallowest high F values are at the Adelphi Forest High. The vertical depth from the SEI contact to F=1.0 contour is only 0.56 km. Once dikes appear in the section, abundance increases with depth very quickly, from F0.25 to F1.0 in only 0.24 km. Within this interval, the increase in dike abundance

Table 4.2.2 Variation of F Contour Depth in Cross Sections

	F0-0.25	F0.25-1.0	F0-1.0
(1)	0.40	0.36	0.76
(2)	0.80	0.52	1.32
(2)	0.32	0.24	0.56
(4)	0.52	1.00	1.52
(5)	0.48	0.32	1.20
(6)	0.40	0.80	1.20

is more rapid in the lower part than in the upper part.

The other two areas of shallow high F values are in the vicinities of the Stavros and Makheras Forest Highs. In these two areas the F0.25 contours are at 0.40 km and 0.48 km respectively, slightly deeper than at the Adelphi Forest High (0.32 km). From F0.25 to 1.0, dike abundance substantially increases within depths of only 0.36 km and 0.32 km, respectively, in the two areas. In contrast to dike abundance quickly increasing with depth, some areas with dike abundance increasing slowly are observed (see Fig. 4.2.4). Two areas, the Kalakhorio Low in the west and Mazovounous High in the east, show thicknesses of 1.0 km and 0.80 km, respectively, between F0.25 and F1.0 contours, which are 2-3 times higher than that in the highs of the SC.

Fig. 4.2.5 shows lateral variation of the F depth contour surfaces. Three values of amplitude of SC and six of F0.25 are obtained. The amplitude of undulations on the upper surface of SC is 0.62 ±0.10 km and of the F0.25 surface 0.48 ±0.19 km (Table 4.2.3). These two amplitudes are indistinguishable within the uncertainties.

4.3 Estimation of volumes of lava flows and dikes

Knowledge of the volumes of lava flows and dikes in an

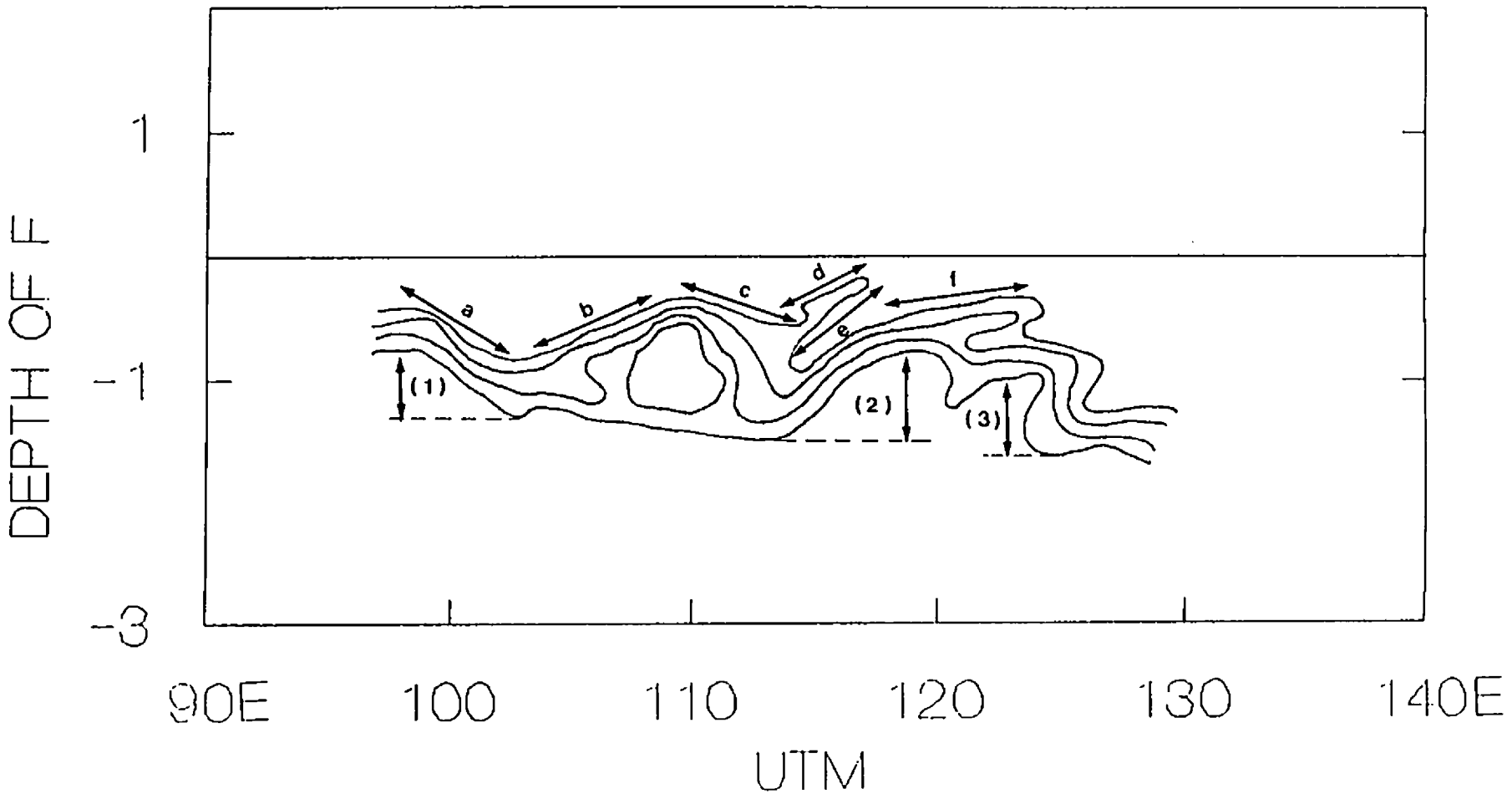

Fig. 4.2.5 Lateral variation of F contour surface. (1), (2) and (3) represent depth variation of SC surface (F1.0); while a, b, c, d, e, and f show the depth variation of F0.25 contour surface. Values are listed in Table 4.2.3.

Table 4.2.3 Lateral variation of F depth contour surface

	Low (km)	High (km)	Difference (km)
F0.25 contour surface			
(a)	0.85	0.40	0.45
(b)	0.85	0.30	0.55
(c)	0.50	0.30	0.20
(d)	0.50	0.15	0.35
(e)	0.90	0.15	0.75
(f)	0.90	0.30	0.60
Average of the six:			0.48 ±0.19
F1.0 contour surface			
(1)	1.30	0.80	0.50
(2)	1.50	0.80	0.70
(3)	1.55	0.90	0.65
Average of the three:			0.62 ±0.10

eruptive formation will provide more information on the nature of crustal formation. The two middle eruptive batches are chosen for volume calculation because of their more complete exposure. The calculation is based on the contour maps of P and F and MODEL 2 thickness calculations. The basic ideas for rock volume calculation are illustrated in Fig. 4.3.1. In brief, to obtain volumes of pillow lavas, sheet flows and dikes in a block, it is first necessary to calculate their areal proportion in a vertical cross section and then it is required to obtain the length of the blocks in the axial direction.

The two blocks chosen for the volume calculation are located in the Xiliatos Formation and Kambia Formation respectively (Fig. 4.3.2). Each is 8 km wide in the E-W direction with partial UTM coordinates from 118E to 126E for the Kambia formation and from 103E to 111E for the Xiliatos Formation on the 1:50,000 topographic maps. There are two steps in the calculation.

First, the cross sectional areas of two irregular blocks are measured in a vertical cross section obtained by thickness calculation using MODEL 2 using a planimeter. The areas of the Extrusive Sequence in the two blocks are 9.2 km^2 each (Fig. 4.3.3).

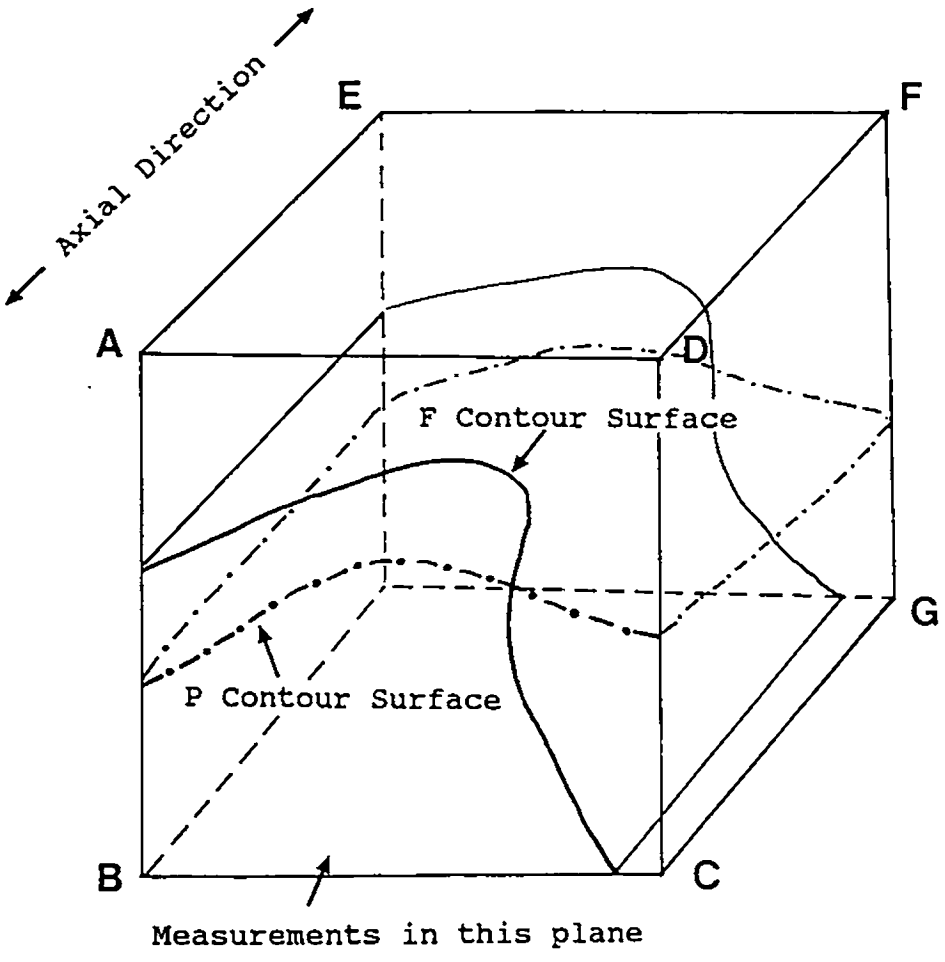

Fig. 4.3.1 Basic ideas for rock volume calculation. Supposing the F and P contour surfaces are observed in the surface ABCD, areas of pillowed flows, sheet flows and dikes then can be calculated from the distribution of the contours in the surface. If the length of the extension of the surface along the axial direction (AE) is known, the volumes of PL, SF and dikes in this block then can be obtained.

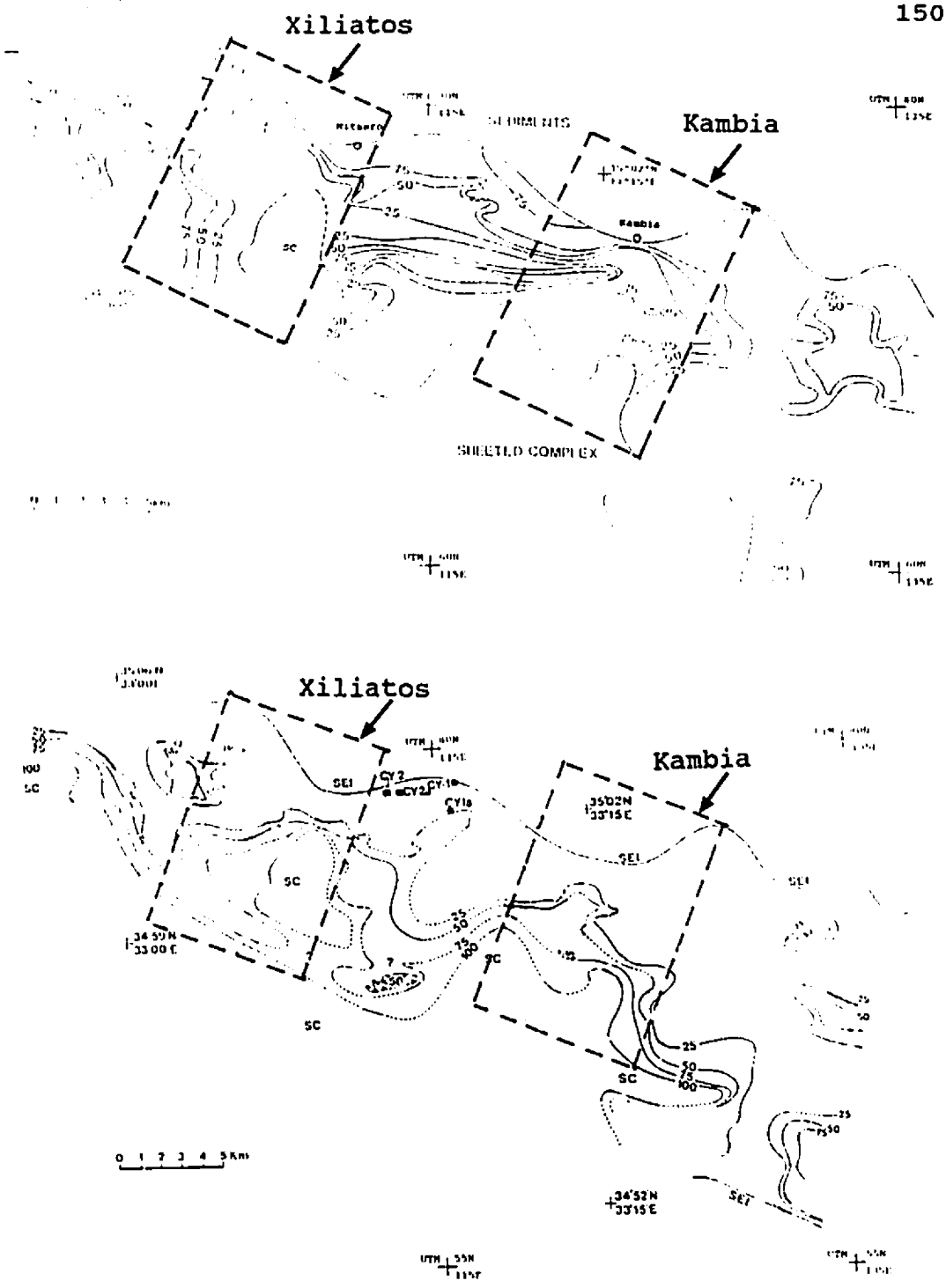

Fig. 4.3.2 Two blocks chosen from Xiliatos Formation in the west and Kambia Formation in the east, respectively, for calculation of rock volume. Each block is 8 km wide in W-E and from SEI to SC in N-S.

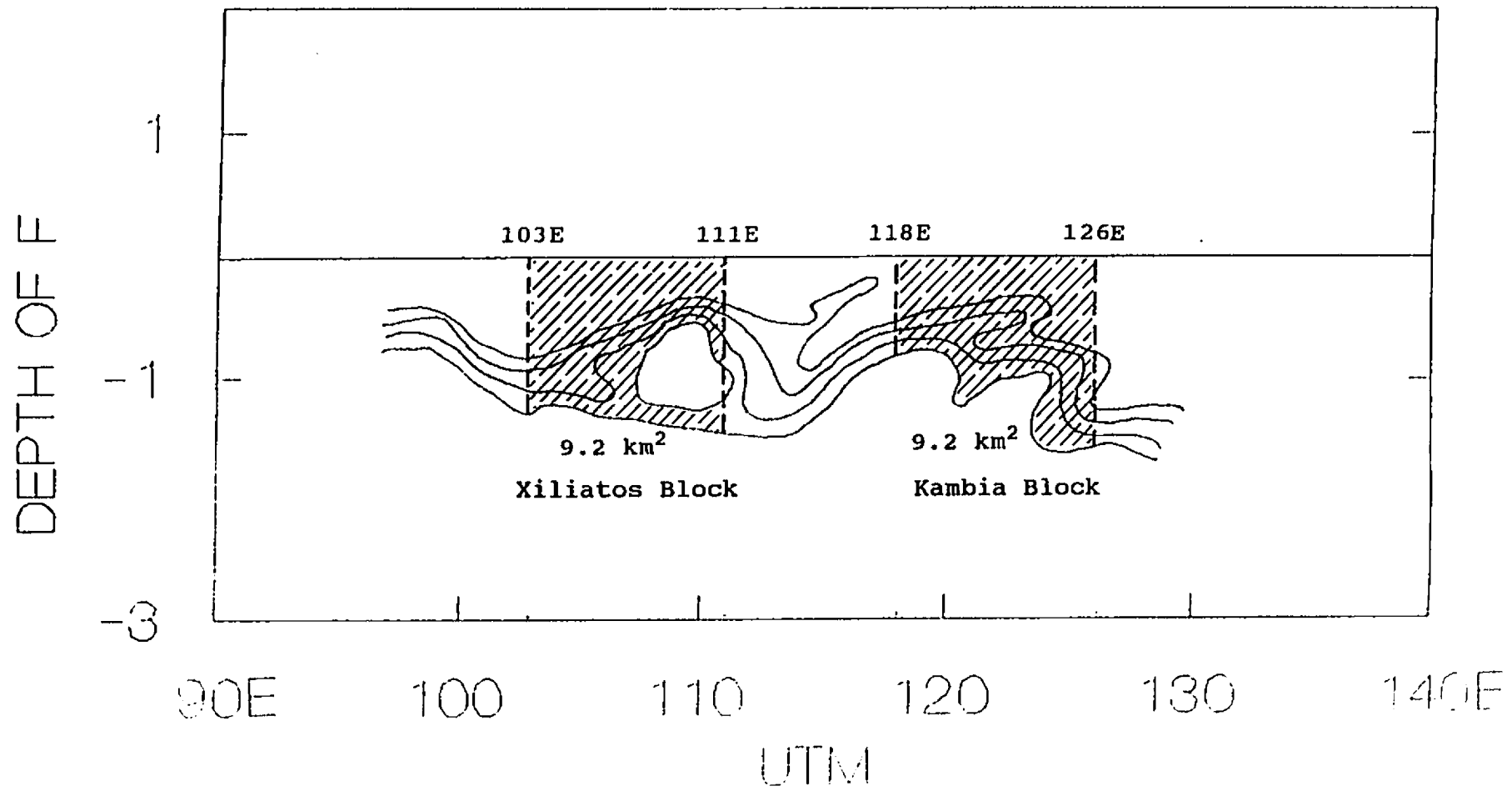

Fig. 4.3.3 Blocks for volume calculation within a depth cross section. The two blocks are at locations in UTM coordinates from 103E to 111E and from 118E to 126E.

Then, areas of individual lithological types SF, PL and dikes in the blocks are measured. A planimeter was used again to measure areas of different proportions of dikes from the F contour map and proportions of pillow lavas and sheet flows from the P contour map. For example, for the Kambia Formation block, the F<0.25 interval occupies about 56.9% of the block. If it is assumed that there is on average 10% dikes in this interval, the area of dikes in F<0.25 interval is equal to 5.7% of the total measured block, while the total dikes in the block as a whole are approximately 33% (Table 4.3.1). In the same way, the pillow flows and sheet flows are 27% and 40%, respectively within the Kambia Formation block.

In the Xiliatos Formation block, although besides dikes, pillow lavas and sheet flows, there is also an area of sheeted complex, the process of calculation is the same. The results show that the dike abundance is about 35%, the pillow lava 17%, the sheet flow 30% and the sheeted dikes 18% (see Table 4.3.1).

Since the length of development of a high volume of sheet flows along axis in these two blocks is unknown, a 1 km length section was taken for each of them for comparison (Table 4.3.2) and the main results are summarised below.

1. The same total volumes of rocks (9.2 km^3) per 1 km-

Table 4.3.1 Proportions of morphological types in the two blocks for volume calculation

Kambia Batch:			
	Area (%)	Dike (%)	Actual Area (%)
F<0.25	56.9	10	5.7
F0.25-0.5	10.7	35	3.7
F0.5-0.75	16.8	60	10.1
F0.75-1.0	15.6	85	13.3
Subtotal	100		32.8
P<0.25	50	10	5
P>0.25	50	70	35
Subtotal			40
Sheet Flow		100-40=	60
Recalculated to 100%:			
	Dike=33%		
	PL =27%		
	SF =40%		
Xiliatos Batch:			
F<0.25	34	10	3.4
F0.25-0.5	9	35	3.2
F0.5-0.75	19	60	10.8
F0.75-1.5	21	85	17.9
Subtotal	82		35.3
Sheeted Dikes	18	100	18
P<0.25	34.4	10	3.4
P>0.25	47.6	70	33.3
Subtotal	82		36.7
Sheet Flows		100-36.7=	63.3
Recalculated to 100%:			
	Dike=35%		
	PL =17%		
	SF =30%		
	SC =18%		

Table 4.3.2 Volumes of Individual Morphological Types in Two Blocks to the Top of the Sheeted Complex

	Kambia Formation		Xiliatos Formation	
Both in 1 km section:				
Pillow Lavas	2.5 km3	(27%)	1.9 km3	(21%)
Sheet Flows	3.7 km3	(40%)	3.3 km3	(36%)
Dikes	3.0 km3	(33%)	4.0 km3	(43%)
Total	9.2 km3		9.2 km3	

interval in the axial direction suggest that the extrusives with included intrusives in the two areas had a similar volume of productivity during their formation, although the proportions of individual morphological types are somewhat different.

2. The extrusives, i.e., the combination of pillowed flows and sheeted flows, in the two blocks are higher than dikes in volume, about twice high in the Kambia Formation and 1.3 times in the Xiliatos Formation respectively. If it is assumed that the volcanic activity in the two areas was comparable in duration, then, relatively speaking, seafloor eruptions in the Kambia area might have been more intense than in the Xiliatos area.

3. On the other hand, both sections show that sheet flows are more abundant than pillow lavas, about 1.7 times in the west and 1.5 times in the east. The higher productivity of sheet flows suggest relatively high magma supply-rate during eruptions during the crustal formation in the two areas.

4.4 Relationship between F value and topography

In the same way as a 3-d perspective diagram for P was obtained, an analogous 3-d diagram for F was obtained (Fig. 4.4.1). In contrast to P, F values in general show an increase

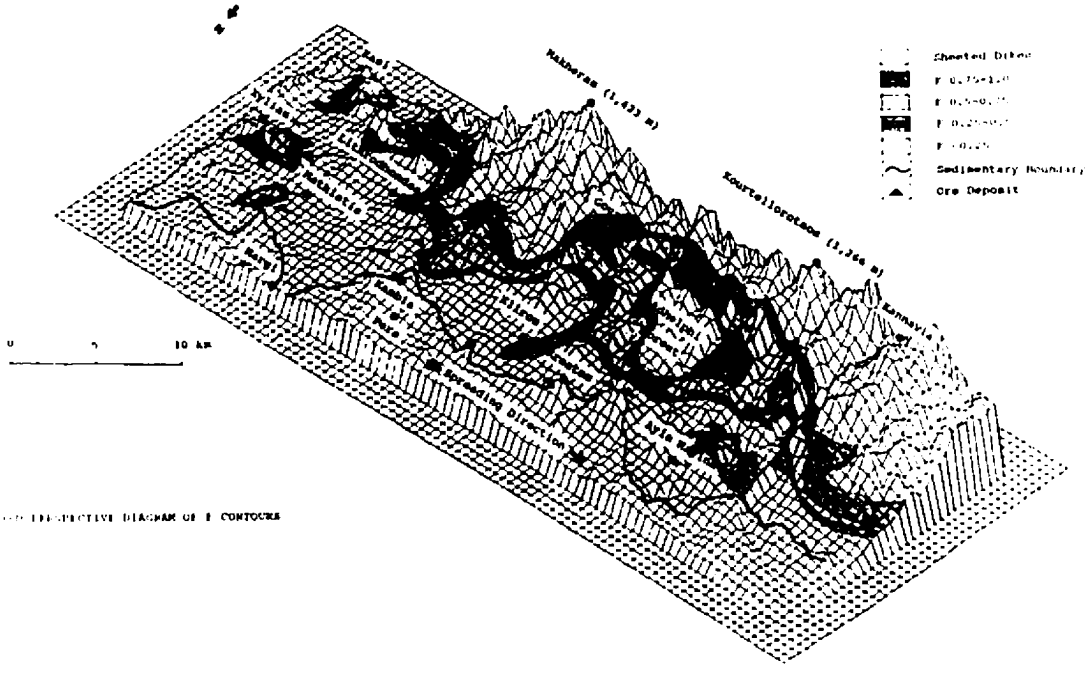

Fig. 4.4.1 3-D perspective diagram of F contours (discussion see text).

from the seafloor with depth in the crust, i.e., towards the south. Although the rates of increase in F are different from place to place in the spreading direction, the increase in F is generally consistent with the increase of elevation of the topography. This is evident from F value vs. elevation diagrams for four profiles from the central part of the area (Fig. 4.4.2) and from cross sections, e.g., from the Nikitari (Stavros) and Adelphi Forest sections (Fig. 4.4.3a and b). It is noted that the curves of increase in elevation with F are different for each line. This shows a real difference in the increase of F with depth within the section. An abrupt increase of elevation frequently occurs at from F=0.5 to F=0.6, which is, spatially, approximately consistent with the transition from zeolite facies to greenschist facies alteration (see Chapter 5 for a detailed discussion), since the two alteration facies have quite different resistant to weathering. The general relationship between dike abundance and topography can be explained by the emplacement structure, i.e., the regional anticlinal structure, and by the previously noted increase of resistance to weathering by screens and dikes showing greenschist facies alteration.

Some isolated areas of high-F contours occur locally, e.g., the Xylias area and Kasi area in the east, the Adelphi Forest area and Klirou area in the middle, and the Ayia Marina area in the west of Figure 4.4.1. Some of them also show

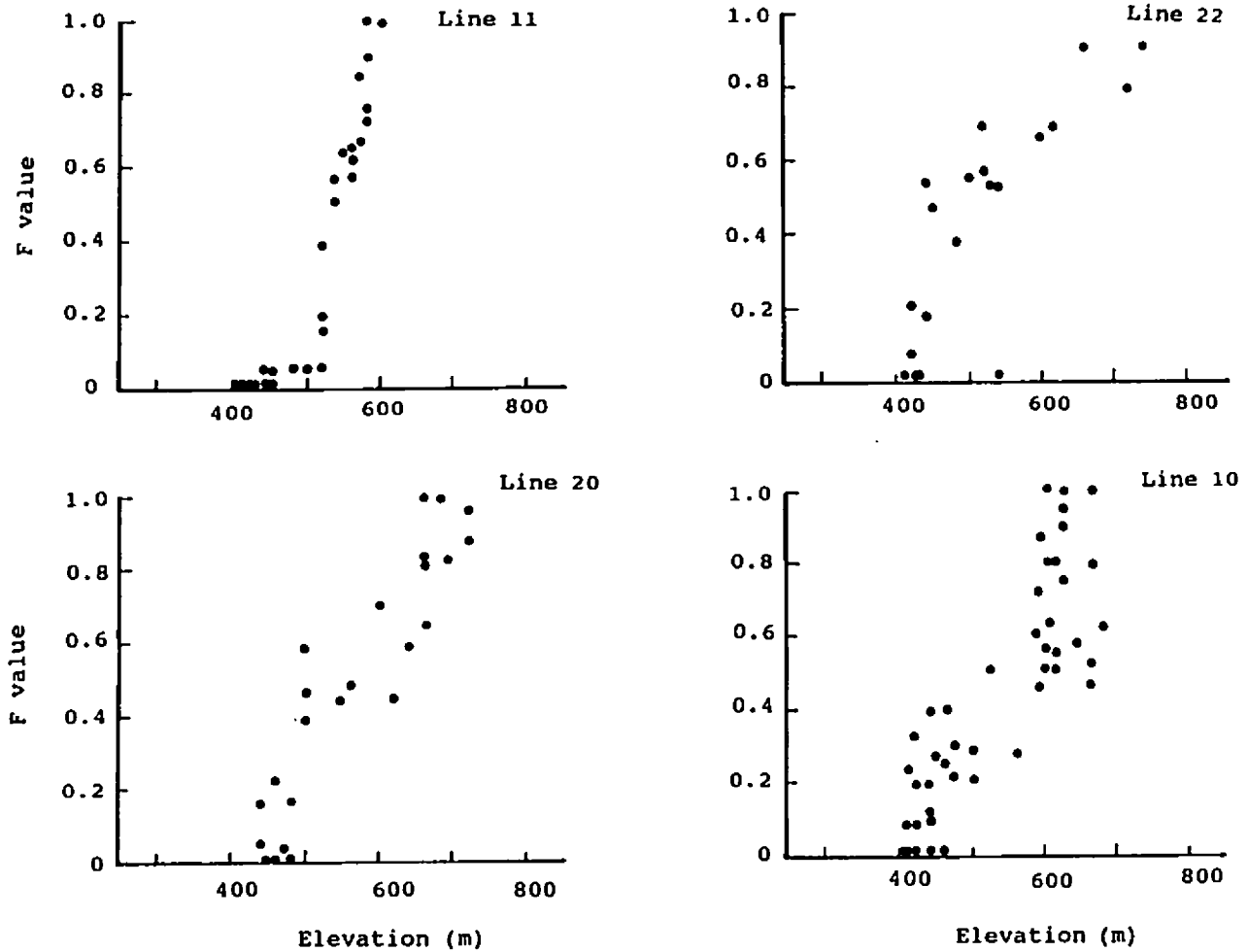

Fig. 4.4.2 F values vs. elevation (m) diagrams of Lines 10, 11, 20 and 22, showing that elevations increase with F value increasing.

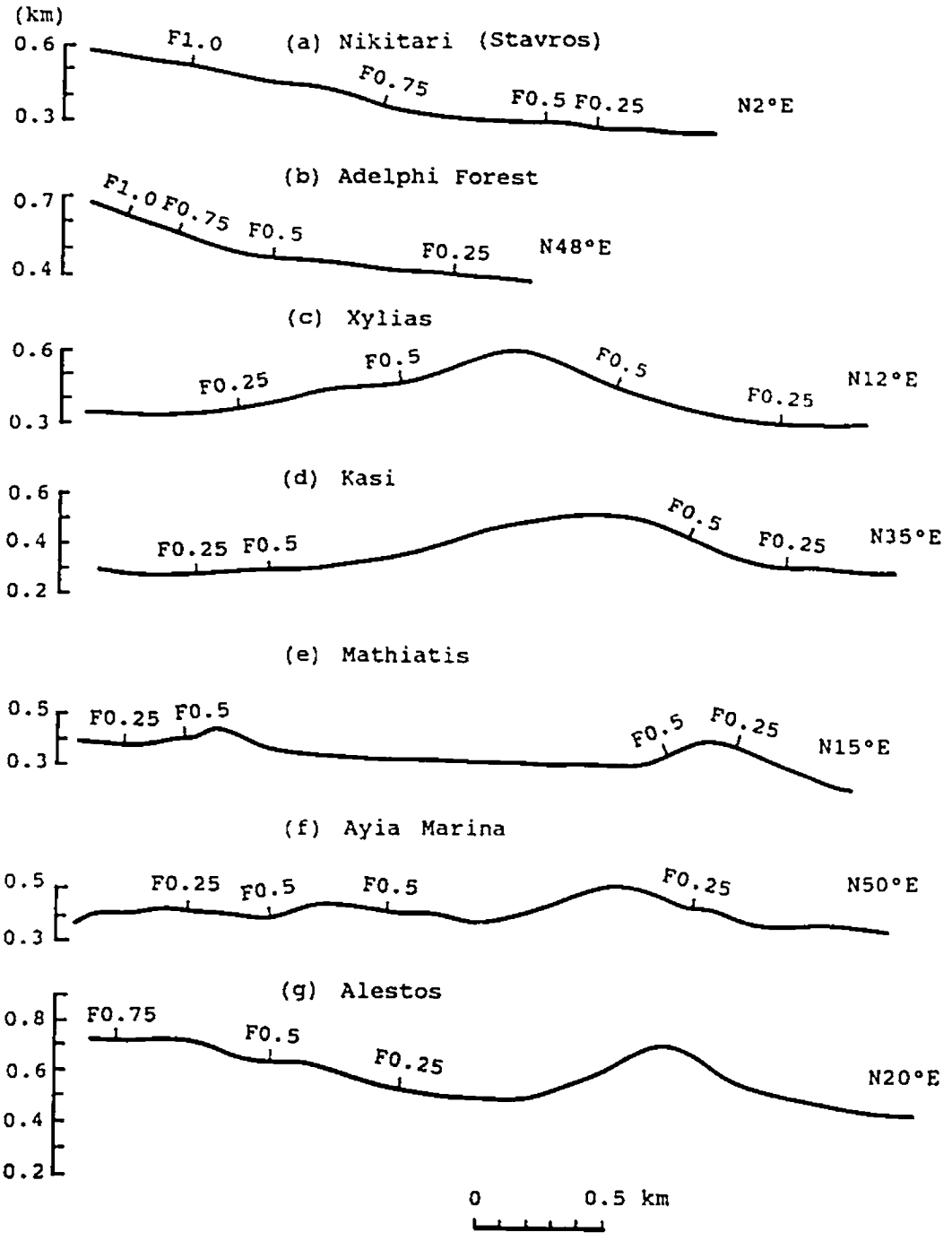

Fig. 4.4.3 Seven profiles showing relationships between topography and F contours. (a) Nikitari; (b) Adelphi Forest; (c) Xylias; (d) Kasi; (e) Mathiatis; (f) Ayia Marina; (g) Alestos; locations of profiles see Fig. 4.2.3.

positive correlation between F values and topography, e.g., the Xylias High and Kasi High (Fig. 4.4.3c and d). Thus it is evident that at least in these areas the variation of F contour surface reflects original constructional features and directly influences the elevation of local topography since a high proportion of dikes ($F \geq 0.5$), because the sections with high F (≥ 0.5) were usually hydrothermally altered into greenschist facies and are much resistant to the weathering than the sections ($F < 0.5$) with zeolite facies alteration (see Chapter 5). However, not all isolated areas with high F correspond a high relief, e.g., the Mathiatis area and Ayia Marina area (e.g. Fig. 4.4.3e and f). In addition, a high relief area even appears in an area with low F, e.g., the Alestos (Fig. 4.4.3g). These suggest that some other factors, such as faults, alteration facies, degree of erosion and lithologic types, may influence the topography locally. For example, observations in Alestos indicate that upper extrusives there were atypically highly silicified and, therefore, also show strong resistance to weathering.

In general, the anticlinal emplacement structure of the Troodos determines the relief of regional topography and the latter controls the essential shape of the F contours rather than of the P contours. Locally, at least, isolated high F areas ($F \geq 0.5$) reflect, in a great degree, original constructional features associated with the formation of the

crust.

There is an alternative way to test the relationship between constructional features and topography. Since it is already clear that P contours have no close relationship with topography, only F contours are considered here for further testing.

This method is, based on the observed F contour, an ideal F surface, topography and regional structure, to build a hypothetical topographically controlled F contour (Boulter, 1989). If the shape of this contour is identical with that of the observed F contour, it indicates that the observed F contour is the outcrop of a flat plane and its variation in shape is then only a result of erosion and is entirely controlled by topography. On the other hand, if the observed and predicted contours are of very different form it indicates that the surface of observed F contour was not planar. The degree of consistency between the two contours may indicate into what degree topography controls the observed contours and, within, will imply the amplitude of real variations in the contour surface.

The method is first based on examination of a particular contour to identify a point at which its location and elevation are close to a median of the belt containing the

contour. Then, on the basis of this point, e.g., station 8.59 for the F0.5 at 500 m elevation contour, a plane is envisioned, which dips towards N18E at 9° and which has station 8.59 at its correct elevation. Then, using the correct elevation of structural contours on this dipping plane surface, a new contour is formed by joining the intersections of the structural contours on this plane and appropriate topographic contours. The new contour thus varies in position following the variation of topography.

The results obtained in this way for both F0.25 and F0.5 contour surfaces indicate that: 1) both the observed F0.25 and F0.5 contour surfaces are distinctly different in form from the relevant contours for a planar surface, so indicating that the observed contours largely reflect original construction of the crust; and 2) the variation of observed contour surfaces suggest that their original constructional surfaces varied in the spreading direction with an average maximum amplitude of about 300 m (Fig. 4.4.4).

Another approach to this problem is illustrated in Figs. 4.4.5a-d which show the variation of elevation of different F contours. All of these diagrams were obtained by the same method. First, a straight reference line which is parallel to the spreading direction, was drawn near to the outcrop of the sediment-extrusive interface (Fig. 4.4.6). Then, parallel

Fig. 4.4.4 Comparison of observed F contours and predicted topography-controlled F contours. Dashed lines are the observed and solid lines are the predicted (discussion see text).

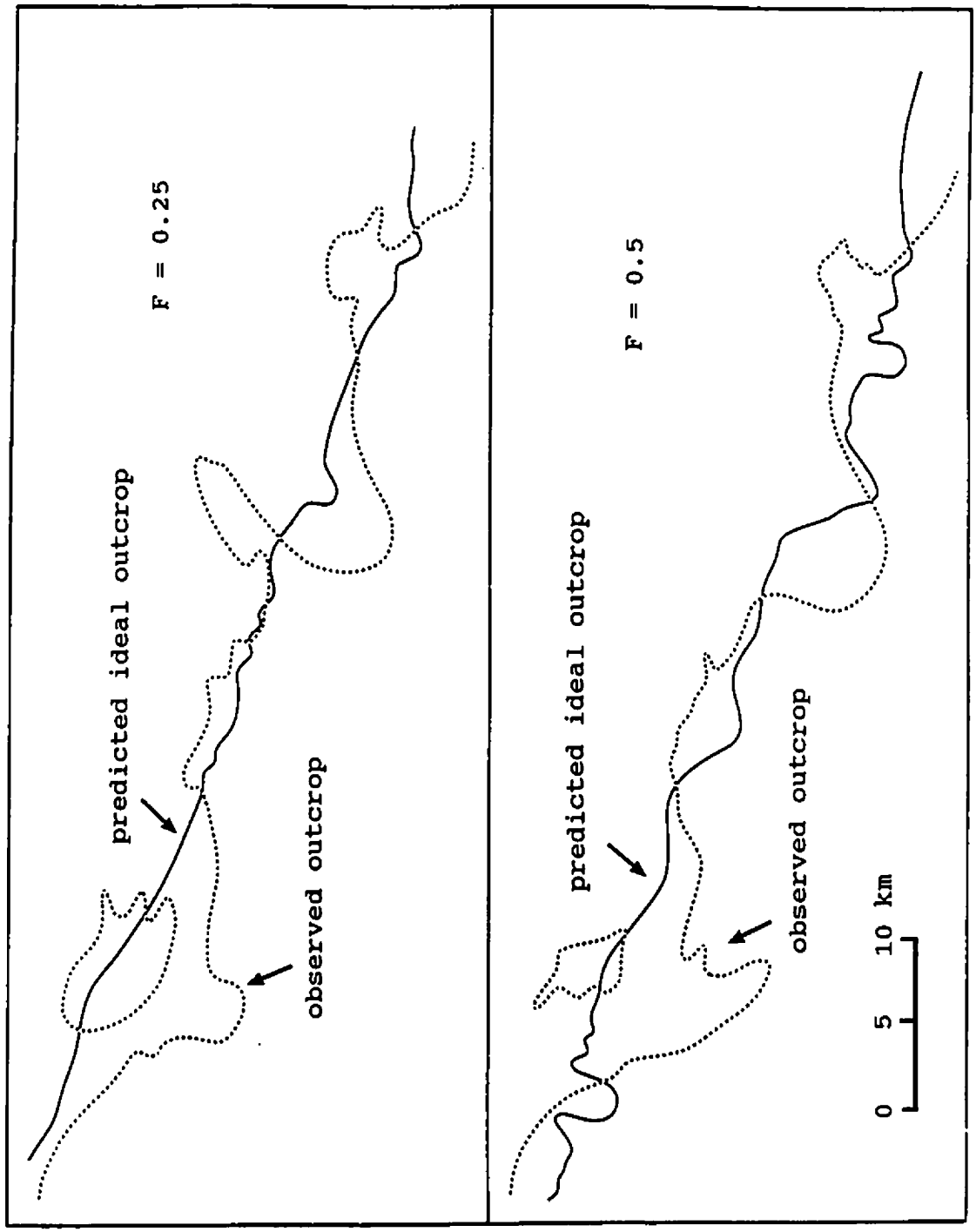
F = 0.25
predicted ideal outcrop
observed outcrop
F = 0.5
predicted ideal outcrop
observed outcrop
0
5
10 km

Fig. 4.4.4

lines normal to the reference line were drawn at 0.5 km intervals, each intersecting the different F contours. Elevations from each crossing point of lines and contours and the distance (km) from each crossing point of the contour and the reference line were measured. The two groups of data, i.e., elevation and distance (km) for each F value contour intersections, were plotted in separate diagrams (Figs. 4.4.5a-d). It is seen from these diagrams that the elevation distributions for each position along any F contour have a significant vertical range of about 300 m at any particular distance from the reference line. If the elevation and distance displayed a closely linear correlation, it would indicate that the surface of the contour was planar. However, in all the diagrams, it seems that there are no closely linear correlations between the elevations and distances, suggesting that the contour positions must also reflect real local variation in the elevation of these F surfaces. The extra information that can be obtained from these diagrams is that the variation of elevation of individual F contour are all in the range of about 300 meters, which suggests that original undulations of F contour surface may be limited to this range, a result similar to that evident from Fig. 4.4.4.

From the above discussion, we know that, to some degree, contour positions may be influenced by topography, but, however, they largely represent real relief of the surfaces of

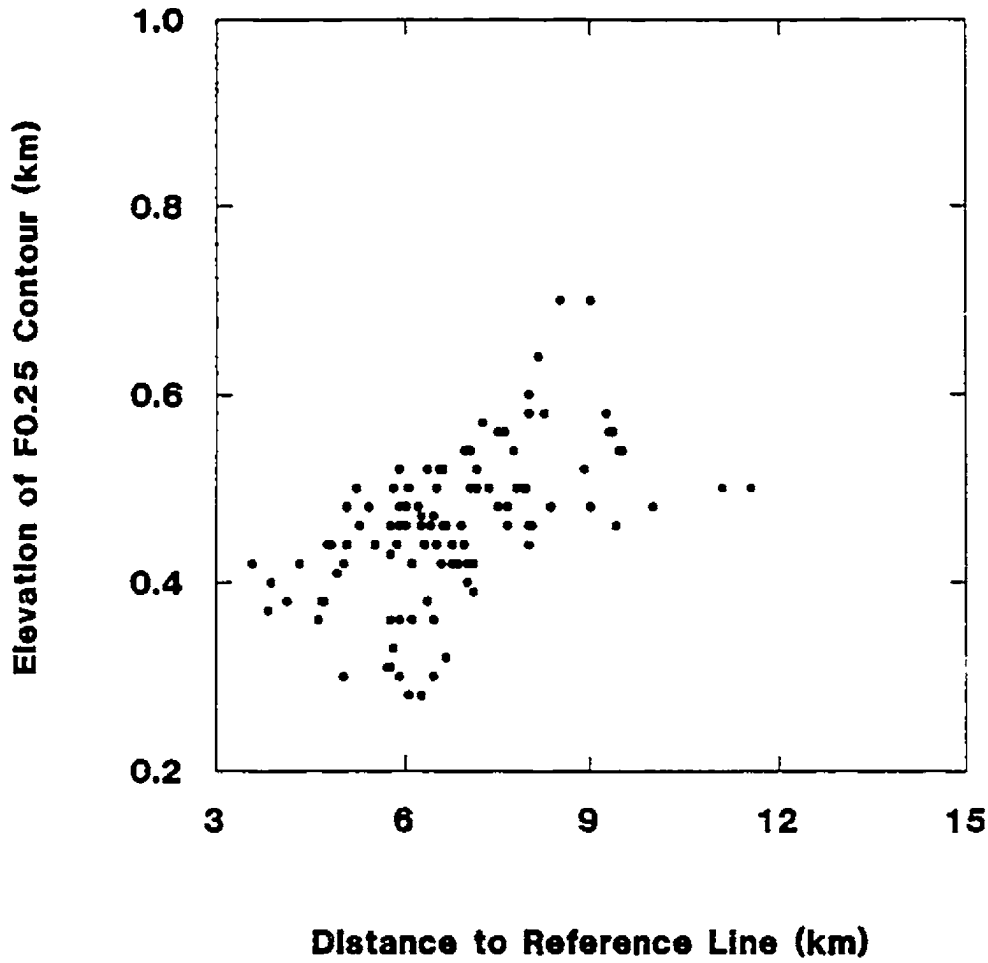

Fig. 4.4.5a Elevation vs. Distance (Km) diagrams of F contours; (a) F0.25 contour; (b) F0.5 contour; (c) F0.5 contour; and (d) F1.0 contour; Reference Line see Fig. 4.4.6; all F contours show no linear correlation between elevations and distances, suggesting the existence of original undulations of F contour surfaces with a general average range of less than 300 m.

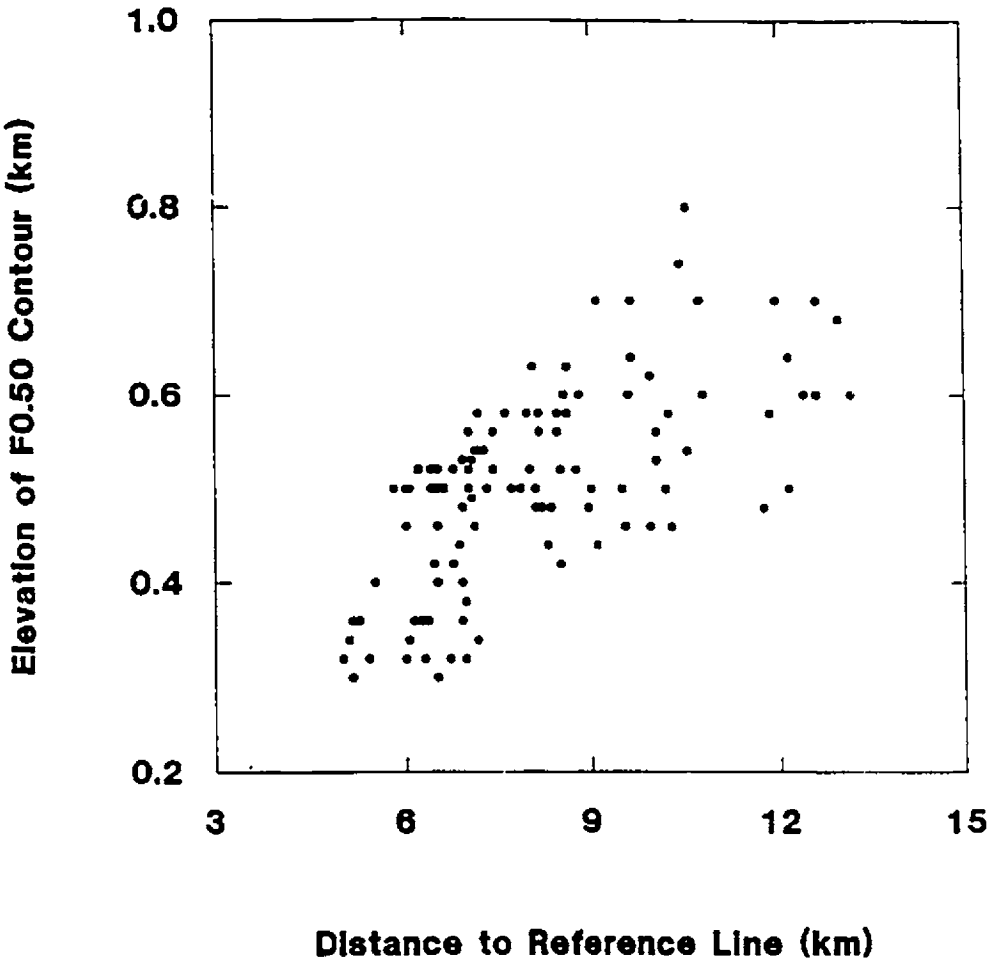
1.0
0.8
0.6
0.4
0.2
Elevation of F0.50 Contour (km)
3
6
9
12
15
Distance to Reference Line (km)

Fig. 4.4.5b

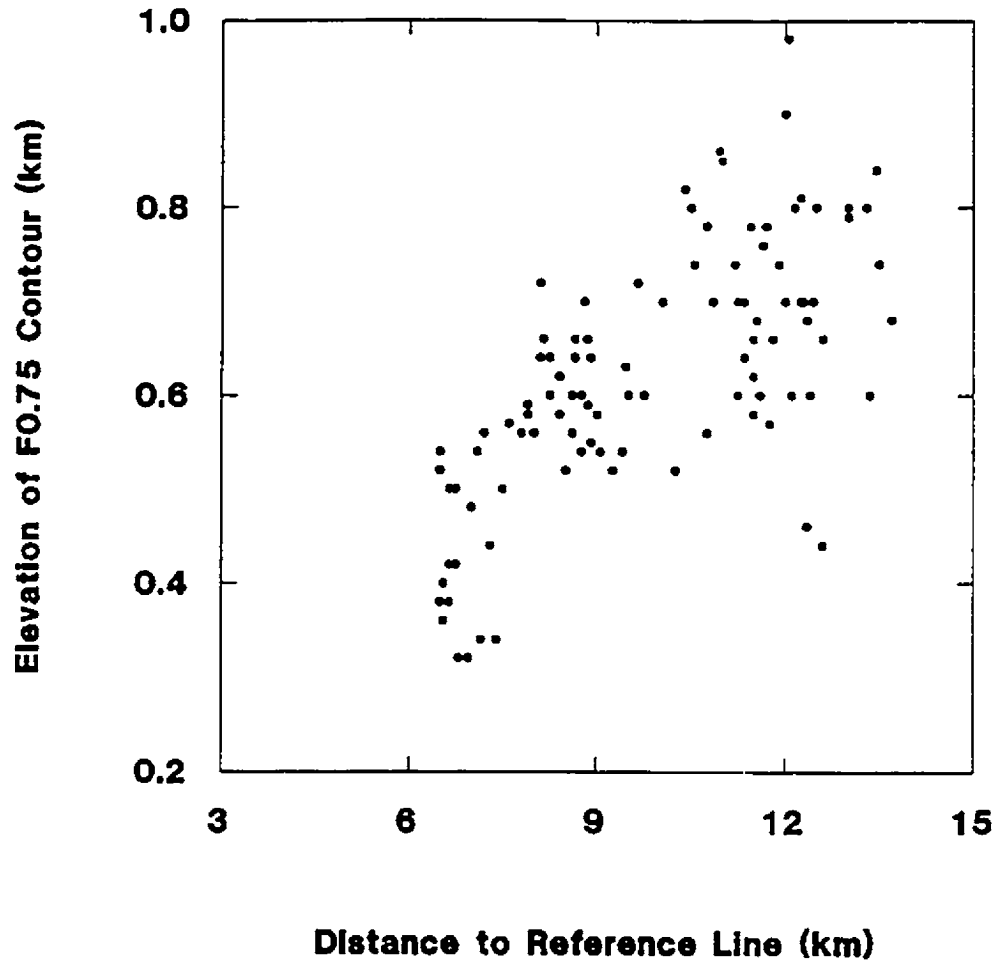
1.0
0.8
0.6
0.4
0.2
Elevation of F0.75 Contour (km)
3
6
9
12
15
Distance to Reference Line (km)

Fig. 4.4.5c

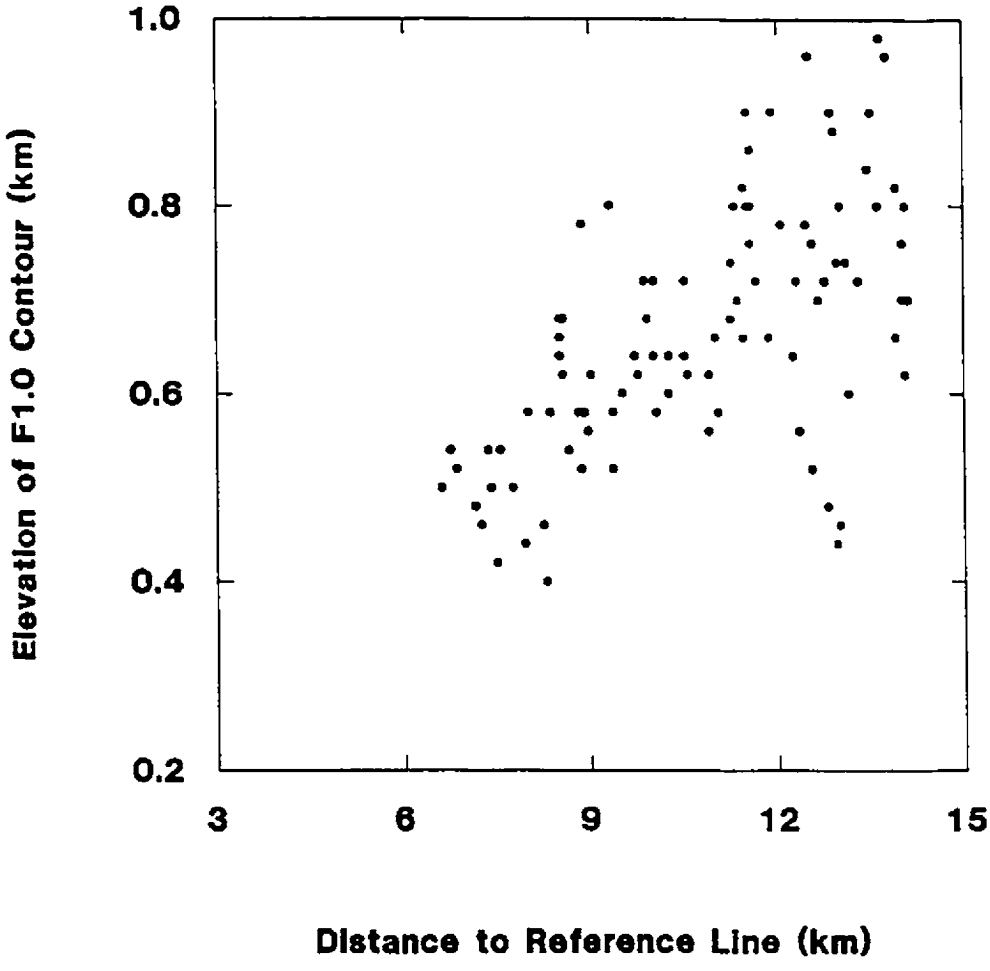
1.0
0.8
0.6
0.4
0.2
Elevation of F1.0 Contour (km)
3
6
9
12
15
Distance to Reference Line (km)

Fig. 4.4.5d

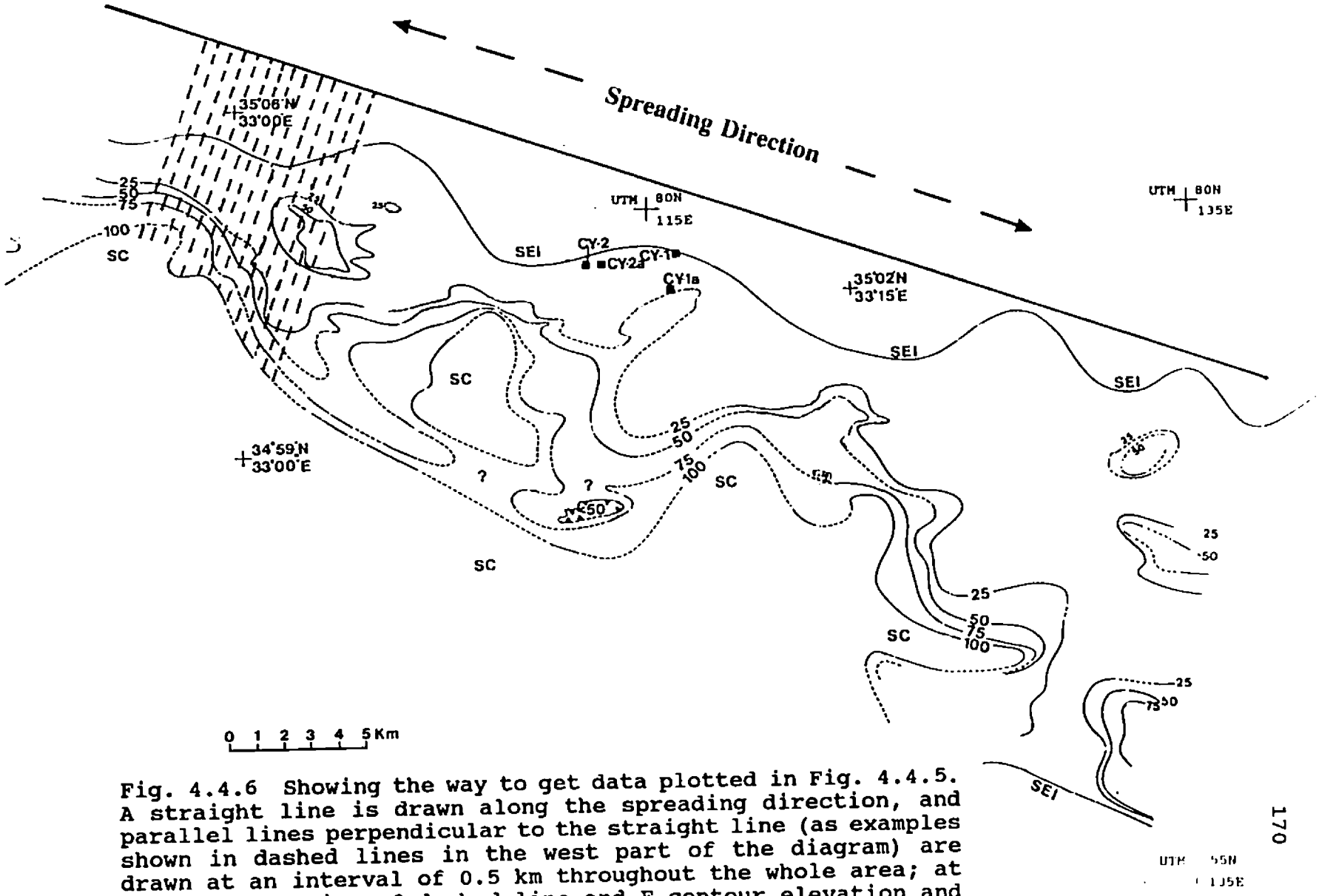

Fig. 4.4.6 Showing the way to get data plotted in Fig. 4.4.5. A straight line is drawn along the spreading direction, and parallel lines perpendicular to the straight line (as examples shown in dashed lines in the west part of the diagram) are drawn at an interval of 0.5 km throughout the whole area; at each intersection of dashed line and F contour elevation and the distance to the straight line are measured.

constructional features. The question now is how to estimate the degree of the influence of the topography to contour position?

Since the Troodos ophiolite occurs approximately as a simple anticline, and the topography of north flank is dipping at 2° to the north and sediment covers on the extrusives have an average dip of 9°, based on the topographic maps (1:50,000) and geological maps (1:31,680) of Cyprus, we can do a simple calculation (Fig. 4.4.7).

Suppose an original geological unit exposed on the horizontal surface along the axial direction was 1.0 km wide with a dip of 9° and, after erosion the topography dips at 2°, the original 1.0 km wide exposure now is 1.3 km, i.e., the width of the exposure increases 0.3 km with a corresponding increase in the spacing of contours. In Troodos, since the topography follows the regular anticline, the geological boundaries, or the contours will, generally change their positions but not the shapes. Since topography and dips of sediment cover have already been considered in MODEL 2, this correction has no influence on the calculated depth of contours.

In addition, a number of original constructional features can be recognized in the study area without general correction

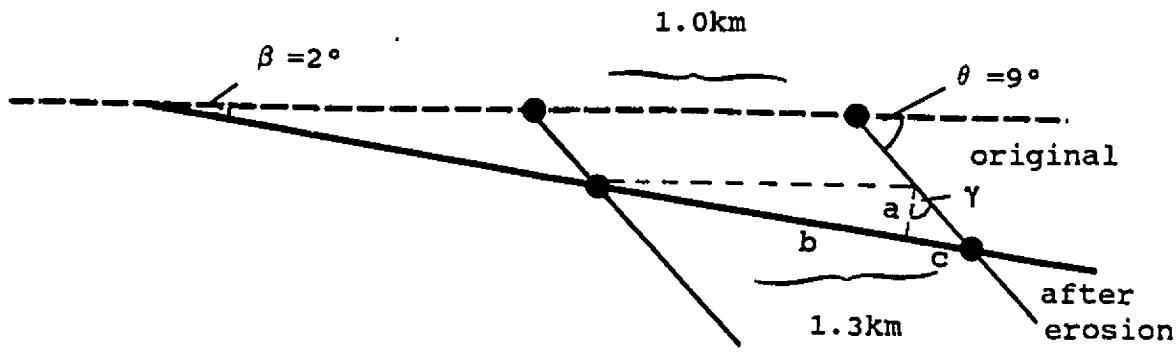

Fig. 4.4.7 Relationship between topography and variation of geological boundary. Suppose a geological section was 1 km wide with a dip of 9° and the original ground was horizontal, then, after erosion the topography now is dipping at 2°, as a result, the geological section is 1.284 km wide.

Calculation is:

$a = 1 \text{ km} \times \sin \beta = 0.035 \text{ km}$
$b = 1 \text{ km} \times \cos \beta = 0.999 \text{ km}$
$\gamma = 180 - 80 - \theta = 83°$
$b + c = 0.999 \text{ km} + a \times \text{tg}\gamma = 1.284 \text{ km}$

for this topographic effect. For example isolated high F areas located within low F areas, must be real features of the original construction of the crust.

4.5 Discussion of the topography of the original seafloor

A question that arises from the discussion of topographic effects is whether the present shape of the boundary between the sediments and the extrusives (the original seafloor) retains its original form or does it merely show the influence of post-emplacement processes such as erosion? This question is also of significance both for discussion of the relationship between the present day topography and original constructional features and for spreading rate estimation, as is carried out in Chapter 7.

If the original seafloor was flat, and then it was tilted uniformly to its present position, say at 9° from the horizontal, and there was no differential erosion but only a simple planar outcrop of the tilted sequence, the shape of the outcrop of the original seafloor should be a straight line. If, in contrast, there was differential erosion, the shape of the outcrop of the original seafloor surface would not be a straight line but would vary with the topography. In other words, if the original seafloor surface was horizontal and afterwards was uniformly tilted, and this surface after

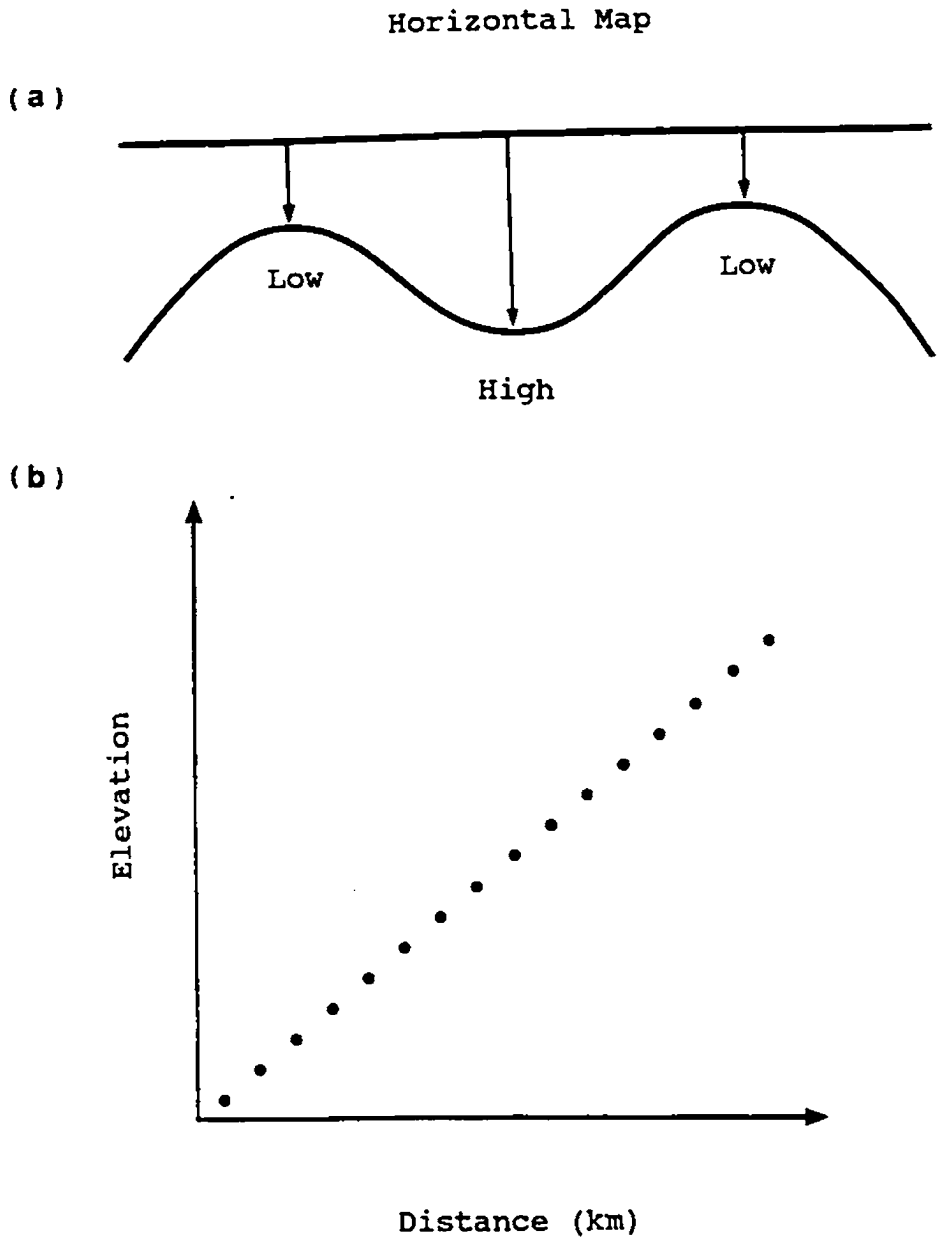

Fig. 4.5.1 Ideas for discussion of original seafloor. Suppose original seafloor was horizontal, after differing erosion, the sedimentary boundary on the seafloor would be curved (a), but the elevation of the boundary and its distance from the boundary to a supposed line would display a linear relationship (b).

erosion displayed a curved outline, or undulations other than a straight line, it would suggest that the position of the boundary has been affected by topography. As erosion proceeded, the position of the contours as well as that of the sedimentary boundary would be moved to the north (Fig. 4.5.1a). but the elevation of the boundary and its distance from the boundary to a supposed line would display a linear relationship (Fig. 4.5.1b)

If, in contrast, original seafloor surface had its own topography and was uniformly tilted to its present position, then evidently, after erosion, there would be no definite relationship between variation of topography and the shape of the sedimentary boundary. The problem is then, again, if the boundary has curved form, to separate the effects of erosion from original seafloor topography.

The elevation of the boundary of the sedimentary cover in the area represents a regular wave in the spreading direction (Fig. 4.5.2). The elevations of the sedimentary boundary in this diagram are obtained as shown in Figure 4.4.6. The smooth curve in the diagram shows that the elevations have a continuous trend of variation. It is necessary to determine if this feature is that of the original seafloor, or has been created by erosion after emplacement.

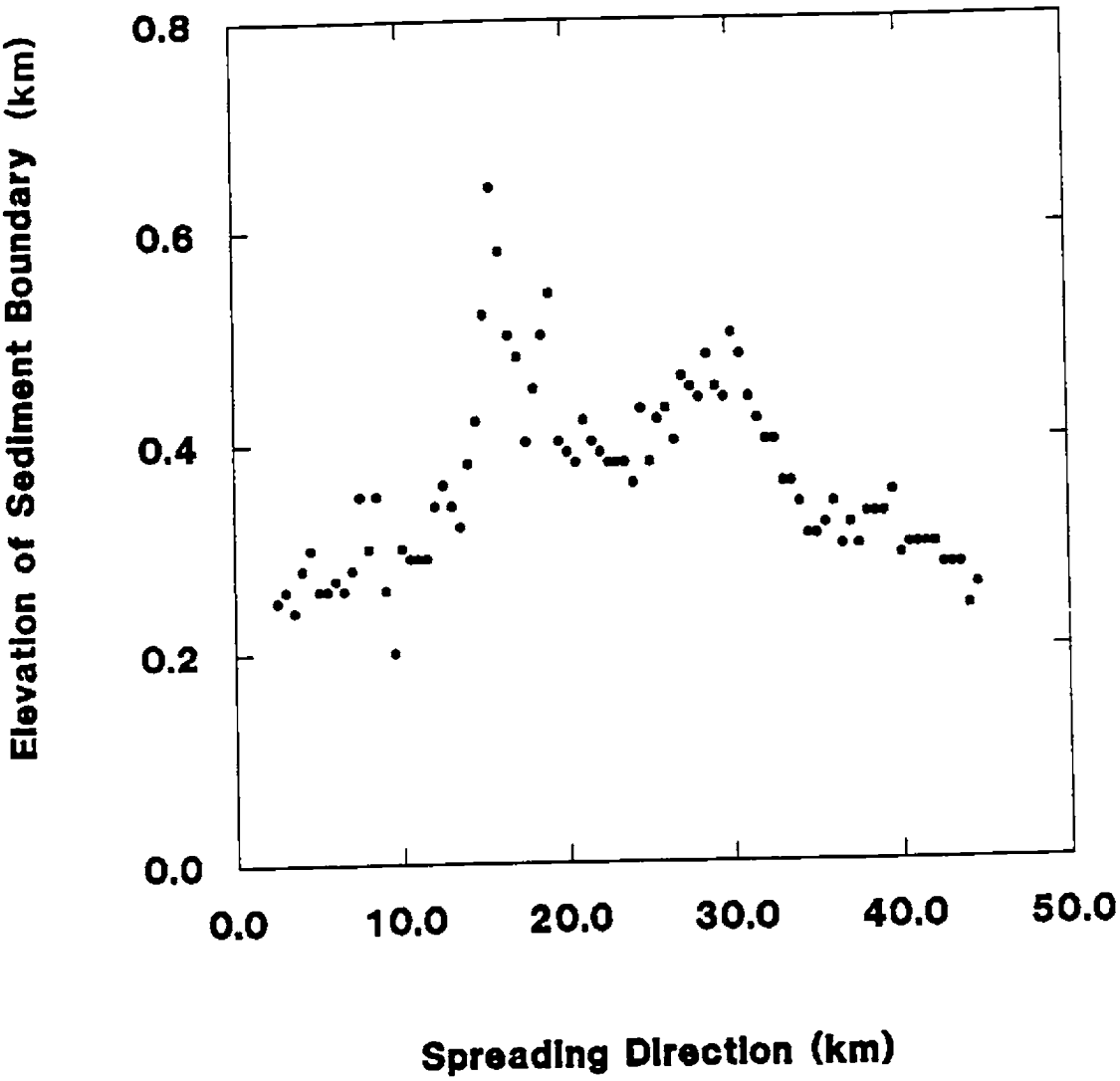

Fig. 4.5.2 Elevation vs. variation of sedimentary boundary along the spreading direction. The elevation of sedimentary boundary along the spreading direction shows a regular variation.

There are two ways to approach this question.

A way to test for the correct situation is, first, to use the reference line in the spreading direction shown in Figure 4.4.6. At each 0.5 km interval along the boundary, elevation and distance from the point on the sedimentary boundary to the reference line within the 45 km of the study area were measured. Then, the two groups of data, i.e., elevation and distance, obtained from the measurements are plotted (Fig. 4.5.3). It seems that, from this diagram, these two groups of data only correlate weakly. The elevation of the boundary has a large range and values of elevation for any particular distance are widely scattered. In this case, it seems that the original seafloor surface was not flat and that the present shape of the seafloor surface was not only controlled by topography, but by original constructional features. The graph suggests an average range of about 120 m in SEI elevation.

The other way to see the interaction between geological boundary and topography is to use the structural contour approach on an ideal planar contact, as described for the F contours (see Fig. 4.4.4). The predicted outcrop for the SEI show general directional similarity with the observed SEI contour (Fig. 4.5.4). However, although minor apparent undulations of the boundary are probably controlled by post-emplacement erosion, most larger undulations of the boundary

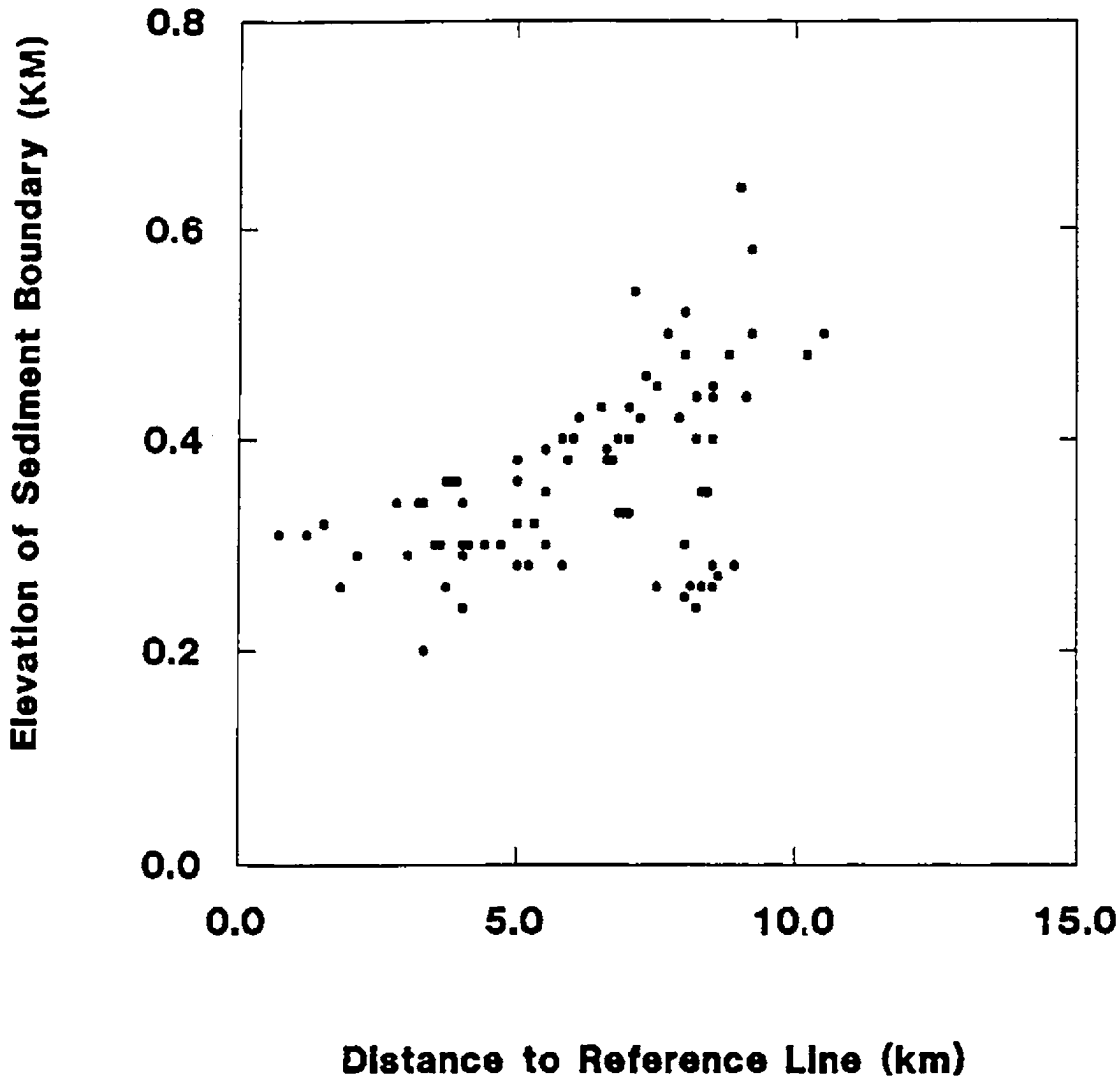

Fig. 4.5.3 Elevation vs. distance (km) of sedimentary boundary to a supposed line (see Fig. 4.4.6 for ref.). The elevations vary in a range of about 120 m, probably showing characteristics of the original seafloor.

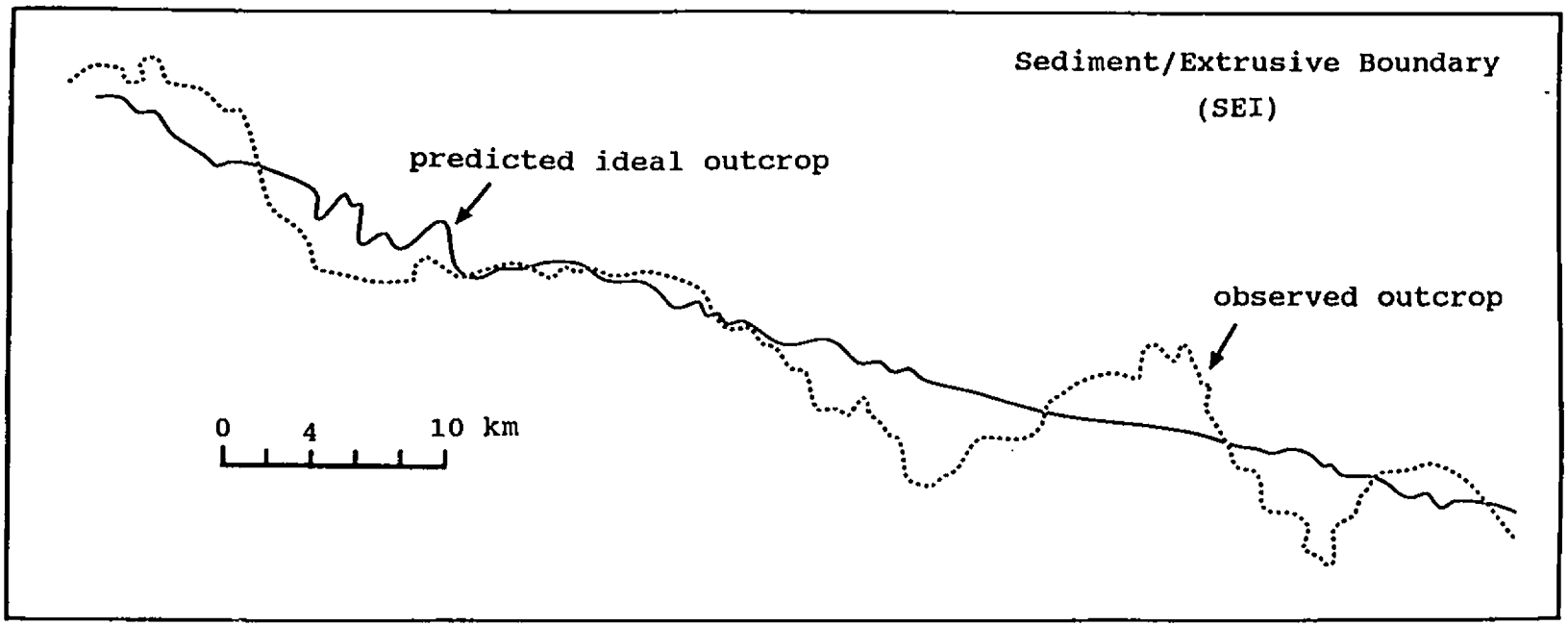

Fig. 4.5.4 Comparison of observed sediment/extrusive boundary (SEI) and predicted topography-controlled SEI. Dashed line is the observed and solid line is the predicted (discussion see text).

in the spreading direction can not be accounted for this way but are likely to represent original variation in the topography of the seafloor. These larger undulations are rather variable in amplitude but have an average value of about 120 m, the same value as obtained by the first approach.

From the above discussion, it is clear that the original seafloor of the Troodos ocean was not flat but undulated with topographic highs and lows. These highs and lows were most probably controlled by structures at depth, e.g., by effects such as extrusion and intrusion during the crustal formation.

To illustrate the situation more simply, a plasticine model of Troodos crust has been constructed with variation in both the SEI and interval features (Fig. 4.5.5a). It is envisioned that after emplacement on land, the block was not dismembered but was slightly titled towards N20E. After erosion, the original structures of the crust were areas of locally high abundance of dikes exposed at the surface, which leads to the undulation of contours on a horizontal map as seen today (Fig. 4.5.5b).

4.6 Influence of faults on constructional contours

In section 2.4, it was noted that there are a number of prominent faults in the northern part of the Troodos

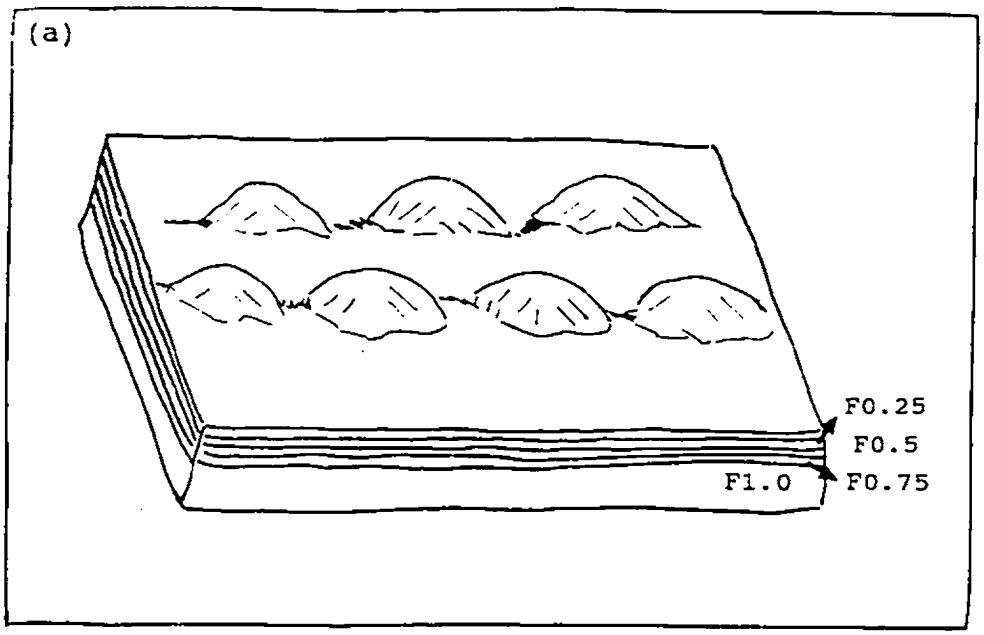

(b)

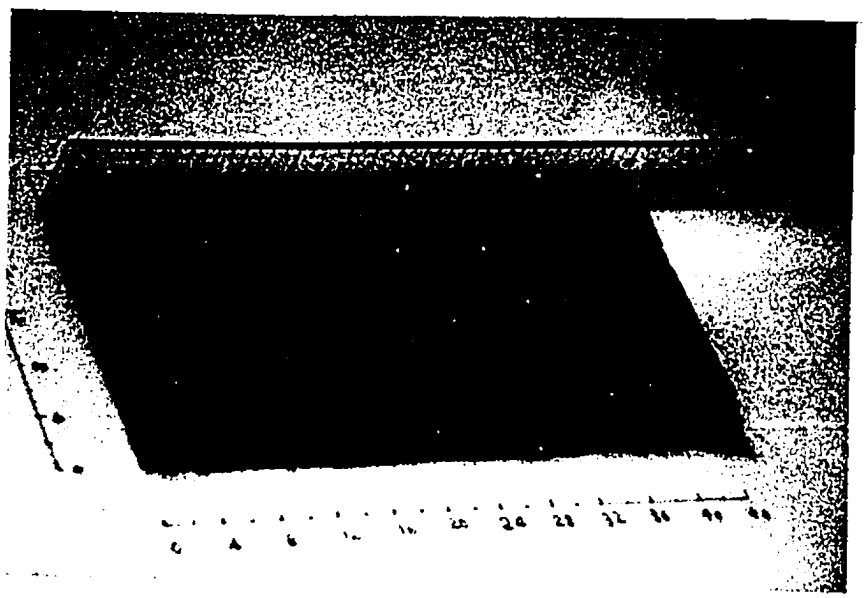

Fig. 4.5.5 A model for the formation of the crustal construction in the study area. (a) Original seafloor was not flat and where the undulations were controlled by structures at depth, e.g., the undulation of the Sheeted Dike Complex (SC); (b) due to the existence of a regional anticlinal structure, erosion reveals the structures at depth.

ophiolite. However, while these faults are shown in the various geological maps of Cyprus (1:250,000 and the 1:31,680 series), no detailed description is given of these faults. For example, it is not known what kind of faults they are or what influences the faults have on the pseudo-stratigraphic sequences of the ophiolite. From the geological maps, these faults only slightly offset geological boundaries, e.g., the boundaries between pillow lavas (UPL + LPL) and BG, or between BG and SC (see Fig. 2.4.1).

On the other hand, since three fault bounded grabens have been reported to occur in the northern part of the ophiolite, it is necessary to consider the possible influence from these grabens on the constructional contours.

The question addressed in this section is whether there are significant influences from structures, such as faults and grabens, on the constructional contours? Since fault data were not obtained for this thesis study, the major faults as indicated in the geological maps of Cyprus will be used here for the discussion of their possible relationship to constructional contours.

To approach this question, possible influence on the positions of the F0.25, F0.5 and P0.5 contours will be explored. F0.25 and F0.5 were chosen here for discussion

because of: 1) their representative nature, the former is a constructional contour within the shallower brownstone alteration zone, and the latter forms the upper boundary of the greenstone alteration zone; 2) both contours are controlled by a high density of measurement in the field. Since P value contours show no regular variation with depth, and different P value contours do not differ much in shape, P0.5, a medium contour was chosen for study.

Structural contours were formed on these three constructional contours. Topographic maps of the 1:50,000 series (Series K717, Sheets 10, 11, 12, 18, 19, 20) were used to obtained the structural contours. The interval between topographic contours was 200 m. Both topographic and constructional contours were first digitized (using the "Autocad" software). Then, structural contours were obtained on the constructional contours. Finally, faults and graben boundaries were digitized in the diagrams to see their relationship with structural and other contours.

Fig. 4.6.1 shows structural contours on F0.25. In the diagram it is seen that the F0.25 contour occur at relatively low elevations (ca. 400-600 m). The structural contours show a regular shape and indicating a generally simple overall structure with a dip gently to the northeast at angles of 3° to 5°. In the west, small isolated areas enclosed by the F0.25

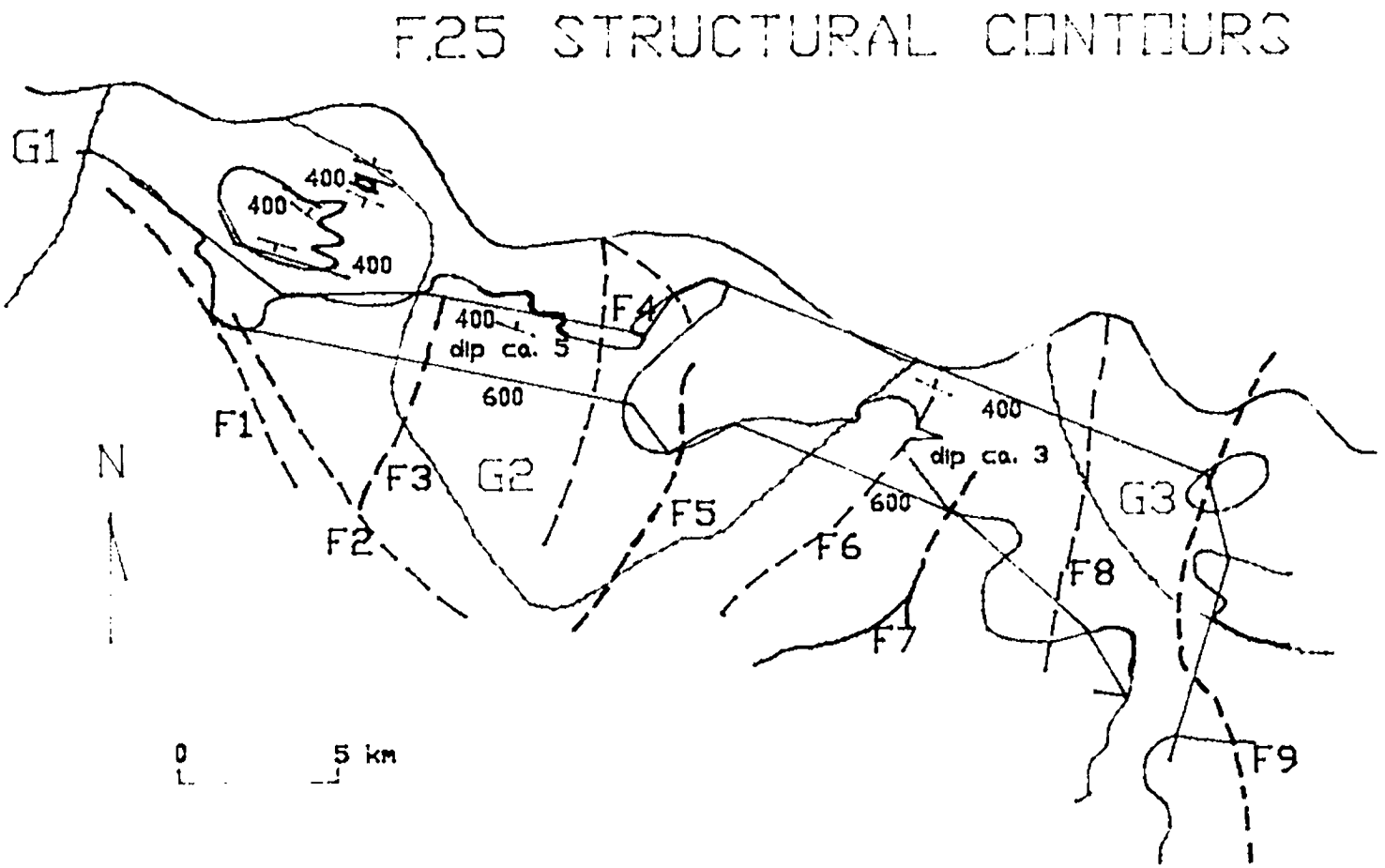

Fig. 4.6.1 Structural contours for F0.25 contour. Green- F0.25 contours; blue- structural contours; brown- faults and inferred faults; orange-graben boundaries; black- sedimentary boundary; F1-fault; G1-Solea Graben; G2-Mitsero Graben; G3-Larnaca Graben; 400- elevation in meter.

contour correspond to local highs of elevation. Structural contours on F0.5 (Fig. 4.6.2) show almost the same pattern as for the F0.25 contour. The difference is that F0.5 contours are located at relatively higher elevation, ranging between ca. 400-800 m, and the dip angles increase from low to high reliefs from ca. 5° to 7°.

Structural contours for P0.5 contour (Fig. 4.6.3) also show a general dip to the northeast, similar to that for F contours.

Major faults in the study area mostly trend northeasterly, i.e. approximately parallel to the axial direction, except two faults in the western part of the area which strike northwesterly. Although most of the faults show no particular spatial relationship with the F contours, it is noted that two of them (described as F2 and F5) are approximately located in southerly directed reentrants in F contours, where the structural contours for the F0.5 constructional contour indicate that the F0.5 surface is relatively steep (see Fig. 4.6.2) but for F0.25 were not (see Fig. 4.6.1). The inconsistent variation of the structural contours for F0.5 and F0.25 contours suggests that the curvature of the F contours most probably represents an original but secondary characteristic of the intrusion of dikes. However, the spatial coincidence between the faults and

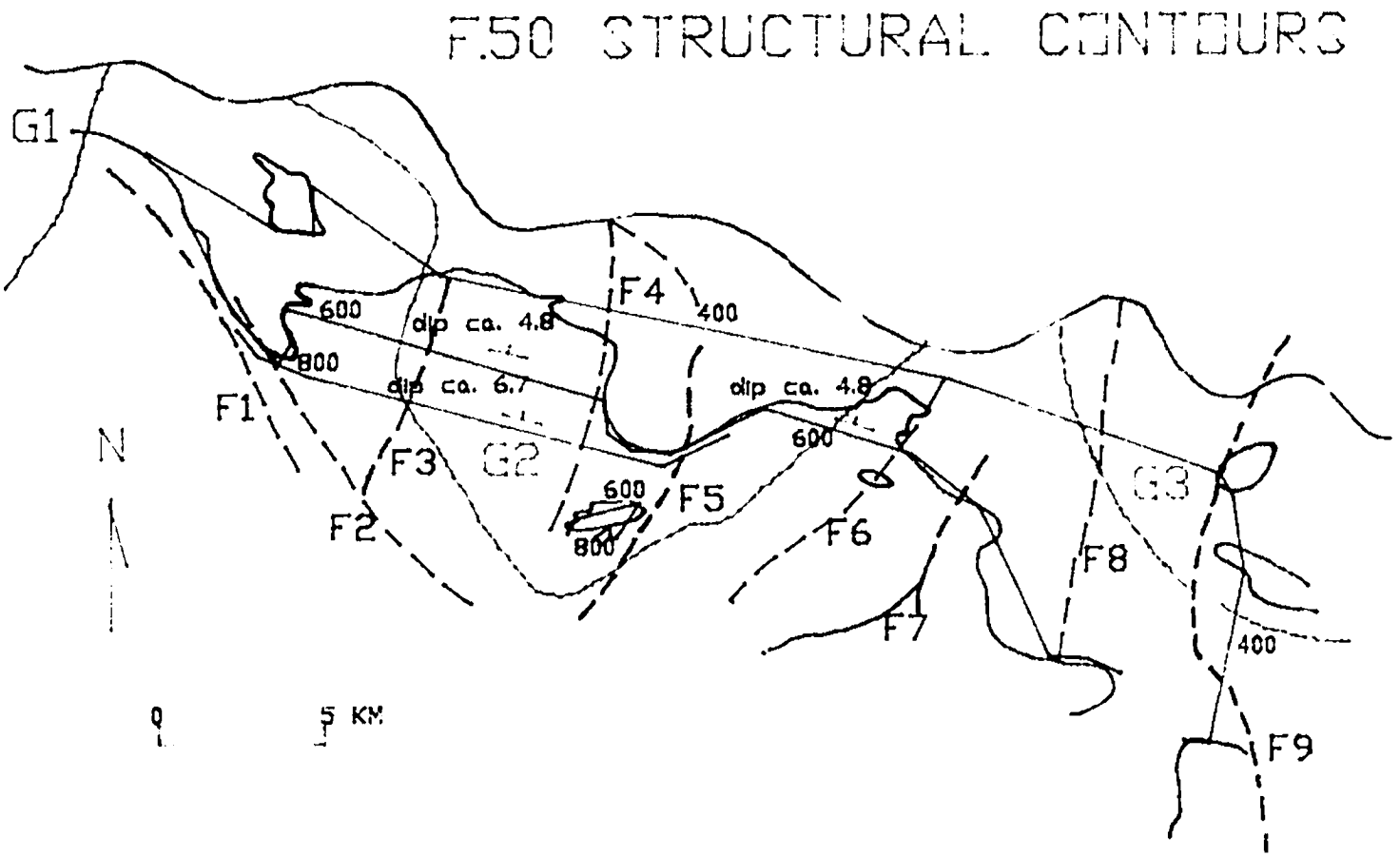

Fig. 4.6.2 Structural contours for F0.5 contour. Green- F0.5 contours; blue- structural contours; brown- faults and inferred faults; orange-graben boundaries; black- sedimentary boundary; F1-fault; G1-Solea Graben; G2-Mitsero Graben; G3-Larnaca Graben; 400- elevation in meter.

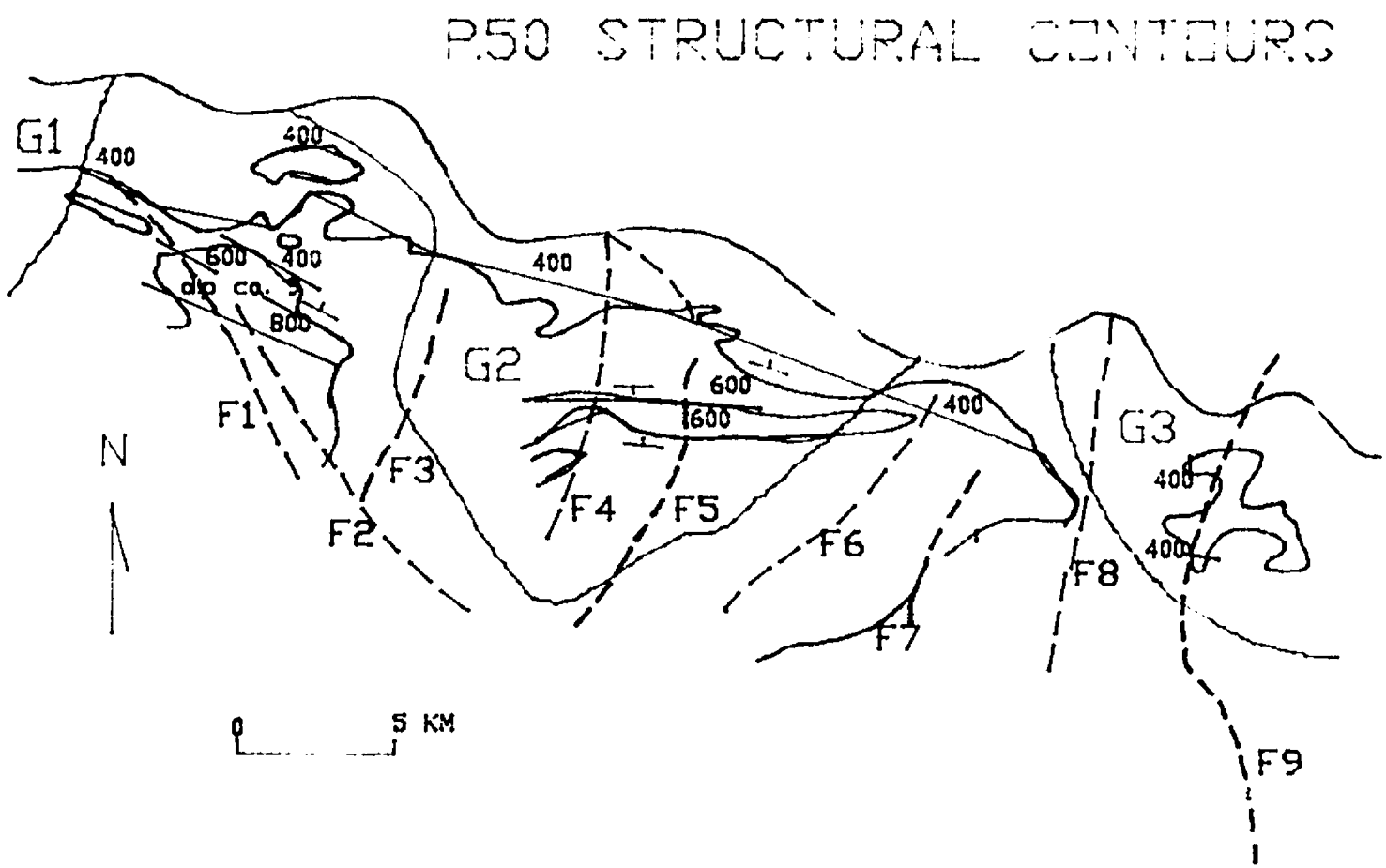

Fig. 4.6.3 Structural contours for P0.5 contour. Green- P0.5 contours; blue- structural contours; brown- faults and inferred faults; orange-graben boundaries; black- sedimentary boundary; F1-fault; G1-Solea Graben; G2-Mitsero Graben; G3-Larnaca Graben; 400- elevation in meter.

F contours may also suggest a possible correlation between changes in the curvature of F contours and faults.

The conclusion is that, although the abrupt variation in the direction of the structural contours at these locations could be explained by an original intrusion of dikes at a relative high level under the seafloor, the influence from the faults on the F contours cannot be excluded. The F contours near to the faults might have been slightly shifted as for the other geological boundaries seen in Fig. 2.4.1. There are no obvious correlations between major faults and P0.5 contours (see Fig 4.6.3), which may provide one more line of evidence to support this conclusion.

The Mitsero Graben (alternatively described as the Ayios Epiphanios Graben in Varga and Moores, 1985) is supposed to be located in the central part of the area (see Fig. 4.6.1 and 2). The graben is defined by opposing dike orientation, i.e., by a north-northwest-trending axis of symmetry across which dikes dip toward each other (Varga and Moores, 1985). However, although the graben boundaries were described as probable faults or intrusive domain boundaries (Varga and Moores, 1985), their paper did not give any evidence or description to show that any faults occurred at so-called graben boundaries. The paper even did not mention on what basis the graben boundaries were drawn and what the field evidence was

involved. On the other hand, the fact that no major faults shown on the geological maps are located at or near the graben boundaries seems to suggest that the existence of these boundaries is questionable. It is noted that the grabens of Varga and Moores do not show any spatial correlation with the F or P constructional contours. In contrast, the constructional contours obtained in this study give a much more detailed and valuable description of constructional variation in the Extrusive Sequence both within and without the supposed grabens.

An interesting thing is that, if the boundary of the Mitsero Graben moves ca. 3 km toward the west, the two sides of the boundary will coincide exactly with the abrupt steep of the structural contours for F0.5 contour and the curvatures of F contours (Fig. 4.6.4). This coincidence may suggest a possible location of the graben boundary, if it existed (N. Culshaw, 1991, personal communication).

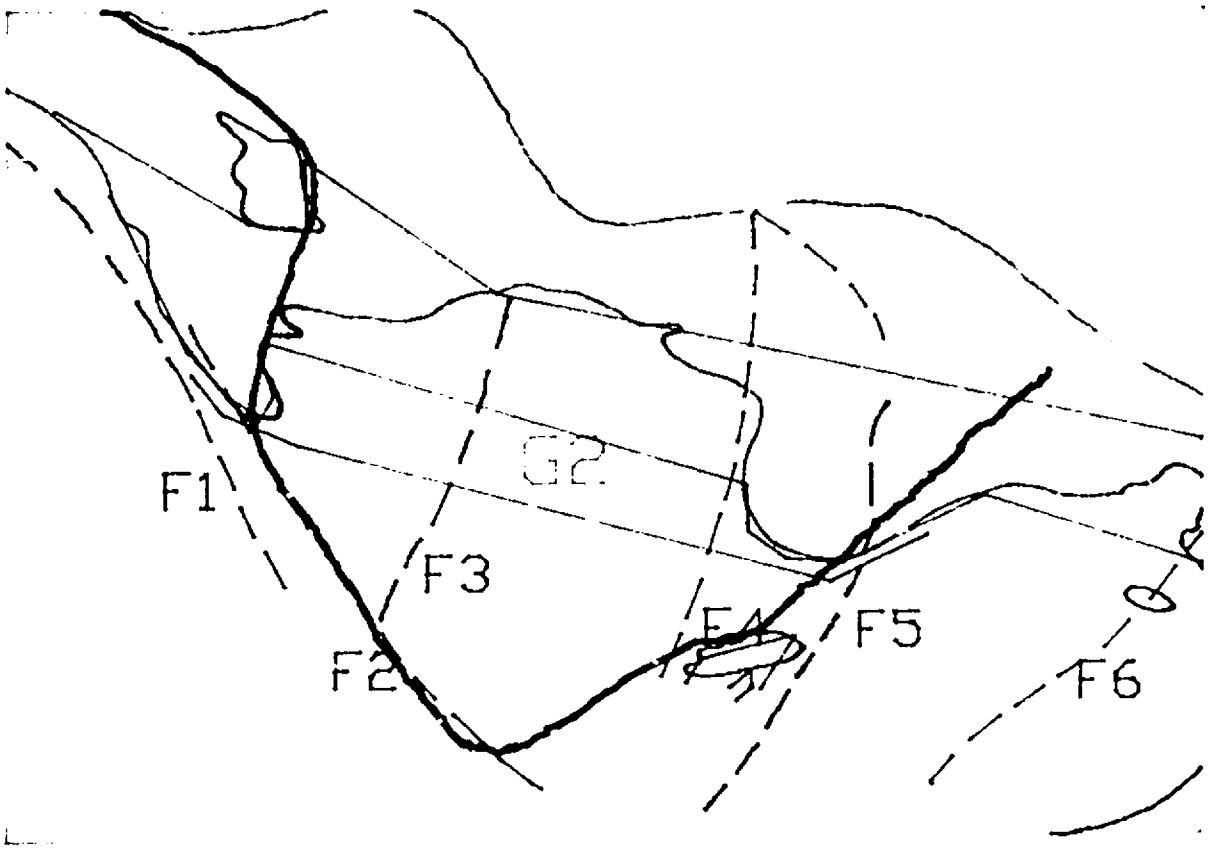

Fig. 4.6.4 After the Mitsero Graben boundary been moved ca. 3 km toward the west, it coincides with the curvature of F0.5 contour and the abrupt steep of the structural contours (symbols see Fig. 4.6.2).

Chapter 5 Regional Alteration Zonation

5.1 Introduction

It is known that Troodos type oceanic crust has undergone very similar types of alteration to that observed in present oceanic crust. A substantial number of studies of alteration minerals and rocks and their alteration zonation in the upper part of the Troodos ophiolite have already been carried out (e.g., Gass and Smewing, 1973; Gillis and Robinson, 1985; Gillis, 1986; Hall et al., 1987; Jamieson and Lydon, 1987; Herzig and Friedrich, 1987).

Early studies of metamorphism (now understood as hydrothermal alteration) of the Troodos ophiolite proposed that the UPL/LPL subdivision corresponded to a metamorphic discontinuity and indicated that this and other metamorphic zones were originally horizontal, with the zeolite facies overlying the greenschist facies (Fig. 5.1.1) and the amphibolite facies occurring at depth (e.g., Gass and Smewing, 1973; Smewing, 1975).

In the 1980s, on the basis of detailed mineralogical and petrological work, Gillis (1986) established six alteration zones in the extrusives of the ophiolite (Fig. 5.1.2), and, later, reduced these to five zones (Gillis and Robinson,

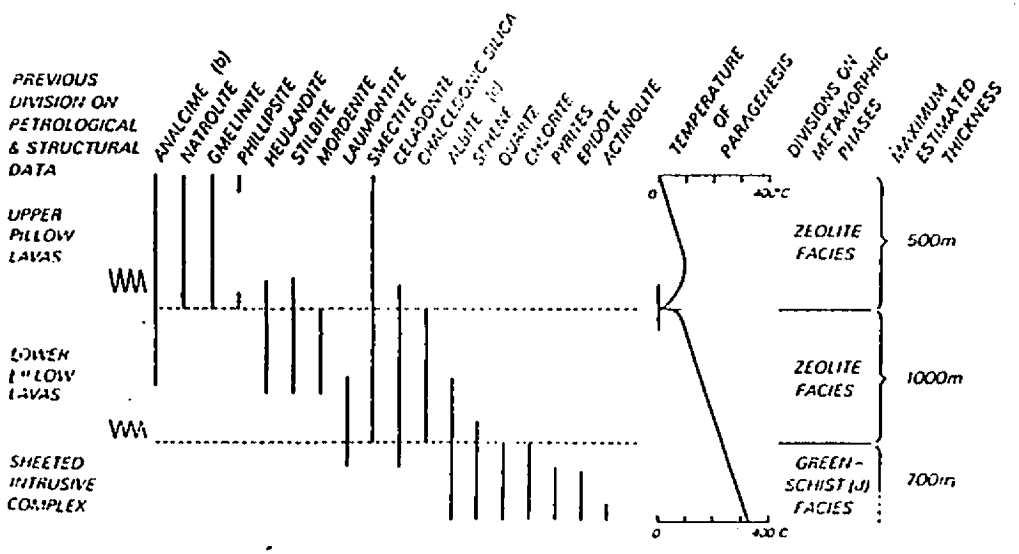

Temperatures of paragenesis when related to maximum thicknesses of facies suggest a minimum thermal gradient of 150° C km^{-1}. *a*, Chabasite, a rare zeolite on Troodos, has been recorded at two localities in the upper division and one in the lower division of the Pillow Lava Series; *b*, analcime occurs as macroscopic, commonly amygdaloidal, crystals in the upper unit but only in the ground mass of the Lower Pillow Lavas; *c*, the anorthite molecule is metastable within the albite stability field near its upper temperature phase boundary; *d*, we retain the term greenschist but appreciate, as others have done[13–15], that it is inappropriate in an oceanic environment.

Fig. 5.1.1 Early division of metamorphic phases (zones) in the Troodos ophiolite by Gass and Smewing (1973).

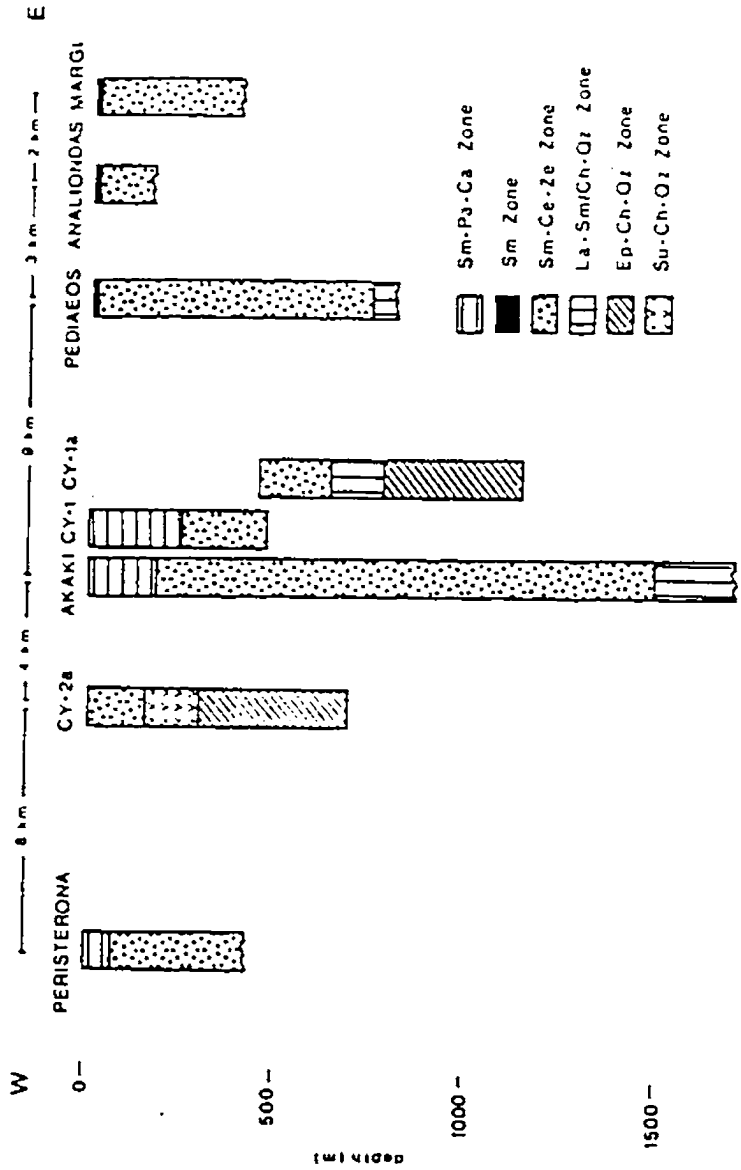

Fig. 5.1.2 Six alteration zones distinguished within the field area by Gillis (1986).

1988). It is noted that these alteration zones were recognized on the basis of the detailed study of several isolated areas along the northern flank of the ophiolite.

Alternatively, some detailed alteration studies were done on several CCSP drill cores from various parts of the Extrusive Sequence of the Troodos ophiolite. Two holes were drilled in the Agrokipia ore deposits in order to investigate the nature of hydrothermal circulation and ore formation in oceanic crust (Robinson, 1987). Although much of these two cores are from a special alteration environment, the alteration features described in the Initial Report for Holes CY-2 and 2a for the parts altered in regional styles (e.g., Kurnosov et al., 1987; Cann et al., 1987; Herzig and Friedrich, 1987; Sunkel et al., 1987) do not show significant difference from those in present oceanic crust. It is interesting that the alteration zonation recognized varies from one author to another. Thus, Kurnosov et al. (1987) recognized two types of alteration in the extrusives, as sampled in Holes CY-2 and CY-2a: low temperature sea water-rock interaction and higher temperature hydrothermal alteration. Again, Cann et al. (1987) divided the rocks of the holes into three different alteration facies and Herzig and Friedrich (1987) distinguished four major alteration zones in Hole CY-2a (Fig. 5.1.3), which are not much different from the four alteration zones based on the cores of CY-2a and CY-2

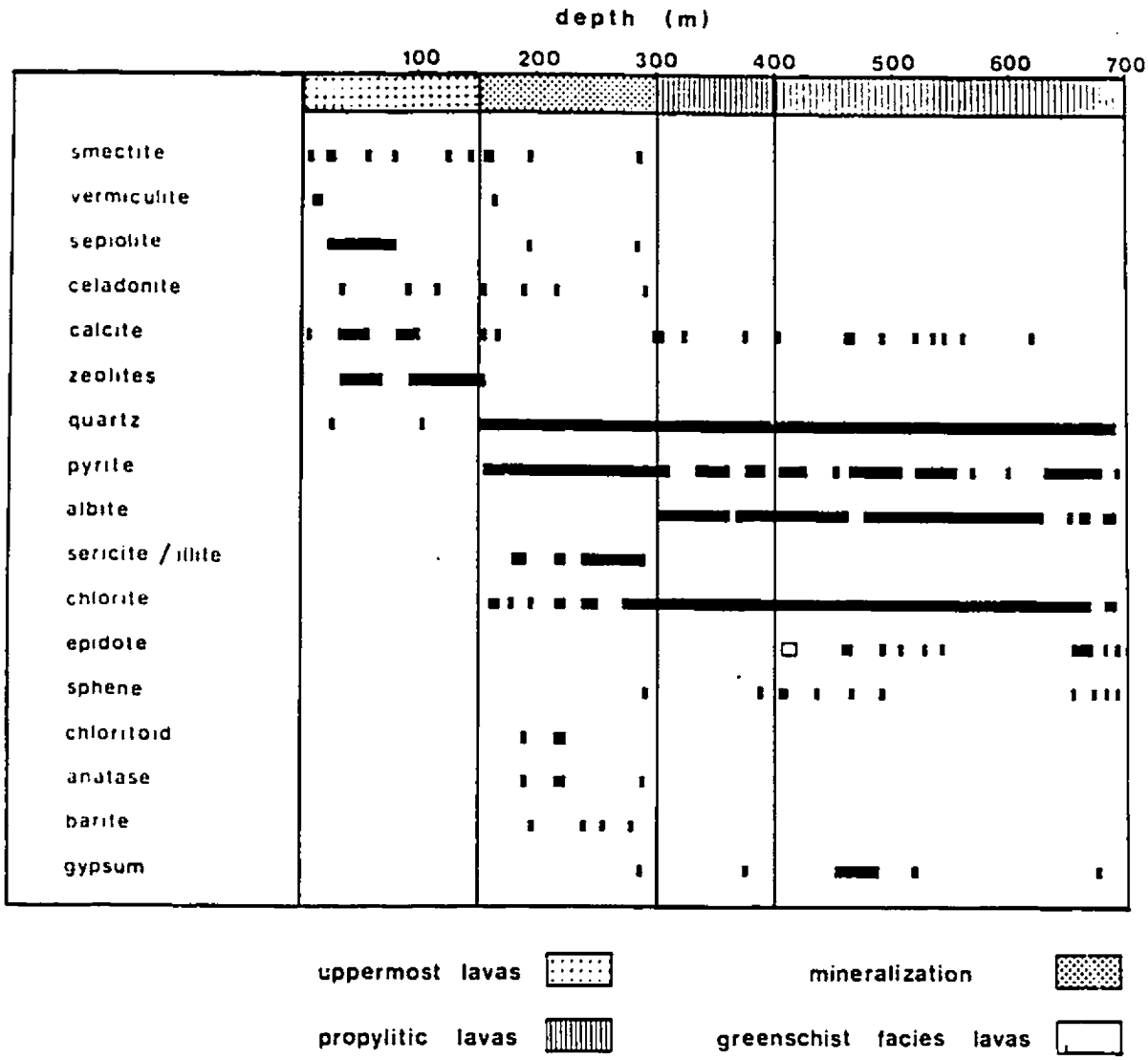

Fig. 5.1.3 Four alteration zones identified in Hole CY-2a by Herzig and Friedrich (1987).

established by Sunkel et al. (1987). Obviously, these alteration zonations only stress some particular local rather than regional characteristics.

Therefore, although all the above zonations were based on the studies of the same secondary minerals, either the scales of division were different, or the points emphasized by each author were different, and, as a result, different zonations of the same section are given by different authors.

A further important point is that these recent publications describing the alteration zonation of the Troodos ophiolite were mostly based on the small number of CCSP drillcores or on results from isolated sections. This means that it is difficult to be sure that the zones reported are of regional extent.

A regional zonation of alteration is likely to represent the general features of alteration of the ophiolite as ancient oceanic crust during its formation. Recognition of a regional alteration zonation, formed almost contemporaneously with construction, is expected to contribute to the constructional study of the Extrusive Sequence of the ophiolite and to comparison with present oceanic crust.

Accordingly, the alteration study in this thesis, as

mentioned in Chapter One, is not intended to address the very detailed mineralogy, chemical composition and isotopic analyses of altered minerals and rocks, as undertaken by many previous workers, e.g., Gillis (1986), Jamieson and Lydon (1988), and Spooner (1977). Neither is the more detailed particular environment of alteration discussed, as in Alt et al. (1986) for the upper oceanic crust of DSDP Hole 504B.

The objective of this alteration study is to identify the zoning of alteration over a relatively large area, its spatial relation to features of the Extrusive Sequence and dikes, as well as its contribution to the development of a model of crustal construction.

5.2 Alteration zonation in this study

Detailed field observation and mapping indicate that the Extrusive Sequence between the sediment/igneous interface (SEI) and the Sheeted Dike Complex (SC) can be divided into an upper, brownstone, and a lower, greenstone alteration intervals, with an abrupt transition between the two intervals. Color and alteration differences are often sufficiently marked that field observation is adequate to recognize these basic intervals.

The rocks in the brownstone alteration interval are

characterized by yellowish, reddish or greenish brown colors, with ubiquitous clays and some carbonate and zeolite. The Upper Pillow Lavas (UPL) forms the most altered upper part of the brownstone interval and usually consists of indurated volcanics that are relatively resistant to subaerial weathering. In contrast, the less altered pillows of LPL in the lower part of the brownstone interval weather down rapidly and often are earthy in appearance. Sheet flows in the brownstone interval are relatively less altered and resistant to weathering, but dikes may commonly show relatively low resistance.

The rocks in the greenstone interval are characterized by greenish grey color, with dominant chlorite and quartz, and minor epidote and secondary pyrite. The greenstone interval consists of the majority of "Basal Group" (BG) and a lesser part of LPL field mapping divisions. With the onset of greenstone alteration, dikes and screens of extrusives show similar resistance to subaerial weathering.

A transition zone between the brownstone and greenstone intervals is not generally evident in megascopic examination but is clearly definable on the basis of microscopic observations.

The alteration study in this thesis is based on

information from 690 rock samples collected from 544 observation stations along 18 lines in the area. From study of these samples 13 main secondary minerals have been identified based on their optical characteristics and microprobe compositions. These are smectite (Sm), celadonite (Ce), calcite (Cal), amorphous silica (Si), zeolite (Ze), quartz (Qtz), chlorite (Chl), epidote (Ep), albite (Ab), sphene (Sph), secondary pyrite (Py), secondary magnetite (Mt) and amphibole (Am).

Recognition of alteration zones is based on the occurrence of the different alteration minerals which are spatially associated. The interval which contains Sm, Ce, Cal, Ze and Si is defined as the brownstone alteration zone. The interval which contains Chl, Qtz, Ab, Ep, Am, Sph, Py and Mt is defined as the greenstone alteration zone. Between these two zones there is a transition zone containing some minerals of both the brownstone and greenstone zones.

The minerals in the brownstone alteration zone imply alteration mainly in the brownstone (Cann, 1979) and zeolite facies (Miyashiro and Shido, 1970) recognized elsewhere in regional metamorphic conditions. Here, the brownstone facies, defined by Cann (1979), is the facies of low temperature ocean floor weathering or cool hydrothermal alteration, with the main secondary minerals being iron-bearing illite, celadonite,

and smectite (saponite). Its products have characteristically a yellowish brown tint or a dark bluish grey. It is the facies of most older upper oceanic crust and persists through most of the drilled sections of oceanic crust (Cann, 1979). The name brownstone alteration zone in this study is derived from both its mineral assemblage and color.

Greenstone in the Glossary of Geology (Bates and Jackson, 1987) is normally a field term applied to any compact dark-green altered or metamorphosed basic igneous rock that owes its color to the presence of chlorite, actinolite, or epidote. Delaney et al. (1987) used "greenstone" to describe a suite of quartz-rich, sulfide-bearing breccias originally related with hydrothermal systems (300°C) discovered on the Mid-Atlantic Ridge south of the Kane Fracture Zone. The name greenstone alteration zone is then adopted in this study due to the presence of a secondary mineral assemblage of greenschist facies minerals and to its color. The secondary mineral assemblage in the greenstone zone suggests alteration in the greenschist facies.

However, it is clearly understood that ophiolite alteration takes place under substantially different physical conditions from regional metamorphism. As a result, almost all of the altered rocks preserve a well-developed igneous texture and a certain amount of primary minerals, and the secondary

minerals were deposited sequentially and are closely related to particular primary phases. In these circumstances they do not represent equilibrium assemblages and mineralogical zones should therefore not be considered as metamorphic zones (Gillis, 1986).

5.2.1 The Brownstone alteration zone

In the brownstone alteration zone smectite is the most widespread and abundant secondary mineral and its occurrence has been described in detail by previous workers (e.g., Gillis and Robinson, 1985; Kurnosov, et al., 1987). It commonly accompanies other secondary minerals but is sometimes the only alteration phase present. Smectite routinely occurs in cavities and in the groundmass, and shows features of both colloform deposition and the replacement of primary silicate minerals. Most smectites present show brownish or occasionally yellow-green color. Brown smectite may occur in fibrous or platy forms while the green smectite only exists in the platy form (Fig. 5.2.1).

The average composition of Troodos smectites (Table 5.2.1) is compatible with that of ferromagnesian trioctahedral smectite (saponite) of Deer et al. (1966), as suggested by Gillis (1986). Most saponites may be formed at temperatures of less than 100°C, but some iron-saponite (Fe/Fe+Mg > 0.5), as

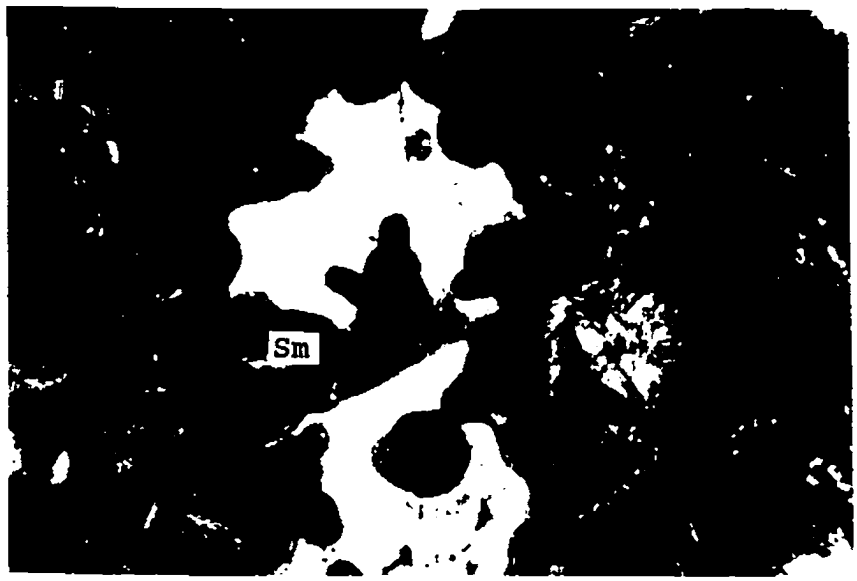

(1.3 x 0.9 mm)

Fig. 5.2.1 Dark brown fibrous smectite occurring at the margin of cavities in the brownstone zone. Calcite (cream) fills in the centre of the cavities (plane polarized light). Sample No. 20.14

Table 5.2.1 Average Microprobe Data of Some Secondary Minerals

	1	2	3	4	5	6	7	8
SiO2	38.40	33.55	35.98	51.88	54.08	26.91	29.55	50.82
TiO2	0.10	0.11	0.10	0.12	0.14	0.09	0.12	0.36
Al2O3	11.31	14.03	12.67	3.56	1.94	18.01	14.42	5.11
FeO*	14.45	13.60	14.02	15.34	24.28	23.61	26.22	16.12
MnO	0.28	0.29	0.28	0.07	0.03	0.51	0.03	0.41
MgO	17.93	21.21	19.75	8.66	4.08	14.73	15.82	11.78
CaO	1.07	0.50	0.78	0.78	0.32	0.43	0.28	9.65
Na2O	0.23	0.13	0.18	0.41	0.18	0.09	0.14	1.01
K2O	1.02	0.16	0.59	6.17	6.80	0.04	0.15	0.05
Total	84.79	83.54	84.22	86.99	92.05	84.42	86.99	95.96
n	4	4	8	4	2	10	2	7

FeO*: total iron; n- number of analyses; 1- brown smectite; 2- yellow green smectite; 3- all smectite; 4- high-Mg celadonite; 5- high-Fe celadonite; 6- chlorite in greenstone zone; 7- chlorite in transition zone; 8- amphibole (actinolite).

identified in this brownstone zone, possibly formed during weathering at ocean bottom water temperature ($20°C \geq T \geq 4°C$) (Velde, 1985). Güven (1988) suggested that some colloform smectite may have precipitated from gels and solutions at temperatures of from 3° to 150°C. Smectites accompanying iron-rich chlorite formed from altered ferromagnesian minerals, mainly in the transition zone, possibly at moderate temperatures of 100°-230°C, may be of this type (Güven, 1988).

Celadonite is relatively less widely distributed than smectites in the brownstone zone and normally only occurs in small amounts. It typically has a fresh green color in thin section and occurs as fine fibrous aggregates (Fig. 5.2.2). Celadonite was mainly deposited at the margins of cavities where it surrounds some spherical amorphous silica, or is accompanied by calcite with the latter usually deposited in the central part of the cavity. Chemical analysis indicates that two sub-types of celadonite occur in the zone, i.e. high ferrous and high magnesian types (see Table 5.2.1 and Appendix 5), possibly suggesting a primary difference in bulk rock composition.

For deep sea basalt alteration, Velde (1985) considered the major elements Al, Fe^{2+}, Fe^{3+} and Mg as being critical in forming secondary phases. In his phase diagrams, nontronite,

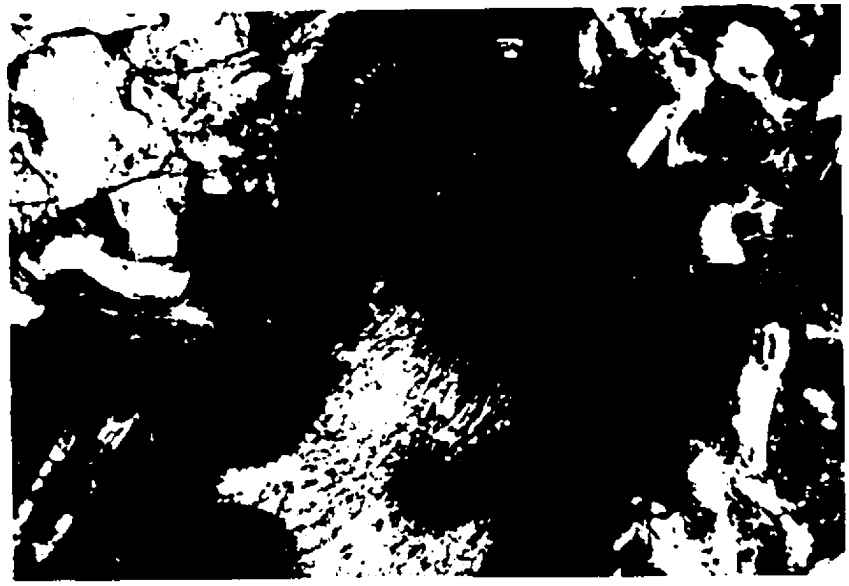

(1.3 x 0.9 mm)

Fig. 5.2.2 Bright green coloured fibrous celadonite occurring at the margins of cavities which are filled with carbonates. Sample No. 20.15

celadonite, zeolite and smectite are all able to form at 80°-200°C during low temperature hydrothermal alteration.

Carbonates are common in this zone, and in the main occur in cavities with minor amounts in veins. Most of the carbonate is calcite occurring in large platy crystals but with the less well developed typical perfect rhombohedral cleavages of calcite. At the top of the zone, some carbonates occur as parallel or radiating aggregates of acicular or fibrous crystals. They are possibly aragonites or pseudomorph of calcite after aragonite. These radiating-pattern carbonates often contain substantial dark-brown impurities, which may occur in zones, indicating the sequence of deposition (Fig. 5.2.3). Chemical analysis indicates that the impurities in the carbonates contain Mn (up to 13%).

It is known that calcite generally has a wide temperature range of formation. The precipitation of $CaCO_3$ from $CaCl_2$ and Na_2CO_3 in solution produces calcite at below 35°C. Calcite is also stable in the greenstone facies, accompanying chlorite and epidote at temperatures as high as about 500°C (Winkler, 1974). The crystallization of aragonite, in general, is favoured by temperatures of between 50°C and 80°C at relatively higher pressures than calcite (Deer et al., 1966).

In this zone amorphous silica is very common, but often

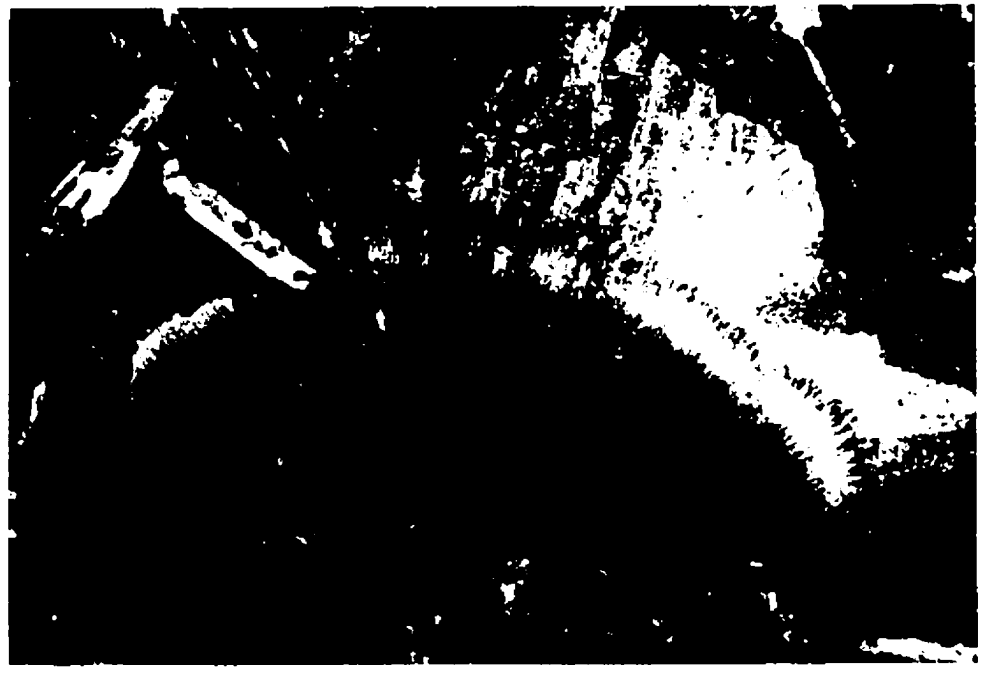

(1.3 x 0.9 mm)

Fig. 5.2.3 Carbonate occurring with radiating habit in cavities. Dark brown impurities are Mn rich. Sample No. 20.15

occurs at low levels (<5%), and in small spherical and radiating aggregates (Fig. 5.2.4). The forms of amorphous silica present are usually opal or chalcedony, i.e., hydrated forms, from a few percent to about 10%. Colloform amorphous silica is largely the by-product of the alteration of feldspars and other silicates to clay minerals.

Several zeolites occur in this zone, including laumontite (Laum), natrolite (Natr), and mordenite (Mord), but they mostly occur in the transition zone and therefore will be described under that heading.

5.2.2 The Transition Zone

The transition zone is defined as that interval containing secondary minerals that are present in both the brownstone and greenstone alteration zones. Only the differences in the secondary minerals of this zone from the other two zones will be discussed in this section.

First, chlorite starts to appear in this zone, typically in the form of small leaves or fibrous radiating aggregates. It mostly occurs at the margins of cavities where it is associated with smectite, amorphous silica, and calcite. This type of chlorite usually shows yellow-green color in plane polarized light and anomalously high birefringence in crossed

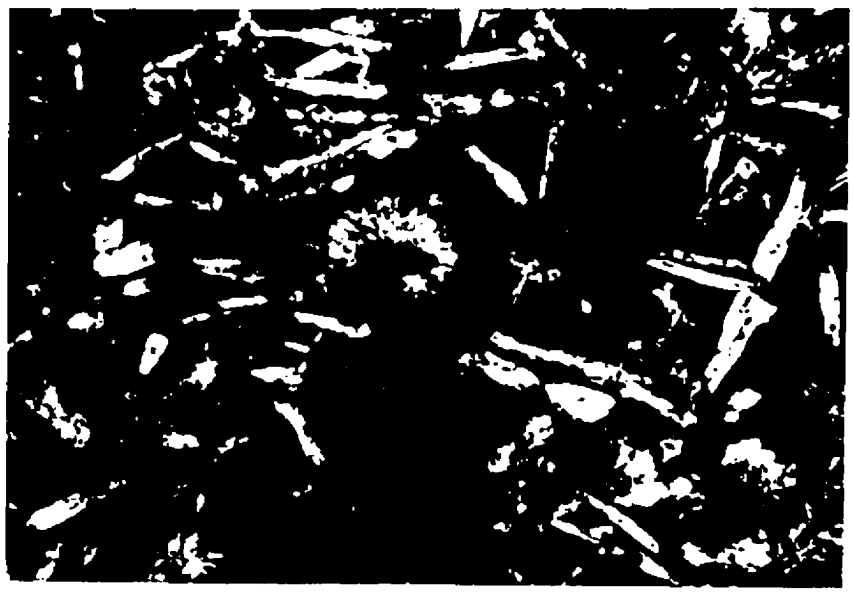

(1.3 x 0.9 mm)

Fig. 5.2.4 Groundmass green celadonite associated with radiating spheroids of chalcedony (white) (plane polarized light). Sample No. 20.11

nicol (Fig. 5.2.5). In these characteristics it differs from typical chlorite in the greenstone zone. In chemical composition chlorite in the transition zone shows higher SiO_2 and lower Al_2O_3 than chlorite in the greenstone zone (Table 5.2.1). The appearance of chlorite in this zone is a very important indicator of zone definition.

Second, amorphous silica in transition zone is different in some aspects from that of the brownstone zone. In particular, it occurs in cavities, deposited in colloform patterns. It is typically fine grained at the margins and coarse grained at the centre of cavities (Fig. 5.2.6), and is distinguishable from the small radiating spherical aggregates in the brownstone zone. Some recrystallized grains of chalcedony at the bottom of this zone show increasingly euhedral morphologies.

Zeolites are common but not abundant in the transition zone. Laumontite, heulandite, natrolite and mordenite are identified and have been reported or studied in detail by previous workers, e.g., Gillis and Robinson (1985) and Sunkel et al. (1987).

Laumontite mainly occurs in this zone and occasionally in the brownstone zone. It usually accompanies the transition minerals of the smectite/chlorite group and occurs in

(1.3 x 0.9 mm)

Fig. 5.2.5 Chlorite in the transition zone showing anomalous high birefringence with crossed nicol, differing from chlorite in the greenstone zone. The latter usually shows anomalous blue birefringence. Sample No. 10.47-E

(1.3 x 0.9 mm)

Fig. 5.2.6 Amorphous silica deposited in zone in cavities and partly recrystallized. A common phenomenon in the transition zone (with crossed nicol). Sample No. 20.31-6

cavities, rather than in the groundmass (Fig. 5.2.7). The most common occurrence of mordenite is in vesicles or vugs with minor occurrence in veins (Fig. 5.2.8). It generally occurs as fibrous aggregates in the form of hemi-spheroids. Natrolite fills vesicles and often accompanies smectite and heulandite in the brownstone zone.

Naturally occurring calcium zeolites, e.g., laumontite, are known to remain stable at higher temperatures than their alkaline counterparts. In active hydrothermal systems, laumontite begins to replace other alkali zeolites at 100°-200°C and is stable to at least 200°C (Kristmannsdottir and Tomasson, 1978). The upper temperature limit of laumontite is about 300°C at an upper pressure limit of 3.4 Kb based on experimental study (Liou, 1971).

Alkali zeolites, e.g., natrolite, heulandite and mordenite, are found to form in most low temperature hydrothermal environments (Velde,1985). Heulandite, mordenite and other alkali zeolites are seldom stable in active systems at temperatures above 100° to 120°C (Kristmannsdottir and Tomasson, 1978).

5.2.3 The greenstone zone

The definition of the onset of the greenstone zone is the

(5.1 x 3.6 mm)

Fig. 5.2.7 Laumonite prisms with well-developed cleavage occurring in cavities mostly in the transition zone (with crossed nicol). Sample No. 9.17

(1.3 x 0.9 mm)

Fig. 5.2.8 Mordenite occurring in radiating spheroids in cavities both in the brownstone and transition zones, showing a dark cross (with crossed nicol). Sample No. 21.07

disappearance of smectite and zeolite, which are common minerals in the transition zone. The greenstone zone includes the major secondary minerals quartz, chlorite, amphibole and calcite, and minor minerals epidote, albite, sphene, pyrite and magnetite.

Chlorite is the most important alteration mineral in this zone and normally constitutes 20% or more of samples. Chlorite in the zone usually occurs as large flat crystals with a typical blue birefringence, differing distinctly from chlorite in the transition zone. Experimentally, the chlorite-smectite to chlorite transition occurs at above 225°C, this result being consistent with reports from geothermal wells in Iceland, where the chlorite-smectite to chlorite transition occurs at between 200° and 240°C (Laird, 1988).

Quartz is another important secondary mineral in the greenstone zone and generally occurs at a significant level (e.g. up to and over 10%). Secondary quartz often shows euhedral forms, occurring both in cavities and in the groundmass, where it is commonly associated with chlorite and calcite (Fig. 5.2.9). It is relatively important volumetrically in the upper part of the zone.

Amphibole abundance increases with depth in this zone. Amphibole shows fibrous to prismatic morphologies.

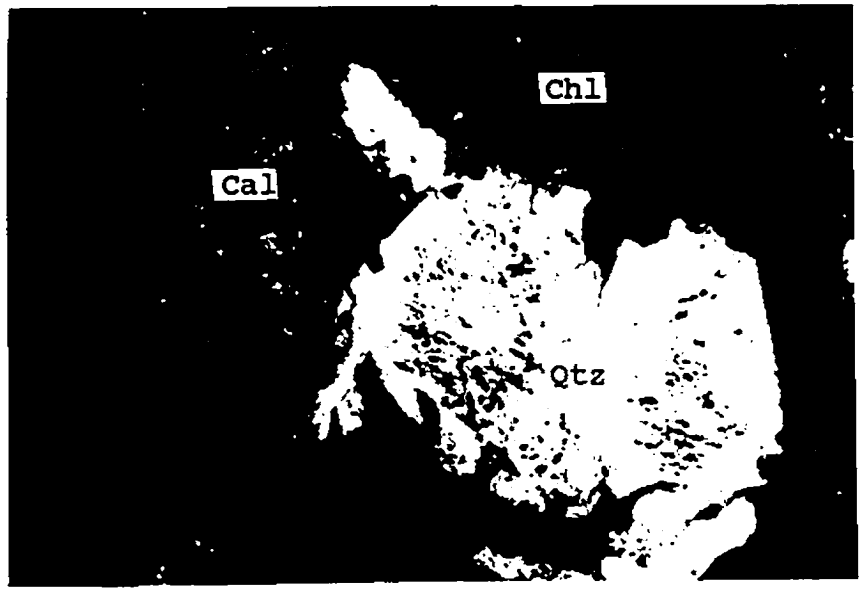

(1.3 x 0.9 mm)

Fig. 5.2.9 Large secondary quartz associated with chlorite and calcite in cavities in the greenstone zone (with crossed nicol). Sample No. 20.27

Volumetrically, it forms as much as 40% of samples, in which case the amounts of chlorite and quartz are reduced. The color of amphibole is variable, from light brownstone in the upper part of the zone to green at depth, suggesting that the composition is possibly variable. Chemically the amphibole is a type of actinolite and belongs to the low grade amphibole phase formed at temperature of 350-400°C (Winkler, 1974).

Calcite is also a very common mineral in the zone. It usually occurs in the groundmass, where it replaces plagioclase. Sphene, pyrite and magnetite are all significant secondary minerals in this zone, but albite and epidote are less important. Sphene forms at a temperature of 300°C and a pressure of 0.5 kb in the greenschist facies when the water/rock ratio is between 2 and 50 (Mottl, 1983). Epidote may begin to appear at 260°C in the greenschist facies (Liou, 1973).

Generally, quartz and associated chlorite, albite, epidote and actinolite are very common greenschist facies minerals. A reasonable temperature range for the greenschist facies is about 250°C to 450°C (Mottl, 1983; Seyfried and Mottl, 1982).

5.3 Evidence of the zonation in seven profiles

To show the existence of threefold alteration zonation, a synthetic diagram of secondary mineral vs. crustal depth is constructed for the study area. Since the central part of the area shows a relatively more regular sequence than both the east and west parts, the central 7 lines of the 18 lines between Mitsero and Kambia, extending for 15 km in the spreading direction, are considered for detailed description and discussion (Fig. 5.3.1a and b), while the data for the rest of the lines will be shown in a general map of alteration zonation in a later section of this chapter. The depth of the locations along the lines used in the diagram is obtained from emplacement anticlinal 'MODEL 2' and is listed in Appendix 6.

In the diagram (Fig. 5.3.1a), each line is divided into several intervals on the basis of secondary mineral assemblages. Numbers present in each individual assemblage in the diagram represent mineral types corresponding the 13 minerals listed in the bottom right corner of the diagram. The three alteration zones, as defined in section 5.2. based on these mineral assemblages, are readily distinguished in each of these seven sections. There are, however, substantial variations in thickness and depth for each individual zone (Fig. 5.3.1b). These three zones quite definitely have physical reality. The main features of the secondary minerals

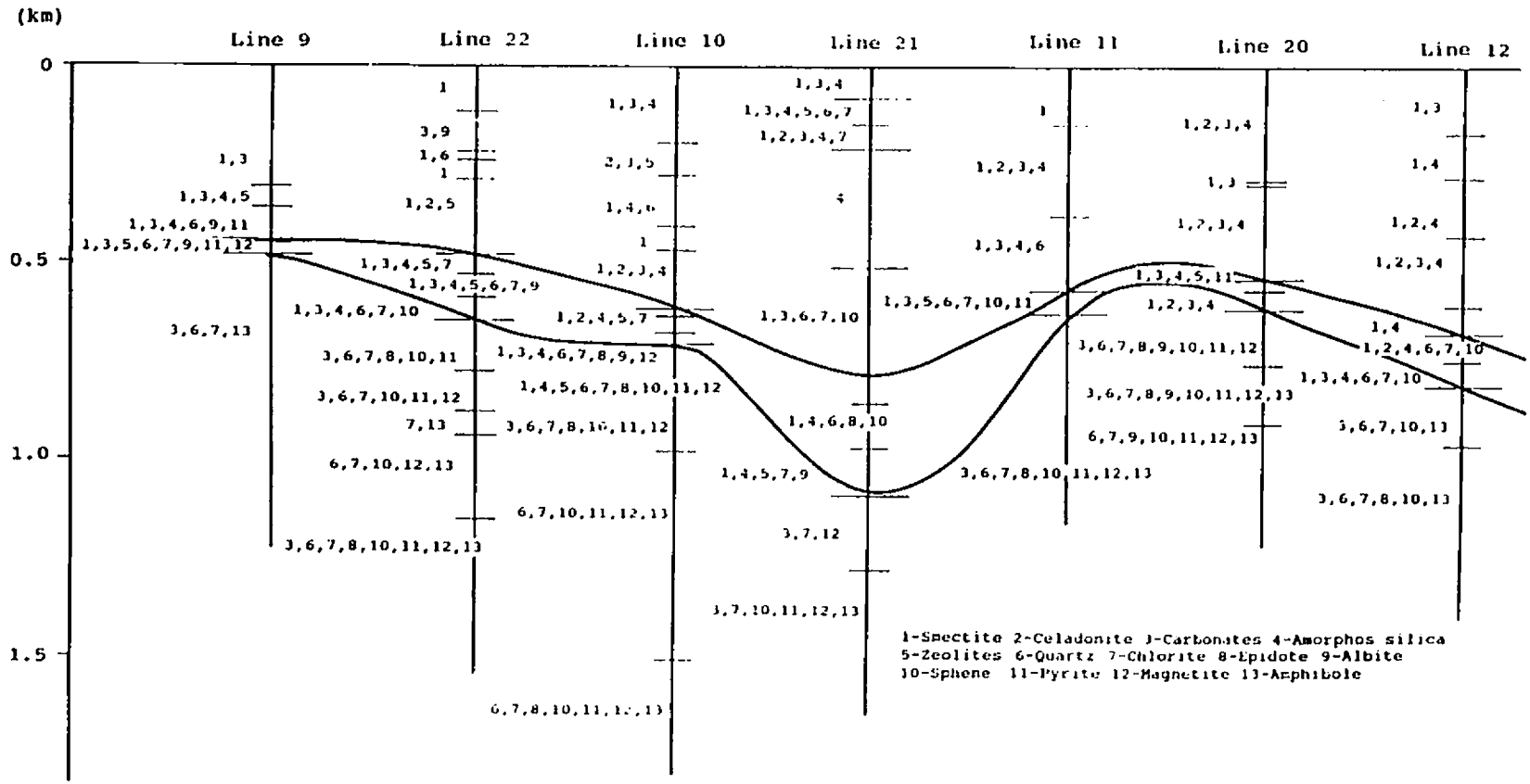

Fig. 5.3.1a Distribution of the thirteen main secondary minerals in the depth diagram.

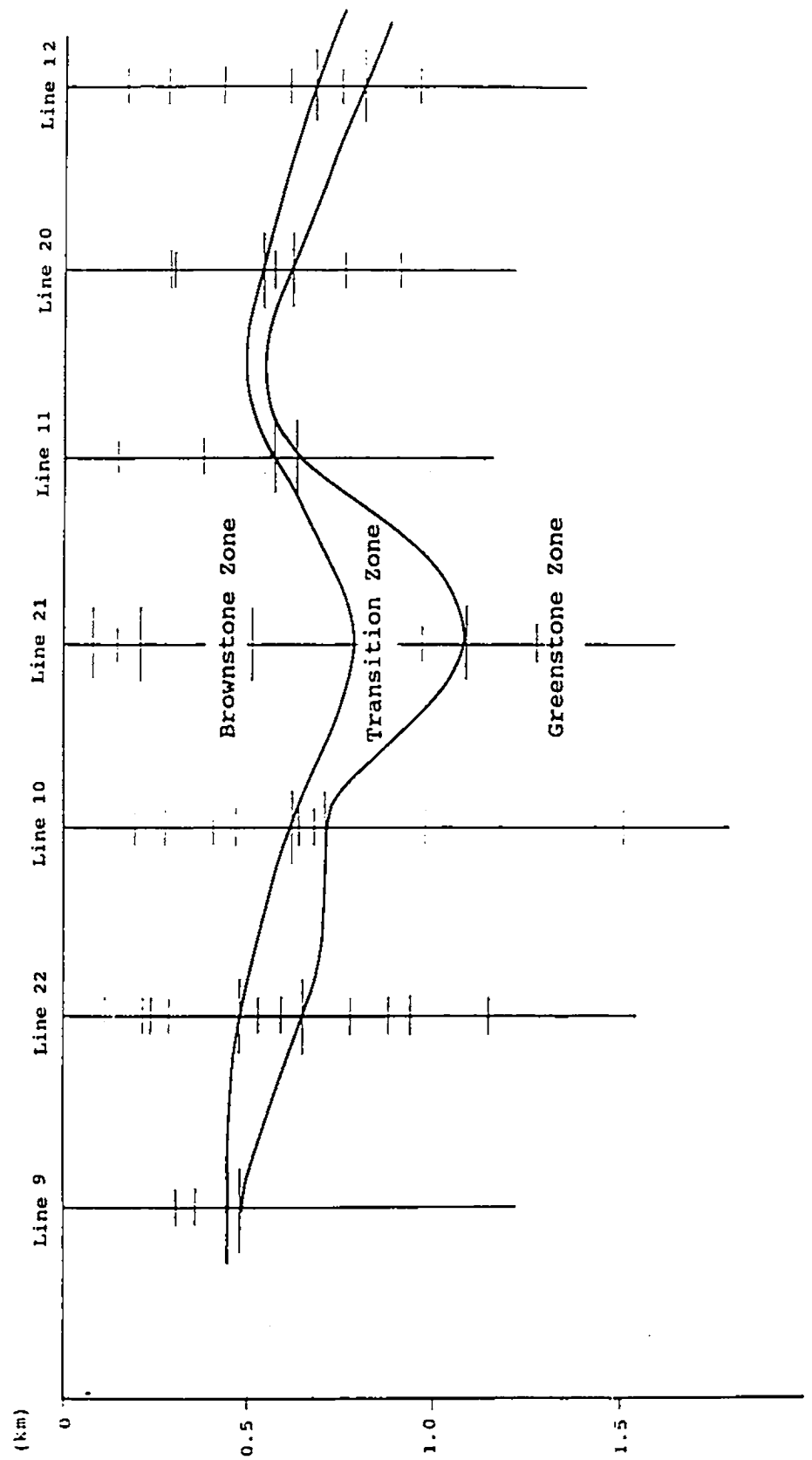

Fig. 5.3.1b Three regional alteration zones, showing depth and thickness variation, are recognizable in the depth diagram.

in each zone have been described above. The only exception to the simple pattern is in the section of Line 21, where the mineral-mixed zone appears two times: one is within the brownstone zone and the other is the transition proper between the brownstone and greenstone zones. The shallower occurrence is possibly controlled by variation in local conditions and will be discussed in the next section of this chapter.

Since three basic alteration zones are recognized based on the types of alteration minerals present, the question now arises as to how representative are the minerals which are used in the diagrams? In other words, how reliable are the diagrams of secondary mineral vs. crustal depth?

The reality of the regional zonation of alteration minerals is determined by the relationship between the density of sampling and the apparent occurrence of alteration zones. First, the distribution of samples shows that most adjacent samples have a separation of less than 100 m between them in depth, and that there are always at least several samples within each zone. Therefore, the possibility can be eliminated that a generally low abundance of unevenly distributed samples has resulted in an apparent zonation. Again, zones generally show regional extent, further supporting their existence. Although in the seven profiles some minerals may occur preferentially in a certain lithology, e.g., zeolites (among

16 occurrences, 56% in pillowed lava flows (PL), 25% in sheet lava flows (SF) and 19% in dikes) and celadonite (among 51 occurrences, 88% in SF, 8% in PL and 4% in dikes), however, all alteration minerals have been found in all lithologic types. On the other hand, although differences exist between the distributions of lithologic types and alteration minerals, the various alteration minerals involved all belong to the same group or assemblage and the existence of an alteration mineral group is thought to be of much more significance than the absence or presence of a particular alteration mineral.

In addition, within these three regional alteration zones, some interesting features appear. First, in the brownstone zone, the mineral assemblage (Ce + Sm ± Cal ± Si) extends horizontally through 6 of the 7 lines and usually has a considerable thickness, suggesting the possible recognition of a regional seawater penetration level. In three lines, 10, 20 and 12, celadonite reappears at a relatively deep level (see Fig. 5.3.1), suggesting the lateral movement of seawater at the levels of the deeper occurrences.

In the transition zone, a generally shallower zeolite-bearing assemblage, i.e., laumontite and /or mordenite occur in 6 of the 7 lines (see Fig. 5.3.1), suggesting an association with relatively low- temperature hydrothermal alteration. Zeolites also show isolated distributions in the

brownstone zone on lines 10 and 21 (See Fig. 5.3.1), where they accompany chlorite and show the features of the transition zone. These occurrences are possibly correlated with a heat source provided by a local high level of dike intrusion (see further discussion below).

In the greenstone zone, although various mineral assemblages can be separated on each individual line (See Fig. 5.3.1), amphibole is usually absent in the upper part of the zone and present in the lower part, suggesting that either the temperature of hydrothermal alteration increased with depth or that the availability of water decreased with depth.

It might be possible to recognize other very local features by the presence or absence of some alteration minerals. However, these only occur on one or two lines within a limited area rather than having a regional extent. Therefore, they possibly indicate some very local variation in alteration conditions. However, since these local variations may involve a certain degree of accidental association (including, for example, in low sample densities, lithological constraints, etc.), they are perhaps only of interest for further more detailed studies of alteration and are of less significance for a discussion involving broad regional alteration zoning and crustal construction. Gillis (1986) has recognized five or six alteration zones locally within some

parts of the larger study area of this thesis and which, in this context, are of local rather than regional significance.

5.4 Relationships between alteration zonation and dike abundance

The three regional alteration zones, based on data from all 18 lines, are plotted on an F contour map in Figure 5.4.1. An immediately obvious and very interesting feature of this map is that the boundaries of three alteration zones are closely coincident with different contours of dike abundance. That is, in general, the brownstone alteration interval is restricted to very low dike densities, usually $F \leq 0.25$, while the transition zone generally lies within the $0.25 \leq F \leq 0.5$ interval and the greenstone zone begins at $F \approx 0.5$.

For a more quantitative expression of these relationships, a set of fourteen cross sections were drawn on the map which cover the major part of the study area (Fig. 5.4.2). The eastern part of the area was not included in the analysis both since the lower part of the Extrusive Sequence is not exposed due to relatively less erosion and the inapplicability of MODEL 2 to the area. Thickness calculations were carried out, based on MODEL 2, for F contours and alteration zones along the 14 cross sections (Table 5.4.1). The average depth of the F0.25 contour on these lines is 0.52

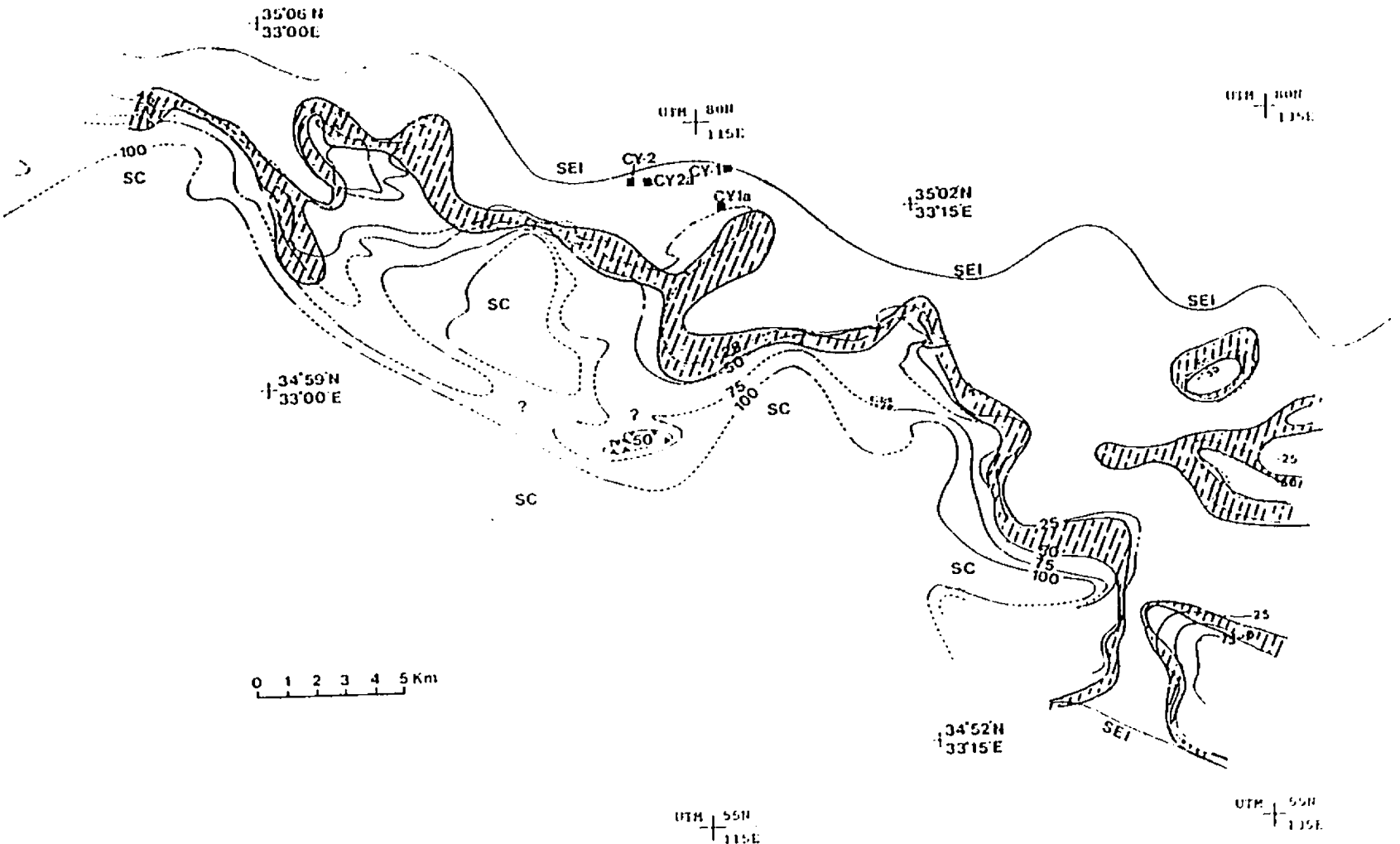

Fig. 5.4.1 The three regional alteration zones showing a good spatial correlation with dike density contours, F. Shaded area is the location of the transition zone, above it is the brownstone zone, and below it is the greenstone zone.

Fig. 5.4.2 14 cross sections chosen to evaluate the relationship between boundaries of alteration zones and dike density contours.

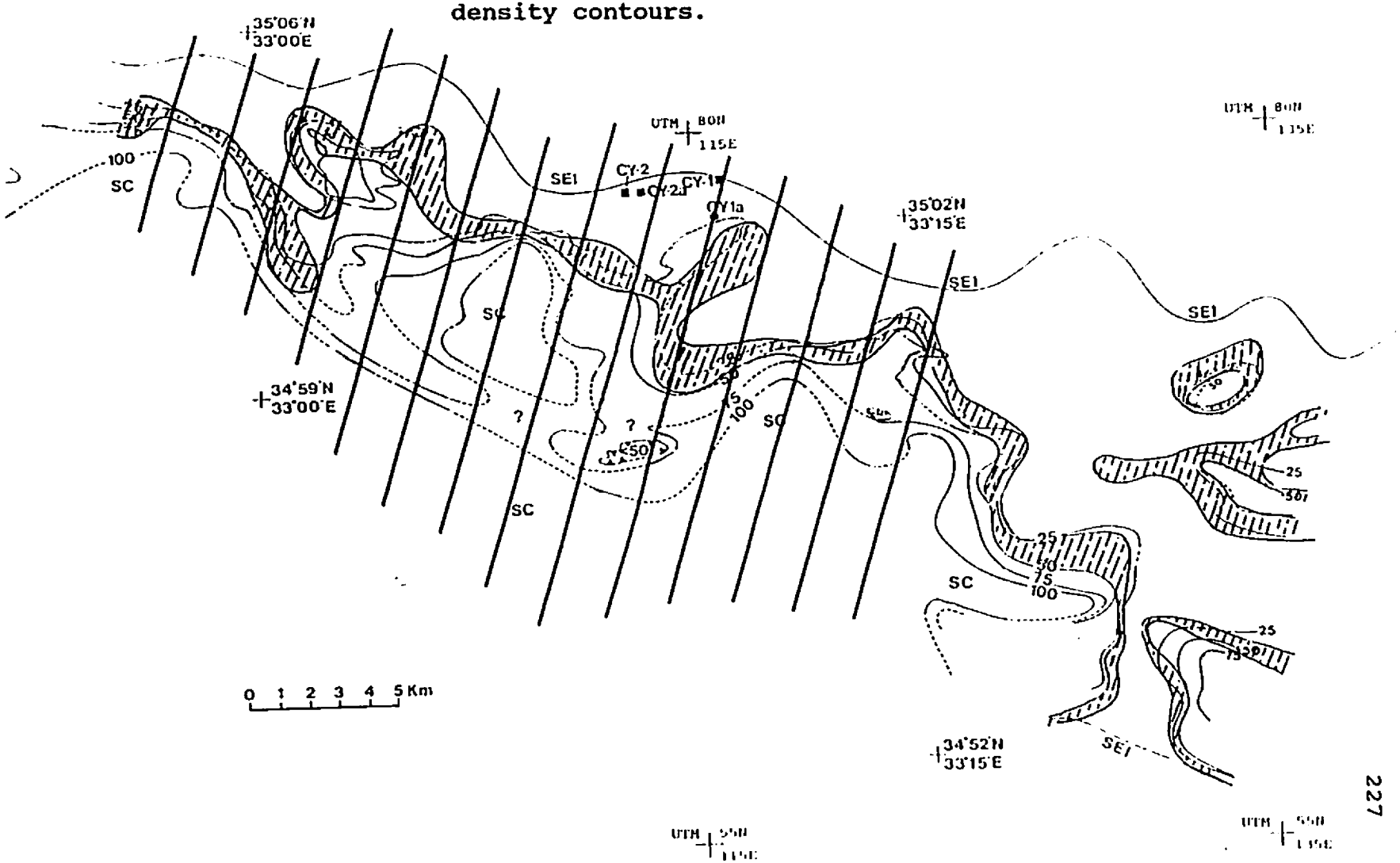

Table 5.4.1 Depth of F Contours and Boundary of Alteration Zones

Line	F0.25	Transision	F0.5	Greenstone
201	0.50(km)	0.47(km)	0.53(km)	0.53(km)
202	0.57	0.58	0.58	0.60
203	0.28	0.25	0.97	1.02
204	0.31	0.31	-	-
205	0.08	0.10	-	-
206	0.61	0.55	0.64	0.67
207	0.44	0.44	0.47	0.46
208	0.51	0.48	0.54	0.65
209	0.50	0.41	0.56	0.53
210	0.80	0.71	1.08	1.08
211	0.78	0.71	0.74	0.74
212	0.58	0.58	0.61	0.62
213	0.51	0.51	0.59	0.59
214	0.35	0.33	0.46	0.41

1) Line: locations see Fig. 5.4.2; 2) F0.25: means depth from seafloor to F0.25 contour surface; 3) Transition: depth from seafloor to boundary of transition zone.

±0.21 km, while the average depth of boundary between the brownstone and transition zones is 0.48 ±0.17 km. The two groups of depths have a coefficient of linear correlation coefficient r=0.986 (Fig. 5.4.3). For the F0.5 contour and boundary between the transition and greenstone zones, 12 of the 14 cross sections provide the depth of F0.5 of the upper and boundary of the greenstone zone. The average depth of the F=0.5 contour between lines is 0.65 ±0.19 km and of the alteration boundary is 0.66 ±0.15 km. The data for the 12 cross sections give a linear correlation coefficient of r=0.981, between the F0.5 contour and the boundary of greenstone zone (Fig. 5.4.4).

Some locally isolated areas of higher dike abundance (F0.25 to F0.5) in the eastern part of the area exactly correspond to isolated areas of the expected relevant alteration zones. These occurrences may reflect the variation of dike abundance along the spreading axis.

These features of the distribution of hydrothermal alteration zones and their correlation with the abundance of dikes are likely to be of considerable significance in the construction of oceanic crust. It was previously thought (e.g., Cann et al., 1985) that a magma chamber beneath the Sheeted Complex provided heat for the hydrothermal circulation and consequent alteration of the newly formed oceanic crust.

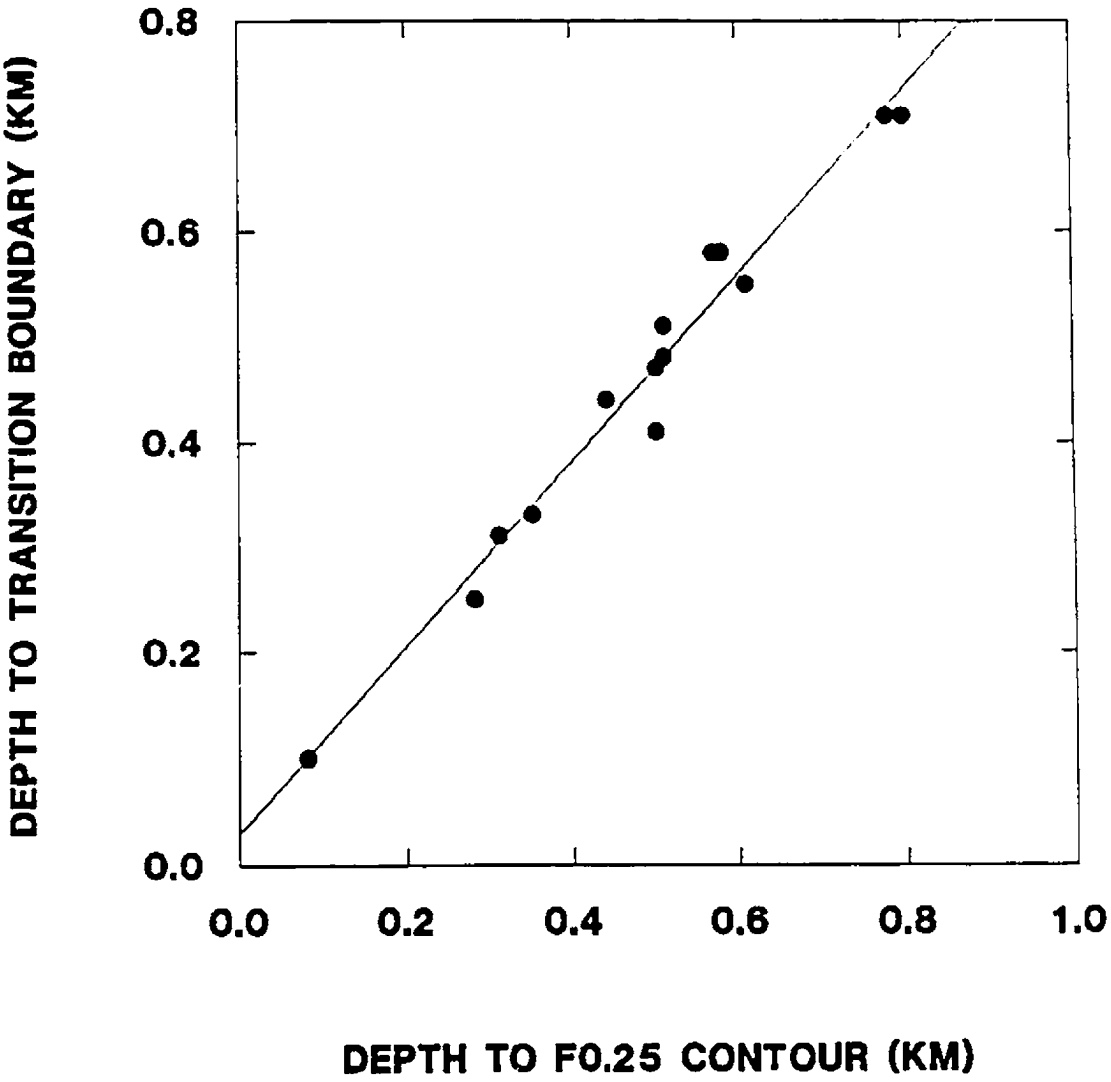

Fig. 5.4.3 The depth of the boundary between the brownstone and transition zones correlated with the F=0.25 contour.

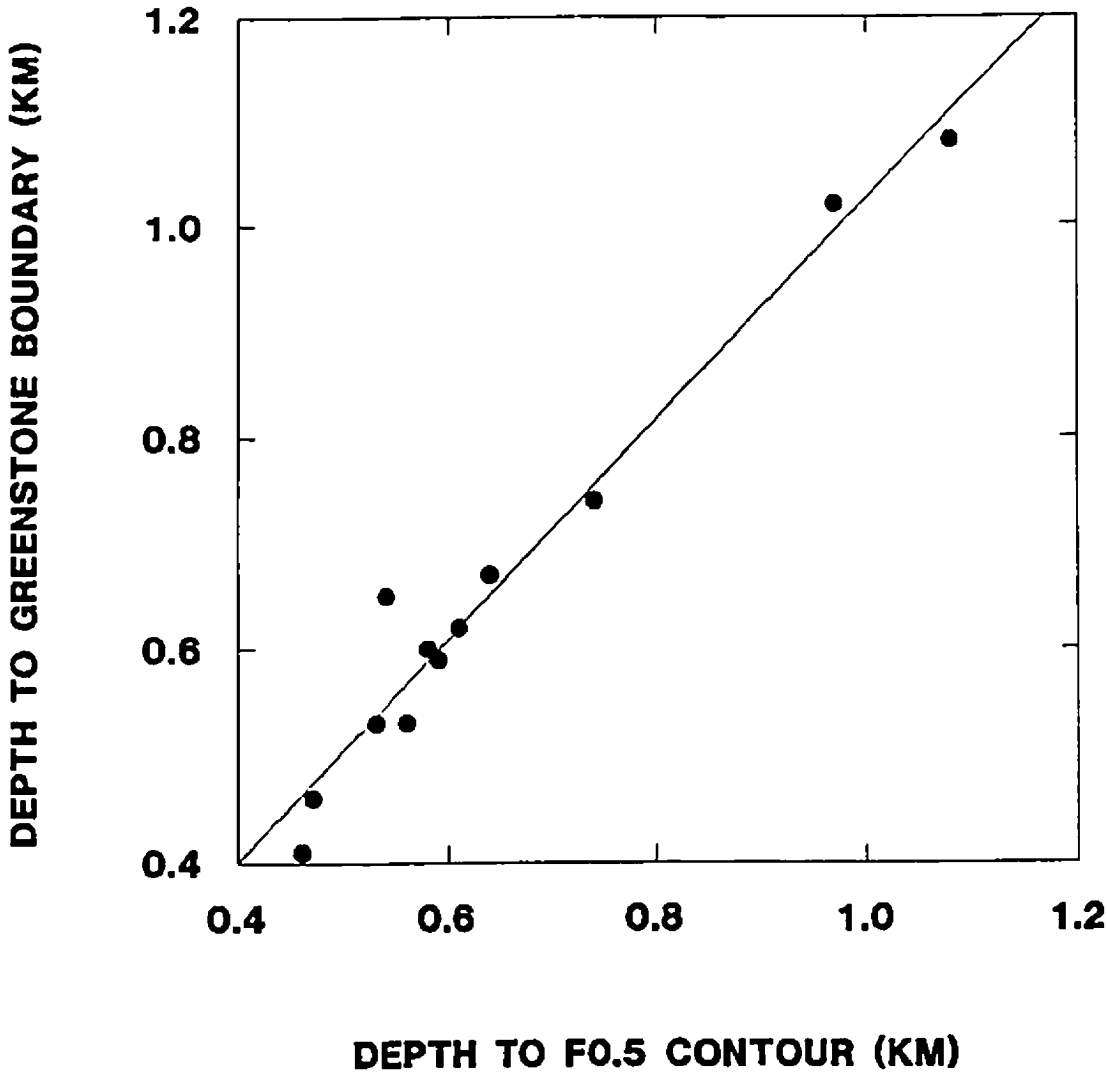

Fig. 5.4.4 The depth of alteration boundary between transition and greenstone zone correlated with the depth of the F=0.5 contour.

However, these new results show that the alteration zoning has instead a remarkably close relationship with dike abundance. There is no report showing the same high degree of spatial correlation with any postulated deep magma chamber. An important question here is whether the sheeted dikes themselves were able to provide all the necessary heat for the hydrothermal alteration, or only a part of it.

The thermal gradient in the different alteration zones appears to be closely related to or controlled by dike abundance. The known stability ranges of the alteration minerals are summarized in Fig. 5.4.5. The secondary minerals of the brownstone zone, such as smectite, celadonite, calcite, chalcedony and various zeolites, show a common low temperature range for their formation of from close to 200°C down to 0°C. Secondary minerals in the transition zone, such as laumontite, calcite by replacement, quartz and albite indicate a temperature range of between 200° and 300°C. The secondary minerals in the greenstone zone indicate a temperature range of 200°-450°C. Thus the variations of hydrothermal alteration temperature are controlled by dike abundance. A similar conclusion was obtained by Schffman and Smith (1988), that they believe that the seawater system resposible for Solea graben massive sulfide deposits was probably driven by hypabyssal intrusions, i.e., heat from dikes.

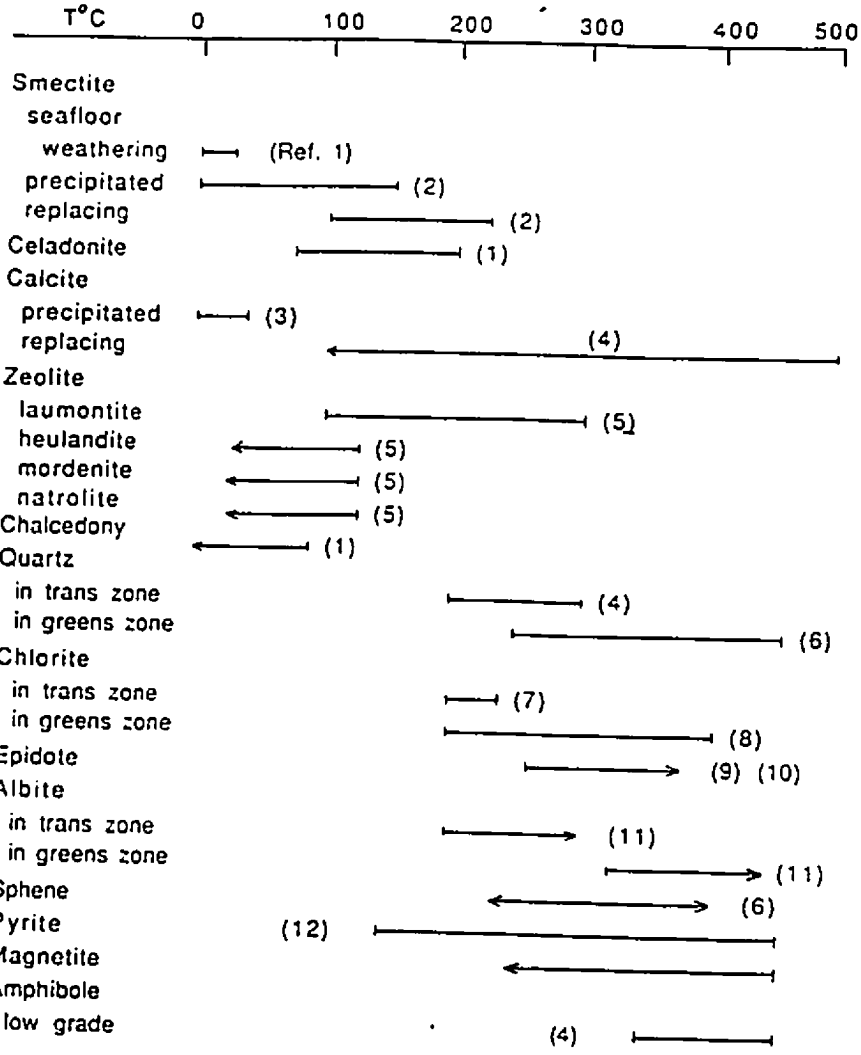

Fig. 5.4.5 Formation and stable range of temperatures of secondary minerals. Refs: 1- Velde, 1985; 2- Güven, 1988; 3- Deer et al., 1966; 4- Winkler, 1974; 5- Kristmannsdottir, 1978; 6- Mottl, 1983; 7- Laird, 1988; 8- Franzson et al., 1986; 9- Cho and Liou, 1987; 10- Liou, 1973; 11- Liou, 1971; 12- Barton and Skinner, 1967.

The new results are different from those of some relevant previous work in several aspects. Coleman (1977), based on work on the Troodos ophiolite by Gass and Smewing (1973), and other ophiolite data, proposed a model of alteration zoning with depth, that is, zeolite facies assemblages are present in the Extrusive Sequence, while greenschist facies assemblages are restricted to the Sheeted Dike Sequence. The new results indicate that: 1) there are three regional alteration zones in the Extrusive Sequence of the ophiolite, instead of one or two as recognized previously; 2) the greenstone alteration zone (largely equivalent to the greenschist facies assemblage) begins to appear at a level close to that of the F=0.5 contour in the Extrusive Sequence rather than at the upper boundary of the Sheeted Dike sequence. It is noted that in the Macquarie island ophiolite the greenschist facies also appears in the pillow lava sequence at ~ 1 km below the Sedimentary/ Extrusive boundary (Cocker et al., 1982).

Chapter 6 Distribution and Preservation of Sulfide Deposits

6.1 Introduction

Ophiolitic massive sulfide deposits are extensively developed in the Troodos complex in Cyprus and appear to be a characteristic feature of ancient oceanic crust everywhere. These deposits show similarities to the sulfide deposits discovered at present mid-oceanic spreading ridges (Constantinou, 1980; Francheteau et al., 1979; Hekinian et al., 1980; Koski, 1987). The Troodos sulfide deposits have been considered typical products of the process involving sea water circulation through oceanic crust leading to the formation of sulfide deposits and metalliferous sediments (e.g., Oudin et al., 1981; Richards and Boyle, 1985).

The history of the mining and mineral industry in Cyprus goes back to prehistoric times, not only to Roman and Phoenician times, but many centuries earlier during the Bronze Age (Bear, 1963). Some sulfide deposits mined in ancient times can still be recognized today by the existence of pits and slag heaps, but some probably cannot, and, also, we cannot estimate how many deposits have been lost by erosion or remain undiscovered. Based on previous publications on sulfide deposits and mineralization in Cyprus, a total of 34 sulfide deposits and 93 mineral prospects are known at present in the

Troodos ophiolite (references listed in Table 6.2.1). The study of the sulfide deposits in this thesis is aimed at determining their distribution and spatial relationships with constructional features of the oceanic crust of the ophiolite. In this chapter the general features of these sulfide deposits and mineral prospects will first be briefly described and then their relationships to other crustal construction processes and a model for their preservation will be discussed.

6.2 General features

The location map of Fig. 6.2.1 shows the sulfide mineralization of the ophiolite with the exception of one deposit and five mineral prospects which are located in the Troulli Inlier to the east of the main map (see insert). The size of the deposits varies from about 45,000 to 16,000,000 tons and the average copper content ranges from less than 0.5 to over 4.5 per cent with local zinc enrichment (Constantinou, 1980). The characteristic features of the 34 deposits are given in Table 6.2.1 and Figure 6.2.2.

Generally, the Cyprus deposits occur as irregular, elongate lenticular or lens-shaped bodies of massive sulfide ore. The sulfide mineralization is mainly confined to the upper part of the Extrusive Sequence, forming, in different places, massive and disseminated copper and iron pyrite

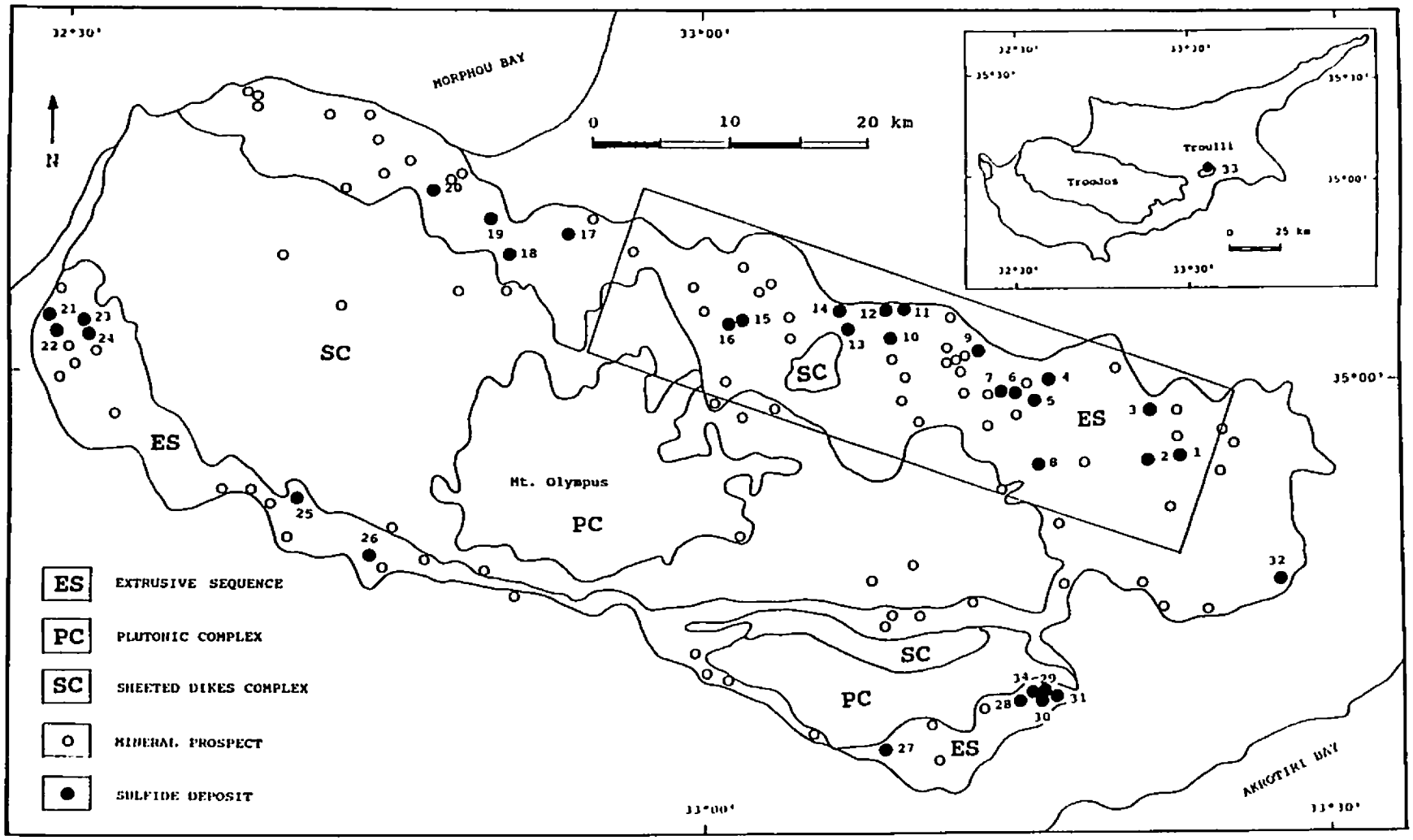

Fig. 6.2.1 Distribution of sulfide deposits and mineral prospects of the Troodos ophiolite (after Geological survey Department of Cyprus, 1982).

Table 6.2.1 ESSENTIAL CHARACTERISTICS OF KNOWN SULFIDE DEPOSITS OF THE TROODOS OPHIOLITE

No.	Name of Deposit	Tonnage (mt)	Grade (%)	Locat.	Refer.
1	Sha	0.35	Cu 0.5-1.2, S 25-30	LPL	1,7
2	S. Mathiati	Unknown	Unknown	LPL	1
3	N. Mathiati	2.8	Cu 0.24, Zn 1.0, S 33	LPL	1,3,5, 6,7,8, 9,10, 11,12
4	Kambia	1.5	S 25-35	LPL	7,1
5	Kapedhes	0.05	Cu <0.5, S 30-35	LPL	1,4
6	Peristerka	0.3	Cu 2.0, Zn 5, S 45	BG	1,2
7	Pytharokhoma	2.25	Cu + Zn 0.5, S 20	LPL	7
8	Lythrodhonda	1.0	S 25	LPL	1
9	E. Klirou	0.5	Cu1.0, Zn1.3, S 22	LPL	15,2
10	S. Agrokipia	<0.5	Zn 2.0, S <40	LPL	2
11	Agrokipia (B)	0.29(Hi) 4.21(Lo)	Cu 4.0, Zn 8-9, S 40	LPL	5,1 ,7
12	Agrokipia (A)	0.77	Cu 1.0, S 30-40	UPL	5,1
13	Kokkinopezoula (Mitsero)	3.5	S 24	UPL	7,1
14	Kokkinoyia	>1.0	Cu1.5, S30	UPL	5,1
15	Memi	1.5	S 26	LPL	1,10, 7,15
16	Alestos	1.5	Cu 1.0, S <40	LPL	2,15
17	Skouriotissa	6.0	Cu 2.25, S 48	UPL	1,3,5, 6
18	Apliki	1.65	Cu 1.8 S 36	LPL	1,15
19	Mavrovouni	15.0	Cu 4.0, Zn 0.5, S 47	UPL	1,3,15

20	Ambelikou	0.016	Cu 1.0 S 45	UPL	1,15
21	Limni	16	Cu 1.0, Zn 0.3, S 14	LPL	15,1, 3,13
22	Evloymeni	<0.5	Cu 1.0, S <40	LPL	1,2
23	Kynousa(Under)	0.3	Cu 2.37, Zn 3.37,S 43.6	LPL	1,15
24	Uncle Charles	0.22	Cu 2.2, S 47	LPL	1,15
25	W. Troodos	<0.5	Cu 1.0, Zn 1.0, S >40	BG	2
26	Peravasa	0.1	Cu 0.75, S 30	UPL	1
27	Maghaleni	<0.5	Cu 2.0, Zn 0.5, S <40	UPL	2
28	Platies	0.045	Cu 2.5-3, S 46	LPL	1,10
29	Lantaria	0.2	Cu 0.5, S 25-35	LPL	1,10
30	Kalavasos (Mavridia)	4.8	Cu 0.5-2.5, S 25-45	LPL	1,6,10
31	Petra	0.5	Cu1.5-2.5, Zn1.5,S35.5	LPL	1,10
32	S. Stavrovauni	<0.5	S <40	LPL	2
33	Troulli	0.05	Cu 1.0, S <40	LPL	1
34	Mavri Sykia	0.35	Cu 1.5-2.5, S 25-45	LPL	1,10

References: 1) Bear, 1963; 2) Geological Survey Department, Cyprus, 1982; 3) Searle, 1972; 4) Robertson and Hudson, 1974; 5) Constantinou and Govett, 1973; 6) Constantinou and Govett, 1972; 7) Richards et al., 1989; 8) Lydon and Galley, 1985; 9) Constantinou, 1980; 10) Pantazis, 1967; 11) Lydon, 1984a; 12) Lydon, 1984b; 13) Spooner, 1980; 14) Boyle and Robertson, 1985; 15) Adamides, 1987.

Fig. 6.2.2 Reserve vs Cu, Zn, S contents (Wt%) of the Troodos sulfide deposits (References see Table 6.2.1).

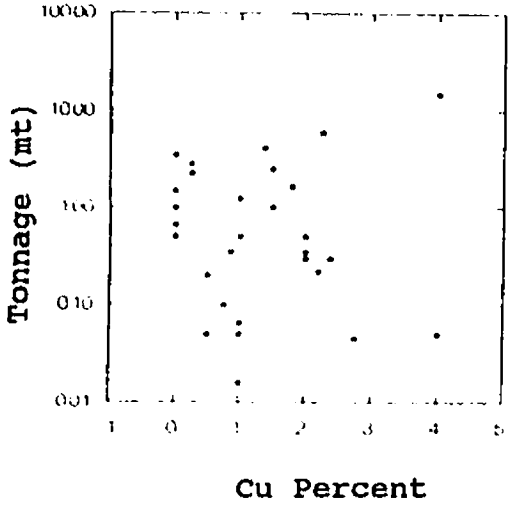

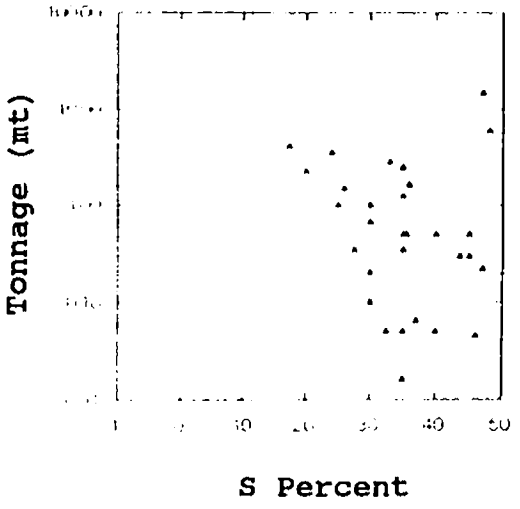

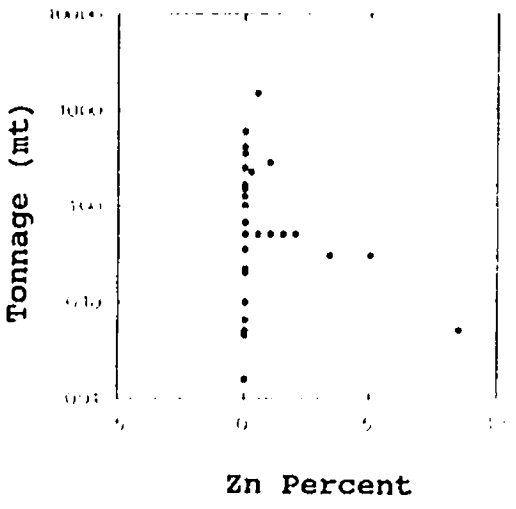

orebodies; small-scale sulfide mineralization is found in the BG and Sheeted Dikes. Formerly, the bodies were believed usually to occur close to the contacts of the BG with the LPL, the LPL with the UPL, or the UPL with the overlying sediments, and that they were restricted to structural lows and accumulated on the sea floor before the first sediments were deposited, or are overlain by pillow lavas and sediments (Searle, 1972; Constantinou, 1980; Adamides, 1987). However, the Cyprus sulfide deposits were not confined to topographic depressions on the seafloor but also formed on the steep slopes of fault scarps, e.g., the Mathiatis deposit (Lydon, 1984).

Hydrothermal vent fragments have been identified in the brecciated ore from the massive sulfide deposits of the Troodos complex (Oudin and Constantinou, 1984). The mineral associations, textures and zonation of the sulfide deposits in Troodos are similar to those observed in recently discovered hydrothermal vents forming on the ocean floor near the East Pacific Rise (Francheteau et al., 1979; Spiess et al., 1980), the Galapagos ridge (Malahoff, 1982), and the Juan de Fuca ridge (Normark et al., 1983; 1987; Kappel and Franklin, 1989). Comparisons of the mineralogy and texture of Cyprus ores with those of EPR deposits confirm that both were formed at or a little below the sea water-basalt interface as the result of hydrothermal circulation in the oceanic crust near a ridge

axis (Oudin and Constantinou, 1984). Geochemical and isotopic data support this conclusion (e.g., Spooner, 1980).

It is a characteristic of the Troodos ophiolite that the Extrusive Sequence is immediately overlain in many places by a variable thickness of ferromanganoan oxide rich sediments known as umber (Robertson, 1975). There also exist thinner, often discontinuous horizons of inter-lava umber within the Extrusive Sequence (Adamides, 1980). Ochre is another "interlava" metalliferous oxide sediment, which is restricted to the upper levels of certain exhalative massive sulfide deposits. The sulfides on Cyprus exhibit primary brecciation textures in the upper part and are massive in the lower part. The massive sulfide ores are underlain by a stockwork zone which consists of mineralized and hydrothermally altered lavas extending to considerable depths.

6.3 Stratigraphic occurrence of sulfide deposits

As mentioned in Chapter 2, the Extrusive Sequence traditionally has been divided into an upward directed succession of Basal Group (BG), Lower Pillow Lavas (LPL) and Upper Pillow Lavas (UPL) (e.g., Wilson and Ingham, 1959; Carr and Bear, 1960; Pantazis, 1967).

According to the traditional division, all 34 sulfide

deposits occur within the Extrusive Sequence (see Fig. 6.2.1), with 7 in the UPL, 25 in the LPL and 2 in the BG (Fig. 6.3.1) (see Table 6.2.1 for the detailed data and references). In contrast, the 93 mineral prospects, i.e., locations of mineralization (Bear, 1963), are distributed with 14 in the UPL, 21 in the LPL, 45 in the BG, 12 in the Sheeted Dikes and one in the Gabbro (Fig 6.3.2), based on the Geological Map of Cyprus (Geological Survey Department of Cyprus, 1979). Although there are no strictly defined boundaries between the UPL and LPL and between the LPL and BG, as mentioned previously (Chapter 2), from the available data shown in Table 6.2.1, there seems to be little doubt that mineralization may occur anywhere within the volcanic sequence, but the most favourable position for the larger and richer orebodies is in the upper levels (UPL + LPL) of the Extrusive Sequence (see Table 6.2.1 for references).

Boyle and Robertson (1984) mapped an area of the eastern Troodos massif in detail to identify stages of volcanism, faulting, and sulfide mineralization. The field relations and comparisons with modern spreading ridges suggest that the pillowed and massive flows making up most of the lava volume in the area were erupted on a relatively flat sea floor at the axis of a well-defined median valley. They inferred that the Mathiati massive sulfide formed in the vicinity of ridge-parallel fractures towards the margins of the rift valley.

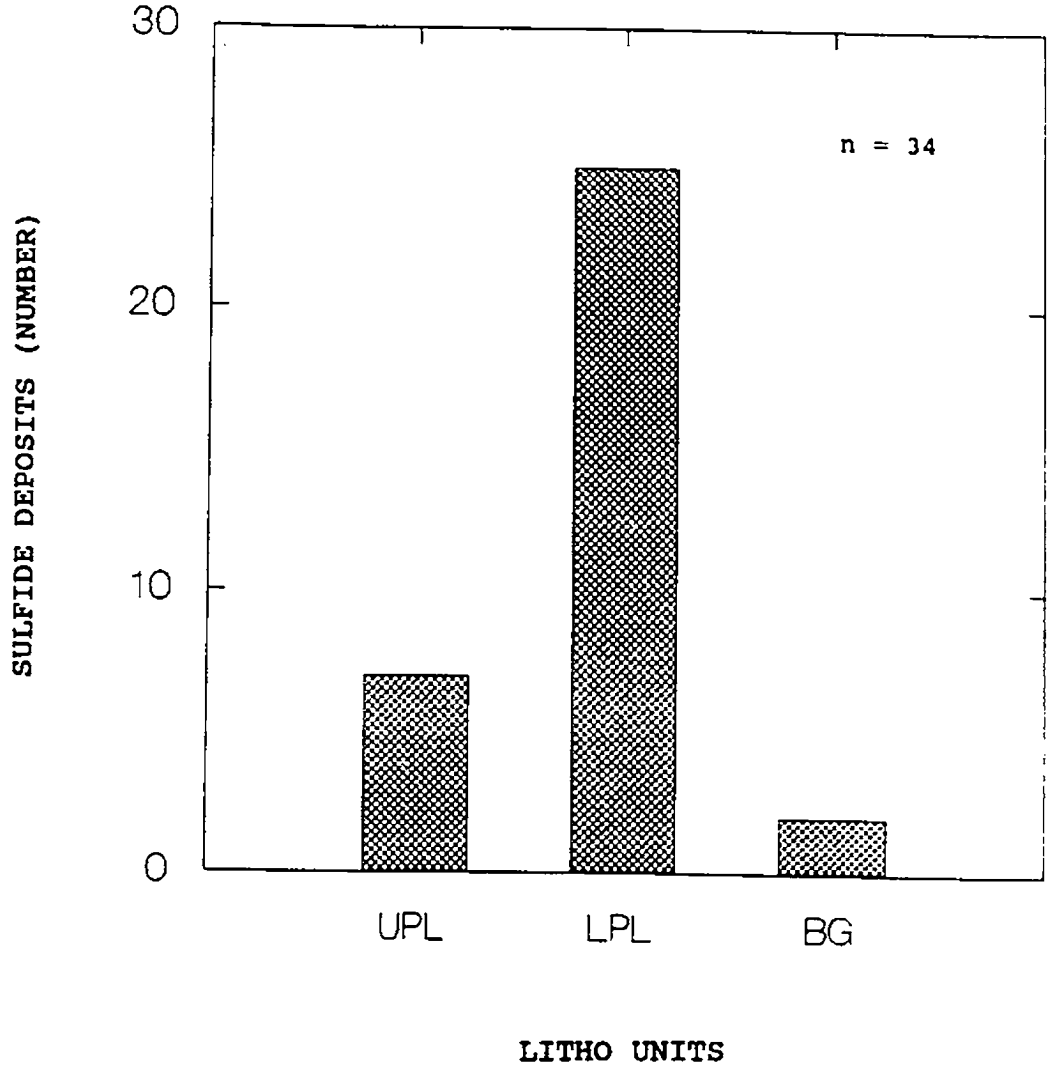

Fig. 6.3.1 Histogram shows sulfide deposits distributed in the each of the traditional divisions of the Extrusive Sequence. Note that by far the largest number are located within the Low Pillow Lavas.

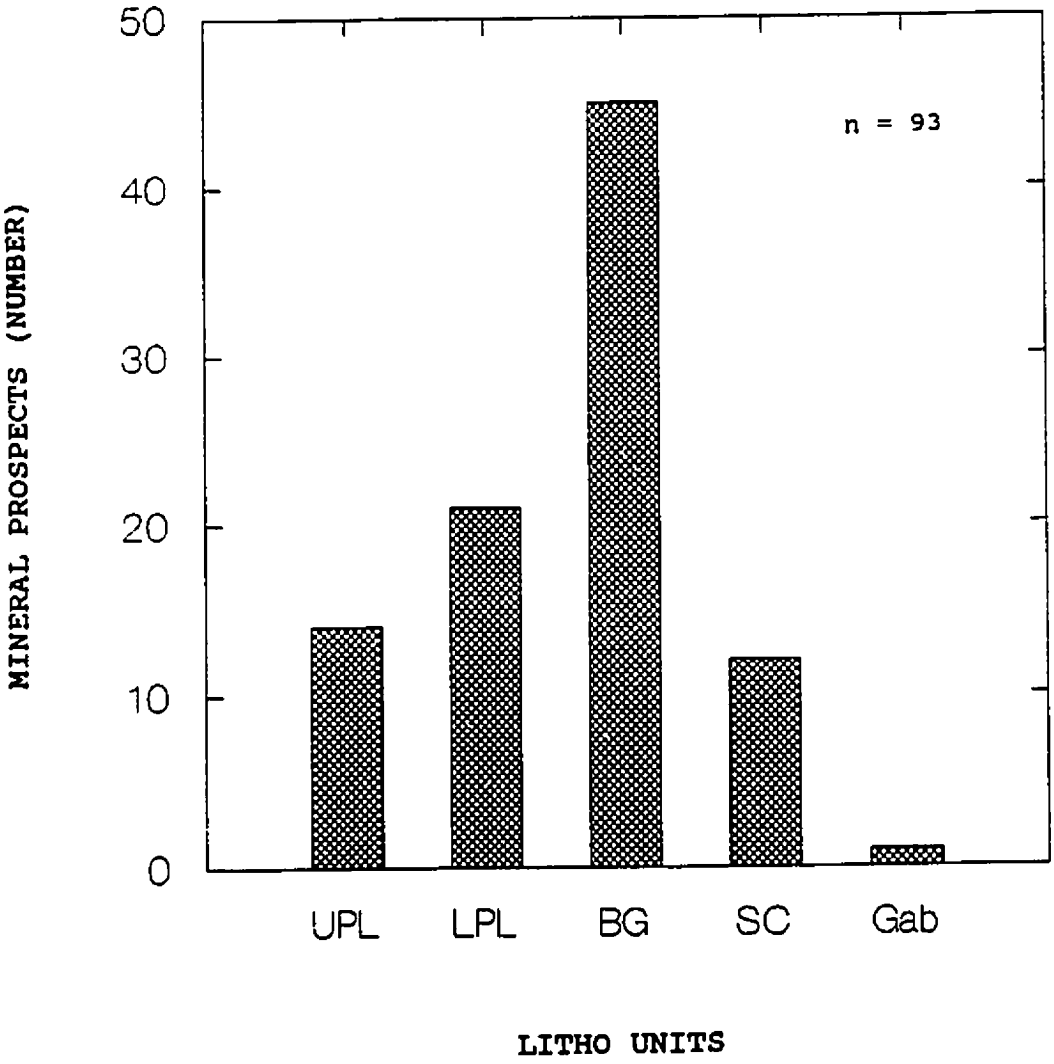

Fig. 6.3.2 Histogram showing the highest percent of mineral prospects, i.e., mineralised occurrences, in the traditional BG (approximately equal to the lower part of the Extrusive Sequence).

This observation is consistent with the mode of formation of black smoker deposits observed on present seafloor, where normal faults parallel to the ridge axis and near-axis seamounts are structurally favorable environments for metallogenesis (Koski, 1987).

On the other hand, it was inferred by Adamides (1987) that faults were not the major determining factor in ore deposition in Cyprus. Some Cyprus deposits (e.g., Agrokipia and Mitsero) apparently formed in unfaulted areas. Elsewhere, however, faults are believed to have acted as the passive recipients of hydrothermal fluids whose circulation is triggered by deeper seated heat sources. Where faulting was active the ore fluids reached the ocean floor and exhalative deposits formed. Where faulting was negligible, ore deposition took place within the lavas (Adamides, 1987).

6.4 Relationships to crustal construction

It has been noted (e.g., Constantinou, 1980; Spooner, 1980; and Hall et al., 1989) that the Cyprus sulfide deposits occur as clusters of two to four or more orebodies in several separated mining districts scattered throughout the Extrusive Sequence. Based on the 1:250,000 mineral resources map of Cyprus (Department of Geology of Cyprus, 1979), several spatial sulfide deposit and sulfide mineralization zones in

Troodos can be recognized with an average spacing in the spreading direction of 13 ±3 km (1sd) (Fig. 6.4.1), the same spacing of other crustal constructional features. This apparently simplified distribution may be the result of quite complex processes. However, it at least suggests that there is a spatial relationship between the distribution of sulfide mineralization and crustal construction.

There are 16 sulfide deposits in the study area (see Fig. 6.2.1 and Table 6.2.1). Among them, 13 were mined or are being mined (e.g., the Memi deposit) and the field relationships of these deposits can be observed from their mine pits. The other three are underground, non-producing deposits which are only indicated on the mineral distribution map and their field relationships can not be observed. The only available information on the mode of occurrence of these three underground deposits is from Adamides (1987). He mentions that drilling in the South Agrokipia deposit disclosed that the mineralization is weak and pyritic, but with locally high zinc content, and the Klirou deposit is similar to it. In these circumstances, only the 13 mined sulfide deposits are large and well known enough to warrant inclusion in a search of relationships between the orebody distribution and crustal construction. These 13 are plotted on an F contour map base (Fig. 6.4.2).

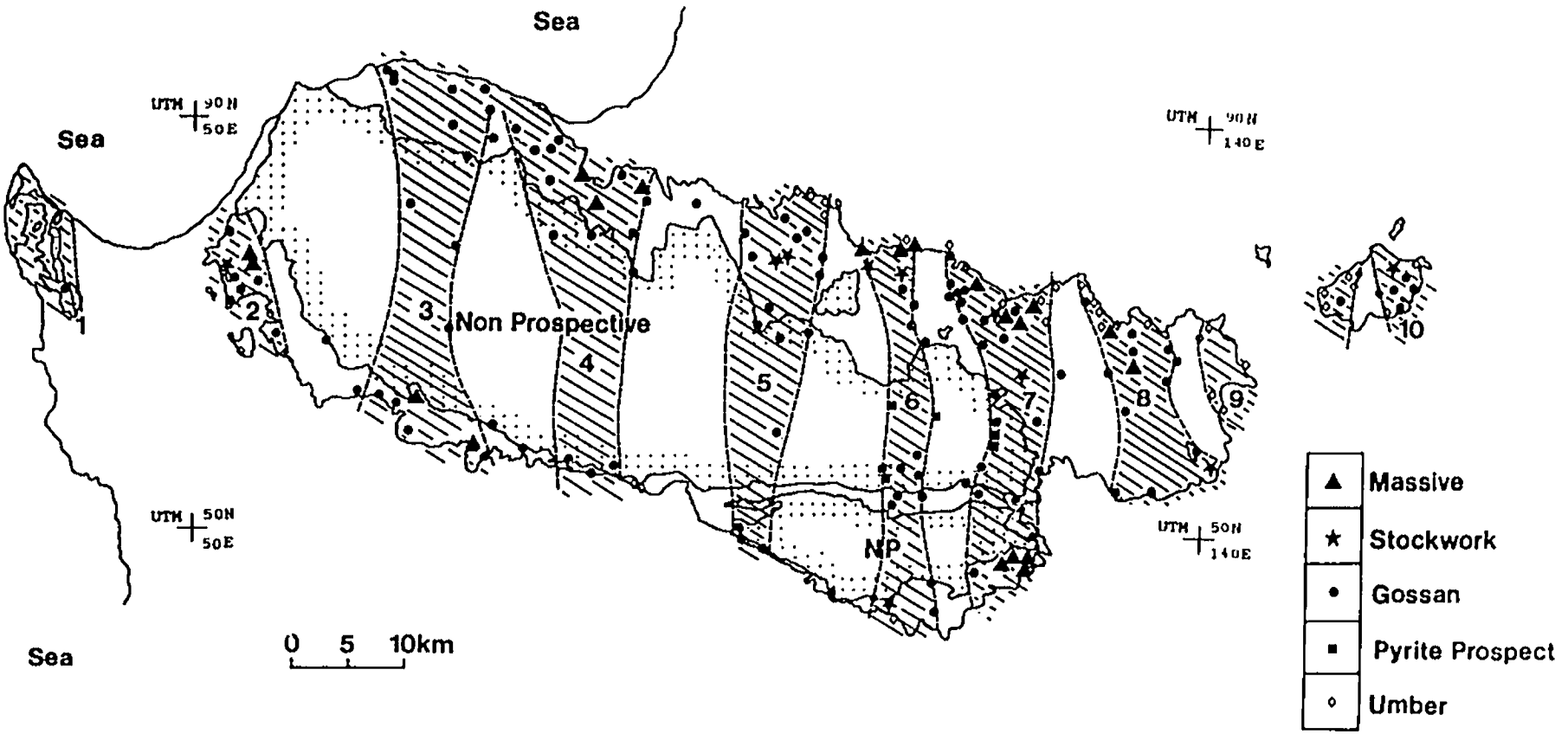

Fig. 6.4.1 The distribution of sulfide orebodies and sulfide mineralization in the Troodos ophiolite. Ten sulfide mineralization zones are distinguished and four, numbered by 5, 6, 7 and 8 are in the study area. The diagram also shows that sulfide orebodies occur in groups (from Hall, unpublished data).

Fig. 6.4.2 Most sulfide deposits in the area are spatially close to the 25% dike abundance contour. See detailed discussion in the text.

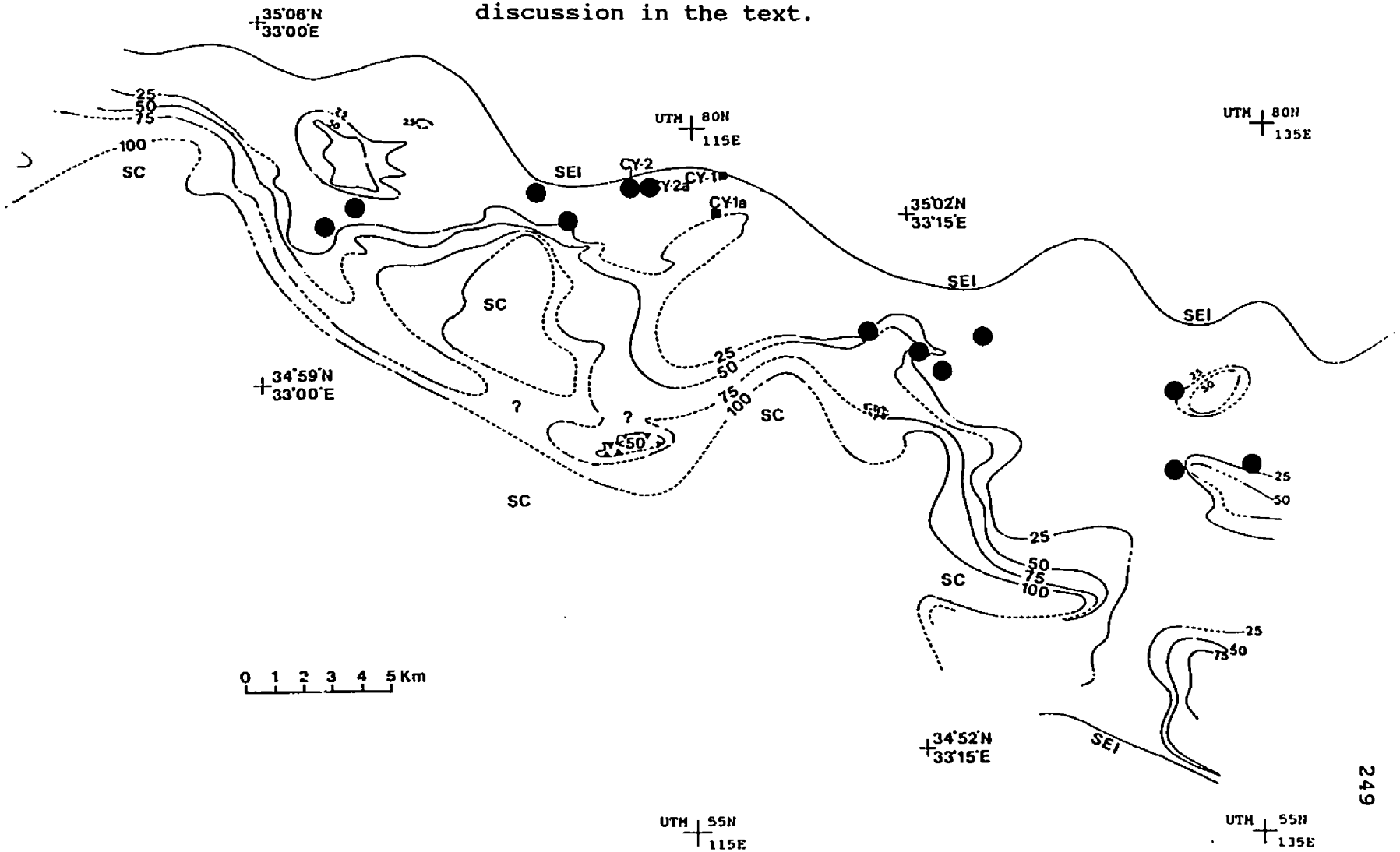

From Fig. 6.4.2, it is evident that at least 10 of the 13 ore deposits are located stratigraphically just above the 0.25 dike abundance level. Depth calculations beneath the SEI of the deposits were based on MODEL 2, except for the three deposits, i.e., the North Mathiatis, the South Mathiatis, and the Sha deposits, located in the east of the area which is not covered by MODEL 2 (Table 6.4.1). The average depth of the ten orebodies beneath the original seafloor, i.e., below the sediment-extrusive interface, is 0.50 ±0.19 km (1sd), while the average depth of the 25% dike surface projected beneath the orebodies is 0.59 ±0.18 km (1sd). The close correlation between these two groups can be seen from the histograms of their distribution (Fig. 6.4.3a,b). The heights of orebodies above the 25% dike surface range between -0.02 and 0.33 km with an average of about 0.10 km.

There is no specific spatial correlation between the sulfide deposits and P values (Fig. 6.4.4). The four groups of deposits in the area occur within the high volume eruption areas (dominant sheet flows), or within the high pillowed flow areas, which suggests that the occurrence of sulfide deposits in Troodos was not spatially constrained by lava forms.

Since three grabens have been reported in the northern part of the Troodos ophiolite, which are believed to act as separate spreading centers (Varga and Moores, 1985; 1990), it

Table 6.4.1 Depth to F0.25 Contour and Orebody

Orebody Name	Depth(Orebody)	Depth(F0.25)	Difference
Memi	0.82 km	0.86 km	0.04 km
Alestos	0.72	0.92	0.20
Kokkinoyia	0.29	0.45	0.16
Kokkinopezoula	0.46	0.44	-0.02
Agrokipia A	0.18	0.51	0.33
Agrokipia B	0.34	0.40	0.06
Pytharokhoma	0.50	0.51	0.01
Peristerka	0.55	0.55	0.00
Kapedhes	0.61	0.63	0.02
Kambia	0.48	0.63	0.15

* Depth calculation based on MODEL 2.

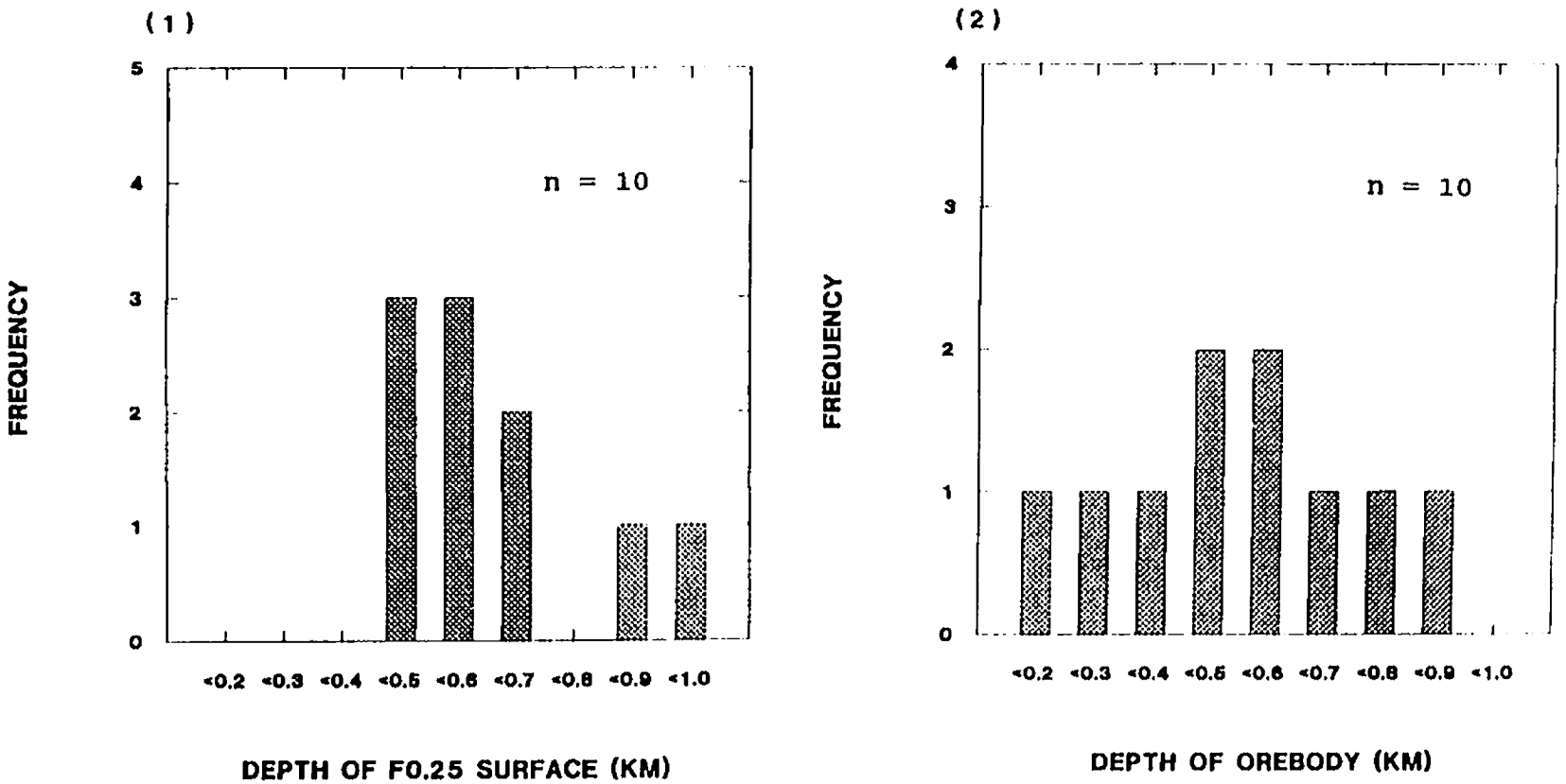

Fig. 6.4.3a Depths from seafloor to F0.25 contour surface (1) and from seafloor to the sulfide deposits in the study area (2).

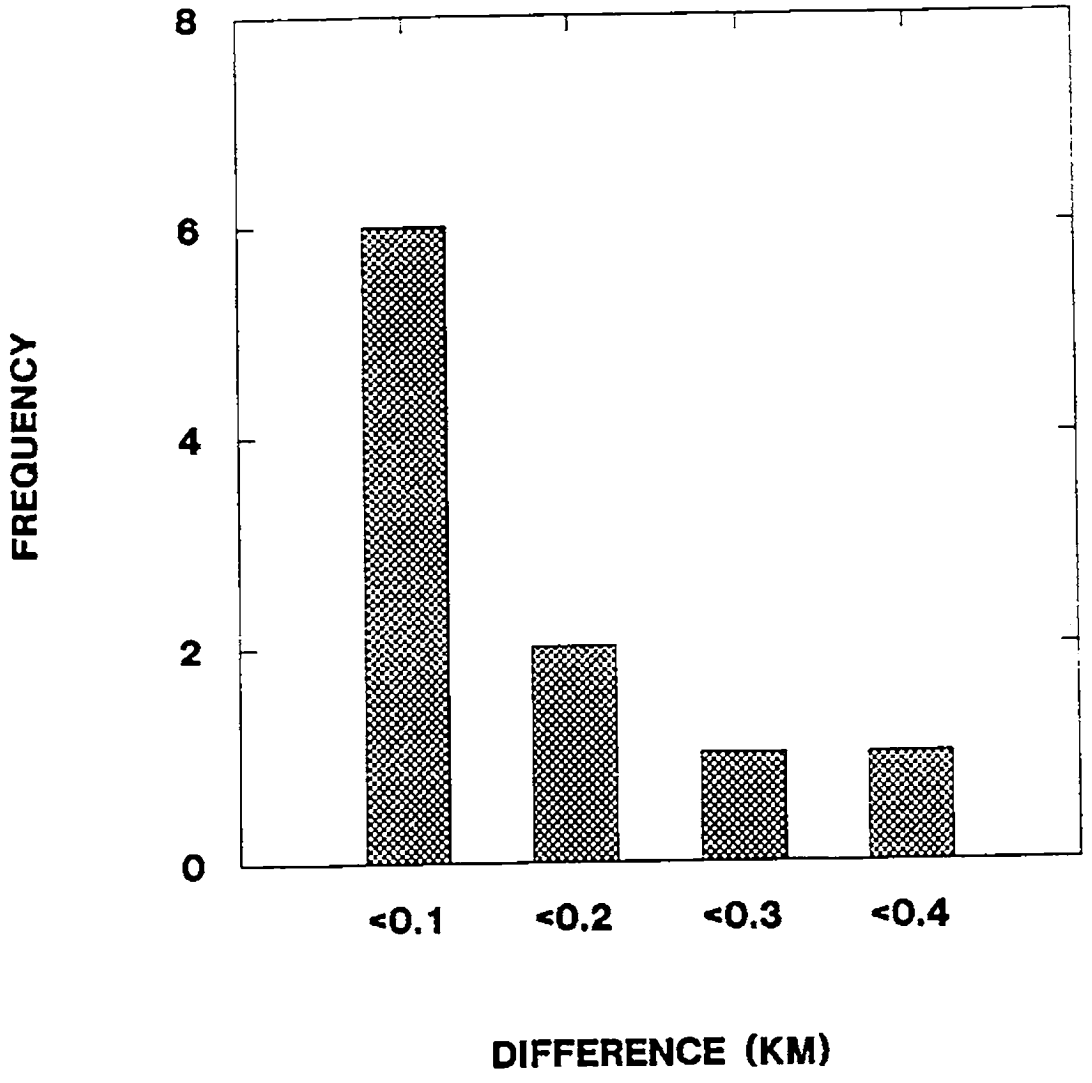

Fig. 6.4.3b Frequency of the depth differences between orebodies and F0.25 contours.

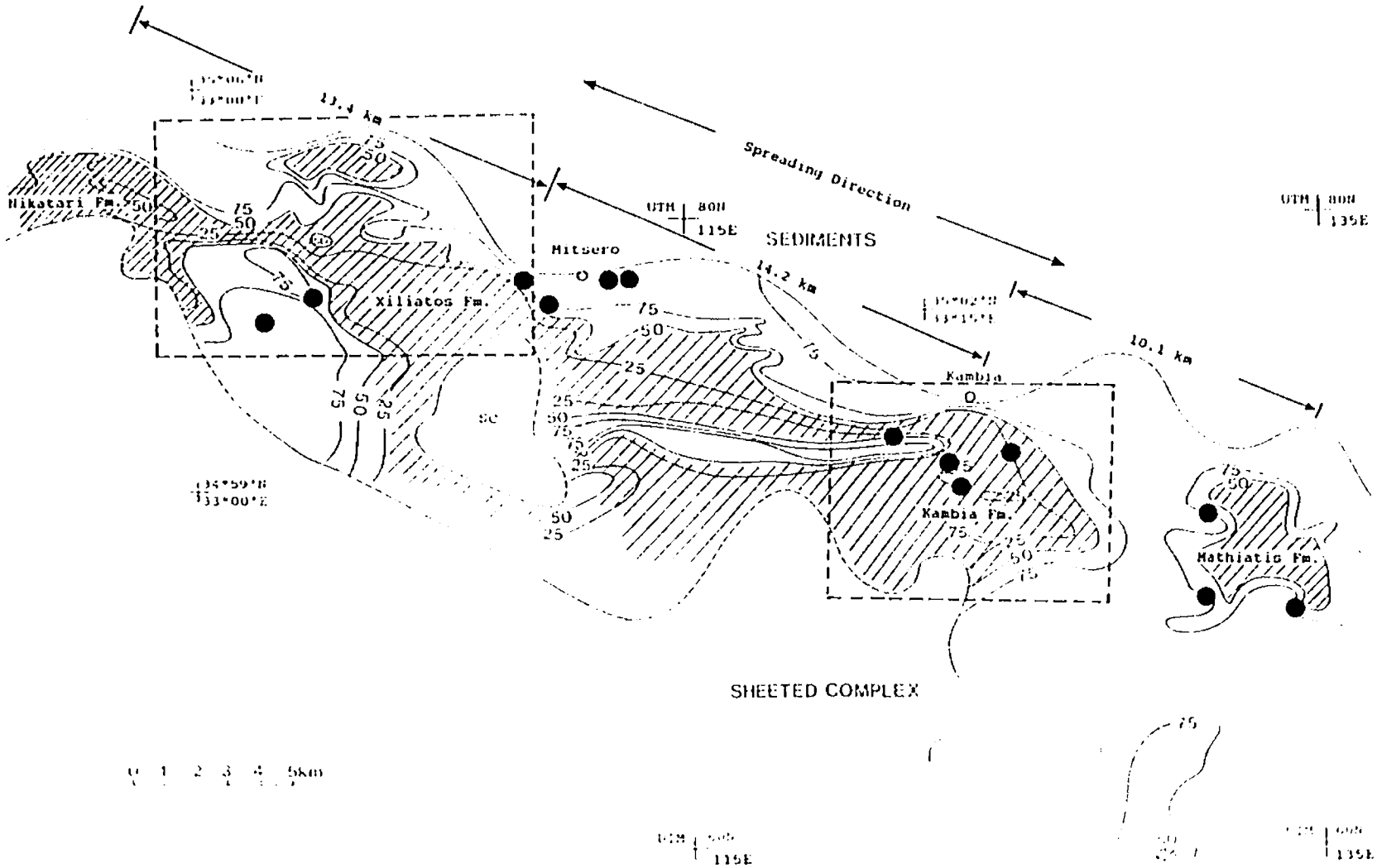

Fig. 6.4.4 Sulfide deposits (block spots) occurring either in sheet-flow dominated (shaded area) or high pillowed flow dominated (blank area).

is interesting to compare the relationship between the grabens, sulfide deposits, and other structural features.

Varga and Moores (1985) proposed that the grabens are fossil axial valleys produced by successive eastward jumps of the spreading axis in steps of 8-13 km. However, it needs to be pointed out that, first, from the graben diagram (Fig. 6.4.5), the two intervals between three grabens are in fact 22-36 km in magnitude with an average of 29 km and, second, several large sulfide deposits in the area (≥0.5 million ton) are not shown in the diagram (see Fig. 6.4.5b). Comparing the distribution of sulfide deposits to the graben structure, in the study area, only the Mitsero Group of ore deposit is in the center of a graben, while the other three groups, the Ayia Marina Group, the Kambia Group and the Mathiati Group, are not (Fig. 6.4.5b). Thus, the occurrence of ore deposits does not correlate simply with the supposed grabens. In contrast, it can be demonstrated that sulfide deposits show a correlation with a high level of volcanic activity which was accompanied by a high level of intrusion of sheeted dikes. In addition, sulfide deposits show a reasonable spatial correlation with major faults (Fig. 6.4.6). Faults and fractures at the spreading centers are important prerequisite conditions for ore-body formation, because fluids must move along pathways that focus discharge at the surface. Otherwise, no significant sulfide masses would be created.

(A)

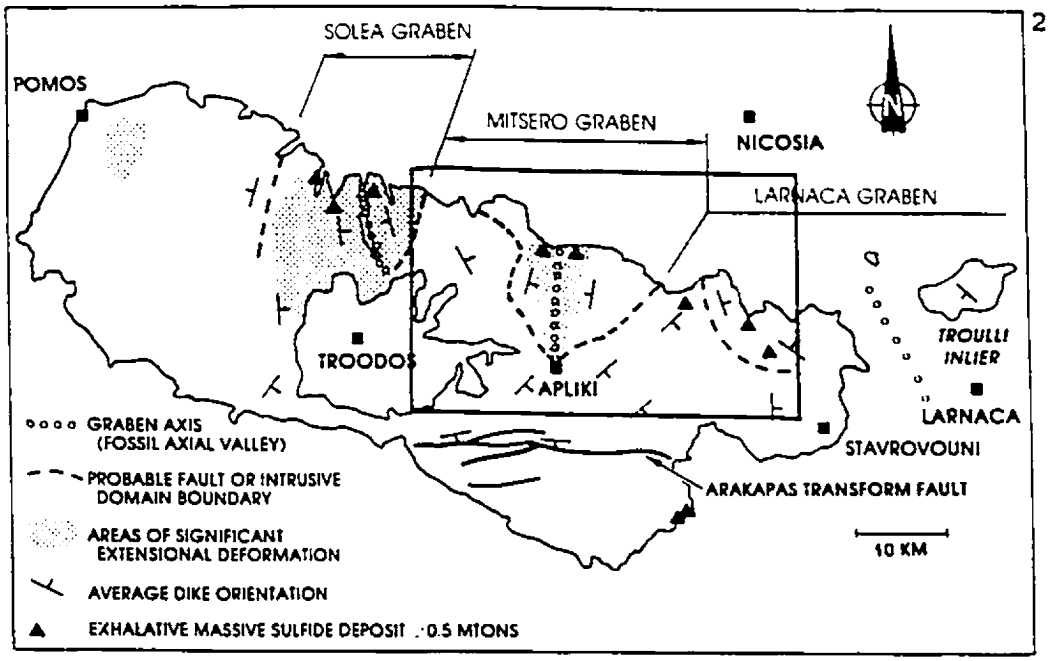

(B)

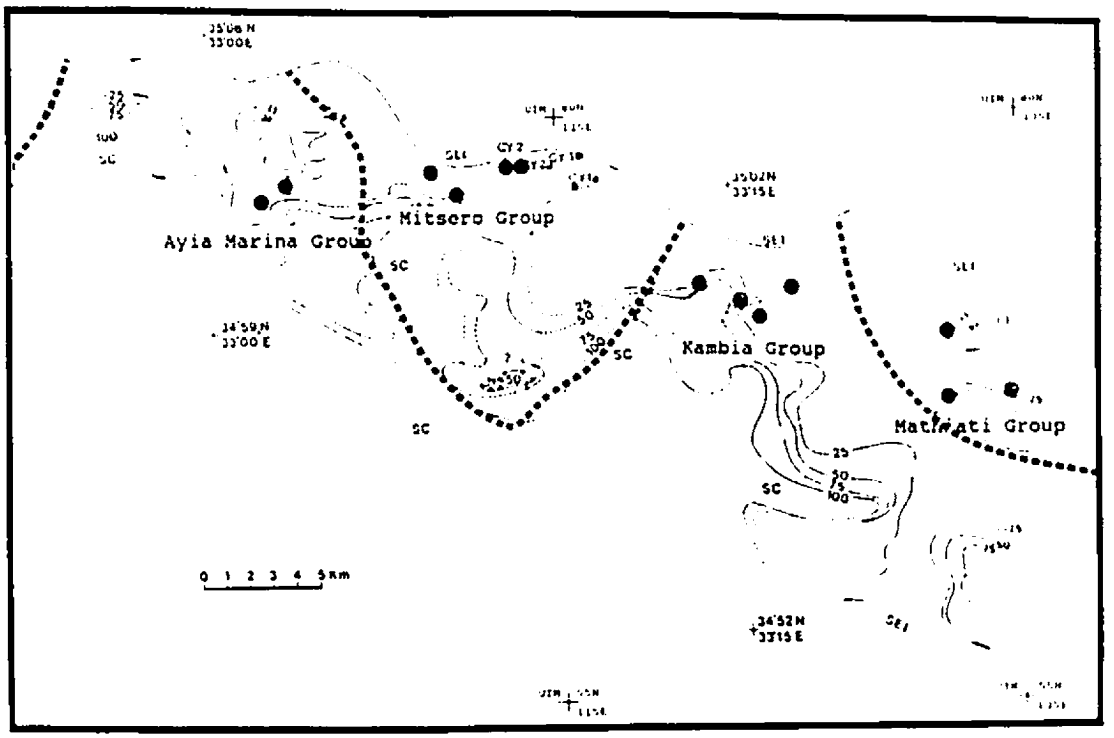

Fig. 6.4.5 (A) Three grabens in Troodos (after Varga and Moores, 1990), black square for location of study area; (B) locations of sulfide deposits (large block stops), for discussion see text.

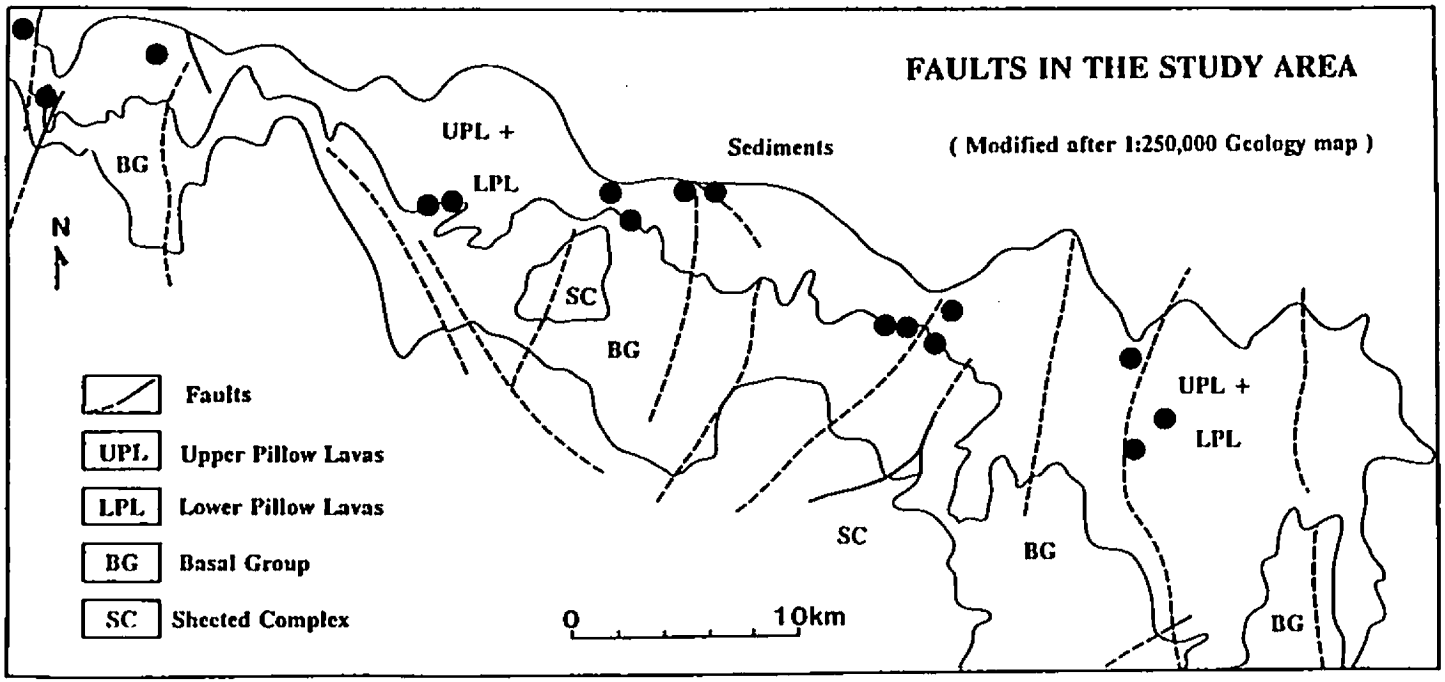

Fig. 6.4.6 Sulfide deposits occur at or near to the main faults in the northern part of the Troodos ophiolite (after Cyprus Geology Survey, 1979; 1982).

6.5 A model for the preservation of the sulfide orebodies

It is evident that sulfide deposits formed at spreading ridges or axes are usually deposited during or at the end of individual eruptive events and accompany hydrothermal activity. Sulfide deposits, after their formation, may be destroyed by erosion on the seafloor, preserved under sediments or younger extrusives, or may be destroyed at depth by continuation of processes of crustal construction involving, for example, dike intrusion. That is, at spreading ridges or centers, as early formed lava flows and intrusions move away from the center with continued spreading, they also subside. As a result, the surface of sheeted dike complex will descend. A sketch showing a possible trajectory is shown in Fig. 6.5.1. Sulfide orebodies deposited both on the seafloor or within the lava flows will undergo the same process. The model for the formation and preservation of sulfide deposits will build on this basic idea. The sources of data for the model are threefold: the spatial distribution of deposits, constructional features of Extrusive Sequence, and the final distribution of metallic elements.

In this model four possible histories for black smoker type orebodies after their formation at the spreading ridges are shown in Fig. 6.5.2.

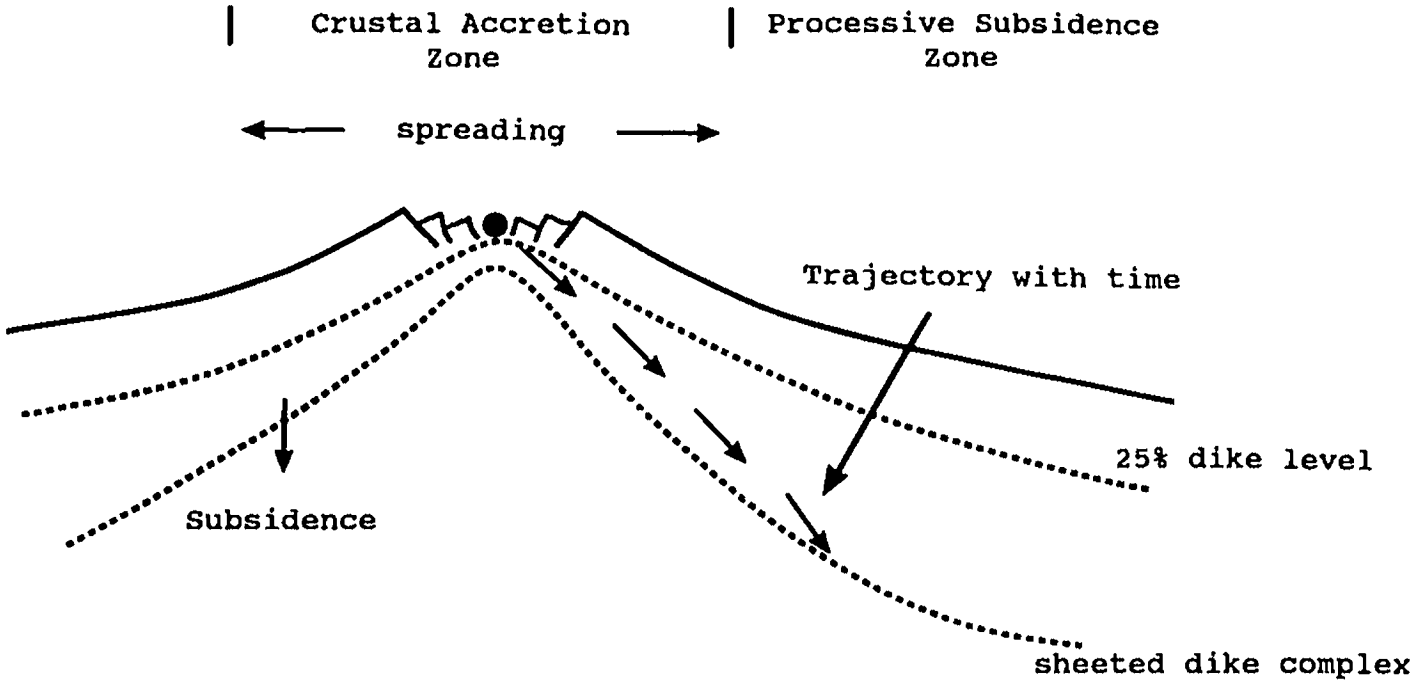

Fig. 6.5.1 Basic idea for orebody preservation. Orebodies, after formation on the seafloor, will be buried by younger lavas or sediments and will become increasingly deeply buried when they move further away from the spreading ridge.

FOUR POSSIBLE HISTORIES FOR BLACK SMOKER TYPE OREBODIES

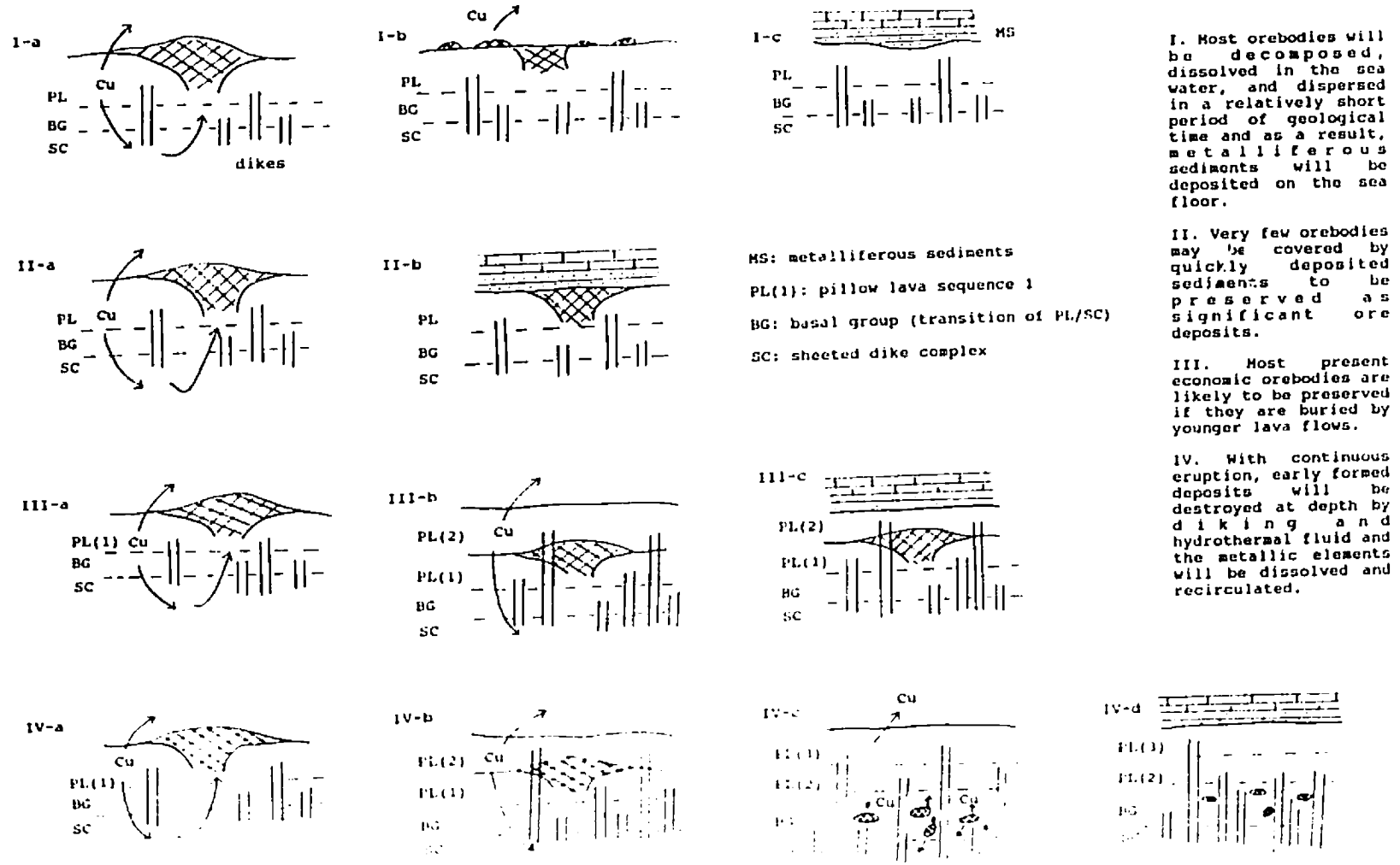

MS: metalliferous sediments

PL(1): pillow lava sequence 1

BG: basal group (transition of PL/SC)

SC: sheeted dike complex

I. Most orebodies will be decomposed, dissolved in the sea water, and dispersed in a relatively short period of geological time and as a result, metalliferous sediments will be deposited on the sea floor.

II. Very few orebodies may be covered by quickly deposited sediments to be preserved as significant ore deposits.

III. Most present economic orebodies are likely to be preserved if they are buried by younger lava flows.

IV. With continuous eruption, early formed deposits will be destroyed at depth by diking and hydrothermal fluid and the metallic elements will be dissolved and recirculated.

Fig. 6.5.2 A model of orebody preservation.

Possibility one: Orebodies will be decomposed by weathering on the seafloor and the metallic elements dissolved in seawater, widely dispersed and redeposited in low concentrations as part of source of the metalliferous sediments that widely occur at the base of the sediment sequence in the present in-situ oceanic basins (Walter and Stoffers, 1985; Bolton et al., 1988; Marchig et al., 1988). For example, Francheteau et al. (1979) and Hekinian et al. (1980) reported that large portions of their sulfide samples obtained from the ocean floor were oxidized and hydrated, i.e., were in the process of being dissolved. The latter authors predicted that most of the deposits lying on the accretion plate boundary of the East Pacific Rise will be altered, deteriorate, and be dispersed in a relatively short period of geologic time. This results from the highly oxygenated environment of deposition and the extremely fragile nature of the massive sulfides. Direct evidence of the existence of metalliferous sediments in Troodos is the deposition of ochre on orebodies and umber on the top of nearly lava flows. Spatially, the latter are usually not far from mineralization zones (e.g., Searle, 1972; Robertson and Hudson, 1973; Hall et al., 1989). Umbers and related radiolarites are largely formed from Fe, Mn and SiO2, the most widely dispersed effluent from sea floor hydrothermal vents (e.g., Hekinian and Fouquet, 1985). However, Searle (1972) has also demonstrated that there is a sharp increase in Cu and Zn

in umber in the vicinity of sulfide deposits compared with umber well away from mineralization. The sulfides probably did contribute some metal to the umber deposited nearby. Direct evidence of some contribution from the sulfides to the umber is the presence of rare pyrite fragments in the Skouriotissa umber (Searle, 1972).

Possibility two: Some seafloor sulfides may be covered by quickly deposited sediments and be preserved in this way as significant ore deposits. Here the preservation of orebodies depends on the periodicity of eruptions and the rate of sediment deposition. The latter is related to spreading rate as well as the distance of the spreading center from a continental margin or other source of sediments. In Troodos, 4 of the total of 34 known deposits are covered directly by sediments. These are the Skouriotissa, Kalavasos (Mavridia), Peravasa, and Troulli (Kokkinopetra) deposits (Bear, 1963 p.51) (see Table 6.2.1). None of these orebodies are in the study area. In this case, the overburden on the orebodies is usually either metallic gossans or metalliferous sediments tending upwards toward shale. For example, at Skouriotissa the covering on the massive sulfide orebody varies from original ochre to a thick sequence of manganiferous and umberiferous shales (Searle, 1972). Small masses of ore are reputed to have been found in the overlying sediments (Bear, 1963).

Possibility three: Massive sulfide orebodies are expected to be preserved if they are buried by younger lava flows, especially if they are of substantial thickness. Most sulfide deposits in Troodos occur within the lava sequence. As described above, 10 of 13 deposits in the study area occur within the lava flows just above the 25% dike abundance surface. Since important hydrothermal activity and sulfide deposition extend into a late stage of individual eruptive events, the eruptive events should be sufficiently long to allow substantial orebodies to accumulate on the seafloor, while the break between the eruptive events might be short, so that successive lava flows, which are possibly large in volume, from the next eruptive event then have the potential to cover the orebodies before they are destroyed by weathering on the seafloor. Some massive sulfide orebodies have upper weathered zones, showing that some loss had occurred before they were covered by successive lava flows. For example, at the Mousoulos (included in the Kalavasos deposit) underground mine in the Kalavasos district, on the top of the orebody there is a layer of ochre ranging in thickness from one-half to several metres (Fig. 6.5.3) followed by a covering of unmineralized UPL (Searle, 1972). In the study area, at the North Mathiatis mine, a similar situation has been observed (Searle, 1972; Constantinou, 1976).

Possibility four: With successive eruptions at a

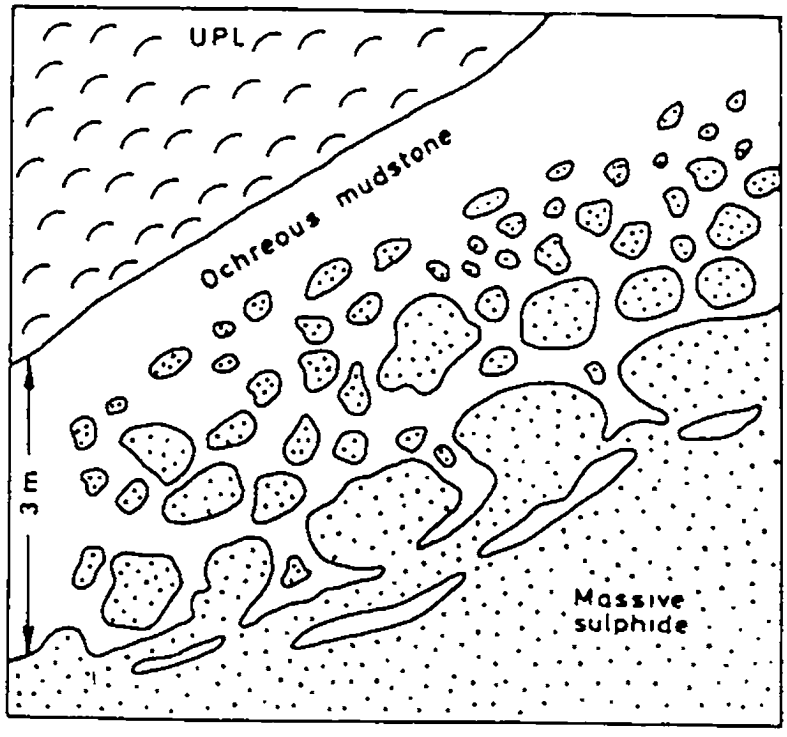

Fig. 6.5.3 Weathering zone on the top of massive sulfide deposit, Mousoulos mine, Cyprus (after Searle, 1972).

spreading ridge, early formed ore deposits and associated rocks will be buried increasingly deeply and will finally be dismembered at depth by both physical and chemical processes, i.e., diking and dissolution by hydrothermal fluids, as an example observed in Oman, where the sulfide orebodies were cut into slices by later dike intrusion (R. Koski, personal communication, 1991). The metallic elements will be dissolved by hydrothermal fluids and probably recirculated. The distribution of the 34 known deposits supports this possibility. If we consider the traditional stratigraphic division of the Extrusive Sequence, the Basal Group (BG), as the stratigraphically lower part contains only 2 small deposits, #6, Peristerka (0.3 Mt) and #25, West Troodos (<0.5 Mt), of the 34 deposits (see Table 6.2.1). In contrast, the number of mineral prospects or gossans is highest in the BG (see Fig.6.3.2). It is suggested that at least some of these BG prospects were originally the parts of larger bodies which were in the process of being dismembered and recycled when crustal construction terminated.

6.6 Distribution of key metallic elements

Abundant geochemical data for the rocks in the Extrusive Sequence and the Sheeted Complex show metallic elemental variation during the alteration and mineralization processes which are useful in testing the predictions of the

preservation model.

A regional geochemical investigation in the Troodos ophiolite in the late 1960's led to more than 2,000 samples of the rocks in the extrusive and dike sequences being collected for analyses along twenty traverse lines (Govett and Pantazis, 1971). The mean values of Cu shows a regular increase with depth (Table 6.6.1). In the lava sequence, i.e., the upper part of the Extrusive Sequence, both lavas and dikes have an average of 69 ppm Cu. In the BG, the concentration of Cu is higher at average of 110 ppm, but the average Cu content (165 ppm) of the dikes in the Sheeted Complex is again higher than that of the BG, although it has a similar range (Govett and Pantazis, 1971).

Analyses of data from the CY-2 and CY-2a drillcores (Bednarz et al., 1987b) yield many similarities to the results of Govett and Pantazis (1971).

In Drillhole CY-2, unmineralized rocks first occur at 100 m depth and extend to the bottom (226 m) of the hole. The 140 analyses from this interval have a mean Cu of 53 ±35 ppm (1sd), similar to that of the interval in Drillhole CY-2a, where 105 samples of the little altered Lower Pillow Lavas above the Agrokipia B orebody (from 4.4 m to 154 m depth) have an average Cu of 62 ±87 ppm, with a relative large standard

Table 6.6.1 Mean Values of Cu, Zn, Ni and Co for Individual Units in the Upper Part of Troodos Ophiolite*

	Numbers of Areas and Mines	Mean Values, ppm			
	n	Cu	Zn	Ni	Co
Lavas	25	69 ±21	67 ±15	71 ±56	36 ±7
Dikes	20	69 ±39	68 ±18	49 ±23	30 ±11
Basal Group	12	110 ±54	77 ±33	48 ±26	31 ±7
Diabase	6	165 ±62	80 ±29	40 ±18	32 ±4

* Calculated on the mean values of individual areas and mines based on over 2000 samples from Govett and Pantazis (1971, Table 4).

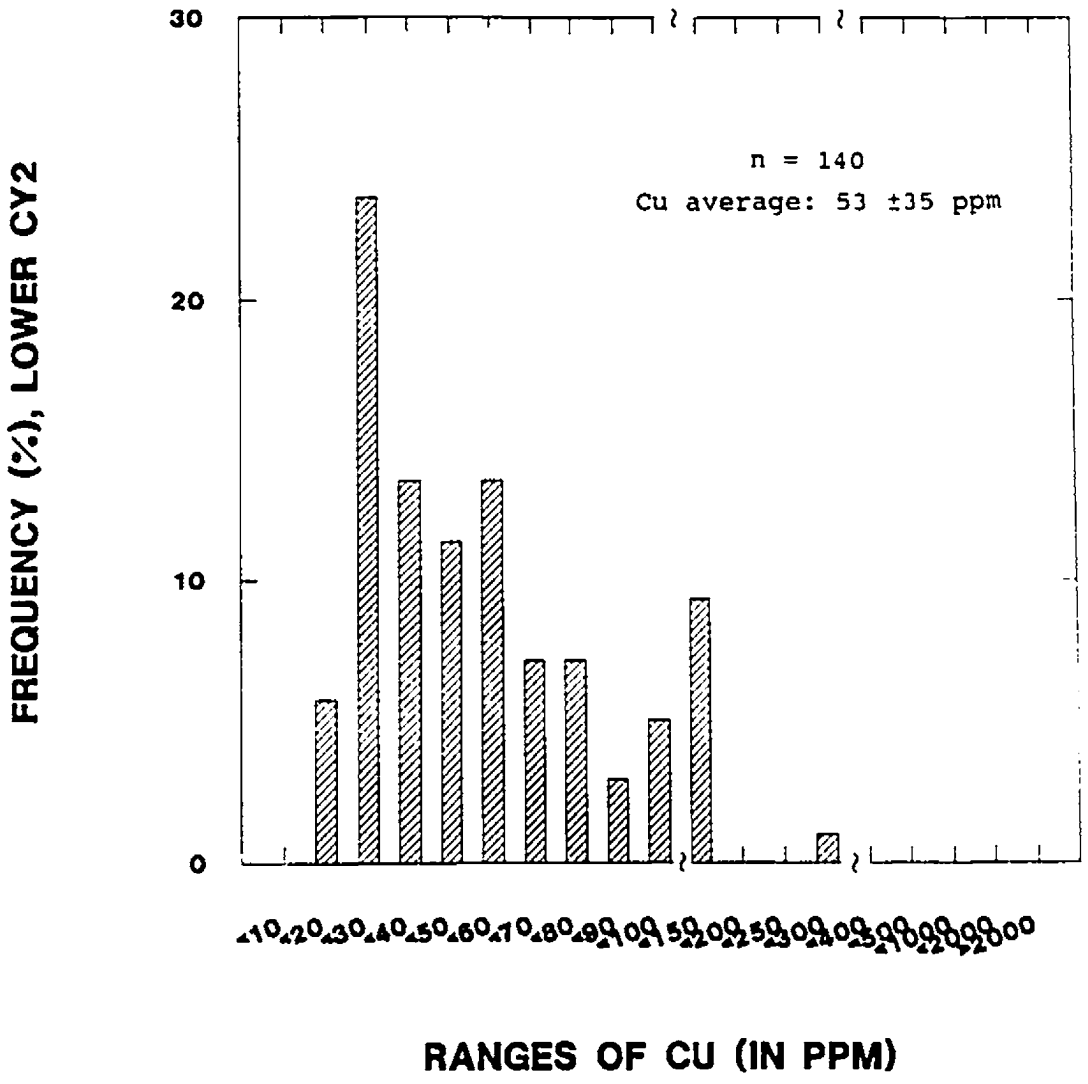

Fig. 6.6.1 Histogram of frequency (%) of Cu abundances in brownstone lavas in drillhole CY-2. Note changes in scale: 0-100 in 10s, 100-300 in 50s, >300 nonlinear (data from Bednarz et al., 1987).

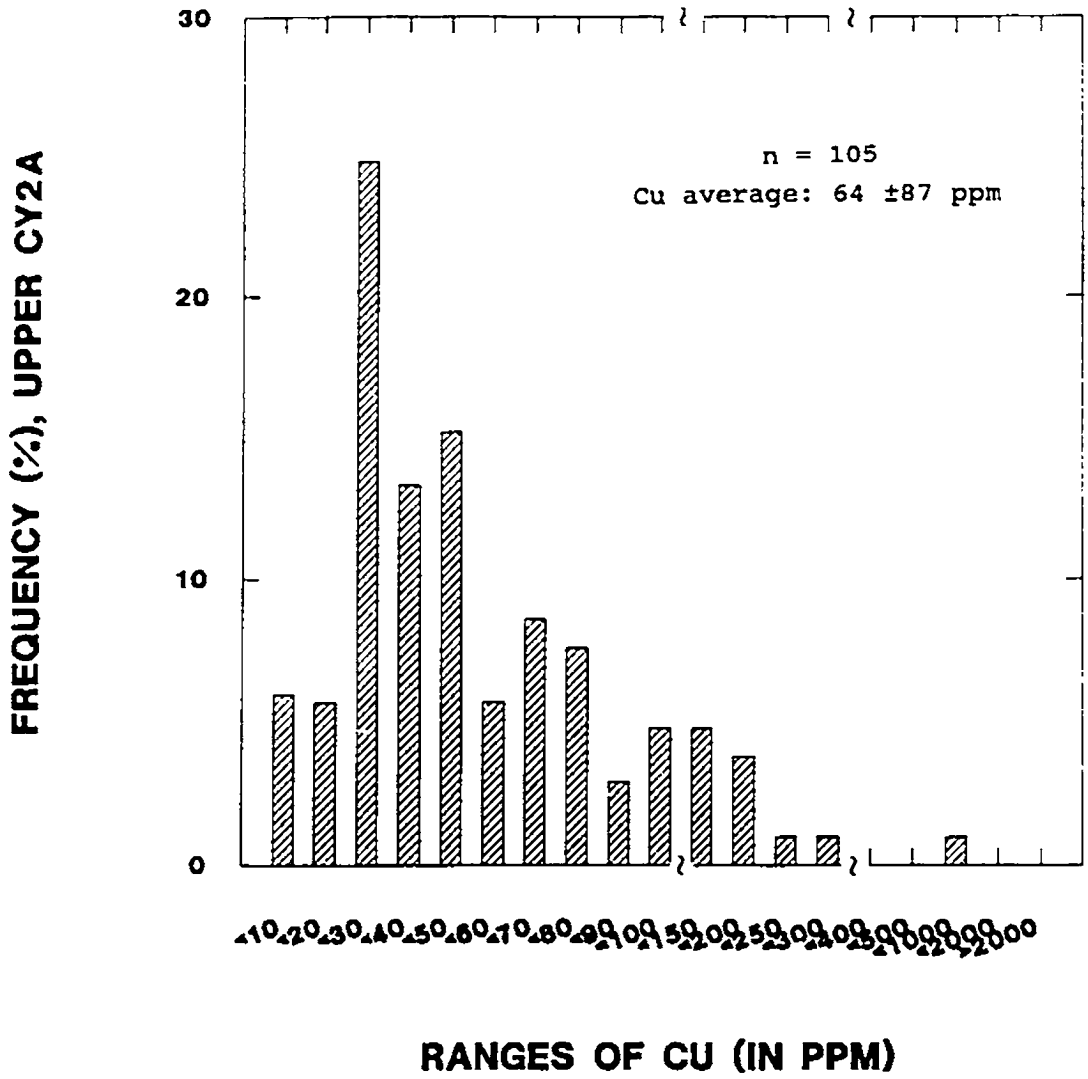

Fig. 6.6.2 Histogram of frequency (%) of Cu abundances in brownstone lavas in drillhole CY-2a. Note changes in scale: 0-100 in 10s, 100-300 in 50s, >300 nonlinear (data from Bednarz et al., 1987).

deviation. Histograms of the ranges of Cu in these two holes display similar trends (Figs. 6.6.1 and 2), which is consistent with the lithological and stratigraphic similarity of the two intervals (Bednarz et al., 1987a; Sunkel et al., 1987). Again, Mehegan (1988) analyzed 153 outcrop lava samples from the extrusives and obtained an average of 58 ±83 ppm in Cu. Both the mean and range of Mehegan's results are similar to those from the drillholes (Fig. 6.6.3).

In the deeper part of the CY-2a drillhole (300-690 m), below the Agrokipia B orebody, 250 analyses of Cu have an average value of 141 ±296 ppm, i.e., between the BG and SC values of Govett and Pantazis (1971). A characteristic of this distribution is that the Cu values vary widely, with a high amplitude peak at low abundances of Cu (<100 ppm) and a relatively higher proportion of high of Cu samples (>500 ppm) than that in the upper part of the CY-2a drillhole and the surface lava of Mehegan (1988) (Fig. 6.6.4). This suggests that in this interval of the crust, although Cu is dominantly depleted relative to the primary abundance it is also locally enriched. Stratigraphically, this interval is equivalent to the traditional BG as is evident from the presence of over 50% dikes and greenschist facies alteration (Bednarz et al., 1987a; Hall and Botros, 1987). By the preservation model, Cu values at this level might be either high or low, depending on the degree of dissolution and redeposition of Cu from a deeply

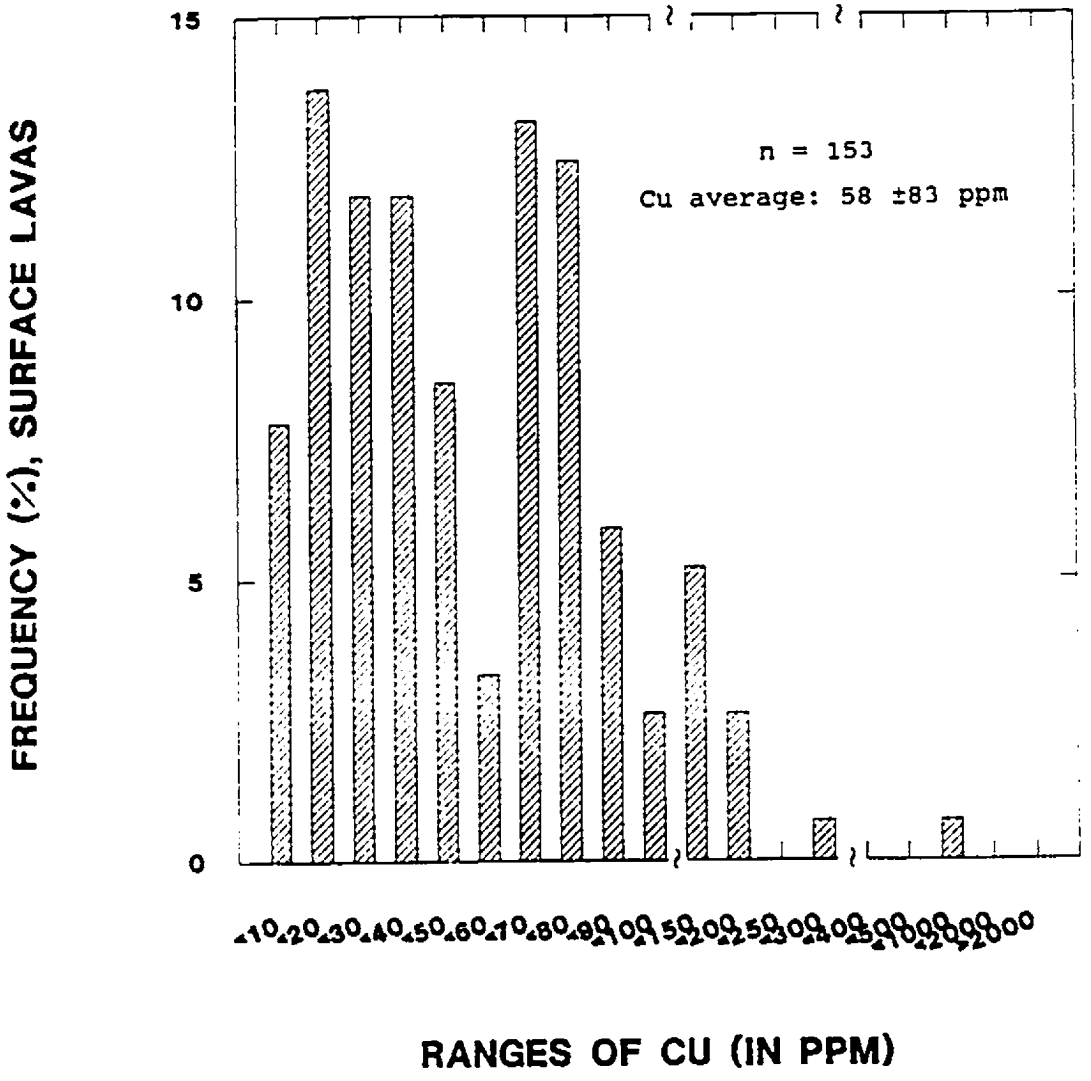

Fig. 6.6.3 Histogram of frequency of Cu abundances of surface lavas. Note changes in scale: 0-100 in 10s, 100-300 in 50s, >300 nonlinear (data from Mehegan, 1988).

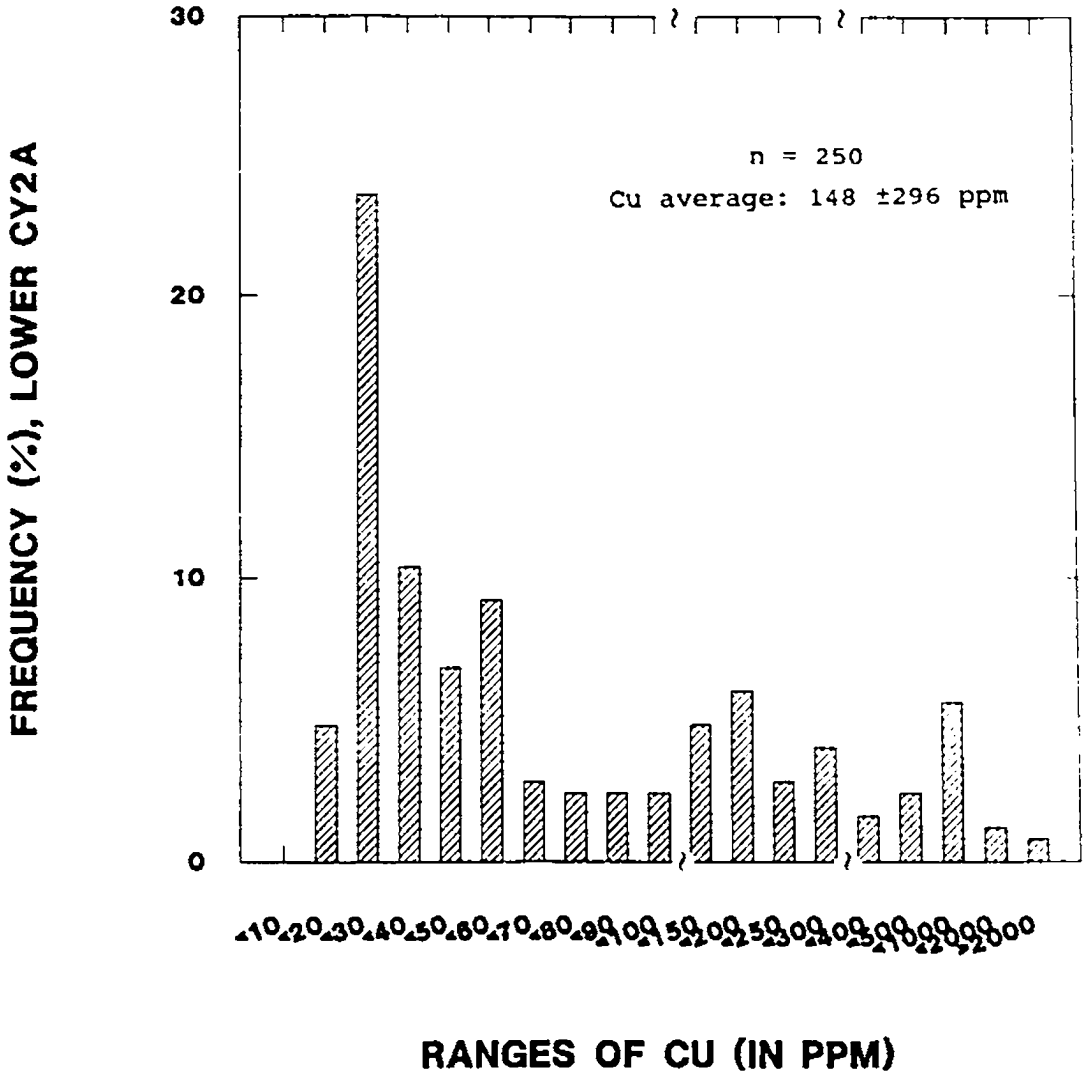

Fig. 6.6.4 Histogram of frequency of Cu abundances in the lower part of drillhole CY-2a. Note changes in scale: 0-100 in 10s, 100-300 in 50s, >300 nonlinear (data from Bednarz et al., 1987).

buried and dismembered orebody or from hydrothermal solutions. As a result, locally, Cu might be as low as less than 20 ppm, or, in contrast, as high as over 2,000 ppm, equivalent to locally high enrichment.

Finally, Baragar et al. (1989) have published a large number of analyses of Cu in dikes from the Sheeted Complex, both from outcrop sections and from drillhole CY-4. The 173 analyses from Hole CY-4 give an average of 305 ±513 ppm Cu and show a similar large range to the BG in CY-2a (Fig. 6.6.5). The Cu distribution in Hole CY-4 shows a similar pattern, i.e., a high peak of Cu-depleted samples and a certain number of Cu-enriched samples, but the Cu-rich group is much more apparent in Hole CY-4 than that in the lower part of Hole CY-2a. It is evident that, first, Cu in the SC has been effected by local loss or addition and, secondly, the SC section in Hole CY-4 is most likely to be in an area locally enriched in Cu. In contrast, the 408 analyses from field sections given in Baragar et al. (1989) give an average of only 56 ppm in Cu, almost 5 times lower than that from CY-4. Careful checking of the locations of the ten profiles from which the samples were collected by Baragar show that, first, three of the profiles are not located in the Sheeted Dike Complex sequence but in the Basal Group, i.e., these three profiles should not be included in the SC. Secondly, in the remaining 7 profiles, three are only about 50 m in length and four range between 100

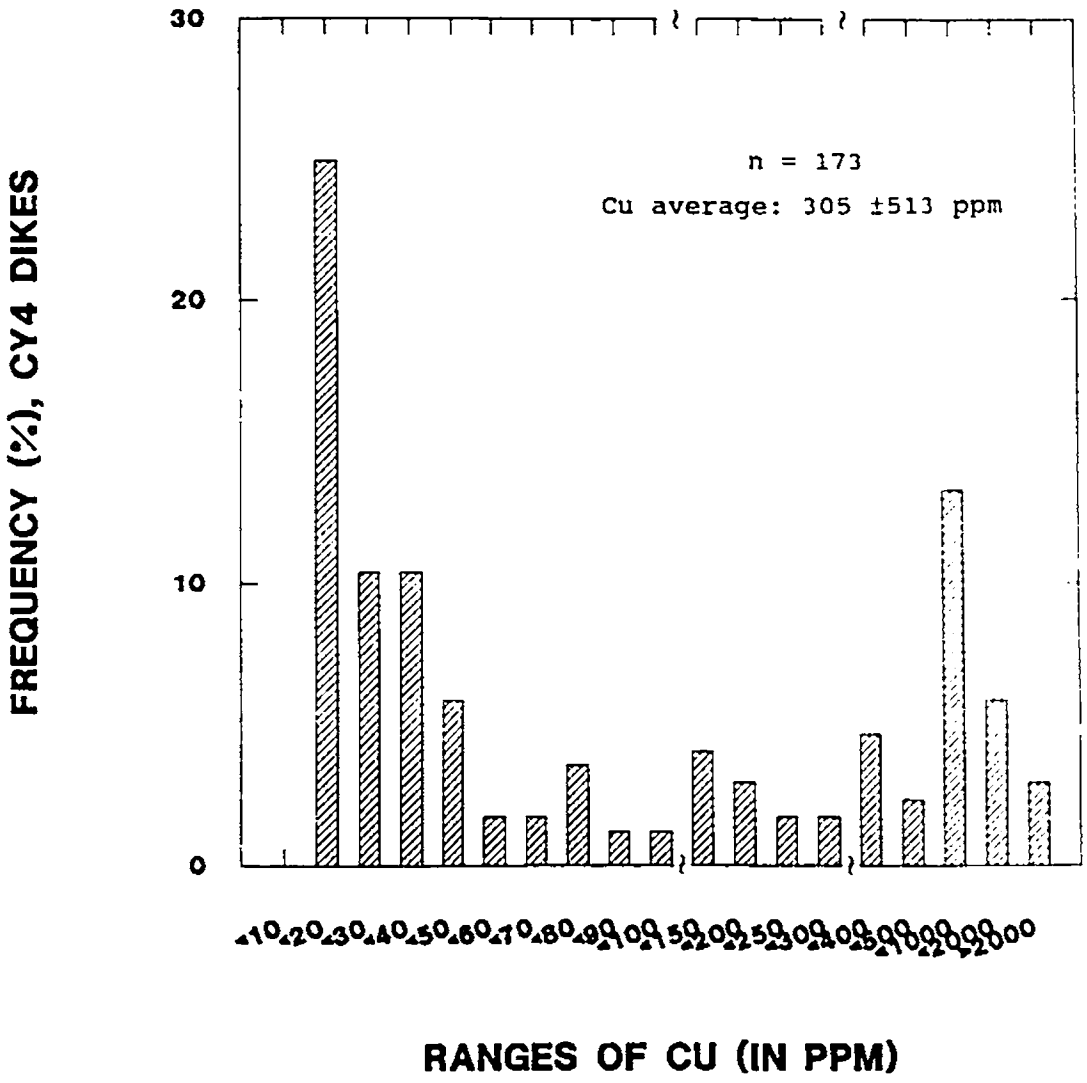

Fig. 6.6.5 Histogram of frequency of Cu abundances in sheeted dikes in hole CY-4. Note changes in scale: 0-100 in 10s, 100-300 in 50s, >300 nonlinear (data from Baragar et al., 1989).

to 250 m. If they are expressed in terms of true thickness, these profiles only represent very limited vertical intervals of the Sheeted Dike sequence, from a few meters to a few tens of meters. These intervals probably represent portions of unmineralized and Cu-depleted SC such as are seen in the CY-4 profile. In comparison with the histogram of Cu in drillhole CY-4, Cu distribution in these profiles represents largely the low abundance peak with only weak indications of the presence of the higher abundance peak (Fig. 6.6.6). The average of the Cu contents of both roadcuts and the CY-4 drillcore is 178 ppm, similar to the mean of SC of Govett and Pantazis (1971).

In summary, from the above discussion, it is clear that although the data from different authors show some numerical differences, most of them display a very similar trend of Cu increase with depth. Since different lithologies (lavas and dikes) all show very similar patterns of variation with depth, and no significant difference at the same level, it is reasonable to assume that when the rocks form on the seafloor or as intrusions below the seafloor they all originally contain the same average content of metallic elements such as Cu, and the present regular variation in abundance with depth was most likely caused by secondary processes. This presumption is also consistent with the view that dikes and intrusions in the ophiolite act as conduits which supply the magma for the extrusives.

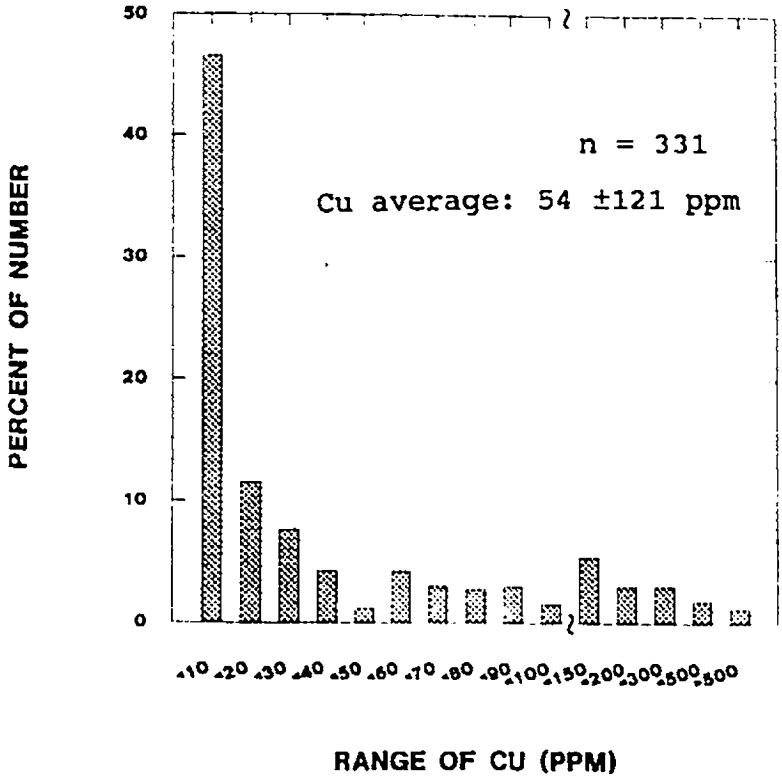

Fig. 6.6.6 Histogram of frequency of Cu abundances in sheeted dikes from road-cut profiles. Since road-cut profiles only are equal to very limited thickness of SC, these low-Cu analyses mostly represent the portions of Cu-depleted SC.

DSDP drillholes and other ophiolites provide analyses of copper in the rocks that support the widespread nature of the vertical variation in Cu described above. Thirty-two analyses of Cu in the lava sequence of DSDP Site 417 have a mean of 90 ±28 ppm (Alt and Honnorez, 1984), while ninety analyses of Cu in the about 500 m thick supposed transition to the SC in Hole 504B contains an average of 102 ±76 ppm (Emmermann, 1985), and the additional 200 m at the bottom of 504B has an average Cu of 112 ±83 ppm (Alt et al., 1989). Analyses from ophiolites are compatible with the oceanic crust recently, e.g., 24 analyses of Cu in the lava sequence of the Josephine ophiolite, Oregon, in USA, have a mean of 85 ±74 ppm (Zierenberg et al., 1988), close to that of the DSDP Site 417 and a mean of 87 ppm for the MAR basalts (Melson et al, 1971; quoted by Coleman, 1977), as well as a mean of 86 ppm for ocean-floor basalts agreed by Basaltic Volcanic Study Project (1981, p.148).

Now, we can do a simple calculation to test the model of orebody preservation proposed above. First, as shown above, the Cu means of Govett and Pantazis (1971) can be simply taken as the average values of Cu in the rocks of the Extrusive Sequence and of the Sheeted Complex. If the general thickness of lava sequence, BG, and SC are considered as 0.6 km, 0.4 km and 1 km (based on Hole CY-4, including transition to Gabbro), respectively, the general mean of Cu in these rocks then is

125 ppm, i.e., the total Cu from the Sheeted Dikes and Extrusive Sequence distributed uniformly over a section 2 km (0.6 + 0.4 + 1.0). This value is close to the mean of 133 ± 38 ppm in Cu in various kinds of basalts of present oceanic crust and on land (calculated based on seven means of Cu from 5 references quoted by Govett and Pantazis, 1971), and is very close to the average 127 ppm of Cu in tholeiites of the world (Prinz, 1967; Manson, 1967; quoted by Coleman, 1977).

The suggested variation of Cu in the Extrusive Sequence and Sheeted Complex during different steps in the formation of Troodos type oceanic crust is shown in Fig. 6.6.7.

At the first stage, when the rocks of the Extrusive Sequence and Sheeted Complex are formed by eruption and intrusion, they are assumed to contain the same amount of Cu, i.e., 125 ppm everywhere, and the lava interval, Basal Group and Sheeted Dikes are assumed to be, respectively, 0.4 km, 0.2 km and 1.0 km in thickness.

At the second stage, Cu, as for many other elements, will be mobilized by the circulating seawater within the sequence. On a regional basis it is supposed that Cu largely moves downwards in the newly formed crust, being leached from the rocks and transported by downwards moving seawater. On the other hand, some Cu will also dissolve in the seawater on the

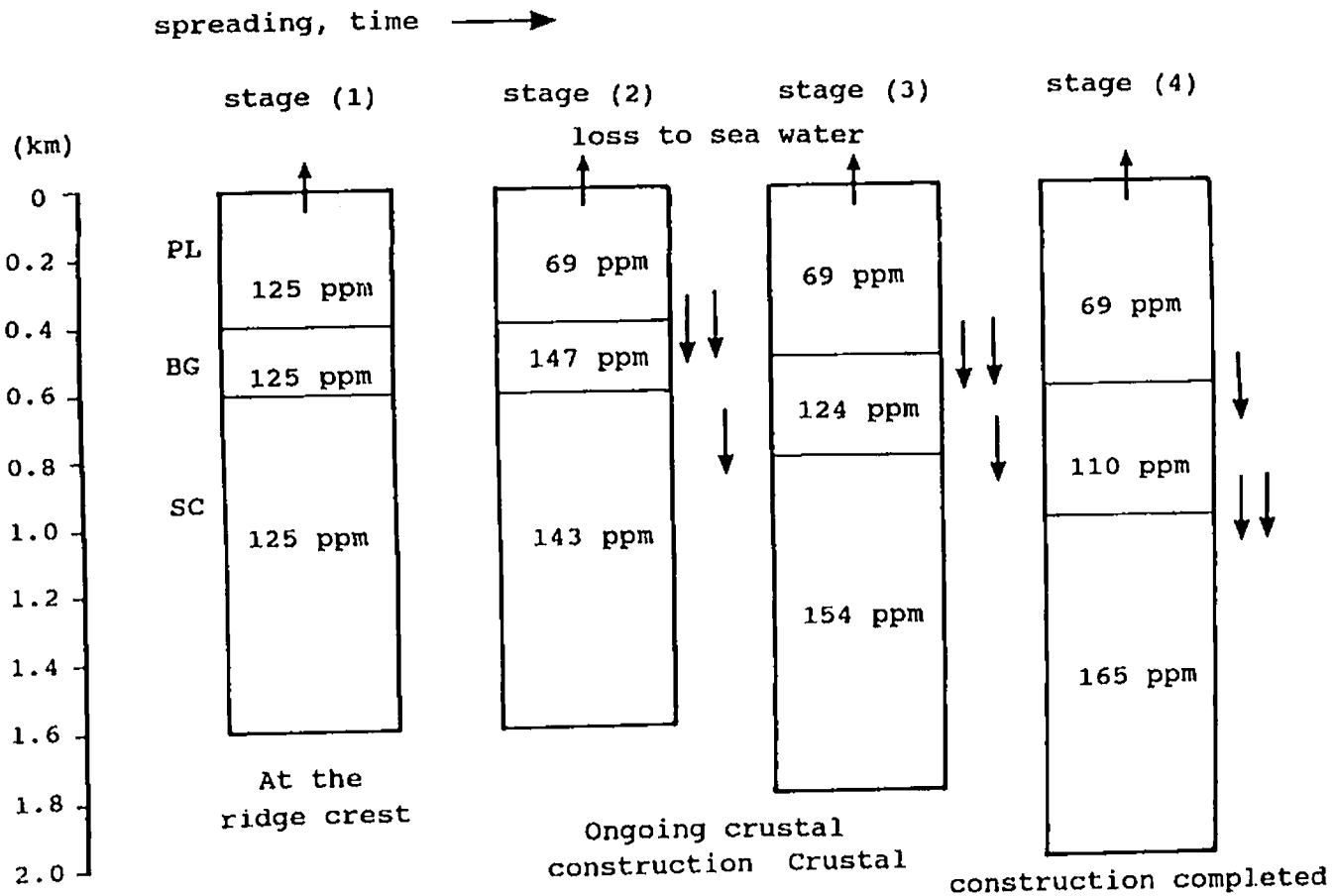

Fig. 6.6.7 Four stages of Cu movement along with hydrothermal circulation during the formation of the in-situ oceanic crust. See discussion in the text. PL-Pillow Lava Sequence; BG-Basal Group; SC-Sheeted Complex.

seafloor, but compared to the downward part, this part is assumed to be much smaller according to the close Cu averages in basalts both in ocean and on land. At the end of this stage of the process, the average Cu is 69 ppm in the lava interval, 147 ppm in the BG and 143 ppm in SC. That is, it is estimated that the downwards circulation at this stage is so intense that Cu increases 17.6% in the BG and 14.4% in the SC. The reason that Cu is higher in the BG than in the SC is that the hydrothermally circulated seawater with high amounts of Cu will meet cold seawater at the upper level of BG and copperiferious sulfide minerals readily precipitate as the environment is abruptly changed. This phenomenon is also noted from the study of present oceanic crust in ODP Hole 504B (Alt et al., 1986).

The mechanism by which Cu in extrusives and intrusives moves downward by circulating seawater from the upper part into deeper part of the crust is not clear. However, several lines of evidence seem to support the possible existence of this process. First, as it has been illustrated above, the average abundance of Cu in the Troodos-type oceanic crust is compatible with that of present oceanic crust, basalts on land and other ophiolites, that is, original basaltic rocks in the world have a similar average Cu abundance. Therefore, both the presently high Cu in the lower part and low Cu in the upper part of the sequence in Troodos are most likely to be the

results of secondary processes. Second, there is no evidence to show that Cu abundance in extrusives is lower than in dikes, because the dikes represent the conduits through which the lavas were transported to the seafloor and they should record the same range of compositions found in the extrusives (Robinson and Malpas, 1990). Third, no evidence shows that Cu abundance is differentiated in dikes, i.e., a lower Cu in higher level of dikes and a higher Cu in lower level of dikes.

At the third stage, new and younger lavas will erupt and cover the relatively older lavas. The younger lava interval is assumed to be 0.2 km thick. Because the total lava interval is getting thicker, the lower part (about 0.1 km thick) of lava interval will gradually change into a part of the BG, i.e., the lava interval now reaches 0.5 km thick, the BG 0.3 km, and SC 1 km (column 3 in Fig. 6.6.7). Again, at this stage, Cu will be leached from the lava interval and added to the BG and SC. After the leaching, Cu in the lava interval stays at 69 ppm in average. In the BG, the new part which was originally from the lava interval may get some Cu from the solution while the old part of BG may lose some Cu to the SC. During this stage, circulating hydrothermal seawater will possibly bring in, as well as take out, almost equivalent amounts of Cu, i.e., by calculation, it will increase about 9% of Cu but decrease around 8%. As a result, the general average of Cu in

the BG will be reduced to 124 ppm. Meanwhile, Cu in the SC will simply increase 11%, and will reach an average of 154 ppm.

At the fourth stage, new lavas again erupt and cover the older ones. Suppose the new lava layer is 0.2 km thick, and again the lowermost 0.1 km of the former lava interval is transformed into BG. As a result, the total lava interval finally reaches 0.6 km thick, the BG 0.4 km and SC 1 km, as observed today. After further seawater circulation, Cu is lost from the new lava interval and finally reaches an average of 69 ppm. In the BG, due to the addition of new material from transformation of the older lava interval (with 69 ppm Cu), Cu will be reduced to an average of 110 ppm. During this period, the circulation of seawater is considered to introduce and remove the same percent of Cu to and from the rocks of BG. In the SC, Cu will increase by a further 11% and reach a final level of 165 ppm, matching the results of analysis.

It needs to be pointed out that, in addition to the formation of black smoker Cu-Fe-Zn deposits on the seafloor, a certain amount of Cu, as well as other metallic and nonmetallic elements, dissolves in seawater during the hydrothermal circulation that occurs when in-situ oceanic crust is formed. This is the Cu deposited as sulfide minerals on the seafloor, and now present in the metalliferous

sediments seen both in the present oceans and in ophiolites. This part of Cu lost from the rocks has been considered in the model. The original average of Cu in the rocks of the Extrusive Sequence and Sheeted Dike Complex is taken as 125 ppm in contrast to the 133 ppm of the world basalts. If difference between them can be considered to be real rather than just part of the uncertainties, then this can be seen as the part of the Cu lost from the rocks to the sea. It is not a small amount considering the volumes involved as is evidenced by the calculation of Cu of the cupriferous deposits in the area.

Among the 16 sulfide deposits, ten deposits are economic cupriferous sulfide deposits (see Table 6.2.1) and the total tonnage of metallic Cu of these deposits is 75,690 tons. The area of study is 40 x 10 km^2 and, if the thickness of the layer (Extrusive Sequence plus Sheeted Dikes) is supposed to be 2 km, then the volume of the block is 800 km^3. According to the average of 125 ppm Cu in the interval, calculation indicates that it contains a total of 250 Mt of Cu. Even if the total Cu metal in the 10 orebodies is doubled, it is only approximately equal to 0.06% of the background copper of country rocks and is equal to a contribution of less than 0.08 ppm towards the Cu of the 125 ppm mean value. The calculation reveals that mineralization and sulfide deposit formation, as well as their redistribution in the rocks, possibly only

locally influences the distribution of metallic elements such as Cu, and is of negligible significance compared to the regional variation of the abundance of Cu.

Richardson et al. (1987) provided some supporting evidence for this conclusion from the study of the metal-depleted root zones in the Troodos ophiolite. They identified epidosite zones in the lower part of the Sheeted Complex. The rocks in these zones are strongly depleted in Cu and Zn, and the metals have been removed to supply the ore deposits. By comparison with lavas and dikes in unmineralized Troodos Pillow Lavas, they proposed that about 75 ppm Cu is lost from the zones of epidosite during their alteration. To supply 0.15 Mt Cu thus requires 2000 Mt of epidosite or about 0.7 km^3. That is, taking the epidosite zones to be 1 km wide and 0.3 km in vertical extent, it only needs to be 2 km in length zone parallel to the ridge axis to provide this amount of Cu. This figure is helpful to understand the above discussion.

6.7 Summary

The high density distribution of massive sulfide deposits and mineralization in the Troodos type ophiolite evidently provides an analog of hydrothermal sulfide deposition on present ocean floor. The well developed anticlinal structure and good exposure further provide an unusual opportunity for

the variations of these deposits at depth to be seen.

The crustal constructional study reveals a close spatial relationship between the 25% dike contour surface and the locations of sulfide deposits. A preservation model is proposed for the orebodies formed on the spreading centers by black smokers and four possibilities are considered. Although metallic elements may have a very complex history when they are transmitted in hydrothermally circulated seawater at spreading centers, features of the copper distribution in the basaltic rocks in Troodos suggest that since Cu displays a regular distribution it is active in the hydrothermal process.

Chapter 7 Summary and Discussion

In the previous chapters, the main constructional features of the Extrusive Sequence of the Troodos ophiolite, such as volcanic cyclicity in vertical sections, dike increase with depth, regional hydrothermal alteration zonation, as well as their spatial relationships to each other and the sulfide deposits, have been characterised and discussed. In this chapter, the main results will first be summarized. Then, questions such as how to apply the results from the Troodos ophiolite to the present oceanic crust and to other ophiolites, as well as what problems and insufficiently defined points remain, will be discussed.

7.1 Summary of main results

1. Extrusives

The extrusives in Troodos mainly consist of two morphological forms, i.e., pillow lava and sheet flows, which show regular variation in proportion laterally and with depth and suggest cyclic eruption at the spreading center responsible for the ophiolite.

The proportion of pillow flows at different stratigraphic

levels is frequently remarkably constant in an east-west, spreading direction, although zones defined by a specific proportion of pillow flows vary in thickness over the same distance. In general, high P values are almost everywhere concentrated at the top of the Extrusive Sequence.

At least two volcanic eruptive cycles, comparable to those recognized at modern mid-ocean ridges (Crane and Ballard, 1981), are apparently represented in the Extrusive Sequence in the central part of the study area by a repetition in vertical variation from high proportion of sheet flows (low P values) to a high proportion of pillow flows (high P values). P generally increases upward from <0.25 to >0.75 much more rapidly in the first, older, cycle than in the second, younger, cycle. On the other hand, in both the eastern and western parts of the study area, P contours are locally variable and isolated areas of high and low P occur. These are also thought to be related to original constructional features of the crust, expressing cyclicity in the axial direction.

Four areas with thick sheet flow sequences and very small contributions from pillow flows are assumed to mark periods of high magma productivity at the spreading axis, where high extension and crustal accretion accompanied by high mamga productivity were benificial for the large scale hydrothermal circulation of modified seawater and sulfide deposition.

Sheeted dikes reached a high crustal level in these areas. The areas are separated by an average of about 12 km in the spreading direction.

2. Dike abundance

Dikes occur through the Extrusive Sequence and generally increase in abundance downward, reaching a maximum in the Sheeted Complex. The abundance of dikes increases with depth at different rates in different areas. Both in the east and west parts of the study area, some isolated areas of high F represent original constructional features of the crust.

The contours of dike abundance in the study area show a close relationship to alteration zonation and to the spatial distribution of sulfide deposits, reflecting most important features of at least Troodos type oceanic crustal construction.

3. Alteration zonation

Three regional alteration zones can be recognized within the Extrusive Sequence, i.e., from top to bottom, a brownstone alteration zone, a transition zone, and a greenstone alteration zone.

Rocks in the brownstone alteration interval are characterized by yellowish, reddish or greenish brown colors, with ubiquitous clays, some carbonate, amorphous silica and zeolite, which suggests low temperature, cold or warm-seawater alteration. The transition zone is defined as that interval containing secondary minerals of both the brownstone and greenstone zones. Some of the secondary minerals in this zone are characteristic, such as the forms of chlorite and quartz, and laumontite. Rocks in the greenstone interval are characterized by a greenish grey color, with dominant chlorite,quartz and, in some areas, with minor epidote and albite, representing pervasive alteration by high temperature, modified seawater.

Alteration temperatures for the transition and greenstone zones, based on secondary minerals, increase rapidly with depth and the boundaries between these zones follow closely contours of dike abundance, suggesting that dikes are the major heat source responsible for hydrothermal alteration accompanying crustal formation in ancient ocean crust.

4. Sulfide deposits

In the Troodos ophiolite as a whole, a total of 34 sulfide deposits are located within the Extrusive Sequence. The deposits occur in groups with a 10-13 km spacing in the

spreading direction between groups. Each group consists of 2-4 deposits. The sulfide deposits in the study area tend to occur on the flanks of high sheet flows areas and show a close relationship with contours of dike abundance. That is, at least 10 of 13 deposits occur at a level just above the 25% dike abundance contour surface. This level is interpreted as the optimal crustal depth for the preservation of ore bodies formed on or very near the sea floor.

This constructional study reveals both first and second order features of the Troodos ophiolite, which will be of significance in comparison with and will improve our knowledge of the present oceanic crust.

7.2 Comparison with knowledge of the present ocean crust

In this section, comparison of constructional features between the Troodos ophiolite and the present oceanic crust covers several aspects: extrusive processes, alteration zonation, the occurrence of sulfide deposits, tectonic environments, and spreading rate.

7.2.1 Extrusive processes

Extrusive processes on the present seafloor have been studied since the 1970s. Pillow flows were the first to be

recognized and have been described in detail (e.g., Ballard and Moore, 1977). Later, sheet flows were also recognized to be a significant component of the extrusives at the accreting plate margin (Lonsdale, 1977). Ballard et al. (1979) defined the term sheet flows to describe extensive flows with surfaces that are smooth in comparison to pillow basalts. "Sheet" for Ballard et al. denotes only the smooth surface form of the flow; it does not describe the mechanics of flow emplacement or the thickness of the flow.

Based on surveys of the Mid-Atlantic Ridge (MAR), the Galapagos Rift at 86°W, and the East Pacific Rise (EPR) at 21°N, Ballard et al. (1981) proposed a tectonic model for volcanism in the rift valley. In this model, the sheet flows represent early, brief but voluminous eruptions, which are followed by more sustained, slower but steadier eruptive phases that produce pillow basalts. For example, on the EPR at 21°N, they observed that sheet flows appear to have been the first product erupted during each of the three cycles recognized there, with pillow lavas formed later in each eruption sequence. The pillowed flows are steep-sided and travelled only a short distance from their eruptive fissures, building stubby volcanic ridges. The youngest sheet flows appear to have flowed rapidly downslope through gaps in the older terrain, ponding at base of faults (Ballard et al., 1981).

Later, Ballard et al. (Argo-Rise Group, 1988) realized that most geologic studies of the Neovolcanic Zone of the EPR have concentrated on topographic highs that are typically marked by recent volcanism and hydrothermal activity, and there is a need to extend detailed studies along the strike of the ridge. The results of geological mapping based on photography and video data along 90 km of the crest of the EPR, north of the Clipperton Fracture Zone, by the Argo-Rise Group (1988) also show episodic magmatic activity along spreading centers on the East Pacific Rise axis (10°19' - 11°53'N). In that particular area the magmatism follows a cyclical pattern, progressing from pillow-lava emplacement, to extrusion of sheet flows, to a waning phase of pillow extrusion, and finally to pelagic sedimentation. Hydrothermal activity seems to be associated only with this second phase of magmatic activity.

The third dimension of the extrusive process on the seafloor can be observed from the drillholes on the seafloor, although there are only few deep drillholes (defined as a penetration of over 500 m in basement) in which pillowed and sheet flows have been generally separated. The three deep drillholes available for comparison with Troodos are holes 418A (on the Bermuda Rise) and 395A (south of the Kane fracture zone near 22°N) in the North Atlantic, and 504B (in the Costa Rica Rift Zone) in the Pacific. Hole 332B in

Atlantic, although it penetrated over 500 m in basement, due to no division of morphology types of lava flows in the cores, is not included here.

Hole 418A is located in 108- to 109 Ma old Cretaceous crust in the North Atlantic and achieved a total penetration of 868 meters of which 544 m was in basement with an average recovery of 72 per cent in basement. The basement section drilled in Hole 418A consists of 72 per cent of pillow basalt and pillow breccia (consisting of pillow fragments) and 28 per cent of massive flows, the latter being most abundant at the top and bottom of the section. The extrusives were cut by high-angle dikes in the deepest levels of the hole (Fig. 7.2.1) (Shipboard Scientific Parties, Legs 51-53, 1980). If we take each 100 m as a unit to measure average P values, the P values vary, from bottom to top, from low to high and then low again (Table 7.2.1), while F generally increases with depth. Therefore, two eruptive cycles, according to Ballard and Francheteau (1981), can be distinguished, which is consistent with the evidence that high magma production rate eruptions, in most cases, appear immediately or very shortly after major noneruptive periods as inferred from breccia zones and magnetic breaks (Shipboard Scientific Parties, Legs 51-53, 1980). Several other drillholes at Sites 418 and 417, e.g., hole 417D, although their sections of basement are relatively short (<500 m), show that lateral variations of lava

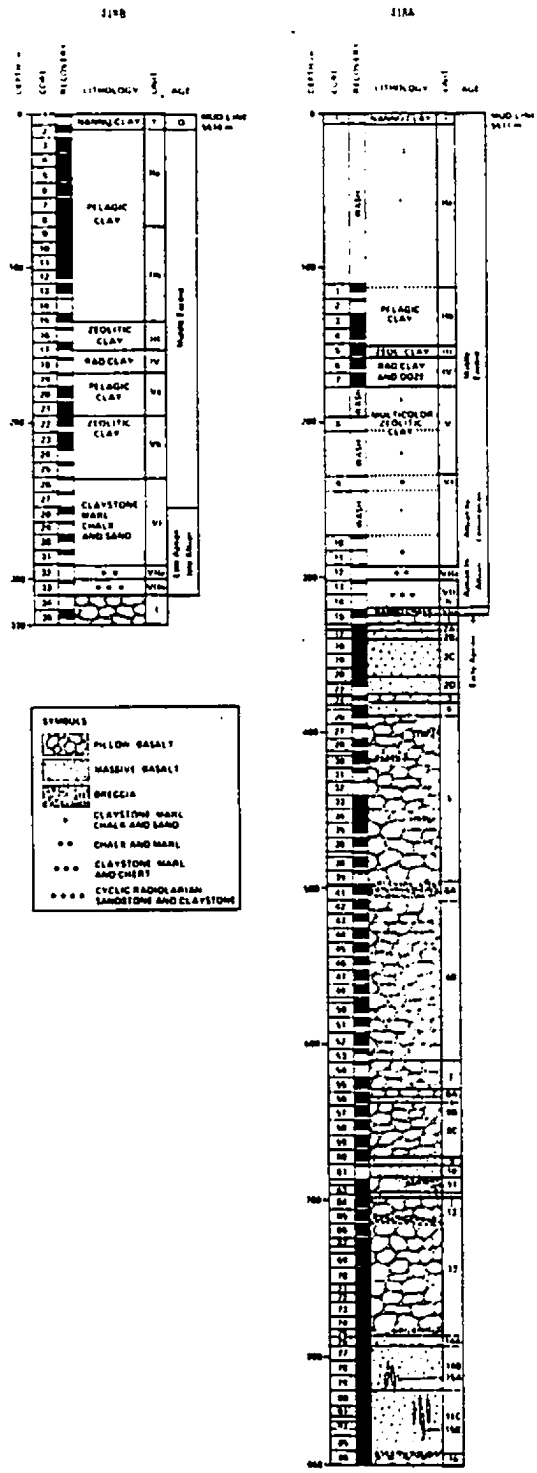

Fig. 7.2.1 Basement stratigraphy, Hole 418A and 418B, in the North Atlantic Ocean (after Shipboard Scientific Parties, Leg 51-53, 1980).

Table 7.2.1 Average P values for 100 m Intervals for Three Deep (>500 m in Basement) DSDP Holes

Depth (m)	504B (780 m)	418A (544 m)	395A (571 m)
0-100 m	0.9	0.5	0.9
100-200 m	0.9	1.0	0.7
200-300 m	0.7	1.0	1.0
300-400 m	0.6	0.8	1.0
400-500 m	0.6	0.6	1.0
500-600 m	0.7	0.2	0.9
600-700 m	0.7		
700-800 m	0.6		

Data sources:
Hole 504B- Shipboard Scientific Parties, Leg 69, 1983; Shipboard Scientific Party, Leg 83, 1985.
Hole 418A- Shipboard Scientific Parties, Leg 51-53, 1980.
Hole 395A- Shipboard Scientific Party, Leg 45, 1979.

morphology and dike abundance occur locally (Shipboard Scientific Parties, Legs 51-53, 1980).

Hole 395A is an example from young crust (less than 10 million years old) on the Mid-Atlantic Ridge. The calculated half spreading rate in the area averages 1.7 cm/year (Hussong et al., 1979). The hole penetrated 571 meters of igneous basement with a recovery of about 19 per cent (Shipboard Scientific Party, Leg 45, 1979). The basalts in this hole occur dominantly as pillow flows (92 per cent, including 10% pillow breccias), and very much less common sheet flows (8 per cent) (Fig. 7.2.2). Sheet flows occur as thin layers intercalated with thick pillow flows and, therefore, P values are consistently high (see Table 7.2.1). Although both Holes 395A and 418A have high ratios of pillow flows to massive flows, relatively speaking, features of eruptive cyclicity in Hole 418A are more obvious than in Hole 395A. The latter is also characterized by more pillow breccias.

Hole 504B is by far the deepest hole yet drilled into the oceanic crust in situ and is located at the Costa Rica Rift, in the eastern equatorial Pacific Ocean, where the crust is 5.9 Ma old (Becker et al., 1989). The half spreading rate of the Costa Rica Rift at the time of formation of the crust at 504B was 3.6 cm/yr (Klitgord et al., 1975, quoted in Langseth et al., 1983). Hole 504B extends to a total depth of 2000.4 m

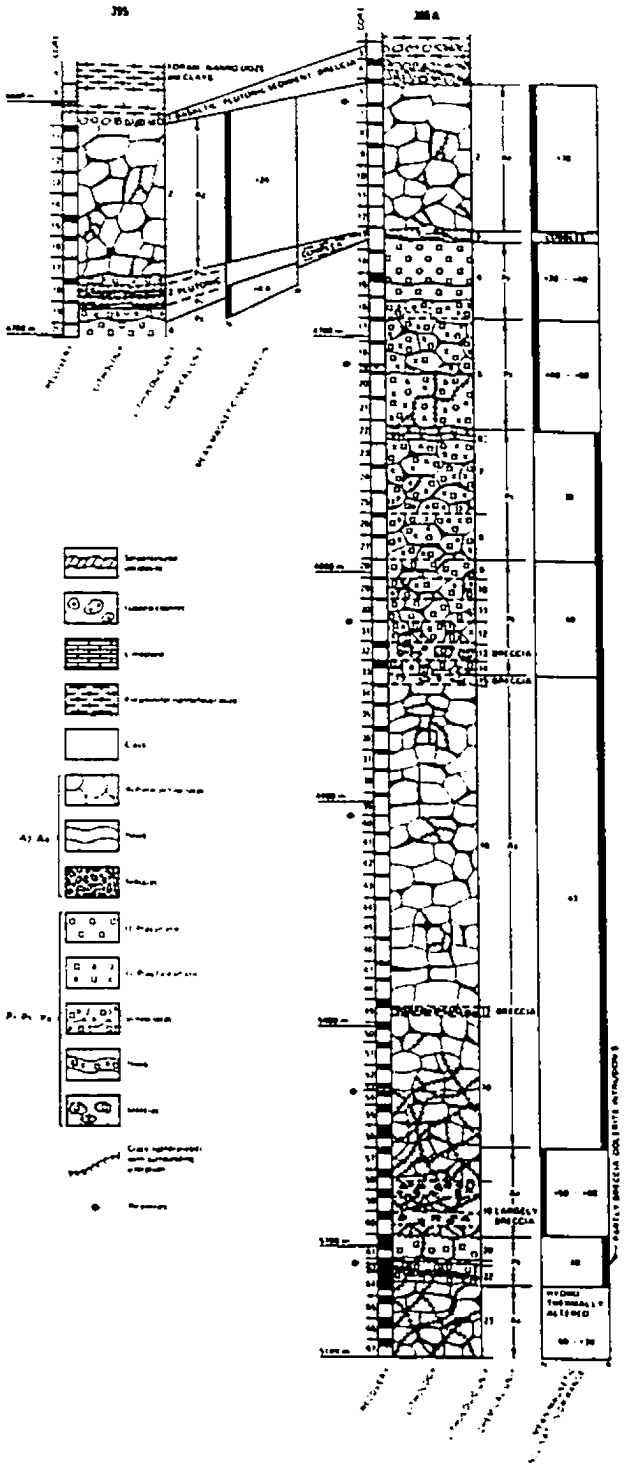

Fig. 7.2.2 Basement stratigraphy, Holes 395 and 395A, in the North Atlantic Ocean (after Shipboard Scientific Parties, Leg 45, 1979).

below the seafloor, penetrating 274.5 m of sediments and 1725.9 m into basement. This section includes 571.5 m of extrusive lavas, underlain by a 209 m transition to 945.4 m of intrusive sheeted dikes (Fig.7.2.3a and b) (Shipboard Scientific Parties, Sites 501 and 504, 1983; Shipboard Scientific Party, Leg 83, 1985; Becker et al., 1989; Shipboard Scientific Party of Leg 140, 1991, personal communication). Within the extrusive sequence, i.e., the 780.5 m interval of extrusive lavas and the transition interval, the proportion of pillow lava flows is higher than that of sheet/massive flows with an average P of 0.7. If we take average values of P for 100 m intervals, it is clear that P values show a gradual increase from the bottom to the top of the section (see Table 7.2.1), which is consistent with the fact that pillow lava units toward the base of the transition zone become thinner, while massive units and/or dikes progressively increase in abundance and frequency toward the base of the transition zone.

In summary, the above three examples from deep drilling on the seafloor show the diversity of igneous sections from in-situ oceanic crust, i.e., from bottom to top, P increases cyclically in Hole 418A, P is almost constantly high in Hole 395A, and P increases gradually in Hole 504B.

One thing is noted that the recoveries of igneous section

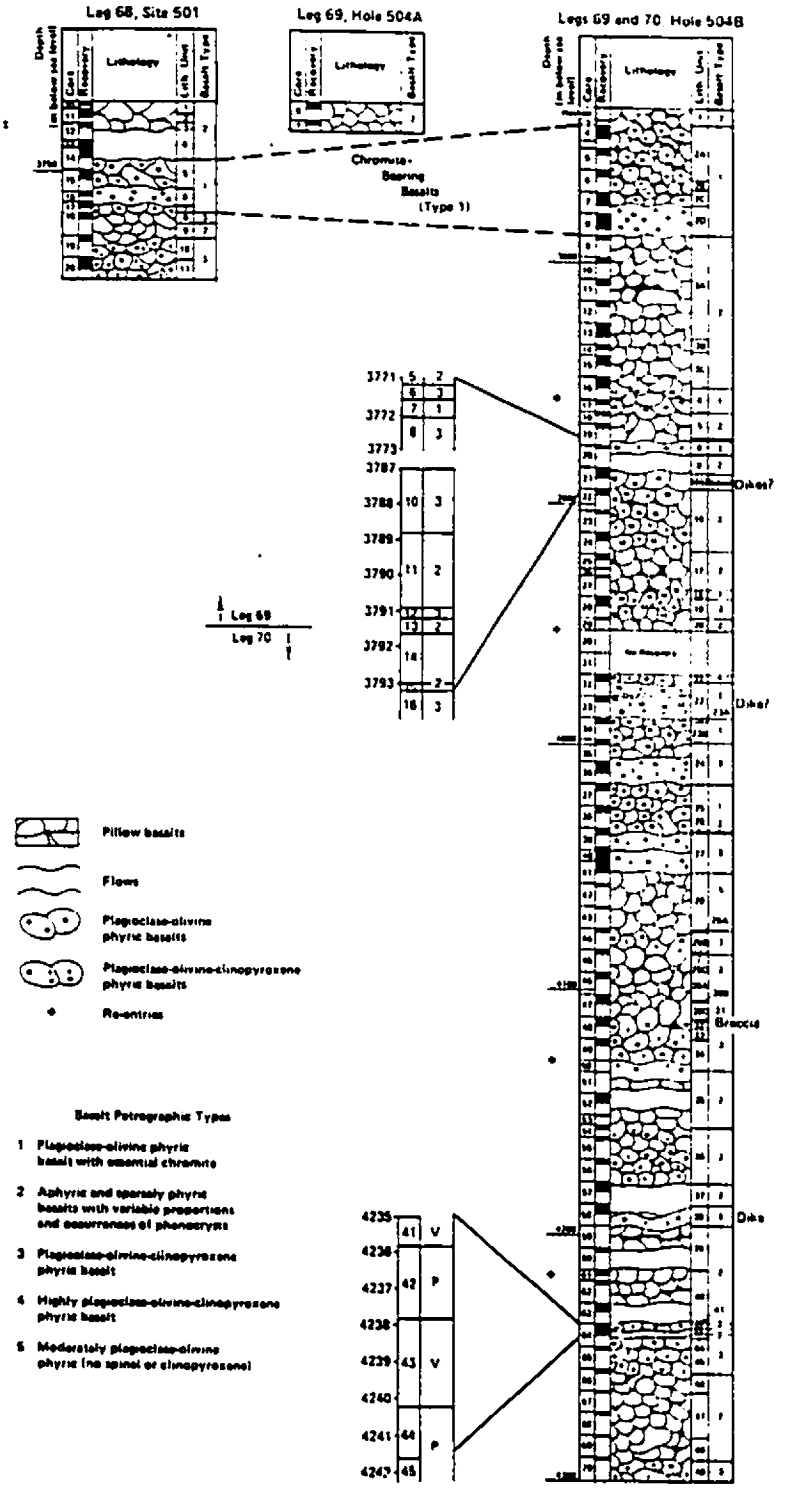

Fig. 7.2.3a Summary of basement stratigraphy, Hole 504B, at Legs 69 and 70, in the Pacific Ocean (after Shipboard Scientific Parties of Leg 68, Leg 69, and Leg 70, 1983).

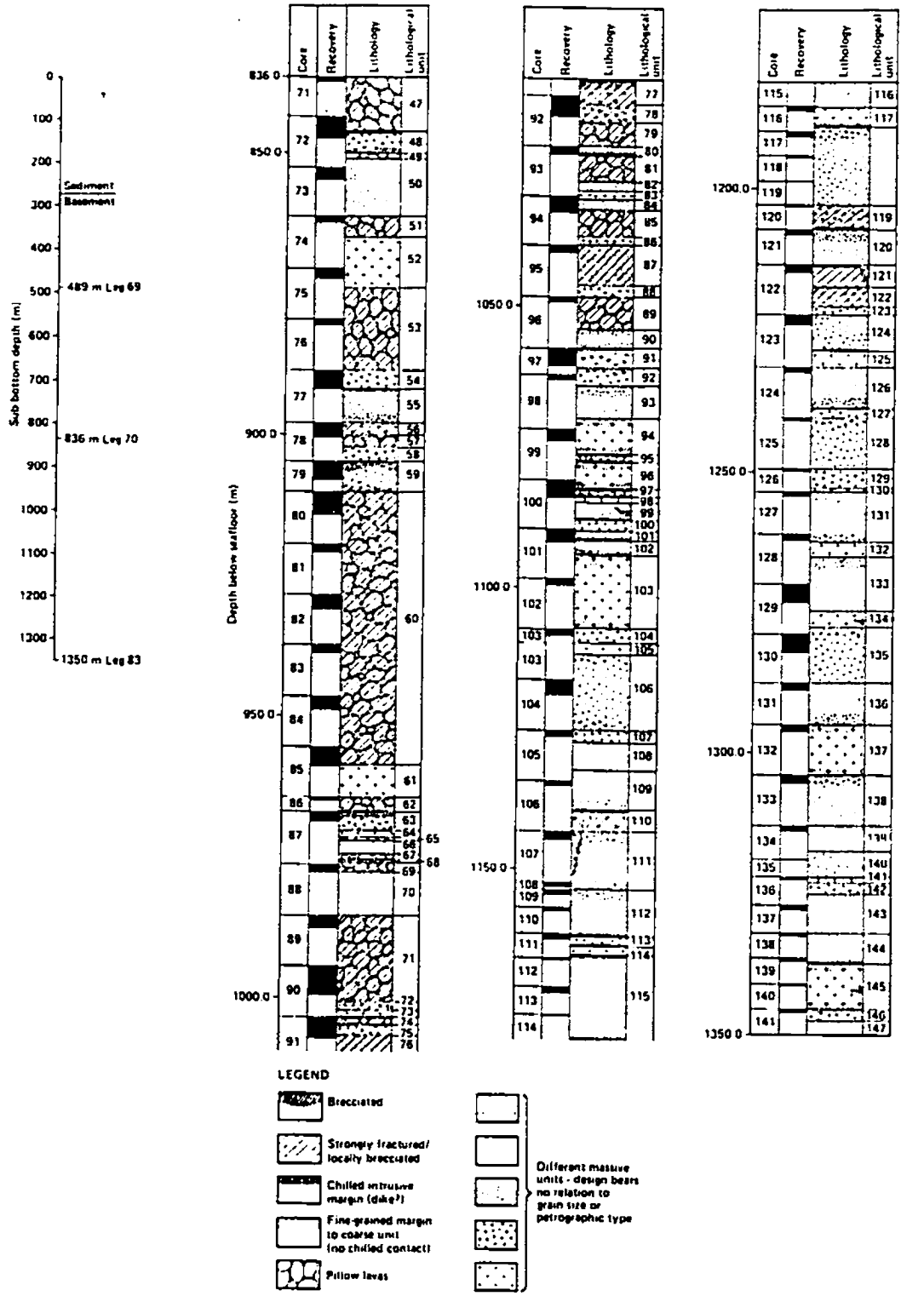

Fig. 7.2.3b Lithostratigraphy of the section of Hole 504B drilled during Leg 83 (after Shipboard Scientific party Leg 83, 1985).

in Holes 395A and 504B only are about 19% and 20% on average, respectively, in contrast to Hole 418A which has a recovery of 72%. The low recovery has seriously affected any attempt to draw an accurate lithological column to represent the rocks drilled in these holes (Shipboard Scientific Party, Leg 83, 1985). It is difficult to judge the possible influence at the low recovery in these holes to the form of the stratigraphic column drawn up by the Shipboard Scientific Parties. Low recovery in these holes may also bring forward another argument for high P ratios. However, a safe assumption is that pillows and sheet flows have an equal chance of recovery, and a high P value (P=0.9) observed on MAR at 37°N (Crane and Ballard, 1981) as well as in Hole 418A at least suggests that a high pillowed lava ratio (P=0.92) in Hole 395A is reasonble.

In comparison with the volcanism at the present mid-ocean ridges, the cyclic eruption in Troodos is most similar to that observed in Hole 418A, a segment of Cretaceous oceanic crust. That is, in each individual cycle the eruptive activity started with bulk sheet flows and ended with pillowed flows. However, the extrusives in Troodos provide quantitative information on the variation of the ratio of pillow to sheet flows both laterally and with depth, which is still generally not available for the present seafloor due to constraints arising from limited recoveries and the isolated nature of

sections.

It is interesting that the average ratio of pillowed flows in Troodos is lower than that reported in all three DSDP holes. Since the most westerly part of the study area shows variations in the axial direction and the most easterly part is less deeply eroded (see Chapter 3), the middle part of the study area is taken as giving a typical section through the whole Extrusive Sequence. The average P value from five profiles from the SEI to the top of the SC for the middle part of the area is 0.4, which is much lower than values from the three DSDP holes, 395A (P=0.9), 418A (P=0.7) and 504B (P=0.7). It is noted here that the holes 418A and 395A did not cover the whole extrusive sequence. However, considering the situation in hole 504B, where P values only show very limited decrease in the lower part of the Extrusive Sequence, the averages of P for the whole extrusive sequence of these two holes may not be significantly different for the value to the SC. Even suppose the whole extrusive sequence in these two holes is 1 km thick in average, as in Troodos, and the unpenetrated part has P<0.25, the averages P of the extrusive sequences in the two holes are still higher than for Troodos. On the other hand, if we consider that most drillholes on the seafloor are located in topographic lows where sediments are relatively thick, needed to stabilize the bottom hole assembly to allow initial penetration of basement, coupled with the

fact that in Troodos high proportions of sheet flows occur in lows in the seafloor, the actual local average P values in the areas where the three DSDP drillholes are located may possibly be even higher. The variation of the P values in these three holes may be related to the spreading rate in in-situ oceanic crust. This possibility will be discussed in section 7.2.5.

In general, the eruptive cyclic model at spreading centers proposed by Ballard and Francheteau (1981) has been little modified after a further ten years study of the ocean floor, both from deep sea drillholes and investigations on the seafloor at many different oceanic ridges. The Extrusive Sequence in Troodos provides a good example of cyclic eruptive activity in the construction of oceanic crust in both vertical and horizontal directions, which can be compared to variation in the vertical direction in present oceanic crust.

7.2.2 Alteration zonation

Alteration zones are known to be formed in both in-situ oceanic crust and in ophiolites. However, since most drillholes on the seafloor only reach shallow depths in basement, only low temperature alteration minerals and zones have been identified in all but one of these drillholes. Examples here are Holes 395A, 418A, and 332B, even though these holes have reached as deep as over 500 m in basement

(e.g., Shipboard Scientific Party, Leg 45, 1979; Shipboard Scientific Parties Legs 51-53, 1979; Shipboard Scientific Party, Leg 37, 1977).

The deepest hole in the present oceanic crust, 504B, provides the only opportunity to see alteration zones deep in the modern oceanic crust. Studies indicate that all of the recovered basalts are altered to some degree (Becker et al., 1989). Alteration in Hole 504B has been divided into three zones with distinct assemblages of secondary minerals (Fig. 7.2.4) (Honnorez et al., 1983; Alt et al., 1985, 1986; Shipboard Scientific Party Site 504B, 1988). The three zones given in Becker et al. (1989) are: 1) the upper 310 m of the pillow lavas, characterized by oxidative alteration; 2) the deeper extrusive section (310-624 m), characterized by smectite and pyrite; and 3) the combined transition zone and dike section (below 624 m), characterized by greenschist-facies minerals but with mixed-layer clays still present. There is possibly a fourth zone with chlorite but no mixed-layer clays from 1250 m down.

A synthesis of results from several DSDP and ODP basement holes (Gillis and Robinson, 1988; Hall and Robinson, 1979) shows that the distribution of alteration zones in the extrusive sequence is systematic but not all zones are ubiquitous. For example, the seafloor weathering zone (closely

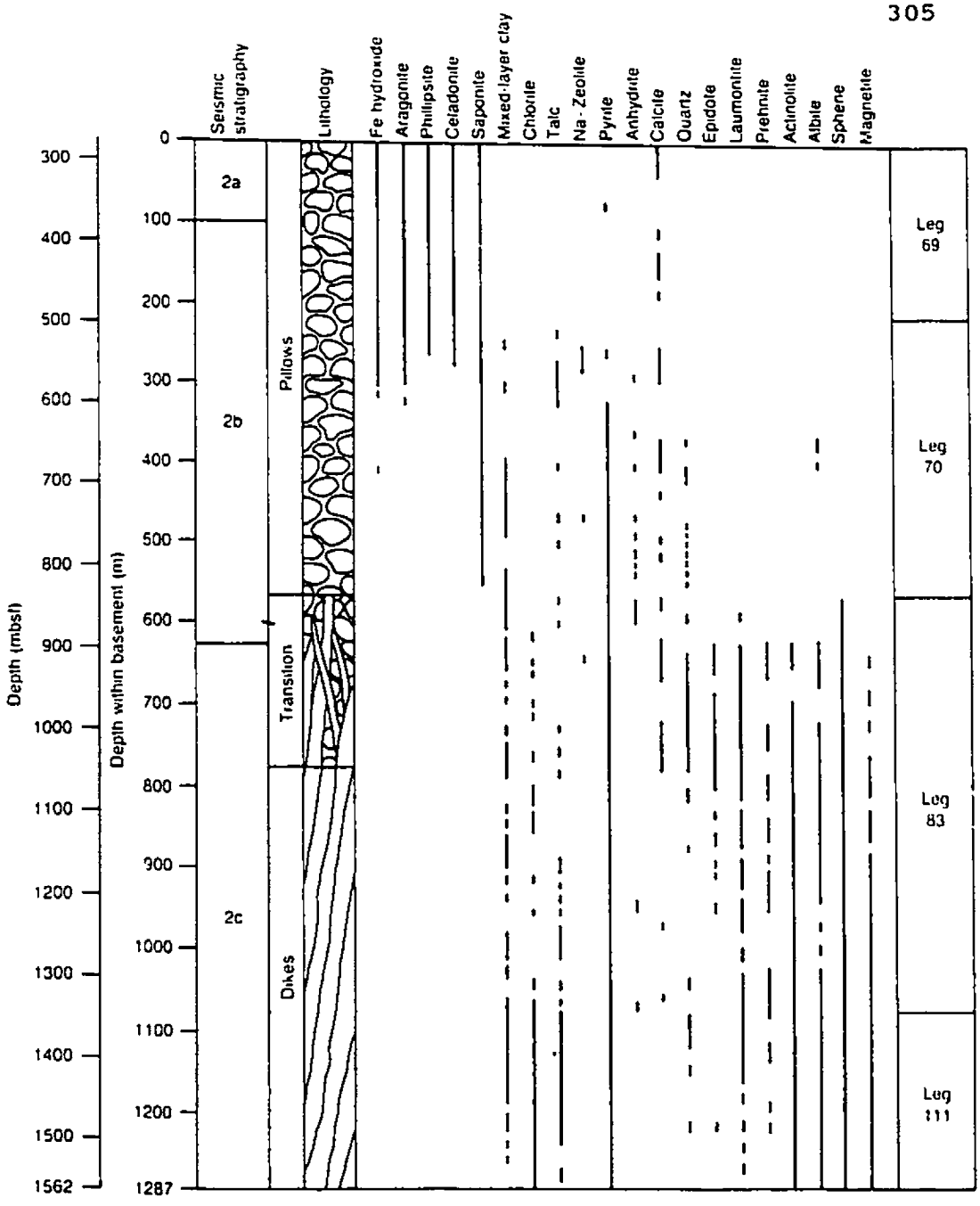

Fig. 7.2.4 Distribution of secondary minerals with depth in Hole 504B (after Becker et al., 1989).

equivalent to the UPL alteration facies in Troodos), identified in the upper part of basalts in Hole 504B, is also found in holes 396B, 417A and 417D, but does not occur in holes 332B, 395A and 418A. The seafloor weathering occurred relatively late, overprinting earlier, less oxidative low temperature alteration on the seafloor, and the thickness and distribution of the weathering zone is dependent on the rate and nature of sedimentation and the morphology of original seafloor (Gillis and Robinson, 1990). Thus, the seafloor weathering zone in oceanic crust is not an essential alteration zone observed everywhere in the ocean, nor does it occur everywhere in ophiolites, e.g., in Troodos (Gillis and Robinson, 1988; this study).

However, at least the three alteration zones, i.e., a brownstone zone (zeolite facies), a transition zone and a greenstone zone (greenschist facies) identified in this study, always exist in the Extrusive Sequence in both present and ancient oceanic crusts, i.e., at the bottom of Hole 504B where mixed-layer clays disappear, Troodos, the Macquarie Island ophiolite (Griffin and Varne, 1980; Cocker et al., 1982), and the Sarmiento ophiolite complex in Chile (Elthon and Stern, 1978) and the other southern Chilean ophiolites (e.g., Stern et al., 1976).

It is interesting that the greenstone alteration zone in

the Troodos ophiolite appears at the levels where F ≈ 0.5 within the Extrusive Sequence. The close relationship between dike abundance and alteration zonation in Troodos suggests that the intrusion of dikes is most likely to have served as the heat source responsible for hydrothermal alteration during the crustal construction. Since quantitative mapping of dike abundance is difficult in present oceanic crust and in most other ophiolites, it is too early to say that the correlation between dike abundance and alteration zones is universal. However, there are several examples which show that greenschist facies alteration begins to appear in the pillow lava sequence at ~ 1 km below from the sedimentary/ extrusive boundary, a situation very similar to that seen in Troodos, although nowhere are quantitative dike abundance data reported. Examples are the Macquarie island ophiolite (Cocker et al., 1982), the Sarmiento ophiolite complex of Chile (Elthon and Stern, 1978) and other southern Chilean ophiolites (Stern et al., 1976), as well as the eastern Iceland crust (Mehegan et al., 1982).

If we suppose that the alteration zoning processes which occurred in the present oceanic crust and Troodos were the same, as other comparisons between them have also been demonstrated, the data from DSDP hole 504B (Alt et al., 1986; Becker et al., 1989) may have more than one interpretation. That is, the so called "Dikes" sequence, which is supposed to

appear at about 800 m depth, contains both zeolite and greenschist facies mineral assemblages, and may in fact belong to an extended transition zone between the Extrusive and Sheeted Dikes sequences. One piece of evidence for this is from Backer et al. (1989) who reported that massive basalt occurs extensively below 800 m. Inspection of three-dimensional images generated from the BHTV (borehole televiewer) record in the lower portion of the borehole reveals the surprising appearance of pillow lavas at a depth (1475 m) previously assumed to be composed of sheeted dikes (Morin et al., 1989). As a result, the transition from lava flows to sheeted dikes may extend over a substantially thicker interval of basement. Therefore, a true Sheeted Dike sequence with 100% dikes, with greenschist facies hydrothermal alteration, could only be located at greater depths than has presently been penetrated. The possibly misleading identification of sheeted dikes was mostly probably caused by the low core recovery, this being only 23.4% on average.

7.2.3 Sulfide deposits

The constructional setting of seafloor sulfide deposits has been widely discussed (e.g., Hekinian et al., 1980, 1983; Lonsdale et al., 1980; Ballard et al., 1981; ODP Leg 106 Scientific Party, 1986; Kappel and Normark, 1987; Davis et al., 1987; Hekinian and Fouquet, 1985; Marchig et al., 1988;

Scott, 1987). Although most observations have been restricted to the seafloor, and usually to a limited and isolated area without sediment cover, these seafloor sulfide deposits appear to be generally compatible in occurrence and distribution with the Cyprus massive sulfide deposits, as already suggested by Spooner (e.g., 1980), Oudin et al., (1981), Oudin and Constantinou (1984), Adamides (1987) and others.

Rona (1988) recently reviewed the global data base and revealed that: 1) a range of hydrothermal mineral-deposit sizes from small to large ($\geq 1 \times 10^6$ tonnes) occurs at all seafloor spreading rates; 2) sulfide deposits on the seafloor can be divided into sediment-hosted and volcanic-hosted types. Larger deposits are more common in sediment-hosted than in volcanic-hosted settings regardless of spreading rate; 3) both volcanic- and sediment-hosted deposits may occur in the tectonic settings of early and advanced stages of opening of an ocean basin. However, in general, knowledge of the size, shape and composition of hydrothermal mineral deposits at seafloor spreading centers is limited by inadequate measurement and sampling techniques. Information on mineral deposits at seafloor spreading centers is incomplete in two dimensions, and almost unknown in the third direction (Rona, 1988).

The sulfide deposits observed on the ocean floor

generally occur within the volcanically active zones of ridges. These volcanically active zones are usually very narrow, e.g., the axis of the East Pacific Rise is marked by a zone of recent volcanism approximately 1 km wide (Spiess et al., 1980), although some rift valleys contain active zones up to 3 km wide. The spreading centers in the Guaymas Basin, where a high-temperature hydrothermal deposit was found on the seafloor, have 3- to 5-km-wide rift valleys (Lonsdale et al., 1980). The groups of ore deposits in the Troodos ophiolite mostly have comparable 2-5 km lateral extent as measured in the spreading direction. However, the Cyprus ore deposits occur in groups separated by much wider barren intervals (~ 12 km) in the spreading direction and it is not known whether hydrothermal sulfide deposits in in-situ oceanic crust are similarly distributed.

Ballard and Francheteau (1983), in their model of the Mid-Ocean Ridge crest and associated sulfide deposition, proposed that at peak elevations in the ridge crest, approximately mid-way between transform offsets, the thermal gradient would be at a maximum, copious sheet flows would be formed, and hydrothermal activity would be at a maximum. This model suggests that large sulfide deposits would be formed regularly in these positions and would be preserved along flow lines away from the ridge crest. Evidence indicates that sulfide deposits in the northeast Pacific ocean are commonly

found along topographically elevated areas of ridge crests that are dominated by young sheet lava flows (e.g., USGS Juan de Fuca Study Group, 1986; Kingston et al., 1984; Scott et al., 1984).

Kappel and Franklin (1989) note that some deposits in the northeast Pacific Ocean do not occur in areas of the youngest lavas and are found in areas dominated by pillowed flows rather than sheet lava flows and, then, propose a tectonic model with three stages accounting for relationships between geologic development of ridge crests and sulfide deposits (Fig. 7.2.5). In their model, the first stage is a period of excessive extrusive axial volcanism and inflated pillow lavas are dominant; at the second stage volcanism is rare to absent; and the third stage is characterized by renewed volcanism with sheet and lobate lava forms dominant. Deposits at stages 1 and 2 are relatively large but at stage 3 are very small.

The above two models, by Ballard and Francheteau (1983) and Kappel and Franklin (1989), are both conceivably correct and consistent with the distribution of ore deposits in Cyprus. From this study, the sulfide deposits in the study area in Cyprus occur at either in sheet flows or in pillow flow areas, or at the transition from dominant sheet flows to more pillow flows (see Fig. 6.4.4). The latter phenomenon has recently been observed in the MARK area at 24°N on the Mid-

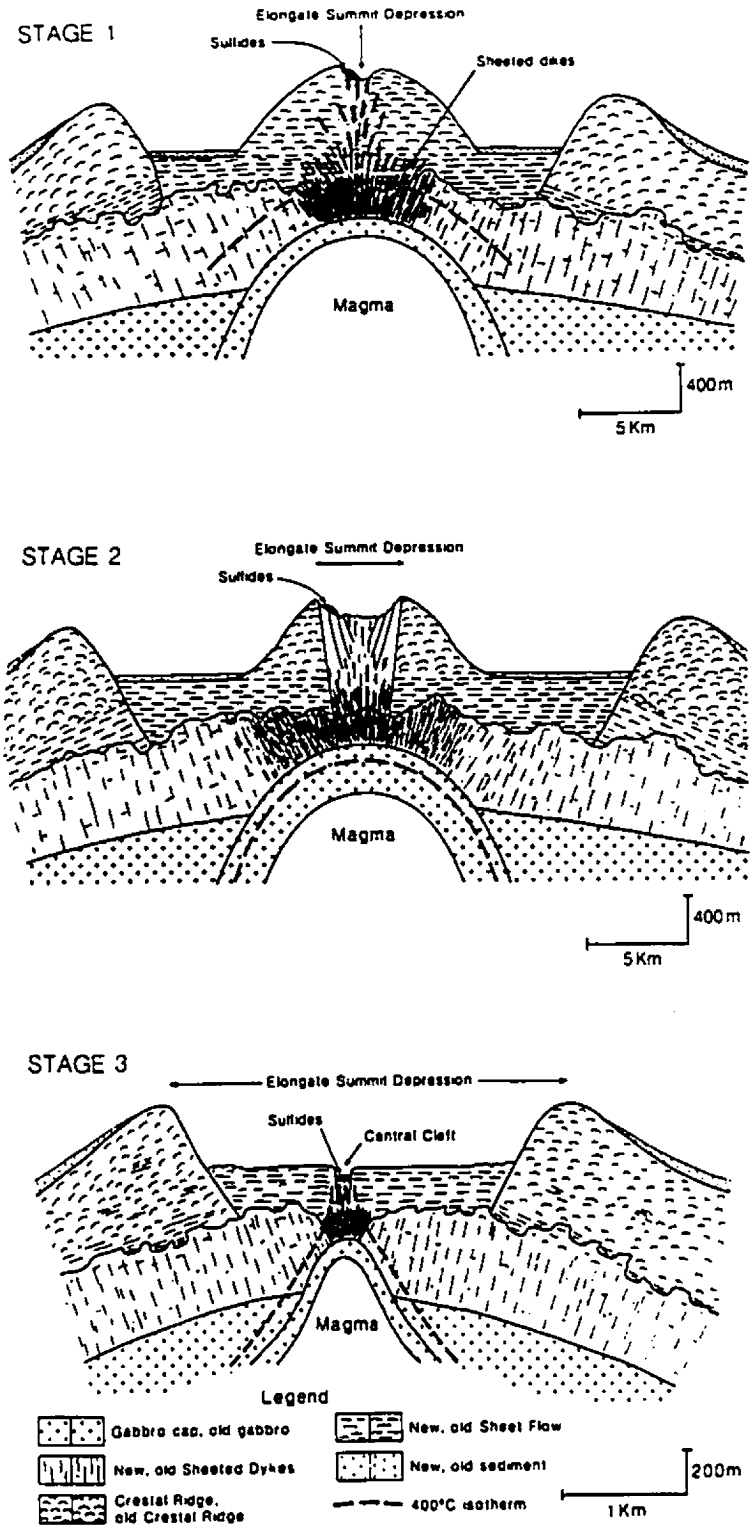

Fig. 7.2.5 A tectonic model proposed by Kappel and Franklin for the formation of sulfide deposits at the northeast Pacific spreading centers (after Kappel and Franklin, 1989).

Ocean Ridge where active vents occur on a neovolcanic ridge close to the Kane transform offset and consisting, at the surface, of both pillowed and sheeted flows (ODP Leg 106 Scientific Party, 1986; Karson et al., 1987). Now we can answer the question of whether large masses of sulfides are uniformly or irregularly distributed along flow lines in in-situ oceanic crust. That is, there is no limitation of lava forms or lithologic types for the formation of sulfide deposit in in-situ oceanic crust, but their preservation is spatially related to dike abundance as has been demonstrated in Chapters 6.

The present study of the Troodos sulfide deposits provides some suggestions about the processes that operate below the ridge crest during sulfide formation. One process of particular interest is the formation and lifespan of shallow magma chambers, which occur, at least periodically, beneath active ridges, and presumably provide heat to drive the seawater circulation for sulfide formation. Generally, the gabbroic rocks in ophiolites are presumed to mark the positions of former shallow magma chambers (e.g., Pallister and Hopson, 1981). From the present study, it can be inferred that magma chambers were locally at a relatively high crustal level in the areas now containing sulfide deposits, although the presence and some aspects of geometry of the chamber are unknown through lack of exposure. In these circumstances, the

behaviour of sheeted and other dikes, which presumably radiated from, and are related to, a nearby magma chamber (Greenbaum, 1972; Thy, 1987), may be used as an indicator of the proximity of a chamber. In the Troodos ophiolite a shallow, high abundance of dikes below or near the sulfide ore deposits appears to be an important requirement in the formation of economic deposits and could provide an indication of a need for a high level magma chamber for the formation of such deposits.

As a summary, a model with four stages for eruptive process and sulfide deposition in Troodos is proposed as below.

Stage 1: Volcanic eruption occurred due to extension at spreading centers on the seafloor. Sheet flows erupted first with a high speed due to an abrupt release of energy at the ridge. During or after the sheet flow eruption, hydrothermal alteration and mineralization are developed but the size of sulfide deposit depends on the length of the period of process. Generally, small size mineralization and few economic ores occur at this stage because during this stage the rate of eruption of magma is fast and the time is relatively short for these processes to operate extensively.

Stage 2: After the intense eruption, the energy of

eruption is reduced and the volume of available magma is decreasing. The lava morphology then gradually changes from sheet flows to pillow flows. The pillow lavas will cover the earlier sheet flows. During this stage, the eruptive process is relatively slow and may last substantially longer than stage 1. This is a good opportunity for hydrothermal alteration and mineralization to develop extensively, since rocks formed in the first stage will start to break due to cooling and faulting, and permeabilities are increasing. This period continues to the end of the eruption, which marks the end of an eruptive cycle.

Stage 3: Generally there is a break before a succeeding eruptive cycle. During this period, lava flows will be mainly faulted and jointed during cooling and thus more channels will be provided for hydrothermal flow, while at the same time the heat source is still at a shallow depth below the ridge. The extent of sulfide deposition depends to a great degree on the duration of this stage.

Stage 4: A new cycle of eruption starts again at the ridge crest with sheet flows erupted first as in stage 1 above. New lava flows will seal older fissures and fill grabens and other shallow depressions, and form lava plains. On the other hand, the massive sulfides formed at early stages will be buried and preserved. New hydrothermal alteration and

mineralization will also follow the pattern described above.

Sulfide deposits can be formed at any stage of an eruptive cycle. The size of individual hydrothermal fields and of mineral deposits depends on local physical and chemical conditions that can occur at any spreading rate (Rona, 1984, 1987), and the duration of volcanic activity and quiescence. Relatively large volcanic-associated deposits may occur near prominent marginal (tectonic) faults, but smaller deposits may occur where the hydrothermal activity is generally related to volcanic structures such as eruptive fissures and caldera walls (Kappel and Franklin, 1989; Malahoff, 1982; Embley et al., 1988; Ballard et al., 1981). It is also noted that the largest sulfide deposits along the northeast Pacific spreading centers are found where sediment cover is greatest, because hundreds of meters of sediment may provide an ideal cap to a hydrothermal system (e.g., Kappel and Franklin, 1989).

After formation, sulfide deposits may be destroyed by erosion or chemical decomposition on the seafloor, or be buried by quickly deposited sediments or successive, younger lava flows. On the other hand, some buried orebodies may also destroyed at depth by later processes, such as dike intrusion, hydrothermal circulation, as discussed for the preservation model described in Chapter 6.

In summary, the tectonic-stratigraphic setting of Cyprus-type massive sulfide deposits can be a valuable guide in evaluation of hydrothermal mineral deposits in modern ocean basins. Land-based ophiolites provide an opportunity to observe the third (vertical) dimension of geothermal systems and their volcanic massive sulfide products that occur in oceanic rift zones. The characteristic spatial relationship between dike and sheet flow abundance and the distribution of sulfide deposits provides the possibility to discover preserved orebodies in Troodos and other ophiolites on land.

7.2.4 Tectonic environment of formation of the Troodos ophiolite

It has been suggested that the Troodos ophiolite formed at an old Tethyan ridge as a fragment of oceanic crust and mantle (e.g., Moores and Vine, 1971), an island arc setting (e.g., Miyashiro, 1973; 1975), a back-arc basin origin (e.g., Muenow et al., 1990), or a subduction-related basin (e.g., Cameron et al., 1979, 1983; McCulloch and Cameron, 1983; Schmincke et al., 1983; Robinson et al., 1983; Rautenschlein et al., 1985; Flower and Levine, 1987; Robinson and Malpas, 1990).

Also, it has been postulated that Troodos formed at a spreading axis or axes above an oblique subduction zone with

the suggestion that the Andaman Sea may provide a modern analog (Moores et al., 1984). However, little is known about the Andaman Sea except a single piece of evidence from only one volcanic rock sample, a differentiated tholeiite, dredged from the Sea (Moores, 1984). Besides, other workers believe that it is more difficult to determine the precise environment of formation within this broad zone (e.g., Robinson and Malpas, 1990).

Since some glasses from the Troodos ophiolite have a clear back-arc-basin affinity (Muenow et al., 1990), and also recent successful submersible investigations were carried out in some contemporary back-arc basins (e.g., Lau basin), it is practible to compare the Troodos ophiolite with a back-arc basin as an alternative of a forc-arc basin, both of them formed in a subduction-related environment.

The Lau Basin is a back-arc basin adjacent to the subduction zone of the Tonga Trench (Fig. 7.2.6). Several spreading axes occur within the basin. The northern spreading axis at the center of the basin consists of tholeiitic basalt. The southern segment is made up of a differentiated series of Fe-Ti basalts, andesites, dacites and rhyolite (Jenner et al., 1987; von Stackelberg and Shipboard Scientific Party, 1988). This area shows the clear influence of the subducted slab on the composition of the lavas (Sunkel, 1990). Very-high-

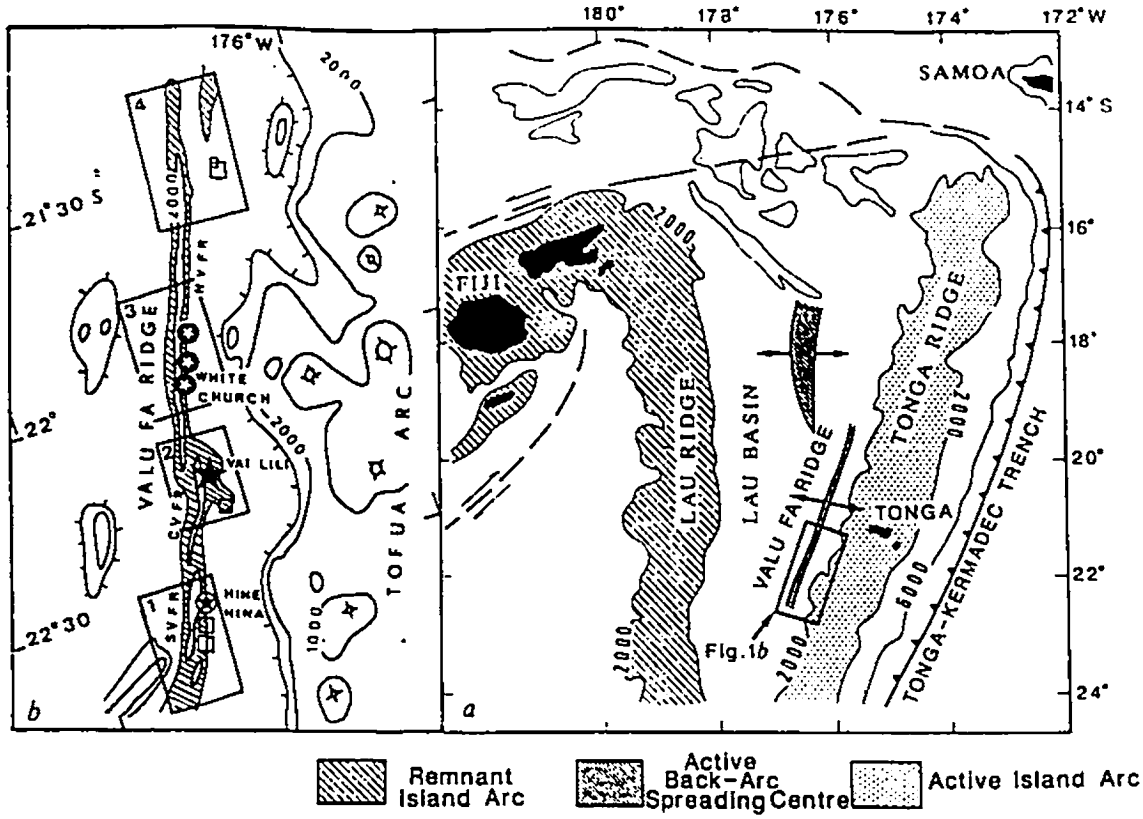

Fig. 7.2.6 General map of the Lau back-arc basin and b) location of hydrothermal fields. Varied symbols such as stars, squares mean sulfides with different compositions (after Fouquent et al., 1991).

temperature black (320-400°C) and white smokers (250-320°C) were discovered at the central Valu Fa Ridge (Fouquet et al., 1990), where the active zone is controlled by a normal fault. The hydrothermal plume rises up to 200 m above the bottom. The temperature anomalies on the bottom are up to 30°C a few meters from the vents, compared with only some tenths of degrees at hydrothermal sites in the MOR systems. Away from the sulfide chimneys there are important zones of widespread low-temperature discharge (Fouquet et al., 1991).

Crusts of manganese oxide (some up to 10 cm thick) have been produced by extensive (several kilometers long) low temperature discharge zones related to the high permeability of the andesites. These Mn deposits are located at the top or next to the sulfide ore bodies (e.g., von Stackelberg et al., 1988), and are thought to be comparable with the umbers in Troodos.

The mean values of sulfide composition from the Lau Basin have been compared with sulfides from mid-ocean ridges and Kuroku by Fouquet et al. (1991) (Table 7.2.2). The most striking contrasts between the Lau Basin and EPR deposits are the importance of barium and high arsenic and lead in the outer part of the Lau Basin deposits, and visible primary grains of native gold are found in the outer part of the Lau Basin barite/sulfides chimneys. Some elements, such as Au and

Table 7.2.2 Comparison of compositions of Lau Basin, mid-ocean ridge, Kuroko and Troodos sulfide deposits

	Lau Basin	Mid-Ocean Ridge	Kuroko	Troodos
n	29	33	39	15
Au (ppm)	1.42	0.26	1.58	0.29
Ag (ppm)	191.34	49	215	10
As (ppm)	1602	154		1775
Pb (wt%)	0.27	0.05	1.78	*0.03
Ba (wt%)	14.16	0.08		*0.09

Data sources:

Lau Basin- Fouquet et al., 1991.

Mid-Ocean Ridge- (East Pacific Rise, 13°N) Fouquet et al., 1988; Fouquet et al., 1991.

Kuroko- Tanimura et al., 1983 (quoted by Fouquet et al., 1991).

Troodos- Hannington et al., 1990; * from Bednarz et al., 1987.

Ag, in the Lau Basin in abundance are close to that in Kuroko. Both mineralogical and geochemical compositions of sulfides and fluids indicate the differences between back-arc and ocean-ridge environments, and because of their volcanic environment, tectonic setting and chemical composition, the Lau Basin deposits are considered by Fouquet et al. (1991) to be a transitional type between Kuroko and mid-ocean types.

The Troodos sulfides have low Au (0.29 ppm), Ag (10 ppm), Ba (0.09 %) and Pb (0.03%) (Hannington et al., 1990) which are close to MOR, but much lower than the Lau Basin. However, some other elements can be compared with the Lau Basin. For example, the average of Se in the Troodos sulfides is 8 ppm, which is obviously lower than EPR (163 ppm) but is close to the Lau Basin, while As in the Troodos sulfides is 1775 ppm much higher than MOR (154 ppm), but matches well with high As, a characteristic of the sulfides in the Lau Basin. Therefore, if we disregard other geological features in Troodos, the chemical composition of sulfides may suggest that the Troodos sulfide deposits are a transitional type between the Lau Basin and mid-ocean types, i.e., are more oceanic than the Lau Basin deposits. This result is consistent with the well organized two dimensional constructional geometry of Troodos type oceanic crust.

The type of ore deposit formed in a back-arc basin

largely depends on the basement rocks, which in turn can be related to the maturity of the back-arc system, although the temperature of deposition was also considered an important factor as controls of ore deposition, e.g., Franklin (1991, personal communication). In an incipient back arc basin the hydrothermal model should include evidence for interaction between continental crust and seawater, while in mature back arc basins, the basaltic oceanic crust that has been created prevents interaction of the seawater with the continental rock and sediments, and the hydrothermal system and associated deposits are therefore expected to be similar to those of mid-ocean ridges (Fouquet et al., 1991). From this point of view, since the Lau Basin environment is thought to be intermediate between oceanic and continental back-arc environments, the Troodos environment therefore should be much closer to oceanic rather than continental dominated back-arc environments.

7.2.5 Spreading rate estimation for Troodos oceanic crust

It is difficult to directly estimate the spreading rate of a paleo-oceanic crust or ophiolite like Troodos because of the insufficient accuracy of radiogenic dating and the absence of either magnetic reversals or fossil-bearing carbonate sediments directly above the SEI. Previous estimates of the spreading rate for the Troodos oceanic crust are conflicting. For example, Varga and Moores (1985) suggested a slow rate

crustal spreading because of the similarity between the grabens in Troodos and Mid-Atlantic rift valleys, while Boyle and Robertson (1984) suggested an intermediate rate of spreading based on comparison of fault throws in Troodos to those on the MOR. From this study, the high proportion of sheet to pillowed flows may indirectly suggest a relatively fast spreading rate during the construction of Troodos oceanic crust.

Studies of spreading centers made so far suggest that sheet flows and pillow flows occur in varying proportions along rift zones differing in spreading rate, pillows being more dominant where spreading rate is low (Ballard and van Andel, 1977). Eruptions along the rift are not continuous but, instead, are fairly short-lived and widely separated in time and space. Eruptions along a slow spreading rift could have high effusion rates but simply do not occur as often as those on a faster spreading rift. There is evidence that sheet flows exist along the MAR but are largely buried by subsequent pillow flows. From this point of view, the proportion of pillow lavas to sheet flows may be taken as an approximate proxy for spreading rate. The initial speculation about the possible relationships between flow morphology and lithospheric spreading rates was proposed by Ballard et al. (1979), but almost ten years later, with the accumulation of more data from the ocean floor, Bonatti and Harrison (1988)

were able to test quantitatively and verify the idea.

Bonatti and Harrison (1988) collected all available lava lakes and sheet lavas versus pillow lavas ratios on spreading ridges. These were obtained from close range, high resolution studies of axial zones of mid-ocean ridges so permitting a semiquantitative estimate of the relative areal distribution of lava lakes and sheet and pillow lavas in a number of accretion zones with different spreading rates.

In this study, I have collected P values from several DSDP drill holes, which can be compared with the results from Bonatti and Harrison and further, and can be used to speculate on the spreading rate during the formation of Troodos oceanic crust.

From earlier chapters, the P values in two deep Holes 395A and 418A in the Atlantic ocean are known to be 0.9 and 0.7, respectively. The spreading full rate for the crustal segment where Hole 395A is located was 3.4 cm/yr. No spreading rate has yet been reported for Hole 418A. However, this can be obtained by calculation from the local linear magnetic anomalies. The calculated spreading full rate for Hole 418A based on magnetic data (Rabinowitz et al., 1979; Vogt, 1986) is 2.4 cm/yr which is the same as the known average spreading full rate (2.4 cm/yr) in the northern of the MAR during the

Cretaceous (Vogt, 1986).

For Hole 504B it is that known the spreading full rate was 7.2 cm/yr, but the average P value (P=0.7) based on previously published work for the upper 800 m section should be modified because pillowed flows have been detected at the much lower depth of 1475 m in the hole (Morin et al., 1989). This new discovery, in conjunction with the use of spatial relationships between alteration zones and dike abundance from Troodos, leads to the assumption of new stratigraphic divisions for Hole 504B (Fig. 7.2.7). That is: 1) at about 700 m depth in basement is the upper boundary of the transition alteration zone is proposed to occur, because secondary minerals of both zeolite and greenschist facies first appear at that level where dike abundance (F) in Troodos would be at about 0.25; 2) at about 1250 m depth the boundary between the transition and greenstone alteration zones occurs, marked by the disappearance of mixed-layer clays, laumontite and other low-temperature secondary minerals, with only the greenschist facies minerals left, where dike abundance F in Troodos would be about 0.5; 3) sheeted dikes (100% dikes) are expected to appear at depths below the bottom of the present level (1287 m in basement). Based on this hypothesis, a new average P value for the Extrusive Sequence in Hole 504B then is 0.43, calculated on the estimation of an average of 90% of sheet flows and 10% pillowed flows below 800 m down to the predicted

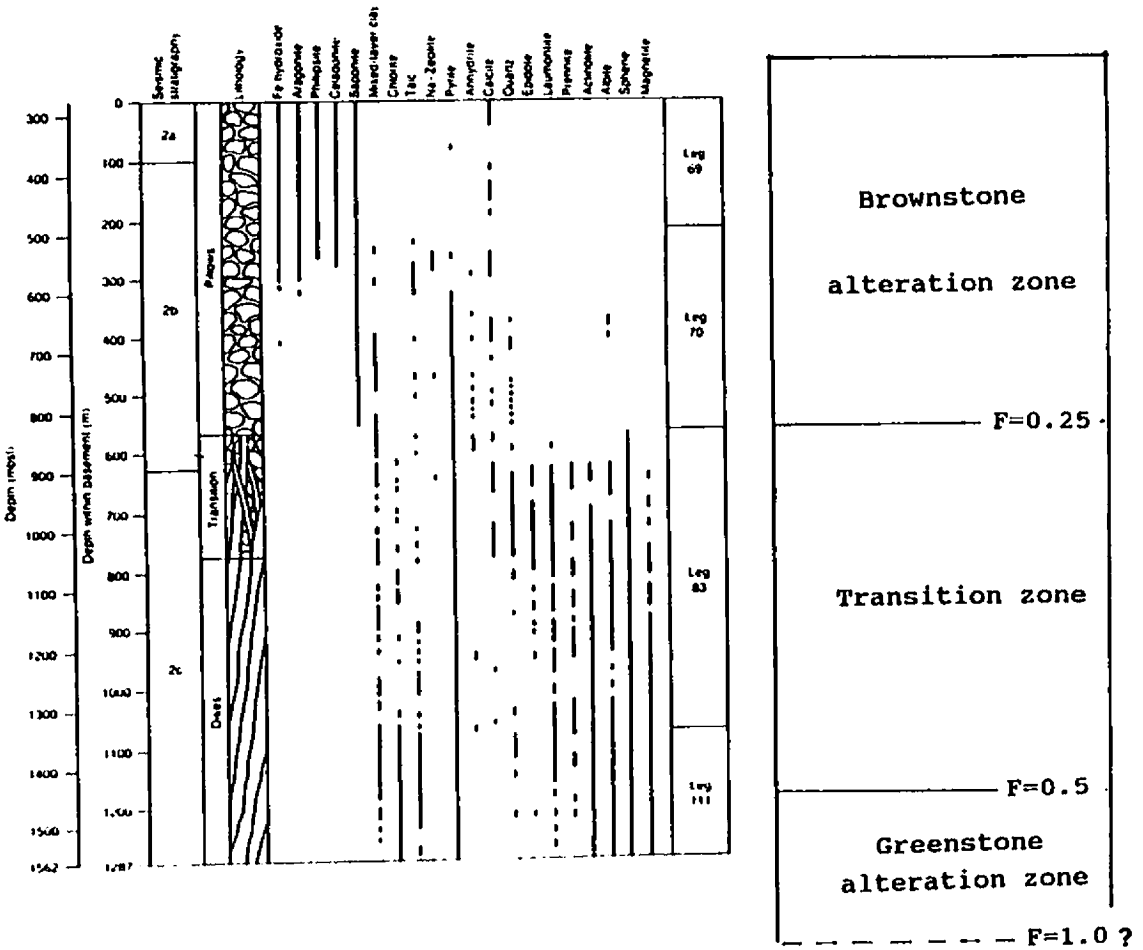

Fig. 7.2.7 (a) Lithologic subdivision of Hole 504B from Becker et al. (1989); (b) A new lithologic subdivision suggested for Hole 504B section. F values are estimated on the lavas of relationships observed in Troodos.

top of the Sheeted Dike Complex at 1400-1500 m.

Figure 7.2.8 displays the relationship between spreading rates and P values both from seafloor observations collected by Bonatti and Harrison (1988) and from the DSDP drill holes collected in this study, with the data listed in Table 7.2.3. Values for Holes 395A and 418A fall within the range of surface P values and spreading rates. The two P values for Hole 504B, one for 800 m of extrusives and the other for 1500 m of extrusives and dikes, fall almost at opposite sides of the range of surface values and suggest the true P value of Hole 504B is possibly between these extremes.

If a continuous relationship is assumed between average P and spreading rate, as shown in the diagram (Fig. 7.2.8), the spreading full rate for Troodos obtained from the average P of 0.4 is 8-15 cm/yr (4-7.5 cm/yr half rate). That is, Troodos oceanic crust most probably formed at an intermediate to fast spreading axis during crustal construction. The existence of a range for the spreading rate is reasonable because P values will be in some degree variable along spreading ridges at different locations with respect to adjacent transforms. If we take the full spreading rate of Troodos as 12 cm/yr (6 cm/yr for half rate), since we know the interval between two major magmatic and spreading events is about 12 km, then, the frequency of major events can be

Table 7.2.3 Relationship between P Values and Spreading Rates

	Half Spreading Rate (cm/yr)	P Value	
395A	1.7	0.92	
418A	1.2	0.72	
504B (1)	3.6	0.71	(0-800 m)
(2)	3.6	0.43	(0-1500 m, estimated)
Troodos	4-7.5 (?)	0.41	

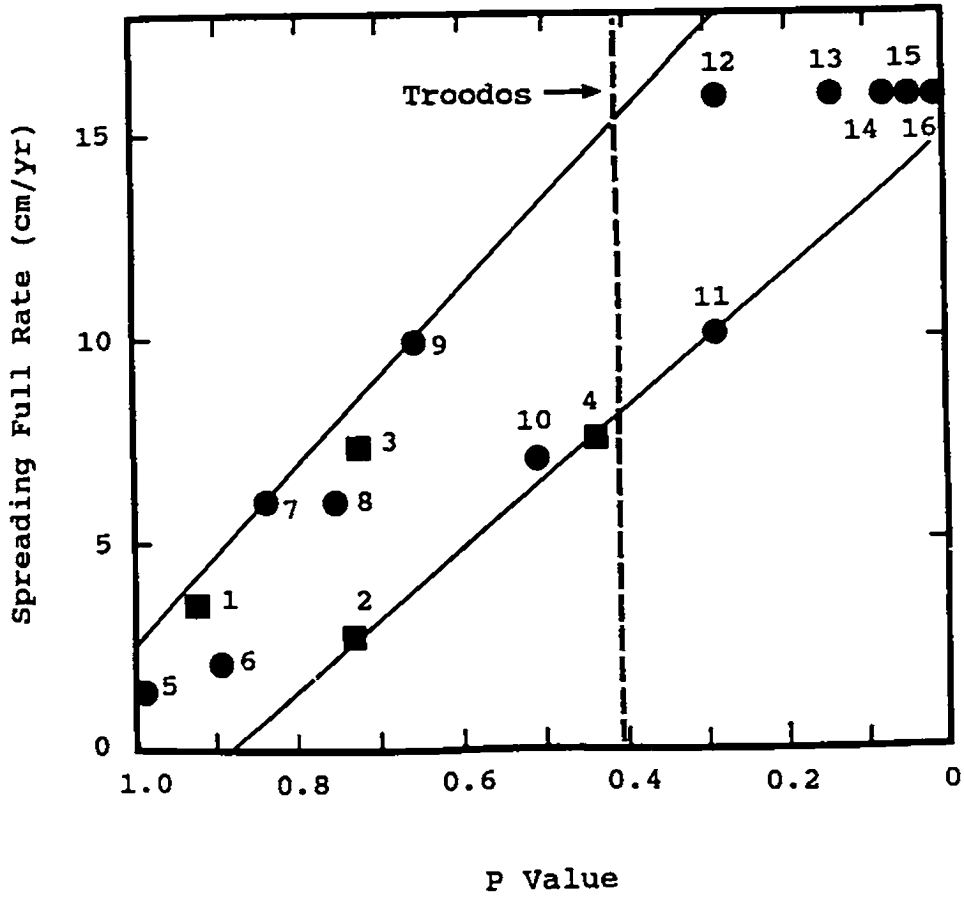

Fig. 7.2.8 Relationship between spreading rates and P values (after Bonatti and Harrison, 1988). Squares are data from this study; circles are from Bonatti and Harrison (1988). 1- Hole 395A, Atlantic; 2- Hole 418A, Atlantic; 3,4- 504B, Pacific; 5- Red Sea; 6- MAR; 7-,8- EPR 21°N; 9- EPR 12°50'N (total); 10- Galapagos Rift 86°W; 11- EPR 12°50'N (axis); 12- EPR 20°S; 13- EPR 21°30'S; 14- EPR 18°30'S; 15- EPR 17°30'S; 16- EPR 20°S.

estimated at 2 x 10^5 yr.

Several additional lines of reasoning support this hypothesis.

1) The topographic amplitude of the sediment/igneous contact (SEI) in Troodos is small, only about 120 m (see Chapter 4). Macdonald (1983) summarized the available data from the present ocean ridges and found that topographic amplitude in the axial zone is small, about 50-100 m for intermediate to fast spreading rate spreading ridges, and large, 100-2000 m for slow spreading rate ridges. The topographic features of the SEI are not in conflict with characteristics of a fast spreading ridge origin although the data of Macdonald show variations along the ridges while the Cyprus data show variations in the spreading direction. Similarly, if the topographic amplitude of the SEI is simply compared to the curve abtained by statistical correlation between topography at ridges and spreading rates by Malinverno (1991) (Fig. 7.2.9), the value of 120 m meets the curve at about 9.5 cm/yr (7.5-14 cm/yr in range), the same as the result from P value. Allerton and Vine (1987) noted the overall subdued topography of the SEI contact and also proposed intermediate to fast rates during the generation of Troodos oceanic crust.

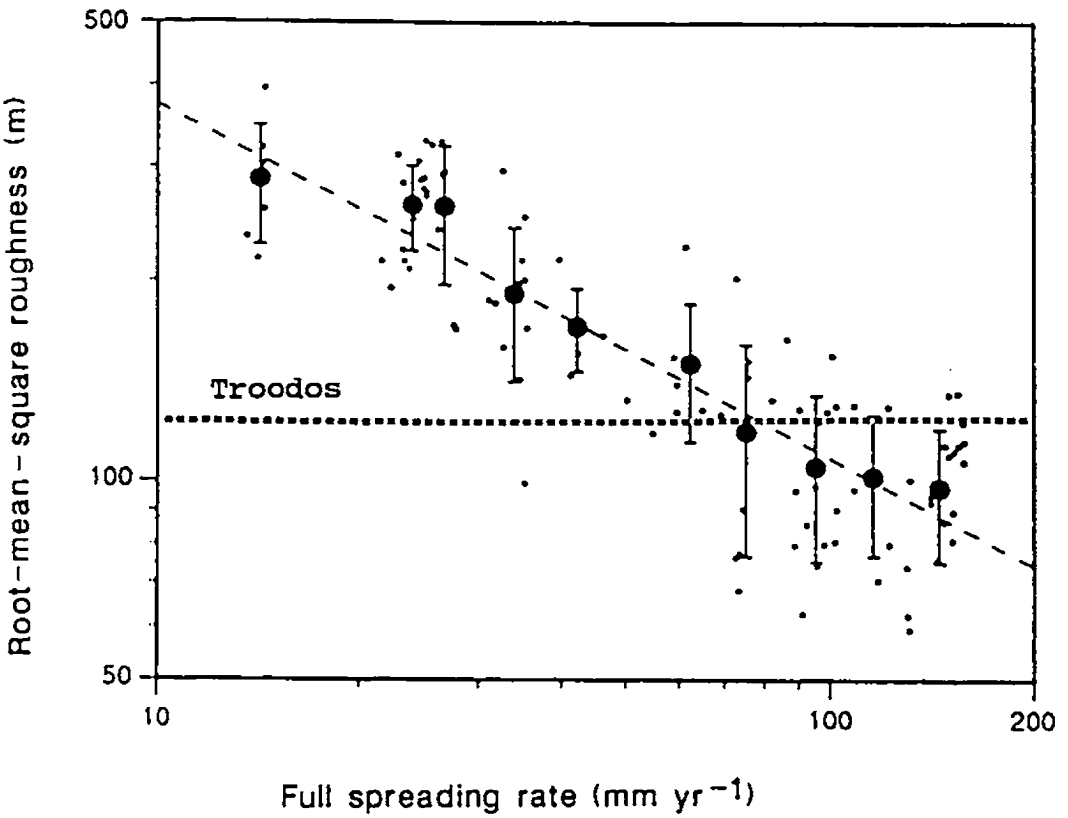

Fig. 7.2.9 Range of roughness of Troodos seafloor topography is about 120 m, and is approximately plotted in the range of about 75-140 mm/yr of full spreading rate (after Malinverno, 1991).

2) The high density of distribution of sulfide mineralization in Troodos is a characteristic of ridges with a relatively fast spreading rate. It is known that in Troodos sulfide deposits and hydrothermal mineralization are concentrated such that in such a small area 34 deposits and 93 mineral prospects have been found. Such high density of distribution of sulfides at present is only known at fast spreading ridges, e.g., the EPR and the Lau Basin, rather than at slow spreading ridges, e.g., the MAR. This indirectly suggests that Troodos formed at a relatively fast spreading axis.

3) Troodos is a harzburgite type ophiolite which it is suggested formed in a relatively fast spreading environment: Nicolas (1989) divides ophiolites into two types: a harzburgite ophiolite type (HOT) and a lherzolite ophiolite type (LOT), on the basis of the existence/lack of harzburgite or lherzolite, as well as some other distinctive characteristics. He suggests that the harzburgite ophiolite type (HOT) is derived from oceanic spreading centers characterized by a half spreading rate greater than approximately 2 cm/yr, while the lherzolite ophiolite type (LOT) is characterized by a slower half spreading rate of below 1-2 cm/yr. This division is explained below.

The crustal section is thicker in HOT than in LOT. The

crustal thickness reflects the degree of melt extraction from the mantle. HOT corresponds to a larger degree (about 20%) of melt extraction in the mantle than LOT (about 15%). As a result, in HOT the layered gabbro unit is thick and continuous suggesting the existence of steady state magma chamber below the ridge, whereas in LOT this unit is absent or discontinuous suggesting the presence of only episodic magma chambers. Moreover, the expected exposure of lherzolitic serpentinites as sea floor in LOT is matched by discoveries made only in slow spreading oceans, e.g., on the Mid-Atlantic Ridge, where among the ultramafic rocks recovered lherzolites or lherzolitic harzburgites are more common than harzburgites (e.g., Aumento and Loubat, 1971; Prinz et al., 1976; Hodges and Papike, 1976; Arai and Fujii, 1979).

Based on these basic ideas, Nicolas et al. (1988) demonstrated several factors which favor a intermediate to fast spreading rate for the case of the Oman paleo-ridge.

According to the criteria of Nicolas (Table 8-1, p.189, 1989), the Troodos ophiolite belongs to the harzburgite type, due to the existence of at least several lines of evidence: 1) harzburgite is dominant in the ultramafic section; 2) the mafic section is thick (3-4 km), the basalts are quartz tholeiite and the layered gabbro sequence is well developed and continuous; 3) intrusive wehrlite bodies occur; 4)

chromite pods are present. This adds to the evidence for a fast (≥2 cm/yr half rate) spreading for the Troodos oceanic crust.

4) Features in the Troodos ophiolite are compared to present marginal basins with fast spreading rates. Several workers have proposed the Andaman Basin, a marginal basin, to be an analog for Troodos (e.g., Moores et al., 1984; Robinson and Malpas, 1990). However, at present, comparison cannot be made since, to date, very little is known about this basin, including spreading rate, tectonics, structures, petrology, magmatic activity, hydrothermal activity and mineralization. In contrast, many other marginal basins currently being investigated are available to provide more information to compare with Troodos, e.g., the Lau Basin and the Fiji Basin.

The Lau Basin is a marginal back-arc region behind the Tonga-Kermadec subduction zone in the SW Pacific. Westward subduction of Pacific crust at a rate of about 10 cm/yr results in the formation of new oceanic lithosphere by back-arc rifting behind the Tonga-Kermadec Trench. Recently volcanic and hydrothermal activity and sulfide mineralization have being observed and studied in the basin (e.g., von Stackelberg and Wiedicke, 1990; Jenner et al., 1987; Stackelberg and Shipboard Scientific Party, 1988; Sunkel, 1990) The half spreading rate in the Lau Basin is 7.5 cm/yr

(Morton and Sleep, 1985; Herzig et al., 1990).

The North Fiji Basin is a back-arc basin behind the active subduction zone of the Vanuatu Arc with a half spreading rate of 7.2 cm/yr (Auzende et al., 1988; Nojiri et al, 1989). Recently volcanic activity and hydrothermal mineralization at the North Fiji Basin spreading axis have been investigated by the Japanese-French Cruise Kaiyo 87 group (e.g. Auzende et al, 1990; LayFoy et al., 1990).

It is interesting that both the North Fiji Basin and Lau Basin are small marginal basins that have fast spreading rates. Rock morphologies have been distinguished from the bottom photographs from active spreading ridges in the two basins (e.g., von Stackelberg and Wiedicke, 1990). Although the main rock types are pillow lavas and sheet flows on some parts of the ridges, it is not uncommon for high brecciated lava and hyaloclastites to occur on the ridges. Based on data from von Stackelberg and Wiedicke (1990), the estimated average P value in the Lau Basin is about 0.5 (not including brecciated lava and hyaloclastites), comparable to an intermediate-fast rate by examination of Fig. 7.2.8. Since Troodos was also most probably formed in a marginal region on a subduction zone (Moores et al., 1984) or in a back-arc basin (Muenow et al., 1990), the intermediate to fast half spreading rate of 4-7.5 cm/yr estimated for Troodos is consistent with

that of both Lau Basin and North Fiji Basin.

6) Some earlier workers have also attempted to demonstrate that the Troodos ophiolite formed by an intermediate to fast spreading process. For example, lack of significant dike rotation throughout much of the Troodos ophiolite probably reflects relatively long periods of time when magmatism kept pace with plate separation, which is a feature usually ascribed to fast-spreading ridge crests (Macdonald, 1982; Varga and Moores, 1990).

In summary, several lines of evidence suggest that Troodos was formed at a intermediate to fast spreading rate (e.g., Allerton and Vine, 1987; Boyle and Robertson, 1984; this study). During the construction of the Troodos oceanic crust, commonplace high-rate eruption rates resulted in a low average P value and strong hydrothermal activity and mineralization, similar to a currently active example, the Lau Basin. One of the possibly more important lines of evidence to lead to a conclusion of a fast spreading rate for Troodos is the P value. Although it is hard to find more data to test the relationship, and to estimate spreading rates during the generation of oceanic crust, results from the present limited number of examples are encouraging.

7.2.6 Summary

From the above discussion and comparison with present oceanic crust, it is concluded that the Troodos ophiolite shows many common features with present in-situ oceanic crust and also provides a series of other features that may be used for prediction of as yet unknown features of in-situ crust.

1. Similarities

1) The Troodos ophiolite shows extensive similarities to present oceanic crust in stratigraphic sequences and physical properties, lithology and rock types.

2) Volcanic cyclicity observed in Troodos is confirmed to exist in the present oceanic crust both by seafloor investigation and deep drillholes, e.g., Hole 418A. Proportion of pillow flows (P value) in Troodos suggests an intermediate to fast spreading rate (4-7.5 cm/yr half rate) and can be compared with Hole 504B and the Lau Basin.

3) Alteration zonation in Troodos is consistent with that in the modern oceanic crust, e.g., Hole 504B.

4) Sulfide deposits associated with hydrothermal activity observed in Troodos can be compared with those on the present

spreading ridges. Similarities include the distribution and size of orebodies, and the composition and texture of ores.

2. Differences

1) The average pillow lava ratio in the Extrusive Sequence on the Troodos ophiolite is relatively lower than that of slow spreading-rate MAR and of intermediate spreading-rate Pacific ridges (e.g., Hole 504B), and suggests a faster spreading rate origin.

2) The compositions of the sulfides of Troodos are intermediate between those from typical oceanic ridges and these from a marginal basin. The sulfide compositions are known to be related mainly to the underlying rock types. Therefore, the differences are consistent with the genetic model of a largely oceanic marginal basin for Troodos.

3) A thin transition alteration zone occurs in Troodos but a much thicker zone occurs in Hole 504B.

7.3.3 Suggestions for future work

The Troodos ophiolite, as a remanent of ancient oceanic crust, provides an exceptional window for us to see the deep sequence of the ocean floor. The almost perfect preservation

and exposure of the whole sequences of the in-situ crust, coupled with varied geological phenomena, such as hydrothermal alteration and mineralization, can contribute many valuable sets of information to support further research.

The pillow lava ratio (P value) and dike abundance (F value) defined and measured in this study are two basic features of crustal construction at the spreading ridges or axes. The approach indicates that these two parameters are related to the stage in the spreading process at the ridge in term of style of magmatic activity, spreading rate, hydrothermal alteration and sulfide mineralization during the generation of the ocean crust. Some results, for example, the close spatial relationship between dike contours and alteration zones, provide information to consider a genetic correlation between them. This, however, provides a subject for laboratory workers to test the implications of this relationship through determination of key thermodynamic and kinetic parameters to explore the implications of this relationship quantitatively. On the other hand, the second order features of construction in Troodos noted in this study are only constrained within the Extrusive Sequence, and are not involved in the Sheeted Dike Complex, Gabbros, and Ultramafic Sequence. Therefore, this study should also be extended elsewhere in Troodos. These lower parts of the ophiolite will provide information at other depths which is

impossible to observe at present for the in-situ seafloor. The constructional study of the Troodos type oceanic crust may provide an analogy of the present ocean floor in the understanding of the formational processes of oceanic crust, and thus will also greatly improve knowledge of plate tectonic processes.

Appendix 1

HOW P AND F WERE MEASURED AND CONTOURED

1. P Measurement

P is the ratio between the thickness of pillowed flows and the total thickness of extrusives in a measured section. It is expressed as below:

P = thickness of pillow flows / total thickness of extrusives in a measured section

In the field, P was measured or estimated in continuously outcropping sections mostly over 100 m in length. Most sections are approximately perpendicular to the spreading direction. Even though some sections are at other angles to the spreading direction, this does not affect the calculation for P, but only results the effective length of the section in the perpendicular to the spreading direction.

For example, at station 11.05, P was obtained from two adjoining sections. Section 1 is 134 paces (1 pace = 0.75 m) in length with a bearing of NE10 and section 2 is 41 paces long with a bearing of N. After being adjusted to the perpendicular to the spreading direction (i.e., NE20), the

total length of the two sections is 128 m. The adjusted section contains 65 m of pillow flows, 60 m of sheet flows and 3 m of dikes. P at this station then is calculated as:

$$65/(65 + 60) = 0.52$$

Field section for 11.05:

Bearing 10°

(unit: pace, 1 pace = 0.75 m)

0-38	sheet flows, LPL;
38-40	dike, dip N, dip angle 50;
40-44	sheet flows, LPL;
44-46	dikes with baked contact;
46-48	sheet flows, LPL;
48-53	pillows, pink
53-66	sheet flows and massive flows;
66-82	sheet flows, LPL;
82-90	massive flows;
90-134	pillows, pink-grey;

New Bearing 0°

0-41 pillows, grey;

End of section.

2. F value

F is the ratio between the thickness of dikes in a section to the total thickness of a measured section. Previous workers called this ratio dike density (e.g., Gass and Smewing, 1975), or abundance of dikes (e.g., Baragar et al., 1989). The F value is expressed as below:

F = thickness of dikes / total thickness of a measured section.

Since the strike of most dikes in the Extrusive Sequence are approximately parallel to the axial direction, the majority of measurement sections for F values are close to the normal to the axial direction, i.e., parallel to the spreading direction. Although minor sections have other angles with the spreading direction, F ratios in these sections were not affected. Sections for F value measurement were mostly over 50 m in length and were usually measured by a tape.

For example, at station 22.08, F ratio was obtained in a continuous section. The total thickness of the section is 42.1 m of which 7.2 m consisted of dikes. Then, F = 7.2 / 42.1 = 0.16.

Field Notes: Station 22.08

Bearing 265°

0-8.3 m	sheet flows;
8.3-8.6 m	dike;
8.6-13.7 m	sheet flows;
13.7-13.9 m	dike;
13.9-16.2 m	sheet flows;
16.2-17.2 m	dikes;
17.2-17.6 m	sheet flow;
17.6-18.8 m	dikes;
18.8-31.1 m	sheet flows;
31.1-31.7 m	dike;
31.7-35.6 m	sheet flows;
35.6-36.6 m	dikes;
36.6-37.3 m	sheet flow;
37.3-38.6 m	dikes;
38.6-39.3 m	dikes;
39.3-41.3 m	sheet flows;
41.3-42.1 m	dikes, dip NE85, dip angle steep;

End the section.

3. P and F contouring

Both P and F data were contoured by hand using the method

of linear interpolation. That is, it was assumed that a property value varied linearly between two stations and the approximate position of a contour was located accordingly. Hand contouring was preferred since experience with machine contouring suggested that the latter approach would not give geologically meaningful contours near the edges of the survey area nor where experience-based choice of contour direction or continuity was required. Where data density was high, and the trend of contours straight or greatly flexural, the uncertainties in contour location is usually small, that is, $\leq$ 100 m. Where these conditions did not apply, and particularly where a judgement had to be made on contour position, larger uncertainties are possible. An example of such an area is the long, northeasterly directed tongue towards Drillhole CY-1a in the F25 contour. It is possible to contour the data in the area on the basis either of continuity with the main F25 contour, as has been chosen here, or such that an isolated area of > F25 occurs. However, the general form of the contour-pattern will not be significantly changed regardless of which choice is made in areas of this type.

Appendix 2 Location of Measured Sections in the Field

SECTION	L(m)	E(km)	P	F	UTM(E)	UTM(N)
6.01	150	0.24	1.00	0.00	96.80	83.20
6.02	300	0.25	1.00	0.00	96.00	82.60
6.03	80	0.25	0.80	0.10	95.80	82.20
6.04	250	0.26	0.20	0.20	95.30	81.90
6.05	70	0.31	0.10	0.30	94.90	81.40
6.06	60	0.34	0.50	0.40	94.40	81.20
6.07	200	0.34	0.30	0.50	94.30	81.20
6.08	100	0.48	-	1.00	91.20	77.20
6.09	100	0.48	-	1.00	91.30	77.70
6.10	200	0.46	0.20	0.90	91.40	78.30
6.11	150	0.44	0.00	0.90	91.40	78.70
6.12	50	0.42	0.80	0.70	91.70	79.10
6.13	100	0.40	0.00	0.80	91.90	79.40
6.14	500	0.37	0.00	0.80	92.10	80.00
6.15	150	0.31	0.00	0.80	92.80	80.80
6.16	80	0.32	0.00	0.70	93.20	80.90
7.01	200	0.36	0.30	0.00	99.20	90.40
7.02	120	0.37	0.50	0.10	99.10	90.30
7.03	100	0.39	0.60	0.60	98.90	90.10
7.04	100	0.40	0.20	0.80	98.70	79.60
7.05	100	0.42	0.00	0.80	98.50	79.40
7.06	150	0.42	0.00	0.80	98.30	78.90
7.07	30	0.46	0.00	0.90	78.10	78.50
7.08	120	0.50	-	1.00	97.30	78.10
7.09	80	0.36	0.50	0.00	99.50	90.70
7.10	150	0.36	1.00	0.00	99.70	90.80
7.11	100	0.30	1.00	0.00	100.60	81.50
7.12	100	0.30	1.00	0.00	101.30	81.60
7.13	50	0.32	1.00	0.00	101.30	82.10
8.01	100	0.33	0.70	0.10	103.60	77.40
8.02	50	0.40	0.80	0.20	103.50	77.70
8.05	80	0.68	0.10	0.00	102.10	76.90
8.10	200	0.42	0.50	0.00	105.30	79.30
8.11	100	0.44	0.90	0.00	105.90	79.60
8.12	150	0.45	0.80	0.00	106.30	79.90
8.13	150	0.40	0.90	0.00	106.20	80.70
8.14	100	0.42	0.40	0.30	105.90	80.40
8.15	70	0.32	0.90	0.00	106.70	82.40
8.16	100	0.31	1.00	0.00	106.70	82.00
8.17	150	0.32	0.50	0.00	106.30	81.70
8.18	100	0.34	0.50	0.00	106.10	81.40
8.19	100	0.33	0.50	0.00	105.40	81.20
8.20	100	0.44	0.50	0.20	105.30	80.80
8.21	170	0.40	0.50	0.20	105.40	80.10
8.22	100	0.42	0.80	0.20	105.40	79.80
8.23	50	0.43	1.00	0.00	105.40	79.60
8.24	100	0.43	0.90	0.00	105.60	79.50
8.25	150	0.48	0.00	0.30	104.50	78.60
8.26	150	0.46	0.00	0.20	104.20	78.40
8.27	25	0.44	0.00	0.60	103.80	78.30
8.28	150	0.42	0.80	0.00	103.50	77.20

Appendix 2 (continued 1)

SECTION	L(m)	E(km)	P	F	UTM(E)	UTM(N)
8.29	100	0.46	1.00	0.60	103.50	76.40
8.30	100	0.50	1.00	0.50	103.70	75.90
8.31	80	0.48	1.00	0.70	103.50	75.50
8.32	120	0.50	1.00	0.70	103.50	75.00
8.33	140	0.53	1.00	0.60	103.60	77.40
8.34	200	0.57	1.00	0.60	103.70	73.60
8.35	100	0.60	1.00	0.70	103.30	73.00
8.36	100	0.66	-	1.00	102.60	71.70
8.37	200	0.72	-	1.00	101.90	71.30
8.38	100	0.65	-	1.00	102.80	72.10
8.39	50	0.60	-	1.00	103.10	72.50
8.40	100	0.50	0.00	0.10	104.80	77.00
8.41	10	0.48	0.10	0.00	105.10	77.30
8.42	100	0.42	0.50	0.00	105.00	79.30
8.43	200	0.34	0.80	0.00	105.60	80.90
8.44	250	0.34	0.80	0.00	105.30	81.10
8.45	100	0.44	0.40	0.20	104.90	79.90
8.46	150	0.36	0.50	0.00	104.30	80.70
8.47	200	0.36	0.80	0.00	104.00	81.20
8.48	100	0.40	0.80	0.10	103.90	80.40
8.49	150	0.44	0.40	0.20	103.90	80.00
8.50	100	0.38	0.70	0.50	103.40	80.00
8.51	100	0.36	0.40	0.50	103.00	80.00
8.52	100	0.34	0.50	0.50	102.60	79.90
8.53	150	0.38	0.60	0.50	103.70	79.20
8.54	50	0.48	0.20	0.20	105.00	77.70
8.55	80	0.58	0.50	0.50	104.85	76.20
8.56	100	0.52	0.50	0.70	105.50	75.70
8.57	100	0.52	0.50	0.70	105.70	75.70
8.58	200	0.44	0.20	0.50	106.20	76.10
8.59	100	0.49	0.20	0.50	106.80	76.60
8.60	200	0.44	0.00	0.20	107.20	76.90
9.01	100	0.48	0.10	0.00	109.40	77.40
9.02	70	0.46	0.00	0.00	109.80	77.40
9.03	50	0.45	0.15	0.10	109.90	77.70
9.04	80	0.47	0.35	0.00	109.80	77.80
9.05	120	0.48	0.40	0.00	109.80	78.00
9.06	25	0.52	0.00	0.95	109.10	76.60
9.07	15	0.52	0.00	0.40	109.00	77.00
9.08	60	0.51	0.00	0.45	109.30	76.70
9.09	10	0.47	0.00	0.11	109.70	77.30
9.10	40	0.46	0.00	0.10	109.60	77.20
9.11	40	0.46	0.00	0.10	109.60	77.10
9.12	50	0.46	0.00	0.10	109.70	77.00
9.13	40	0.48	0.00	0.00	109.60	76.90
9.14	45	0.49	0.00	0.40	109.60	76.70
9.15	50	0.50	0.00	0.45	109.60	76.60
10.01	200	0.72	-	1.00	110.80	65.60
10.02	80	0.64	-	1.00	111.30	66.90
10.03	100	0.62	-	1.00	111.50	67.70
10.04	60	0.64	-	0.95	111.40	67.80

Appendix 2 (continued 2)

SECTION	L(m)	E(km)	P	F	UTM(E)	UTM(N)
10.05	40	0.62	-	0.90	111.50	68.10
10.07	45	0.62	-	0.75	111.60	68.30
10.08	60	0.62	-	0.72	111.60	68.40
10.09	50	0.62	-	0.87	111.60	68.60
10.10	60	0.61	-	0.50	111.60	68.80
10.12	40	0.61	-	0.80	111.60	68.90
10.13	70	0.57	-	0.50	111.80	69.10
10.14	60	0.58	-	0.60	111.90	69.10
10.15	100	0.58	-	0.56	111.80	69.40
10.16	100	0.57	-	0.79	111.80	70.00
10.17	80	0.58	0.00	0.57	111.80	70.20
10.18	50	0.57	-	0.45	111.80	70.70
10.19	50	0.57	-	0.55	111.80	70.80
10.20	80	0.58	-	0.63	111.90	71.00
10.21	120	0.55	0.63	0.52	111.80	71.70
10.22	80	0.54	0.63	0.46	111.80	71.90
10.23	90	0.50	-	0.62	112.30	72.80
10.24	80	0.48	0.00	0.27	112.80	73.10
10.25	60	0.48	0.50	0.28	113.00	73.30
10.26	60	0.50	-	0.20	113.10	73.80
10.27	90	0.47	-	0.29	113.50	74.30
10.28	70	0.47	0.20	0.40	113.80	74.70
10.29	100	0.46	-	0.26	114.10	75.00
10.30	70	0.44	0.30	0.09	114.30	75.30
10.31	80	0.44	0.30	0.39	114.40	75.60
10.32	80	0.45	-	0.21	114.60	75.80
10.33	70	0.44	-	0.25	114.70	76.00
10.34	80	0.43	-	0.19	114.80	76.30
10.35	80	0.43	-	0.23	115.00	76.50
10.36	80	0.42	-	0.08	115.20	76.70
10.37	70	0.42	-	0.08	115.30	77.00
10.38	70	0.41	-	0.11	115.50	77.20
10.39	100	0.41	-	0.32	115.70	77.40
10.40	80	0.40	-	0.19	115.80	77.70
10.41	200	0.36	0.90	-	116.30	78.20
10.42	120	0.40	0.80	-	115.80	76.90
10.43	150	0.40	0.60	-	115.40	76.50
10.44	80	0.44	0.30	-	114.60	76.20
10.45	70	0.46	0.30	-	114.20	75.40
10.46	600	0.45	0.15	0.40	114.10	74.60
10.47	900	0.47	0.10	0.50	113.40	74.20
10.48	100	0.52	0.00	0.70	112.30	72.60
10.49	80	0.52	0.00	-	111.90	72.10
10.50	120	0.59	0.50	-	111.90	71.10
10.51	70	0.58	0.25	-	111.70	70.30
10.52	40	0.59	0.20	-	111.70	69.00
10.53	60	0.63	-	0.80	111.50	68.20
10.54	60	0.63	-	1.00	111.50	67.60
10.55	100	0.65	-	1.00	111.40	67.20
10.56	70	0.52	0.00	-	112.00	72.40
10.57	60	0.50	0.00	-	112.50	73.00

Appendix 2 (continued 3)

SECTION	L(m)	E(km)	P	F	UTM(E)	UTM(N)
10.58	50	0.51	0.80	-	113.00	73.50
10.59	80	0.46	0.00	-	113.70	74.50
10.60	70	0.50	0.25	-	113.15	74.00
10.61	110	0.70	-	1.00	111.10	66.00
11.01	215	0.42	0.58	0.00	120.00	76.10
11.02	687	0.40	0.54	0.00	120.00	75.80
11.03	70	0.42	0.95	0.00	119.90	75.30
11.04	298	0.42	0.80	0.00	119.60	74.80
11.05	161	0.44	0.52	0.05	119.70	74.50
11.06	326	0.44	0.75	0.05	119.60	74.20
11.07	278	0.51	0.15	0.05	119.60	73.40
11.18	100	0.56	-	1.00	118.60	71.70
11.19	71	0.57	-	0.75	118.60	71.90
11.20	135	0.57	0.00	0.72	118.70	72.10
11.21	76	0.56	0.00	0.66	118.70	72.10
11.22	35	0.55	0.00	0.67	118.80	72.10
11.23	38	0.55	0.00	0.57	118.90	72.10
11.24	64	0.54	0.27	0.61	118.90	72.20
11.25	62	0.54	0.43	0.63	118.90	72.30
11.26	50	0.54	0.85	0.56	119.10	72.50
11.27	274	0.52	1.00	0.15	119.20	72.50
11.28	75	0.51	0.51	0.38	119.30	72.60
11.29	136	0.51	0.00	0.19	119.30	72.70
11.30	62	0.53	0.56	0.05	119.40	72.90
11.31	555	0.55	0.25	0.05	119.50	73.10
11.32	183	0.50	0.65	0.05	119.60	73.30
11.33	124	0.43	0.42	0.00	119.80	74.70
11.34	94	0.42	0.83	0.00	119.90	75.20
11.35	250	0.41	0.71	0.00	119.90	75.40
11.50	168	0.56	-	0.50	119.00	72.30
11.51	100	0.56	-	0.99	118.50	71.60
11.52	72	0.56	0.00	0.90	118.60	71.80
11.53	134	0.57	0.00	0.84	118.80	72.00
12.01	10	0.46	1.00	0.00	124.30	74.20
12.02	12	0.46	0.10	0.00	124.20	74.10
12.03	15	0.45	0.00	0.00	124.30	74.10
12.04	15	0.44	0.00	0.00	124.30	73.90
12.05	15	0.43	0.00	0.00	124.30	73.90
12.06	15	0.45	0.00	0.00	124.30	73.80
12.07	13	0.46	0.00	0.00	124.30	73.70
12.08	8	0.44	0.00	0.00	124.30	73.60
12.09	13	0.42	0.03	0.00	124.30	73.50
12.10	15	0.42	0.00	0.00	124.40	73.40
12.11	13	0.44	0.00	0.00	124.40	73.30
12.12	10	0.44	0.00	0.00	124.40	73.20
12.13	12	0.43	0.00	0.00	124.40	73.20
12.14	15	0.44	0.00	0.00	124.40	73.10
12.15	8	0.46	0.00	0.00	124.30	73.00
12.16	10	0.46	0.00	0.00	124.40	72.90
12.17	15	0.47	0.00	0.00	124.40	72.80
12.18	9	0.45	0.00	0.00	124.50	72.70

Appendix 2 (continued 4)

SECTION	L(m)	E(km)	P	F	UTM(E)	UTM(N)
12.19	15	0.47	0.00	0.00	124.40	72.60
12.20	15	0.45	0.00	0.00	124.50	72.50
12.21	15	0.45	0.00	0.00	124.50	72.40
12.22	9	0.46	0.00	0.00	124.50	72.30
12.23	9	0.47	0.00	0.00	124.50	72.20
12.24	12	0.47	0.00	0.00	124.50	72.00
12.25	11	0.47	0.00	0.00	124.50	71.90
12.26	8	0.49	0.00	0.00	124.40	71.80
12.27	8	0.49	0.00	0.00	124.50	71.70
12.28	7	0.50	0.00	0.00	124.50	71.60
12.29	11	0.49	0.05	0.00	124.60	71.60
12.30	8	0.48	0.00	0.00	124.60	71.50
12.31	6	0.48	0.00	0.00	124.60	71.40
12.32	15	0.46	0.33	0.00	124.70	71.30
12.33	7	0.48	0.00	0.00	124.70	71.20
12.34	13	0.48	0.00	0.00	124.70	71.00
12.35	5	0.48	0.00	0.00	124.70	70.90
12.36	6	0.50	0.00	0.00	124.70	70.80
12.37	3	0.50	0.00	0.00	124.50	70.80
12.38	10	0.51	0.00	0.00	124.50	70.70
12.39	11	0.52	0.00	0.00	124.50	70.60
12.40	7	0.50	0.00	-	124.40	70.50
12.41	15	0.48	0.00	0.06	124.40	70.40
12.42	15	0.49	0.00	0.00	124.30	70.30
12.43	20	0.48	0.95	-	124.30	70.10
12.44	6	0.48	0.00	-	124.30	70.20
12.45	11	0.48	0.00	0.57	124.50	70.30
12.46	12	0.46	0.00	0.67	124.60	70.20
12.60	13	0.48	-	0.77	124.20	70.00
12.61	10	0.49	-	1.00	124.00	69.80
12.62	8	0.51	-	0.69	123.40	69.60
12.63	7	0.56	-	1.00	123.00	68.20
12.64	7	0.54	-	0.96	122.50	68.00
12.65	5	0.54	-	1.00	121.80	67.60
12.66	8	0.60	-	1.00	121.30	67.50
12.67	8	0.63	-	1.00	120.70	67.00
12.68	10	0.54	-	1.00	123.20	68.40
12.69	15	0.50	-	1.00	123.20	68.70
12.70	11	0.52	-	1.00	123.10	69.00
12.71	11	0.52	-	1.00	123.20	69.30
12.72	12	0.50	-	1.00	123.20	69.40
12.73	11	0.55	-	1.00	122.10	67.70
12.74	14	0.64	-	1.00	120.80	67.30
12.75	11	0.68	-	1.00	120.50	66.70
12.76	10	0.65	-	1.00	120.30	66.60
12.77	10	0.75	-	1.00	120.00	66.50
12.78	13	0.72	-	1.00	119.90	66.40
12.79	11	0.75	-	1.00	119.80	66.10
13.01	100	0.36	0.95	0.00	129.30	70.70
13.02	150	0.39	0.85	0.00	128.30	71.20
13.03	80	0.42	0.80	0.00	127.90	71.50

Appendix 2 (continued 5)

SECTION	L(m)	E(km)	P	F	UTM(E)	UTM(N)
13.04	100	0.35	0.80	0.00	128.10	72.60
13.05	60	0.36	0.90	0.00	128.80	74.30
13.06	80	0.33	0.75	0.00	129.20	74.70
13.07	40	0.34	0.75	0.00	129.10	75.10
13.08	100	0.32	1.00	0.00	129.60	75.60
13.09	200	0.42	-	1.00	124.80	63.10
13.10	150	0.50	-	1.00	125.10	63.80
13.11	200	0.44	0.80	0.80	125.10	64.40
13.12	100	0.48	0.80	0.50	125.30	65.00
13.13	100	0.50	0.80	0.80	125.60	65.70
13.14	200	0.46	0.80	0.10	125.90	66.70
13.15	100	0.40	0.80	0.00	129.00	67.90
14.01	200	0.29	1.00	0.00	134.70	73.20
14.02	100	0.32	0.80	0.00	134.10	71.80
14.03	170	0.36	1.00	0.00	133.80	68.10
14.04	200	0.36	0.50	0.10	134.20	67.80
14.05	150	0.34	1.00	0.10	134.30	67.60
14.06	28	0.34	0.90	0.26	134.60	67.40
14.07	100	0.29	1.00	0.00	134.70	71.00
14.08	70	0.36	0.50	0.20	132.80	69.50
14.09	100	0.43	0.90	0.00	129.70	58.20
14.10	200	0.30	1.00	0.00	130.60	58.00
14.11	100	0.24	1.00	0.50	130.80	58.30
14.12	50	0.20	1.00	0.70	131.20	59.10
14.13	200	0.20	0.50	0.00	130.80	59.80
14.14	150	0.22	0.40	0.00	130.30	59.90
14.15	150	0.24	0.60	0.00	129.80	60.80
14.16	200	0.32	0.70	0.00	129.30	62.20
14.17	100	0.34	0.60	0.10	129.70	62.30
14.18	200	0.38	0.60	0.00	130.00	62.40
14.19	50	0.40	0.30	0.00	130.20	62.80
14.20	200	0.40	0.60	0.00	130.20	63.30
14.21	200	0.42	0.90	0.00	131.80	67.70
14.22	120	0.44	0.90	0.00	132.30	67.00
14.23	100	0.38	0.80	0.00	132.60	66.40
14.24	80	0.36	0.80	0.20	132.30	66.20
14.25	100	0.36	0.40	0.00	132.30	68.70
14.26	250	0.30	0.90	0.00	131.80	70.70
14.27	80	0.44	0.50	0.60	132.20	67.70
14.28	100	0.40	0.50	0.50	132.30	69.70
14.29	150	0.34	0.20	0.00	133.90	71.30
14.30	100	0.38	0.20	0.60	133.70	71.10
14.31	100	0.36	0.50	0.00	131.80	71.10
17.01	200	0.30	0.50	0.00	135.70	67.90
17.02	100	0.32	0.60	0.00	135.60	68.80
17.03	150	0.28	0.80	0.00	136.20	69.80
17.04	200	0.25	0.80	0.10	136.40	70.60
17.05	100	0.30	1.00	0.00	136.30	71.10
17.06	150	0.16	1.00	0.20	132.50	57.20
17.07	200	0.14	1.00	0.60	132.30	57.30
17.08	100	0.40	1.00	0.80	131.80	60.20

Appendix 2 (continued 6)

SECTION	L(m)	E(km)	P	F	UTM(E)	UTM(N)
17.09	100	0.42	1.00	0.80	131.00	60.80
17.10	150	0.42	1.00	0.80	131.90	61.30
17.11	200	0.24	1.00	0.30	133.30	61.70
17.12	250	0.26	1.00	0.20	133.00	62.40
17.13	150	0.30	1.00	0.00	133.80	63.50
17.14	140	0.35	0.90	0.00	133.90	64.70
17.15	100	0.40	1.00	0.30	134.60	65.40
17.16	200	0.56	0.90	0.60	134.90	66.30
17.17	200	0.46	0.90	0.50	134.70	66.70
18.01	100	0.34	0.75	0.00	131.00	71.00
18.02	200	0.33	0.85	0.00	130.90	71.70
18.03	100	0.32	0.85	0.00	130.90	71.90
18.04	50	0.32	1.00	0.00	131.00	72.20
18.05	100	0.34	1.00	0.00	131.00	72.60
18.06	150	0.38	0.65	0.10	131.30	69.80
18.07	100	0.39	0.80	0.00	130.80	68.50
18.08	200	0.40	0.70	0.00	131.00	67.00
18.09	112	0.38	0.90	0.10	131.20	66.30
18.10	100	0.32	0.90	0.00	131.10	65.30
18.11	68	0.32	1.00	0.10	131.00	64.90
18.12	100	0.54	0.90	0.00	128.00	59.20
18.13	80	0.51	0.90	0.10	128.00	59.40
18.14	100	0.36	0.90	0.10	128.20	60.10
18.15	100	0.28	0.90	0.30	128.30	60.70
18.16	100	0.26	0.90	0.00	128.70	61.10
18.17	150	0.28	0.90	0.00	128.80	61.60
18.18	39	0.30	1.00	0.50	128.70	62.00
18.19	18	0.32	1.00	0.40	128.00	62.20
18.20	21	0.36	1.00	0.50	127.90	62.80
18.21	60	0.42	-	1.00	127.90	63.20
18.22	50	0.48	1.00	0.70	128.00	63.80
18.23	100	0.53	1.00	0.50	128.00	64.30
18.24	100	0.46	1.00	0.20	127.20	65.90
18.25	50	0.38	0.80	0.00	129.40	70.00
18.26	50	0.36	0.80	0.00	129.50	69.50
18.27	100	0.38	0.80	0.00	128.50	68.90
18.28	100	0.41	0.80	0.00	128.00	67.90
19.01	150	0.35	1.00	0.00	127.60	75.60
19.02	200	0.36	0.90	0.00	126.80	74.80
19.03	100	0.38	0.80	0.00	126.80	73.90
19.04	150	0.39	0.90	0.00	127.00	73.20
19.05	100	0.40	0.50	0.00	127.20	71.10
19.06	100	0.42	0.10	0.00	126.80	70.20
19.07	150	0.42	0.90	0.10	127.00	69.00
19.08	100	0.43	0.90	0.00	126.40	67.60
19.09	100	0.47	0.80	0.10	125.40	67.30
19.10	50	0.50	0.80	0.50	124.60	67.90
19.11	100	0.52	0.80	0.60	125.00	68.30
19.12	100	0.46	0.80	0.30	125.00	67.00
19.13	50	0.50	0.90	0.60	124.80	66.80
19.14	70	0.52	0.80	0.80	124.30	66.40
19.15	100	0.60	0.80	0.80	123.70	66.10

Appendix 2 (continued 7)

SECTION	L(m)	E(km)	P	F	UTM(E)	UTM(N)
19.16	100	0.62	0.80	0.80	123.20	66.00
19.17	100	0.66	-	1.00	122.80	66.20
19.18	100	0.68	-	1.00	122.30	65.30
19.19	100	0.56	-	1.00	122.50	63.70
19.20	200	0.54	0.80	0.80	123.10	63.30
19.21	200	0.50	-	1.00	123.60	63.40
19.22	100	0.66	-	1.00	122.30	64.90
19.23	200	0.66	-	1.00	122.10	64.80
19.24	200	0.68	-	1.00	121.80	62.30
19.25	200	0.94	-	1.00	122.50	60.70
20.01	29	0.50	0.00	0.44	122.40	71.40
20.02	41	0.52	0.00	0.48	122.30	71.30
20.03	21	0.59	0.00	0.88	121.20	68.70
20.04	80	0.57	-	1.00	121.30	69.50
20.05	5	0.56	0.00	0.45	121.70	69.90
20.06	29	0.54	0.10	0.65	122.00	70.60
20.07	200	0.70	-	1.00	119.70	68.30
20.08	200	0.64	-	0.95	120.90	68.30
20.09	150	0.58	0.00	0.83	121.30	68.90
20.10	180	0.58	0.00	0.80	121.40	69.30
20.11	100	0.56	0.00	0.80	121.40	69.70
20.12	9	0.55	0.00	0.59	121.80	70.20
20.13	8	0.54	0.00	0.70	122.10	70.80
20.30	42	0.46	0.82	0.16	121.20	72.70
20.31	71	0.49	0.51	0.59	121.10	72.50
20.32	153	0.50	0.43	0.39	121.00	72.40
20.33	35	0.50	0.00	0.46	120.80	72.40
20.34	80	0.41	-	0.00	122.50	74.20
20.35	40	0.42	0.99	0.00	122.40	74.20
20.36	100	0.44	0.95	0.00	122.30	74.00
20.37	90	0.46	1.00	0.00	122.10	73.70
20.38	110	0.46	0.50	0.05	122.00	73.60
20.39	150	0.44	0.50	0.05	121.60	73.30
20.40	72	0.44	0.16	0.16	121.30	73.20
20.41	58	0.44	0.68	0.22	121.30	73.00
20.60	100	0.50	0.00	0.50	122.50	71.50
20.61	50	0.50	0.00	0.40	122.50	71.60
20.62	150	0.48	0.00	0.50	122.60	71.80
20.63	1000	0.47	0.00	0.50	122.70	72.00
20.64	150	0.44	0.00	0.50	122.70	72.60
20.65	50	0.45	0.00	0.40	122.70	72.70
20.66	30	0.45	0.50	0.50	122.60	72.70
20.67	30	0.44	0.90	-	122.70	72.70
20.68	100	0.44	0.80	0.50	122.60	72.80
20.69	100	0.42	0.50	0.45	122.60	72.90
20.70	100	0.42	0.60	0.40	122.60	73.00
20.71	70	0.43	0.40	0.35	122.60	73.10
20.72	100	0.43	0.20	0.30	122.60	73.20
20.73	200	0.43	0.00	0.10	122.50	73.30
20.74	300	0.45	0.00	0.00	122.50	73.50
20.75	150	0.42	0.00	0.10	122.60	73.70

Appendix 2 (continued 8)

SECTION	L(m)	E(km)	P	F	UTM(E)	UTM(N)
21.01	100	0.36	0.70	0.00	117.90	78.00
21.02	150	0.37	0.70	0.00	117.80	77.90
21.03	100	0.36	0.70	0.00	117.70	77.70
21.04	150	0.38	0.60	0.00	117.60	77.50
21.05	100	0.38	-	0.00	117.60	77.40
21.06	100	0.39	-	0.00	117.60	77.30
21.07	200	0.39	0.90	0.00	117.60	77.30
21.08	100	0.39	-	0.10	117.60	77.20
21.09	24	0.40	-	0.11	117.60	77.10
21.10	50	0.40	0.90	0.19	117.50	77.00
21.11	29	0.41	0.51	0.21	117.30	76.70
21.12	100	0.41	0.90	0.10	117.30	76.60
21.13	250	0.42	1.00	-	117.30	76.60
21.14	80	0.42	-	0.00	117.30	76.50
21.15	22	0.42	0.50	0.06	117.30	76.40
21.16	4	0.42	-	0.23	117.30	76.30
21.17	100	0.42	1.00	-	117.20	76.30
21.18	110	0.43	1.00	0.05	117.30	76.20
21.19	5	0.43	1.00	0.10	117.20	76.20
21.20	100	0.44	0.67	0.10	117.20	76.00
21.21	300	0.44	0.50	0.10	117.20	75.80
21.22	100	0.46	0.10	0.10	117.20	75.70
21.23	200	0.44	0.10	-	117.30	75.60
21.24	100	0.44	0.33	0.05	117.30	75.50
21.25	100	0.45	0.75	0.05	117.30	75.30
21.26	21	0.66	0.20	0.80	113.70	68.00
21.27	15	0.66	0.00	0.83	113.70	68.30
21.28	50	0.66,	0.00	0.84	113.80	68.40
21.29	15	0.65	0.00	0.80	113.70	68.60
21.30	50	0.65	0.00	0.73	113.60	68.70
21.31	50	0.64	0.12	0.49	113.60	68.80
21.32	50	0.62	0.16	0.56	113.80	69.40
21.33	25	0.62	0.20	0.79	113.70	69.80
21.34	50	0.40	0.00	0.62	113.90	70.20
21.36	44	0.54	0.10	0.64	114.00	70.70
21.39	51	0.56	0.00	0.39	114.50	71.50
21.40	94	0.56	0.33	0.13	114.50	72.00
21.41	200	0.55	0.60	0.00	114.70	72.80
21.42	100	0.52	0.70	0.00	115.00	73.30
22.01	52	0.47	0.28	0.53	111.40	76.00
22.02	41	0.45	0.66	0.37	111.30	75.80
22.03	31	0.48	0.00	0.52	111.00	75.10
22.04	16	0.50	0.00	0.68	111.20	74.70
22.05	17	0.45	0.00	0.56	111.20	75.60
22.06	49	0.46	0.07	0.54	111.00	75.70
22.07	23	0.45	0.00	0.46	110.90	76.20
22.08	42	0.43	0.00	0.17	111.10	76.30
22.09	52	0.42	0.75	0.20	110.90	77.00
22.10	150	0.44	0.90	0.10	110.60	77.20
22.11	19	0.60	-	0.90	111.10	72.60
22.12	100	0.58	-	0.89	111.40	70.10

Appendix 2 (continued 9)

SECTION	L(m)	E(km)	P	F	UTM(E)	UTM(N)
22.13	12	0.64	-	0.78	111.80	70.00
22.14	24	0.60	0.89	0.65	110.80	73.00
22.15	33	0.54	0.37	0.52	110.70	73.90
22.16	115	0.56	1.00	0.68	111.40	72.80
22.17	100	0.42	0.80	0.00	112.80	77.50
22.18	75	0.42	0.80	0.00	112.70	77.70
22.19	250	0.42	0.95	0.00	112.30	78.00
22.20	200	0.52	0.95	0.00	112.40	78.40
23.01	200	0.34	0.80	0.00	107.30	80.10
23.02	100	0.35	0.90	0.00	107.30	79.70
23.03	100	0.38	0.50	0.00	107.00	79.20
23.04	50	0.40	0.50	0.00	107.50	79.30
23.05	150	0.38	0.90	0.00	108.20	80.00
23.06	100	0.42	0.60	0.00	107.70	78.70
23.07	100	0.44	0.40	0.10	107.40	77.80
23.08	50	0.42	0.20	0.20	107.60	77.10
23.09	50	0.46	-	1.00	107.70	76.00
23.10	100	0.51	-	1.00	106.90	73.90
23.11	100	0.59	-	1.00	106.50	72.50
23.12	150	0.60	0.00	0.70	106.00	71.80
23.13	32	0.58	0.00	0.60	105.90	71.70
23.14	100	0.70	-	1.00	104.80	69.80
23.15	100	0.64	-	1.00	105.40	70.70
23.16	100	0.60	-	1.00	105.50	71.20
23.17	50	0.60	0.00	0.60	106.30	72.10
23.18	50	0.51	-	1.00	106.80	73.50
23.19	150	0.48	-	1.00	107.40	76.60
23.20	100	0.38	0.80	0.00	107.10	80.90
23.20	40	0.43	0.00	0.80	107.60	75.60
23.21	50	0.43	0.00	0.60	107.80	76.40
23.23	50	0.35	0.90	0.00	107.00	81.30
23.24	100	0.42	0.00	0.60	107.70	76.70
23.25	50	0.43	0.00	0.80	107.80	76.00
23.26	50	0.44	0.00	0.20	107.60	77.60
23.27	30	0.42	0.00	1.00	107.50	78.20
24.01	200	0.27	1.00	0.00	104.60	82.80
24.02	150	0.26	0.50	0.00	104.40	82.40
24.03	100	0.28	0.80	0.00	103.60	82.30
24.04	150	0.31	0.50	0.00	103.10	81.90
24.05	100	0.36	0.80	0.00	102.80	81.30
24.06	120	0.31	1.00	0.00	101.70	81.00
24.07	100	0.31	1.00	0.00	101.90	80.60
24.08	50	0.35	0.00	0.60	102.60	79.40
24.09	15	0.34	1.00	0.50	102.50	79.00
24.10	40	0.35	1.00	0.50	102.40	78.70
24.11	300	0.35	1.00	0.50	102.30	78.50
24.12	100	0.37	0.50	0.10	102.20	78.30
24.13	150	0.40	0.60	0.10	102.10	77.80
24.14	100	0.40	1.00	0.10	101.80	77.70
24.15	50	0.42	1.00	0.10	101.70	77.30
24.16	150	0.44	1.00	0.10	101.30	76.80
24.17	200	0.45	0.70	0.20	101.00	76.30

Appendix 2 (continued 10)

SECTION	L(m)	E(km)	P	F	UTM(E)	UTM(N)
24.18	50	0.45	0.80	0.50	100.90	76.10
24.19	120	0.48	1.00	0.60	100.80	75.70
24.20	150	0.52	1.00	0.80	100.70	75.20
24.21	200	0.54	-	1.00	100.50	74.70
24.22	150	0.55	-	1.00	100.20	74.10
24.23	100	0.60	0.00	0.90	99.80	73.50
24.24	40	0.60	-	1.00	99.50	73.00
24.26	150	0.44	1.00	0.30	100.70	77.40
24.27	120	0.44	0.50	0.20	100.90	78.10
24.28	100	0.44	0.50	0.20	100.70	78.70
24.29	50	0.40	0.50	0.50	100.40	77.90
24.30	50	0.58	0.50	0.60	99.70	78.30
24.31	80	0.58	0.50	0.70	99.90	77.90
24.32	50	0.60	0.00	0.80	99.30	77.70
24.33	200	0.62	-	1.00	98.80	77.80
24.34	10	0.43	0.50	0.50	100.60	77.70
24.35	30	0.42	0.50	0.20	100.70	78.70
24.36	20	0.40	0.50	0.10	100.80	79.40
24.37	140	0.40	0.10	0.10	100.90	79.90
24.38	100	0.36	0.50	0.10	100.90	79.90
24.39	200	0.33	0.90	0.00	100.60	80.50
25.01	100	0.22	1.00	0.00	98.30	83.50
25.02	150	0.23	1.00	0.00	97.90	83.10
25.03	30	0.27	0.90	0.00	97.70	82.70
25.04	50	0.28	1.00	0.00	97.70	82.30
25.05	50	0.29	0.50	0.10	97.30	82.10
25.06	100	0.29	0.10	0.00	96.90	82.00
25.07	150	0.30	0.50	0.20	96.70	81.60
25.08	100	0.32	0.20	0.30	96.80	81.50
25.09	100	0.34	0.70	0.50	96.90	81.20
25.10	200	0.38	0.20	0.70	97.00	80.80
25.11	200	0.40	0.00	0.80	96.90	80.60
25.12	100	0.42	0.30	0.80	96.90	80.30
25.13	80	0.46	0.00	0.90	97.20	80.10
25.14	100	0.47	-	1.00	97.60	89.80

1) Total 18 lines and 547 stations. 25.14 means the 14th station of Line 25.
2) L- Length of sections.
3) E- Elevation at the station, measured from 1:50,000 topographic maps.
4) Symbol "-" in P or F values means no value measured at the station.
5) UTM (E) and (N) are reduced coordinates.

UTM (E)	UTM (N)	Elevation(km)	Depth(km)
108.000,	79.500,	0.390,	-0.100
108.500,	79.000,	0.420,	-0.113
109.000,	78.500,	0.510,	-0.049
109.500,	78.100,	0.520,	-0.074
110.000,	77.800,	0.460,	-0.173
110.500,	77.300,	0.500,	-0.176
111.000,	77.080,	0.420,	-0.289
111.500,	77.150,	0.410,	-0.265
112.000,	77.300,	0.410,	-0.215
112.500,	77.400,	0.440,	-0.134
113.000,	77.350,	0.460,	-0.091
113.500,	77.250,	0.420,	-0.133
114.000,	77.100,	0.420,	-0.131
114.500,	77.000,	0.400,	-0.148
115.000,	76.900,	0.440,	-0.086
115.500,	76.800,	0.410,	-0.115
116.000,	76.800,	0.400,	-0.103
116.500,	76.850,	0.420,	-0.045
117.000,	76.850,	0.440,	0.005
117.500,	76.700,	0.400,	-0.045
117.100,	76.700,	0.420,	-0.038
117.450,	76.500,	0.430,	-0.039
116.600,	76.250,	0.450,	-0.093
117.000,	76.050,	0.440,	-0.117
117.500,	75.950,	0.440,	-0.108
118.100,	75.500,	0.460,	-0.122
117.700,	75.300,	0.440,	-0.200
118.000,	74.750,	0.500,	-0.195
118.500,	74.600,	0.500,	-0.193
119.000,	74.450,	0.480,	-0.217
119.500,	74.350,	0.470,	-0.220
120.000,	74.150,	0.480,	-0.213
120.500,	74.000,	0.470,	-0.225
121.000,	73.900,	0.500,	-0.176
121.500,	73.800,	0.480,	-0.191
122.000,	73.800,	0.440,	-0.217
122.500,	74.000,	0.440,	-0.160
123.000,	74.100,	0.470,	-0.079
123.500,	74.150,	0.480,	-0.033
124.000,	74.100,	0.460,	-0.042
124.500,	74.000,	0.420,	-0.085
125.000,	73.800,	0.400,	-0.116
125.500,	73.500,	0.400,	-0.138
126.000,	73.400,	0.400,	-0.128
126.500,	73.200,	0.380,	-0.160
127.000,	73.000,	0.380,	-0.166
110.000,	72.800,	0.640,	-0.756
110.500,	73.050,	0.600,	-0.743
111.000,	73.300,	0.580,	-0.704
111.500,	73.500,	0.600,	-0.619
112.000,	73.500,	0.560,	-0.645
112.500,	73.600,	0.560,	-0.602
113.000,	73.600,	0.540,	-0.601
113.500,	73.500,	0.500,	-0.643

(to be continued)

Appendix 3a P0.75 Contour Depth (Continued)

UTM (E)	UTM (N)	Elevation(km)	Depth(km)
114.000,	73.450,	0.550,	-0.559
114.500,	73.450,	0.520,	-0.572
115.000,	73.350,	0.520,	-0.561
115.500,	73.300,	0.560,	-0.491
116.000,	73.300,	0.680,	-0.308
116.500,	73.200,	0.560,	-0.454
117.000,	73.100,	0.520,	-0.495
117.500,	72.950,	0.520,	-0.493
118.000,	72.900,	0.540,	-0.449
118.500,	72.800,	0.540,	-0.438
119.000,	72.750,	0.540,	-0.420
119.500,	72.750,	0.500,	-0.445
120.000,	72.750,	0.540,	-0.366
120.500,	72.750,	0.500,	-0.391
121.000,	72.800,	0.510,	-0.343
121.500,	72.800,	0.520,	-0.303
122.000,	72.850,	0.510,	-0.281
122.500,	72.850,	0.520,	-0.241
122.800,	72.800,	0.500,	-0.260
122.000,	72.650,	0.520,	-0.301
121.500,	72.500,	0.500,	-0.379
121.000,	72.500,	0.520,	-0.380
120.500,	72.400,	0.520,	-0.423
120.000,	72.350,	0.540,	-0.432
119.500,	72.300,	0.560,	-0.442
119.000,	72.400,	0.520,	-0.504
118.500,	72.600,	0.560,	-0.446
118.000,	72.700,	0.570,	-0.443
117.500,	72.850,	0.540,	-0.484
117.000,	73.000,	0.520,	-0.512
116.500,	73.050,	0.560,	-0.478
116.000,	73.100,	0.580,	-0.471
115.500,	73.150,	0.600,	-0.464
115.000,	73.200,	0.540,	-0.560
114.500,	73.300,	0.540,	-0.570
114.000,	73.350,	0.540,	-0.589
113.500,	73.500,	0.500,	-0.643
113.000,	73.500,	0.520,	-0.644
112.500,	73.350,	0.560,	-0.643
112.000,	73.050,	0.580,	-0.692
111.500,	72.700,	0.560,	-0.800
111.000,	72.500,	0.640,	-0.752
110.500,	72.150,	0.680,	-0.779

Appendix 3b P0.5 Contour Depth

UTM (E)	UTM (N)	Elevation(km)	Depth(km)
108.000,	78.600,	0.420,	-0.201
108.500,	78.600,	0.460,	-0.124
109.000,	78.400,	0.520,	-0.052
109.500,	78.200,	0.480,	-0.110
110.000,	77.750,	0.420,	-0.233
110.500,	76.850,	0.460,	-0.301
111.000,	76.900,	0.440,	-0.292
111.500,	76.850,	0.410,	-0.313
112.000,	76.500,	0.420,	-0.331
111.300,	75.800,	0.460,	-0.431
112.000,	75.750,	0.480,	-0.376
112.500,	76.000,	0.440,	-0.360
113.000,	76.300,	0.480,	-0.233
113.500,	76.600,	0.440,	-0.210
114.000,	76.700,	0.420,	-0.194
114.500,	76.550,	0.420,	-0.192
115.000,	76.450,	0.430,	-0.169
115.500,	76.450,	0.400,	-0.183
116.000,	76.500,	0.410,	-0.137
116.500,	76.600,	0.440,	-0.057
117.100,	76.500,	0.420,	-0.069
116.400,	76.200,	0.440,	-0.124
117.000,	75.950,	0.440,	-0.133
117.700,	75.700,	0.440,	-0.137
117.000,	75.300,	0.420,	-0.263
117.500,	74.700,	0.430,	-0.321
118.000,	74.300,	0.500,	-0.269
118.500,	74.100,	0.500,	-0.275
119.000,	73.950,	0.480,	-0.299
119.500,	73.800,	0.500,	-0.271
120.000,	73.700,	0.510,	-0.248
120.500,	73.600,	0.520,	-0.225
121.000,	73.500,	0.480,	-0.267
121.500,	73.500,	0.460,	-0.266
122.000,	73.550,	0.460,	-0.232
122.500,	73.950,	0.460,	-0.142
123.000,	74.000,	0.460,	-0.108
123.500,	74.050,	0.470,	-0.062
124.000,	74.000,	0.440,	-0.084
124.500,	73.800,	0.420,	-0.115
125.000,	73.700,	0.400,	-0.132
125.500,	73.500,	0.400,	-0.138
126.000,	73.000,	0.400,	-0.190
117.300,	78.100,	0.400,	0.146
117.500,	77.500,	0.400,	0.072
118.000,	77.000,	0.420,	0.049
118.500,	76.500,	0.410,	-0.013
119.000,	76.000,	0.420,	-0.051
119.500,	75.400,	0.420,	-0.118
120.000,	75.000,	0.460,	-0.104
120.500,	74.950,	0.460,	-0.086
121.000,	74.900,	0.460,	-0.069
121.500,	74.900,	0.460,	-0.044
122.000,	74.900,	0.470,	-0.006

(to be continued)

Appendix 3b P0.5 Contour Depth (Continued 1)

UTM (E)	UTM (N)	Elevation(km)	Depth(km)
110.500,	73.500,	0.600,	-0.672
111.000,	73.700,	0.560,	-0.665
111.500,	73.800,	0.660,	-0.492
112.000,	73.900,	0.560,	-0.579
112.500,	73.900,	0.540,	-0.578
113.000,	73.850,	0.520,	-0.586
113.500,	73.800,	0.500,	-0.593
114.000,	73.700,	0.540,	-0.531
114.500,	73.600,	0.500,	-0.573
115.000,	73.500,	0.520,	-0.536
115.500,	73.400,	0.540,	-0.500
116.000,	73.350,	0.700,	-0.274
116.500,	73.300,	0.560,	-0.437
117.000,	73.250,	0.520,	-0.470
117.500,	73.150,	0.520,	-0.460
118.000,	73.050,	0.540,	-0.424
118.500,	73.000,	0.520,	-0.431
119.000,	72.950,	0.540,	-0.386
119.500,	72.950,	0.500,	-0.411
120.000,	72.950,	0.520,	-0.359
120.500,	73.000,	0.540,	-0.298
121.000,	73.050,	0.520,	-0.288
121.500,	73.050,	0.520,	-0.262
122.000,	73.050,	0.500,	-0.261
122.500,	73.000,	0.520,	-0.217
123.200,	72.900,	0.600,	-0.092
122.500,	72.600,	0.500,	-0.309
122.000,	72.600,	0.540,	-0.283
121.500,	72.400,	0.520,	-0.369
121.000,	72.400,	0.500,	-0.422
120.500,	72.300,	0.530,	-0.427
120.000,	72.250,	0.580,	-0.397
119.500,	72.250,	0.560,	-0.450
119.000,	72.250,	0.560,	-0.477
118.500,	72.300,	0.560,	-0.495
118.000,	72.300,	0.580,	-0.496
117.500,	72.350,	0.580,	-0.515
117.000,	72.350,	0.620,	-0.490
116.500,	72.300,	0.600,	-0.550
116.000,	72.300,	0.700,	-0.447
115.500,	72.300,	0.680,	-0.500
115.000,	72.400,	0.580,	-0.640

(to be continued)

Appendix 3b P0.5 Contour Depth (Continued 2)

UTM (E)	UTM (N)	Elevation(km)	Depth(km)
114.500,	72.700,	0.540,	-0.669
114.000,	72.900,	0.580,	-0.611
113.500,	73.200,	0.580,	-0.588
113.000,	73.350,	0.540,	-0.642
112.500,	73.200,	0.540,	-0.693
112.000,	72.900,	0.540,	-0.768
111.500,	72.500,	0.580,	-0.805
111.000,	72.500,	0.620,	-0.778
110.500,	71.900,	0.760,	-0.713
111.000,	71.500,	0.700,	-1.035
111.500,	71.900,	0.600,	-1.051
112.000,	72.000,	0.580,	-1.031
112.650,	71.700,	0.640,	-0.985
112.000,	71.250,	0.560,	-1.164
111.500,	71.000,	0.640,	-1.144

UTM (E)	UTM (N)	Elevation(km)	Depth(km)
108.000,	78.400,	0.440,	-0.207
108.500,	78.350,	0.460,	-0.163
109.000,	78.300,	0.500,	-0.093
109.500,	78.100,	0.520,	-0.074
110.000,	76.800,	0.500,	-0.284
110.500,	76.600,	0.460,	-0.342
111.000,	76.550,	0.460,	-0.324
111.500,	76.400,	0.430,	-0.361
111.000,	75.800,	0.460,	-0.448
111.500,	75.700,	0.500,	-0.385
112.000,	75.550,	0.450,	-0.448
112.500,	75.400,	0.480,	-0.407
113.000,	75.300,	0.520,	-0.345
113.500,	75.200,	0.520,	-0.335
114.000,	75.100,	0.480,	-0.376
114.500,	75.000,	0.420,	-0.444
115.000,	74.900,	0.460,	-0.382
115.500,	74.700,	0.480,	-0.362
116.000,	76.700,	0.460,	-0.041
116.500,	76.500,	0.460,	-0.047
117.000,	76.300,	0.480,	-0.027
117.500,	76.250,	0.490,	0.004
118.000,	74.000,	0.500,	-0.318
118.500,	73.900,	0.500,	-0.308
119.000,	73.800,	0.500,	-0.298
119.500,	73.700,	0.500,	-0.287
120.000,	73.550,	0.500,	-0.285
120.500,	73.400,	0.480,	-0.309
121.000,	73.300,	0.460,	-0.325
121.500,	73.250,	0.460,	-0.307
122.000,	73.400,	0.480,	-0.230
122.500,	73.700,	0.460,	-0.181
123.000,	73.900,	0.480,	-0.098
123.500,	74.000,	0.480,	-0.057
124.000,	74.000,	0.440,	-0.084
124.500,	73.900,	0.460,	-0.048
125.000,	73.200,	0.420,	-0.184
125.500,	72.300,	0.460,	-0.250
126.000,	71.100,	0.420,	-0.473
126.500,	70.700,	0.420,	-0.512
127.000,	70.500,	0.410,	-0.532
127.300,	70.000,	0.420,	-0.586
126.500,	69.950,	0.420,	-0.637
126.000,	69.900,	0.440,	-0.646
125.500,	69.850,	0.460,	-0.655
125.000,	69.750,	0.480,	-0.673
124.500,	69.500,	0.550,	-0.649
124.000,	69.000,	0.600,	-0.692
110.500,	74.200,	0.540,	-0.636
111.000,	74.250,	0.520,	-0.627
111.500,	74.250,	0.520,	-0.600
112.000,	74.200,	0.480,	-0.633
112.500,	74.250,	0.480,	-0.598
113.000,	74.050,	0.500,	-0.579

(to be continued)

Appendix 3c P0.25 Contour Depth (Continued 1)

UTM (E)	UTM (N)	Elevation(km)	Depth(km)
113.500,	74.100,	0.460,	-0.595
114.000,	74.200,	0.480,	-0.526
114.500,	74.250,	0.480,	-0.491
115.000,	74.250,	0.500,	-0.438
115.500,	74.200,	0.490,	-0.432
116.000,	74.150,	0.490,	-0.414
116.500,	74.050,	0.540,	-0.338
117.000,	74.000,	0.490,	-0.385
117.500,	73.800,	0.520,	-0.352
118.000,	73.700,	0.520,	-0.342
118.500,	73.600,	0.540,	-0.305
119.000,	73.400,	0.500,	-0.364
119.500,	73.200,	0.560,	-0.292
120.000,	73.150,	0.500,	-0.351
120.500,	73.100,	0.480,	-0.359
121.000,	73.100,	0.480,	-0.332
121.500,	73.100,	0.460,	-0.332
122.000,	73.100,	0.480,	-0.279
122.500,	73.100,	0.440,	-0.304
123.000,	73.100,	0.400,	-0.330
123.400,	73.000,	0.520,	-0.169
123.000,	72.600,	0.500,	-0.282
122.500,	72.500,	0.500,	-0.325
122.000,	72.400,	0.560,	-0.290
121.500,	72.400,	0.500,	-0.395
121.000,	72.300,	0.500,	-0.439
120.500,	72.200,	0.540,	-0.430
120.000,	72.100,	0.580,	-0.422
119.500,	72.000,	0.560,	-0.491
119.000,	72.000,	0.580,	-0.492
118.500,	72.000,	0.590,	-0.506
118.000,	71.950,	0.620,	-0.502
117.500,	71.950,	0.600,	-0.555
117.000,	71.900,	0.640,	-0.537
116.500,	71.900,	0.640,	-0.564
116.000,	71.850,	0.660,	-0.572
115.500,	71.900,	0.700,	-0.538
115.000,	72.000,	0.680,	-0.574
114.500,	72.200,	0.560,	-0.724
114.000,	72.300,	0.500,	-0.812

(to be continued)

Appendix 3c P0.25 Contour Depth (Continued 2)

UTM (E)	UTM (N)	Elevation(km)	Depth(km)
113.500,	72.800,	0.600,	-0.628
113.000,	73.100,	0.500,	-0.735
112.500,	73.050,	0.520,	-0.743
112.000,	72.800,	0.540,	-0.784
111.500,	72.[illegible]3,	0.580,	-0.836
111.000,	71.950,	0.640,	-0.837
110.500,	71.650,	0.800,	-0.698
110.500,	71.400,	0.820,	-0.953
111.000,	71.750,	0.660,	-1.038
111.500,	72.000,	0.600,	-1.036
112.000,	72.200,	0.520,	-1.060
112.500,	72.250,	0.600,	-0.947
113.000,	72.200,	0.620,	-0.909
113.500,	71.750,	0.700,	-0.874
113.000,	71.100,	0.680,	-1.019
112.500,	70.750,	0.600,	-1.174
112.000,	70.600,	0.560,	-1.258
111.500,	70.300,	0.620,	-1.262
111.000,	70.100,	0.680,	-1.250

Appendix 4 Strikes and Dips of Sheet Flows in the Xiliatos Formation

Strikes	Dip Direction*	Strikes	Dip Direction*
57.000,	2.000	359.000,	2.000
58.000,	2.000	5.000,	2.000
356.000,	2.000	358.000,	2.000
322.000,	2.000	356.000,	2.000
295.000,	2.000	43.000,	2.000
305.000,	2.000	54.000,	2.000
87.000,	2.000	50.000,	2.000
75.000,	2.000	48.000,	2.000
90.000,	2.000	38.000,	2.000
31.000,	1.000	25.000,	2.000
31.000,	1.000	59.000,	2.000
38.000,	1.000	30.000,	2.000
12.000,	2.000	11.000,	2.000
66.000,	1.000	10.000,	2.000
51.000,	1.000	14.000,	2.000
359.000,	1.000	10.000,	2.000
27.000,	1.000	3.000,	2.000
28.000,	1.000	20.000,	2.000
8.000,	1.000	18.000,	2.000
10.000,	1.000	24.000,	2.000
22.000,	1.000	49.000,	2.000
344.000,	2.000	13.000,	2.000
2.000,	1.000	360.000,	2.000
28.000,	2.000	341.000,	2.000
18.000,	1.000	353.000,	2.000
8.000,	1.000	87.000,	1.000
2.000,	2.000	342.000,	1.000
37.000,	2.000	356.000,	1.000
350.000,	2.000	2.000,	1.000
5.000,	2.000	19.000,	1.000
343.000,	2.000	358.000,	1.000
2.000,	2.000	349.000,	1.000
360.000,	2.000	358.000,	1.000
18.000,	2.000	354.000,	1.000
15.000,	2.000	352.000,	1.000
305.000,	1.000	342.000,	2.000
359.000,	2.000	345.000,	2.000
23.000,	2.000	346.000,	2.000
350.000,	2.000	338.000,	1.000
357.000,	2.000	61.000,	1.000
353.000,	2.000	58.000,	2.000
306.000,	2.000	82.000,	1.000
320.000,	2.000	29.000,	1.000
303.000,	2.000	56.000,	1.000
322.000,	2.000	48.000,	2.000
13.000,	2.000	18.000,	1.000
270.000,	2.000	18.000,	2.000
352.000,	2.000	15.000,	1.000

(to be continued)

Appendix 4 Strikes and Dips of Sheet Flows in the Xiliatos Formation (continued 1)

Strikes	Dip Direction*	Strikes	Dip Direction*
15.000,	2.000	21.000,	2.000
36.000,	2.000	19.000,	2.000
32.000,	2.000	42.000,	2.000
347.000,	1.000	43.000,	2.000
21.000,	2.000	12.000,	1.000
64.000,	2.000	28.000,	2.000
70.000,	2.000	20.000,	2.000
27.000,	2.000	3.000,	2.000
9.000,	1.000	2.000,	2.000
24.000,	2.000	3.000,	2.000
35.000,	1.000	18.000,	1.000
35.000,	2.000	60.000,	2.000
32.000,	2.000	36.000,	2.000
7.000,	2.000	23.000,	1.000
49.000,	2.000	8.000,	1.000
23.000,	2.000	51.000,	1.000
37.000,	2.000	52.000,	2.000
13.000,	2.000	52.000,	2.000
28.000,	2.000	34.000,	2.000
46.000,	2.000	29.000,	2.000
310.000,	1.000	46.000,	2.000
12.000,	2.000	2.000,	2.000
25.000,	1.000	298.000,	1.000
72.000,	2.000	2.000,	2.000
37.000,	2.000	1.000,	1.000
37.000,	2.000	12.000,	2.000
66.000,	2.000	12.000,	2.000
40.000,	2.000	43.000,	2.000
39.000,	2.000	25.000,	2.000
40.000,	2.000	35.000,	2.000
22.000,	2.000	20.000,	2.000
38.000,	1.000	12.000,	1.000
57.000,	1.000	8.000,	2.000
19.000,	2.000	32.000,	2.000
27.000,	2.000	5.000,	2.000
17.000,	2.000	28.000,	1.000
15.000,	1.000	28.000,	1.000
18.000,	2.000	22.000,	2.000
9.000,	2.000	36.000,	2.000
40.000,	2.000	24.000,	2.000
23.000,	2.000	64.000,	2.000
18.000,	1.000	49.000,	2.000
22.000,	1.000	30.000,	2.000
25.000,	1.000	26.000,	2.000
46.000,	1.000	51.000,	2.000
6.000,	2.000	28.000,	2.000
6.000,	2.000	36.000,	2.000
20.000,	2.000	28.000,	2.000

(to be continued)

Appendix 4 Strikes and Dips of Sheet Flows in the Xiliatos Formation (continued 2)

Strikes	Dip Direction*	Strikes	Dip Direction*
5.000,	1.000	11.000,	2.000
42.000,	2.000	360.000,	2.000
43.000,	2.000	70.000,	2.000
7.000,	1.000	10.000,	2.000
8.000,	2.000	348.000,	2.000
65.000,	2.000	38.000,	2.000
30.000,	2.000	61.000,	2.000
20.000,	2.000	64.000,	2.000
355.000,	1.000	58.000,	2.000
349.000,	2.000	1.000,	2.000
70.000,	2.000	353.000,	2.000
59.000,	2.000	313.000,	2.000
34.000,	2.000	310.000,	2.000
30.000,	2.000	27.000,	2.000
72.000,	2.000	342.000,	2.000
350.000,	1.000	297.000,	1.000
5.000,	2.000	38.000,	2.000
16.000,	1.000	43.000,	2.000
23.000,	2.000	2.000,	2.000
318.000,	2.000	3.000,	1.000
4.000,	2.000	8.000,	2.000
4.000,	2.000	5.000,	1.000
4.000,	2.000	22.000,	1.000
5.000,	1.000	8.000,	2.000
30.000,	2.000	357.000,	1.000
34.000,	2.000	8.000,	2.000
30.000,	2.000	357.000,	1.000
18.000,	1.000	9.000,	2.000
25.000,	2.000	37.000,	2.000
14.000,	2.000	352.000,	1.000
9.000,	2.000	348.000,	2.000
360.000,	1.000	63.000,	2.000
32.000,	2.000	50.000,	2.000
50.000,	2.000	55.000,	2.000
356.000,	2.000	45.000,	2.000
355.000,	2.000	18.000,	2.000
353.000,	2.000	25.000,	2.000
40.000,	2.000	57.000,	2.000
9.000,	2.000	13.000,	2.000
360.000,	2.000	310.000,	2.000
30.000,	2.000	328.000,	1.000
356.000,	2.000	63.000,	2.000
2.000,	2.000	77.000,	1.000
2.000,	2.000	298.000,	1.000
2.000,	2.000	52.000,	2.000
38.000,	2.000	20.000,	2.000
18.000,	2.000	320.000,	2.000
15.000,	2.000	54.000,	2.000

(to be continued)

Appendix 4 Strikes and Dips of Sheet Flows in the Xiliatos Formation (continued 3)

Strikes	Dip Direction*	Strikes	Dip Direction*
54.000,	2.000	42.000,	2.000
2.000,	2.000	46.000,	2.000
355.000,	2.000	359.000,	2.000
8.000,	2.000	6.000,	2.000
30.000,	2.000	1.000,	2.000
316.000,	1.000	44.000,	2.000
4.000,	2.000	4.000,	1.000
86.000,	1.000	349.000,	2.000
13.000,	2.000	64.000,	2.000
310.000,	1.000	69.000,	2.000
90.000,	2.000	347.000,	1.000
62.000,	2.000	349.000,	1.000
8.000,	2.000	24.000,	2.000
324.000,	2.000	352.000,	2.000
360.000,	2.000	16.000,	2.000
330.000,	2.000	354.000,	2.000
61.000,	2.000	70.000,	2.000
328.000,	1.000	24.000,	2.000
350.000,	2.000	8.000,	1.000
316.000,	2.000	7.000,	1.000
348.000,	2.000	60.000,	2.000
346.000,	1.000	30.000,	2.000
348.000,	2.000	46.000,	2.000
72.000,	2.000	18.000,	2.000
360.000,	2.000	51.000,	2.000
40.000,	2.000	13.000,	2.000
360.000,	2.000	36.000,	2.000
360.000,	2.000	11.000,	2.000
13.000,	2.000	3.000,	2.000
15.000,	1.000	4.000,	2.000
15.000,	1.000	7.000,	2.000
360.000,	2.000	18.000,	2.000
360.000,	2.000	7.000,	2.000
351.000,	2.000	7.000,	2.000
353.000,	2.000	6.000,	2.000
12.000,	2.000	6.000,	2.000
24.000,	1.000	18.000,	2.000
293.000,	2.000	3.000,	2.000
338.000,	1.000	51.000,	2.000
328.000,	2.000	50.000,	2.000
4.000,	2.000	360.000,	1.000
45.000,	1.000	10.000,	2.000
20.000,	2.000	24.000,	2.000
11.000,	1.000	43.000,	2.000
3.000,	2.000	40.000,	2.000
316.000,	2.000	22.000,	2.000
662.000,	1.000	25.000,	2.000
343.000,	1.000	37.000,	2.000

(to be continued)

Appendix 4 Strikes and Dips of Sheet Flows in the Xiliatos Formation (continued 4)

Strikes	Dip Direction*	Strikes	Dip Direction*
86.000,	2.000	5.000,	1.000
84.000,	2.000	7.000,	2.000
355.000,	1.000	85.000,	2.000
37.000,	2.000	9.000,	2.000
6.000,	2.000	355.000,	2.000
61.000,	2.000	12.000,	2.000
350.000,	2.000	43.000,	2.000
360.000,	2.000	12.000,	2.000
3.000,	2.000	44.000,	1.000
2.000,	0.000	65.000,	2.000
2.000,	2.000	67.000,	2.000
4.000,	2.000	46.000,	2.000
11.000,	2.000	91.000,	2.000
12.000,	2.000	74.000,	2.000
64.000,	2.000	32.000,	2.000
335.000,	1.000	35.000,	1.000
16.000,	2.000	35.000,	1.000
70.000,	2.000	32.000,	2.000
69.000,	2.000	59.000,	2.000
73.000,	1.000	24.000,	2.000
83.000,	2.000	22.000,	2.000
85.000,	2.000	32.000,	2.000
6.000,	2.000	40.000,	2.000
3.000,	2.000	7.000,	2.000
61.000,	2.000	11.000,	2.000
1.000,	2.000	35.000,	2.000
24.000,	1.000	20.000,	2.000
360.000,	2.000	37.000,	2.000
59.000,	2.000	63.000,	2.000

* Dip Direction: 1-east; 2-west.

UTM (E)	UTM (N)	Elevation(km)	Depth(km)
113.800,	73.200,	0.540,	-0.786
114.000,	72.150,	0.460,	-1.026
115.000,	71.700,	0.610,	-0.896
116.000,	71.850,	0.660,	-0.770
116.750,	72.300,	0.580,	-0.737
117.550,	72.500,	0.570,	-0.671
118.600,	72.650,	0.560,	-0.599
119.350,	72.450,	0.540,	-0.612
120.250,	72.650,	0.520,	-0.550
121.200,	72.600,	0.500,	-0.528
121.150,	73.200,	0.460,	-0.471
122.700,	71.750,	0.500,	-0.588
121.700,	73.300,	0.480,	-0.406
122.350,	73.350,	0.470,	-0.373
122.800,	73.200,	0.460,	-0.384
114.100,	73.950,	0.500,	-0.686
114.600,	74.600,	0.480,	-0.571
115.200,	75.200,	0.460,	-0.459
104.950,	76.700,	0.540,	-0.681
105.800,	76.650,	0.480,	-0.704
106.800,	76.800,	0.480,	-0.625
107.400,	76.900,	0.420,	-0.636
108.250,	77.500,	0.500,	-0.412
109.100,	77.200,	0.480,	-0.436
110.000,	76.800,	0.500,	-0.433
110.900,	76.700,	0.470,	-0.432
111.500,	76.200,	0.460,	-0.492
111.900,	75.500,	0.450,	-0.596
112.800,	75.200,	0.500,	-0.548
113.800,	75.000,	0.480,	-0.547
114.050,	75.700,	0.490,	-0.409
114.800,	76.300,	0.410,	-0.352
115.750,	76.750,	0.400,	-0.243
116.600,	76.950,	0.380,	-0.191
116.800,	76.300,	0.440,	-0.220
116.000,	76.700,	0.420,	-0.218
100.000,	79.400,	0.400,	-0.639
100.600,	78.600,	0.420,	-0.720
100.900,	78.000,	0.460,	-0.763
101.000,	77.150,	0.460,	-0.898
100.950,	76.350,	0.460,	-1.030
101.750,	75.900,	0.500,	-1.020
102.550,	76.300,	0.460,	-0.955
103.300,	76.900,	0.440,	-0.837
104.300,	76.800,	0.480,	-0.760
105.300,	76.550,	0.500,	-0.727
106.300,	76.650,	0.490,	-0.667
107.250,	76.900,	0.440,	-0.624
101.300,	80.500,	0.300,	-0.490
101.400,	79.600,	0.360,	-0.571
102.000,	78.650,	0.400,	-0.656
102.800,	78.150,	0.420,	-0.676
103.750,	77.850,	0.400,	-0.695

(to be continued)

Appendix 5a (continued 1)

UTM (E)	UTM (N)	Elevation(km)	Depth(km)
104.700,	77.800,	0.440,	-0.612
104.250,	78.400,	0.470,	-0.507
105.000,	78.700,	0.440,	-0.447
104.400,	79.300,	0.440,	-0.382
105.100,	79.800,	0.420,	-0.286
103.400,	80.300,	0.400,	-0.314
102.500,	80.800,	0.380,	-0.301
101.750,	80.900,	0.310,	-0.393
105.500,	80.500,	0.350,	-0.228
106.100,	80.400,	0.420,	-0.144
122.900,	73.200,	0.500,	-0.339
123.100,	72.400,	0.500,	-0.459
123.900,	72.000,	0.500,	-0.482
123.000,	72.000,	0.520,	-0.510
123.100,	71.050,	0.540,	-0.643
123.700,	70.100,	0.540,	-0.768
124.500,	69.500,	0.530,	-0.834
125.500,	69.400,	0.460,	-0.867
126.300,	68.900,	0.440,	-0.927
125.800,	68.050,	0.470,	-1.060
125.400,	67.300,	0.470,	-1.196
125.200,	66.400,	0.480,	-1.327
125.400,	65.700,	0.520,	-1.375
126.600,	65.500,	0.540,	-1.330
127.700,	65.700,	0.520,	-1.272
128.700,	65.800,	0.500,	-1.230
129.800,	65.650,	0.400,	-1.300
129.800,	64.700,	0.440,	-1.397
129.700,	63.700,	0.540,	-1.434
129.100,	62.700,	0.420,	-1.694
128.800,	61.800,	0.300,	-1.914
128.400,	61.050,	0.260,	-2.027
128.000,	60.400,	0.320,	-2.020
133.900,	71.200,	0.340,	-0.253
133.000,	71.000,	0.330,	-0.338
132.100,	70.500,	0.400,	-0.393
131.800,	69.800,	0.370,	-0.553
132.700,	69.400,	0.350,	-0.591
133.600,	69.800,	0.340,	-0.488
134.300,	70.500,	0.280,	-0.400
134.800,	67.400,	0.320,	-0.840
133.800,	67.600,	0.360,	-0.820
132.800,	68.050,	0.410,	-0.749
132.000,	68.100,	0.400,	-0.794
132.200,	67.300,	0.440,	-0.876
132.800,	66.500,	0.370,	-1.045
132.500,	66.000,	0.340,	-1.170
133.400,	65.400,	0.350,	-1.209
134.350,	65.250,	0.370,	-1.164
133.300,	62.000,	0.280,	-1.759
132.300,	62.200,	0.280,	-1.774

(to be continued)

Appendix 5a (continued 2)

UTM (E)	UTM (N)	Elevation(km)	Depth(km)
131.300,	62.300,	0.380,	-1.700
130.400,	61.900,	0.360,	-1.794
130.300,	60.900,	0.280,	-1.970
130.900,	60.000,	0.220,	-2.085
130.700,	59.400,	0.220,	-2.127
130.500,	58.600,	0.260,	-2.129
107.700,	77.200,	0.480,	-0.510
107.800,	77.400,	0.440,	-0.512
110.950,	76.250,	0.440,	-0.533
111.950,	76.000,	0.450,	-0.511
114.400,	75.350,	0.430,	-0.507

UTM (N)	UTM (E)	Elevation(km)	Depth(km)
81.250,	96.800,	0.320,	-0.585
81.100,	97.700,	0.330,	-0.552
80.500,	98.800,	0.460,	-0.462
78.500,	100.000,	0.500,	-0.689
77.500,	100.550,	0.500,	-0.825
76.400,	100.700,	0.480,	-1.015
75.500,	101.400,	0.600,	-1.001
74.700,	102.150,	0.740,	-0.946
74.100,	103.100,	0.580,	-1.149
75.000,	103.000,	0.660,	-0.938
75.900,	103.000,	0.500,	-0.956
76.000,	103.700,	0.500,	-0.903
76.400,	103.300,	0.420,	-0.939
76.400,	104.300,	0.500,	-0.806
76.100,	105.300,	0.500,	-0.802
76.100,	106.100,	0.540,	-0.719
76.700,	107.000,	0.460,	-0.651
76.850,	108.000,	0.470,	-0.562
76.750,	109.000,	0.520,	-0.475
76.400,	110.000,	0.500,	-0.499
76.000,	110.500,	0.480,	-0.559
76.000,	111.500,	0.460,	-0.525
75.800,	111.100,	0.450,	-0.590
75.000,	112.000,	0.480,	-0.644
74.600,	113.000,	0.540,	-0.597
74.000,	113.150,	0.500,	-0.728
73.000,	112.900,	0.500,	-0.906
72.300,	112.800,	0.520,	-1.004
71.300,	113.400,	0.680,	-0.969
71.000,	114.500,	0.580,	-1.060
71.250,	115.300,	0.700,	-0.861
71.700,	116.400,	0.700,	-0.733
72.200,	117.300,	0.600,	-0.704
72.500,	118.400,	0.550,	-0.645
72.400,	119.500,	0.560,	-0.592
79.600,	99.600,	0.460,	-0.567
72.300,	120.500,	0.530,	-0.585
72.600,	121.300,	0.520,	-0.502
73.000,	122.000,	0.520,	-0.399
72.300,	123.000,	0.500,	-0.481
71.550,	122.250,	0.540,	-0.606
71.300,	121.950,	0.570,	-0.633
70.600,	121.500,	0.600,	-0.743
69.900,	123.500,	0.540,	-0.811
69.300,	124.500,	0.570,	-0.827
68.700,	125.400,	0.580,	-0.866
68.000,	124.700,	0.500,	-1.093
67.200,	124.800,	0.500,	-1.210
66.500,	125.000,	0.520,	-1.282
65.500,	125.100,	0.480,	-1.454
64.700,	126.000,	0.480,	-1.519
64.500,	127.000,	0.600,	-1.384
64.400,	128.000,	0.520,	-1.435

(to be continued)

Appendix 5b (continued)

UTM (N)	UTM (E)	Elevation(km)	Depth(km)
63.700,	129.050,	0.600,	-1.400
81.600,	101.900,	0.360,	-0.228
80.800,	102.500,	0.360,	-0.321
80.300,	102.200,	0.320,	-0.455
79.800,	102.500,	0.340,	-0.500
79.400,	102.400,	0.320,	-0.591
79.250,	103.200,	0.380,	-0.513
79.100,	104.100,	0.420,	-0.450
80.100,	103.700,	0.420,	-0.310
81.000,	103.300,	0.420,	-0.190
81.200,	102.700,	0.360,	-0.249
70.300,	120.800,	0.700,	-0.729
70.200,	121.500,	0.600,	-0.808
69.900,	121.800,	0.600,	-0.841
69.900,	121.400,	0.600,	-0.862
69.300,	112.300,	0.540,	-1.439
69.500,	113.200,	0.700,	-1.215
69.100,	114.000,	0.700,	-1.234
68.800,	113.100,	0.780,	-1.229
68.600,	112.300,	0.700,	-1.363
68.700,	111.500,	0.640,	-1.441
69.000,	111.800,	0.580,	-1.455

Appendix 5c F0.75 Contour Depth

UTM (N)	UTM (E)	Elevation(km)	Depth(km)
63.400,	128.500,	0.500,	-1.558
63.800,	127.500,	0.600,	-1.449
64.100,	126.500,	0.550,	-1.502
64.500,	125.500,	0.160,	-1.583
65.100,	124.800,	0.470,	-1.528
66.100,	124.500,	0.600,	-1.280
67.000,	124.300,	0.500,	-1.263
68.000,	124.300,	0.520,	-1.093
69.000,	124.250,	0.630,	-0.828
69.600,	123.450,	0.500,	-0.903
69.700,	122.300,	0.630,	-0.817
69.800,	121.300,	0.600,	-0.883
70.300,	120.500,	0.620,	-0.824
71.000,	119.700,	0.640,	-0.733
71.700,	119.000,	0.590,	-0.705
72.000,	118.100,	0.600,	-0.694
71.600,	117.150,	0.620,	-0.790
70.900,	116.400,	0.620,	-0.940
70.400,	115.600,	0.800,	-0.877
70.000,	114.700,	0.760,	-1.019
69.900,	114.000,	0.600,	-1.226
69.800,	113.300,	0.660,	-1.211
69.300,	114.250,	0.680,	-1.217
68.700,	113.700,	0.660,	-1.337
68.350,	112.700,	0.800,	-1.277
68.300,	111.750,	0.700,	-1.417
68.500,	110.800,	0.800,	-1.328
69.000,	110.100,	0.820,	-1.279
69.600,	110.000,	0.780,	-1.253
69.700,	110.900,	0.740,	-1.246
69.800,	111.800,	0.600,	-1.336
70.700,	111.400,	0.660,	-1.172
71.700,	111.450,	0.620,	-1.064
72.500,	111.900,	0.560,	-0.978
72.700,	110.900,	0.620,	-0.938
73.300,	110.200,	0.600,	-0.899
74.500,	110.900,	0.520,	-0.746
75.250,	110.400,	0.520,	-0.649
76.100,	110.050,	0.520,	-0.526
76.600,	109.100,	0.520,	-0.494
76.200,	108.100,	0.540,	-0.595
76.000,	107.150,	0.540,	-0.679
75.550,	106.200,	0.560,	-0.784
75.400,	105.100,	0.560,	-0.867
75.300,	104.150,	0.540,	-0.952
74.400,	104.250,	0.640,	-0.988
73.700,	104.700,	0.700,	-1.012
73.000,	105.300,	0.860,	-0.926
72.400,	106.300,	0.660,	-1.165
71.900,	107.100,	0.660,	-1.198
71.000,	107.900,	0.740,	-1.204
70.800,	107.000,	0.700,	-1.306
71.250,	106.300,	0.700,	-1.278

(to be continued)

Appendix 5c (continued)

UTM (N)	UTM (E)	Elevation(km)	Depth(km)
71.700,	105.300,	0.720,	-1.242
72.300,	104.400,	0.960,	-0.962
72.700,	103.500,	0.720,	-1.188
73.200,	102.750,	0.800,	-1.073
73.800,	102.100,	0.640,	-1.179
74.600,	101.400,	0.840,	-0.897
75.300,	100.800,	0.560,	-1.101
76.050,	100.500,	0.520,	-1.041
77.000,	100.200,	0.560,	-0.865
77.900,	99.850,	0.520,	-0.776
78.500,	99.100,	0.500,	-0.737
79.500,	9.050,	0.400,	-0.050
80.200,	98.500,	0.360,	-0.627
80.600,	97.750,	0.310,	-0.651
80.800,	96.800,	0.300,	-0.679

UTM (N)	UTM (E)	Elevation(km)	Depth(km)
80.000,	96.700,	0.500,	-0.617
79.700,	97.800,	0.500,	-0.608
79.000,	97.700,	0.580,	-0.649
78.200,	97.500,	0.500,	-0.872
78.100,	98.500,	0.620,	-0.715
77.400,	99.300,	0.540,	-0.867
76.600,	99.700,	0.620,	-0.895
75.700,	100.100,	0.640,	-0.995
74.800,	100.600,	0.540,	-1.206
74.000,	101.300,	0.800,	-1.028
73.300,	102.100,	0.800,	-1.088
72.700,	103.000,	0.700,	-1.229
72.100,	104.000,	0.800,	-1.165
71.600,	104.800,	0.760,	-1.235
71.200,	105.700,	0.620,	-1.388
70.700,	106.700,	0.760,	-1.270
70.200,	107.400,	0.800,	-1.262
69.700,	108.300,	0.700,	-1.386
69.100,	109.200,	0.860,	-1.259
68.700,	110.100,	0.980,	-1.151
68.100,	110.900,	0.720,	-1.446
67.600,	111.900,	0.720,	-1.463
67.300,	112.800,	0.800,	-1.384
67.300,	113.800,	0.760,	-1.392
67.800,	114.700,	0.800,	-1.266
68.700,	115.250,	0.860,	-1.073
69.300,	115.800,	0.860,	-0.968
70.100,	116.300,	0.740,	-0.948
70.700,	116.800,	0.700,	-0.871
71.300,	117.700,	0.660,	-0.770
71.400,	118.500,	0.580,	-0.791
70.750,	119.200,	0.700,	-0.740
69.750,	119.700,	0.740,	-0.833
68.900,	120.200,	0.660,	-1.019
68.250,	120.000,	0.640,	-1.144
68.300,	121.800,	0.640,	-1.051
68.800,	122.300,	0.560,	-1.030
69.200,	122.250,	0.600,	-0.930
69.250,	123.300,	0.500,	-0.967
68.400,	123.900,	0.600,	-0.971
67.500,	123.700,	0.580,	-1.138
66.700,	123.200,	0.560,	-1.296
65.670,	123.250,	0.580,	-1.409
65.100,	123.800,	0.500,	-1.537
64.450,	124.600,	0.460,	-1.622
64.100,	125.600,	0.520,	-1.565
63.750,	126.700,	0.560,	-1.524
63.500,	127.700,	0.500,	-1.576
63.200,	128.300,	0.420,	-1.668
74.500,	107.000,	0.550,	-0.922
73.800,	107.000,	0.500,	-1.083
73.100,	106.200,	0.600,	-1.129
72.500,	106.700,	0.560,	-1.232

(to be continued)

Appendix 5d (continued)

UTM (N)	UTM (E)	Elevation(km)	Depth(km)
72.000,	107.600,	0.780,	-1.042
71.400,	108.600,	0.600,	-1.260
71.000,	109.700,	0.720,	-1.146
70.700,	110.700,	0.820,	-1.043
71.500,	110.900,	0.720,	-1.020
72.300,	110.800,	0.640,	-0.985
73.000,	109.900,	0.640,	-0.921
74.000,	110.000,	0.540,	-0.856
75.000,	110.100,	0.530,	-0.696
75.800,	110.000,	0.500,	-0.599
76.400,	109.300,	0.580,	-0.457
76.000,	108.400,	0.480,	-0.672
75.300,	107.700,	0.480,	-0.825

Appendix 6a Microprobe Analyses of Smectite

	1	2	3	4	5	6
SiO2	35.06	42.40	35.95	40.19	32.94	33.77
TiO2	0.08	0.17	0.05	0.10	0.06	0.18
Al2O3	13.24	11.12	13.64	7.25	15.37	14.77
FeO*	14.10	13.91	14.61	15.18	9.01	10.42
MnO	0.39	0.24	0.39	0.10	0.21	0.55
MgO	21.17	13.59	22.58	14.37	24.15	22.57
CaO	0.61	0.89	0.59	2.20	0.22	0.29
Na2O	0.24	0.28	0.24	0.24	0.11	0.13
K2O	0.19	3.11	0.13	0.65	0.03	0.00
Total	85.08	85.71	88.18	80.30	82.10	82.68
Sample	20.14	20.14	20.14	9.14	20.12	20.12

	7	8	9	10
SiO2	33.12	34.38	40.46	39.92
TiO2	0.09	0.10	0.00	0.08
Al2O3	15.17	10.83	10.15	5.37
FeO*	20.62	14.55	4.89	0.28
MnO	0.23	0.16	0.24	0.00
MgO	19.75	18.40	20.71	0.93
CaO	0.45	1.02	1.94	2.46
Na2O	0.10	0.16	0.25	0.00
K2O	0.17	0.45	0.32	0.00
Total	89.70	80.05	82.52	78.50
Sample	9.17	9.18	Ref.	Ref.

* 1,2,3,6- brown Sm; 4,5- yellow-green Sm; 7,8- Sm in transion zone; 9- Saponite, from Deer et al. (1966); 10- Nontronite, from Deer et al., (1966).

Appendix 6b Microprobe Analyses of Celadonite (Ce)

	1	2	3	4	5	6	7
SiO2	54.30	53.85	52.80	50.87	53.04	50.82	52.55
TiO2	0.16	0.11	0.16	0.11	0.16	0.04	0.14
Al2O3	2.42	1.45	4.39	3.20	3.36	3.30	3.90
FeO*	23.47	25.48	14.96	15.21	15.21	15.99	17.20
MnO	0.00	0.06	0.00	0.11	0.10	0.05	0.00
MgO	4.29	3.87	7.67	8.75	9.37	8.84	6.34
CaO	0.21	0.43	1.53	0.59	0.65	0.33	0.21
Na2O	0.19	0.16	0.44	0.46	0.39	0.34	0.15
K2O	6.23	7.36	4.99	6.25	6.25	7.18	9.07
Total	91.27	92.77	86.94	85.55	88.53	86.89	89.56
Sample	20.07	20.07	20.15	20.11	20.09	20.11	Ref.

* 7- Celadonite, from Buckley et al. (1978).

Appendix 6c Microprobe Analyses of Carbonate (Cal)

	1	2	3	4	5	6
SiO2	0.00	0.00	0.00	0.15	0.00	0.00
TiO2	0.02	0.08	0.03	0.00	0.00	0.06
Al2O3	0.00	0.01	0.05	0.04	0.04	0.01
FeO*	0.19	0.15	0.20	0.22	0.73	0.23
MnO	0.24	0.30	1.43	2.60	13.03	6.19
MgO	0.08	0.05	0.08	0.44	0.91	0.12
CaO	54.39	59.04	57.92	57.38	39.43	54.72
Na2O	0.08	0.05	0.04	0.07	0.12	0.07
K2O	0.05	0.03	0.04	0.03	0.00	0.06
Total	55.05	59.71	59.79	60.93	54.26	61.46
Sample	21.04	11.25	20.27	20.27	20.15	12.21

* 1- Calcite in brownstone groundmass; 2- Calcite in vein in transition zone; 3-calcite in cavity in greenstone zone; 4- Calcite after plagioclase in greenstone zone; 5,6- Aragonite in cavity in brownstone zone.

Appendix 6d Microprobe Analyses of Mordenite (Mord)

	1	2	3	4	5	6	7
SiO2	76.90	70.80	71.65	68.11	65.99	63.13	64.78
TiO2	0.00	0.03	0.07	0.07	0.05	0.06	0.05
Al2O3	12.38	9.68	9.83	10.64	10.33	11.89	12.68
FeO*	0.28	0.11	0.09	0.07	0.06	0.09	0.08
MnO	0.00	0.01	0.00	0.00	0.00	0.00	0.00
MgO	0.15	0.12	0.12	0.07	0.06	0.08	0.08
CaO	3.53	3.05	3.08	1.71	1.75	1.96	1.90
Na2O	0.88	1.70	1.82	5.57	4.79	6.20	6.15
K2O	0.19	0.39	0.23	0.44	0.47	0.15	0.11
Total	94.31	85.89	86.89	86.68	83.50	83.56	85.83
Sample	20.04	11.17	11.17	21.07	21.07	21.06	21.06

	8	9	10	11	12
SiO2	62.97	65.14	66.83	66.06	70.41
TiO2	0.04	0.04	0.05	0.00	0.00
Al2O3	12.53	12.64	11.37	12.32	11.01
FeO*	0.10	0.09	0.11	0.00	0.09
MnO	0.01	0.00	0.00	0.00	0.00
MgO	0.07	0.06	0.09	0.36	0.08
CaO	1.89	2.22	2.34	3.02	2.88
Na2O	6.40	5.05	4.06	3.86	2.15
K2O	0.16	0.13	0.25	0.50	0.48
Total	84.17	85.37	85.10	86.12	87.10
Sample	21.06	21.05	Average	Ref.	Ref.

* 10- Average of 9 (1-9); 11- Mordenite, from Deer et al. (1966); 12- Mordenite (average of 6), from Gillis (1986).

Appendix 6e Microprobe Analyses of Heulandite (Heul)

	1	2	3	4	5	7	8
SiO2	60.34	58.41	61.21	58.36	67.06	62.47	64.83
TiO2	0.05	0.05	0.03	0.04	0.06	0.07	0.00
Al2O3	15.07	15.84	14.82	14.89	9.42	12.57	12.44
FeO*	0.06	0.06	0.05	0.07	0.14	0.24	2.55
MnO	0.00	0.00	0.00	0.00	0.00	0.00	0.00
MgO	0.76	0.91	1.15	0.88	0.06	0.11	0.00
CaO	2.46	2.85	3.15	2.56	3.45	5.09	5.51
Na2O	2.12	1.22	1.11	1.42	1.75	0.97	1.15
K2O	2.06	1.67	1.39	1.47	1.14	0.45	0.30
Total	82.92	81.01	82.91	79.69	83.08	81.97	83.78
Sample	21.04	21.04	21.04	21.04	11.17	11.17	Ref.

* 7- Heulandite, from Deer et al.(1966).

Appendix 6f Microprobe Analyses of Natrolite (Natro)

	1	2	3	4	5
SiO2	51.21	50.10	48.39	47.17	48.33
TiO2	0.04	0.03	0.09	0.00	0.00
Al2O3	26.90	27.92	27.04	26.84	26.61
FeO*	0.05	0.00	0.09	0.07	0.27
MnO	0.00	0.01	0.00	0.00	0.00
MgO	0.04	0.06	0.07	0.05	0.18
CaO	0.06	0.46	3.99	0.12	0.43
Na2O	12.46	11.84	7.97	15.89	6.24
K2O	0.06	0.06	0.06	0.00	1.42
Total	90.82	90.53	87.70	90.14	83.48
Sample	22.21	22.21	22.21	Ref.	Ref.

* 4- Natrolite, from Deer et al. (1966); 5- Natrolite, average of 3, from Gillis (1986).

Appendix 6g Microprobe Analyses of Laumontite (Laum)

	1	2	3	4	5	6	7	8
SiO2	52.79	52.50	53.16	53.60	50.70	54.00	53.21	53.12
TiO2	0.07	0.02	0.06	0.04	0.00	0.00	0.00	0.04
Al2O3	21.47	20.11	21.53	20.57	22.53	20.13	20.10	21.83
FeO*	0.09	0.11	0.09	0.08	0.04	0.00	0.14	0.05
MnO	0.00	0.05	0.03	0.00	0.00	0.00	0.00	0.02
MgO	0.05	0.05	0.06	0.04	0.00	0.00	0.01	0.05
CaO	10.18	8.39	10.08	8.43	11.54	10.28	7.86	9.92
Na2O	0.69	0.84	0.58	1.15	0.40	0.00	0.79	0.45
K2O	0.53	1.02	0.56	1.02	0.30	0.29	1.01	0.66
Total	85.87	83.06	86.15	84.93	85.51	84.70	83.12	86.14
Sample	9.17	9.17	9.17	9.17	Ref.	Ref.	Ref.	Ref.

* 6- Laumontite, from Deer et al. (1960); 7- Laumontite, Iceland, from Viereck et al. (1982); 8- Laumontite, average of 5, from Gillis (1986).

Appendix 6h Microprobe Analyses of Chlorite (Chl)

	1	2	3	4	5	6
SiO2	25.86	26.94	26.94	26.18	25.13	27.14
TiO2	0.08	0.07	0.08	0.02	0.06	0.09
Al2O3	18.05	17.11	18.61	18.20	18.99	18.17
FeO*	25.14	24.29	25.27	18.89	21.83	22.17
MnO	0.48	1.37	0.15	0.64	0.11	0.59
MgO	15.00	14.10	13.30	20.50	18.45	18.98
CaO	0.09	0.05	0.07	0.07	0.20	0.18
Na2O	0.07	0.12	0.07	0.09	0.00	0.06
K2O	0.06	0.00	0.00	0.00	0.00	0.06
Total	84.83	84.05	84.49	84.59	84.79	87.49
Sample	20.27	20.16	20.32	20.26	20.38	11.46

	7	8	9	10	11	12
SiO2	28.57	26.87	25.41	30.09	30.44	28.66
TiO2	0.13	0.12	0.14	0.15	0.11	0.12
Al2O3	17.83	17.62	19.33	16.16	13.30	15.53
FeO*	22.77	26.18	25.63	23.92	25.08	27.36
MnO	0.61	0.44	0.37	0.38	0.30	0.28
MgO	19.85	14.78	15.41	14.78	16.78	14.97
CaO	0.13	0.85	0.12	2.55	0.37	0.19
Na2O	0.07	0.16	0.08	0.17	0.16	0.11
K2O	0.05	0.07	0.07	0.04	0.19	0.10
Total	90.01	87.09	86.56	88.24	86.71	87.32
Sample	11.46	22.14	21.16	21.16	9.18	9.18

* 1-10 Chlorite in greenstone zone; 11-12 chlorite in transition zone.

Appendix 6i Microprobe Analyses of Amphibole (Am)

	1	2	3	4	5	6
SiO2	55.51	54.06	51.15	47.68	49.35	50.71
TiO2	0.14	0.24	0.45	0.39	0.59	0.30
Al2O3	9.29	4.65	4.80	3.74	3.79	2.96
FeO*	9.95	11.99	18.99	15.47	20.15	17.66
MnO	0.26	0.46	0.43	0.35	0.38	0.50
MgO	11.03	13.12	11.24	10.49	12.05	12.28
CaO	8.93	10.81	8.11	8.18	10.13	10.87
Na2O	3.33	0.38	0.76	0.69	0.93	0.47
K2O	0.02	0.00	0.01	0.00	0.06	0.10
Total	98.46	95.71	95.94	86.99	97.43	95.85
Sample	20.29	20.29	20.32	20.32	20.30	21.16

	7	8
SiO2	47.29	50.82
TiO2	0.38	0.36
Al2O3	6.53	5.11
FeO*	18.66	16.12
MnO	0.47	0.41
MgO	12.27	11.78
CaO	10.52	9.65
Na2O	0.53	1.01
K2O	0.13	0.05
Total	96.78	95.56
Sample	21.16	Ave.

* 8- Average of 7 (1-7).

Appendix 7 Depth of Seven Cross Sections in the Central Part of the Study Area

Station no.	Elevation(km)	UTM (E)	UTM (N)	Depth(km)
9.01,	0.48,	109.40,	77.40,	-0.39
9.02,	0.46,	109.80,	77.40,	-0.39
9.03,	0.45,	109.90,	77.70,	-0.34
9.04,	0.47,	109.80,	77.80,	-0.31
9.05,	0.48,	109.80,	78.00,	-0.27
9.06,	0.52,	109.10,	76.60,	-0.49
9.07,	0.52,	109.00,	77.00,	-0.43
9.08,	0.51,	109.30,	76.70,	-0.48
9.09,	0.47,	109.70,	77.30,	-0.40
9.10,	0.46,	109.60,	77.20,	-0.43
9.11,	0.46,	109.60,	77.10,	-0.45
9.12,	0.46,	109.70,	77.00,	-0.46
9.13,	0.48,	109.60,	76.90,	-0.46
9.14,	0.49,	109.60,	76.70,	-0.48
9.15,	0.50,	109.60,	76.60,	-0.49
10.01,	0.72,	110.80,	65.60,	-1.64
10.02,	0.64,	111.30,	66.90,	-1.62
10.03,	0.62,	111.50,	67.70,	-1.57
10.04,	0.64,	111.40,	67.80,	-1.54
10.05,	0.62,	111.50,	68.10,	-1.53
10.07,	0.62,	111.60,	68.30,	-1.50
10.08,	0.62,	111.60,	68.40,	-1.49
10.09,	0.62,	111.60,	68.60,	-1.47
10.10,	0.61,	111.60,	68.80,	-1.46
10.12,	0.61,	111.60,	68.90,	-1.44
10.13,	0.57,	111.80,	69.10,	-1.45
10.14,	0.58,	111.90,	69.10,	-1.44
10.15,	0.58,	111.80,	69.40,	-1.41
10.16,	0.57,	111.80,	70.00,	-1.34
10.17,	0.58,	111.80,	70.20,	-1.31
10.18,	0.57,	111.80,	70.70,	-1.24
10.19,	0.57,	111.80,	70.80,	-1.23
10.20,	0.58,	111.90,	71.00,	-1.19
10.21,	0.55,	111.80,	71.70,	-1.12
10.22,	0.54,	111.80,	71.90,	-1.10
10.23,	0.50,	112.30,	72.80,	-0.97
10.24,	0.48,	112.80,	73.10,	-0.92
10.25,	0.48,	113.00,	73.30,	-0.87
10.26,	0.50,	113.10,	73.80,	-0.76
10.27,	0.47,	113.50,	74.30,	-0.69
10.28,	0.47,	113.80,	74.70,	-0.61
10.29,	0.46,	114.10,	75.00,	-0.56
10.30,	0.44,	114.30,	75.30,	-0.51
10.31,	0.44,	114.40,	75.60,	-0.46
10.32,	0.45,	114.60,	75.80,	-0.41
10.33,	0.44,	114.70,	76.00,	-0.38
10.34,	0.43,	114.80,	76.30,	-0.33
10.35,	0.43,	115.00,	76.50,	-0.29

Station no.	Elevation(km)	UTM (E)	UTM (N)	Depth(km)
10.36,	0.42,	115.20,	76.70,	-0.26
10.37,	0.42,	115.30,	77.00,	-0.21
10.38,	0.41,	115.50,	77.20,	-0.18
10.39,	0.41,	115.70,	77.40,	-0.14
10.40,	0.40,	115.80,	77.70,	-0.10
10.41,	0.36,	116.30,	78.20,	-0.04
10.42,	0.40,	115.80,	76.90,	-0.22
10.43,	0.40,	115.40,	76.50,	-0.30
10.44,	0.44,	114.60,	76.20,	-0.35
10.45,	0.46,	114.20,	75.40,	-0.48
10.46,	0.45,	114.10,	74.60,	-0.63
10.47,	0.47,	113.40,	74.20,	-0.71
10.48,	0.52,	112.30,	72.60,	-0.98
10.49,	0.52,	111.90,	72.10,	-1.08
10.50,	0.59,	111.90,	71.10,	-1.16
10.51,	0.58,	111.70,	70.30,	-1.29
10.52,	0.59,	111.70,	69.00,	-1.45
10.53,	0.63,	111.50,	68.20,	-1.51
10.54,	0.63,	111.50,	67.60,	-1.57
10.55,	0.65,	111.40,	67.20,	-1.59
10.56,	0.52,	112.00,	72.40,	-1.03
10.57,	0.50,	112.50,	73.00,	-0.93
10.58,	0.51,	113.00,	73.50,	-0.81
10.59,	0.46,	113.70,	74.50,	-0.66
10.60,	0.50,	113.15,	74.00,	-0.73
10.61,	0.70,	111.10,	66.00,	-1.63
11.01,	0.42,	120.00,	76.10,	-0.11
11.02,	0.40,	120.00,	75.80,	-0.18
11.03,	0.42,	119.90,	75.30,	-0.24
11.04,	0.42,	119.60,	74.80,	-0.33
11.05,	0.44,	119.70,	74.50,	-0.36
11.06,	0.44,	119.60,	74.20,	-0.41
11.07,	0.51,	119.60,	73.40,	-0.47
11.18,	0.56,	118.60,	71.70,	-0.76
11.19,	0.57,	118.60,	71.90,	-0.72
11.20,	0.57,	118.70,	72.10,	-0.68
11.21,	0.56,	118.70,	72.10,	-0.69
11.22,	0.55,	118.80,	72.10,	-0.69
11.23,	0.55,	118.90,	72.10,	-0.69
11.24,	0.54,	118.90,	72.20,	-0.68
11.25,	0.54,	118.90,	72.30,	-0.66
11.26,	0.54,	119.10,	72.50,	-0.62
11.27,	0.52,	119.20,	72.50,	-0.63
11.28,	0.51,	119.30,	72.60,	-0.62
11.29,	0.51,	119.30,	72.70,	-0.60
11.30,	0.53,	119.40,	72.90,	-0.54
11.31,	0.55,	119.50,	73.10,	-0.49
11.32,	0.50,	119.60,	73.30,	-0.50
11.33,	0.43,	119.80,	74.70,	-0.33
11.34,	0.42,	119.90,	75.20,	-0.26

Station no.	Elevation(km)	UTM (E)	UTM (N)	Depth(km)
11.35,	0.41,	119.90,	75.40,	-0.23
11.50,	0.56,	119.00,	72.30,	-0.64
11.51,	0.56,	118.50,	71.60,	-0.78
11.52,	0.56,	118.60,	71.80,	-0.74
11.53,	0.57,	118.80,	72.00,	-0.69
12.01,	0.46,	124.30,	74.20,	-0.15
12.02,	0.46,	124.20,	74.10,	-0.17
12.03,	0.45,	124.30,	74.10,	-0.17
12.04,	0.44,	124.30,	73.90,	-0.22
12.05,	0.43,	124.30,	73.90,	-0.23
12.06,	0.45,	124.30,	73.80,	-0.22
12.07,	0.46,	124.30,	73.70,	-0.23
12.08,	0.44,	124.30,	73.60,	-0.26
12.09,	0.42,	124.30,	73.50,	-0.30
12.10,	0.42,	124.40,	73.40,	-0.31
12.11,	0.44,	124.40,	73.30,	-0.30
12.12,	0.44,	124.40,	73.20,	-0.32
12.13,	0.43,	124.40,	73.20,	-0.33
12.14,	0.44,	124.40,	73.10,	-0.34
12.15,	0.46,	124.30,	73.00,	-0.34
12.16,	0.46,	124.40,	72.90,	-0.35
12.17,	0.47,	124.40,	72.80,	-0.35
12.18,	0.45,	124.50,	72.70,	-0.39
12.19,	0.47,	124.40,	72.60,	-0.39
12.20,	0.45,	124.50,	72.50,	-0.42
12.21,	0.45,	124.50,	72.40,	-0.43
12.22,	0.46,	124.50,	72.30,	-0.44
12.23,	0.47,	124.50,	72.20,	-0.45
12.24,	0.47,	124.50,	72.00,	-0.48
12.25,	0.47,	124.50,	71.90,	-0.50
12.26,	0.49,	124.40,	71.80,	-0.50
12.27,	0.49,	124.50,	71.70,	-0.51
12.28,	0.50,	124.50,	71.60,	-0.52
12.29,	0.49,	124.60,	71.60,	-0.52
12.30,	0.48,	124.60,	71.50,	-0.55
12.31,	0.48,	124.60,	71.40,	-0.56
12.32,	0.46,	124.70,	71.30,	-0.60
12.33,	0.48,	124.70,	71.20,	-0.59
12.34,	0.48,	124.70,	71.00,	-0.63
12.35,	0.48,	124.70,	70.90,	-0.64
12.36,	0.50,	124.70,	70.80,	-0.64
12.37,	0.50,	124.50,	70.80,	-0.65
12.38,	0.51,	124.50,	70.70,	-0.66
12.39,	0.52,	124.50,	70.60,	-0.66
12.40,	0.50,	124.40,	70.50,	-0.70
12.41,	0.48,	124.40,	70.40,	-0.74
12.42,	0.49,	124.30,	70.30,	-0.75
12.43,	0.48,	124.30,	70.10,	-0.80
12.44,	0.48,	124.30,	70.20,	-0.78
12.45,	0.48,	124.50,	70.30,	-0.75

Station no.	Elevation(km)	UTM (E)	UTM (N)	Depth(km)
12.46,	0.46,	124.60,	70.20,	-0.78
12.60,	0.48,	124.20,	70.00,	-0.82
12.61,	0.49,	124.00,	69.80,	-0.85
12.62,	0.51,	123.40,	69.60,	-0.90
12.63,	0.56,	123.00,	68.20,	-1.09
12.64,	0.54,	122.50,	68.00,	-1.16
12.65,	0.54,	121.80,	67.60,	-1.25
12.66,	0.60,	121.30,	67.50,	-1.23
12.67,	0.63,	120.70,	67.00,	-1.29
12.68,	0.54,	123.20,	68.40,	-1.07
12.69,	0.50,	123.20,	68.70,	-1.06
12.70,	0.52,	123.10,	69.00,	-1.00
12.71,	0.52,	123.20,	69.30,	-0.94
12.72,	0.50,	123.20,	69.40,	-0.95
12.73,	0.55,	122.10,	67.70,	-1.22
12.74,	0.64,	120.80,	67.30,	-1.24
12.75,	0.68,	120.50,	66.70,	-1.29
12.76,	0.65,	120.30,	66.60,	-1.34
12.77,	0.75,	120.00,	66.50,	-1.27
12.78,	0.72,	119.90,	66.40,	-1.31
12.79,	0.75,	119.80,	66.10,	-1.32
20.01,	0.50,	122.40,	71.40,	-0.66
20.02,	0.52,	122.30,	71.30,	-0.66
20.03,	0.59,	121.20,	68.70,	-1.07
20.04,	0.57,	121.30,	69.50,	-0.96
20.05,	0.56,	121.70,	69.90,	-0.89
20.06,	0.54,	122.00,	70.60,	-0.78
20.07,	0.70,	119.70,	68.30,	-1.09
20.08,	0.64,	120.90,	68.30,	-1.09
20.09,	0.58,	121.30,	68.90,	-1.04
20.10,	0.58,	121.40,	69.30,	-0.98
20.11,	0.56,	121.40,	69.70,	-0.93
20.12,	0.55,	121.80,	70.20,	-0.84
20.13,	0.54,	122.10,	70.80,	-0.74
20.30,	0.46,	121.20,	72.70,	-0.55
20.31,	0.49,	121.10,	72.50,	-0.56
20.32,	0.50,	121.00,	72.40,	-0.57
20.33,	0.50,	120.80,	72.40,	-0.58
20.34,	0.41,	122.50,	74.20,	-0.29
20.35,	0.42,	122.40,	74.20,	-0.28
20.36,	0.44,	122.30,	74.00,	-0.30
20.37,	0.46,	122.10,	73.70,	-0.34
20.38,	0.46,	122.00,	73.60,	-0.36
20.39,	0.44,	121.60,	73.30,	-0.45
20.40,	0.44,	121.30,	73.20,	-0.48
20.41,	0.44,	121.30,	73.00,	-0.52
20.60,	0.50,	122.50,	71.50,	-0.64
20.61,	0.50,	122.50,	71.60,	-0.62
20.62,	0.48,	122.60,	71.80,	-0.61
20.63,	0.47,	122.70,	72.00,	-0.58

Station no.	Elevation(km)	UTM (E)	UTM (N)	Depth(km)
20.64,	0.44,	122.70,	72.60,	-0.51
20.65,	0.45,	122.70,	72.70,	-0.48
20.66,	0.45,	122.60,	72.70,	-0.49
20.67,	0.44,	122.70,	72.70,	-0.49
20.68,	0.44,	122.60,	72.80,	-0.48
20.69,	0.42,	122.60,	72.90,	-0.48
20.70,	0.42,	122.60,	73.00,	-0.47
20.71,	0.43,	122.60,	73.10,	-0.44
20.72,	0.43,	122.60,	73.20,	-0.42
20.73,	0.43,	122.50,	73.30,	-0.41
20.74,	0.45,	122.50,	73.50,	-0.36
20.75,	0.42,	122.60,	73.70,	-0.35
21.01,	0.36,	117.90,	78.00,	-0.00
21.02,	0.37,	117.80,	77.90,	-0.01
21.03,	0.36,	117.70,	77.70,	-0.05
21.04,	0.38,	117.60,	77.50,	-0.06
21.05,	0.38,	117.60,	77.40,	-0.08
21.06,	0.39,	117.60,	77.30,	-0.08
21.07,	0.39,	117.60,	77.30,	-0.08
21.08,	0.39,	117.60,	77.20,	-0.10
21.09,	0.40,	117.60,	77.10,	-0.10
21.10,	0.40,	117.50,	77.00,	-0.12
21.11,	0.41,	117.30,	76.70,	-0.16
21.12,	0.41,	117.30,	76.60,	-0.18
21.13,	0.42,	117.30,	76.60,	-0.17
21.14,	0.42,	117.30,	76.50,	-0.18
21.15,	0.42,	117.30,	76.40,	-0.20
21.16,	0.42,	117.30,	76.30,	-0.22
21.17,	0.42,	117.20,	76.30,	-0.22
21.18,	0.43,	117.30,	76.20,	-0.22
21.19,	0.43,	117.20,	76.20,	-0.23
21.20,	0.44,	117.20,	76.00,	-0.25
21.21,	0.44,	117.20,	75.80,	-0.28
21.23,	0.44,	117.30,	75.60,	-0.30
21.24,	0.44,	117.30,	75.50,	-0.32
21.25,	0.45,	117.30,	75.30,	-0.34
21.26,	0.66,	113.70,	68.00,	-1.42
21.27,	0.66,	113.70,	68.30,	-1.39
21.28,	0.66,	113.80,	68.40,	-1.37
21.29,	0.65,	113.70,	68.60,	-1.36
21.30,	0.65,	113.60,	68.70,	-1.35
21.31,	0.64,	113.60,	68.80,	-1.35
21.32,	0.62,	113.80,	69.40,	-1.28
21.33,	0.62,	113.70,	69.80,	-1.23
21.34,	0.40,	113.90,	70.20,	-1.39
21.36,	0.54,	114.00,	70.70,	-1.17
21.39,	0.56,	114.50,	71.50,	-1.01
21.40,	0.56,	114.50,	72.00,	-0.92
21.41,	0.55,	114.70,	72.80,	-0.79
21.42,	0.52,	115.00,	73.30,	-0.73

Station no.	Elevation(km)	UTM (E)	UTM (N)	Depth(km)
22.01,	0.47,	111.40,	76.00,	-0.52
22.02,	0.45,	111.30,	75.80,	-0.58
22.03,	0.48,	111.00,	75.10,	-0.68
22.04,	0.50,	111.20,	74.70,	-0.72
22.05,	0.45,	111.20,	75.60,	-0.62
22.06,	0.46,	111.00,	75.70,	-0.61
22.07,	0.45,	110.90,	76.20,	-0.54
22.08,	0.43,	111.10,	76.30,	-0.53
22.09,	0.42,	110.90,	77.00,	-0.43
22.10,	0.44,	110.60,	77.20,	-0.40
22.11,	0.60,	111.10,	72.60,	-0.96
22.12,	0.58,	111.40,	70.10,	-1.33
22.13,	0.64,	111.80,	70.00,	-1.27
22.14,	0.60,	110.80,	73.00,	-0.92
22.15,	0.54,	110.70,	73.90,	-0.84
22.16,	0.56,	111.40,	72.80,	-0.96
22.17,	0.42,	112.80,	77.50,	-0.26
22.18,	0.42,	112.70,	77.70,	-0.23
22.19,	0.42,	112.30,	78.00,	-0.20
22.20,	0.52,	112.40,	78.40,	-0.04

REFERENCES

Adamides, N. G., 1980, The form and environment of the Kalavasos ore deposits, Cyprus. In: Panayiotou, A. (ed.), Ophiolite, Proceedings, International Ophiolite Symposium, Cyprus 1979, Ministry of Agriculture and Natural Resources, Geological Survey Department, p. 117-127.

Adamides, N. G., 1987, Diverse modes of occurrence of Cyprus Sulfide Deposits and comparison with recent analogues. In: P. T. Robinson, I. L. Gibson, and A. Panayiotou (ed.), Cyprus Crustal Study Project: Initial Report, Holes CY-2 and 2a. Geological Survey of Canada, p. 153-168.

Allerton, S., and Vine, F. J., 1987, Spreading structure of the Troodos ophiolite, Cyprus: Some palaeomagmnetic constrains. Geology, 15, 593-597.

Alt, J. C., and Honnorez, J., 1984, Alteration of the upper oceanic crust, DSDP site 417: minealogy and chemistry. Contributions to Mineralogy and Petrology, 87, 149-169.

Alt, J. C., Laverne, C., and Muehlenbachs, 1985, Alteration of the upper oceanic crust: mineralogy and processes in Deep Sea Drilling Project Hole 504B, Leg 83. Initial Reports of DSDP, 83: Washington (U.S. Government Printing Office), p. 217-248.

Alt, J. C., Honnorez, J., Laverne, C., and Emmermaun, R., 1986, Hydrothermal alteration of a 1 km section through the upper oceanic crust, Deep Sea Drilling Project Hole 504B: Mineralogy, chemistry and evolution of seawater-basalt interactions. Journal of Geophysical Research, v.91. 10309-10335.

Alt J. C., Anderson, T. F., Bonnell, L., and Muehlenbechs, K., 1989, Mineralogy, chemistry, and stable isotopic compositions of hydrothermally altered sheeted dikes: ODP Hole 504, leg 111. In Becker, K., Sakai, H., et al., Proceedings of the Ocean Drilling Program, Scientific Results, 111: College Station, TX (Ocean Drilling Program), 27-40.

Arai, S., and Fujii, T., 1979, Petrology of ultramafic rocks from Site 395. Initial Reports of the Deep Sea Drilling Project, v. 45: Washington (U.S. Government Printing Office), p. 587-594.

Arcyana, 1975, Transform fault and rift valley from bathyscaph and diving saucer. Science, 190, 108-116.

Argo-Rise Droup, 1988, Geological mapping of the East Pacific Rise axis (10°19' - 11°53'N) using the Argo and Angus imaging systems. Canadian Mineralogist, 26, 467-486.

Auclair, F., and Ludden, J. N., 1987, Cyclic geochemical variation in the Troodos Pillow Lavas: evidence from the CY-2a Drill Hole. In: P. T. Robinson, I. L. Gibson, and A. Panayiotou (ed.), Cyprus Crustal Study Project: Initial Report, Holes CY-2 and 2a. Geological Survey of Canada, p 221-235.

Aumento, F., and Loubat, H., 1971, The mid-Atlantic Ridge near 45°N. XVI. Serpentinized ultramafic intrusions. Canadian Journal of Earth Science, 8, 631-663.

Auzende, J. M., Eissen, J. P., Lafoy, Y., Gente, P., and Charlou, J. L., 1988, Sea-floor spreading in the North Fiji Basin (SW Pacific). In: Tectonophysics, special issue 146, Wezel, F. C.(ed.), p. 317-351.

Auzende, J.-M, et al., 1989, Direct observation of a section through slow-spreading oceanic crust. Nature, 373, 726-729.

Auzende, J.-M. et al., 1990, Active spreading and hydrothermalism in North Fiji Basin (SW Pacific): Results of Japanese French Cruise Kaiyo 87. Marine Geophysical Researches, 12, 269-283.

Bagnall, P. S., 1960, The Geology and Mineral Resources of the Pano Lefkara-Larnaca Area. Geological Survey Department Cyprus, Memoir 5, 116 pp.

Bailey, D. G., 1984, Stratigraphy and geochemistry of the Troodos ophiolite extrusive sequence in the Margi area, Cyprus. Unpublished M.Sc thesis, Dalhousie University, Halifax, Nova Scotia, Canada, 215 pp.

Ballard, R. D., Bryan, W. B., Heirtzler, J. R., Keller, G. R., Moore, J. G., and van Andel, Tj. H., 1975, Manned submersible observations in the Famous area. Science, 190, 103-108.

Ballard, R. D., and Moore, J. G., 1977, Photographic Altas of the Mid-Atlantic Ridge. Springer, New York, 114 pp.

Ballard, R. D., Holcomb, R. T., and Van Andel, T. H., 1979, The Galapagos Rift at 86° W, 3, sheet flows, collapse pits, and lava lakes of the rift. Journal Geophysical Research, 84, 5407-5422.

Ballard, R. D., Francheteau, J., Juteau, T., Rangan, C. and Normark, W., 1981, East Pacific Rise at 21° N: The volcanic, tectonic, and hydrothermal processes of the central axis. Earth and Planetary Science Letters, 55, 1-10.

Ballard, R. D., van Andel, Tj. H., and Holcomb, R. J., 1982, The Galapagos Rift at 86 W: 5. Variation in volcanism,

structure, and hydrothermal activity along a 30 km segment of the rift valley. Journal Geophysical Research, 87, 1149-1161.

Ballard, R. D., and Francheteau, J., 1983, Geologic processes of the Mid-Ocean Ridge and their relation to sulphide deposition. In: Rona, P. A., Bostrom, K., Laubier, L., and Smith, K. L., ed., Hydrothermal Processes at Seafloor Spreading Centres, Series IV: Marine Sciences, NATO CONFERENCE SERIES, Plenum Press, New York and London, p. 17-25.

Baragar, W. R. A., Lambert, M. B., Baglow, N., and Gibson, I. L., 1989, Sheeted Dikes from CY-4 and surface sections: Troodos ophiolite.In: Cyprus Crustal Study Project: Initial Report, Hole CY-4, (eds.) I. L. Gibson, J. Malpas, P. T. Robinson and C. Xenophontos, Geologial Survey of Canada, Paper 88-9. p. 69-106.

Baragar, W. R. A., Lambert, M. B., Baglow, N., and Gobson, I. L., 1990, The sheeted dike zone in the Troodos ophiolite. In: Ophiolites, Oceanic Crustal Analogues, Proceedings of the Symposium "Troodos 1987", eds. by J. Malpas, E. Moores, A. Panayiotou, C. Xenophontos, Cyprus, p. 37-52.

Basaltic Volcanic Study Project, 1981, Basaltic Volcanism on the Terrestrial Planets. Pergamon Press, Inc., New York. p. 132-160.

Bates, R. L., and Jackson, J. A., 1987, Glossary of Geology, Third Edition. American Geological Institute, Alexandria, Virginia, 788 pp.

Bear, L. M., 1960, The geology and mineral resources of the Akaki-Lythrodonda area. Cyprus Geological Survey Department Memoir, 3, 122 pp.

Bear, L. M., 1963, The Mineral Resources and Mining Industry of Cyprus. Geological Survey Department, Cyprus, Bulletin No.1, 208 pp.

Becker, K., Sakai, H., Adamson, A. C., Alexandrovich, L., Alt, J. C., Anderson, R. N., Bideau, D., Gable, R., Herzig, P. M., Houghton, S., Ishizuka, H., Kawahata, H., Kinoshita, H., Langseth, M. G., Lovell, M. A., Malpas, J., Masuda, H., Merrill, R. B., Morin, R. H., Mottl, M. J., Pariso, J. E., Pezard, P., Phillips, J., Sparks, J., and Uhlig, S., 1989, Drilling deep into young oceanic crust, Hole 504B, Costa Rica Rift. Reviews of Geophysics, 27, 79-102.

Bednarz, U., Sunkel, G., and Schmincke, H.-U., 1987, The basaltic andesite-andesite and the andesite-dacite series from the ICRDG Drill Holes CY-2 and CY-2a. I. Lithology, petrology and geochemistry. In: P. T. Robinson, I. L. Gibson, and A.

Panayiotou (ed.), Cyprus Crustal Study Project: Initial Report, Holes CY-2 and 2a. Geological Survey of Canada, p. 183-204.

Bellaiche, G., Cheminee, J. L., Francheteau, J., Hekinian, R., LePichon, X., Needham, H. D., and Ballard, R. D., 1974, Rift valley's inner floor: First submersible study. Nature, 250, 558-560.

Benn, K., and Laurent, R., 1987, Intrusive suite documented in the Troodos ophiolite plutonic complex, Cyprus. Geology, 15, 821-824.

Bolton, B. R., Both, R., Exon, N.F., Hamilton, T. F., Ostwald, J., and Smith, J. D., 1988, Geochemistry and mineralogy of seafloor hydrothermal and hydrogenetic Mn oxide deposits from the manus Basin and Bismarck Archipelago Region of the southernwest Pacific Ocean, Marine Geology, 85, 65-87.

Bonatti, E., and Harrison, C. G. A., 1988, Eruption styles of basalt in oceanic spreading ridges and seamounts: effect of magma temperature and viscosity. Journal of Geophysical Research, 93, 2967-2980.

Boulter, C.A., 1989, Four Dimensional Analysis of Geological Maps, Techniques of Interpretation. Hohn Wiley & Sons, Chichester. P. 12-40.

Boyle, J. F., and Robertson, A. H. F., 1984, Evolving metallogenesis at the Troodos spreading axis. In: I. G. Gass, S. J. Lippard and A. W. Shelton (ed.), Ophiolites and Oceanic Lithosphere, Geological Society Special Publications, p. 169-181.

Bryan, W. B., and Grove, T. L., 1986, Contrasting Atlantic and Pacific MORB modal phenocryst assemblages (abstract), Eos Trans. AUG. 67, 1225.

Burnett, M. S., Caress, D. W., and Orcutt, J. A., 1989, Tomographic image of the magma chamber at 12°50'N on the East Pacific Rise. Nature, 339, 206-208.

Byers, C. D., Garcia, M. O., and Muenow, D. W., 1986, Volatiles in basaltic glasses from the East Pacific Rise at 21°N: implications for MORB sources and submarine lava flow morphology. Earth and Planetary Science Letters, 79, 9-20.

Cameron, W. E., 1985, Petrology and origin of primitive lavas from the Troodos ophiolite, Cyprus. Contribution to Mineralogy and Petrology, 89, 239-255.

Cameron, W. E., Nisbet, E. G., and Dietrich, V. J., 1979,

Boninites, komatiites and ophiolitic basalts. Nature, 280, 550-553.

Cameron, W. E., McCulloch, M. T., and Walker, D. A., 1983, Boninite petrogenesis: chemical and Nd-Sr isotopic constraints. Earth and Planetary Sciences Letters, 65, 75-89.

Campsie, J., Johnson, G. L., Rasmusssen, M. H., and Laursen, J., 1984, Dredged basalts from the western Nazca plate and the evolution of the East Pacific Rise. Earth and Planetary Sciences Letters, 68, 271-285.

Cann, J. R., 1979, Metamorphism in the ocean crust. In: Deep Drilling Results in the Atlantic ocean: Ocean Crust, (eds.) M. Talwani, C. G. Harrison, and D. E. Hayes, American Geophysical Union, Washington, D. C., p. 230-238.

Cann, J. R., Strens, M. R., and Rice, A., 1985, A simple magma-driven thermal balance model for the formation of volcanogenic massive sulfides. Earth and Planetary Science Letters, 76, 123-134.

Cann, J. R., Oakley, P. J., Richards, H. G., and Richardson, C. J., 1987, Geochemistry of hydrothermally altered rocks from Cyprus Drill Holes CY-2 and CY-2a, Troodos Ophiolite, Cyprus. In: P. T. Robinson, I. L. Gibson and A. Panayiotou (ed.), Cyprus Crustal Study Project: Initial Report, Holes CY-2 and 2a, Geological Survey of Canada, Paper 95-29, p 87-102.

Carr, J. M., and Bear, L. M., 1960, The Geology and Mineral Resources of the Peristerona-Lagoudhera Area. Geological Survey Department Cyprus, Memoir 2, 79 pp.

Christie, D., and Sinton, 1981, Evolution of abyssal lavas along propagating segments of the Galapagos spreading centre. Earth and Planetary of Science Letters, 56, 321-335.

Coch, N. K., and Ludman, A., 1991, Physical Geology. Macmillan Publishing Company, USA, p. 430-432.

Cocker, J. D., Griffin, B. J., and Muejlenbachs, K., 1982, Oxygen and carbon isotope evidence for seawater-hydrothermal alteration of the Macquarie Island ophiolite. Earth and Planetary Science Letters, 61, 112-122.

Coleman, R. G., 1977, Ophiolites. Springer-Verlag. p. 108-114.

Collier, J., and Sinha, M., 1990, Seismic images of a magma chamber beneath the Lau Basin back-arc spreading centre. Nature, 346, 646-648.

Constantinou, G., 1976, Genesis of the conglomerate structure,

porosity and collomorphic textures of the massive sulfide ores of Cyprus. Geological Association of Canada, Special Paper 14, 188-209.

Constantinou, G., 1977, Hydrothermal alteration of the basaltic lavas of the Troodos ophiolite complex associated with the formation of the massive sulfide deposits. Geological Society of London Special Publications, no 7, 77.

Constantinou, G., 1980, Metallogenesis associated with the Troodos ophiolite. In: Panayiotou, A. (ed.), Ophiolite, Proceedings, International Ophiolite Symposium, Cyprus 1979, Ministry of Agriculture and Natural Resources, Geological Survey Department, p. 663-674.

Crane, k. and Ballard, R. D., 1981, Volcanics and structure of the FAMOUS Narrowgate rift: Evidence for cyclic evolution: AMAR 1. Journal Geophysical Research, 86, 5112-5124.

Crane, K., Aikman, F., Embley, R. W., Hammond, S., Malahoff, A., and Lupton, J., 1985, The distribution of geothermal fields on the Juan de Fuca Ridge. Journal of Grophysical Research, 90, 727-744.

Deer, W. A., Howie, R. A., and Zussman, J., 1966, An Introduction to the Rock Forming Minerals. Longman Group Ltd., London, 528 pp.

Delaney, H. R., Mogk, D. W , and Mottle, M. J., 1987, Quartz-cemented breccias from the Mid-Atlantic Ridge: samples of a high salinity hydrothermal upflow zone, Journal of Geophysical Research, 92, 9175-9192.

Desmons, J., Delaloye, M., Desmet, A., Gagny, C., Rocci, G., and Voldet, P., 1980, Trace and rare earth element abundances in Troodos lavas and sheeted dikes, Cyprus. Ofioliti, 5, 35-56.

Detrick, R. S., Buhl, P., Vera, E., Mutter, J., Orcutt, J., Madsen, J., and Brocher, T., 1987, Multi-channel seismic imaging of a crustal magma chamber along the East Pacific Rise. Nature, 326, 35-41.

Detrick, R. S., Mutter, J., Buhl, P., and Kim, I. I., 1990, No evidence from multichannel reflection data for a crustal magma chamber in the MARK area on the Mid-Atlantic Ridge. Nature, 347, 61-64.

Dilek, Y., Thy, P., Moores, E. M., and Ramsden, T. W., 1990, Tectonic evolution of the Troodos ophiolite within the Tethyan framework. Tectonics, 9, 811-823.

Douma, L., and Robinson, P. T., 1984, Cyprus Crustal Study Project, Hole CY-1, edited core descriptions. Unpublished report, Dalhousie University, Halifax, 1000 pp.

Embley, R. W., Jonasson, I. R., Perfit, M. R., Franklin, J. M., Tivey, M. A., Malahoff, A., Smith, M. F., and Francis,,T. J. G., 1988, Submersible investigation of an extinct hydrothermal system on the Galapagos Ridge: sulfide mounds, stockwork zone and differential lavas. Canadian Mineralogist, 26, 517-539.

Emmermann, R., 1985, Basement geochemistry, Hole 504B. In: Anderson, R. N., Honnorez, J., Becker, K., et al., Init. Repts. DSDP, 83: Washington (U.S. Govt. Printing Office), p. 183-200.

Elthon, D., and Stern, C., 1978, Metamorphic petrology of the Sarmiento ophiolite complex, Chile. Geology, 6, 464-468.

Flower, M. F. J., and Levine, H. M., 1987, Petrogenesis of a tholeiite-boninite sequence from Ayios Mamas, Troodos ophiolite: evidence for splitting of a volcanic arc? Contribution to Mineralogy and Petrology, 97, 509-524.

Fouquet, Y., Von Stackelberg, U., Charlou, J. L., Donval, J. P., Erzinger, J., Foucher, J. P., Herzig., P., Muhe, R., Soakai, S., Wiedicke, M., and Whitechurch, H., 1991, Hydrothermal activity and metallogenesis in the Lau back-arc basin. Nature, 349, 778-781.

Francheteau, J., Needham, H. D., Choukroune, P., Juteau, T., Seguret, M., Ballard, R. D., Fox, P. J., Normark, W., Carranza, A., Cordoba, D., Guerrero, J., Rangin, C., Bougault, H., Comcon, P., and Hekinnian, R., 1979, Massive deep-sea sulfide ore deposits discovered on the East Pacific Rise. Nature, 277, 523-528.

Francheteau, J., and Ballard, R. D., 1983, The East Pacific Rise near 21° N, 13° N and 20° S: Inferences for along-strike variability of axial processes of the Mid-Ocean Ridge. Earth and Planetary Science Letters, 64, 93-114.

Gass, I. G., 1960, The geology and mineral resources of the Dhali area. Cyprus Geological Survey Department, Memoir 4, 116 pp.

Gass, I. G., 1980, The Troodos Massif: Its role in the unravelling of the understanding of constructive plate margin processes. In: Panayiotou, A. (ed.), Ophiolite, Proceedings, International Ophiolite Symposium, Cyprus 1979, Ministry of Agriculture and Natural Resources, Geological Survey Department, p. 23-35.

Gass, I. G., and Smewing, J. D., 1973, Intrusion, extrusion and metamorphism at constructive margins: evidence from the Troodos massif, Cyprus. Nature, 242, 26-29.

Geological Survey Department of Cyprus, 1960, Geological Map of the Periserona-Lagoudhera Area. Geological Survey Department, Government of Cyprus.

Geological Survey Department of Cyprus, 1979, Geological Map of Cyprus (1:250,000). Geological Survey Department, Government of Cyprus.

Gillis, K., 1986, Multistage alteration of the extrusive sequence, Troodos ophiolite, Cyprus. Unpublished PhD Thesis, Dalhousie University, Halifax, Nova Scotia, Canada, 387 pp.

Gillis, K. M. and Robinson, P. T., 1985, Low-temperature alteration of the extrusive sequence, Troodos ophiolite, Cyprus. Canadian Mineralogist, 23, 431-441.

Gillis, K. M., and Robinson, P. T., 1988, Distribution of alteration zones in the upper oceanic crust. Geology, 16, 262-266.

Gillis, K. M., and Robinson, P. T., 1990, Patterns and processes of alteration in the lavas and dikes of the Troodos ophiolite, Cyprus, Journal of Geophysical Research, 95, 21523-21548.

Govett, G. J. S., and Pantazis Th. M., 1971, Distribution of Cu, Zn, Ni and Co in the Troodos Pillow Lava Series, Cyprus. Trans. Inst. Min. Mettall. (section B), 80, B27-B46.

Griffin, B. J., and Varne, R., 1980, The Macquarie Island ophiolite complex: Mid-Tertiary oceanic lithosphere from a major ocean basin. Chemical Geology, 30, 285-308.

Güven, N., 1988, Smectites. In: Hydrous Phyllosilicates (exclusive of micas), Reviews in Mineralogy, v. 19, (ed) S. W. Bailey, Mineralogist Society of America, p. 497-559.

Hall, J. M., and Robinson, P. T., 1979, Deep crustal drilling in the North Atlantic Ocean. Science, 204, 573-586.

Hall, J. M., Fisher, B. E., Walls, C. C., Hall, S. L., Johnson, H. P., Bakor, A. R., Agrawal, V., Persaud, M., and Sumaiang, R. M., 1987, Vertical distribution and alteration of dikes in a profile through the Troodos ophiolite. Nature, 326, 780-782.

Hall, J. M., and Botros, 1987, Evidence relevant to the

hydrothermal discharge pattern during formation of the Agrokipia 'B' Ore Deposit, Cyprus. In: P. T. Robinson, I. L. Gibson, and A. Panayiotou (ed.), Cyprus Crustal Study Project: Initial Report, Holes CY-2 and 2a. Geological Survey of Canada, p. 29-38.

Hall, J. M., Walls, C. C., and Yang, J-S., 1989a, Constructional features of Troodos type oceanic crust and implications for the distribution of economic ore bodies and for in-situ oceanic crust. Canadian Journal of Earth Sciences, 26, 1172-1184.

Hall, J. M., Fisher, B., Walls, C., Ward, T., Hall, L., Johnson, H. P., and Pariso, J., 1989b, Magnetic properties, oxide petrography, and alteration in the Cyprus Crustal Study Project Drill Hole CY-4 section through the Lower Sheeted Complex and Upper Plutonic Complex of the Troodos, Cyprus, ophiolite. In: Cyprus Crustal Study Project: Initial Report, Hole CY-4, (eds.) I. L. Gibson, J. Malpas, P. T. Robinson and C. Xenophontos, Geologial Survey of Canada, Paper 88-9. p. 235-278.

Hall, J. M., Walls, C. C., and Yang, J-S., 1990, Constructional features of the Troodos ophiolite and implications for the distribution of orebodies and the generation of oceanic crust: Reply. Canadian Journal of Earth Sciences, 27, 1139-1141.

Hall, J. M., Walls, C. C., Yang, J-S., Hall, L., and Bakor, A. R., 1991, The magnetization of oceanic crust: contribution to knowledge from Troodos, Cyprus, ophiolite. Canadian Journal of Earth Sciences. (in press)

Hannington, M. D., Herzig, P. M., and Alt, J. C., 1990, the distribution of gold in sub-seafloor stockwork mineralization from DSDP hole 504B and the Agrokipia B deposit, Cyprus. Canadian Journal of Earth Science, 27, 1409-1417.

Hekinian, R., and Bideau, D., 1985, Volcanism and mineralization of the oceanic crust on the East Pacific Rise. In: Metallogeny of Basic and Ultrabasic Rocks. Edinburg: Institute of Mining and Metallurgy. p. 3-20.

Hekinian, R., Fevrier, M., Bischoff, J. L., Picot, P., and Shanks, W. C., 1980, Sulfide deposits from the East Pacific Rise near 21° N. Science, 207, 1433-1444.

Hekinian, R., and Fouquet, Y., 1985, Volcanism and metallogenesis of axial and off-axial structures on the East Pacific Rise near 13°N. Economic Geology, 80, 221-249.

Herzig, P. M., and Friedrich, G. H., 1987, Sulfide

mineralization, hydrothermal alteration and chemistry in the drill hole CY-2a, Agrokipia, Cyprus. In: P. T. Robinson, I. L. Gibson and A. Panayiotou (ed.), Cyprus Crustal Study Project: Initial Report, Holes CY-2 and 2a, Geological Survey of Canada, Paper 95-29, p. 103-138.

Herzig, P. M. von Stackelberg, U., and Petersen, S., 1990, Hydrothermal mineralization from the Valu Fa Ridge, Lau back-arc basin (SW Pacific), Marine Mining, 9, 271-301.

Hodges, F. N., and Papike, J. J., 1976, DSDP Site 334: Magmatic cumulates from oceanic Layer 3. Journal of Geophysical Research, 81, 4135-4151.

Honnorez, J., Emmermann, R., Hubberten, H. W., Laverne, C., and Muehlenbachs, K., 1983, Alteration processes in layer 2 basalts, DSDP hole 504B, Costa Rica Rift. Initial Report of Deep SEA Drilling Project, 69, 509-546.

Horibe, Y., Kim, K. -R., and Craig, H., 1986, Hydrpthermal methane plumes in the Mariana back-arc spreaidng centre. Nature, 324, 131-133.

Horne, L., and Robinson, P. T., 1986, Cyprus Crustal Study Project, Hole CY-1a, edited core descriptions. Unpublished report, Dalhousie University, Halifax, Nova Scotia, 700 p.

Hughes, C. J., 1982, Igneous Petrology. Developments in Petrology 7, Elsevier, Amsterdam-Oxford-New York, p. 147-155.

Hussong, D. M., Fryer, P. B., Tuthill, L. D., and Wipperman, L. K., 1979, The geological and geophysical setting near DSDP Site 395, North Atlantic Ocean. Initial Reports of the Deep Sea Drilling Project, v. 45: Washington (U.S. Government Printing Office), p.23-38.

Hussong, D.M., and Uyeda, S., 1982, Tectonic processes and history of the Mariana Arc: A synthesis of the results of Deep Sea Drilling Project Leg 60. Initial Report of Deep Sea Drilling Project, 60, 909-929.

Jamieson, H. E., Lydon, J. W., 1987, Geochemistry of a fossil ore-solution aquifer: chemical exchange between rock and hydrothermal fluid recorded in the lower portion of research drill hole CY-2a, Agrokipia, Cyprus. In: P. T. Robinson, I. L. Gibson and A. Panayiotou (ed.), Cyprus Crustal Study Project: Initial Report, Holes CY-2 and 2a, Geological Survey of Canada, Paper 95-29, p. 139-152.

Jenkyns, H. C., and Winterer, E. L., 1982, Paleoceanography of Mesozoic ribbon radiolarites. Earth and Planetary Science Letters, 60, 351-375.

Jenner, G. A., 1981, Geochemistry of high-Mg andesites from Cape Vogel, Papua New Guinea. Chemical Geology, 33, 307-332.

Jenner, G. A., Cawood, P. A., Rautenschlein, M., and White, W. M., 1987, Composition of back-arc basin volcanics, Valu Fa Ridge, Lau Basin: evidence for a slab-derived component in their mantle source. Journal of Volcanology and Geothermal Research, 132, 209-222.

Juteau, T., Eissen, J. P., Francheteau, J., Needham, D., Choukroune, P., Rangin, C., Seguret, M., Ballard, R. D., Fox, P. J., Normark, W. R., Carranza, A., Cordoba, D., and Guerrero, J., 1980, Homogeneous basalts from the East Pacific Rise at 21°N: Steady state magma reservoirs at moderately fast spreading centres. Oceanol. Acta, 3, 487-503.

Kappel, E. S., and Normark, W. R., 1987, Morphometric variability within the axial zone of the Southern Juan de Fuca Ridge: interpretation from Sea MARC II, Sea MARC I, and Deep-Sea photography, Journal of Geophysical Research, 92, 11291-11302.

Kappel, E.S. and Ryan, W.B.F., 1986, Volcanic episodicity and a non-steady state rift valley along Northeast Pacific Spreading Centres: evidence from sea MARC I. Journal Geophysical Research, v. 91, 13925-13940.

Kappel, E. S., and Franklin, J. M., 1989, Relationships between geologic development of ridge crests and sulfide deposits in the Northerneast Pacific Ocean. Economic Geology, 84, 485-505.

Karson, J. A., Thompson, G., Humphris, S. E., Edmond, J. M., Bryan, W.B., Brown, J. R., Winters, A. T., Pockalny, R. A., Casey, J. F., Campbell, A. C., Klinkhammer, G., Palmer, M. R., Kinzler, R. J., and Sulanowska, M. M., 1987, Along-axis variations in seafloor spreading in the MARK area. Nature, 328, 681-685.

Karson, J. A., and Rona, P. A., 1990, Block-tilting, transfer faults, and structural contral of magmatic and hydrohermal processes in the TAG areas, Mid-Atlantic Ridge 26°N. Grological Society of America Belletin, 102, 1635-1645.

Kelley, D. S., 1990, Fluid circulation in a submarine paleohydrothermal system, Troodos ophiolite, Cyprus: fluid inclusion evidence for deep-seated circulation of brine in the oceanic crust. Unpublished PhD thesis.

Kent, G. M., Harding, A. J., and Orcutt, J. A., 1990, Evidence for a smaller magma chamber beneath the East Pacific Rise at 9°30'N. Nature, 344, 650-653.

Kennett, J. P., 1982, Marine Geology. Prentice-Hall, Inc., Englewood Cliffs, N. J. p. 203-232.

Koski, R. A., 1987, Sulfide deposits on the sea floor: geological models and resource perspectives based on sulfides in ophiolite sequences. Marine Minerals, (eds.) P. G. Teleki, M. R. Dobson, J. R. Moore, and U. von Stackelberg, D. Reidel Publishing Company, p. 301-316.

Kristmannsdottir, H., and Tomasson, J., 1978, Zeolite zones in geothermal areas iceland. In: Natural Zeolites, (eds) L. B. Sand and F. A. Mumpton, Pergamon, Oxford, p. 277-284.

Kurnosov, V. B., Robinson, P. T., Chudaev, O. V., Kholodkevich, I. V., and Petachenko, E. D., 1987, Secondary minerals in the CCSP Drill Holes CY-2 and CY-2a, Agrokipia, Cyprus. In: P. T. Robinson, I. L. Gibson and A. Panayiotou (ed.), Cyprus Crustal Study Project: Initial Report, Holes CY-2 and 2a, Geological Survey of Canada, Paper 95-29, p. 69-78.

Lafoy, Y., Ausende, J. M., Ruellan, E., Huchon, P., and Honza, E., 1990, The 16°40'S triple junction in the North Fiji Basin (SW Pacific). Marine Geophysical Researches, 12, 285-296.

Laird, J., 1988, Chlorites: metamorphic petrology. In: Hydrous Phyllosilicates (exclusive of micas), Reviews in Mineralogy v. 19, (ed.) S. W. Bailey, Mineralogist Society of America, p. 405-453.

Langmuir, C., and Bender, J., 1984, The geochemistry of oceanic basalts in the vicinity of transform faults: observations and implications. Earth and Planetary of Sciences Letters, 69, 107-127.

Langmuir, C. H., Bender, J. F., and Batiza, R., 1986, Petrological and tectonic segmentation of the East Pacific Rise, 5°30'-14°30'N. Nature, 322, 422-429.

Langseth, M. G., Cann, J. R., Natland, J. H., and Hobart, M., 1983, Geochemical phenomena at the Costa Rica Rift: background and objectives for drilling at Deep Sea Drilling Project Sites 501, 504, and 505. Init. Repts. DSDP, 69: Washington (U.S. Govt. Printing Office), p. 5-30.

Laurent, R., 1990, Parental magma and crystal fractionation modeling of the CY-4 plutonic rocks, Troodos ophiolite, Cyprus. In: Ophiolites, Oceanic Crustal Analogues, Proceedings of the Symposium "Troodos 1987", eds. by J. Malpas, E. Moores, A. Panayiotou, C. Xenophontos, Cyprus. p. 139-148.

Lewis, B. T. R., 1979, Periodicities in volcanism and longitudinal magma flow on the East Pacific Rise at 23° N.

Geophysical Research Letters, v. 6, 753-756.

Leitch, E. C., 1984, Island arc elements and arc-related ophiolites. Tectonophysics, 106, 177-203.

Lichtman, G. S., and Eissen, J-P., 1983, Time and space constraints on the evolution of medium-rate spreading canters. Geology, v. 11, 592-595.

Liou, J. G., 1971, P - T stabilities of laumontite, wairakite, lawsonite and related minerals in the system $CaAl_2Si_2O_8$ - SiO_2 - H_2O. Journal of Petrology, 12, 379-411.

Liou, J. G., 1973, Synthesis and stability relations of epidote, $Ca_2Al_2FeSi_3O_{12}(OH)$. Journal of Petrology, 14, 381-413.

Lonsdale, P. F., 1977, Abyssal pshoehoe with lava coils at the Galapagos Rift. Geology, 5, 147-152.

Lonsdale, P. F., Bischoff, J. L., Burns, V. M., and Sweeney, R. E., 1980, A high-temperature hydrothermal deposit on the seabed at a gulf of California spreading centre. Earth and Planetary Science Letters, V. 49, 8-20.

Lydon, J. W., 1984, Some observations on the morphology and ore textures of volcanogenic sulfide deposits of Cyprus. In: Current Research, Part A, Geological Survey of Canada, Paper 84-1A, p. 601-610.

Maaloe, S., and Petersen, T. S., 1981, Petrogenesis of oceanic andesites. Journal of Geophysical Research, 86, 10273-10286.

Macdonald, K. C., 1982, Mid-ocean ridges: Fine scale tectonic, volcanic and hydrothermal processes within the plate boundary zone. Annual Reviews of Earth and Planetary Science, 10, 155-190.

Macdonald, K.C., 1983, A geophysical comparison between fast and slow spreading canters: constrains on magma chamber formation and hydrothermal activity. In: Rona, P.A., Bostrom, K., Laubier, L., and Smith, K.L., Hydrothermal Processes at Seafloor Spreading Centres, Series IV: Marine Science, NATO CONFERENCE SERIES, New York and London, p 27-52.

Macdonald, K. C., 1986, The crest of the Mid-Atlantic Ridge: models for crustal generation processes and tectonics. in The Geology of North America, Vol. M, The Western North Atlantic Region, (eds) by P. R. Vogt and B. E. Tucholke, The Geological Society America, pp 51-68.

Macdonald, K. C., Haymon, R., and Chor, A., 1989, A 220 km_2 recent erupted lava field on the East Pacific Rise near lat

8°S. Geology, 17, 212-226.

Macdonald, K. C., Fox, P. J., Perram, L. J., Eisen, M. F., Haymon, R. M., Miller, S. P., Carbotte, S. M., Vormier, M.-H., and Shor, A. N., 1988, A new view of the mid-ocean ridge from the behaviour of rodge-axis discontinuities. Nature, 335, 217-225.

Macdonald, K. C., 1990, A slow but restless ridge. Nature, 348, 108-109.

Machado, N., Ludden, J., Brooks, C., and Thompson, G., 1982, Fine scale isotopic heterogeneity in the sub-Atlantic mantle. Nature, 295, 226-228.

Malahoff, A, 1982, A comparison of the massive submarine polymetallic sulfides of the Galapagos Rift with some continental deposits. Marine Technical Society Journal, 16, 39-45.

Malinverno, A., 1991, Inverse square-root dependence of mid-ocean-ridge flank roughness on spreading rate. Nature, 352, 58-60.

Malpas, J., and Langdon, G., 1984, Petrology of the Upper Pillow Lava suite, Troodos ophiolite, Cyprus. In: I. G. Gass, S. J. Lippard and A. W. Shelton (ed.), Ophiolites and Oceanic Lithosphere, Geological Society Special Publications, 155-167.

Malpas, J., Brace, T., and Dunsworth, S. M., 1989, Structural and petrologic relationships of the CY-4 drill hole of the Cyprus Crustal Study Project. In: I. L. Gibson, J. Malpas, P. T. Robinson and C. Xenophontos (ed.), Cyprus Crustal Study Project: Initial Report, Hole CY-4, Geological Survey of Canada, Paper 88-9, p. 39-67.

Marchig, V., Gundlach, H., Holler, G., and Wilke, M., 1988, New discoveries of massive sulfides on the East Pacific Rise. Marine Geology, 84, 179-190.

Maruyama, S., and Liou, J. G., 1988, Ocean floor metamorphism at different tectonic settings: a review on the DSDP drilling projects. Eos, Transitions American Geophysical Union, 69, (44), p. 1403.

McCulloch M. T., and Cameron, W. E., 1983, Nd-Sr isotopic study of primitive lavas from the Troodos ophiolite, Cyprus: evidence for a subduction-related setting. Geology, 11, 727-731.

Mehegan, J. M., and Robinson, P. T., 1982, Secondary mineralization and hydrothermal alteration inthe Reydarfjordur

drill core, Eastern Iceland. Journal of Geophysical Research, 87, 6511-6524.

Mehegan, J. M., and Robinson, P. T., 1985, Lava compositions of the Troodos ophiolite, Cyprus. Eos, American Geophysical Union Transactions, 66, 1123.

Mehegan, J. M., 1988, Temporal, spatial, and chemical evolution of the Troodos ophiolite lavas, Cyprus: supra-subduction zone volcanism in the Tethys Sea. Unpublished PhD thesis, Dalhousie University, Halifax, Nova Scotia, Canada, 700 pp.

Mehegan, J. M., and Robinson, P. T., Lava group and volcanic stratigraphy of the CCSP boreholes Cy-1 and Cy-1a, Troodos ophiolite, Cyprus. Cyprus Crustal Study Project: Initial Report, Holes CY-1 and 1a. (in press)

Meijer, A., Anthony, E., and Reagan, M., 1981, Petrology of volcanic rocks from the fore-arc sites. Initial Report of Deep Sea Drilling Project, 60, 709-729.

Miyashiro, A., 1973, The Troodos ophiolite complex was probably formed in an island arc. Earth and Planetary Sciences Letters, 19, 218-224.

Miyashiro, A., 1975, Origin of Troodos and other ophiolites: a reply to Hynes. Earth and Planetary Science Letters, 25, 217-222.

Moores, E. M., and Vine, F. J., 1971, the Troodos massif, Cyprus and other ophiolites as volcanic crust: evaluation and implications. Royal Society of London Philosophical Transaction, series A, v. 268, 443-466.

Moores, E. M., 1982, Origin and emplacement of ophiolites. Reviews in Geophysics and Space Physics, 20, 735-760.

Moores, E. M., Robinson, P. T., Malpas, J., Xenophonotos, C., 1984, Model for the origin of the Troodos massif, Cyprus, and other mideast ophiolites. Geology, 12, 500-503.

Morton, J. L., and Sleep, N. H., 1985, Seismic reflections from a Lau Basin magma chamber. In: D. Scholl and T. Vallier, eds., Geology of offshore resources of Pacific Island Arcs-Tonga region. Earth Science Series 2, p. 441-453.

Morin, R. H., Anderson, R. N., and Barton, C. A., 1989, Analysis and interpretation of the borehole televiewer log: information on the state of stress and the lithostratigraphy at Hole 504B. In: Becker, K., Sakai, H., et al., Proceedings of the Ocean Drilling Program, Scientific Results, 111:

College Station, TX (Ocean Drilling Program), 109-118.

Mottl, M. J., 1983, Metabasalts, axial hot springs and the structure of hydrothermal systems at mid-ocean ridges. Geological Society of American Bulletin, 94, 161-180.

Muenow, D. W., Garcia, M. O., Aggrey, K. E., Bednarz, U., and Schmincke, H. U., 1990, Volatiles in submarine glasses as a discriminant of tectonic origin: application to the Troodos ophiolite. Nature, 343, 159-161.

Mukasa, S. B., and Ludden, J. N., 1987, Uranium-lead isotopic ages of plagiogranites from the Troodos ophiolite, Cyprus, and their tectonic significance. Geology, 15, 825-828.

Nicolas, A., Ceuleneer, G., Boudier, F., and Misseri, M., 1988, A structural mapping in the Oman ophiolites: mantle diapirism along an oceanic ridge. Tectonophysics, 151, 27-56.

Nicolas, A., 1989, Structures of Ophiolites and Dynamics of Oceanic Lithosphere. Kluwer Academic Publishers, p. 37-90.

Nisbet, E. G., and Fowler, C. M. R., 1978, Mid-Atlantic Ridge at 37-42°N and some geophysical and petrological constrains. The Geophysical Journal of the Royal Astronomical Society, 54, 631-660.

Nojiri, Y., Ishibashi, J., Kawai, T., Otsuki, A., and Sakai, H., 1989, Hydrothermal plumes along the North Fiji Basin spreading axis. Nature, 342, 667-670.

Normark, W. R., Morton, J. L., Koski, R. A., and Clague, A, 1983, Active hydrothermal vents and sulfide deposits on the southern Juan de Fuca Ridge. Geology, 11, 158-163.

Normark, W. R., Morton, J. L., and Ross, S. L., 1987, Submersible observations along the southern Juan de Fuca Ridge: 1984 Alvin program. Journal of Geophysical Research, 92, 11283-11290.

Ocean Drilling Program, Leg 106 Scientific Party, 1986, Drilling the Snake Pit hydrothermal sulfide deposit on the Mid-Atlantic Ridge, lat 23°22'N. Geology, 14, 1004-1007.

Oudin, E., Picot, P., and Pouit, G., 1981, Comparison of sulfide deposits from the East Pacific Rise and Cyprus. Nature, 291, 404-407.

Oudin, E., and Constantinou, G., 1984, Black smoker chimney fragments in Cyprus sulfide deposits. Nature, 308, 349-353.

Pantazis, Th. M., 1967, The Geology and Mineral Resources of

the Pharmakas-Kalavasos Area. Geological Survey Department Cyprus, Memoir 8, 190 pp.

Prinz, M., Keil, K., Green, J. A., Reid, A. M., Bonatti, E., and Honnorez, J., 1976, Ultramafic dregded samples from the equatorial Mid-Atlantic Ridge and fracture zones. Journal of geophysical Research, 81, 4087-4103.

Rautenschlein, M., Jenner, G. A., Hertogen, J., Hofmann, A. W., Kerrich, R., Schmicke, H.-U., and White, W. M., 1985, Isotopic and trace element composition of volcanic glasses from the Akaki Canyon, Cyprus: implications for the origin of the Troodos ophiolite, Earth and Planetary Science Letters, 75, 369-383.

Richards, H. G., and Boyle, J. F., 1985, Origin, alteration and mineralization of inter-lava metalliferous sediments of the Troodos ophiolite, Cyprus. In: Metallogeny of Basic and Ultrabasic Rocks. Edinburg: Institute of Mining and Metallurgy, p. 21-31.

Richards, H. G., Cann, J. R., Jensenius, 1989, Mineralogical zonation and metasomatism of the alteration pipes of Cyprus sulfide deposits. Economic Geology, 84, 91-115.

Richardson, C. J., Cann, J. R., Richards, H. G., and Cowan, J. G., 1987, Metal-depleted root zones of the Troodos ore-forming hydrothermal systems, Cyprus. Earth and Planetary Science Letters, 84, 243-253.

Robertson, A. H. F., 1975, Cyprus umbers: basalt-sediment relations in Mesozoic ocean floor. Journal of Geological Society of London, 131, 511-531.

Robertson, A. H. F., and Hudson, J. D., 1973, Cyprus umbers: chemical precipitates on a Tethyan ocean ridge. Earth and Planetary Science Letters, 18, 93-101.

Robinson, P. T., 1987, Holes CY-2 and CY-2a of the Cyprus Crustal Study Project: an outline of objectives and operations. In: P. T. Robinson, I. L. Gibson and A. Panayiotou (ed.), Cyprus Crustal Study Project: Initial Report, Holes CY-2 and 2a, Geological Survey of Canada, Paper 95-29, p. 1-17.

Robinson, P. T., Melson, W. G., O'Hearn, T., and Schmincke, H-U., 1983, Volcanic glass compositions of the Troodos ophiolite, Cyprus. Geology, 11, 400-404.

Robinson, P. T., and Malpas, J., 1990, The Rroodos ophiolite of Cyprus: New perspectives on its origin and emplacement. In: Ophiolites, Oceanic Crustal Analogues, Proceedings of the Symposium "Troodos 1987", eds. by J. Malpas, E. Moores, A.

Panayiotou, C. Xenophontos, Cyprus. p. 13-26.

Rona, P. A., 1984, Hydrothermal mineralization at seafloor spreading centers. Earth Science Review, 20, 1-104.

Rona, P. A., 1987, Hydrothermal mineralization at slow-spreading centers: The Atlantic model. Marine Mining, 6, 1-7.

Rona, P. A., 1988, Hydrothermal mineralization at oceanic ridges. Canadian Mineralogist, 26, 431-465.

Rona, P. A., and Clague, D. A., 1989, Geologic control of hydrothermal discharge on the northern Gorda Ridge. Geology, 17, 1097-1101.

Salisbury, M. H., Christensen, N. I., Vine, F. J., Smith, G. C. and Eleftheriou, S., 1989, Geophysical structure of the Troodos ophiolite from downhole logging. In: I. L. Gibson, J. Malpas, P. T. Robinson and C. Xenophontos (ed.), Cyprus Crustal Study Project: Initial Report, Hole CY-4, Geological Survey of Canada, Paper 88-9, p. 351-369.

Schiffman, P., and Smith, B. M., 1988, Petrology and oxygen isotope geochemistry of a fossil seawater hydrothermal system within the Solea Graben, northern Troodos ophiolite, Cyprus. Journal of Geophysical Research, 93, 4612-4624.

Schilling, J-G., Kingsley, R., and Devine, J., 1982, Galapagos hot spot-spreading centre system 1. Spatial petrological and geochemical variations (83°W-101°W). Journal of Geophysical Research, 87, 5593-5610.

Schmincke, H.-U., Rautenschlein, M., Robinson, P. T., Mehegan, J. M., 1983, Troodos extrusive series of Cyprus: A comparison with oceanic crust. Geology, 11, 405-409.

Schouten, H., and Klitgord, K., 1982, The memory of the accreting plate boundary and the continuity of fracture zones. Earth and Planetary of Sciences Letters, 59, 255-266.

Scott, S. D., 1987, Seafloor polymetallic sulfides: Scientific curiosities or mines of the future? Marine Minerals, (eds.) P. G. Teleki, M. R. Dobson, J. R. Moore, and U. von Stackelberg, D. Reidel Publishing Company, 277-300.

Searle, D. L., 1972, Mode of occurrence of the cupriferous pyrite deposits of Cyprus. Tran. Inst. Min. Metall. (Section B), 81, B189-B197.

Searle, D. L., and Panayiotou, A., 1980, Structural implications in the evolution of the Troodos massif, Cyprus. In: Panayiotou, A. (ed.), Ophiolite, Proceedings,

International Ophiolite Symposium, Cyprus 1979, Ministry of Agriculture and Natural Resources, Geological Survey Department,

Seyfried Jr., W. E., and Mottl, M. J., 1982, Hydrothermal alteration of basalt by seawater under seawater-dominated conditions. Geochim. Cosmoschim. Acta, 46, 985-1002.

Shipboard Scientic Party, Leg 37, 1977, Initial Reports of the Deep Sea Drilling Project, v. 37: Washington (U.S. Government Printing Office), 1008 pp.

Shipboard Scientific Party, Leg 45, 1979, Site 395: 23°N, Mid-Atlantic Ridge, Initial Reports of the Deep Sea Drilling Project, v. 45: Washington (U.S. Government Printing Office), p. 131-264.

Shipboard Scientic Parties, Leg 51-53, 1980, Part I: Site reports, site surveys, and downhole geophysical experiments. Initial Reports of the Deep Sea Drilling Project, v. 51, 52, 53: Washington (U.S. Government Printing Office). p. 3-626.

Shipboard Sceintific Parties, Sites 501 and 504, 1983, Sediments and ocean crust in an area of high heat flow on the southern flank of the Costa Rica Rift, Initial Report of the Deep Sea Drilling Project, 69, p. 31-173.

Shipboard Sceintific Party, Hole 504B, Leg 83, 1985, Initial Report of the Deep Sea Drilling Project, 83, p. 13-118.

Shipboard Scientific Party, Site 504, Proceedings of the Ocean Drilling Program, Initial Report, Part A, 111, pp. 253-346, Ocean Drilling Program, College Station, Tex., 1988.

Shipboard Scientific Party, Site 786, 1990, Site 786. In:Fryer, P., Pearce, J. A., Stokking, L. B., et al., Proc. ODP, Init. Repts., 125: College Station, TX (Ocean Drilling Program), 313-366.

Simonian, K. O., and Gass, I. G., 1978, Arakapas fault belt, Cyprus, a fossil transform fault, Geological Society of America Bulletin, 89, 1220-1230.

Smewing, J. D., Simonian, K. O., and Gass, I. G., 1975, Metabasalts from the Troodos Massif, Cyprus: genetic implication deduced from petrography and trace element geochemistry. Contribution to Mineralogy and Petrology, 51, 49-64.

Smith, D. K., and Cann, J. R., 1990, Hundreds of small volcanoes on the median valley floor of the Mid-Atlantic Ridge at 24-30°N. Nature, 348, 152-155.

Smith, G. C., and Vine, F. J., 1987, Seismic velocities in basalts from CCSP dill holes Cy-2 and CY-2a at Agrokipia Mines, Cyprus. In: P. T. Robinson, I. L. Gibson and A. Panayiotou (ed.), Cyprus Crustal Study Project: Initial Report, Holes CY-2 and 2a, Geological Survey of Canada, Paper 95-29, p. 295-306.

Smith, G.M., and Banerjee, S.K., 1986, Magnetic structure of the upper kilometre of the marine crust at DSDP Hole 504B, Eastern Pacific Ocean. Journal of Geophysical Research, 91, 10337-10354.

Spiess, E. N., Macdonald, K. C., Atwater, T., Ballard, R., Carranza, A., Cordba, D., Cox, C., Diaz Garcia, V. M., Francheteau, J., Guerrero, J., Hawkins, J., Hayman, R., Hessler, R., Juteau, T., Kastner, M., Larson, R., Luyendyk, B., MacDougall, J. D., Muller, S., Normark, W., Orcott, J., and Rangin, C., 1980, East Pacific Rise: Hot springs and geophysical experiments. Science, 207, 1421-1433.

Spooner, E. T. C., 1977, Hydrodynamic model for the origin of the ophiolite cupriferous pyritic ore deposits of Cyprus. Geological Society of London Special Publications, no.7, 58-71.

Spooner, E. T. C., 1980, Cu-Pyrite mineralization and seawater convection in oceanic crust: the ophiolite ore bodies of Cyprus. Geological Association of Canada, Special Paper 20, 685-704.

Stakes, D. S., Shervais, J. W., and Hopson, C. A. J., 1984, The volcanic-tectonic cycle of the FAMOUS and AMAR valleys, Mid-Atlantic Ridge (36° 47' N): Evidence from basalt glass and phenocryst compositional variations for a steady state magma chamber beneath the valley midsections, AMAR 3. Journal of Geophysical Research, v. 89, 6,995-7,028.

Stern, C, de Wit, M. J., and Lawrence, J. R., 1976, Igneous and metamorphic procrsses associated with the formation of Chilean ophiolites and their implication for ocean floor metamorphism, seismic layering, and magnetism. Journal of Geophysical Research, 81, 4370-4380.

Stoffa, P., and Talwani, M., 1978, Exploring the crust beneath the oceans. In: Lamont-Doherty Geol. Observ. Yearbook. New York, Columbia University.

Sunkel, G., Bednarz, U., and Schmincke, H.-U., 1987, The basaltic andesite-andesite and the andesite-dacite series from the ICRDG Drill Holes CY-2 and CY-2a. II. Alteration. In: P. T. Robinson, I. L. Gibson and A. Panayiotou (ed.), Cyprus Crustal Study Project: Initial Report, Holes CY-2 and 2a,

Geological Survey of Canada, Paper 95-29, pp. 205-220.

Sunkel, G., 1990, Origin of petrological and geochemical variations of Lau Basin lavas (SW Pacific). Marine Mining, 9, 205-234.

Taylor, R. N., 1990, Geochemical stratigraphy of the Troodos extrusive sequence: temporal developments of a spreading center magma chamber. In: Ophiolites, Oceanic Crustal Analogues, Proceedings of the Symposium "Troodos 1987", eds. by J. Malpas, E. Moores, A. Panayiotou, C. Xenophontos, Cyprus. p. 173-183.

Thompson, G., Bryan, W. B., Ballard, R., Hamuro, K., and Melson, W. G., 1985, Axial processes along a segment of the East Pacific Rise, 10°12'N. Nature, 318, 429-433.

Thompson, G., Humphris, S. E., Schroeder, B., Sulanowska, M., and Rona, P. A., 1988, Active vents and massive sulfides at 26°N (TAG) and 23°N (Snakepit) on the Mid-Atlantic Ridge. Canadian Mineralogist, 26, 697-712.

Thy, P., 1987a, Petrogenetic implications of mineral crystallization trends of Troodos cumulates, Cyprus. Geological Magazine, 124, 1-11.

Thy, P., 1987b, Magmas and magma chamber evolution, Troodos ophiolite, Cyprus. Geology, 15, 316-319.

Thy, P., Brooks, C. K., and Walsh, J. N., 1985, Tectonic and petrogenetic implications of major and rare earth element chemistry of Troodos glasses, Cyprus. Lithos, 18, 165-178.

Thy, P., and Moores, E. M., 1988, Crustal accretion and tectonic setting of the Troodos ophiolite, Cyprus. Tectonophysics, 147, 221-245.

Toomey, D. R., Purdy, G. M., Solomon, S. C., and Wilcock, S. D., 1990, The three-dimensional seismic velocity structure of the East Pacific Rise near latitude 9°30'. Nature, 347, 639-645.

van Andel, T.H., 1983, The four dimensions of spreading axis. In: Rona, P. A., Bostrom, K., Laubier, L., and Smith, K. L., ed., Hydrothermal Processes at Seafloor Spreading Canters, Series IV: Marine Sciences, New York, p. 1-16.

Varga, R. J., and Moores, E. M., 1985, Spreading structure of the Troodos ophiolite, Cyprus. Geology, v. 13, 846-850.

Varga, R. J., and Moores, E. M., 1990, Intermittent magmatic spreading and tectonic extension in the Troodos ophiolite:

implications for exploration for black smoker-type ore deposits. In: Ophiolites, Oceanic Crustal Analogues, Proceedings of the Symposium "Troodos 1987", eds. by J. Malpas, E. Moores, A. Panayiotou, C. Xenophontos, Cyprus, p. 53-64.

Velde, B., 1985, Clay Minerals, A physical-Chemical Expanation of Their Occurrence. Elsevier, Amsterdam-Oxford-New York-Tokyo, p. 45-252.

Vine, F. J., and Smith, G. C., 1990, Structure and physical properties of the Troodos crustal section at ICRDG drillholes CY1, 1a and 4. In: Ophiolites, Oceanic Crustal Analogues, Proceedings of the Symposium "Troodos 1987", eds. by J. Malpas, E. Moores, A. Panayiotou, C. Xenophontos, Cyprus. p. 113-124.

Vogt, P. R., 1986, Magnetic anomalies and crustal magnetization. in The Geology of North America, Vol. M, The Western North Atlantic Region, (eds) by P. R. Vogt and B. E. Tucholke, p. 229-256.

von Stackelberg, U., and Shipboard Scientic Party, 1988, Active hydrothermalism in the Lau Back-Arc basin (SW-Pacific): first results from the SONNE 48 Cruise (1987). Marine Mining, 7, 431-442.

von Stackelberg, U., and Wiedicke, M., 1990, Interpretation of bottom photographs from active spreading ridges in the Lau Basin. Marine Mining, 9, 247-270.

Walker, G. P. L., 1966, Acid volcanic rocks in Iceland. Bulletin of Volcanology, 29, 375-402.

Walker, G. P. L., 1972, Compound and simple lava flows and flood basalts. Bull. Volcanol. 35, 579-590.

Walker, G. P. L., 1973, Lengths of lava flows. Royal Society of London Philosophical Transaction, series A 274, 107-118.

Walter, P., and Stoffers, P., 1985, Chemical characteristics of metalliferous sediments from eight areas on the Galapagos and East Pacific ise between 2°N and 42°S. Marine Geology, 65, 271-287.

White, D. J., and Clowes, R. M., 1990, Shallow crustal structure beneath the Juan de Fuca Ridge from 2-D seismic refraction tomography, Geophysic J. Int. 100, 349-367.

White, R. S., Detrick, R. S., Mutter, J. C., Buhl, P., Minshull, T. A., and Morris, E., 1990, New seismic imagines of oceanic crustal structure. Geology, 18, 462-465.

Wilson, R. A. M., and Ingham, F. T., 1959, The Geology og the Xeros-Troodos Area with an Account of the Mineral Resources. Geological Survey Department Cyprus, Memoir 1, 184 pp.

Winkler, H. G. F., 1974, Petrogenesis of Metamorphic Rocks, Third Edition. Springer, New York-Heidelberg-Berlin, 310 pp.

Yang, J-S., Hall, J. M., Walls, C. C., and Fisher, B. E., 1988, Variation of crustal constructional and alteration features in the spreading direction in Troodos type oceanic crust. Geological Association of Canada-Mineralogical Association of Canada, Program with Abstract, 13, A137.

Yang, J-S. and Hall, J. M., Alteration zoning in the upper part of Troodos type oceanic crust and its correlation with dike density. Regional Metamorphism of Ore Deposits and Genetic Implications (eds) P. G. Spry and L. T. Bryndzia, Proceedings of the 28th International Geological Congress, 9-19 July, 1989. 171-195.

Zierenberg, R. A., Shanks III, W. C., Seyfried, Jr., W. E., Koski, R. A., and Strickler, M. D., 1988, Minralization, alteration, and hydrothermal metamorphism of the ophiolite-hosted Turner-Albright sulfide deposit, southwestern Oregon. Journal of Geophysical Research, 93, 4657-4674.

Map 2

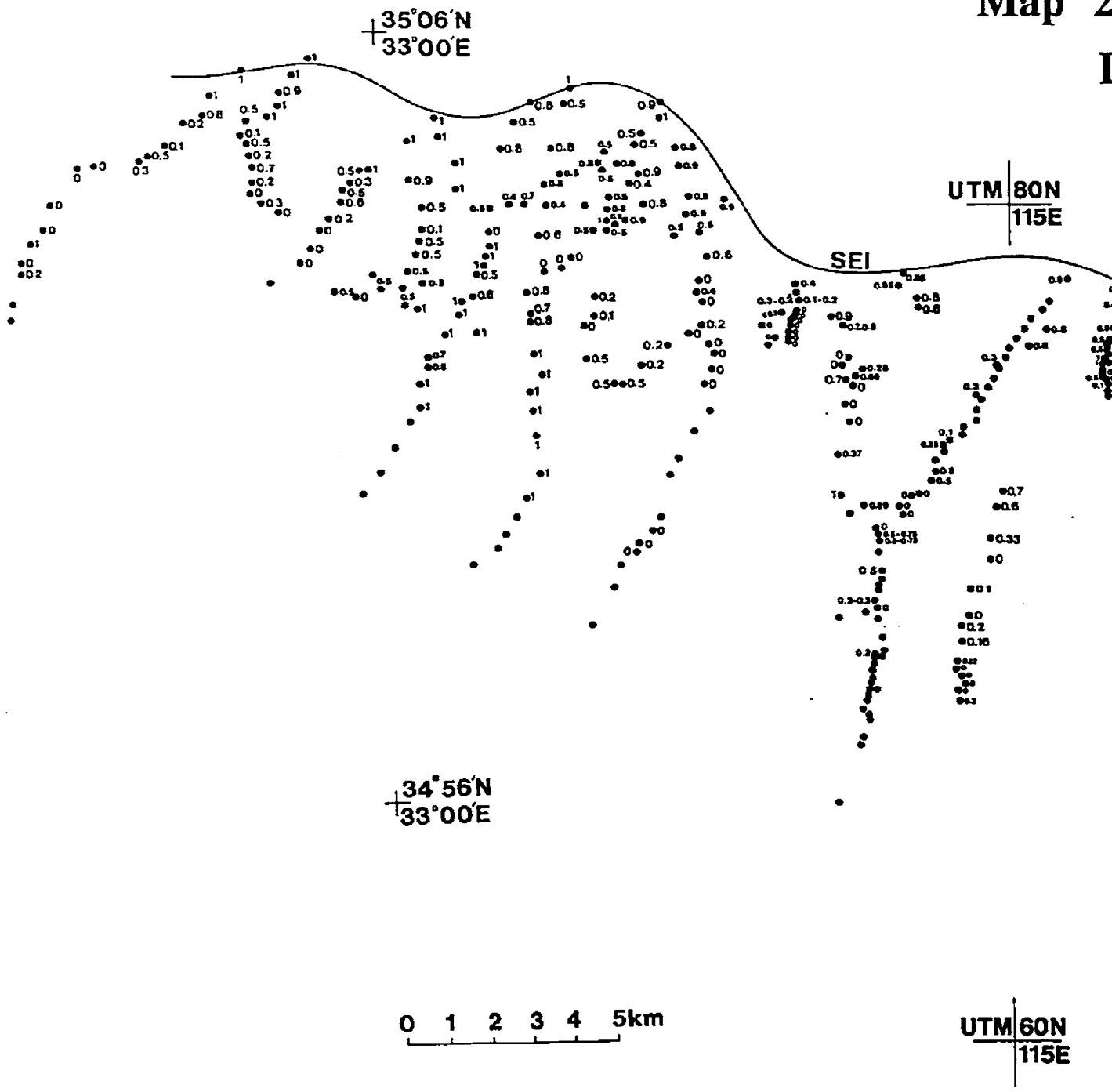
35°06′N
33°00′E
UTM 80N
115E
SEI
34°56′N
33°00′E
0 1 2 3 4 5km
UTM 60N
115E

Map 2:

Location Map For P Values

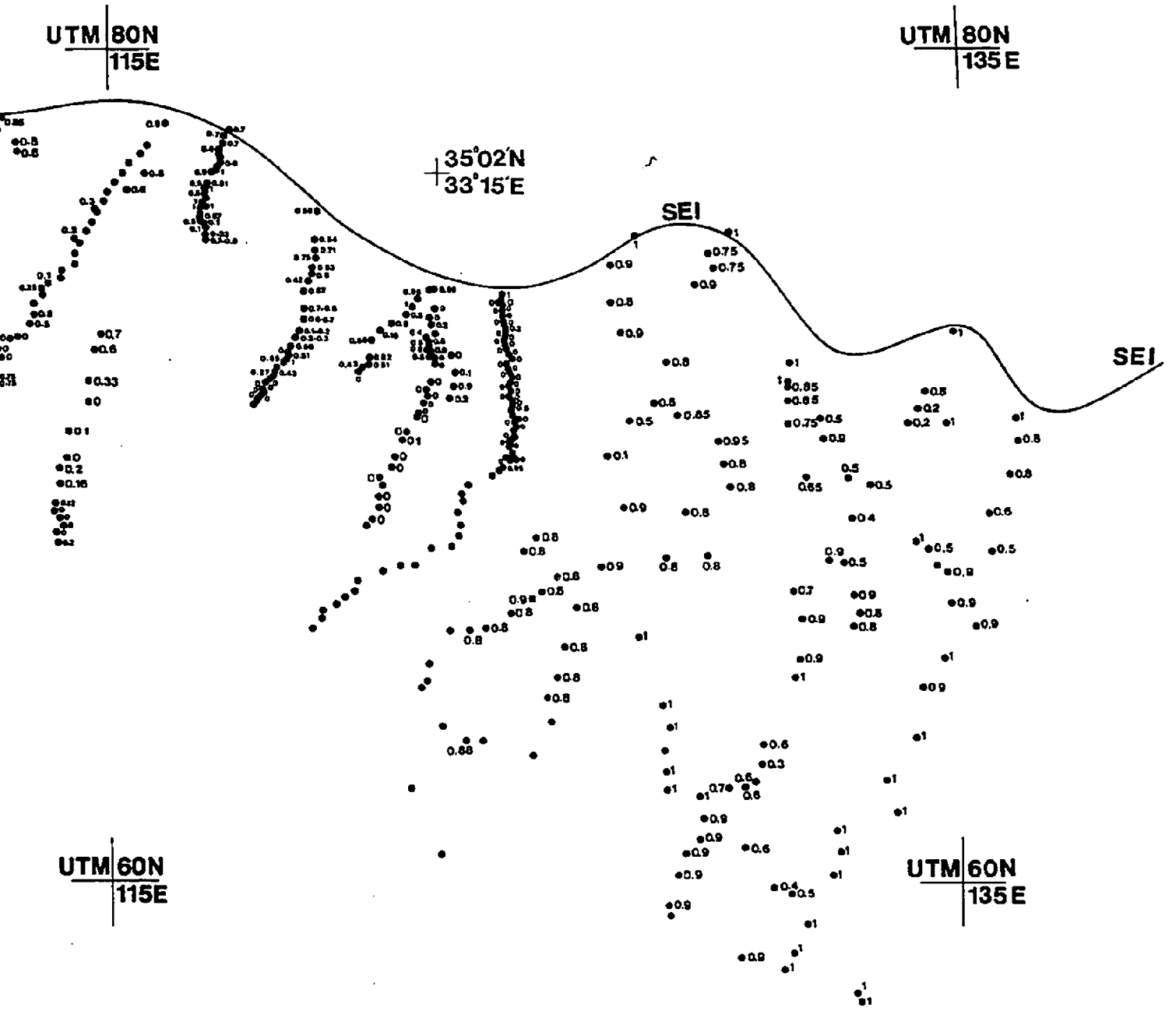

Map 3:

Loc

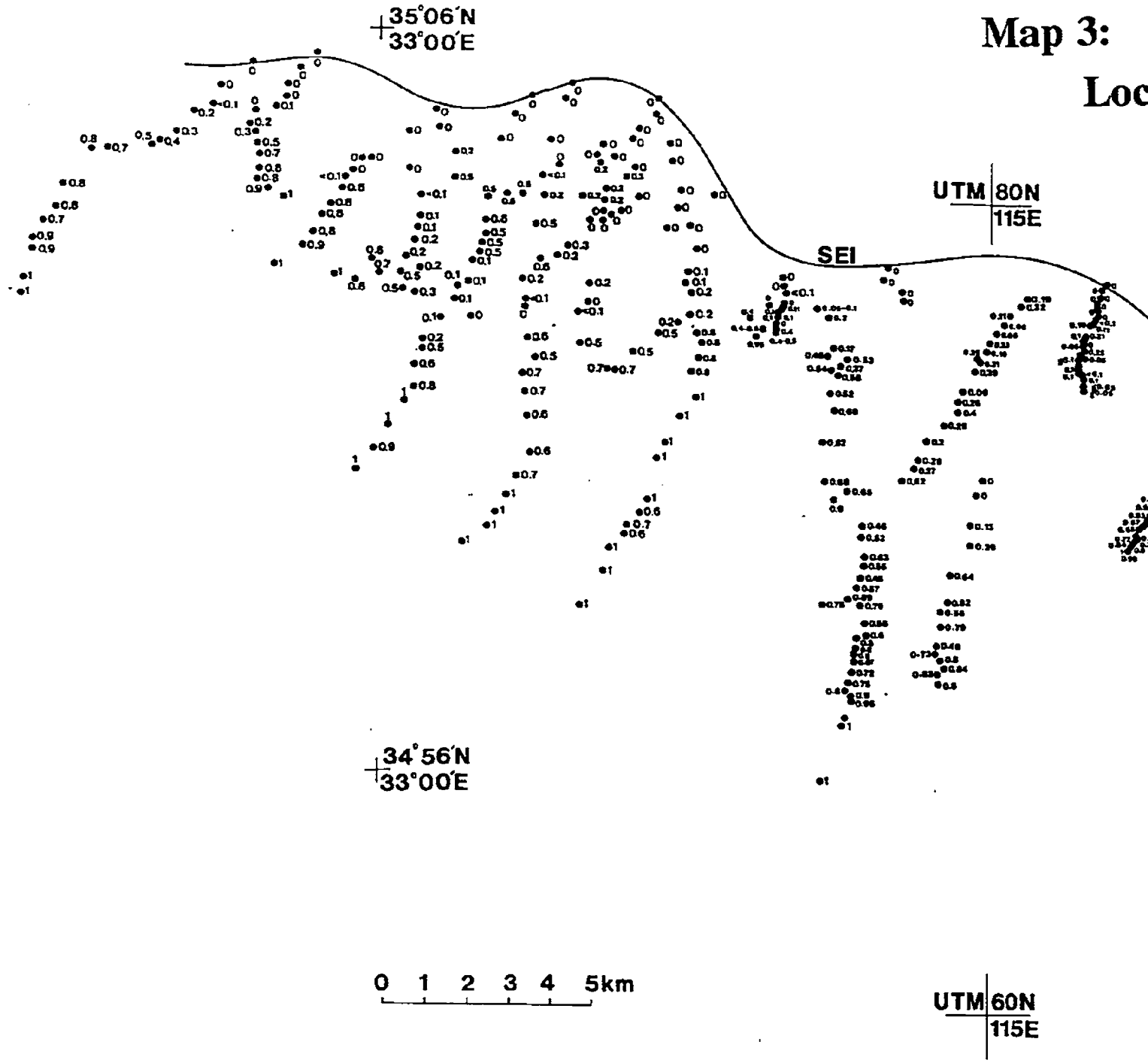
35°06'N
33°00'E
UTM 80N
115E
SEI
34°56'N
33°00'E
0 1 2 3 4 5km
UTM 60N
115E

Map 3:

Location Map For F Values

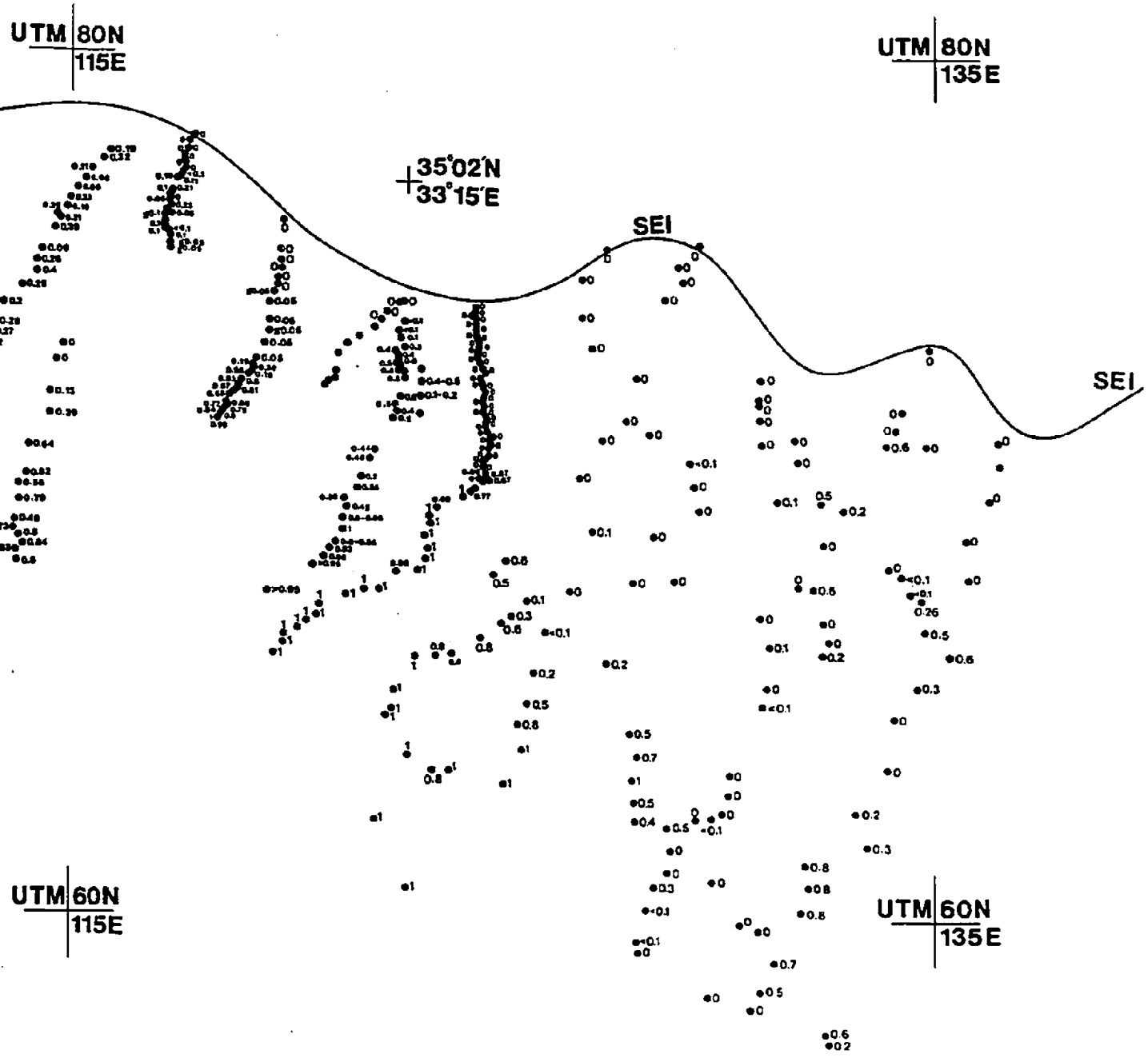

Map 1: Loc

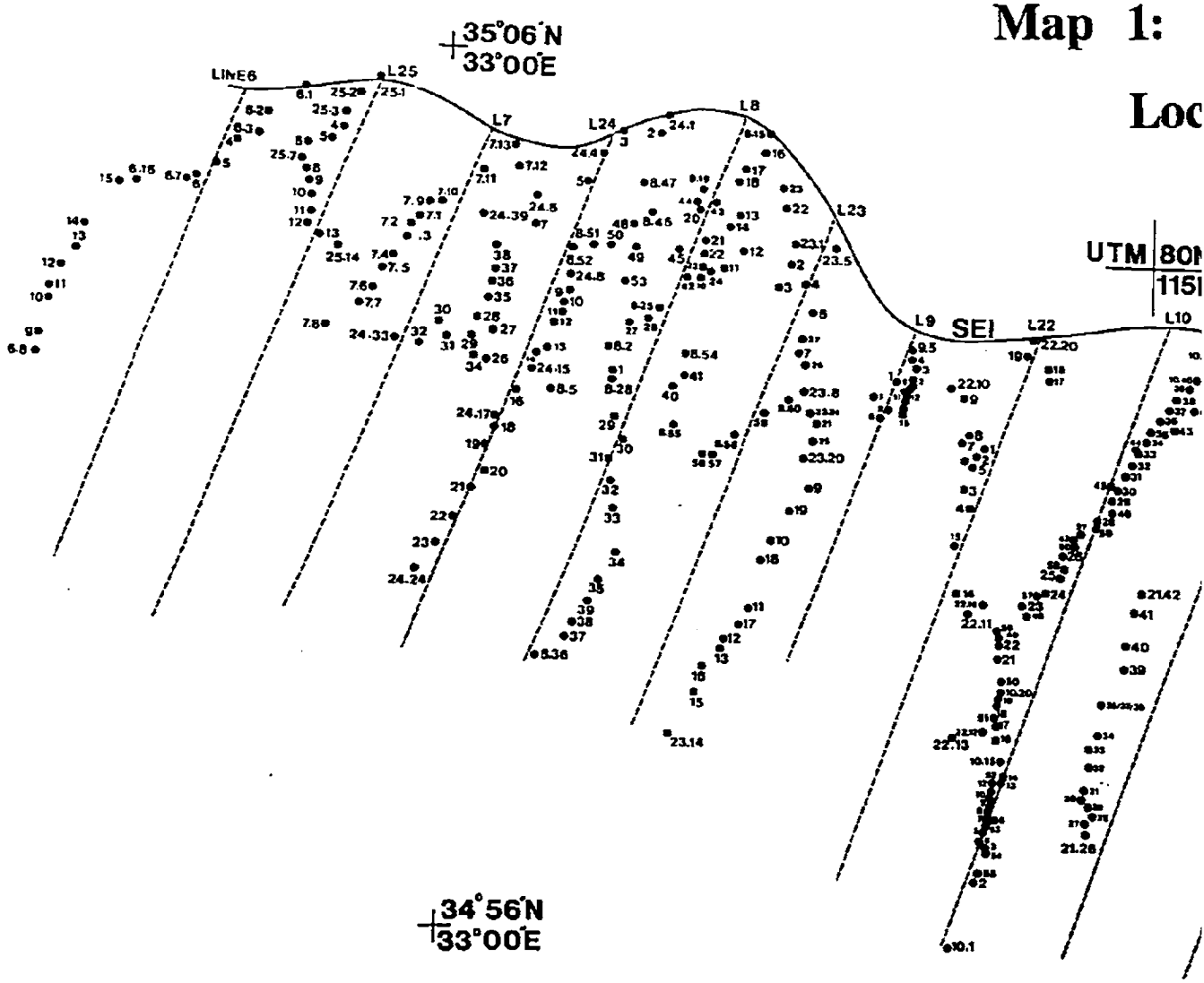
35°06'N
33°00'E
LINE6
L25
L7
L24
L8
L23
L9
SEI
L22
L10
34°56'N
33°00'E
0 1 2 3 4 5km
UTM 80N
115E
UTM 60N
115E

Map 1:

Location of Stations Measured in the Field